Bull. Min. Res. Exp. (2016) 153:1-44

Bulletin of the Mineral Research and Exploration

http://bulletin.mta.gov.tr

UPPER CRETACEOUS-TERTIARY GEOLOGY/STRATIGRAPHY OF PERTEK AND ITS VICINITY (TUNCELİ, TURKEY)

Erdal İ. HERECE[a*] and Şükrü ACAR[a]

[a] *General Directorate of Mineral Research and Exploration Department of Geological Research, Ankara, Turkey*

Research Article

Keywords:
Elazığ Magmatics, Harami formation, Kırkgeçit formation, Alibonca formation, Karabakır formation, Pertek Andesites, Pertek Fault.

ABSTRACT

The basement units of the study area are Paleozoic-Mesozoic Keban metamorphics and Late Cretaceous Elazığ magmatics. As a result of tectonic events caused by final collision in Middle Maastrichtian, all these basement units were juxtaposed, uplifted, eroded and acted as a source area for the Maastrichtian-Paleogene basins. Upper Cretaceous-Paleogene deposits were systematically sampled in order to determine their ages and lithologies. Due to new age findings and stratigraphical positions the marine units were identified as; Harami, Seske and Kırkgeçit formations. Late Oligocene-Early Miocene Alibonca formation and Pliocene Karabakır formation are the other units of the study area. Maastrichtian-Thanetian Harami formation is formed by grainstone intercalated with sandstone at the bottom and white limestone at the top. Early Lutetian Seske formation consists of conglomerate at the bottom and much nummulitic, carbonate cemented sandstone with ophiolitic fragments at the top. Kırkgeçit formation consists of sandstone-siltstone-limestone intercalation, and it is early Bartonian-early Chattian. Late Chattian-middle Burdigalian Alibonca formation consists of conglomerate at the bottom, reefal limestone in the middle and clayey limestone intercalated with algal limestone at the top. Pliocene Karabakır formation is formed by conglomerate-mudstone and locally by intercalations of pyroclastics and lavas. Pertek Andesite and Basalt Members are both vertically and laterally transitional with sedimentary lithologies of the Karabakır formation. There is no data to date the lithology; however, it was assumed that it had been Pliocene in age according to the lithostratigraphical succession. In the study area, macrotectonic events were experienced in Late Cretaceous, Early Eocene, middle-late Lutetian, Middle?-Late Miocene and in the Latest Pliocene. During the last tectonic phase, the Anatolian plate bounded by the East Anatolian Fault (EAF) in E-SE began to move westward, and the right lateral strike slip Pertek Fault activated in the study area.

Received: 08.02.2016
Accepted: 09.07.2016

1.Introduction

This study was initiated in order to prepare Elazığ K42 sheet in 1/100.000 scale. Although; c-d sheets in 1/25.000 scale consisting the southern part of K42 sheet have been studied by Herece et al. (1992), a-b sheets forming the northern part have not been studied at all. To prepare the geological maps and define the geological units of the non-investigated areas, short term field studies were carried out in the region. Within scope of the study; first 1/35 000 scale aerial photos of the region were investigated in the office; discriminated geological units were transferred on to map then checked on the field. In the study; Keban metamorphics and Elazığ magmatics, which are the basement units of the region and the unconformably overlying Tertiary units were distinguished. In order to determine the rock types of Elazığ magmatics and stratigraphical relationships and ages in Tertiary units, the basin deposits were collected from bottom to top in systematically. Rock types in the Elazığ magmatics were distinguished based on petrographical descriptions. The age intervals of the formations were determined following the paleontological studies, and the units were defined based on formational nomenclature in the region and their surrounding (Figures 1 and 2).

Preliminary studies were carried out in the region which were started in 1940's and the regional geology and stratigraphy in wide areas were investigated (Ketin, 1946; Tolun, 1955; Altınlı, 1966). Later on; the allochthonous units cropping out along the belt, Yüksekova complex (Perinçek, 1979), Keban metamorphics (Özgül, 1976; Kipman, 1976, 1981; Yazgan, 1981, 1983, 1984; Özgül and Turşucu, 1984) and Baskil magmatics (Asutay, 1988) have been studied in the following years. The sedimentary outcrops around Pertek, Yüksekova complex (Bingöl, 1984) and Cretaceous volcanics and ophiolitic rocks

* *Corresponding author: Erdal HERECE eherece@hotmail.com*
http://dx.doi.org/10.19111/bmre.38353

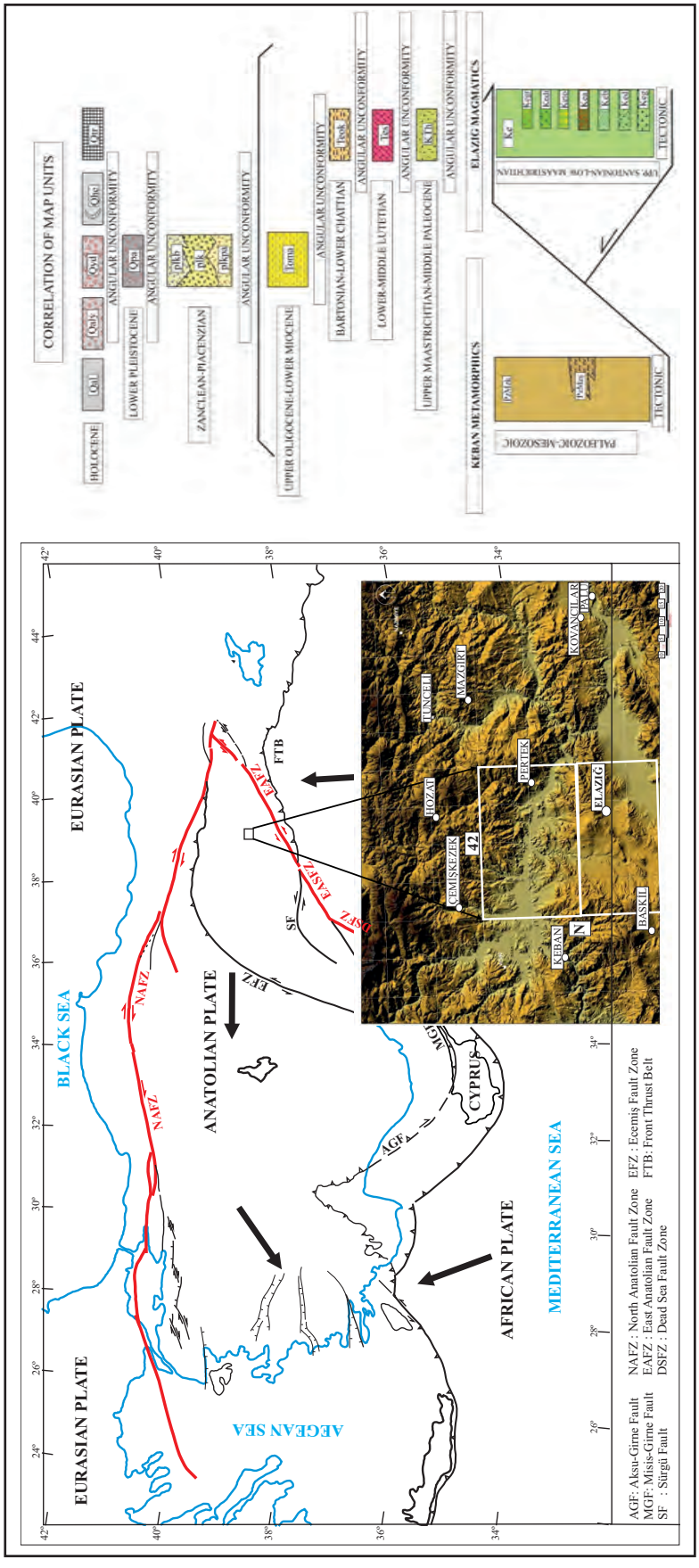

Figure 1- Location of the study area and the explanation of distinguished geological units (Herece, 2016).

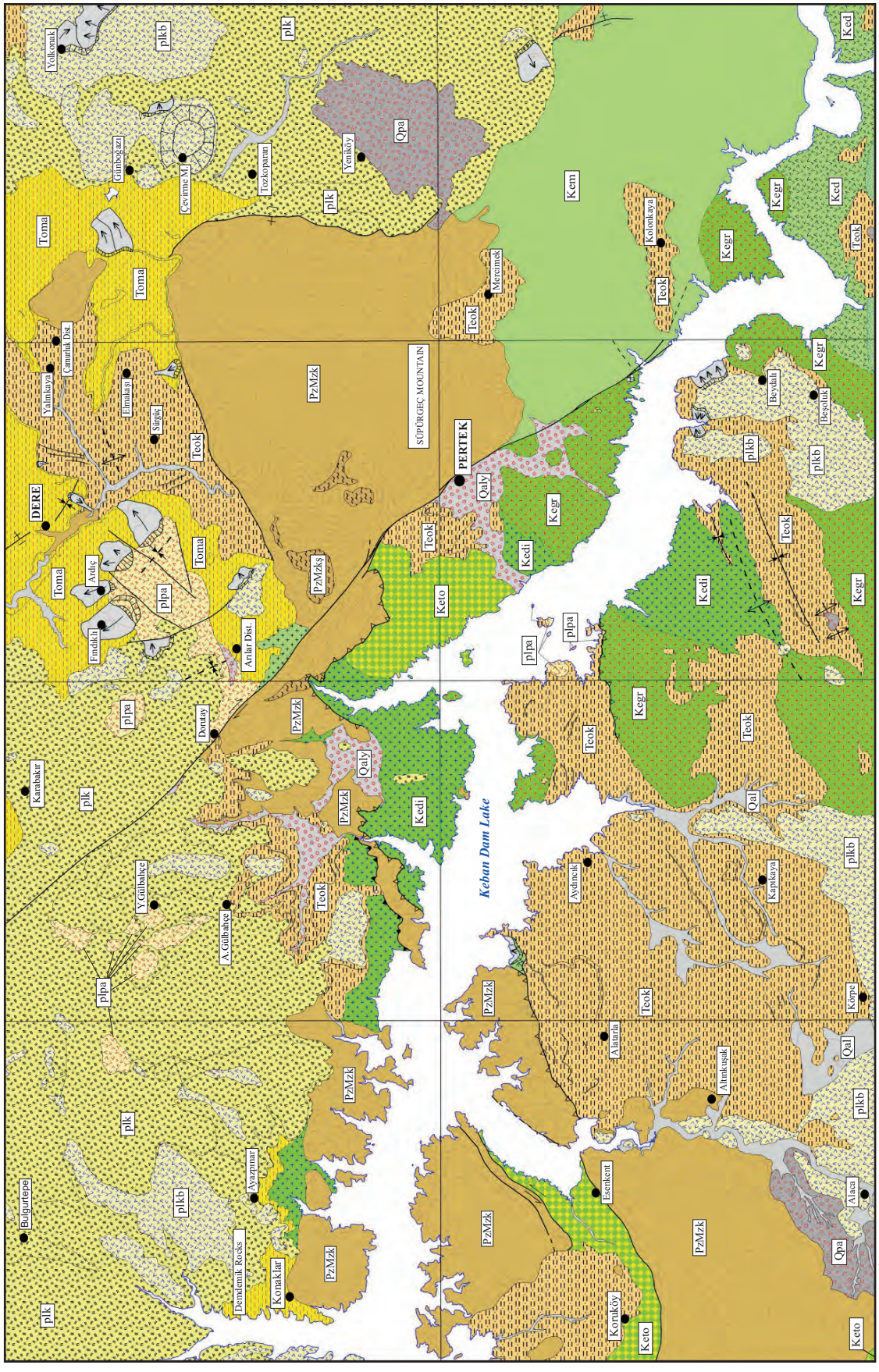

Figure 2- Geological map of the study area (modified from Herece, 2016).

around Elazığ were studied (Hempton and Savcı, 1982; Hempton, 1984, 1985). Besides; the fossils of a section within the Kırkgeçit formation in local areas in west of Pertek were described based on species (Avşar, 1991, 1996).

2. The Stratigraphy Of The Region In Pre-Late Maastrichtian

Keban metamorphics and Elazığ magmatics cropping out around Pertek which are the basements units of the region. Harami, Seske and Kırkgeçit formations are Late Cretaceous-Tertiary in age. Adilcevaz formation is Late Oligocene-Early Miocene and the Karabakır formation and its members are Pliocene.

2.1. Keban Metamorphics (PzMzk)

Keban metamorphics are generally composed of schist and marble. It outcrops in north of the Keban Dam Lake between Konaklar-Tuzbaşı districts, around Eğer Tepe in south of the dam lake, the east of Kolbaşı district, the north of Esenkent and in west of Altınkuşak (Figure 3a).

The unit was first named by Kipman (1976), Özgül (1976), Perinçek (1979) and Erdoğan (1982), and the same nomenclature was used in other studies (Özgül and Turşucu, 1984). The exposures of metamorphics in Pertek and its surround were shown as one unit since the rock type discrimination had not been studied before. The outcrops of the unit in different places are similar in character and formed dominantly from grayish, white marbles and seldom amphibolite schists. The unit was defined as basic amphibolites in sections which can be distinguished by its dark color in the outcropped areas and in section which displays schistose structure. Amphibolites are composed of nematoblastic textured hornblende, plagioclase, quartz, sphene and opaque minerals (Herece, 2016).

Keban metamorphics overlie Late Cretaceous Elazığ magmatics with reverse fault at the bottom and is unconformably overlain by Maastrichtian deposits on top.

There is not age data within study area; however, Özgül (1976) obtained Permian-Triassic age from the bottom of the unit. Özgül and Turşucu (1984), detected ages ranging from Permian and Upper Triassic to Cretaceous from recrystallized limestones which are in the form of two layers. Kipman (1976) detected Permo-Carboniferous ages based on fossils described in samples in schists beneath marbles. Yılmaz et al. (1993) detected Campanian age from the topmost part of the metamorphics. According to these age data, the marbles were deposited as limestone between Permian to Cretaceous, then metamorphosed in greenschist facies between Campanian-early Maastrichtian.

2.2. Elazığ Magmatics (Kem)

Elazığ magmatics, which have extensive spreads along the belt, were defined as Yüksekova complex (Perinçek, 1979), İspendere-Kömürhan ophiolites (Yazgan, 1983, 1984; Poyraz, 1988), Elazığ complex (Hempton and Savcı, 1982), Elazığ igniyıs complex (Hempton, 1984, 1985), four units belonging to Yüksekova complex (Bingöl, 1984), Elazığ magmatics (Turan et al., 1995; Beyarslan and Bingöl, 1996; 2000)

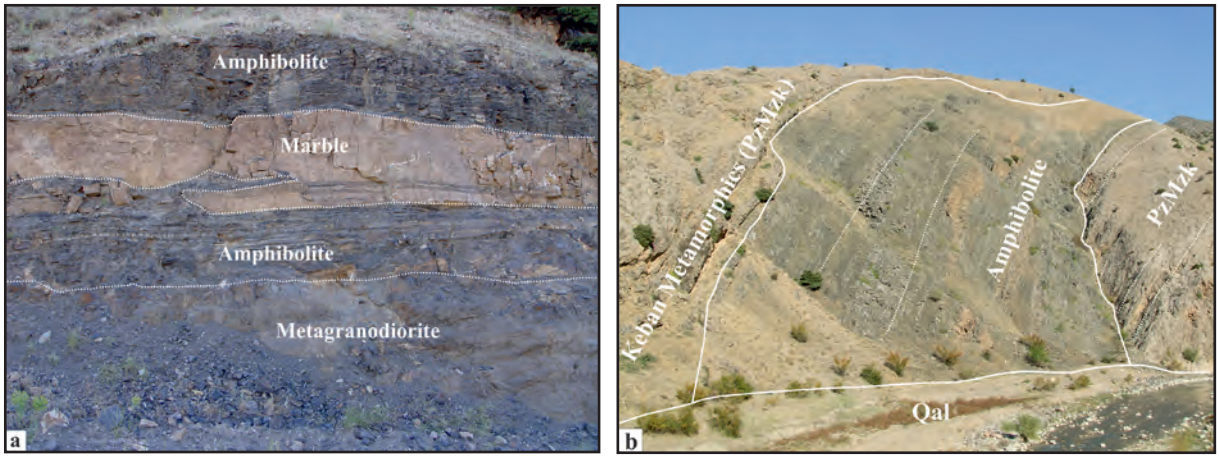

Figure 3- Views of amphibolites, which are distinctive with their dark colors and schistose structures, observed in limited area within Keban metamorphics; a) K42 a2, 21285-07968, looking south and b) K42 a2, 21630-07400, looking northwest.

and Elazığ-Baskil magmatic complex (Robertson et al., 2007). Elazığ magmatics cropping out in Elazığ surround are formed by ophiolitic succession which developed in the intra-oceanic supra subduction zone and by the overlying ensimatic island arc units. The ophiolites present a successive deposit and consist of gabbro, diabase, basalt and andesitic volcanics-tuff and agglomerates from bottom to top. Diabase unit, which outcrop in limited locality in the study area, is observed with basalt units, arc volcanics (andesite, andesitic volcano-clastics, tuff and agglomerate), and with intrusive diorite, monzodiorite, tonalite, granite and granodiorites of the widespread ensimatic island arc.

2.2.1. Diabase (Ked)

The unit outcrops around Sarıbük village in south of the Keban Dam Lake and observed as widespread and massive masses. It has sheeted dykes parallel to each other at 500 meters east of the Kilise Tepe at 1 km SW of Yeşildere outside the study area. Diabases have sometimes ophitic and intersertal textures of which plagioclase microliths have formed. Generally; chloritization, carbonation and epidotization are observed and it consists of sphene as accessory mineral.

The lower contact of the unit is not observed in the study area, and it is transitional with the underlying gabbro outside the study area (Hempton, 1985; Herece et al., 1992). However; it is transitional with the basalt unit cropping out in limited area in its upper contact. There is not any radiometric data for the unit. It is Late Senonian according to the pelagic fauna detected in the overlying basalts (Herece et al., 1992). It is a unit of the supra subduction zone ophiolite which developed on the intra-oceanic subduction zone.

2.2.2 Basalt (Keb)

The unit is composed of basalt and it crops out in a limited area in east of Sarıbük village at the south of the Keban Dam Lake. The unit was named as Basalt Unit based on lithological name within scope of this study. The unit is composed of maroon like green lavas at 4 km's northwest of the Osmanağa village in southwest outside the study area. Rarely, it consists of pelagic limestone interlayers and is intruded by small gabbro intrusives and diabase dykes. It has been much disintegrated in occasion, and flow and pillow structures are deteriorated. However; pillow structures along the road from Barge stream in south of the Karodağ to the Yeşildere village are widespread and distinctive outside the study area, and flow directions can also be seen by flow structures in places. The pillow structures were cut by dasitic and andesitic dykes in this area. Basalts are amygdoidal in texture and pores are filled by mineral. It has rare, red and fossilliferous limestone interlayers (Herece et al., 1992). Basaltic pillow lavas, lava flows and diabase dykes, rhyolitic and andesitic pyroclastic intercalations in few amounts comprise andesitic dykes, lava flows and gabbro and diorite stocks (Hempton, 1985).

Basalt unit is generally observed as tectonically associated with diabase unit. However; it is transitional with diabase in the lower boundary and andesitic volcanics in the upper boundary outside the study area (Herece, 1992). There is not any thickness data in the studied area. The unit thickness is 1000 m around Karodağ in southeast and outside the study area (Herece et al., 1992) and 375 m around Hazar Lake (Hempton, 1985). There is also not any radiometric age data for the unit, and it is unconformably overlain by the late Maastrichtian Harami Formation (Herece et al., 1992). The unit is Santonian-early Campanian based on *Marginotruncana coronata* Bolli, *Globotruncana carinata* Dalbiez and *Globotruncana linneiana* (d'Orbigny) fauna in samples collected from pelagic limestones blocks, which has been formed with basalts and of which their primary location failed by the flow, outside the study area (Herece et al., 1992).

Samples collected from the blocks in lavas (Herece et al., 1992), *Globotruncanita* cf. *stuarti* (de Lapparent) and *Globotruncanita stuartiformis* (Dalbiez) fauna are also early Maastrichtian. The basalts are Senonian "late Senonian" according to these age data, and these are the part of ophiolites forming in the intra-oceanic supra subduction zone.

2.2.3. Andesitic Volcanics (Kea)

Andesitic volcanics, though have limited spread in the study area, crop out over wide areas in south of the study area. The unit generally consists of lithologies of andesite, andesitic agglomerate and tuffite, and rarely consists of pelagic limestone intercalations. The whole succession is green to pale green in color. However; the fresh and decayed colors of andesitic rocks are white. Agglomerates are moderately sorted

and well cemented. The succession consists of laterally lensoidal pyroclastic layers. Occasionally; diabase and dacitic dyke intrusions and rare pelagic intercalations take place within the unit (Figure 4).

Andesitic volcanics are transitional with the underlying basalts of the Elazığ magmatics at its lower contact (Herece et al., 1992); however, it is unconformably overlain by the late Maastrichtian Harami Formation at its upper contact. Its thickness is unknown since the measured stratigraphical section could not be taken in the unit. Nevertheless; in south and outside the study area it is approximately 1800 m thick (Herece et al., 1992). There is no age data for the unit in the investigated area; however, its age outside the study area was detected as early Maastrichtian (Herece et al., 1992). The presence of clayey limestone intercalations and blocks requires indicates that they have been deposited in open marine environment.

2.2.4. Ensimatic Island Arc Rocks

The rocks of the ensimatic island arc together with Intra Oceanic Supra Subduction ophiolites outcrop within the study area. Ophiolites and the overlying andesitic volcanics were distinguished; however, the rocks of widespread ensimatic island arc were named based on the petrographical descriptions of samples collected from the area. These rocks are generally beige, pink or pale and occasionally have lineation and fracture system. Rock types in exposures covering wide areas were distinguished as Tonalite (Keto), Diorite (Kedi) and Granite-Granodiorite (Kegr) (Herece, 2016).

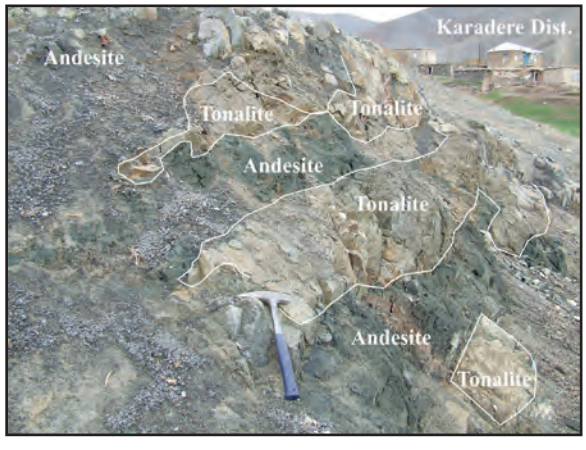

Figure 4- Views of intrusive tonalite dykes with the andesites of Elazığ magmatics on the road cut of the auto road in west of the Karadere District (K42 b1, 2407-03847, looking NNE).

Tonalite (Keto) : It is an intrusive rock in andesites, which outcrops on the road cut in west of the Karadere district in NW of Pertek (Figure 4). The andesite has hypidiomorphic texture (pilotaxitic texture) and consists of plagioclase, hornblende, quartz, biotite and opaque minerals. The groundmass consists of plagioclase, hornblende, very few biotite microliths, amorphous quartz grains and opaque minerals. However; tonalite has hypidiomorphic holocrystalline granular texture and consists of plagioclase, quartz, orthoclase, hornblende, biotite, apatite and opaque minerals. Chloritization, argillization, calcification in plagioclases; chloritization and argillization in the orthoclases; chloritization in biotites are widespread (Herece, 2016).

Towards west, it is formed by NE-SW extending Eğer Tepe metamorphics in south of Koruköy; however, the NW looking slope of the hill is formed by intrusive rocks. In the cut of water canal, which vertically crosscut the hill, Keban metamorphics and Elazığ magmatics are tectonically and intrusively associated with each other (Figure 5a-b). Elazığ magmatics consist of tonalite and granodiorite; however, the latter intrusives are basalt and diabase (Figure 6a-b). These dyke intrusions consist of enclave fragments detached from previously formed magmatics. Tonalite is holocrystalline granular textured, and consists of plagioclase, quartz, hornblende, biotite, zircon, apatite and opaque minerals. Granodiorite has holocrystalline granular texture and consists of plagioclase, quartz, orthoclase, hornblende, biotite, zircon and opaque minerals. Some plagioclases consist of quartz, alkaline feldspar, hornblende and chloritized biotite inclusions. Minerals are; clinopyroxene, biotite and serpentinized olivine as the secondary mineral around epidote at the center as phenocrystals; and clinopyroxene, secondary carbonate, secondary chlorite minerals among plagioclase microliths in the groundmass. Intrusive basalt has hypocrystalline porphyritic texture and the groundmass is intergranular textured. Intrusive diabase porphyry is holocrystalline porphyritic and intergranular textured. Minerals are; clinopyroxene, plagioclase, quartz, and plagioclase with secondary rod like calcite phenocrystals, quartz and opaque minerals, and they are observed within intergranular textured groundmass which consists of secondary chlorite and secondary calcite.

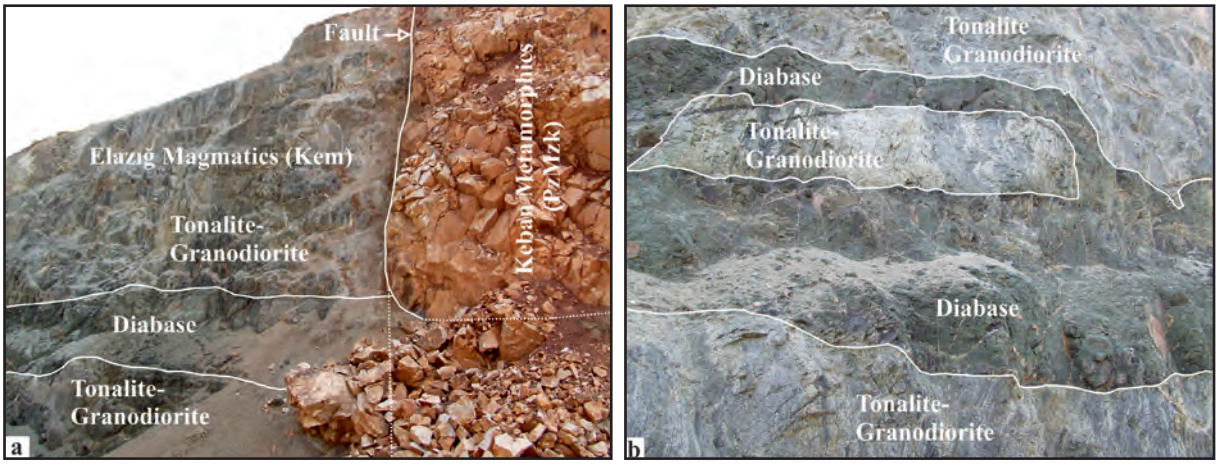

Figure 5- a) Views of Elazığ magmatics tectonically associated with Keban metamorphics in the cut excavated in water canal, in SW of Koruköy (K42 a4, 00300-96025, looking east), b) views of tonalites cut by diabase dykes in Elazığ magmatics (K42 a4, 00300-96025, looking east).

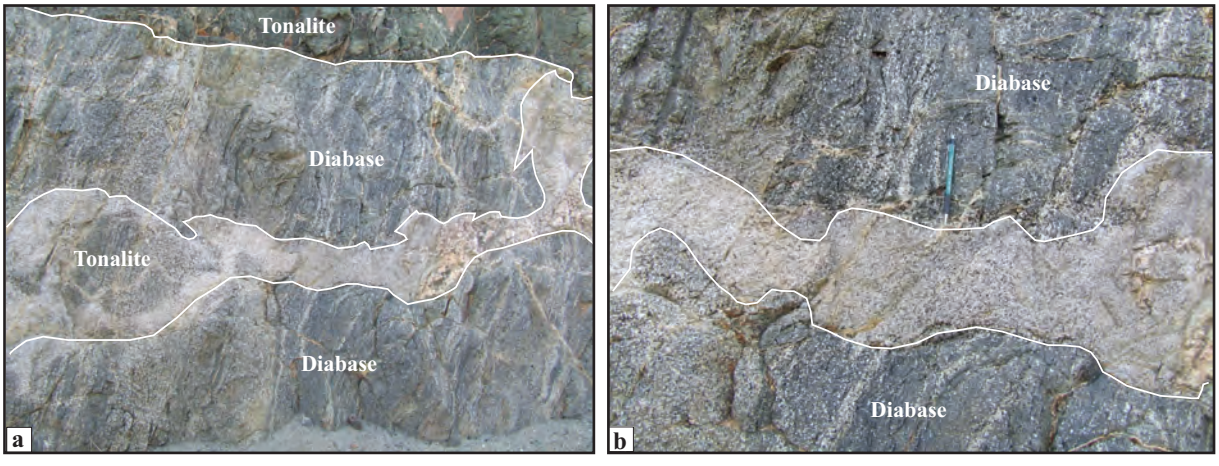

Figure 6- General views of diabases and intrusive tonalites in Elazığ magmatis in the cut excavated in the water canal in SW of Koruköy (K42 a4, 00300-96025, looking east).

On the other hand, norite and gabbronorite were identified in magmatic rocks exposing in the area towards the north of Pertek Fault (Herece, 2016). Norite is holocrystalline in texture and consists of plagioclase, orthopyroxene and opaque minerals. Plagioclases have polysynthetic twinning and rarely observed opaque minerals are in the form of fine grains. Gabbronorite is holocrystalline textured and consists of medium-fine grained plagioclase, orthopyroxene, clinopyroxene and opaque minerals.

Diorite (Kedi): It is the tectonically associated rock type beneath Keban metamorphics in northeast of the Hasır district. Diorite is holocrystalline and poikilitic textured and is formed by plagioclase, amphibole (hornblende) and opaque minerals. Plagioclase minerals are partly sericitized and argillized, and amphiboles are carbonated.

Magmatic rocks cropping out in south of the Hasır district are quartized diorite, microdiorite and metadiorite (Herece, 2016). Quartz diorite is granular textured and consists of plagioclase, amphibole, quartz and zircon minerals. Argillization and sericitization are widespread in plagioclase minerals. Diorite and alkaline feldspar granite are the other intrusive related rocks in the same region. Diorite is holocrystalline granular textured, and it consists of plagioclase, orthoclase, quartz, hornblende, clinopyroxene and opaque minerals.

Granite (Kegr): These are holocrystalline granular textured magmatics and located in Hodinik Mountain in south of Pertek (Herece, 2016). Granite

is holocrystalline textured and consists of orthoclase, quartz, hornblende, augite, biotite, titanite, apatite, zircon and opaque minerals. There are observed argillization, sericitization and chloritization in plagioclases, and sericitization and argillization in orthoclases. Basic and intrusive rocks, along with road cuts towards Edincik district in southwest of Pertek, are metagabbro and granites, respectively (Figure 8). Metagabbro is holocrystalline textured and consists of plagioclase, augite, hornblende, tremolite-actinolite, opaque minerals and uralitic hornblende minerals. However; the granophyre is holocrystalline in texture and consists of plagioclase, quartz, alkaline feldspar, biotite, zircon and opaque minerals. There are observed argillization and sericitization in plagioclases and alkaline feldspars.

Ultrabasic rocks and intrusive dykes are remarkable along the road cut at 2.6 km southeast of the Kolbaşı district along the auto road heading westward from Pertek. The dominant rock types observed on the cut are metagabbro, metagranitoid and moreover granite in intrusive dykes (Figure 7). Metagabbro is blastoporphyritic in texture and consists of plagioclase, orthoclase, hornblende, clinopyroxene, biotite, titanite, spinal and opaque minerals. Plagioclases are chloritized, sericitized, carbonated, epidotized and argillized; and orthoclases are chloritized, sericitized and argillized. It has probably been altered from pyroxene mineral in octagonal minerals which area completely infilled by amphibole. Most of the minerals resembling to that have been medium carbonated, chloritized and the edges have been altered into amphibole. In some of these minerals the residual pyroxene and fully chloritized biotite residuals are observed.

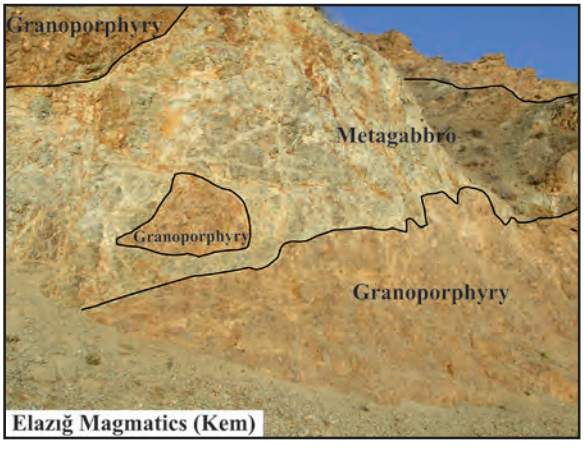

Figure 7- General views of granoporphyries, which are located with metagabbro in Elazığ magmatics and form wide alteration zone, along the road cut of the auto road in NW of the Edincik district (K42 b3, 31882-96900, looking north).

The intrusive gabbro of Elazığ magmatic was cut by granodiorites along Pertek-Hozat auto road (Figure 8), and the microdiorites were cut by diabase rocks along Elazığ-Pertek auto road (Figure 9a-b). In southern areas of the Keban Dam Lake, monzodiorite outcrops at the west of Çolaklı district; and granite, altered syenite/altered monzonite and metabasic rocks crop out in the south of Tilağası district.

There is not any age data in the area investigated for magmatic, and late Maastrichtian Harami formation unconformably overlies the unit. Santonian-early Campanian age was detected from pelagic limestones in which basalts are located, and early Maastrichtian age was taken from pelagic limestone blocks located in lavas (Herece, 1992). These data indicate that the age of magmatics could more probably be late Senonian.

On the other hand, Late Senonian basalts and Early Maastrichtian andesitic volcanics are cut by granitoid intrusions or by the youngest intrusives, and are unconformably overlain by the late Maastrichtian Harami formation. If the youngest granitoids cutting andesitic volcanics have developed with andesites then their ages should be early Maastrichtian or even younger.

3. The Upper And Post Maastrichtian Stratigraphy Of The Region

Late Cretaceous-Tertiary units are formed by Harami formation, Seske formation, Kırkgeçit formation, Alibonca formation, Karabakır formation and its Pertek andesite member and basalt member.

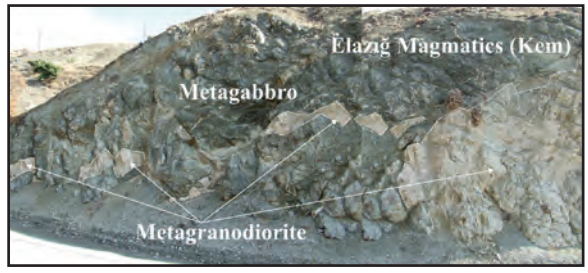

Figure 8- Intrusive views of metagabbros with metagranitoids in SE of the Kolbaşı district on Pertek-Hozat auto road cut (K42 a2, 21492-06625, looking north).

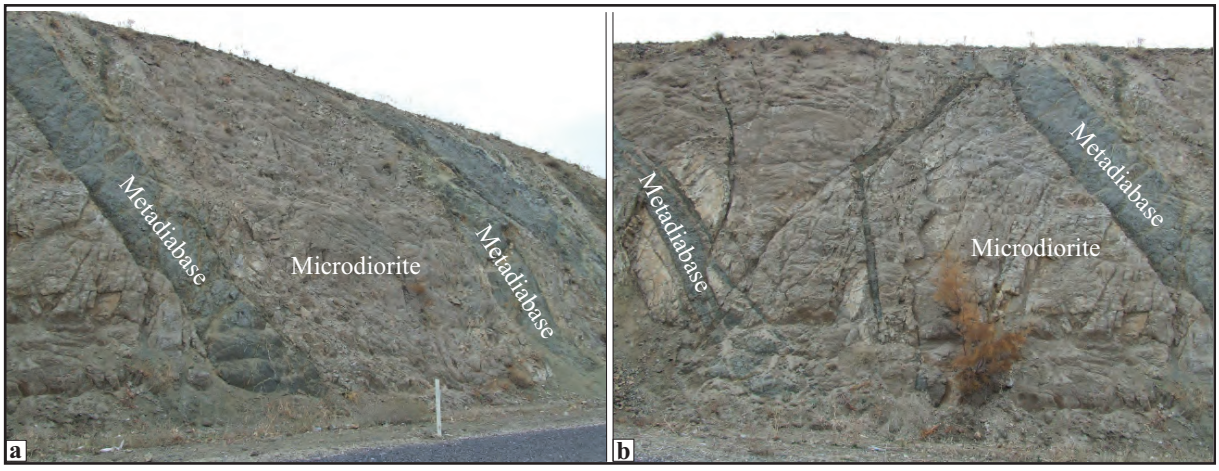

Figure 9- a-b. Views of microdiorites and intrusive metadiabases on Elazığ-Pertek road cut (K42 a3, 17608-95485, looking east).

3.1. Upper Late Cretaceous – Paleogene Units

3.1.1. Harami Formation (KTh)

The unit was first named by Perinçek (1979) and Erdoğan (1982), and the same nomenclature was used in other studies carried out in the region. The formation outcrops at high elevations of the ridges located on the southern boundary of the Kurbankapan village (Figure 10).

The unit at the bottom consists of reddish, pale brown basal conglomerate intercalating with carbonate cemented, angular, pebbly sandstone and algal fragmented grainstone (Figure 11a-b). The succession continues with white, thick to very thick bedded limestones towards upper layers.

The unit unconformably overlies Elazığ magmatic and unconformably overlain by Seske and Kırkgeçit formations. The thickness of the formation is not

Figure 10- General view of the Harami formation which unconformably overlies the Elazığ magmatics (K42 b4-c1; 27365-87915, looking south).

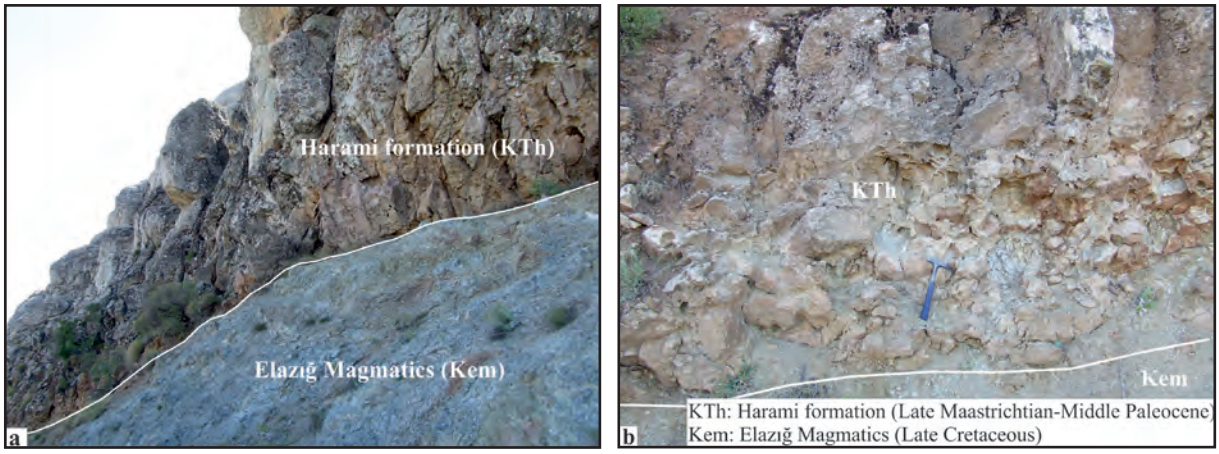

Figure 11- a) The unconformable relationship of the Harami formation with Elazığ magmatics, b) close up view of 2 m thick conglomerate which forms the bottom (K42 b4-c1; 27365-87915, looking south).

known in the study area; however, the measured stratigraphical sections taken from the unit in the near south of the area were estimated about 60 m (Herece et al., 1992).

In samples collected from the bottom of the unit on road cuts in south of the Kurbankapan district, the late Maastrichtian age was obtained by benthic foraminifers; *Siderolites calcitrapoides* Lamarck, *Sirtina orbitoidiformis* Bronnimann and Wirtz, *Hellenocyclina beotica* Reichel, *Siderolites* spp. and *Omphalocyclus* sp. (Herece, 2016).

In samples collected from the southern part of the study area (Herece et. al., 1992), the Selandian age was obtained according to the fauna such as; *Cuvillierina sireli* İnan or *Pseudocuvillierina sireli* (İnan), *Miscellanea* sp., *Sistanites* sp. for the upper part of the succession. According to these data the Harami Formation is late Maastrichtian-Late Paleocene (Selandian) and it was deposited in shallow shelf environment.

3.1.2. Seske Formation (Tes)

Seske formation was first named by Erdoğan (1975) in the vicinity of Seske village of Adıyaman. It consists of bioclastic packstone and algal grainstone in the bottom, and angular pebbly conglomerate and clastic sandstone in the top. The unit, which was first named by Herece (2016) around Pertek, was observed in the southern part of the ferry pier at south of Keban Dam Lake (Figure 12). This outcrop, which was formerly beneath the water, emerged as a result of 20 m decrease in water level in the dam lake.

The unit does not have wide outcrops to nomenclature for a new formation. Eastern and western extensions of the succession observed in the limited area remain below the dam lake. However, it was defined in order to detect that the formation is present in this region. The extension of the formation at east is formed by the medium bedded sandy limestone-limestone alternation. In the western extension, the conglomerate made up of angular pebbles derived from ophiolites at the bottom grades into many nummulitic sandstones with much ophiolitic clastics (Figure 13a-b). The unit unconformably overlies Elazığ metamorphics at the bottom at ferry pier; however, the upper contact is paraconformably overlain by the Kırkgeçit Formation (Herece, 2016). Approximately; 10-15 m thick section of the unit could be observed in the outcrop at the southern edge of the Pertek ferry pier. Since the lateral extension of the succession remains below the dam lake, its thickness is unknown.

In samples collected from the lower part of the succession exposing in the area (Herece, 2016) the late Kuvizian age was detected by *Nummulites manfredi* Schaub (spp) fauna. However; *Nummulites messinae* Schaub (spp), *Gyroidinella* sp. (n.sp?), *Neorotalia* sp., Belemnitidae fauna gave early Lutetian age in samples collected from the upper part of the succession (Herece, 2016).

On the other hand, *Nummulites messinae* Schaub (spp.), *Fabiania cassis* Oppenheim, *Gyroidinella* sp. (n.sp?, grain forms available), *Discocyclina* sp., *Praefabiania?* sp. and Belemnitide form (plenty) fauna assemblage described in the sample collected

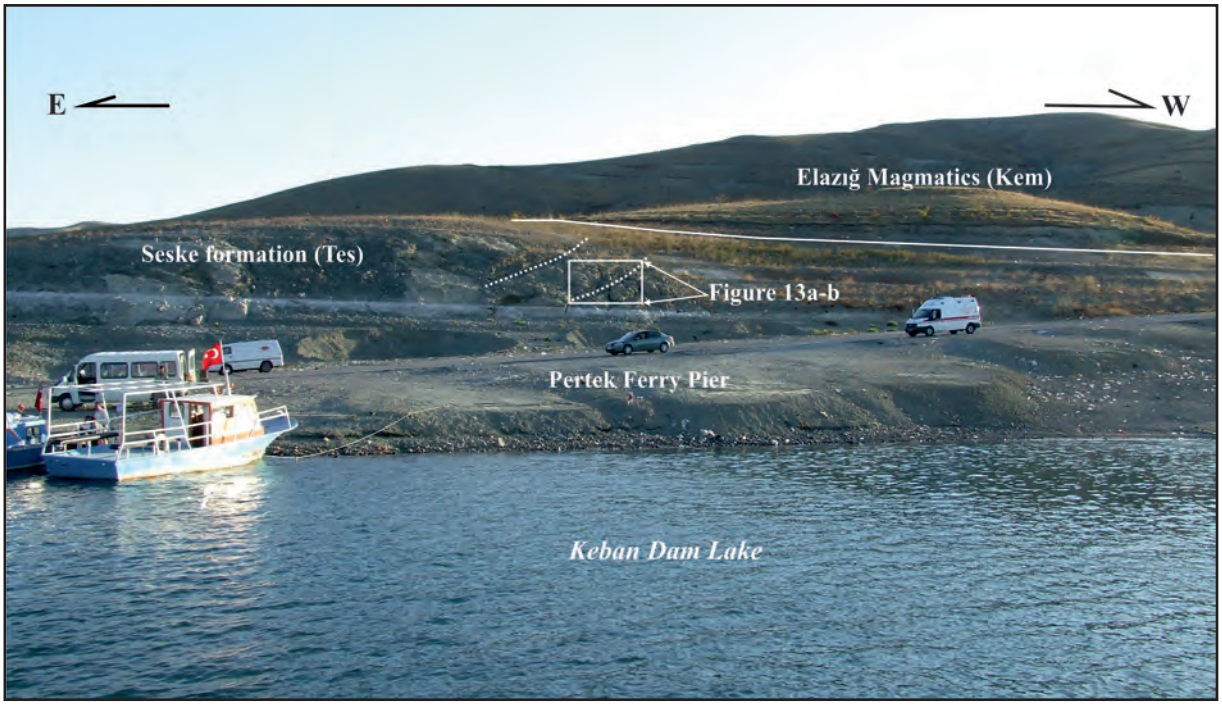

Figure 12- General view of the Seske formation on the southern edge of the Pertek ferry pier (K42 b4; 23820-98025, looking SSW).

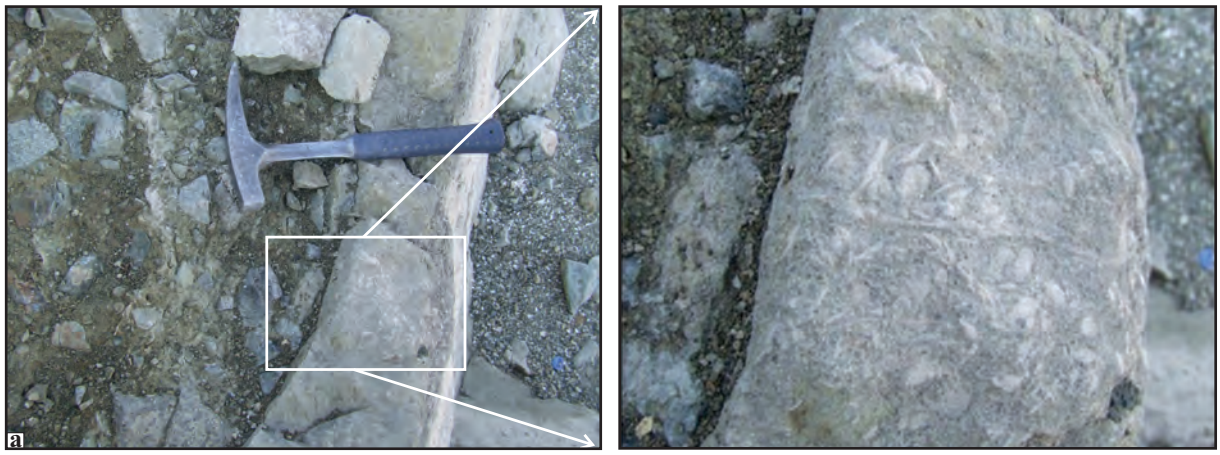

Figure 13- a-b. The close up view of much nummulitic grainstone overlying the coarse conglomerate in the lower part closer to the bottom of the Seske Formation on the southern edge of the Pertek ferry pier (K42 b4; 23820-98025, looking SW).

from algal and bryozoan fragmented grainstone, which is located below the Kırkgeçit formation around Tilağası district, give upper early Lutetian-early middle Lutetian age.

According to these data, the age of the formation cropping out in areas around Pertek ranges from late Kuvizian to early middle Lutetian. In exposures outside the study area, Yazgan (1984) investigated the Seske formation together with Harami formation under the name of Upper Paleocene-Lower Eocene limestones. Turan and Bingöl (1991) and Türkmen et al. (2001) defined the Seske formation as Late Paleocene-Early Eocene. The unit was deposited in fore reef environment.

3.1.3. Kırkgeçit Formation (Teok)

The formation, which consists of the alternation of basal conglomerate, sandstone, siltstone and limestone, crops out in wide areas from north to south. The unit, which is formed by sedimentary deposits in similar characteristics, is observed as separate

outcrops as a result of effective tectonical events in the region after sedimentation.

The unit which was first named by Perinçek (1979) was defined under the same name. The outcrops of the Kırkgeçit Formation are observed in near west of Pertek, between the Cevizlik Tepe (hill) and Taht Tepe (hill), in west of Pertek, between Aşağı Gülbahçe and Karşıyaka District, in near east of Pertek, around Mercimek village, in SE of Pertek, between Kabasakal District- Kolonkaya, in south of Pertek, between Karacalar District – Kabakçılar District, in SW of Pertek, between Altınkuşak and Tilağası District.

The formation, which outcropped in 6 different areas, was mapped for the first time and successions were systematically sampled from bottom to top in order to determine rock type characteristics and ages of each exposure.

Kırkgeçit Formation outcropping between Cevizlik Tepe and Taht Tepe: The formation generally trends in NW-SE direction. The bottom of the basin is located in the west of Soğukpınar district and begins with the alternation of fine and coarse grained grainstone. Grainstone is grayish-pale brown, medium-thick bedded, flaky and with conglomerate-pebblestone intercalations. First; the sedimentary deposit is laterally transitional with pale green claystones, then continues as pale yellowish, brown, fine to medium bedded limestone with plenty of *Gypsina,* and algal and spar cemented boundstone and algal fragmented grainstone in upper layers. However; the uppermost part of the succession is formed by reddish-brown, medium to thick bedded, medium to fine textured boundstone with highly porous algae and bryozoans (Figure 14).

The age of the unit was determined according to fauna described in samples collected systematically from bottom to top at the outcrop in the west of Pertek (Herece, 2016).

In samples collected from the grainstone with much *Gypsina* in the section at the bottom of the unit, boundstone with algea and *gypsina*, grainstone with algae fragments and clastic packstone-grainstone (Herece, 2016); *Nummulites ptukhiani* Kacharava, *Chapmanina gassinensis* (Silvestri) (spp), *Fabiania cassis* (Oppenheim) (spp), *Schlosserina asterites (*Gümbel), *Gypsina mastalensis* Bursh, Praecalcarina tohmaensis Alan *Alveolina* gr. *fusiformis* Sowerby, *Nummulites* cf. *dufrenoyi* d'Archiac and Haime, *Penarchaias* sp., *Borelis?* sp., *Eoannularia* sp., *Heterostegina* sp., *Discocyclina* sp., *Peneroplis* sp. and *Opertorbitolites* sp. benthic foraminiferal assemblage was detected which gives Bartonian age.

In samples collected from clastic packstone-grainstone in the succession gives Latest Bartonian according to *Borelis wonderschmitti* (Schweighauser), *Chapmanina gassinensis* (Silvestri) / n.sp?, *Planorbulina bronnimanni* Bignot and Decrouez, *Schlosserina asterites* (Gumbel) and *Borelis* sp./n. sp?, fauna (Herece, 2016).

In samples collected from clayey limestones located on the grainstone (Herece, 2016*a*); Late Bartonian-Lower Early Priabonian age was given detecting *Silvestriella tetraedra* (Gumbel), *Chapmanina gassinensis* (Silvestri), *Halkyardia minima* (Liebus), *Planorbulina bronnimanni* Bignot and Decrouez, *Fabiania cassis* (Oppenheim), *Nummulites* gr. *ptukhiani* Kacharava and Miliolidae fauna (Figure 14).

In samples collected from packstone located on the grainstone in the middle part of the succession (Herece, 2016), *Nummulites fabiani* (Prever), *Nummulites striatus* (Bruguiere), *Nummulites incrassatus* De La Harpe, *Nummulites boullei* De La Harpe and *Silvestriella tetraedra* (Gumbel) fauna was determined, and the early Priabonian age was given (Figure 14).

In samples collected from the boundstone close to the upper part of the unit (Herece, 2016); the early Rupelian age was given by *Halkyardia minima* (Liebus) (spp), *Halkyardia* cf. *maxima* Cimerman, *Nummulites* gr. *vascus* Joly and Leymerie, fA), *Nummulites* spp. (with flat radiated mesh), *Amphistegina* spp., *Planorbulina* sp. and Miliolidae (plenty) benthic foraminiferal assemblage (Figure 14).

In samples collected from the algal and bryozoan fragmented grainstone in the uppermost part of the succession (Herece, 2016); late Rupelian-early Chattian age was given with benthic foraminifers of *Nummulites vascus* Joly and Lymerie, *Borelis merici* Sirel and Gündüz, *Bullalveolina bulloides* (d'Orbigny) (spp), *Borelis* spp., *Halkyardia* sp., *Archaias?* sp., *Heterostegina* sp. and *Peneroplis* sp. (Figure 14).

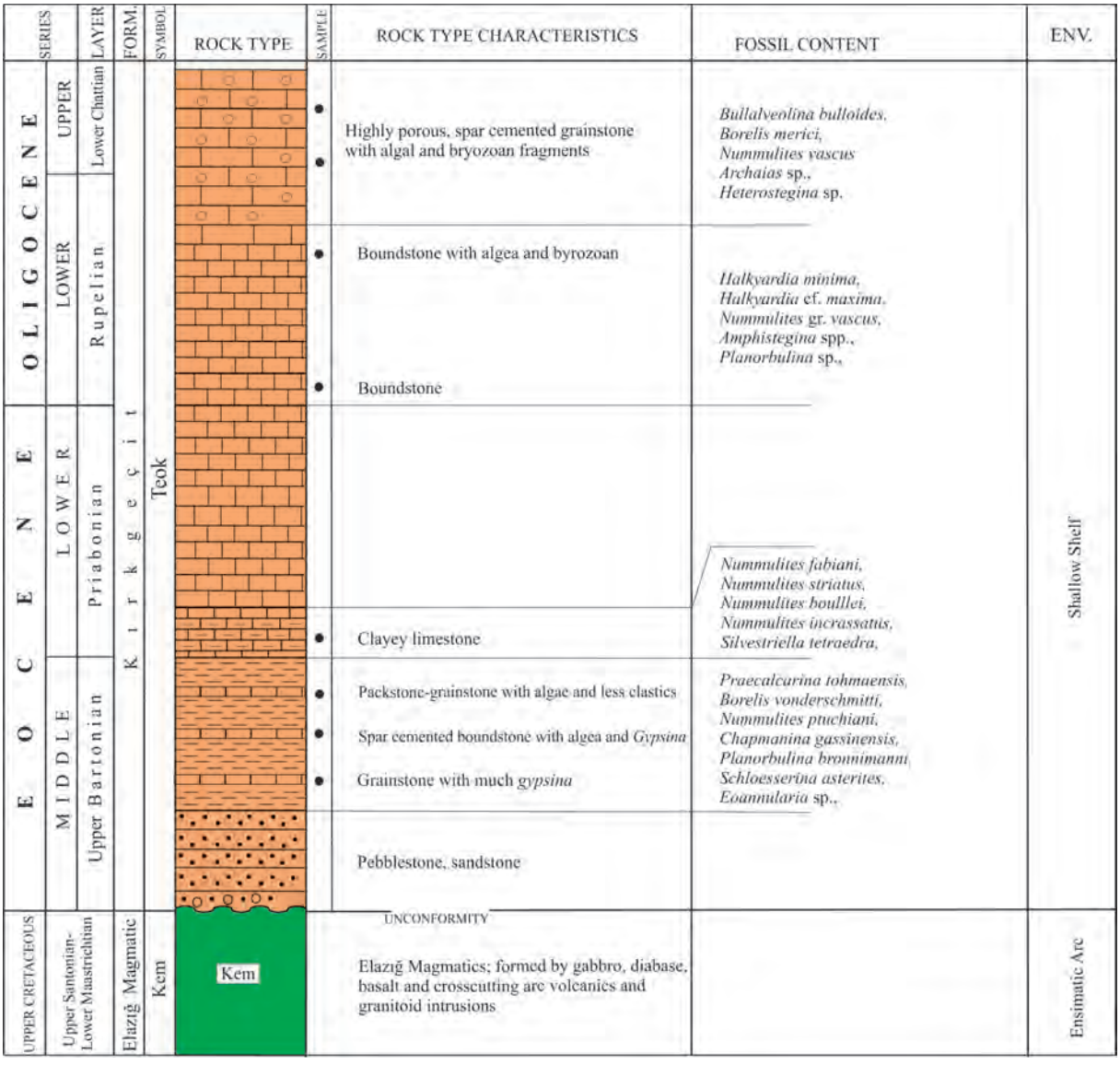

Figure 14- The columnar section showing the rock type characteristics and locations of the samples collected from the succession of the Kırkgeçit formation outcropping between Cevizlik Tepe and Taht Tepe in west of Pertek (Herece, 2016).

According to these data, the age of the Kırkgeçit formation outcropping between Cevizlik Tepe and Taht Tepe in west of Pertek continuously ranges from late Bartonian to early Chattian. The whole succession can clearly be observed in this region (Herece, 2016).

The lower contact of the unit is unconformable with the underlying Elazığ magmatics in this area; however, the upper contact is unconformably overlain by younger units.

Both benthic and planktonic foraminifers are observed within the succession forming the formation. Therefore; the depositional environment of the unit is wide reefal flat which is in contact with the fore reef and back reef. The exact thickness of the unit is not known since the measured stratigraphical section could not be performed, but it is approximately assumed to be 250 meters according to topographical data.

Kırkgeçit Formation between Aşağı Gülbahçe and Karşıyaka Districts: The deposit begins with basal conglomerate at the bottom then grades into sandstones in upper layers. Most of the conglomerates originate from well-rounded Keban metamorphics and seldom from ophiolites which do not show any sorting-grading. The deposit is formed by much miliolitic grainstone with algal fragments, widespread

limestone and by the alternation of algal fragmented grainstone with plenty of *Gypsina*, claystone, silty grainstone, grainstone-boundstone (Figure 15).

In samples collected from algae fragmented and much miliolitic grainstone overlying the basal conglomerate cropping out between Aşağı Gülbahçe and Karşıyaka Districts in the west of Pertek (Herece, 2016*a*) the age of the unit was given as late Bartonian according to; *Malatyna drobneae* Sirel and Acar, *Halkyardia minima* (Liebus), *Peneroplis dusenbory* Henson, *Fabiania cassis* (Oppenheim), *Gyroidinella magna* Le Calvez, *Medocia blayensis* Parvati, *Austrotrillina* cf. *eocenica* Hottinger, *Haymanella* cf. *huberi* (Henson) (spp), *Penarchaias* cf. *glynnjonesi* (Henson) (spp), *Alveolina (Alveolina)* gr. *fusiformis* Sowerby, *Borelis* sp./n.sp?, *Nummulites* spp., *Discocyclina* spp., *Schlosserina* sp., *Rhabdorites* sp., *Orbitolites* sp. benthic assemblage (Figure 15).

In samples collected from the upper continuation of the grainstone (Herece, 2016), *Chapmanina gassinensis* (Silvestri), *Praecalcarina tohmaensis* Alan *Asterigerina rotula* (Kaufmann), *Halkyardia minima* (Liebus), *Alveolina* (Alveolina) gr. *fusiformis* Sowerby), *Nummulites* sp., *Schlosserina* sp. and Miliolidae fossil assemblage was detected which give the upper late Bartonian age (Figure 15).

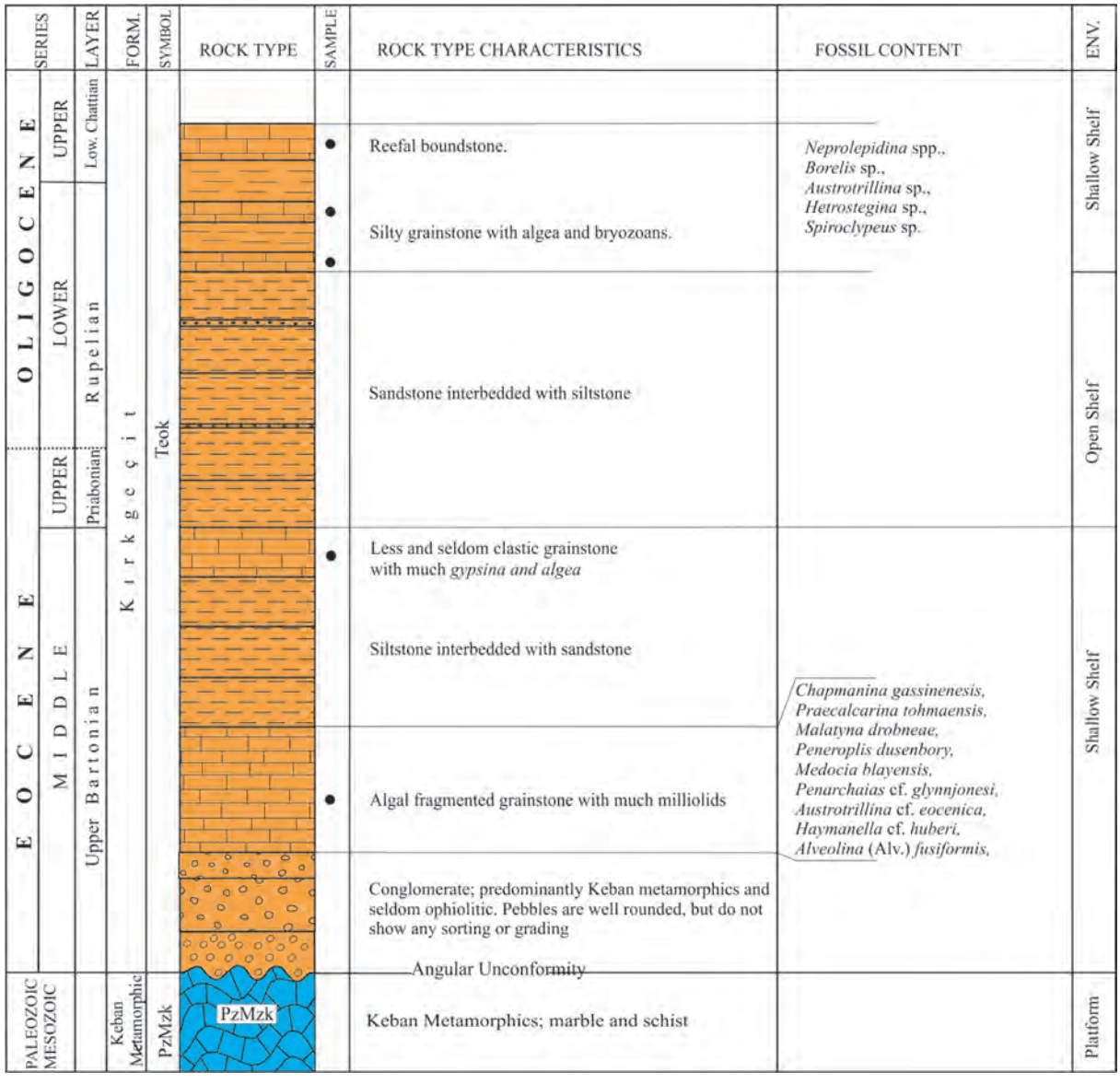

Figure 15- Generalized stratigraphical section showing the lithological characteristics, sample locations and fossil content of the Kırkgeçit formation outcropping between A. Gülbahçe village and the north of Karşıyaka District (Herece, 2016).

Samples collected from the upper part of the succession (Herece, 216) belong to late Rupelian-early Chattian with *Nephrolepidina* spp., *Borelis* sp./n. sp?, *Austrotrillina* sp., *Pararotalia* spp., *Neorotalia* spp. and Miliolidae fauna. According to these data, the age of the formation ranges from late Bartonian-early Chattian (Figure 15).

The lower contact of the unit is unconformable with Keban Metamorphics; however, the upper contact is unconformably overlain by younger deposits. The thickness is not known as the measured stratigraphical section could not be performed for the formation. The unit was deposited in shelf environment.

Kırkgeçit Formation outcropping around Mercimek village: The unit begins to deposit with pebblestone and coarse sandstone at the bottom. Then it grades into much algal detritic limestone with bryozoan fragments, highly porous boundstone with coarse algal fragments and claystone intercalating with laterally lensoidal limestone (Figure 16). The bottom and lower contact relationship of the formation is not distinctive because of the overlying unstable basement unit. However; lithologies near the bottom are grayish pale yellow and consist of medium bedded much algal and bryozoan detritic limestones and coarse algal fragmented boundstones on coarse sandstone (Figure 16).

According to the samples collected from much algal and bryozoan fragmented detritic limestone located at the bottom of the formation (Herece, 2016*a*); the basement age of the basin was detected as the late Bartonian according to *Halkyardia minima* (Liebus), *Chapmanina gassinensis* (Silvestri) (spp), *Schlosserina asterites* (Gumbel), *Gyroidinella magna* Le Calvez (fB), *Alveolina* (Alv) sp. and *Discocyclina* sp. fauna (Figure 16). As sufficient sampling could not be carried out in Late Oligocene-Oligocene transitional-conformable deposits because of special conditions of the region, the fossil-fauna assemblage could not detected.

The unit unconformably overlies Elazığ magmatics (Figure 17a-b), and it is unconformably overlain by younger units. Its thickness is not known as the measured stratigraphical section could not be done. It was deposited in open shelf environment.

Kırkgeçit formation between Kabasakal District and Kolonkaya Village: The sedimentary deposit

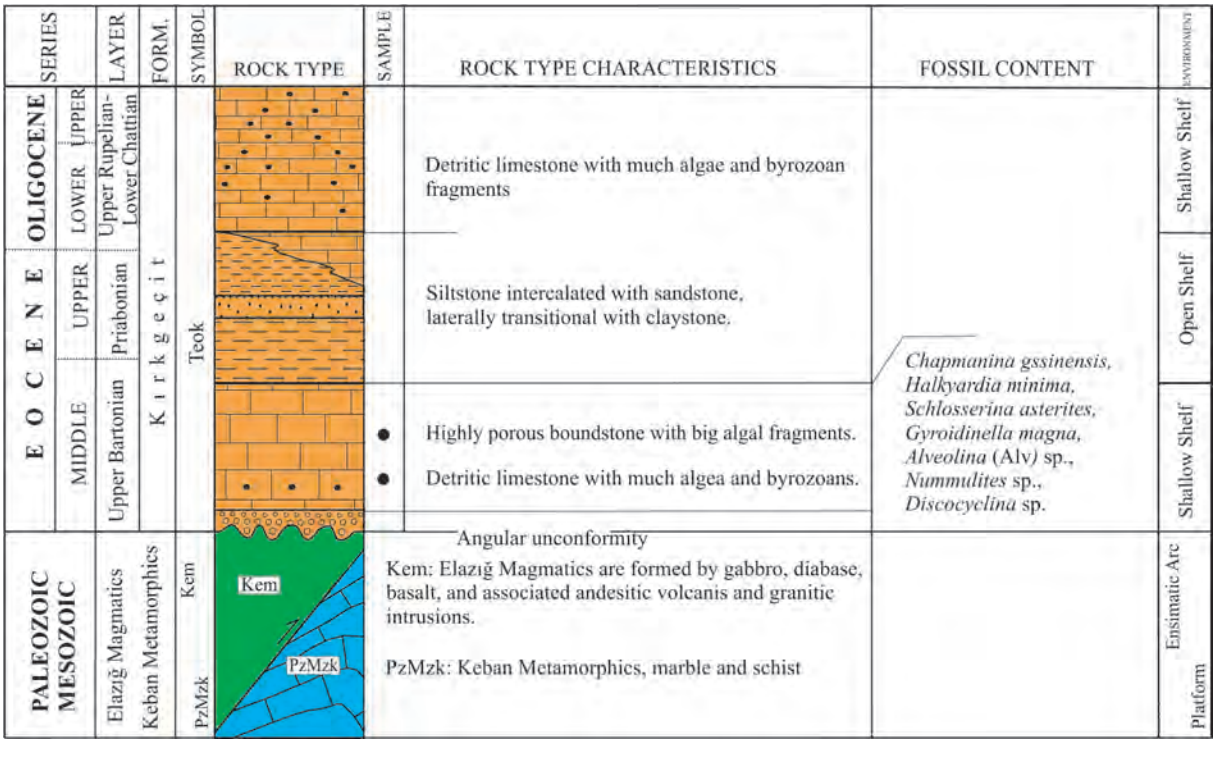

Figure 16- The columnar section showing the lithological characteristics of the Kırkgeçit formation outcropping in the vicinity of Mercimek village and lower sampled part of the unit (Herece, 2016).

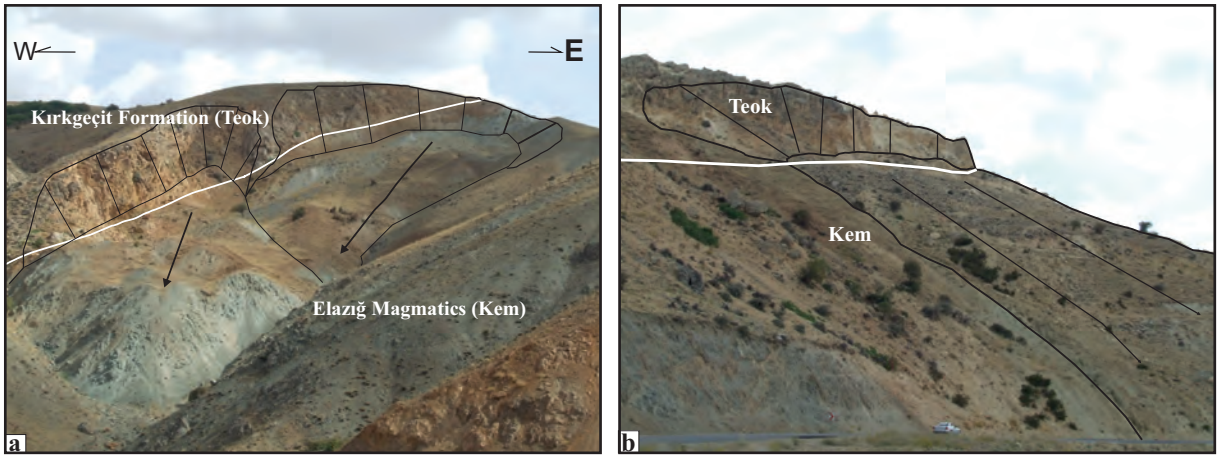

Figure 17- a-b. The bottom contact relationship of the Kırkgeçit formation outcropping i the vicinity of Mercimek village and the view of widespread landslides developed near the bottom of Elazığ magmatics (Kem) (K42 b3, 33100-00850, looking NNE).

in this region begins with basal conglomerate and coarse sandstone on the northern edge of the basin. Sandstones are fine-medium bedded, fine grained and clastic textured. Grains are medium-poorly rounded, well sorted and carbonate-cemented. Sandstones continue with algal, reefal, clastic wackestone, packstone and claystone intercalated with laterally lensoidal limestone. The uppermost part of the succession consists of fine-medium grained, much algal and bryozoan fragmented, well-compacted sandstones with angular pebbles and much gypsinides.

In samples collected from wackestone-packstone overlying the basal conglomerate in the unit which outcrops between Kabasakal district and Kolankaya village in the southeast of Pertek (Herece, 2016); *Chapmanina gassinensis* (Silvestry), *Fabiania cassis* (Oppenheim), *Gyroidinella magna* Le Calvez (spp), *Planorbulina* cf. *bronnimanni* Bignot and Decrouez, *Halkyardia* cf. *minima* (Liebus), *Nummulites* cf. *incrassatus* De La Harpe, *Nummulites* gr. *boullei* De La Harpe, *Nummulites* gr. *biedai* Schaub, *Nummulites* gr. *biaritzensis* d'Archiac and Haime, *Nummulites* gr.*striatus* (Bruguiere), *Alveolina* (Alveolina) sp. (fusiform type) and Microcodium? fauna assemblage was determined which gives the Upper Late Bartonian as the basement age of the unit (Figure 18). The formation unconformably overlies Elazığ magmatic, and is unconformably overlain by the Quaternary alluvial deposits. The unit was deposited in open shelf- shelf front environment.

Kırkgeçit Formation between Karacalar and Kabakçılar Districts: The bottom of the formation is observed in the near north of the Kabakçılar district (Figure 18). The lowermost part of the unit in this area begins with fine grained, intraclastic, steeply dipping sandstone and grades into medium bedded much fossilliferous limestone consisting of 5-8 cm thick sandy limestone interlayers (Figure 19a-b). Sandstone is badly sorted, angular, fine to medium grained, with metamorphic and volcanic pebbles. This bottom succession presents approximately 4 m thickness and grades into laterally lensoidal, algal fragmented, very few clastic grainstone, and grainstone-claystone alternation in upward direction. This part of the outcropping succession is formed by limestones intercalating with packstone-wackestone.

The age of the unit is early Bartonian according to *Halkyardia minima* (Liebus), *Nummulites biaritzensis* d'Archiac and Haime, *Nummulites* cf. *discorbinus* (Schlotheim), *Nummulites* cf. *beamonti* d'Archiac and Haime, *Nummulites* cf. *perforatus* (De Montfort), *Linderina* spp., *Neorotalia* sp. (spinal form), *Pararptalia* sp. (abdomen and ridge much pillared), *Schlosserina* sp. and Rotalidae fauna in samples collected from the fine grained sandstone located at the bottom of the unit near the Kabakçılar district.

Samples were collected from rare clastic grainstone overlying the pebbly packstone, from laterally lensoidal, NE-SW trending, fine grained clastic limestone and from fine-grained sandstone located in the southern part of the road heading to Kabakçılar district in 300 m SSW of the Kurtoğlu district (Herece, 2016). According to these collections; *Austrotrillina eocenica* Hottinger,

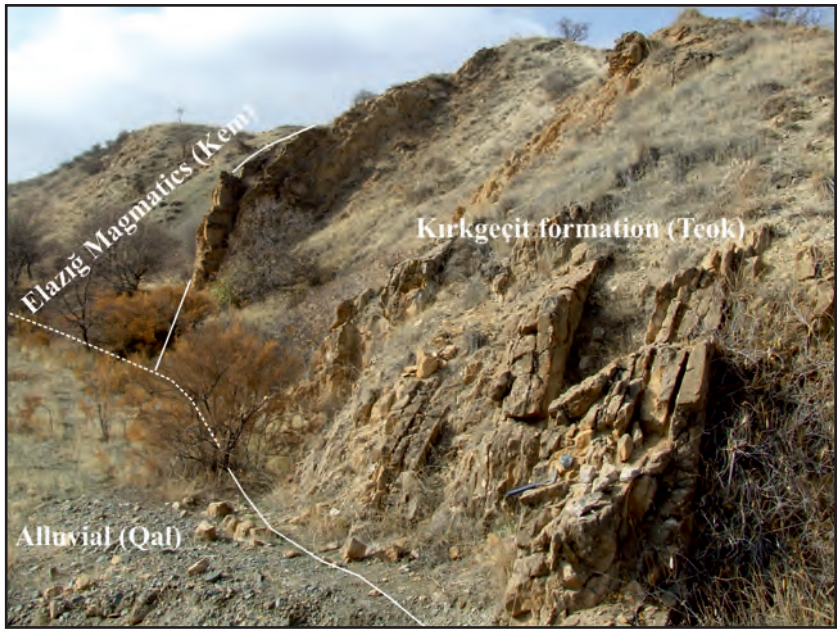

Figure 18- General view of the Kırkgeçit formation which unconformably overlies the Elazığ magmatics between Kabakçılar district and Kolankaya village (K42 b4, 26528-93459, looking NW).

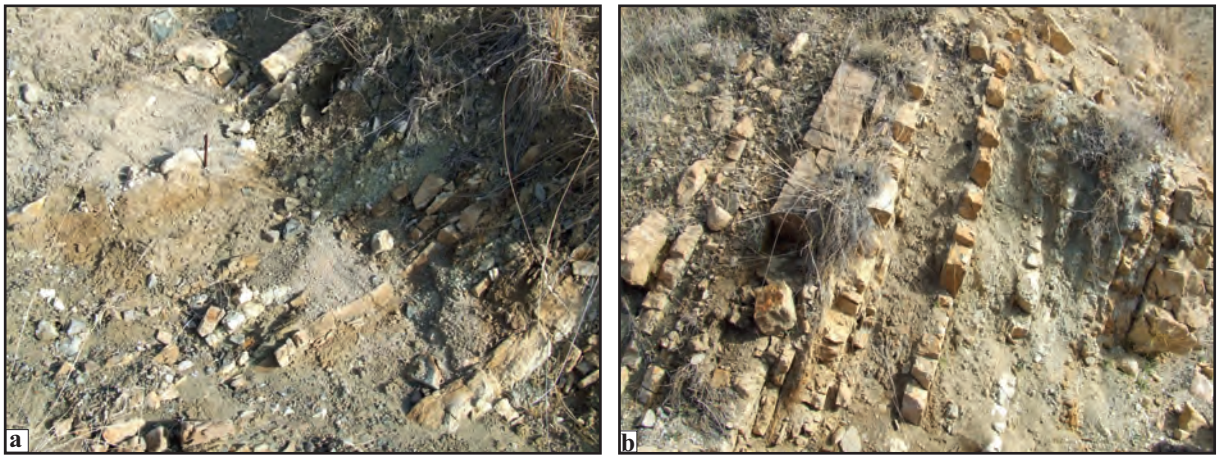

Figure 19- a) Fine grained sandstone, sandstone intercalated with limestone forming the basement of the Kırkgeçit formation in NW of the Kabakçılar district, and b) the overlying limestone-sandstone alternation (K42 b4, 26534-93450).

Chapmanina gassinensis (Silvestri), *Praecalcarina tohmaensis* Alan, *Gypsina mastalensis* Bursh, *Schlosserina asterites* (Gumbel), *Nummulites* cf. *dufrenoyi* d'Archiac and Haime or *Nummulites* cf. *lyelli* d'Archiac and Haime, *Alveolina (Alveolina)* gr. *fusiformis* Sowerby (badly preserved), *Borelis* sp., *Maslinella?* sp. and *Linderina* sp. fauna were described which give the late Bartonian age.

According to nannoplankton samples collected from claystones in the upper part of the sedimentary deposit (Herece, 2016) such as; *Helicosphaera compacta* Bramlette and Wilcoxon, *Cyclicargolithus floridanus* (Roth and Hay), *Dictyococcites bisectus* (Hay, Mohler and Wade), *Reticulofenestra reticulata* (Gartner and Smith), *Discoaster saipanensis* Bramlette and Riedel the Late Eocene (Priabonian) age was given.

According to these data, the depositional conditions began in early Bartonian in the Kırkgeçit basin outcropping between Karacalar and Kabakçılar districts in SE of Pertek and continued in Priabonian (Figure 20). However; the late Rupelian?-early Chattian deposits, which should be located in the upper part of the succession, could not be observed

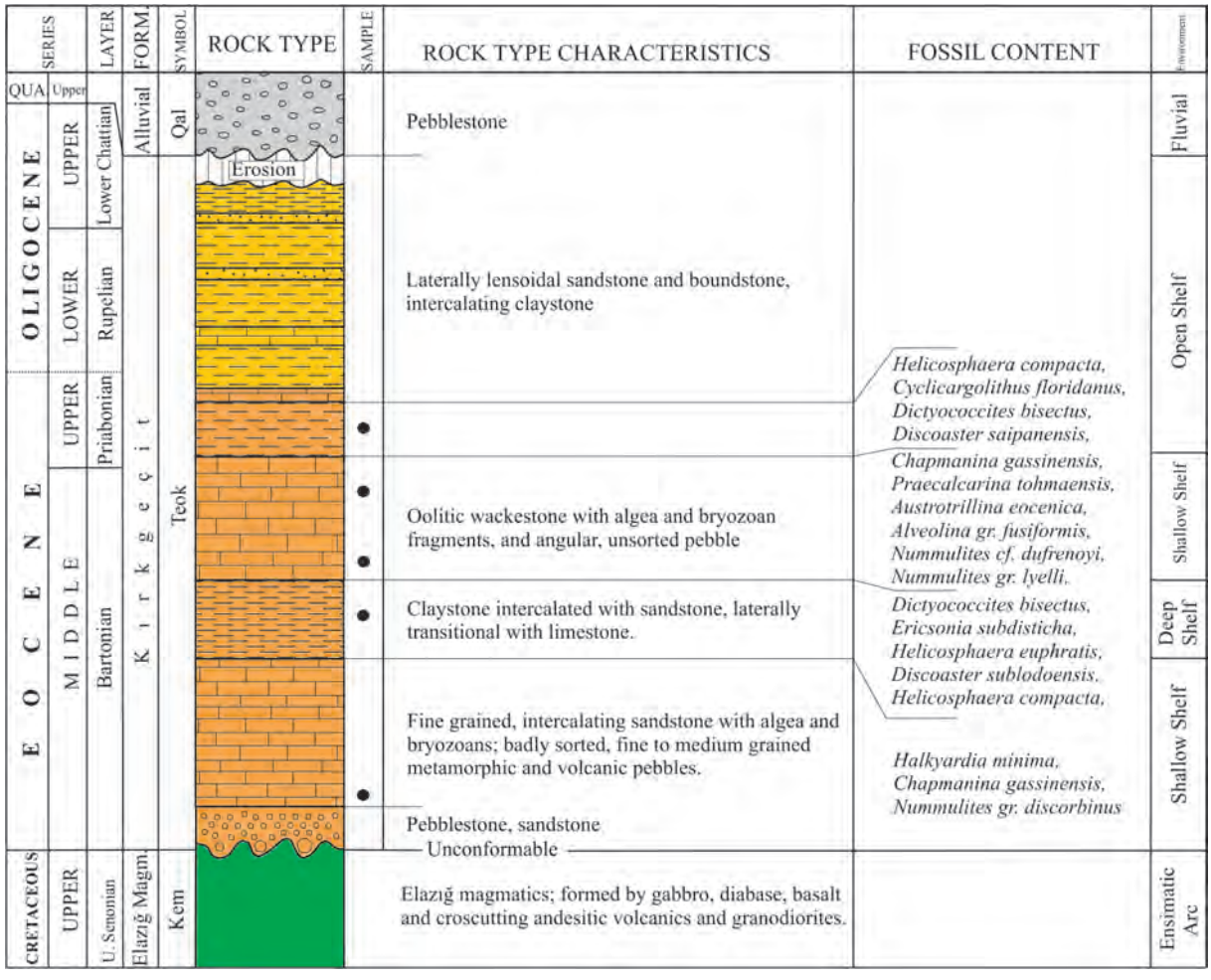

Figure 20- Generalized stratigraphical section showing the lithological characteristics of the Kırkgeçit formation outcropping between Karacalar and Kabakçılar districts and the locations of collected samples.

probably because of insufficient sampling. The formation unconformably overlies Elazığ magmatic and unconformably overlain by Pliocene volcanics. The unit was deposited in open shelf environment.

Kırkgeçit formation between Altınkuşak-Tilağası Districts: The formation outcrops in a wide area between Alatarla district at north and Körpe district at the south. The basin extends in NE-SW directions and presents a successive deposit which gives a type section from SE to NW. The deposit is distinctively traced along the section in NNW-SSE directions in the western part of the basin and in the area between the Körpe District and Keban Dam Lake.

The bottom of the unit is observed in west of Çömlek village and in southeast of the Körpe District. It begins with fine grained sandstone and algal and bryozoan grainstones then grades into sandy limestone and limestone in west of the Çömlek village. The lowermost section of the unit, which can be observed in the vicinity of the Körpe village, begins with algal and bryozoan grainstones and fine grained intraclastic sandstones, then grades into flysch facies in upper layers. Sandstones are poorly sorted, angular, fine to medium grained, metamorphic and pebbly. Flysch consists of 80% claystone and 20% sandstone. Claystones are grayish green, fine and laminated, and the sandstone is fine to medium bedded and consists of rare macro fossil and much small nummulites. The deposit grades into laterally lensoidal, thick bedded-massif limestone and coarse grained, thick bedded sandstone, sandstone-claystone alternation. Reddish, pale brown conglomerate, which formed as result of shoaling of ENE-WSW trending basin, comprises intercalated mudstone-sandstone interlayers. Afterwards; the deposit ends with algal, bryozoan fragmented grainstone, algal, bryozoan and

reefal boundstone and algal fragmented, rare clastic grainstone (Figure 21).

The observable lowermost part of the formation in the east of Körpe district consists of grayish-dirty white colored, medium to thick bedded grainstone and is overlain by Pliocene volcanics. Grainstones are overlain by claystone intercalating with ~25 m thick sandstone. It is then overlain by thick bedded boundstone with occasional massive grainstone which form Cankurtaran Tepe and Kaplıkaya Tepe extending from the Körpe district to Kaplıkaya. The grayish-dirty yellow, medium to thick bedded, fine textured, blocky disintegrated grainstone among Yukarıdirektepe, Aşağıdirek and Çakılburnu hills in NE of the Ebil district; and grayish-pale brown, fine to medium bedded grainstone outcropping in Kale Tepe (hill) in north of Çatalharman are located in the lower part of the succession. The middle and the upper part of the deposit cropping out in the area extending from Alatarla to North are formed by the grainstones consisting of boundstone interlayers (Figure 21).

According to samples collected from the basal conglomerate, which unconformably overlies magmatics and the lowermost part of the sandstone in the vicinity of Ebil district, in the west of Çömlek district and in the Körpe district (Herece, 2016); the late Bartonian age was taken from *Penarchaias glynnjonesi* (Henson), *Chapmanina gassinensis* (Silvestri), *Praecalcarina tohmaensis* Alan, *Gypsina mastalensis* Bursh (fA), *Planorbulina bronnimanni* Bignot and Decrouez, *Fabiania cassis* (Oppenheim), *Halkyardia minima* (Liebus) (spp), *Asterigerina rotula* (Kaufmann), *Malatyna* cf. *vicensis* Sirel and Acar, *Medocia* cf. *blayensis* Parvati, *Alveolina (Alveolina)* gr. *fusiformis* Sowerby, *Nummulites* gr. *lyelli* d'Archiac and Haime, *Nummulites* gr. *perforatus* (De Montfort), *Nummulites* sp. (*Nummulites* gr. *ptukhiani* Kacharava), *Schlosserina* spp., *Haymanella* sp., *Eoannularia* sp. (piece), *Malatyna* sp. (n.sp?) and *Linderina* sp. (coarse form, axial section) fauna assemblage (Figure 21).

From the algal grainstone collected in northeast of the Çatalharman village (Herece, 2016a); *Planorbulina bronnimanni* Bignot and Decrouez, *Halkyardia minima* (Liebus), *Nummulites* cf. *fabianii* (Prever), *Gypsina* cf. *mastalensis* Bursh, *Peneroplis spp*. fauna was detected which gives the late Bartonian?-early Priabonian age (Figure 21).

In samples collected from grainstone in the vicinity of the Çakıl district and the north of Alatarla village (Herece, 2016a); the Priabonian age was given with *Nummulites fabianii* (Prever) (spp), *Chapmanina gassinensis* (Silvestri) (spp, n.sp?), *Penarchaias glynnjonesi* (Henson), *Silvestriella tetraedra* (Gumbel), *Eoannularia eocenica* Cole and Bermudez, *Halkyardia minima* (Liebus), *Schlosserina asterites* (Gumbel), *Planorbulina bronnimanni* Bignot and Decrouez, *Fabiania cassis* (Oppenheim), *Nummulites* cf. *striatus* (Bruguiere), *Peneroplis* spp., *Praebullalveolina*? sp., *Borelis?* sp.

Due to samples were taken from the grainstone in the upper part of the section (Herece, 2016); the Rupelian age was given with *Planorbulina bronnimanni* Bignot and Decrouez, *Halkyardia* cf. *maxima* Cimerman, *Nummulites* cf. *fichteli* Michelotti, fA), *Nummulites* gr. *vascus* Joly and Leymerie, (fA), *Peneroplis* spp. fauna.

According to samples taken from spar cemented boundstone and grainstone around Alatarla (Herece, 2016); *Nummulites vascus* Joly and Leymerie, *Borelis inflata* Adams (spp) (small, bulky and ovoid forms), *Borelis merici* Sirel and Gündüz, *Halkyardia minima* (Liebus), *Nummulites* cf. *fichteli* Michelotti, *Victoriella* cf. *conoidea* (Rutten), *Borelis* cf. *pygmaea* Hanzawa, *Amphistegina* spp., *Heterostegina* spp. (X=3), *Eulepidina* sp., *Schlosserina* sp. *Bullalveolina?* sp. faunal assemblage were detected which give the late Rupelian-early Chattian age.

According to all these data, the depositional conditions began in Bartonian and continued until late Rupelian?-early Chattian in the Kırkgeçit formation.

The formation unconformably overlies Keban metamorphics and Elazığ magmatic, but are overlain by younger units with angular unconformity. The outcrops in the Pertek fortress and its northern side are intruded by volcanic necks where andesitic volcanics erupt. Whereas; the outcrops located between Altınkuşak and Aydıncık districts are overlain by reverse fault striking from north to south by Keban metamorphics along its northern boundary. Since SW extension of the unit was covered by the Pliocene volcanics in the east of Körpe district, the lower contact can not be observed.

Thickness of the unit is not known as the measured stratigraphical section could not be done, but based on

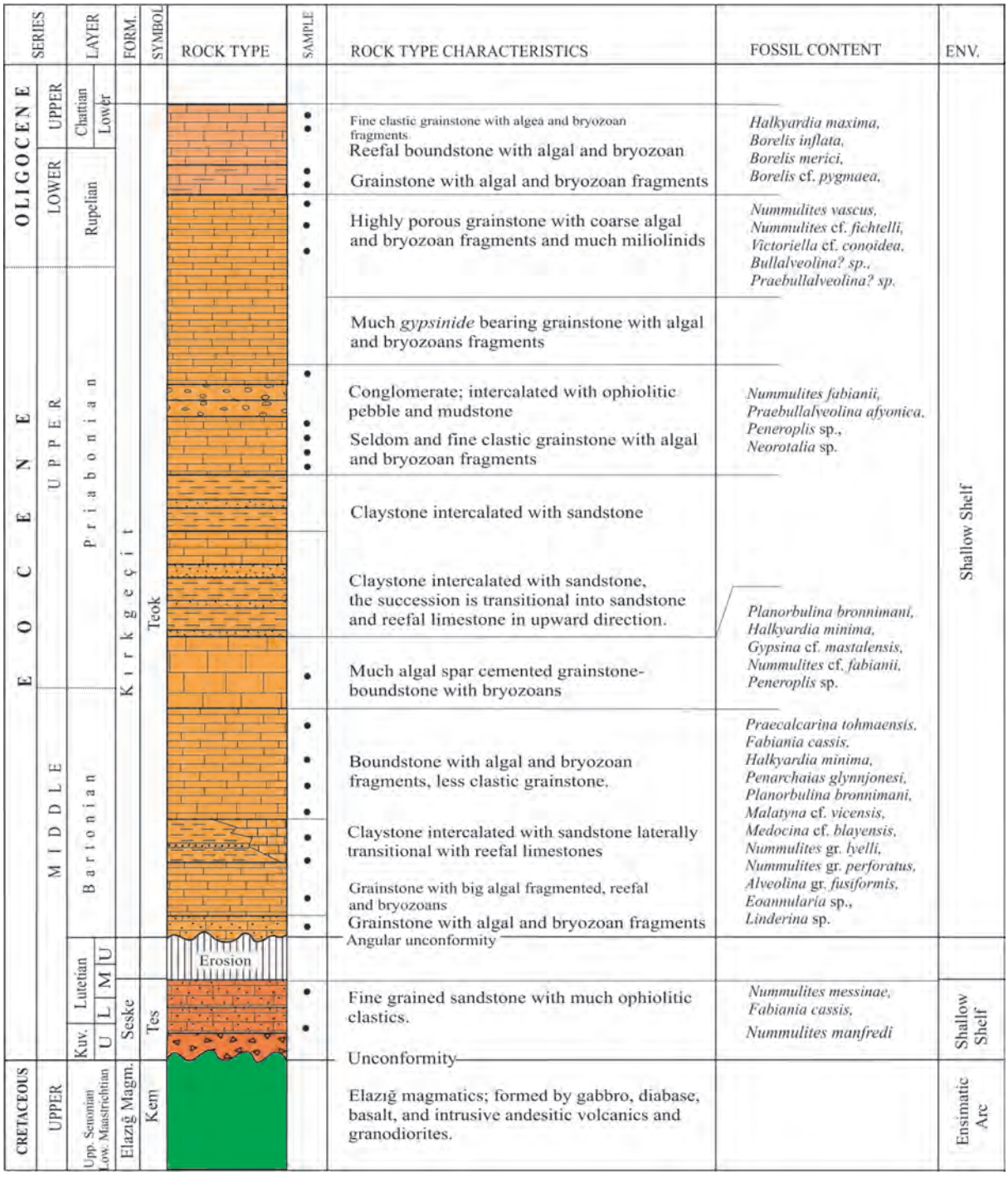

Figure 21- Generalized stratigraphical section showing the lithological characteristics of the Kırkgeçit formation outcropping between Altınkuşak-Tilağası districts and the locations of collected samples.

areal distribution of the basin, the thicknesses which can vary from region to region should mostly occur in the outcrop between Altınkuşak-Tilağası districts. The unit was deposited in fore reef and open shelf environment.

3.2. Upper Paleogene-Neogene Units

Late Oligocene-Neogene deposits widely cropping out in north of the Keban Dam Lake are represented by Alibonca formation, Karabakır formation and by the Pertek andesite and Basalt member.

3.2.1. Alibonca Formation (Toma)

The unit, which consists of conglomerate, sandstone, boundstone and claystone, extends towards Dere town through Dağarcık district by enlarging through Ayazpınar in the northern edge of the Keban Dam Lake and Arılar, Çukurbağ, Kaballı districts in NNW of Pertek and towards Çamurluk district at east.

The unit, defined first by Soyutürk (1973) in the vicinity of Alibonca village of the Muş city was defined under the same nomenclature also in studies around Elazığ and Malatya. The formation is the lateral equivalent of the Adilcevaz formation around Van Lake which was named by Demirtaşlı and Pisoni (1965).

The outcrops of the unit are observed in two different areas separated by the Pertek fault. The SW outcrop of the Pertek fault is between Ayazpınar and Çukurca villages (Figure 22). It begins to deposit with basal conglomerate (Figure 23a), continues with medium to thick bedded boundstone (Figure 23b) and ends with clayey limestone in the area. In the outcrop, which is located nearly at 930-950 m elevations, 4 meter thick boundstone makes distinctive moldings and is observed 3 km long in the lateral direction. Pale green, clayey limestone in the upper part of the sedimentary deposit, which unconformably overlies

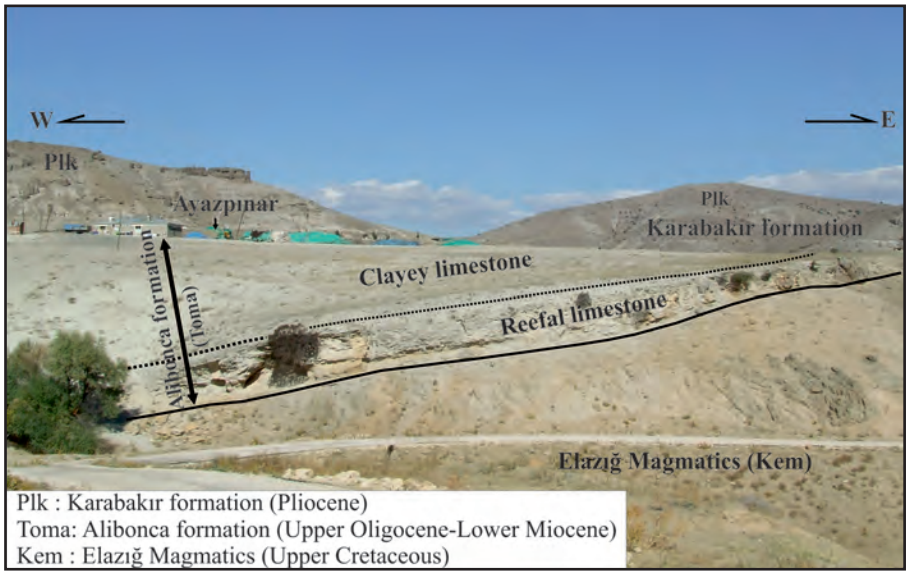

Figure 22- General view of the Alibonca formation exposing in the vicinity of Ayazpınar (K42 a1, 05168-08397, looking north).

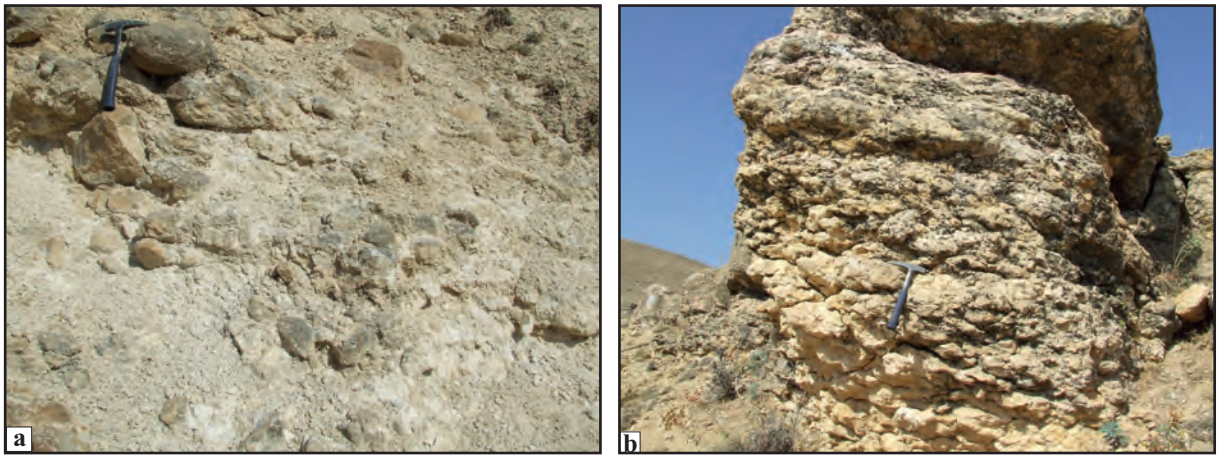

Figure 23- General views of the pebbly conglomerate derived from Elazığ magmatics, which is located at the bottom of the outcropping unit between Ayazpınar and Çukurca villages, and the overlying boundstone (K42 a1, 05087-08320, looking north).

the Elazığ magmatics, is paraconformably overlain by Pliocene volcanogenic sediments.

The exposures in the N-NE side of the Pertek fault are wider and spread on larger areas. The sedimentary deposit here is narrower in the west but widens eastward and its thickness increases. The exposures in the westernmost side are in the vicinity of Arılar, Çukurbağ and Kaballı districts in north of Sağman. The unit in these exposures begins with conglomerate-sandstone and ends with algal and bryozoan boundstone, grainstone-boundstone and clayey limestones (Figures 24 and 25). Conglomerate is thick bedded, loose-medium compacted, mostly derived from Keban platform, Elazığ magmatics and less from Kırkgeçit formation pebbles. The dominant rock type of the outcropping sedimentary deposit is boundstone, and it forms steep and thick moldings in the lateral direction on topography. It is also interlayered with clayey limestone in its western extension. The upper part of the succession consists of grayish-pale green clayey limestones, and it is interlayered with laterally lensoidal sandstone and limestone.

It extends first northward from the Dağarcık district then westward and eastward. The eastern extension of this outcrop is cut by N-S trending Değirmen Stream which was excavated at a depth of 250 m It is subhorizontally deposited in the outcrop in the west of Değirmen stream and consists of 40-50 m thick boundstone and the overlying clayey limestone (Figure 26a-b). The outcrops located on the eastern side of the Değirmen stream have the same lithological characteristics (Figure 27a-b); however, the clayey limestones are more widespread.

The unit unconformably overlies Elazığ magmatics and Keban metamorphics. It also unconformably overlies magmatics with 60 cm thick, loose compacted, rapid deposited, angular, pebbly conglomerates derived from Elazığ magmatics in the eastern slope of the Kara Tepe (hill) looking towards Tandır stream in the south of the Arılar district (Figures 28 and 29). The unit again unconformably overlies Keban metamorphics on the western part of the Dere town (Figures 30 and 31a-b). There is an angular unconformity on Keban metamorphics in the east of the Söğütlütepe district. However; it is unconformably overlain by younger sediments (Figure 32). Since the measured section could not be carried out its thickness is not known, but is considered to be more than 100 meters changes through in lateral direction.

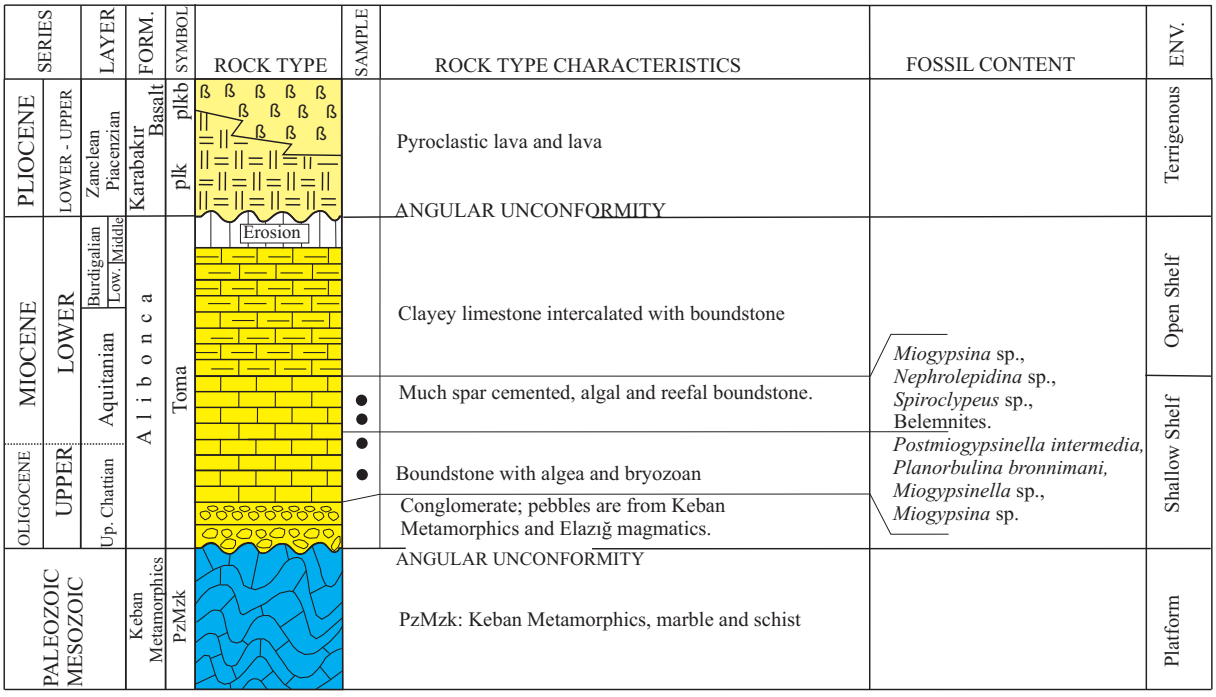

Figure 24- Generalized stratigraphical section showing the lithological characteristics of the Alibonca formation on the eastern edge of Uygun Tepe (hill), south of the Kaballı district and the sampled section (Herece, 2016).

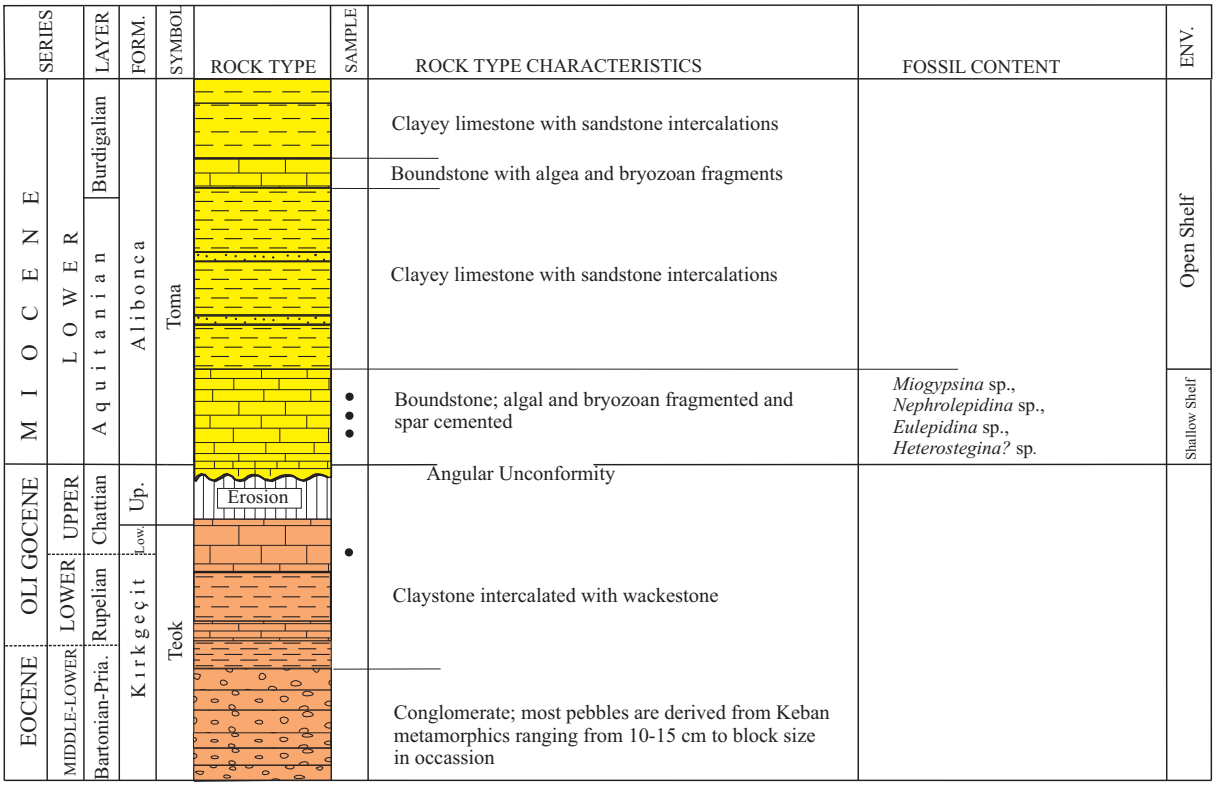

Figure 25- The generalized stratigraphical section showing the lithological characteristics of the Alibonca gormation cropping out in 1 km south of the Dağarcık district, the north of Sağman village, and sampled section of the succession (K42 b1, 25700-09500) (modified from Herece, 2016).

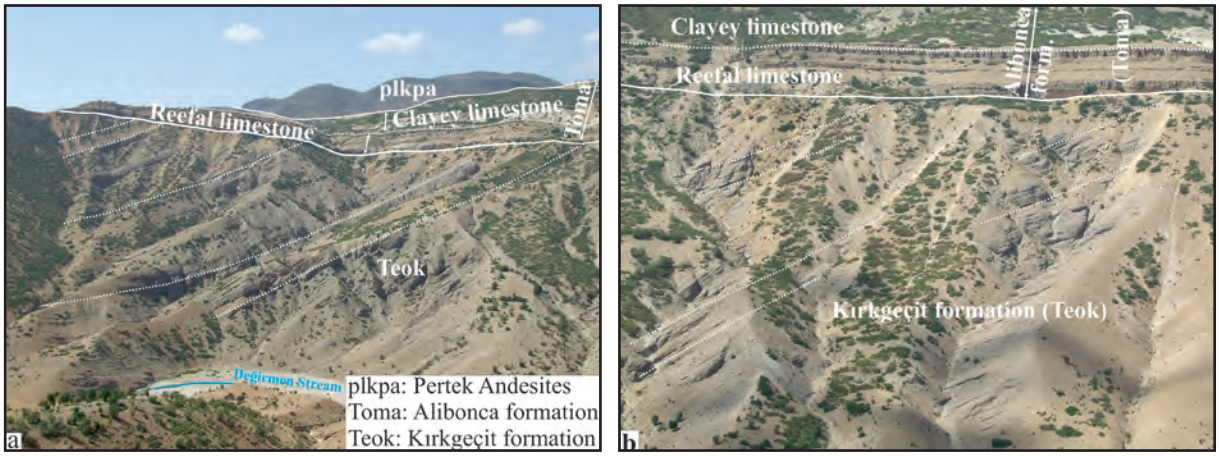

Figure 26- a-b. Horizontally deposited lithologies of the Alibonca formation extending northeastward from Sağman and the general views of the Kırkgeçit formation overlain by the angular unconformity (K42 b1, 27800-08900, looking NW).

The age of the Alibonca formation was determined by benthic, planktonic fauna and nannoplankton descriptions carried out in several samples collected at different elevations of the exposures in different areas (Herece, 2016).

The unit spreads over the wide region from east to west and the lithologies of the succession thickens with lateral facies changes. Therefore; a type location representing the whole unit could not be found. On the other hand, the western exposures of the boundstone forming the bottom of the formation are a few meters thick; however, this thickness reaches 50 meters towards east and forms steep cuts. Samplings in reefal limestones were carried out at different levels, which can be traced and reached in

Figure 27- a-b. General views of; a) the outcrop on the Kazıkbaba ridge in southeast of the Karabulut district (K42 b1, 32.500-14.400, looking west), south of the Yalınkaya village of the Alibonca formation, and b) the angular unconformities on the Kırkgeçit formation (K42 b1, 31.200-15.400, looking NW).

Figure 28- The general view of the lower contact relationship of the Alibonca formation which unconformably overlies the Elazığ magmatics (K42 b1, 22660-08663, looking WNW).

Figure 29- The general view of the basal conglomerate located at the bottom of the Alibonca formation and originated from angular, coarse ophiolitic pebbles, which unconformably overlies Elazığ magmatics in south of the Arılar district (K42 b1, 22660-08663, looking west).

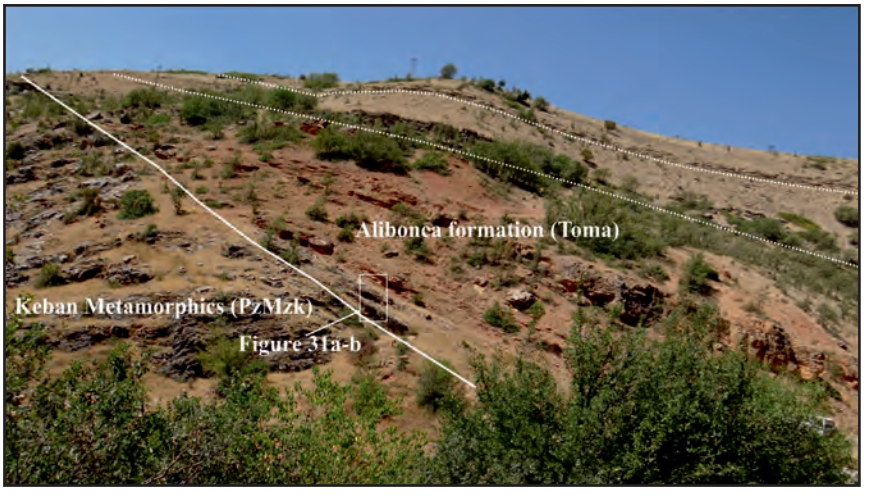

Figure 30- The general view of the Alibonca formation, which unconformably overlies the Keban metamorphics, and its lower contact relationship (K42 b1, 26425-15897, looking NW).

Figure 31- a-b. General views of the ~2 m thick basal conglomerates from pebbles of the Keban metamorphics at the bottom of the Alibonca formation (K42 b1, 26425-15897).

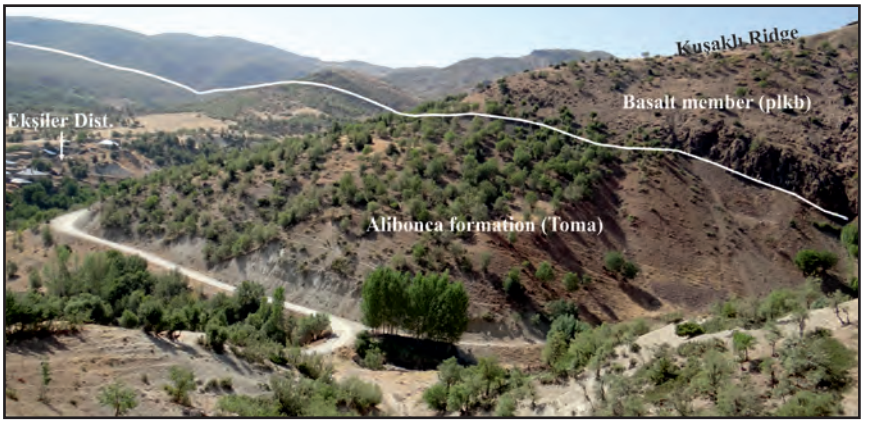

Figure 32- The contact relationship between the basalt member of the Alibonca and Karabakır formations in NE of the Ekşiler district (K42 b1, looking SSW).

the lateral direction, and the age data obtained were given below (Figures 33 and 34).

Samples taken from the first levels corresponding to the bottom of the unit in Dağarcık and Akmezra districts in Pertek NW and Çevirme district in the south of Tunceli city; *Postmiogypsinella intermedia* Sirel and Gedik, *Nephrolepidina morgani* Lemoine & Douville, *Planorbulina brönnimanni* Bignot and Decrouez, *Miogypsinella* cf. *complenata* (Schlumberger) foraminiferal assemblage was described which are late Chattian in age.

According to samplings made from bottom to top in reefal limestones, which are located at the lower part of the succession, from 1 km south of the Dağarcık district in NW of Pertek and from the Çamurluk district in the NW of the Günboğazı village (Figure 33); Early Miocene (early Aquitanian) age was taken from *Planobulina bronnimanni?* Bignot and Decrouez (piece), *Miogypsina* spp. (1, 2, 3), *Miogypsinoides* sp., *Nephrolepidina* sp., *Eulepidina* sp. and *Spiroclypeus* sp. fossil assemblage.

Boundstones are laterally transitional into clayey limestones in their upward and eastward extending exposures. Clayey limestone samples consisting the upper part of the succession in NW of the Dere town are Early Miocene (late Aquitanian-Burdigalian) with *Globoquadrina dehiscens* (Chapman, Parr and Collins), *Paragloborotalia semivera* (Hornibrook), *Globigerinoides trilobus* (Reuss) planktonic foraminifers. Samples collected from the north of Yalıkaya village at 5 km east of the Dere town are early Miocene (Burdigalian) with *Sphenolithus heteromorphus* Deflandre, *Cyclicargolithus abisectus* (Müller) nannoplanktons; and the samples collected from the boundstone in the vicinity of Günboğaz are Early Miocene (Burdigalian) with *Nephrolepidina tournoueri* Lemoine and Douville, *Miolepidocyclina* sp., *Miogypsina* spp. and *Eulepidina* sp. benthic fauna.

On the other hand, the levels forming the upper part of the clayey limestone deposit are observed around Karaveli. In several samples collected on these levels; *Globigerinoides trilobus* (Reuss), *Globigerinoides quadrilobatus* (d'Orbigny), *Catapsydrax dissimilis* (Cushman and Bermudez), *Globigerinoides sacculifer* (Brady), *Globoturborotalita euapertura* (Jenkins), *Globigerinoides altiaperturus* Bolli, *Globoquadrina venezuelana* (Hedberg), *Neogloboquadrina continuosa* (Blow), *Globigerina praebulloides occlusa* Blow and Banner, *Globigerinella obesa* (Bolli), *Globoquadrina* cf. *dehiscens* (Chapman, Parr and Collins), *Globigerinella* cf. *praesiphonifera* (Blow) and *Globigerinoides* cf. *quadrilobatus* (d'Orbigny) planktonic fauna gave Early Miocene (early-middle

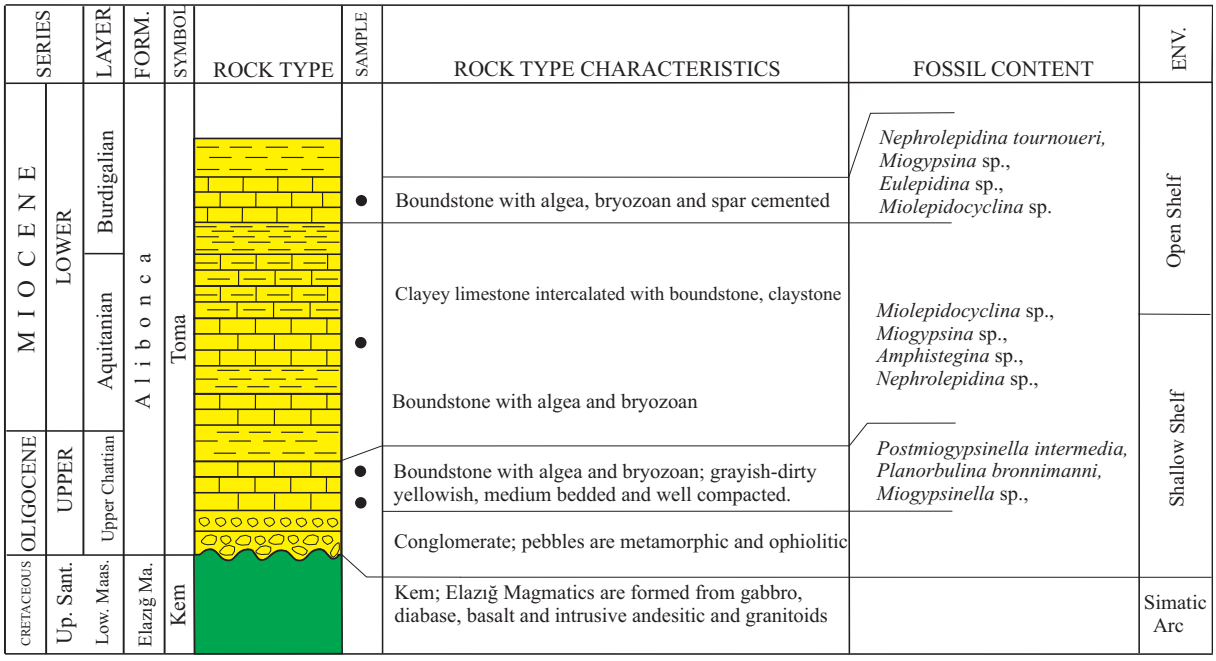

Figure 33- Stratigraphical section showing the rock type characteristics and sampled sections of the Alibonca formation in the vicinity of the Çamurluk district (K42 b1-b2).

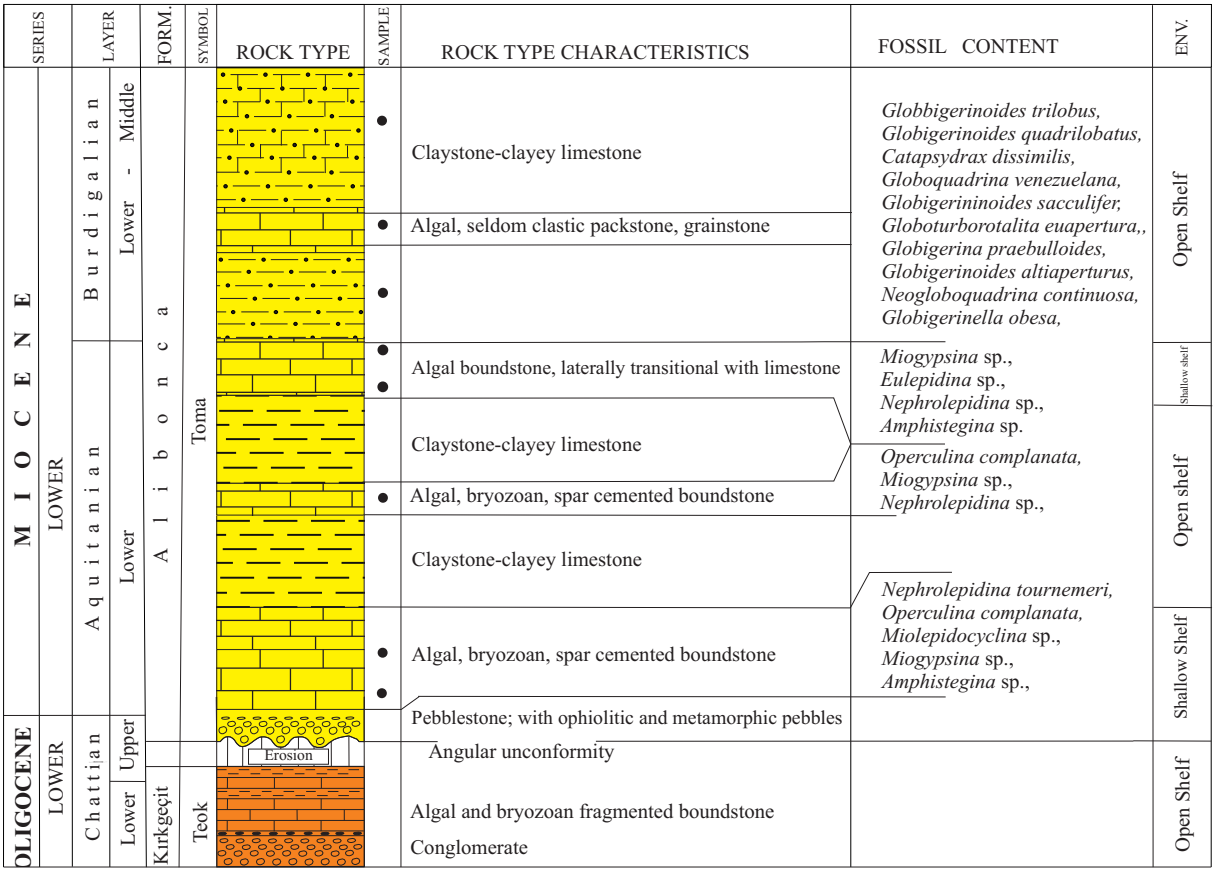

Figure 34- The generalized stratigraphical section showing the lithological characteristics, sampled sections of the succession and ages of the deposits of the Alibonca formation outcropping in north of Pertek.

Burdigalian) age. According to all these data the Alibonca formation is Late Oligocene-Early Miocene (late Chattian-middle Burdigalian) (Figure 34).

Conglomerate and sandstone located at the bottom of the succession were deposited in fluvial-shallow marine environment, the reefal limestone, clayey limestone and claystone were deposited in fore reef and open shelf conditions.

3.2.2. Karabakır Formation (plk)

Karabakır formation is outcropping in the region consists of volcanoclastics, pyroclastics, epiclastics, lava flows and lacustrine limestones, which are both laterally and vertically transitional, and fluvial deposits. Andesitic volcanic rocks, which have large exposures around Pertek within unit, and andesitic volcanics were named as the Pertek Andesite member and Basalt Member, respectively (Herece, 2016).

Pyroclastics cropping out in the vicinity of Aşağı Gülbahçe begins with coarse grained tuffs, continues with andesitic tuffs; afterwards, they present a deposit in the form of nearly 12 m thick lapillistones and pyroclastic breccia. Thicknesses of pyroclastic breccias increase towards Y. Gülbahçe village in the north. In poorly sorted breccias; the material forming the breccia is mostly andesitic and few basaltic in origin. In north of A. Gülbahçe village, reddish lapillistones outcropping in limited areas present distinctive structures as fairy chimneys in topography (Figure 35a-b). Reddish color is most probably because of ferric content in cement material (Figure 36a-b). Dominant pebbles in subhorizontally deposited lapillistone are andesitic and in minor amount basaltic in origin.

Volcanoclastics exposing in large areas present different characteristics based on depositional environment and on distances to volcanic centers. The lower part of the deposit crops out as tuff-ignimbrite alternation on the southwest end of the Demdemik rocks in northeast of the Konaklar district (Figure 37a-b). Tuffs are grayish white and ignimbrites are grayish-pale brown and massive. In the eastward lateral continuation

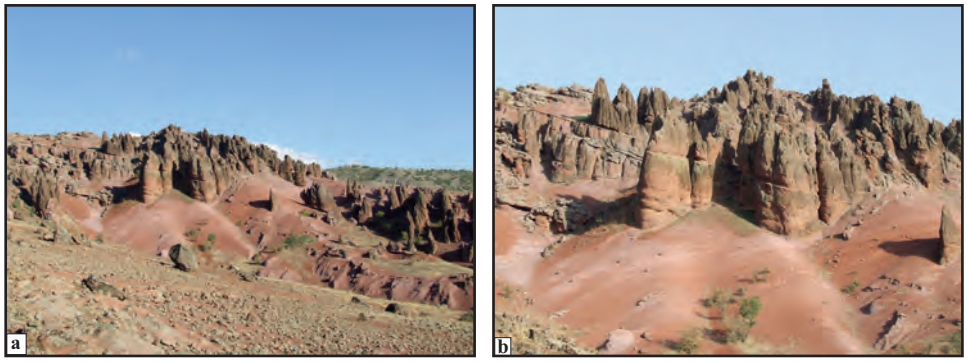

Figure 35- Views of lapillistones in N-NE of Aşağı Gülbahçe resembling to fairy chimneys on topography (K42 a2, 14750-09500, looking ENE).

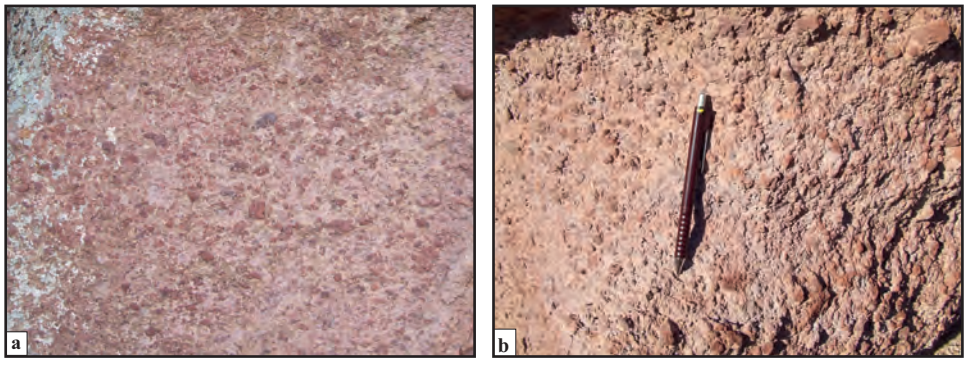

Figure 36- Close up views of the lapillistones cropping out in N-NE of Aşağı Gülbahçe (K42 a2, 14750-09500).

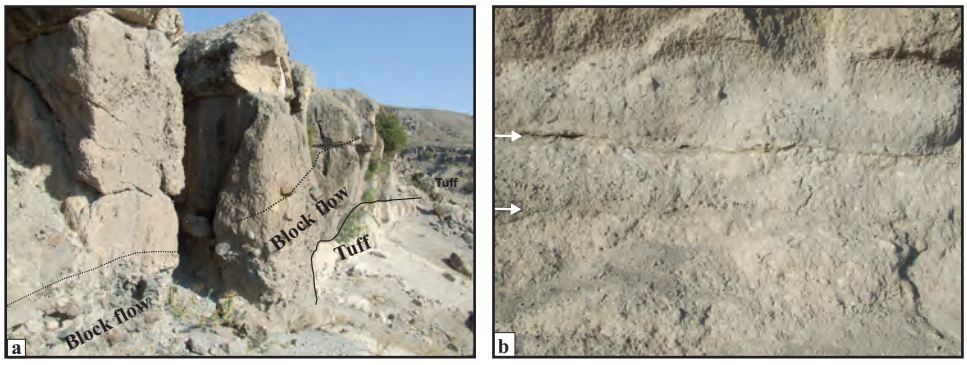

Figure 37- a) Views of ash and block flows during eruptions in SW end of Demdemik rocks, the NE of Konaklar, and b) eruptive volcanic products transported into the depositional environment (arrows indicate the sedimentary deposits of the basin).

of the same deposit, the debris flow and blocks from north to south during volcanic eruptions are observed on tuffs (Figure 38a-b). Similarly; eruptive volcanic products and pumice accretions in lapilli type on 3-6 cm thick mudstone bands are observed (Figures 39a-b and 40a-b). There is also observed the presence of lacustrine environment in the close vicinity of volcanic centers during volcanic activity.

Epiclastics are represented by agglomerate, sandstone, claystone and lacustrine limestones. Agglomerates are poorly sorted and angular pebbly in various sizes (Figure 41a-b). Most pebbles are andesitic and in few amounts basaltic origin. Sandstone interlayers deposited as alternating with agglomerate were formed by sub-horizontal, coarse grained sand accretion in ophiolitic and metamorphic origin. The groundmass among grains are formed by clay size material. Claystone interlayers are greenish brown with capillary caliche and loose textured.

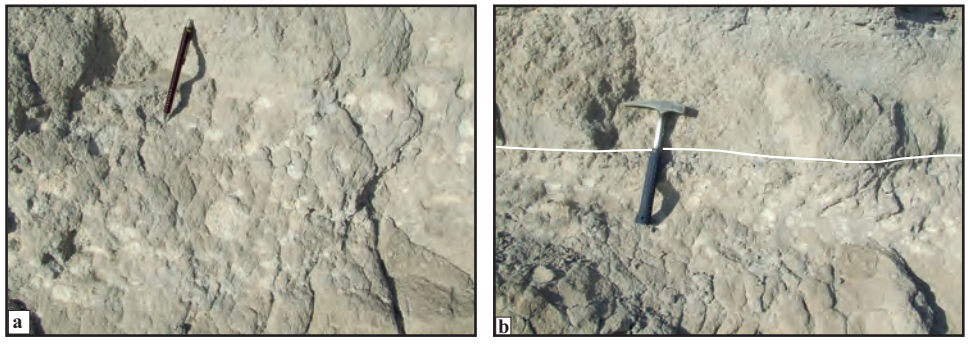

Figure 38- a-b. Volcanic products transported into the lacustrine environment during eruption (in tuff and lapilli sizes) (K42 a1, looking north).

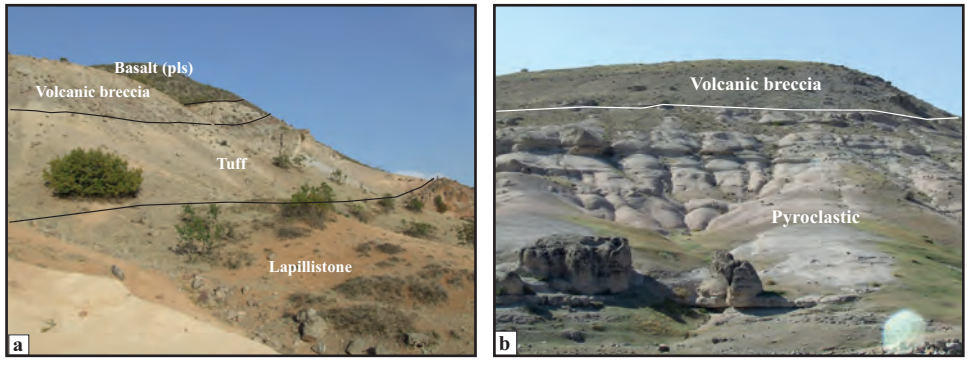

Figure 39- Views of; a) lapillistone and the overlying tuff, volcanic breccia and basaltic lava flows in Aşağı Gülbahçe NW (K42 a2), and b) volcanic breccias located on pyroclastics in the lower part of the succession in 1 km NE of Konaklar (K42 a1).

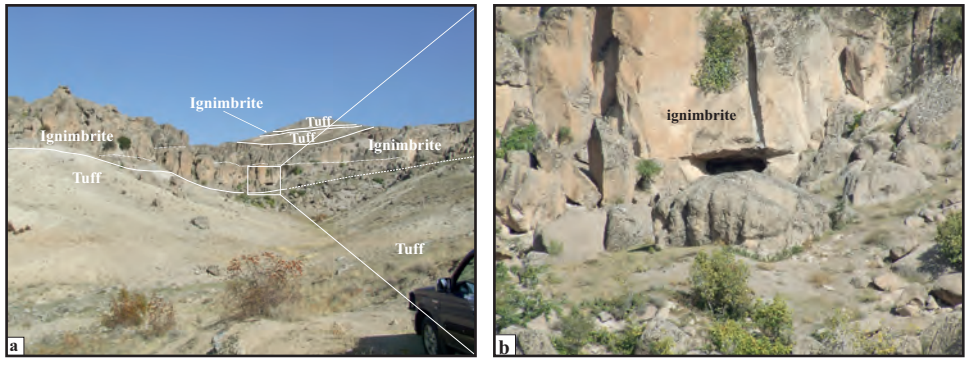

Figure 40- a-b. Views of tuff-ignimbrite alternation in the southwest end of Demdemik Rocks in NE of Konaklar (K42 a1, looking north).

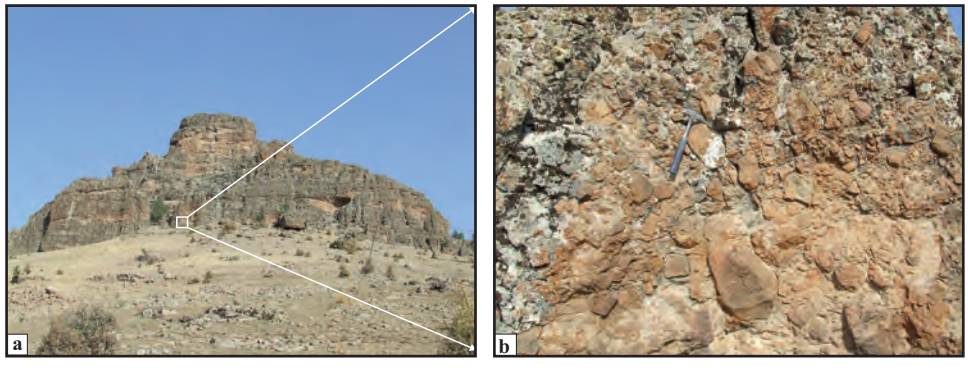

Figure 41- a) Massive agglomerates which have wide spread and outcrop in north of Yukarı Gülbahçe, and b) the close up views from agglomerates (K42 a2).

Undistinguished epiclastics are also observed within the study area. These are represented by conglomerate (agglomerate), sandstone, mudstone and lacustrine deposits. Coarse layered, massive agglomerate is badly sorted and matrix supported. Pebbles are of variable size, and blocks in 1 m size are encountered. Pebbles are generally angular, and most of them are andesite and the remaining is basalt.

Karabakır formation is stratigraphically deposited below the basalt member in 2 km northwest of the Günboğazı village. In the locality, the eastern part of the study area, the thickness of deposit becomes thinner compared to outcrops in west, and basalt exposures become widespread. The deposit of the formation cropping out along the road cut consists of the alternation of loose compacted, cross bedded, channel filled, coarse sandstone-pebblestone and conglomerate (Figure 42a), and it covers the rounded pebbles of the Alibonca formation (Figure 42b). The outcrops in east of the Tozkoparan village are located on the eastern slopes of the Karaçalı hills. The outcrop here consists of the alternation of grayish milky white, loose compacted, coarse sandstone and reddish bordeaux claystone.

Karabakır formation, which is located below the basalt in the near south of the study area along the cuts of Pertek-Elazığ road, is channel filled mudstone which is not thick (Figure 47a), and it comprises rounded, coarse pebbles of the basement units with Alibonca formation (Figure 47b).

The Karabakır formation has unconformable lower contact relationship with the underlying older units, but the upper contact is unconformably overlain by Quaternary deposits.

There was not made any fossil dating in the Karabakır formation. However; in the middle part of the lacustrine deposit, which consists of the Çaybağı basin located between Elazığ and Palu in near south of the study area without volcanics Micro Mammals Fauna (MMF) was determined as; *Promimomys moldavicus*, *Apodemus* cf. *dominans* and Castoridae gen. et. sp. indet. (big form) and the Early Pliocene age (MN-14) was detected representing 5.3-4.2 my interval. Similarly; *Mimomys occitanus*, *Occitanomys brailloni*, *Apodemus* sp. (cf. *dominans?*), Cricetidae gen. et sp. indet MMF fauna was detected from the Sürsürü district in south of Elazığ gives Early Pliocene (MN-15) which represents 4.2-3.4 my age interval (Herece et al., 1992). In Muş and its surrounding, the Late Pliocene-Early Pleistocene (MN-17) representing 2.6-1.95 my age interval was obtained from the lateral equivalence of the similar deposits (Akay et al., 1989).

On the other hand, the basalt, which outcrops in large areas in east and outside the study area and named as Solhan volcanics, were radiometrically dated. These radiometric ages were taken as; 4.4±1.08my and 6.0±1.0my (Pearce et al., 1990), in Karakoçan surround as; 4.1±0.32my (Sanver, 1968) and in Muş surrounding as; 4.4±1.3my and 6.0±0.6my (Türkecan, 1991). The ages corresponding to upper Late Miocene-lower Early Pliocene most probably match with the lower age boundary of volcanics, and the lower age limit of the volcanics may drop down to upper Late Miocene (Messinian).

According to these data, the volcanism in the Karabakır formation began in the upper Late Miocene and the depositional conditions have continued until Late Pliocene as transitionally in horizontal-vertical directions with the active volcanism and depositional

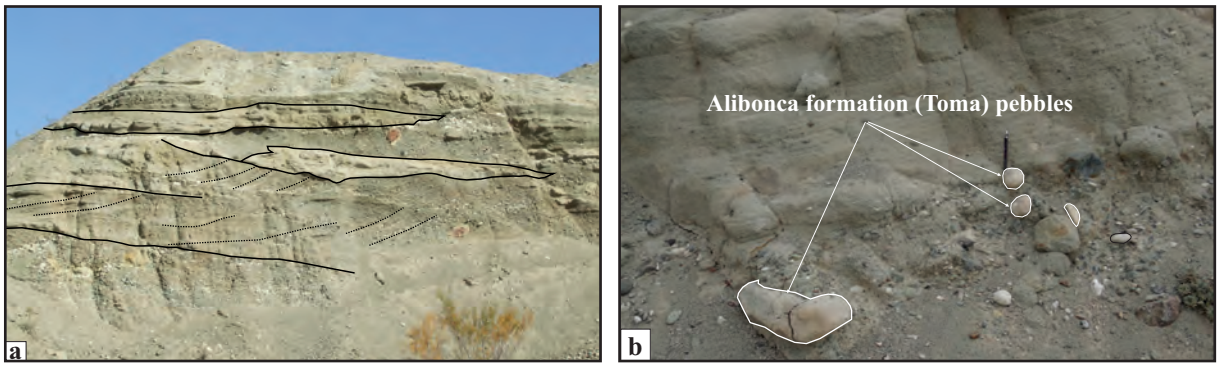

Figure 42- a) Coarse sandstone-conglomerate alternation forming the bottom of the Karabakır formation (K42 b2, 37384-14207), and b) lime pebbles of the Alibonca formation within conglomerate (K42 b2, 37384-14207).

environments of the unit are fluvial, fluvial-lake and lake environments in which the volcanism is active.

Pertek Andesite Member (plkpa): It consists of andesitic volcanics and was first defined and named by Herece (2016a). The exposures of andesitic volcanics around Pertek are located in south and north of the Keban Dam Lake. Type locality is observed on Karataş Tepe (hill) in the south of the dam lake and in Pertek fortress in Dam Lake (Figure 43a-b). The exposures in north of the Keban Dam Lake are observed in north of Yukarı Gülbahçe village and as volcanic neck (Figure 44a) in Kale Tepe and as large dyke in east (Figure 44b). The outcrop of andesites in Pertek NW are the Büyük Tepe located among the Çıkıntı district in south, Ardıç village in north and Söğütlütepe in east, Eşikmeydanı Tepe and other elevated areas. Most of the unit in this area is massive and sustainable to eroding and weathering.

Andesitic volcanics were sampled in the field and collected samples were petrographically described (Herece, 2016). Samples collected from the northern slope of the Büyük Tepe in the Fındıklı district of Pertek were defined as hornblende andesite. Andesite is microlithic porphyric and occasionally glassy, microlithic porphyric in texture and consists of plagioclase, amphibole (hornblende), biotite and opaque minerals. The groundmass of the rocks is formed by volcanic glass, plagioclase, amphibole, biotite microliths and rare opaque minerals.

The outcrop in the south of Pertek-Söğütlü Tepe was defined as andesite porphyry. The rock is glassy microlitic porphyritic in texture and consists of plagioclase, amphibole and biotite minerals. The groundmass is amphibole opacitized with plagioclase microliths. Another andesite sample is microlitic porphyritic in texture and contains plagioclase,

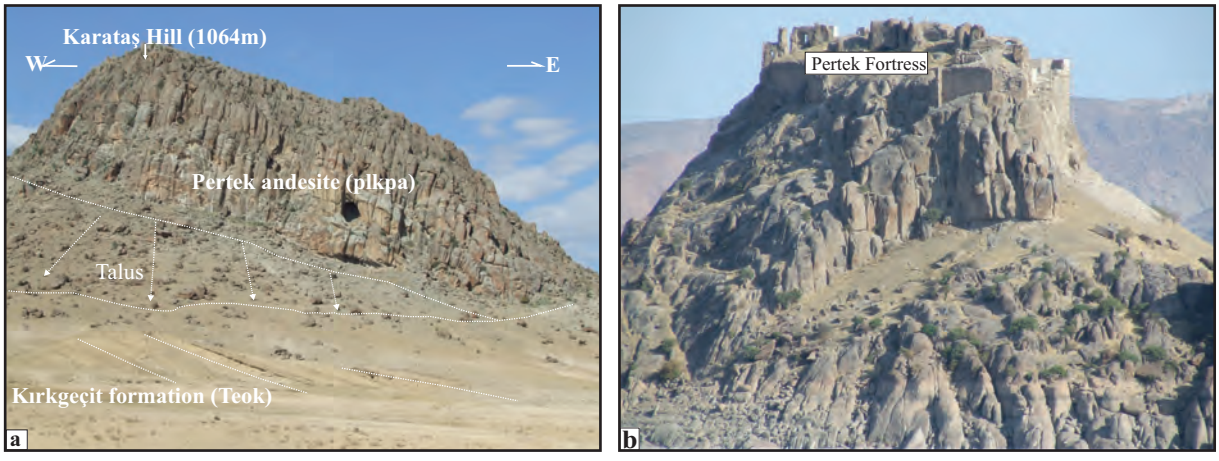

Figure 43- Views of volcanic chimneys formed by outcropping Pertek andesites a) in Karataş Tepe in Pertek SW (K42 b4, 22000-99000) and b) in Pertek fortress (K42 b4, 23500-99500).

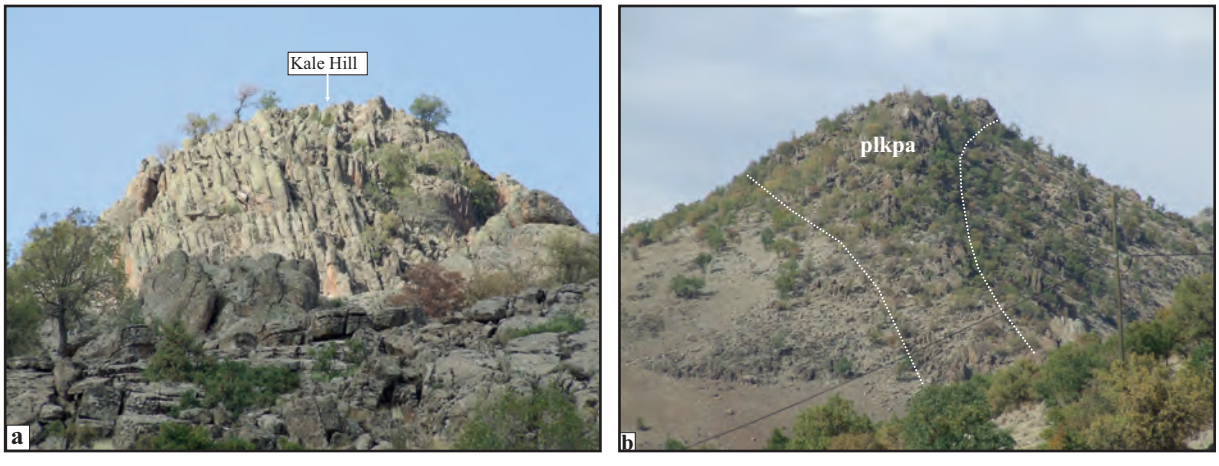

Figure 44- a-b. General views of the Pertek andesites outcropping in Kale Tepe and its east side in north of the Yukarı Gülbahçe village (K42 a2, 14075-12100, looking north).

pyroxene (clinopyroxene) and amphibole minerals. The groundmass is formed by plagioclase and tiny opaque minerals which are in radiated form with amphibole microliths.

The northeastern end of the Pertek fortress, as the location of volcanic neck, in south of Pertek was sampled (Figure 45b). All these samples were described as andesite. The rock consists of plagioclase, amphibole (hornblende), biotite, opaque mineral, apatite and zircon minerals, and the groundmass is formed by plagioclase and opaque minerals which are radiated with amphibole microliths. Sericitization and argillization are observed among the plagioclase microliths in the groundmass.

There is not any data on age and the formational period of Pertek andesites. Lower and upper age boundaries are hypothetically determined according to the contact and stratigraphical relationships of the rocks with respect to its surrounding.

Andesite outcrops in Pertek fortress and its close vicinity is intrusively associated with Kırkgeçit and Alibonca formations (Figure 45a-b). According to these stratigraphical relationships the andesitic volcanism is younger than Kırkgeçit and Alibonca formations. Besides; agglomerates in the volcanoclastic deposit of the Karabakır formation widely comprises andesitic pebbles (Figure 46a), and the andesitic volcanics in west of the Çıkıntı district in Pertek are also overlain by sub horizontally bedded tuff and basalts of the Pliocene Karabakır formation (Figure 46b). Also the lapillistone in lower part of the deposit forming the formation is much andesitic pebbly. Moreover; thin andesitic lava flows are observed also within pyroclastics. Pertek andesites are stratigraphically located in the lower part of the volcanic succession and in the upper part of the succession on the other side. Besides; they support volcanic products to volcanoclastics and pyroclastics located in upper part of the deposit, and the youngest ones of the volcanism cut Pliocene Karabakır formation as dykes.

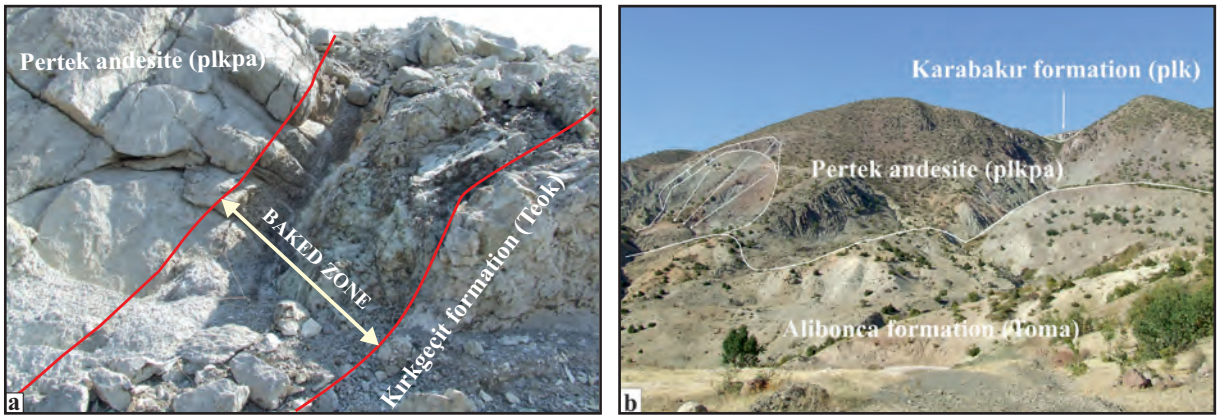

Figure 45- a) Baked zone between Pertek andesite and Kırkgeçit formation in NE end of Karataş Tepe on the southern boundary of the Keban Dam Lake (K42 b4) and b) the crosscut of the Alibonca formation in N-NE of the Çıkıntı District by Pertek andesites (K42 b2).

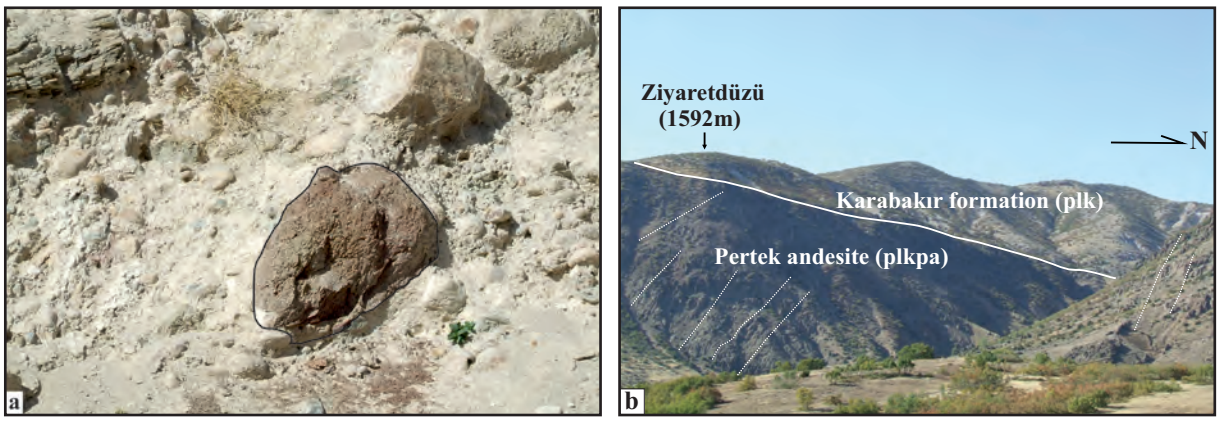

Figure 46- a) Views of andesitic volcanic pebbles in the agglomerates of the Karabakır formation and b) the coverage of the Karabakır formation of the Pertek andesites in 1 km west of the Çıkıntı District (K41 b1).

According to all these stratigraphical and contact relationships, the volcanism forming Pertek andesites should have begun in pre Pliocene, most probably in Late Miocene and continued its activity during Pliocene.

Basalt Member (plkb): Sub horizontally deposited basalts overlying the Karabakır formation are the dominant rock type in their eastward and westward extensions. Basalts, which have the first primary relationship with the Karabakır formation, were distinguished as the member and named based on the lithology (Herece, 2016). The locations of the volcanic centers were defined as basalt member in exposures which are not distinctive or in places outside the study area. Basalt outcrops located in north of the Keban Dam Lake are in the vicinity of the Çevirme District in east and Gülbahçe and Konaklar villages in west. The outcrops in south of the dam lake are observed between Alaca-Körpe and around Beydalı-Beşoluk.

Basalt exposures in north of the Keban Dam Lake and the eastern part of the mapping area are observed in the Çevirme district and its east. The outcrops in this locality originated from E-W trending volcanic crater with sizes of 1.7x2.5 km. Type localities of the unit are in the vicinities of Günboğazı, Yolkonak and Beydamı villages. The basalt that had flown from the Korucak Tepe (hill) located at an elevation of 1383 m in 2.25 km of the Bulgurtepe village to S-SW direction have reached the Demdemik rocks at 1020 m in 1.5 km NE of the Konaklar village. Volcanics in this area are between ~100-110 m thick according to topographical data.

Basalt outcrops in south of the Keban Dam Lake are located in east and west of the Körpe district in the west and between Beydalı-Beşoluk in east. The exposures around the Körpe district originates from the volcanic center in the south and outside the mapping area and continues northward. However; the volcanic centers of exposures in east are the hill with elevation of ~970 m in the south of Beşoluk village. Basalt that had flown northward starting from the center has formed Çakmaközü and Beydalı plains today. Basaltic flows in the area are ~40-50 m thick, and this thickness flows towards centers in south. Type localities of the unit are road cuts along Elazığ-Pertek highway (Figure 47a-b).

Samples collected from basaltic lava flows are glassy, microlitic porphyritic textured. The groundmass of the rock consists of plagioclase microliths and opaque minerals in radiated form. It contains plagioclase, pyroxene (augite), olivine and much olivine residuals with opaque minerals (Herece, 2016).

Basalt member is laterally transitional in vertical-horizontal directions with sedimentary lithologies of the Karabakır formation at its lower boundary; however, it is unconformably overlain by the Early Pliocene deposits.

There is not any radiometric dating performed for the Basalt member within the study area. However; the

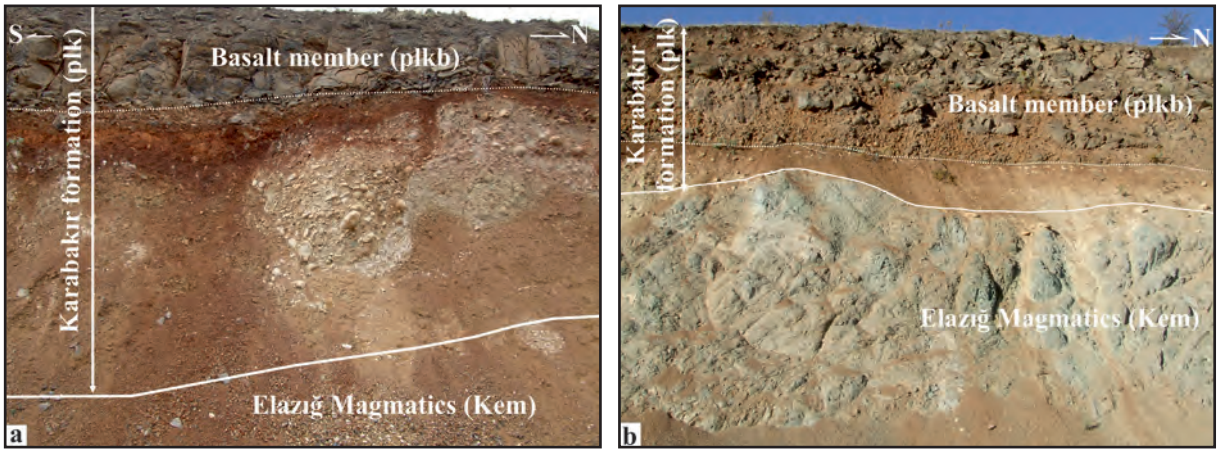

Figure 47- General views of; a) the basalt member of the Karabakır formation and the underlying mudstone and channel fill conglomerate in road cuts of the Pertek-Elazığ highway (K42 d2, 18223-88326, looking west), and b) lower contact relationships of the thin Karabakır formation and Basalt member (K42 a3, 17400-89925, looking west).

basalts outcropping in Elazığ NW were radiometrically dated, and 1.8±0.05my and 1.9±0.08my (Sekrek et al., 2008); 1.47±0.09my and 1.87±0.07my (Arger et al., 2000) were taken. These ages correspond to the Late Pliocene.

The depositional environment of volcanic and volcanoclastic rocks are fluvial and lacustrine that are horizontally-vertically transitional with volcanic center.

3.3. Palu Formation (Qpa)

The unit, which is rounded, grain supported pebble stocks, was first named by Herece et al. (1992). Type locality of the unit, which outcrops in Pertek NE and Alaca Village NW, are the road cuts of the Pertek-Tunceli highway in the south of Yeniköy. The unit consists of conglomerate and the overlying pale brown sandstone and thin mudstone layers. The formation has an angular unconformity with the underlying Karabakır formation and other older units.

There is not any age data but most probably it should be early Pleistocene. Mostly; they are alluvial fan deposits.

3.4. Quaternary (Qal)

Forms mapped as terraces, alluvial deposits, talus, alluvial fans have been formed as a result of river and stream activities in the region. The alluvial deposits, which formed by loosely compacted silt, clay and fine sand-intra block material, develop on river sides and rivers.

4. Structural Geology

4.1. Faults

The abvious faults in the region were observed. Significant faults are right lateral strike slip Pertek fault and left lateral strike slip Koruköy fault.

4.1.1. Pertek Fault

The fault restricts the Pertek settlement area from east (Bingöl, 1984; Aksoy, 1994), forms distinctive structures at the surface and can laterally be traced from SE to NW. SE extension of the fault remains beneath the Keban Dam Lake and NW extension of it can be traced until NW of Çağlarca town. Fault scarps, fault plains and slickensides preserved on plains indicate that movement along the fault zone is right lateral strike slip (Herece, 2014). According to fault scarps, plains formed and offsets in the drainage perpendicular to the fault zone, destructive earthquakes with magnitudes more than 7 (M≥7.0) could develop along the zone (Herece, 2014). However; the slip-rate to be low in the fault zone shows that the recurrence intervals of earthquakes could be quite long.

4.1.2. Koruköy Fault

This fault is formed by two distinctive segments on the eastern facing slopes of the Keban metamorphics in north of Koruköy. NE extensions of the faults are below the Keban Dam Lake, and SW extensions could not be traced due to agricultural activity. The eastern segment is between Keban metamorphics and Elazığ magmatics, and restricts magmatics from the west.

4.1.3. Esenkent Fault

The fault restricting Esenkent settlement area from east extends linearly toward NE, and its SW extension makes a smouth curve. The fault restricts Elazığ magmatics from the east and separates from Keban metamorphics. There was not found any data about the recent activity of the fault.

Faults have most probably developed as reverse faults on the NNW boundary of the Kırkgeçit formation outcropping in south of the Keban Dam Lake during NNW-SSE directed compression which ends the basin forming process in the Kırkgeçit formation. Keban metamorphics in north of Alatarla overlies Elazığ magmatics and Kırkgeçit formation with reverse fault. In addition; probable left lateral strike slip faults with the strike of N30°-40°E are observed located within Keban metamorphics and between Keban metamorphics and Elazığ magmatics in NE of Koruköy. There is observed another fault with similar strike located between Keban metamorphics and Elazığ magmatics in east of these faults. NE extensions of the fault systems in this area remain below the Keban Dam Lake; SW extensions on the other hand fall outside the study area and remain as a problem to be solved.

4.1.4. Folds

Folds with an axial strike of N65°E in the Kırkgeçit formation is observed in the vicinity of the Kabakçılar district. The convergence that has been effective in the region is N25°W in direction. The folding in this area has not affected basalts of the horizontally bedded Pliocene Karabakır formation. Besides; the Alibonca formation is horizontally bedded as well. Accordingly; the regional compression generating the folding should have occurred during early Chattian.

4.3. Mass Movements

Remarkable landslide areas are observed within the study area. The first of the landslides is along Pertek-Tunceli road, the south of the Mercimek village. The landslide here originates from heavily crushed zones developed in Elazığ magmatics and the hill slope (Figure 48a-b).

The second landslide is in the last section of Pliocene volcanics in south of the Keban Dam Lake (K42 b4). It is nearly 500 meters wide and occurs in the NE end of the Çakmaközü Plain and the NW end of the Beydali Plain (Figure 49a). Both landslides develop towards Keban Dam Lake. The reason that causes the landslide is lithologies which are not well compacted below thick basalts.

NW-SE extending ridge in Sorkun District in NW of Pertek is formed by Pliocene basalts. The presence of fault extending along the NE boundary of the ridge and loose lithologies of the Alibonca formation give rise to landslide (Figure 49b).

In 4 km NW of the Sorkun District, four different landslides 1 km width take place on the northern slope of the Eşikmeydanı hill that formed by andesitic volcanics (Figure 50a). Fındıklı (Figure 50b), Ardıç and Söğütlütepe villages (K42 b1) are located on

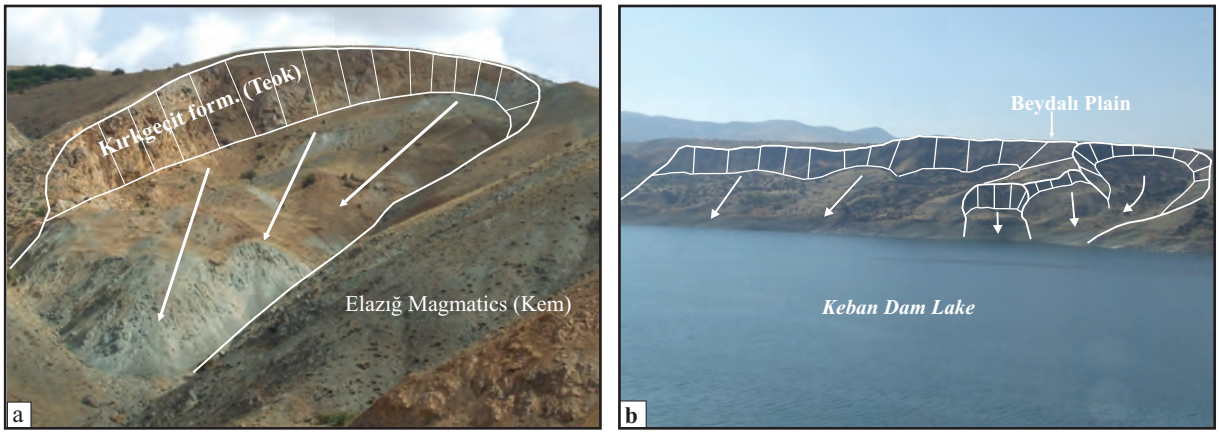

Figure 48- Views of; a) ophiolites of the Kırkgeçit formation and widespread landslides that have formed in the lower boundary around Mercimek village (K42 b3, looking NE), and b) the landslide that developed on NE slope of the Beydalı Plain in north of the Beydalı village (K42 b4, looking SW).

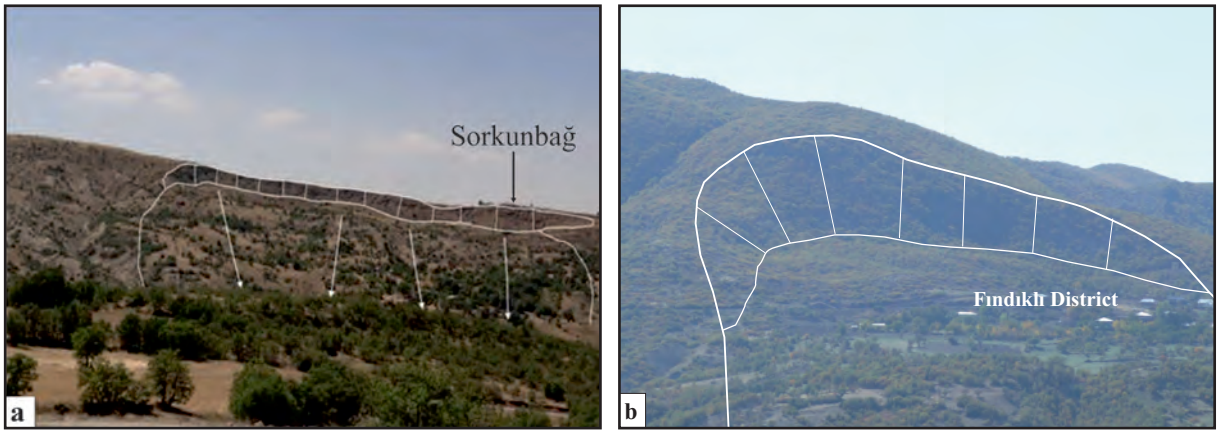

Figure 49- The general view of the landslide that developed; a) along a distinctive fault on NW boundary of Pliocene volcanics outcropping in near north of the Sorkunbağ village (K42 b1, Sorkunbağ district, looking south), and b) towards NW in Kengerlik locality located in NW slope of Eşikmeydanı Tepe (K42 b1, looking SE).

landslides that have developed from steeply sloping hills in the south towards north.

4.4. Deformation Phases

There have been some macrotectonic events during Maastrichtian, Lower Eocene, middle-upper Lutetian, Middle Oligocene, Middle-Late Miocene and Late Pliocene corresponding to periods in which the unconformities in sedimentary deposits had formed in the study area.

4.4.1. Macrotectonics during Maastrichtian Phase

Rifting of Neotethys ocean which separates the northern and southern continents that began during the Middle?-Late Triassic and continued during the Late Jurassic-Early Cretaceous to form the ophiolites. On the supra-subduction zone dipping north in the ocean that began during the Late Cretaceous, SSZ ophiolites and Elazığ magmatic and by the subduction of the oceanic crust beneath the Keban platform in the north, Baskil magmatics were formed.

Keban-Malatya metamorphics, Baskil and Elazığ magmatics that form the northern continent are being overlain by late Maastrichtian-Middle Paleocene Harami formation while the Pütürge metamorphics and Guleman ophiolites located in the south are being covered by late Maastrichtian-Middle Paleocene Simaki formation with angular unconformity.

All these basements units have been juxtaposed due to tectonic events as a result of the collision occurred in middle Maastrichtian; they have been uplifted and eroded and have formed source areas for the Paleogene basins that begin with late Maastrichtian deposits. In the study area there are no data to indicate subduction during Paleogene.

All these basements units have been juxtaposed due to tectonic events as a result of the collision occurred in middle Maastrichtian; they have been uplifted and eroded and have formed source areas for the Paleogene basins that begin with late Maastrichtian deposits.

4.4.2. Macrotectonics during Lower Eocene Phase

During Early Eocene, the region has been uplifted and depositional conditions in the Harami formation were terminated. The uplifted region has re-subsided and caused the formation of the Seske formation which has exposures in limited areas.

4.4.3. Macrotectonics during middle-upper Lutetian Phase

The second deformation affecting the region occurred in middle-late Lutetian. Distinctive deformations of this phase is observed in the south of Elazığ.

The tectonic line which is known as Uluova fault in the south of Elazığ begins in Palu and extends westward on Çaybağı, Mollakendi and south of Akçakale and juxtaposes different basement units of different ages and the Paleogene basins. In the area north of the Uluova fault Keban-Malatya platform, Elazığ magmatics and Andezitik volcanoclastics, and in the south of the fault Pütürge metamorphics and Guleman ophiolites are located. The basement units located in the north are unconformably being overlain by late Maastrichtian-Middle Paleocene Harami formation, late Cuvisien-middle Lutetien Seske formation and early Bartonian-early Chattian Kırkgeçit formation. The basement units on the south of the fault, on the other hand, are unconformably being overlain by late Maastrichtian-Paleocene Simaki formation, Paleocene-Early Eocene Gehroz formation and Lutetian Melefan and Karadere formations.

By N-S directing compression during Middle-late Lutetian, areas in south of the Uluova fault were uplifted and the depositional conditions terminated. Consequently, while block formations in Melefan formation were occurring, volcanic facies in Karadere formation developed. In the area to the north of the fault the Seske basin first uplifted and became terrestrial and the Kırkgeçit basin which began forming during the early Bartonian continued its development until early Chattian with a new angular unconformity.

4.4.4. Middle Oligocene Stage Macrotectonics

In this deformation period, the region uplifted and depositional conditions in the Kırkgeçit basin has ended. Although the deformation has occurred due to the compression of the region in NNW-SSE directions, the reason is not clearly known. Late Oligocene-Early Miocene Alibonca formation developed in the basin formation that has formed due to the termination of compression.

4.4.5. Macrotectonics During Middle?-Late Miocene Phase

Another deformation period that has been effective in the region occurred in Middle-Late Miocene and the region was uplifted; so the depositional conditions ended in the Alibonca formation. The deformation occurred due to the compression in N-S directions. It has most probably occurred by the northward movement of the African-Arabian plate (Herece, 2008). As a result of the decrease in N-S convergence velocity in this deformation period, the lacustrine deposits and widespread volcanic activity in local areas have occurred.

4.4.6. Macrotectonics During Uppermost Pliocene Phase

The most remarkable structure of this deformational period is the development of the EAF. Continental convergence rate which continued slower during the Pliocene has increased during the Latest Pliocene and the region was uplifted by compression. The most effective N-S convergence before the development of the EAF in the region has caused east-west trending compressive folds in the Çaybağı Pliocene basin located in the east of Elazığ; therefore, the basement in north of the basin has been uplifted and locally thrusted on Pliocene units.

Based on the activity of the EAF which began moving after this folding and deposition, Early Pleistocene deposits were developed. Due to this compression, the right lateral movement along the Pertek fault should have begun to gain activity. Aksoy (1994) investigated one segment of the fault around Pertek and stated that it had been right lateral strike slip fault with reverse fault component. The position of the fault within regional tectonism, its extension and activity was also asserted (Ozaner et al., 2010; Herece, 2014).

The 40 km section of the Pertek fault cropping out within study area was mapped for the first time based on field data. However; the extensions of the fault towards NW and SE have not adequately been investigated. The right lateral strike slip fault also covers the reverse slip component in few amounts. Besides; 6.0 km and 3.25 km offsets were detected in basement units and Pliocene deposits, respectively (Herece, 2014). The regional compression forming the fault is ~350°, and right-lateral offsets varying in between 75-975 meters have occurred in streams that are flowing perpendicular to the fault (Herece, 2014).

5. Discussion

Keban metamorphics and Elazığ magmatics are the basement units of the region. Keban metamorphics are generally observed as; marble, schist and amphibolites. They were deposited as limestone within interval of Permian-Cretaceous and metamorphosed in green schist facies during Campanian-early Maastrichtian.

Elazığ magmatics were formed by ensimatic island arc units developed on the ophiolitic deposit which formed in the intra-oceanic supra subduction zone. Ophiolites present a successive deposit and consist of gabbro, diabase, basalt and andesitic volcanics-tuff and agglomerates from bottom to top. Ensimatic island arc consists of intrusive diorite, monzodiorite, tonalite, granite and granodiorite and it is Late Cretaceous.

Keban platform was intruded by Baskil magmatics due to the northward subduction in Senonian. The intrusives of the Baskil magmatic also intruded into the tectonic contacts of metamorphics with ophiolites (Yazgan and Chessex, 1991). The bottom of metamorphics in and around the study area cannot be observed and they overlie Elazığ magmatics with reverse fault. The succession, which deposited under environmental conditions, are most probably the lateral equivalence of Malatya metamorphics.

Elazığ magmatics are the unit discussed in limited studies within the study area and defined under various names. The unit, which has a wide spread along a belt, have been defined as; Yüksekova complex (Perinçek, 1979), Elazığ complex (Hempton and Savcı 1982), Elazığ igniyıs complex (Hempton 1984, 1985), and as 4 units belonging to Yüksekova complex (Bingöl 1984). However; Turan et al. (1995) investigated Elazığ magmatics cropping out in this region under the name of "Elazığ magmatics" as they are in a successive internal structure.

There is not any radiometric age determination in Elazığ magmatics within study area. The unit is unconformably overlain by late Maastrichtian Harami formation. The basalt unit, which is on top of diabases located in the upper part of magmatics, is Late Senonian based on planktonic fossils as described in samples collected from pelagic limestones (Herece et al., 1992). On the other hand; the ophiolitic deposit, which is located below and in the western extension of Elazığ magmatics in the vicinity of Hazar Lake,

was named as Kömürhan ophiolites (Yazgan, 1983; Poyraz, 1988). Kömürhan ophiolites consist of three tectonic slices (Yazgan 1983; Poyraz 1988; Yazgan and Chessex 1991; Beyarslan and Bingöl 1996; Beyarslan and Bingöl, 2000) and its upper tectonic slice is the basement unit of the Baskil arc unit (Yazgan an Chessex, 1991). The lower tectonic slice was dated as; 127±14my, 89.5±5my by K/Ar method. Besides; 85±3 my age was taken by means of biotite dating from leucodiorites, which formed by the partial melting of amphiboles; and 78.5±2.5 My age was taken from trondjhemitic granophyre by means of muscovite dating (Yazgan and Chessex, 1991).

Baskil magmatics, which cut Keban metamorphic, were as well dated by K/Ar method as; 76±2,5 My, 78,5±2,5 My; and from biotite, muscovites in granodioritic intrusives 75±2,5 My, 75,4±2,5 My ages were obtained. The ages taken are explained by the partial melting of the continental crust below the ophiolitic nappes due to ophiolitic obduction (Yazgan and Chessex, 1991).

Kömürhan ophiolite around Hazar Lake overlies Pütürge metamorphics by 40° northerly dipping reverse fault. However, it is underlain by Elazığ magmatics with a similarly dipping reverse fault (Robertson et al., 2007) and transitional with Elazığ magmatics in the west of Hazar Lake (Herece et al., 1992). On the other hand, both units are then unconformably overlain by late Maastrichtian Harami formation (Herece et. al., 1992).

It is stated that the depositional environment of Elazığ magmatics are products of arc-backarc (Hempton, 1985), arc-forearc (Yazgan and Chessex, 1991) of the ensimatic island arc, and the ensimatic island arc products of the supra subduction zone ophiolites due to intraoceanic subduction-obduction (Beyarslan and Bingöl 2000; Robertson, 2002).

Supra-subduction zone ophiolites and ensimatic island arc volcanics are unconformably overlain by late Maastrichtian-Selandian Harami formation. On the other hand, it is asserted that there is not any unconformity between Harami formation and Elazığ magmatics in studies carried out by Aksoy et al. (1999). It is also emphasized that the depositional conditions in the Harami formation began in late Campanian and continued in Maastrichtian as well in which the arc magmatism had stopped. In studies carried out by Herece et al. (1992) and Herece (2008) in the same region, the Harami formation was sampled, and the forms with Campanian?-Maastrichtian age and the late Maastrichtian fauna were determined. Therefore; there is significant unconformity between the Harami formation and Elazığ magmatic.

6. Results

Following results were reached when available age data had been assessed for the geodynamical evolution of the region (Figures 50 and 51). The preliminary breaks in the ocean before the collision began in Cenomanian-Turonian (Yazgan and Chessex, 1991; Robertson et. al., 2007). The first subduction has started in the ocean and supra subduction zone ophiolites have developed with the subduction (İspendere, Kömürhan and Guleman). While Kömürhan ophiolites developed as oceanic crust on the supra subduction zone (Turan et al., 1995; Beyarslan and Bingöl, 1996; Bingöl and Beyarslan, 1996; Beyarslan and Bingöl, 2000), the gabbro, diabase, basalt and andesitic volcanics developed in the upper part (Herece et al., 1992). The basalts, which consists of the upper part of the Kömürhan ophiolites, are late Senonian according to pelagic fauna described in samples (Santonian-early Maastrichtian) and early Maastrichtian in andesitic volcanics (Herece et al., 1992).

Another subduction has occurred along the southern edge of the Keban platform and Baskil arc magmatics cutting the platform have formed. Baskil magmatics, which outcrop in 25 km NW outside the map area, are represented by depth, vein and surface rocks (Asutay, 1988). Magmatics show development with plutonic rocks compound, which is represented by gabbros in early stages of the magmatism, and with monzodiorite, quartz monzodiorite, quartz diorite, tonalite, granodiorite, quartz monzodiorite, quartz monzonite compound in latter stages (Yazgan and Asutay, 1981). Basic and acidic vein rocks, which frequently cut granitoids and syenite porphyries, are significant compounds of the Baskil magmatics. Baskil magmatics end generally with andesitic, basaltic volcanic rocks represented by lava flow, pillow lava and tuffs. They are Santonian-Campanian (85-76 my) according to radiometric dating (Yazgan and Chessex, 1991) and they are the lateral equivalences of 85 my Elazığ magmatic with these characteristics (Yu-Chin et al., 2015).

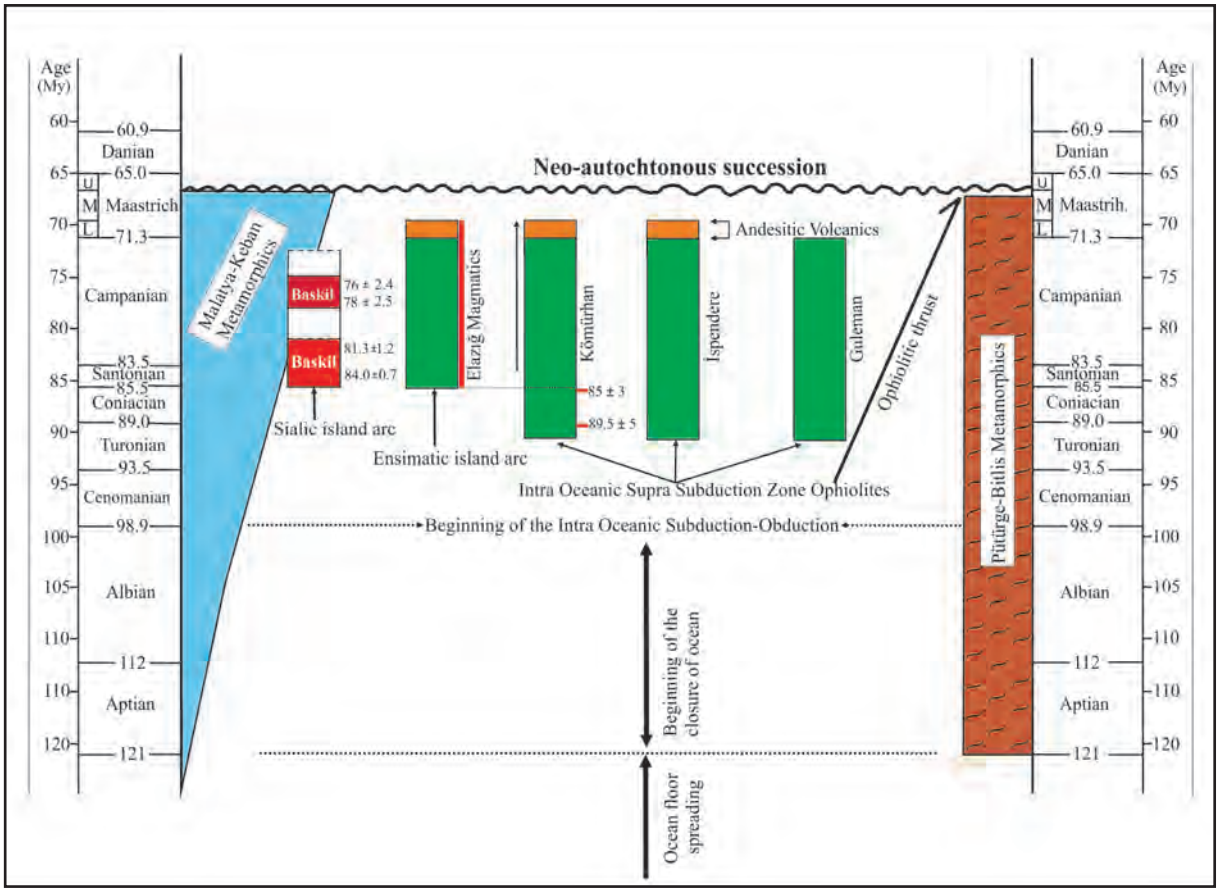

Figure 50- Relationships of the ophiolitic rocks outcropping in Elazığ and the vicinity of Pertek with basement rocks and dating within units (Yazgan and Chessex, 1991; Herece et al., 1992; Robertson et al., 2007).

Baskil magmatics are 75 my and 86 my according to isotopic age determination by K/Ar method. These calc-alkaline magmatics, which are defined as I type granitoid, cut Keban platform and affect them as the contact metamorphism (Asutay, 1988). The contact metamorphic zone is represented by easily breaking, sugar textured marbles. In contacts of marbles, which are formed by calcite and dolomite, especially with magmatic rocks the mineral assemblages reflecting the conditions of pyroxene-hornfels facies metamorphism such as; olivine, garnet, spinal and magnetite were encountered (Asutay, 1988).

Elazığ and Baskil magmatics are similar in age and rock type, and they are the lateral equivalences of each other. Baskil arc magmatics were formed in Coniacian-Santonian-Campanian, the ophiolite obduction in Campanian, and the arc-continent collision in late Campanian-early Maastrichtian (Yazgan and Chessex, 1991) and the last emplacement of ophiolites occurred in middle Maastrichtian. All basement units in the region are unconformably overlain by late Maastrichtian Harami formation. The stratigraphical relationships between the basement units and Paleogene deposits indicate that the final collision ended in the middle Maastrichtian.

On the other hand, the location and the time of the subduction zone during the closure of the ocean is still in debate. In preliminary suggested models, it was asserted that supra subduction zone ophiolites had occurred by the northern intra-oceanic subduction and Baskil granitoid had been formed by the extension of the subduction beneath the Keban platform (Hall, 1976; Aktaş and Robertson, 1984, 1990; Yılmaz et al., 1993; Robertson, 2000). In two subductional models, one of the subduction submerges beneath the Keban platform and forms Baskil magmatics, and the another subduction has occurred within the ocean and formed supra subduction zone ophiolites (İspendere, Guleman, Kömürhan) (Robertson, 2000). A third model is suggested as multi staged subduction (Robertson et al., 2007; Parlak et al., 2009). Another problem to be solved is the beginning period of the

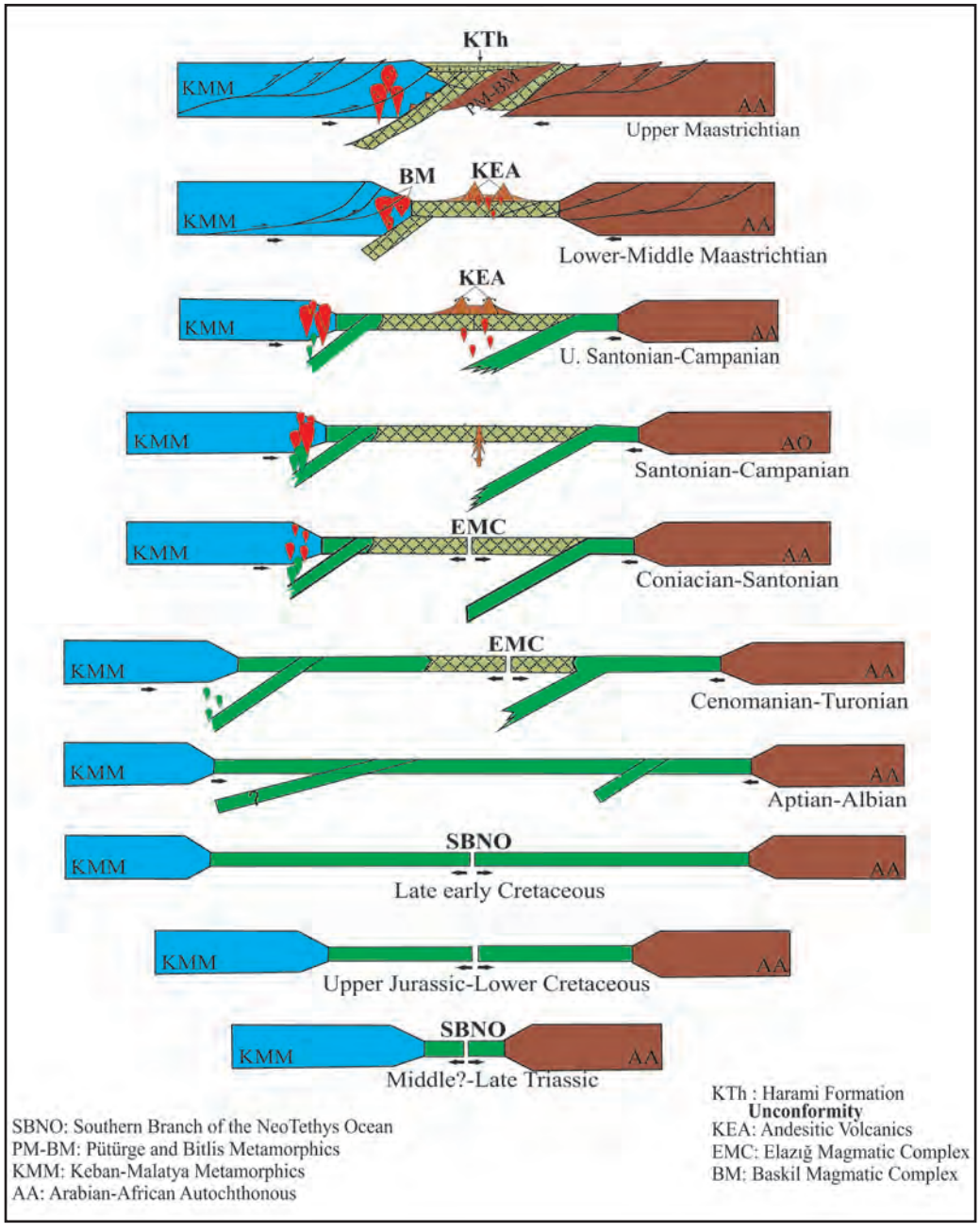

Figure 51- Hypothetically geological evolution model of basement models from Middle?-Late Triassic to late Maastrichtian (modified from Yazgan and Chessex, 1991; Bingöl and Beyarslan, 1996; Herece, 2008).

subduction and the formation ages of the supra subduction zone ophiolites.

Late Cretaceous-Paleogene marine deposits in the region were mapped and defined for the first time. Faunal assemblages collected from field were described based on species. Late Cretaceous-Paleogene deposits begin with late Maastrichtian-Selandian Harami formation. The unit, which begins with the deposition of basal conglomerate, is the first neo-autochtonous deposit unconformably overlying the Elazığ magmatics in post collision at the same time. The depositional conditions in the Harami formation ended with the regional uplift in Late Paleocene-Lower Eocene. Due to decreasing or diminishing in the regional compression affecting in the region, the Seske formation was deposited. Seske formation, which has not widespread exposure, was defined in the region for the first time and it is late Kuvizian- early middle Lutetian.

The nomenclature of formations and their ages carried out in previous studies and its close vicinity are given in Figure 52.

The effective tectonism in the region occurred in middle-upper Lutetian. In this time, the depositional conditions in Seske formation finished by regional uplifts, and the basin forming conditions of the Kırkgeçit formation, which had been deposited in the early Bartonian, occurred. Very thick and widespread deposits occurred in the Kırkgeçit formation in Early Bartonian-early Chattian. In mid Chattian, the Kırkgeçit formation was folded and outcropped at another deformation affecting in the region. This deformation phase terminated at the beginning of Upper Chattian, and the late Chattian-Burdigalian Alibonca formation was deposited. Typical deposits of this marine environment are reefal limestones and clayey limestones laterally transitional with them. In the deformation period, which was active in Middle-Upper Miocene, the depositional conditions of the formation finished. The extensive volcanism, which started at the end of Upper Miocene-Lower Pliocene, caused the development of andesitic at the beginning and pyroclastics that are transitional with lacustrine deposits and the basaltic volcanism.

In the last deformation period affected in the region, the Pertek fault formed in Late Pliocene was mapped. It was detected that the fault zone had been active and the offset values developed along the zone were given.

Acknowledgement

We would like to thank to Dr. Aynur Hakyemez, for the description of planktonic foraminifers in Oligocene- Miocene sediments in paleontological

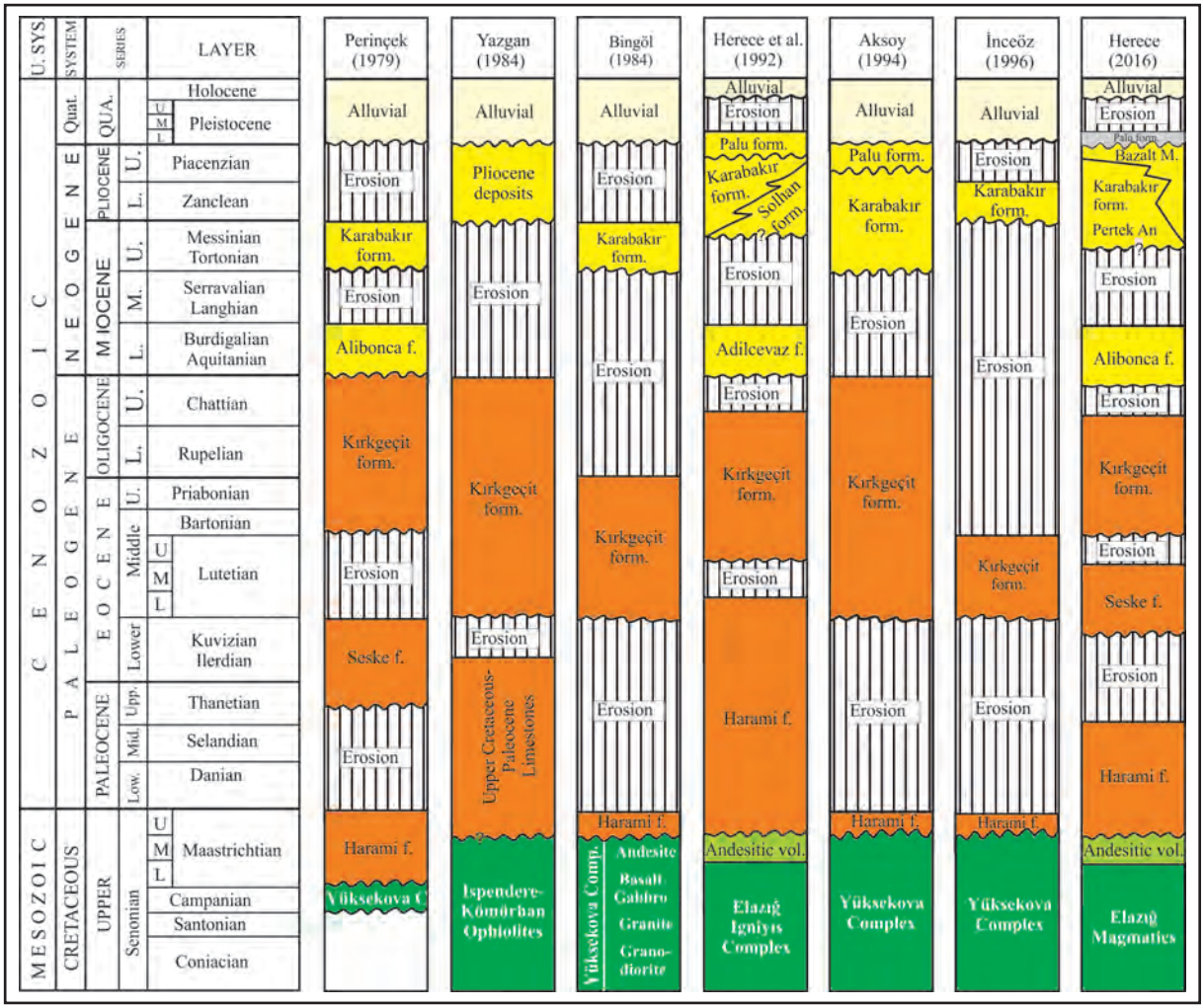

Figure 52- The nomenclature of formations made in the study area and its surrounding and their age correlations (Herece, 2016).

samples collected from the area; to Dr. Fatma Gedik, for the description of benthic foraminifers; to Ayşegül Aydın (M.Sc.), for the description of nannoplanktons; to Dr. Ayla Hanedan Nar, for petrographical descriptions of ophiolitic-magmatic rocks; and to Yelda Ilgar (M.Sc.) and Esra Esirtgen (M.Sc.) for their invaluable contributions in the study.

Besides; we are thankful to Prof. A. Fevzi Bingöl and Prof. Ercan Aksoy for their contributions and criticisms in this article.

References

Akay, E., Erkan, E., Ünay, E. 1989. Muş Tersiyer havzasının stratigrafisi, *Bulletin of Mineral Research and Exploration*, 109, 59-76.

Aksoy, E. 1994. Pertek (Tunceli) çevresinin jeolojik özellikleri, *F.Ü. Fen ve Müh. Bilimleri Dergisi*, 6(2), 1-18.

Aksoy, E., Türkmen, İ., Turan, M., Meriç, E. 1999. Harami Formasyonu'nun (Üst Kampaniyen-Maastrihtiyen) stratigrafik konumu ve çökel ortamıyla ilgili yeni bulgular, Elazığ güneyi, *TPJD Bulletin*, 11(1), 1-15.

Aktaş, G., Robertson, A.H.F. 1984. The Maden Complex, SE Turkey: evolution of a Neotethyan continental margin. In: Dixon, J.E., Robertson, A.H.F. (eds). The Geological Evolution of the Eastern Mediterranean. *Geol. Soc. London, Spec. Publ*., 17, 375-402.

Aktaş, G., Robertson, A.H.F. 1990. Tectonic evolution of the Tethys suture zone in SE Turkey: evidence from the petrology and geochemistry of Late Cretaceous and Middle Eocene extrusive, In Ophiolites oceanic crustal analogues, (Edited by Moores, E.M., Panayiotou, A and Xenophontos), Proceeding of the International Symposium "Troodos 1987", Nicosia, Cyprus, *Cyprus Geological Survey Department*, 311-328.

Asutay, H.J. 1988. Baskil (Elazığ) çevresinin jeolojisi ve Baskil magmatitlerinin petrolojisi, *Bulletin of Mineral Research and Exploration*, 107.

Arger, J., Mitchell, J., Westaway, R. 2000. Neogene and Quaternary volcanism of South-Eastern Turkey, Bozkurt, E.. Winchester, J.A. Piper, J.D.A. (Eds), Tectonics and Magmatism of Turkey and Surrounding Area, *Geological Society of London, Special Publications*, 173, 459-487.

Avşar, N. 1991. Elazığ Bölgesinde *Nummulites fabianii* (Prever) Grubunun (*Nummulites* Ex gr. *fabianii*) varlığı ile ilgili foraminiferler, *Bul.Min.Res.Exp*, 112, 155-160.

Avşar, N. 1996. Inner Platform sediments with Praebullaveolina afyonica Sirel and Acar around Elazığ Region (E. Turkey), *Bulletin of Mineral Research and Exploration.*, 118, 9-14.

Beyarslan, M., Bingöl, A.F. 1996. Kömürhan ofiyolit biriminin petrografik ve petrolojik incelenmesi, *F.Ü. Fen ve Müh. Bilimleri Dergisi*, 8(2), 1-16.

Beyarslan, M., Bingöl, A.F. 2000. Petrology of a supra-subduction zone ophiolite (Elazığ, Turkey), *Canadian Journal Earth Science*, 37, 1411-1423.

Bingöl. A.F. 1984. Geology of the Elazığ Area in the Eastern Taurus Regıon: in the *Geology of the Taurus Belt*; International Symposium Proceedings, O. Tekeli and M.C. Göncüoğlu (eds.), 209-216, MTA, Ankara.

Bingöl, A.F. 1998. Petrographical and petrological features of the intrusive rocks of Yüksekova Complex in the Elazığ region (Eastern Taurus-Turkey), *Journal of Fırat Univ*., 3(2), 1-17.

Demir, T., Seyrek, A., Guillou, H., Scalliet, S., Westaway, R., Bridgland, D. 2009. Preservation by basalt of a staircase of latest Pliocene terraces of the River Murat in Eastern Turkey: Evidence for rapid uplift of the Eastern Anatolian Plateau, *Global and Planetary Change 68*, 254-269.

Demirtaşlı, E.. Pisoni, C. 1965. Ahlat-Adilcevaz bölgesinin jeolojisi (Van gölü kuzeyi), *Bulletin of Mineral Research and Exploration*, 64, 22-23, Ankara.

Erdoğan, B. 1982. Ergani-Maden yöresindeki güneydoğu Anadolu ofiyolit kuşağının jeolojisi ve volkanik kayaları, *TJK Bulletin*., 25(1), 49-60.

Erdoğan, T. 1975. Gölbaşı yöresinin jeolojisi, *TPAO Report*, Archive No, 229, 18.

Hall, R. 1976. Ophiolite emplacement and the evolution of the Taurus suture zone, South-east Turkey, *Geological Society of America Bulletin*, 87, 1078-1088.

Hempton, M.R. 1984. Results of detailed mapping near Lake Hazar, in: O. Tekeli and M.C. Göncüoğlu (eds.), *Geology of the Taurus Belt*; International Symposium Proceedings, 223-228, MTA, Ankara.

Hempton, M.R. 1985. Structural and deformation history of the Bitlis suture near Lake Hazar, Southeast Turkey, *Geol. Soc. of Amer. Bull*., 96, 233-243.

Hempton, M.R., Savcı, G. 1982. Petrological and structural features of the Elazığ Complex: *Bull. Geol. Soc. Turkey*, 25/2, 143-150.

Herece, E. 2008. Atlas of East Anatolian Fault, *General Directorate of Mineral Research and Exploration, Special Publication Series-13*, 359, 13 appendices as separate maps.

Herece, E. 2014. Pertek Fayı, *67. Türkiye Jeoloji Kurultayı*, Abstracts, 648.

Herece, E. 2016. Altınkuşak (Elazığ) ile Pertek (Tunceli) arasındaki alanın Jeolojisi, *Maden Tetkik ve Arama, Derleme Rapor No*. (unpublished).

Herece, E., Akay, E., Küçümen, Ö., Sarıaslan, M. 1992. Elazığ-Sivrice-Palu dolayının jeolojisi, *Maden Tetkik ve Arama Report No. 9634, Ankara* (unpublished).

İnceöz, M. 1996. Elazığ yakın kuzeyinde Harami Formasyonu'nun (Üst Maastrihtiyen) stratigrafisi ve çökelme ortamları, *Bull. of Association of Turkish Petroleum Geologist*, 8(1), 130-136.

Ketin, İ. 1946. Elazığ-Palu ve Pertek yörelerinin jeolojik etüdüne ait rapor, *Maden Tetkik ve Arama, Derleme Rapor No,* 1708, Ankara (unpublished).

Kipman, E. 1976. Keban'ın jeolojisi ve volkanitlerinin petrolojisi, *PhD Thesis, İstanbul University*, İstanbul, Turkey, 91.

Kipman, E. 1981. Keban'ın jeolojisi ve Keban şaryajı, İ.Ü, Yerbilimleri Dergisi, 1(1/2), 75-81, İstanbul.

Naz, H., 1979. Elazığ-Palu dolayının jeolojisi, *TPAO Report*, 1360 (unpublished).

Ozaner, H., Arpat, E., Ergintav, S., Doğru, A., Çakmak, R., Turgut, B., Doğan. U. 2010. Kinematics of the eastern part of the North Anatolian Fault Zone, *Journal of Geodynamics,* 49, 141–150.

Özgül, N. 1976. Torosların bazı temel jeoloji özellikleri, *TJK Bull.*., 19(1), 65-78.

Özgül, N., Turşucu, A. 1984. Stratigraphy of the Mesozoic carbonate sequence of the Munzur Mountain: In: O. Tekeli and M.C. Göncüoğlu (eds.), *Geology of the Taurus Belt*; International Symposium Proceedings, 173-180, Maden Tetkik ve Arama, Ankara.

Parlak, O., Rızaoğlu, T., Bağcı, U., Karaoğlan, F., Höck, V. 2009. Tectonic significance of the geochemistry and petrology of ophiolites in southeast Anatolia, Turkey, *Tectonoophysics*, 473, 173-187.

Pearce, J.A., Bender, JF., De Song, S.E, Kidd, W.S.F., Low, P.F., Şaroğlu, F., Yılmaz, Y., Moorbath, S., Mitchell, J.J. 1990. Genesis of collision volcanism in eastern Anatolia, Turkey, *Journal of Volcanology, Geothermal Res*., 44, 189-229.

Perinçek, D. 1979. The Geology of Hazro-Korudağ-Çüngüş-Maden-Ergani-Hazar-Elazığ-Malatya area: Guide Book, *TJK yayını*, 33.

Poyraz, N. 1988. İspendere-Kömürhan (Malatya) ofiyolitlerinin jeolojisi ve petrografisi: *PhD. Thesis, Gazi Üniversitesi Fen Bilimleri Enstitüsü*, Ankara, 151. (unpublished).

Robertson, A.H.F. 2000. Mesozoic-Tertiary tectonic-sedimentary evolution of a South Tethyan oceanic basin and its margins in southern Turkey, In: Bozkurt, E., Winchester, J.A, Piper, J.D.A. (Eds), Tectonic and magmatism in Turkey and the surrounding area, *Geol., Soc., London, Spec., Pub*., 173, 97-138.

Robertson, A.H.F. 2002. Overview of the genesis and emplacement of Mesozoic ophiolites in the Eastern Mediterranean Tethyan region, *Lithos*, 65, 1-67.

Robertson, A.H.F., Parlak, O., Rızaoğlu, T., Ünlügenç, Ü., İnan, N., Taşlı, K., Ustaömer, T. 2007. Tectonic evolution of the South Tethyan ocean: evidence from the Eastern Taurus Mountain (Elazığ region, SE Turkey), In: Ries, A.C, Butler, R.W.H. and Graham, R.H. (Eds), Deformation of the Continental Crust: The Legacy of Mike Coward, *Geological Society, London, Special Publications*, 272, 231-270.

Sanver, M., 1968. A palaeomagmatic study of Quaternary volcanic rocks from Turkey, *Physics of the Earth and Planetary Interiors 1*, 403-421.

Seyrek, A., Westaway, R., Pringle, M., Yurtmen, S., Demir, T., Rowbotham, G. 2008. Timing of the Quaternary Elazığ volcanism, Eastern Turkey, and its significance for constraining landscape evolution and surface uplift, *Turkish Journal of Earth Science 17*, 497-541.

Soyutürk, N. 1973. Murat baseni jeolojisi ve hidrokarbon imkanları, *TPAO Arama Grubu*, Report No. 791 (unpublished).

Tolun, N. 1955. Elazığ-Keban-Çemişkezek ve Pertek bölgesinin jeolojik etüdü, *Maden Tetkik ve Arama Derleme, Report No*, 2227, Ankara (unpublished).

Turan, M., Aksoy, E., Bingöl, A.F. 1995. Doğu Toroslar'ın jeodinamik evriminin Elazığ civarındaki özellikleri, *Fırat Üniversitesi, Fen ve Mühendislik Bilimleri Dergisi*, 7(2), 177-199.

Turan, M., Bingöl, A.F.1991. Kovancılar-Baskil (Elazığ) arası bölgenin tektonostratigrafik özellikleri, Çukurova Üniversitesi, Ahmet Acar Simpozyumu, Proceedings, 213-227.

Türkecan, A. 1991. Muş yöresindeki Pliyosen yaşlı volkanitlerin petrolojisi, *Bulletin of Mineral Research and Exploration*, 112, 85-102.

Türkmen, İ., İnceöz, M., Aksoy, E., Kaya, M. 2001. Elazığ yöresinin Eosen stratigrafisi ve paleocoğrafyası ile ilgili yeni bulgular, *Yerbilimleri*, 24, 81-95.

Yazgan, E. 1981. Doğu Toroslarda etkin bir Paleo-kıta kenarı etüdü (Üst Kretase-Orta Eosen): *Yerbilimleri*, 7, 83-104.

Yazgan, E. 1983. A geotraverse between the Arabian platform and the Munzur nappes. Int. Symp., On the Geology of the Taurus Belt, *Field Guide Book*, Excursion, Ankara.

Yazgan, E. 1984. Geodynamics Evolution of the Eastern Taurus Region: In: O. Tekeli and M.C. Göncüoğlu (eds.), *Geology of the Taurus Belt*; International Symposıum Proceedings, 199-208, MTA, Ankara.

Yazgan, E., Asutay, H.J. 1981. Definition of structural units located between Arabian platform and Munzur Mountains and their significance in the geodynamic evolution of the area, 35th Congress of the Geological Society of Turkey, abstract, 44-55.

Yazgan, E., Chessex, R., 1991. Geology and Tectonic Evolution of the Southeastern Taurides in the region of Malatya, *Bull. of Assoc. of Turkish Petroleum Geologists*, 3(1), 1-42.

Yılmaz, Y., Şaroğlu, F., Güner, Y. 1987. Initation of the neomagmatism in East Anatolia, *Tectonophysics*, 134, 177-199.

Yılmaz, Y., Yiğitbaş, E., Genç, S.C., 1993. Ophiolitic and metamorphic assemblages of South-East Anatolia and their significance in the geological evolution of the orogenic belt, *Publication of Istanbul Teknik Üniversitesi, Maden Fakültesi*, 12, 1280-1297.

Yu-Chin Lin, Sun-Lin Chung, Bingöl, A.F.,Beyarslan, M., Hao-Yang, Lee, Jin-Hui Yang. 2015. Petrogenesis of Late Cretaceous Elazig Magmatic rocks from SE Turkey: New age and geochemical and Sr-Nd-Hf isotopic constraints, *Goldschmidt 2015*.

Bull. Min. Res. Exp. (2016) 153:45-61

Bulletin of the Mineral Research and Exploration

http://bulletin.mta.gov.tr

TECTONIC DEFORMATIONS IN THE QUATERNARY DEPOSITS OF THE LAKE VAN (EDREMİT BAY), EASTERN ANATOLIA, TURKEY

Selim ÖZALP[a*], B. Serkan AYDEMİR[b], Şeyda OLGUN[a], Barbaros ŞİMŞEK[b], Hasan ELMACI[a], Murat EVREN[b], Ömer EMRE[c], M. Burak AYDIN[b], Oktar KURTULUŞ[b], Füsun ÖCAL[b], Aslı Z. CAN[b], Mehmet N. YANMAZ[d], Ramazan APA[b] and Tamer Y. DUMAN[a]

[a] *General Directorate of Mineral Research and Exploration, Department of Geological Research, 06800 Ankara*
[b] *General Directorate of Mineral Research and Exploration, Department of Marine Research, 06800 Ankara*
[c] *Fugro-Sial Geosciences Consulting and Engineering Ltd., Farabi Sokak No: 40/4, Çankaya/Ankara*
[d] *General Directorate of Mineral Research and Exploration, Istanbul Liaison Office, Beyoğlu / İstanbul*

Research Article

Keywords:
Active Tectonics, Deformation Structures, Seismic Reflection, Lake Van, Eastern Anatolia

ABSTRACT

The 23 October 2011 Van Earthquake (Mw: 7.2) was generated by the Van Fault Zone (VFZ) with reverse fault characteristics. The earthquake on the fault caused surface deformation with 10 cm displacement observed in engineering structures. On land the VFZ has general E-W strike and 28 km length. The western end of the fault is within Lake Van. This study aimed to determine the tectonic structures and evolution in the Quaternary of Edremit Bay using detailed mapping of the VFZ with land and underwater research methods, investigation of its continuation into Lake Van and common assessment of land and underwater data. Continental data showed the presence of E-W fold axes affecting Quaternary units in the hanging-wall and footwall of the VFZ. Offshore studies using shallow seismic profiling (GeoAcoustics) and multibeam bathymetric data acquisition determined that the underwater section of the VFZ had similar characteristics to those on land. Quaternary successions on the lake floor observed on seismic sections clearly showed folds in both blocks of the fault with axes parallel to the strike of the fault. The underwater ridge that is an extension of Çarpanak Cape coincides with the ridge structure on the hanging-wall block of the fault on land. Surface deformation related to the 23 October 2011 earthquake developed in a broad zone of the hanging wall of the VFZ. The research findings show the deformation along the VFZ in the Quaternary is in accordance with the deformations developing during the last earthquake.

Received: 04.12.2015
Accepted: 10.02.2016

1. Introduction

Turkey is located in the Alpine-Himalayan earthquake belt. This area is a result of the continental collision between Arabia and Eurasia along the Bitlis-Zagros Thrust Zone, and presents active tectonic structures related to intracontinental approach in Eastern Anatolia and tectonic escape deformation in Central/Western Anatolia (Figure 1). Eastern Anatolia has been under a N-S directional compressional tectonic regime for nearly 12 million years (Middle-Upper Miocene) (Ketin, 1977; Şengör and Kidd, 1979; Şengör and Yılmaz, 1983; Dewey et al., 1986; Şaroğlu and Yılmaz, 1986; Yılmaz et al., 1987; Koçyiğit et al., 2001). The Van Earthquake (Mw: 7.2), occurred east of Lake Van on 23 October 2011 caused the death of more than 600 people and injured nearly 2000 people (AFAD) in addition to cause severe damage, is the most recent event showing the continuation of this compressional regime in the present day. Studies after the earthquake showed the source of the earthquake was the Van Fault Zone (VFZ) (Emre et al., 2011, 2012, 2013; Özalp et al., 2011; Özkaymak et al., 2011; Doğan and Karakaş, 2013; Koçyiğit, 2013). Although little information about activity of the fault at literature, the remaining area of the VFZ has been stated to be a nearly E-W trending, north-dipping active thrust/reverse fault cutting and deforming Late Pleistocene-Holocene age lake/stream units in previous studies (Özkaymak, 2003; Özkaymak et al., 2004). The earthquake did not produce a clear surface rupture on land, with deformation structures at the surface reflecting the thrust nature of the faulting mechanism and with this deformation affecting nearly 8 to 12 km on land (Emre et al., 2011, 2013; Özalp et al., 2011; Özkaymak et al., 2011; Doğan and Karakaş, 2013; Koçyiğit, 2013). The deformation structures observed on land ended northwest of Bardakçı village

* *Corresponding Author: Selim ÖZALP, selim.ozalp@mta.gov.tr*
http://dx.doi.org/10.19111/bmre.58034

Figure 1- Active tectonic map of Turkey. Lines with filled triangles are active subduction zones, lines with empty triangles are active thrust belts on land, thick lines are strike-slip faults and notched thin lines are normal faults. Large dark arrows indicate direction of motion of lithospheric plates, values show GPS velocity relative to Eurasia (adapted from Okay et al., 2000; GPS velocity values taken from Reilinger et al., 2006).

on the shore of Lake Van and after the main shock the distribution of aftershocks in the region showed that the fault causing the earthquakes may continue toward the west on the floor of Lake Van (Figure 2).

According to earthquake catalogues, it is known that the study area and close surroundings experienced many destructive earthquakes in the historical period (<1900) (Ergin et al., 1967; Soysal et al., 1981; Tan et al., 2008; Ambraseys, 2009). The natural records relating to these earthquakes may be better preserved in unconsolidated or semi-consolidated sediments on the lake floor compared to on land. This study used high resolution shallow seismic marine geophysics and multibeam bathymetric mapping data for the eastern half of Lake Van to discuss and interpret the continuation of the VFZ, source of the 23 October 2011 Van Earthquake, on the lake floor and the deformation structures due to tectonics observed in Edremit Bay.

2. Neotectonic Setting

The world's largest sodic lake, Lake Van, is surrounded by the provinces of Van and Bitlis. In the north and west entirely volcanic in the south metamorphic and east are predominantly outcrops of sedimentary rocks are covered with fields that it is located in a region with many bays and capes. With area of 3,522 km² and volume of 607 km³, the lake circumference is 430 km (Kadıoğlu et al., 1997). At its widest point the distance from Van to Tatvan is 130 km, with a mean water level 1648 m above sea level, mean depth of 171 m and maximum depth of 460 m (Kempe et al., 1991; Kadıoğlu et al., 1997).

Neotectonic regime of Turkey began Middle-Upper Miocene about 12 million years ago as a result of continent-continent collision of the Arabian and Eurasian plates at Eastern Anatolia (Şengör and Kidd, 1979; Şengör, 1980; Şengör and Yılmaz, 1983; Dewey et al., 1986; Şaroğlu and Yılmaz, 1986; Yılmaz et al., 1987; Bozkurt, 2001; Koçyiğit et al., 2001). The right lateral strike-slip North Anatolian Fault (NAF), left lateral strike-slip East Anatolian Fault (EAF) and the active subduction zone formed by the subduction of African oceanic lithosphere under the Aegean Sea along the Hellenic-Cyprus Arc developing after the collision are the neotectonic structures playing major roles in shaping the Anatolian plate and surroundings (Figure 1) (Hempton, 1987; Koçyiğit et al., 2001). After continental collision in Eastern Anatolia the region entered a very active period tectonically

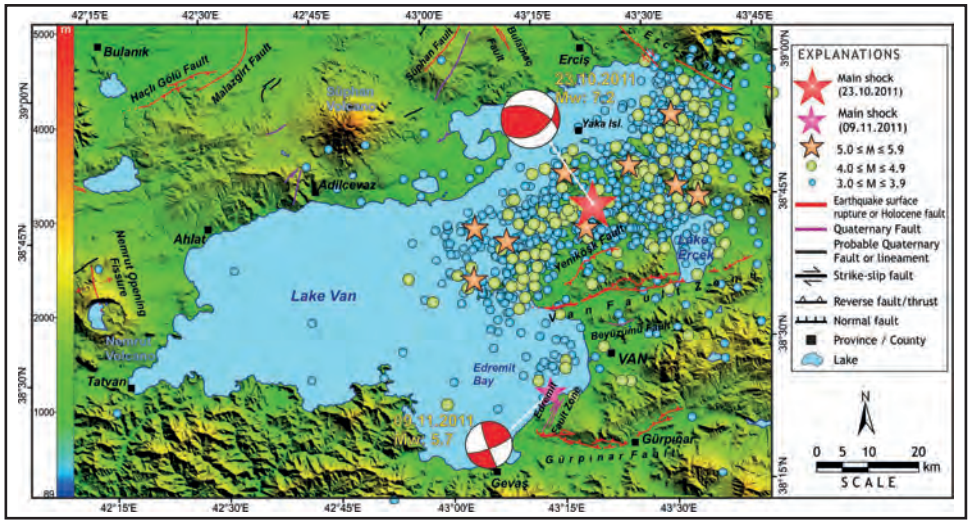

Figure 2- Map showing active faults in Lake Van and surroundings and distribution of main shock and aftershocks of the 23 October 2011 Van and 9 November 2011 Edremit earthquakes. Gürpınar Fault and Edremit Fault zone taken from Özalp et al. (2015); Beyüzümü Fault from Ateş et al. (2007); other active faults from Emre et al. (2013) and seismological data from Kandilli Observatory (KRDAE) records.

with simultaneous volcanic activity began. During the neotectonic period, the result of dominant N-S directed compression was a complicated tectonic structures comprising diagonal NE-SW left lateral and NW-SE right lateral strike slip faults, E-W fold axes, reverse faults and thrusts, N-S oriented normal faults or extensional fractures, were formed in the Eastern Anatolia high plateau (Şaroğlu, 1985; Şaroğlu and Yılmaz, 1986; Şaroğlu et al., 1987, 1992; Bozkurt, 2001; Koçyiğit et al., 2001; Emre et al., 2013). Parallel to the compression direction, the N-S oriented extensional fractures controlled volcanic output. After continent-continent collision, crustal shortening developed in this period and the regional elevation increased (Şaroğlu and Yılmaz, 1986; Yılmaz et al., 1987; Şengör et al., 2003, 2008; Dhont and Chorowicz, 2006; Zor, 2008; Tezel et al., 2013).

One of the most important geological structures formed by continent-continent collision is the Bitlis Zagros Thrust Belt (Şengör, 1979; Şengör and Yılmaz, 1981), extending to the Iranian border (Figure 1). The Lake Van Basin, immediately north of the Bitlis Zagros Thrust Belt, is located east of the Karlıova triple junction where the NAF and EAF intersect (Figure 1). The basin began to form in the Late Pliocene and it is proposed that the effect of volcanism gained its current form at the beginning of the Quaternary (Blumenthal et al., 1964; Wong and Finckh, 1978; Degens et al., 1984). Lake Van contains three important basins called Tatvan, North and Deveboynu, separated by ridges (Cukur et al. 2013, 2014). The deepest of these, the Tatvan Basin, has been determined to contain 600,000 years of lacustrine sediments (Litt et al., 2014; Cukur et al., 2013, 2014). The Deveboynu Basin is smaller than Tatvan with 1.5 km E-W extension and 6 km N-S extension and average water depth of 300 m (Cukur et al. 2013, 2014). The study area placed on a section, nearly 18 km shelf with E-W orientation and nearly 8 km of slope feeding the Deveboynu Basin from the east.

One of the important records of the tectonism playing an effective role in shaping Lake Van Basin is seismites. The term seismite defined for the first time by Seilacher (1969) is generally used for fine gravel, sandy and silty deposits and deformation structures that may form due to earthquakes. These structures develop due to liquefaction of unconsolidated sediments which are important in terms of reflecting the occurrence of ancient earthquakes. Seismites are commonly observed within Quaternary-aged lacustrine sediments outcropping east of Lake Van (Üner et al., 2010), indicating the region has a very active structure in terms of seismicity.

There are many active faults in the Eastern Anatolia regions that are sources of earthquakes. 13 September 1924 Pasinler (Ms: 6.8), 6 September 1975 Lice (Ms: 6.6), 24 November 1976 Çaldıran (Ms: 7.5), and 30 October 1983 Horasan-Narman (Ms 6.9) earthquakes are all large earthquakes which

occurred in the instrumental period, apart from the 2011 Van earthquake. Before the 2011 Van earthquake the number of mapped active faults in the region was so few as to be insignificant (Ketin, 1977; Şaroğlu et al., 1987, 1992; Koçyiğit et al., 2001; Özkaymak, 2003; Özkaymak et al., 2004). However, the focal mechanism results from some moderate earthquakes occured east and southeast of Lake Van in the years between 1988-2003 indicated the presence of almost E-W thrust/reverse faults in this area producing earthquakes (Özkaymak et al., 2004; Üner et al., 2010). The 23 October 2011 Van earthquake (Mw: 7.2) indicated the region is still being formed by the effect of a N-S oriented compressional tectonic regime and is the most recent event proving the presence of the VFZ. After this earthquake many studies were carried out about the active tectonics of the region (Emre et al., 2011, 2012, 2013; Özalp et al., 2011; Özkaymak et al., 2011; Doğan and Karakaş, 2013; Koçyiğit, 2013; Görür et al., 2015). Of the current tectonic structure in the region and surroundings where the 23 October 2011 Van earthquake occurred, the Erciş, Çaldıran, Hasantimur Gölü, Süphan and Malazgirt faults are strike-slip. The Muş thrust forms the northern boundary of the Muş Basin, the western continuation of the Lake Van Basin. The Nemrut extensional fissure, where Nemrut volcanism outcrops, is the best example of extensional structures in Eastern Anatolia (Şaroğlu, 1985; Şaroğlu et al., 1987, 1992).

3. Onshore Features of 23 October 2011 Van Earthquake Surface Rupture

About 10 km north of the Van City, the VFZ extends in a nearly E-W direction on land between Lake Erçek and Lake Van (Figure 2). Fault was firstly named and mapped as an active fault by Emre et al. (2012), the total length of the fault on land is 28 km. The eastern tip of the fault is within Lake Erçek while the western tip is located within Lake Van. Morphologically, the north block of the fault is higher than the south block (Figure 3a). On land a 12 km section extending east from Lake Van is a single fault, while toward the east it bifurcate into two parallel sections 17 km long and 2 km wide (Figure 2 and 3b).

In the east the VFZ is geologically observed within an accretionary prism (Sümengen, 2008) comprised of ophiolitic, metamorphic, volcano-sedimentary, sedimentary and carbonate rocks developed in the age between the Late Permian and Early Miocene. The western segment cuts Early Eocene-Pliocene sedimentary and carbonate rocks (Sümengen, 2008), Quaternary age slope debris, alluvial fans and fluvial deposits and sequences comprised of terrace and delta deposits from Lake Van (Özalp et al., 2015). Morphologically though the fault is defined by broken slope terrain in the field, findings of old surface faulting showing Holocene activity is not clear. Additionally folding observed in Quaternary lacustrine-fluvial deposits, elevated lake terraces and ancient coastal markings are formations in the hanging-wall block documenting the activity of the fault.

The 23 October 2011 Van earthquake (Mw: 7.2) was originated from the E-W oriented VFZ between Lake Van and Lake Erçek nearly 10 km north of the city of Van and at 16 km depth (Figure 2; Emre et al., 2011, 2012, 2013). The earthquake caused nearly 12 km of surface rupture in the western section of the VFZ. The surface ruptures that developed were observed as uncontinuous hairline fractures, causing deformation of asphalt and stabilized roads and concrete water canals perpendicular to the fault (Emre et al., 2011, Özalp et al., 2011; Doğan and Karakaş, 2013). The fault plane solutions of the main shock of 23 October 2011 earthquake, aftershock earthquake distribution and field findings revealed that the source fault had nearly E-W oriented reverse fault/thrust characteristics (Figure 2).

Fault planes preserved within basement units N-NE of the Van Organized Industrial Zone were measured (Table 1) and kinematic analysis was performed. Analysis of fault planes used the method recommended by Marrett and Allmendinger (1990) in FaultKinWin 1.2 [computer program developed for analysis of fault plane data by Almendinger vd. (2001)] and results are presented as fault plane solutions (Figure 3c). Accordingly results obtained from measurements taken for kinematic analysis of the VFZ show that in this section of the zone the fault segment developed under the effect of NW-SE compressional forces and is a dip-slip reverse fault with a very small right lateral strike-slip component.

4. Offshore Studies

4.1. Data Acquisition and Processing

To analyze the continuation of the VFZ on the floor of Lake Van and all details of other tectonic

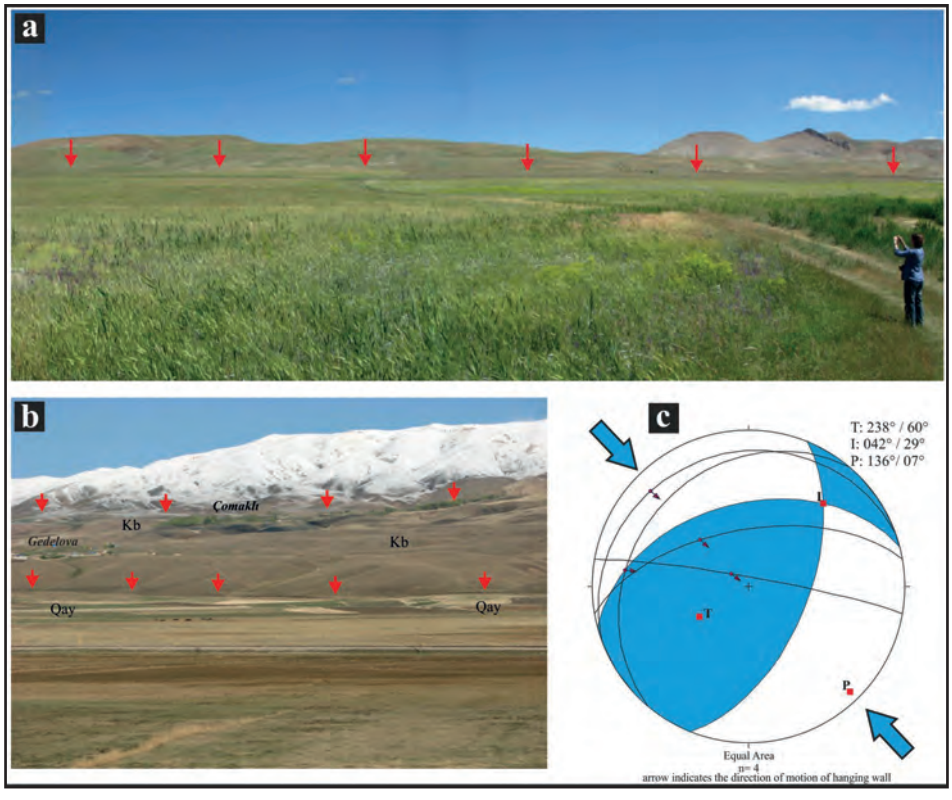

Figure 3- (a) General appearance of VFZ (view N-NW) observed between basement units and ancient alluvial fan sediments (Qey) east of Van Organized Industrial Zone. (b) General appearance of VFZ splitting (view N-NW) between the Bakışık melange (Kb) and alluvial fan sediments (Qay) west of Erçek Lake. (c) Equal-area lower-hemisphere of plane data belonging to the VFZ (P: compression axis; T: extension axis; I: central axis). Fault plane solutions used FaultKinWin (V. 1.2.2, Allmendinger, 2001).

Table 1- Data related to fault planes measured in the field for kinematic interpretations of the VFZ.

No	Longitude E	Latitude N	Strike	Dip Degree and Direction	Rake Angle and Direction	Strike-Dip Value (Right Hand Rule)
1	352835	4272770	N70°E	15°NW	60° West	250/15
2	352800	4273080	N40°E	25°NW	60° West	220/25
3	352517	4272953	N80°W	85°NE	80° West	280/85
4	352500	4272943	N80°E	60°NW	60° West	260/60

deformation structures in Edremit Bay, geophysical studies were completed in the area between Çarpanak Island and Edremit. The gathered data were compared with structures observed on land with the aim of ensuring a holistic view. During the study completed in 2012, high resolution shallow seismic data were gathered along the planned lines with the 14 m Fatih65 boat (Figure 4). The line directions were selected to be perpendicular to the extension of the VFZ on land where it entered the lake at the shore. Due to shallowing of the lake in the eastern section of Edremit Bay, seismic records could not be gathered due to the proximity of the shore. Additional to this study, a multibeam echo sounder was used to determine traces and effects of faults or deformation that may be visible on the floor of the lake and floor morphology was investigated with the gathered data.

During this data acquisition stage, the data were collected by a GeoAcuoustics system consisting of a Boomer energy source, a single channel hydrophone, a receiver with filters, a recorder, and a power supply. The pulse of energy was between 175–280J depending on the depth and the frequency of the pulse

was 200Hz–7 kHz. According to vertical resolution theory at this frequency interval, is about 5-20 cm. The sampling interval was 40 microseconds. During data processing, the mean water velocity (1475-1490 m/s) measured by CTD which was used time to depth. Additionally as it was a single channel system, the basic data processing modules of filtering and gain processing were applied to data. For bathymetry a multibeam echo sounder (Elac SeaBeam 1050D) with 180 kHz transducer was used. During recording, navigation was ensured by using the Hypack program with the aid of GPS.

4.2. Bathymetry and Underwater Morphology

Depth data were collected along seismic lines determined at 2 km intervals and this data was assessed to investigate morphology variations. The map was created by evaluating data, not by the method of multibeam depth measurements of full coverage, that is created not only line data collected with multibeam echo sounder but also previously completed bathymetry maps (Wong and Degens, 1978; SHOD, 1985) were investigated to prepare a map ensuring a general approach to bathymetry in the study area (Figure 4).

To research the continuation on the lake floor of surface deformations observed on land on the fault causing the earthquake, the effects of freshwater and sediment inputs into the lake and wind and currents were evaluated together. The results of this investigation did not encounter clear deformation due to the fault at the resolution of the obtained map on the lake floor morphology similar to on land.

When the map is examined, at the most eastern of Edremit Bay, it is observed that the depths gradually increase westward from the shore. Depth is parallel to the shore first -25 m, then -50 m and continues to increase to -100 m and after reaching depth of -300 m towards the Deveboynu Basin (Figure 4).

4.3. Seismic Stratigraphy

This study was performed by using seismic reflection methods recorded structures observed on the floor of Edremit Bay forming the southeast section of Lake Van and presents significant data for interpretation. This data provides a significant contribution to observations of the effects of forces affecting the region in the neotectonic period on the floor of Lake Van and to research of the western extension of the VFZ on the lake floor.

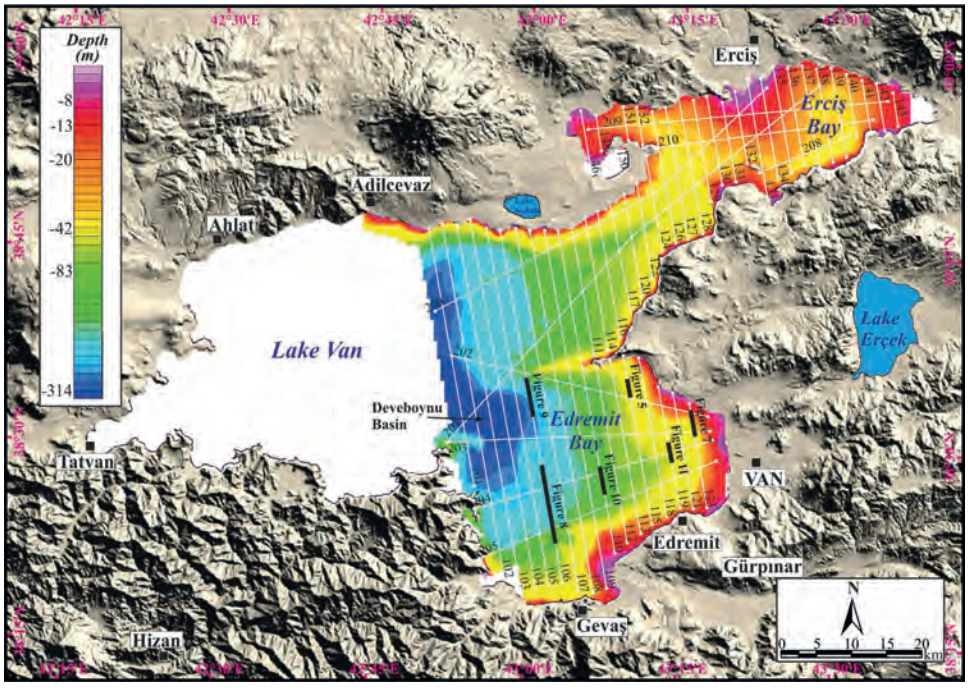

Figure 4- Location of bathymetry and seismic and hydrographic lines in Lake Van. Bathymetry was produced from data collected during this study using a multi-beam depth sounder at line intervals of ~2 km and previous studies.

On seismic lines two main stratigraphic types of reflection data were observed; (1) seismic units with clear or semiclear continuous reflection (Figure 5; seismic units shown with orange and red) and (2) seismic units that are unclear or not continuous (Figure 5; seismic units between the orange and red units). The seismic units in the first group were interpreted as geological lacustrine sedimentary sequences. The seismic units in the second group were assessed as mass flows due to tectonic or volcanic shaking of sediments that found on slightly more inclined surfaces or basement rock units overlain by basin sediments.

4.4. Faults and Other Tectonic Deformations

4.4.1. Van Fault Zone

Line 115 is the most clear profile that VFZ is observed on the lake floor (Figure 4). Along the line the deformation structure with reverse fault/thrust character with fallen southern block along the nearly E-W oriented fault is very clearly observed. When the seismic units presenting clear and continuous reflection affected by the fault are investigated, within the upper young sediments the dip slip amount on the fault has a very small value, while at lower levels in older sediments, the slip amount reaches higher values (Figure 5). This deformation structure in the fault zone is the most important data that showing the fault continuously produced earthquakes from past to present. Additionally along the zone the deformation structures in the current sediments on the footwall and hanging-wall blocks are other important structures showing current activity of the fault (Figure 5). The fold structure related to compressional deformation close to north of the upthrust block of the fault is noteworthy. According to the investigated seismic lines, the VFZ is interpreted to extend along the lake floor toward the west for nearly 9 km (Figure 6).

South of the VFZ the zone of faults striking between E-W and N70°W with observable length from 7-15 km with variable reverse fault/thrust character is noteworthy (Figure 6). Along Line 123 where this fault zone is clearly observed, the reverse fault/thrust faults are clearly seen to cut basement and overlying younger seismic units (Figure 7). Within the thrust belt when placement of seismic units clearly distinguished due to different reflection characteristics are evaluated, it appears that the northern blocks of all faults are elevated. According to seismic data and the tectonic structure of the region, all structures in the fault belt are interpreted as slices belonging to a system thrusting from north to south.

4.4.2. N-S Fault

The structure on seismic sections bounding the east of Deveboynu Basin in the west of Edremit Bay was remarkable. This tectonic structure with nearly NNE-SSW orientation is clearly observed on Line 106 (Figure 8). On the profile representing the area between Gevaş and Sodalı Lake, the structure appears to be a fault zone with length of 10 km (Figure 6) and width of 500 m (Figure 8). Three different seismic units are observed at the North section of the fault zone. The uppermost unit has a semi-prominent non-continuous reflection profile. Below this is a level of seismic units with very clear, continuous and parallel reflections. At the bottom there is a seismic unit with semi-prominent appearance and lacking continuation in all areas. Taking account of the location within the region's tectonic regime, the geometry of the structure and the seismic units it cuts, it was interpreted as a left lateral strike-slip fault zone (Figure 6). Though not clear on seismic profiles, it is considered that this structure may continue for a certain length to the SW.

4.4.3. Çarpanak Ridge

The ridge known as Çarpanak Island at the west of Çitiören village northwest of Van city continues into Lake Van in the form of a cape. Seismic reflection and multibeam bathymetry studies observed that this ridge on land continues toward the west on the lake floor (Figure 6). On seismic sections, the sections including the western extension of the Çarpanak Ridge are observed to contain deformation structures. In the central section of Line 106, in the area south of the Çarpanak Ridge a reverse fault/thrust structure is noted (Figure 9). Interpretation of seismic units (yellow and orange lines) differentiated by reflection characteristics and used as marker horizons found the fault, with a strike-slip component, appears to affect current sediments on the lake floor.

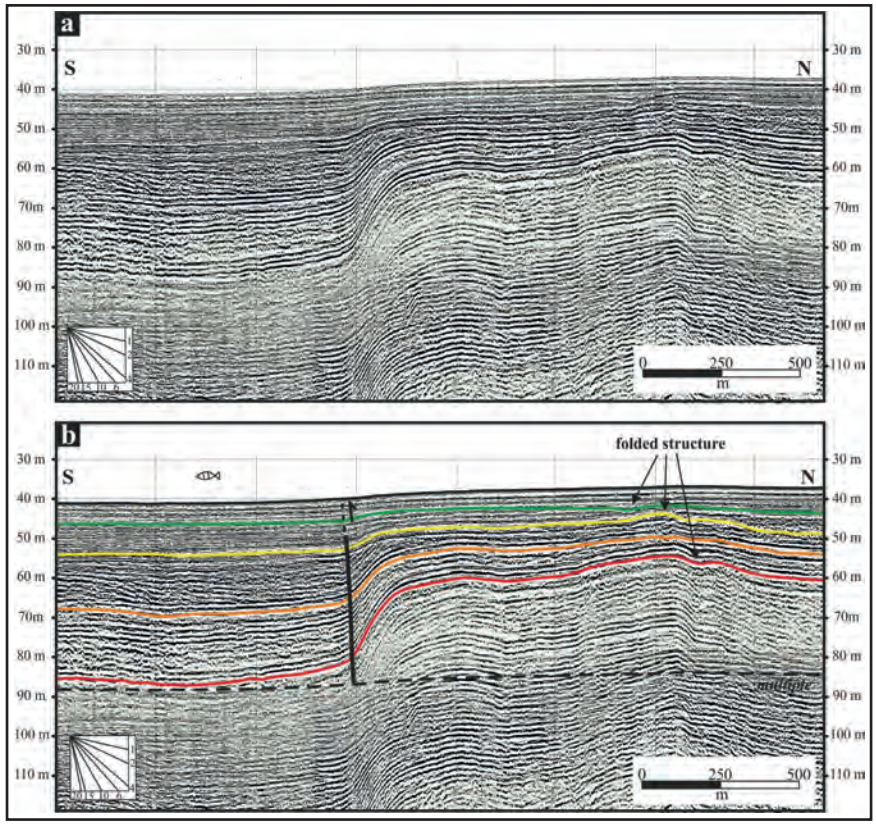

Figure 5- (a) Single channel high resolution shallow seismic system (GeoAcoustics) profile of the north section of Line 115 taken between Çarpanak Cape and Edremit (for profile location see figure 4). (b) Interpretation of the profile. The western extension of the VFZ in this section on the lake floor is shown with a thick black line. Moving to previous periods the slip amount in seismic units shown in different colors cumulatively increased and the development of a fold structure is observed in the hanging-wall.

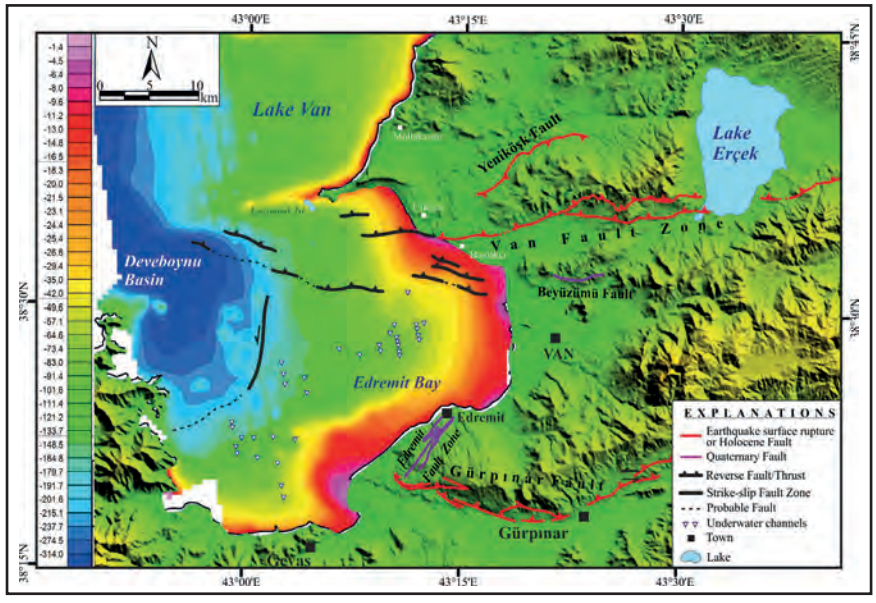

Figure 6- Map showing western continuation of the Van Fault Zone and other structures within Lake Van interpreted from seismic profiles and active faults observed on land. Depth map was produced using multibeam sounder on lines at intervals of 2 km and mapping from previous years. On land the Beyüzümü Fault was taken from Ateş et al. (2007); Van Fault Zone and Yeniköşk Fault from Emre et al. (2013); and Gürpınar Fault and Edremit Fault Zone from Özalp et al. (2015).

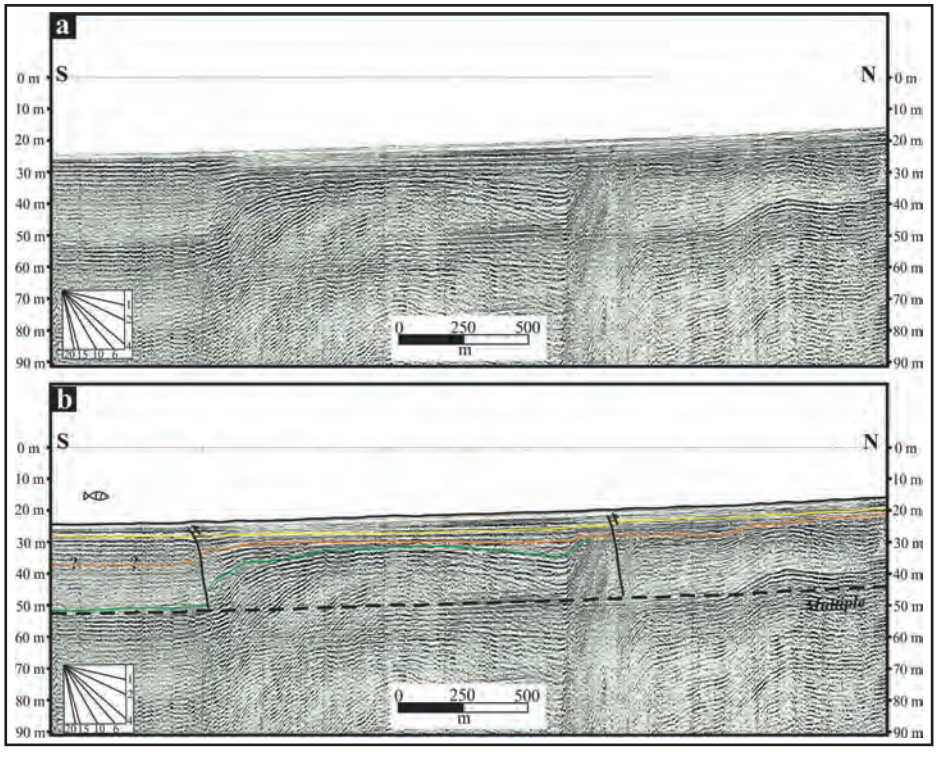

Figure 7- (a) Single channel high resolution shallow seismic system (GeoAcoustics) profile of the north section of Line 123 taken from Bardakçı village to Edremit (for profile location see figure 4). (b) Interpretation of the profile. In this section structures related to the fault zone observed on the lake floor south of the VFZ are shown with thick black lines and the seismic units affected by these structures are shown with colored lines.

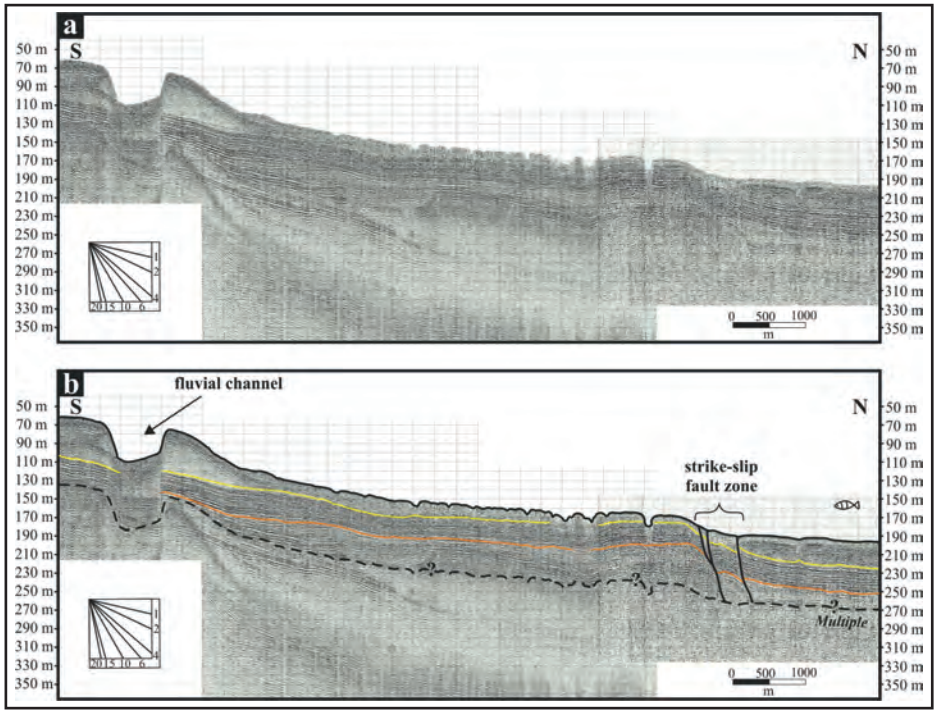

Figure 8- (a) Single channel high resolution shallow seismic system (GeoAcoustics) profile of the south section of Line 106 taken between Gevaş and Sodalı Lake (for profile location see figure 4). (b) Interpretation of the profile. In the south of this section a broad and deep fluvial channel is observed on the lake floor, in the north structures related to a strike-slip fault zone are mapped in thick black lines and the seismic units affected by these structures are shown with colored lines.

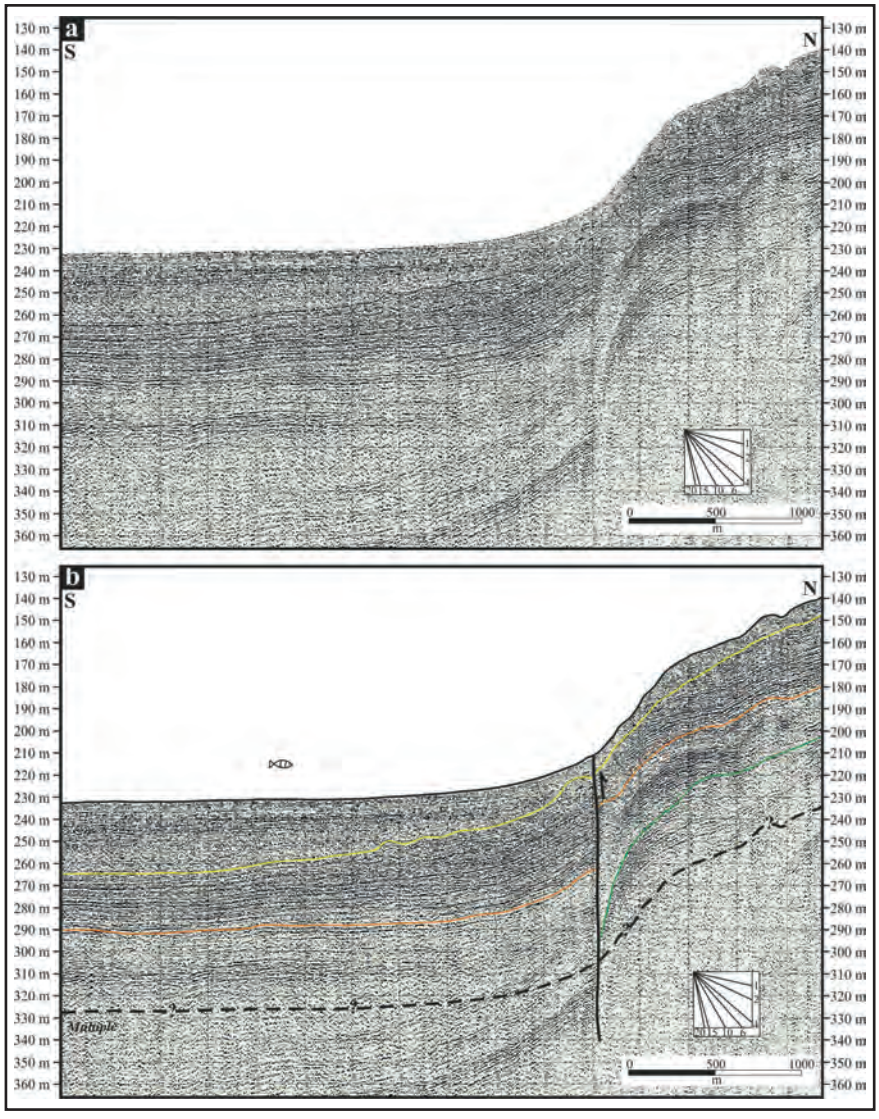

Figure 9- (a) Single channel high resolution shallow seismic system (GeoAcoustics) profile of the west section of Line 106 between Gevaş and Sodalı Lake (for profile location see figure 4). (b) Interpretation of the profile. A reverse fault/thrust immediately south of the Çarpanak Ridge is observed on the lake floor. Within units in the footwall and hanging-wall of the fault folded structures are found to develop linked to the direction of compression.

4.4.4. Paleo-Drainage Channels

On seismic sections there are fluvial channels commonly observed on the shelf. These channels are evaluated as structures that developed due to the shelf being above water until recent times as a result of climatic or tectonic effects. On seismic lines, there are channel structures observed in many different areas of the lake floor (Figure 6). The channels observed on the floor of Edremit Bay on Lines 106 and 110, generally have a U-shaped geometry with depths of nearly 40 m and widths up to 900 m (Figures 8 and 10). Another example of a channel observed on seismic lines are buried sediment-filled channels. The example on Line 119 of a buried fluvial channel defines paleogeographic changes in the lake water level linked to climate. These structures are important to indicate periods when the lake level fell and the shelf became land. On figure 11 the discordance between seismic units distinguished by different reflection characteristics is clearly observed. Above the older seismic units shown with purple and green lines, a V-shaped fluvial channel developed shown with a red line and representing an erosion surface during a period when the lake level fell. After this period, the fluvial channel observed on this section was drowned again and was filled and

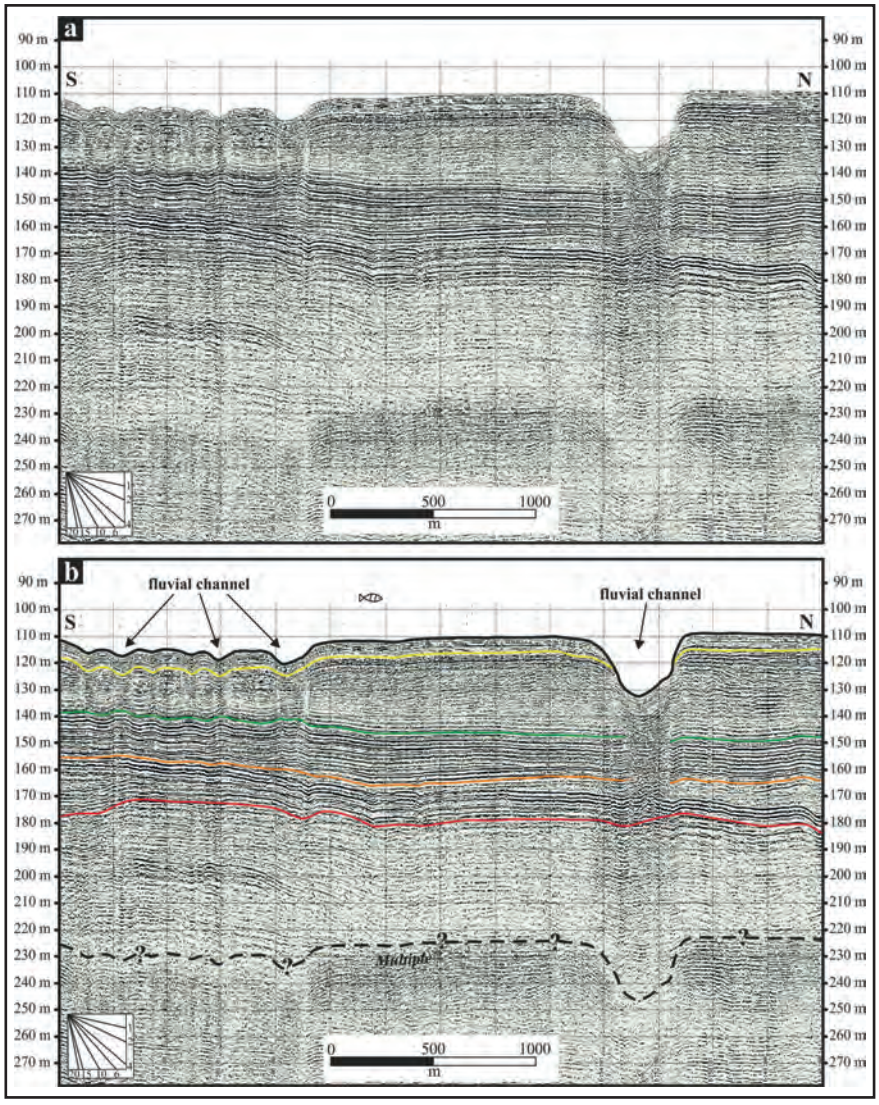

Figure 10- (a) Single channel high resolution shallow seismic system (GeoAcoustics) profile of the south section of Line 110 between Gevaş and Sodalı Lake (for profile location see figure 4). (b) Interpretation of the profile. In this section of slope portions of Edremit Bay, in the very south many fluvial channels are observed. Additionally in deeper areas to observe seismic reflection units more easily they are shown in different colors.

buried by younger sedimentary packets shown with blue and yellow lines.

5. Discussion and Conclusions

The Eastern Anatolian region, containing Lake Van, has been compressed in a N-S direction since the Late Miocene (Şaroğlu and Yılmaz, 1984; Dewey et al., 1986; Bozkurt, 2001; Şengör et al., 2003, 2008; Dhont and Chorowicz, 2006; Elitok and Dolmaz, 2008; Zor, 2008; Tezel et al., 2013). As a result, extensional fractures parallel to the N-S compression direction, E-W fold axes, reverse faults and thrusts and NW-SE oriented right lateral and NE-SW left lateral strike-slip faults have begun to form (Şaroğlu, 1985; Şaroğlu and Yılmaz, 1986; Bozkurt, 2001; Koçyiğit et al., 2001; Özkaymak et al., 2011; Koçyiğit, 2013). One of these structures and the source of the 23 October 2011 Van earthquake is the VFZ, without clear old surface faulting proving activity during the Holocene but with slope breaks in morphology allowing recognition of the fault. This situation may be explained in three ways; (1) the recurrence interval for earthquakes resulting with surface rupture on the fault is very long, (2) previous earthquakes developed similar surface deformations with the last earthquake as described above and (3) the active erosion processes in the region are more rapid than tectonic effects. The 23 October

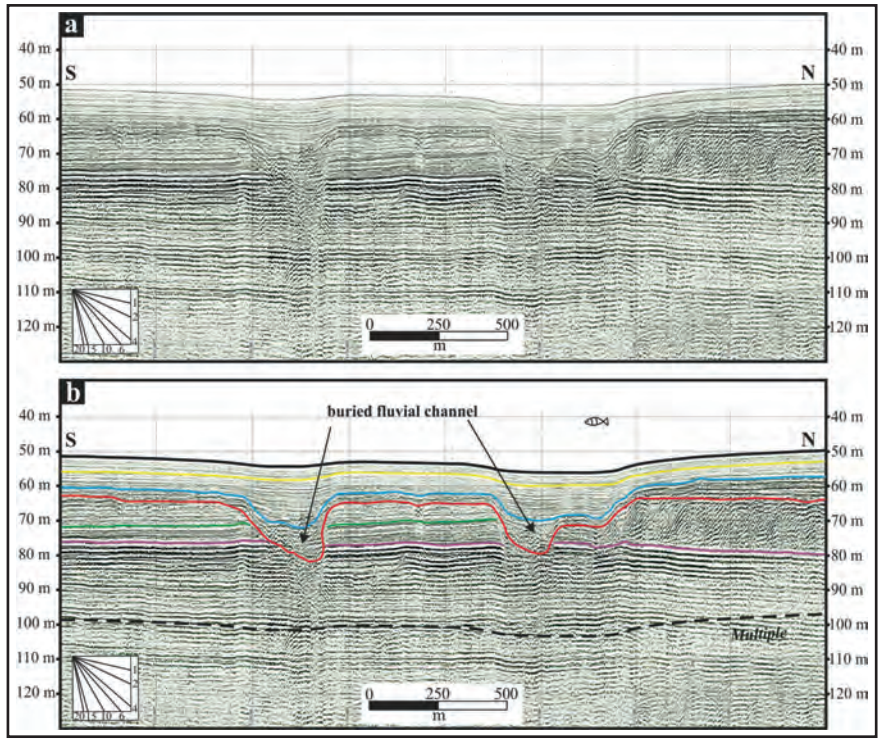

Figure 11- (a) Single channel high resolution shallow seismic system (GeoAcoustics) profile of the central section of Line 119 taken between Edremit and Çitören village (for profile location see figure 4). (b) Interpretation of the profile. In the eastern section of Edremit Bay buried fluvial channels are observed on the lake floor. To observe the structure seismic units are shown in different colors. The V-shaped valley formation in older units is filled with current sediment packets from a later period.

2011 Van earthquake is the most current example proving the presence of N-S compressional tectonic processes affecting Eastern Anatolia, and showing that the earthquake hazard in Eastern Anatolia is at least as high as in other regions of the country. After the earthquake, field studies along the VFZ and shallow seismic profiling studies in Edremit Bay in the lake have mapped structures (Figure 6).

Investigation of seismic data collected from the eastern half of Lake Van observed similar characteristics underwater as on land and mapped these structures on the lake floor. Accordingly, the source fault for the 23 October 2011 Van Earthquake was determined to continue nearly 9 km to the west based on deformation structures observed on the lake floor. However, due to the properties of the systems used no clear findings were obtained related to surface rupture. Additionally in accordance with the tectonic structure of the region, south of the VFZ a zone comprising reverse component faults with nearly E-W orientation and length reaching 15 km was determined. This fault zone mapped by this study (Figure 6) and the reverse fault bounding the north of Deveboynu Basin (Figure 12) interpreted during studies in the west of Lake Van by Cukur et al. (2014) are concordant with each other in terms of strike and mechanism. Another important tectonic structure in the same area is the nearly N-S fault bounding the east of the Deveboynu Basin. This structure, interpreted as a strike-slip fault according to seismic sections and regional tectonic setting, was mapped as an east-dipping normal fault zone by Cukur et al. (2014) (Figures 6 and 12). Apart from these tectonic structures folds in young sediments especially on land are widely observed on seismic lines on the lake floor (Figure 5). These structures mapped in the hanging-wall and footwall of the VFZ have E-W strikes in accordance with reverse fault/ thrust structures developed by N-S compression.

In the western section of Lake Van, studies of the Ahlat Basin have identified the age of the oldest sediment in the lake basin as 600,000 years (Litt et al., 2014; Cukur et al. 2013, 2014). As a result the units over the basement observed within Edremit Bay must be deposited from the Holocene-Middle Pleistocene.

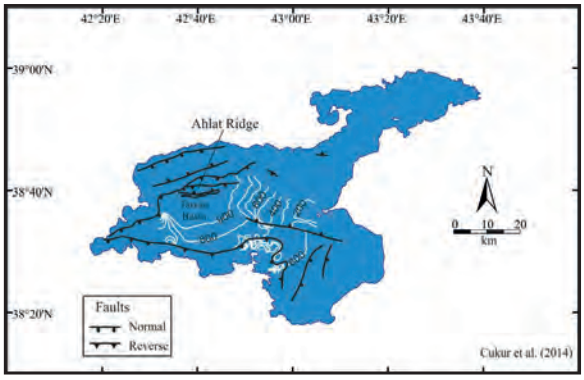

Figure 12- Depth of the upper section of acoustic basement of the southwest of Lake Van. Acoustic basement deepens toward the west. E-W striking reverse faults are observed locally. Acoustic basement was not resolved in the northwest and northeast sections of the lake. Contour interval is 50 m (adapted from Cukur et al., 2014).

Studies completed in the region after the 23 October 2011 Van earthquake observed shoreline changes that may cause in the physical geography of Lake Van (Emre et al., 2011; Özalp et al., 2011). The most important of these was a rise in the shoreline of nearly 40 cm observed near Çarpanak Island closest to the earthquake epicenter. Additionally near Mollakasım village, satellite images clearly observed elevated shorelines from previous periods (Emre et al., 2011). During studies, nearly ENE-WSW striking reverse faults and fold axes affecting Miocene-Late Quaternary sedimentary deposits were observed north and south of the Çarpanak Ridge on land and on the lake floor and active structures cutting Quaternary-Holocene age units were observed on seismic sections of the lake floor (Figure 6). Koçyiğit (2013) mentioned the presence of an active reverse fault with significant left lateral strike-slip component immediately south of the ridgewith ENE strike and 25 km length. This situation is explained by active structures observed on land and on the lake floor south of the Çarpanak Ridge being affected by similar tectonic activity to the latest earthquake during the recent geologic past (Late Quaternary-Holocene).

Important data to show seismic activity in the historical or prehistorical period of a region are seismites. Seismites are structures developing linked to liquefaction of unconsolidated sediments. According to Atkinson (1984), in order for liquefaction to occur, an earthquake must have magnitude (M) of at least 5. However, according to a study by Moretti (2000) investigating the correlation between earthquake source and liquefaction, more than 90% of liquefaction areas are within 40 km of the earthquake epicenter, while the remaining 10% are found at maximum 100 km distance related to large earthquakes. Our studies on land have encountered seismites in the Plio-Quaternary age Büyükçay Formation SE of Andaç village on the Van-Gevaş road (Figure 13) (UTM: 0341721 E, 4244340 N). These structures, while drawing attention to the current tectonic situation of the region, show that earthquakes of M 5.0 or above due to active faults or volcanism have frequently occurred.

Seismic reflection data offer significant clues related to the lake's recent history apart from structural interpretations. On lines in the section forming the study area of the lake, fluvial channels were very clearly observed on the lake floor. While Wong and Degens (1978) and Wong and Finckh (1978) assessed these structures as similar to karst structures, Cukur et al. (2013) interpreted them as braided channel systems forming as a result of erosion

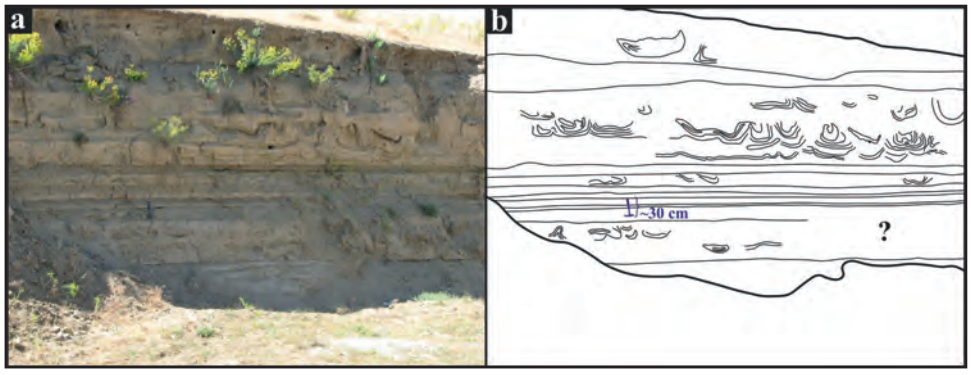

Figure 13- (a) General appearance of seismites (view SW) observed within sandstone, siltstone and conglomerate forming Plio-Quaternary lacustrine and fluvial sediments SE of Andaç village on the Van-Gevaş road in the study area. (b) Interpretative sketch of the photograph.

by sediment-loaded flows within horizontally layered fan sediments based on new seismic data. According to a morphology map created by Cukur et al. (2015) using multi-beam bathymetry data, they proposed these structures are normal channel structures of a drainage system. According to Wong et al. (1978) and Wong and Degens (1978), during the last low level of the lake from 7500 to 4500 years ago erosion was very active and from that time channels were probably preserved and flattened. We observed two different fluvial channels on the lake floor. The first of these developed in parallel to climatic changes in previous times when the water level in the lake fell and then when the lake level rose, was drowned and then filled with young sediments and buried. The other developed on land formed in the period when the lake level last fell, and when the lake level rose remained as fluvial channels without infilling by sediment packets. These structures provide important data in terms of proving the many climatic falls and later rises in lake level in previous times.

According to the results of this study obtained from land and offshore data from Lake Van basin, deformation structures are observed over a very wide area, the region is very active tectonically and active faults have the potential to produce large earthquakes. In terms of regional earthquake risk analysis, in addition to the VFZ, all active faults in the region are significant. As a result it is recommended that fault parameters such as the slip rate and recurrence interval of these active structures be determined by paleoseismology and GPS studies.

Acknowledgements

This study was supported by General Directorate of Mineral Research and Exploration (MTA) (Project Code No: 2012-30-14-02-3). We wish to thank the following reviewers for their valuable assessment and constructive criticism of the manuscript: Prof.Dr. Günay Çifci (Dokuz Eylül University) and Doç.Dr. Çağlar Özkaymak (Afyon Kocatepe University).

References

AFAD, Afet ve Acil Durum Yönetim Başkanlığı internet sitesi; *https://www.afad.gov.tr/*

Allmendinger, R.W., Marrett, R., Cladouhos, T. 2001. FaultKin Version 1.2, Copyrighted Software.

Ambraseys, N. 2009. Earthquakes in the Mediterranean and Middle East, A Multidisciplinary Study of Seismicity up to 1900. *Cambridge University Press*, 946 p.

Ateş, S., Mutlu, G., Özerk, O.C., Çiçek, İ., Karakaya Gülmez, F., Bulut Üstün, A., Karabıyıkoğlu, M., Osmançelebioğlu, R., Özata, A., Aksoy, A. 2007. Van İlinin yerbilim verileri. *Maden Tetkik ve Arama Genel Müdürlüğü*, Rapor No: 10961, 158 s., Ankara (unpublished).

Atkinson, G. 1984. Simple computation of liquefaction probability for seismic hazard applications. *Earthquake Spectra*, 1, 107–123.

Blumenthal, M.M., Van der Kaaden, G., Vlodavetz, V.I. 1964. Catalogue of the active volcanoes of the World including solfatara fields: Part XVII Turkey and the Caucasus. *International Association of Volcanology*, 17, 1-23.

Bozkurt, E. 2001. Neotectonics of Turkey—a synthesis. *Geodinamica Acta*, 14, 3–30.

Cukur, D., Krastel, S., Demirel-Schlüter, F., Demirbağ, E., İmren, C., Niessen, F., Toker, M., PaleoVan-Working Group. 2013. Sedimentary evolution of Lake Van (Eastern Turkey) reconstructed from high-resolution seismic investigations. *International Journal of Earth Sciences (Geologische Rundschau)*, 102(2), 571-585.

Cukur, D., Krastel, S., Schmincke, H-U., Sumita, M., Çağatay, M.N., Meydan, A.F., Damcı, E., Stockhecke, M. 2014. Seismic stratigraphy of Lake Van, eastern Turkey. *Quaternary Science Reviews*, 104, 63-84.

Cukur, D., Krastel, S., Çağatay, M.N., Damcı, E., Meydan, A.F., Kim, S.-P. 2015. Evidence of extensive carbonate mounds and sublacustrine channels in shallow waters of Lake Van, eastern Turkey, based on high-resolution chirp subbottom profiler and multibeam echosounder data. *Geo-Marine Letters*, 35, 329-340.

Degens, E.T., Wong, H.K., Kempe, S., Kurtman, F. 1984. A geological study of Lake Van, Eastern Turkey. *Geologische Rundschau*, 73, 701-734.

Dewey, J.F., Hempton, M.R., Kidd, W.S.F., Şaroğlu, F., Şengör, A.M.C. 1986. Shortening of Continental Lithosphere: The Neotectonics of Eastern Anatolia-A Young Collision Zone. *Geological Society Special Publication*, 19, 3-37.

Dhont, D., Chorowicz, J. 2006. Review of the neotectonics of the Eastern Turkish–Armenian Plateau by geomorphic analysis of digital elevation model imagery. *International Journal of Earth Sciences (Geologische Rundschau)*, 95, 34-49, doi: 10.1007/s00531-005-0020-3

Doğan, B., Karakaş, A. 2013. Geometry of co-seismic surface ruptures and tectonic meaning of the 23 October 2011 Mw 7.1 Van earthquake (East Anatolian Region, Turkey). *Journal of Structural Geology*, 46, 99-114.

Elitok, Ö., Dolmaz, M.N. 2008. Mantle flow-induced crustal thinning in the area between the easternmost part of the Anatolian plate and the Arabian Foreland (E Turkey) deduced from the geological and geophysical data. *Gondwana Research*, 13, 302–318.

Emre, Ö., Duman, T.Y., Özalp, S., Elmacı, H. 2011. 23 Ekim 2011 Van Depremi saha gözlemleri ve kaynak faya ilişkin ön değerlendirmeler. *Maden Tetkik ve Arama Genel Müdürlüğü Jeoloji Etütleri Dairesi*, 20 s., Ankara.

Emre, Ö., Duman, T.Y., Özalp, S., Olgun, Ş., Elmacı, H. 2012. 1:250.000 Ölçekli Türkiye Diri Fay Haritası Serisi, Van (NJ 38-5) Paftası. Seri No: 52, *Maden Tetkik ve Arama Genel Müdürlüğü*, Ankara.

Emre, Ö., Duman, T.Y., Özalp, S., Elmacı, H., Olgun, Ş., Şaroğlu, F. 2013. Açıklamalı Türkiye Diri Fay Haritası. Ölçek 1:1.250.000, VI+89s.+bir pafta, *Maden Tetkik ve Arama Genel Müdürlüğü*, Özel Yayın Serisi-30, Ankara.

Ergin, K., Güçlü, U., Uz, Z. 1967. Türkiye ve civarının deprem kataloğu (MS.11-1964). İTÜ *Maden Fakültesi*, Arz Fiziği Enstitüsü Yayınları No:24, 169 s., İstanbul.

Görür, N., Çağatay, M.N., Zabcı, C., Sakınç, M., Akkök, R., Şile, H., Örçen, S. 2015. Van Gölü'nün Geç Kuvaterner tektono-stratigrafik evrimi. *Maden Tetkik ve Arama Dergisi*, 151, 1-47.

Hempton, M.R. 1987. Constraints on Arabian plate motion and extensional history of the Red sea. *Tectonics*, 6, 687-705.

Kadıoğlu, M., Şen, Z., Batur, E. 1997. The greatest soda-water lake in the world and how it is influenced by climatic change. *Annales Geophysicae*, 15, 1489-1497.

Kempe, S., Kazmierczak, J., Landmann, G., Konuk, T., Reimer, A., Lipp, A. 1991. Largest known microbialites discovered in Lake Van, Turkey. *Nature*, 349, 605-608.

Ketin, İ. 1977. Van Gölü ile İran Sınırı arasındaki bölgede yapılan jeoloji gözlemlerinin sonuçları hakkında kısa bir açıklama. *Türkiye Jeoloji Kurumu Bülteni*, 20, 79-85.

Koçyiğit, A. 2013. New field and seismic data about the intraplate strike-slip deformation in Van region, East Anatolian plateau, E. Turkey. *Journal of Asian Earth Sciences*, 62, 586–605.

Koçyiğit, A., Yılmaz, A., Adamia, S., Kuloshvili, S. 2001. Neotectonics of East Anotolian Plateau Transition From Thrusting to Strike-Slip Faulting. *Geodinamica Acta*, 14, 177-195.

KRDAE: Kandilli Rasathanesi ve Deprem Araştırma Enstitüsü, *http://www.koeri.boun.edu.tr/*

Litt, T., Pickarski, N., Heumann, G., Stockhecke, M., Tzedakis, P.C. 2014. A 600,000 year long continental pollen record from Lake Van, eastern Anatolia (Turkey). *Quaternary Science Reviews*, 104, 30-41.

Marrett, R.A., Allmendinger, R.W. 1990. Kinematic analysis of fault slip data. *Journal of Structural Geology*, 12, 973–986.

Moretti, M. 2000. Soft sediment deformation structures interpreted as seismites in middle-late Pleistocene aeolian deposits (Apulian foreland, southern Italy). *Sedimentary Geology*, 135, 167-179.

Okay, A.İ., Kaşlılar-Özcan, A., İmren, C., Boztepe-Güney, A., Demirbağ, E., Kuşçu, İ. 2000. Active faults and evolving strike-slip basins in the Marmara Sea, northwest Turkey: a multichannel seismic reflection study. *Tectonophysics*, 321, 189-218.

Özalp, S., Zabcı, C., Elmacı, H., Sançar, T. 2011. 23 Ekim 2011 Van ve 09 Kasım 2011 Edremit (Van) Depremleri. *TÜBİTAK Bilim ve Teknik*, Aralık 2011, 529, 16-20, Ankara.

Özalp, S., Aydemir, B.S., Olgun, Ş., Şimşek, B., Elmacı, H., Evren, M., Emre, Ö., Aydın, M.B., Duman, T.Y., Öcal, F., Kurtuluş, O., Yanmaz, M.N., Can, A.Z. ve Apa, R. 2015. Van Gölü Doğu Yarısının Kuvaterner Tektoniği ve 23 Ekim 2011 Van Depremi'nin (Mw: 7,2) Kaynak Fay Özellikleri. *Maden Tetkik ve Arama Genel Müdürlüğü*, Rapor No: 11845, 108 s., Ankara (unpublished).

Özkaymak, Ç. 2003. Van Şehri ve Yakın Çevresinin Aktif Tektonik Özellikleri. Yüksek Lisans Tezi, *Yüzüncü Yıl* Üniversitesi, Fen Bilimleri Enstitüsü, 76 s. (unpublished).

Özkaymak, Ç., Yürür, T., Köse, O. 2004. An example of intercontinental active collisional tectonics in the Eastern Mediterranean region (Van, Eastern Turkey). *Fifth International Symposium on Eastern Mediterranean Geology (5th ISEMG)*, 14-20 Nisan 2004, 153-156, Selanik, Yunanistan.

Özkaymak, Ç., Sözbilir, H., Bozkurt, E., Dirik, K., Topal, T., Alan, H., Çağlan, D. 2011. 23 Ekim 2011 Tabanlı-Van Depreminin Sismik Jeomorfolojisi ve Doğu Anadolu'daki Aktif Tektonik Yapılarla İlişkisi. *Jeoloji Mühendisliği Dergisi*, 35 (2), 175–199.

Reilinger, R., McClusky, S., Vernant, P., Lawrence, S., Ergintav, S., Çakmak, R., Özener, H., Kadirov, F., Guliev, I., Stepanyan, R., Nadariya, M., Hahubia, G., Mahmoud, S., Sakr, K., ArRajehi, A., Paradissis, D., Al-Aydrus, A., Prilepin, M., Guseva, T., Evren, E., Dmitrotsa, A., Filikov, S.V., Gomez, F., Al-Ghazzi, R., Karam, G. 2006. GPS constraints on continental deformation in the Africa-Arabia-Eurasia continental collision zone and implications for the dynamics of plate interactions. *Journal of Geophysical Research*, 111, B05411.

Seilacher, A. 1969. Fault-graded beds interpreted as seismites. *Sedimentology*, 13, 155–159.

SHOD, 1985. 1:150.000 Ölçekli Türkiye, Doğu Anadolu Van Gölü Seyir Haritası. Harita no: 8006, *Seyir, Hidrografi ve Oşinografi Dairesi Başkanlığı*, İstanbul.

Soysal, H., Sipahioğlu, S., Kolçak, D., Altınok, Y. 1981. Türkiye ve Çevresinin Tarihsel Deprem Kataloğu (2100 B.C.–1900 A.D.). *TÜBİTAK Raporu*, No. TBAG-341, 87 s.

Sümengen, M. 2008. 1:100.000 ölçekli Türkiye Jeoloji Haritaları Serisi Van K50 Paftası. No: 65, *Maden Tetkik ve Arama Genel Müdürlüğü*, 16 s., Ankara.

Şaroğlu, F. 1985. Doğu Anadolu'nun neotektonik dönemde jeolojik ve yapısal evrimi. Doktora Tezi, İstanbul Üniversitesi, Fen Bilimleri Enstitüsü, 240 s., İstanbul.

Şaroğlu, F., Yılmaz, Y. 1984. Doğu Anadolu'nun Neotektoniği ve İlgili Mağmatizması. *Türkiye Jeoloji Kurumu*, Ketin Simpozyumu bildiriler kitabı, 142-162.

Şaroğlu, F., Yılmaz, Y. 1986. Doğu Anadolu'da Neotektonik Dönemdeki Jeolojik Evrim ve Havza Modelleri. *Maden Tetkik ve Arama Dergisi*, 107, 73-94, Ankara.

Şaroğlu, F., Emre, Ö., Boray, A. 1987. Türkiye'nin Diri Fayları ve Depremsellikleri. *Maden Tetkik ve Arama Genel Müdürlüğü*, Rapor No:8174, 394 s., Ankara (unpublished).

Şaroğlu, F., Emre, Ö., Kuşçu, İ. 1992. Türkiye Diri Fay Haritası (Ölçek 1:2.000.000). *Maden Tetkik ve Arama Genel Müdürlüğü*, Ankara.

Şengör, A.M.C. 1979. The North Anatolian Transform Fault: Its age, ofset and tectonic significance. *Journal of Geological Society of London*, 136, 269-282.

Şengör, A.M.C. 1980. Türkiye'nin neotektoniğinin esasları. *TJK Yayını*, 40s.

Şengör A.M.C., Kidd W.S.F. 1979. Postcollisional Tectonics of the Turkish Iranian Plateau and a Comparison with Tibet. *Tectonophysics*, 55, 361-376.

Şengör, A.M.C., Yılmaz, Y. 1981. Tethyan evolution of Turkey: a plate tectonic approach. *Tectonophysics*, 75, 181-241.

Şengör, A.M.C., Yılmaz, Y. 1983. Türkiye'de Tetis'in Evrimi: Levha Tektoniği Açısından bir Yaklaşım. *TJK Yerbilimleri* Özel *Dizisi*, No. 1, İstanbul.

Şengör, A.M.C., Özeren, S., Genç, T., Zor, E. 2003. East Anatolian high plateau as a mantle-supported, north-south shortened domal structure. *Geophysical Research Letters*, 30 (24), 8045.

Şengör, A.M.C., Özeren, M.S., Keskin, M., Sakınç, M., Özbakır, A.D., Kayan, İ. 2008. Eastern Turkish high plateau as a small Turkic-type orogen: Implications for post-collisional crust-forming processes in Turkic-type orogens. *Earth-Science Reviews*, 90, 1-48.

Tan, O., Tapırdamaz, M.C., Yörük, A. 2008. The earthquake catalogues for Turkey. *Turkish Journal of Earth Sciences*, 17, 405-418.

Tezel, T., Shibutani, T., Kaypak, B. 2013. Crustal thickness of Turkey determined by receiver function. *Journal of Asian Earth Sciences*, 75, 36–45.

Üner, S., Yeşilova, Ç., Yakupoğlu, T., Üner, T. 2010. Pekişmemiş sedimanlarda depremlerle oluşan deformasyon yapıları (sismitler): Van Gölü Havzası, Doğu Anadolu. *Yerbilimleri*, 31(1), 53-66.

Wong, H.K., Degens, E.T. 1978. The bathymetry of Lake Van; a preliminary report. In: E.T. Degens, F. Kurtman (Eds.), *The Geology of Lake Van*, Maden Tetkik ve Arama Publication No: 169, 6-10, Ankara.

Wong, H.K., Finckh, P. 1978. Shallow structures in Lake Van. In: E.T. Degens, F. Kurtman (Eds.), *The Geology of Lake Van*, Maden Tetkik ve Arama Publication No: 169, 20-28, Ankara.

Wong, H.K., Degens, E.T., Finckh, P. 1978. Structures in modern Lake Van sediments as revealed by 3.5 KHz high resolution profiling. In: E.T. Degens, F. Kurtman (Eds.), *The Geology of Lake Van*, Maden Tetkik ve Arama Publication No: 169, 11-19, Ankara.

Yılmaz Y., Şaroğlu F., Güner Y. 1987. Initiation of the Neomagmatism in East Anatolia. *Tectonophysics*, 134, 177-199.

Zor, E. 2008. Tomographic evidence of slab detachment beneath eastern Turkey and the Caucasus. *Geophysical Journal International*, 175, 1273–1282.

Bull. Min. Res. Exp. (2016) 153:63-90

Bulletin of the Mineral Research and Exploration

http://bulletin.mta.gov.tr

DIAGENETIC HISTORY OF THE ROCK UNITS OF BOZKIR UNIT CONTROLLED BY THE TRIASSIC RIFTING, BOZKIR-KONYA

Hüseyin YALÇIN[a*], Ömer BOZKAYA[b] and Mine TAKÇI[c]

[a]*Cumhuriyet University, Dept. of Geol. Eng., 58140 Sivas, Turkey*
[b]*Pamukkale University, Dept. of Geol. Eng., 20070 Denizli, Turkey*
[c]*Cumhuriyet University, Graduate School of Sciences, 58140 Sivas, Turkey*

Research Article

Keywords:
Taurus Belt, Extensional basin, Phyllosilicate, Mineralogy and Geochemistry

ABSTRACT

The Bozkır Unit representing the northern edge of the Taurus Belt comprises, from bottom to top, three distinct structural entities; the Upper Triassic pre-rift (Korualan Group), the Upper Triassic-Upper Cretaceous syn-rift (Huğlu Group) and the Jurassic-Cretaceous Boyalı Tepe Group as to their structural settings. The Korualan Group is represented by the alternations of carbonate (limestone, dolomitic limestone, dolomite) with radiolarite and chert intercalations and clastic rocks (sandstone, siltstone, mudstone, shale). The Huğlu Group is made up of volcanic (basalt, andesite) and pyroclastic (tuffaceous sandstone) rocks including radiolarite, limestone and clastic rock (sandstone, siltstone, shale) intercalations. The Boyalı Tepe Group is completely made of carbonate rocks. The carbonate-silisiclastic-volcanogenic rocks of the Bozkır Unit contain carbonate (calcite, dolomite), quartz, feldspar (plagioclase, anorthoclase), phyllosilicate (illite, chlorite, mixed-layered illite-chlorite / I-C, chlorite-vermiculite / C-V, chlorite-smectite / C-S, rare smectite), augite, hematite, analcime and heulandite in order of abundance. On the basis of illite Kübler Index data; Korualan and Huğlu Group reflect low grade diagenetic, high grade diagenetic and high grade diagenetic-anchizonal characteristics, respectively. The illite/micas of the pre-rift units and units related to the rifting have muscovitic, and phengitic and seladonitic compositions, respectively. The distributions of chondrite-normalized trace and rare earth element (*REE*) contents in illites present similar trends for Korualan ve Huğlu groups, but the quantities of these elements slightly increase in the Huğlu Group. $\delta^{18}O$–δD isotopic compositions of water forming the illite minerals are different than that of sea water and are found to be between the Eastern Mediterranean Meteoric Water (EMMW) and magmatic water compositions. It also shows that temperature of the water forming illite minerals varies from low to high values. The findings from the rocks of Bozkır Unit suggest that pre- and syn-rift units have different mineralogical-petrographic and geochemical properties. The younger units within the rift due to extension and crustal thinning related to rifting must have been exposed in higher diagenetic conditions by more burial and heat with respect to older units on the edges.

Received: 05.02.2016
Accepted: 29.03.2016

1. Introduction

In diagenetic-low grade metamorphic rocks, the mineralogical parameters such as; the mineral assemblages, illite crystallinity, *b* cell dimension of white K-micas, phyllosilicate polytypes and etc. (Bozkaya and Yalçın, 1996) are extensively used in world literature for the last 30 years at an increasing rate in order to establish the geological evolution of related rocks (Frey, 1987; Liou et al., 1987; Merriman and Frey, 1999; Merriman and Peacor, 1999). The studies, which are about autochthonous and allochthonous units especially in Taurus belt in our country (Bozkaya and Yalçın, 1997*a*, 1997*b*, 1998, 2000, 2004, 2005, 2010; Bozkaya et al., 2002, 2006*a*) provided significant contributions for the interpretation of tectono-stratigraphic units. Besides; the opening/extension related to rifting and the following inversion has significantly influenced the diagenetic/metamorphic evolution of the rocks with detailed mineralogical-petrographic studies carried out successively in Triassic (Antalya Unit) and Eocene (Maden Group) diagenetic/metamorphic deposits in western Taurus and the southeastern Anatolian regions (For example; Bozkaya et al., 2006*b*; Bozkaya and Yalçın, 2010).

The Bozkır Unit, which consists of rock block and slices in different dimensions and appear as mélange deposited between Triassic-Cretaceous time intervals, forms the northernmost unit of the Taurus Belt (Özgül, 1997, Alan et al., 2014). It also comprises sedimentary and volcanic rocks related with the Triassic rifting similar to the Alakırçay Nappe of the Antalya Unit. The Triassic rifting restricting the northern (Bozkır

* *Corresponding Author: Hüseyin YALÇIN yalcin44@gmail.com*
http://dx.doi.org/10.19111/bfmre.266051

Unit) and southern (Antalya Unit) edges of the Taurus Platform is an important geological event in terms of the evolution of the northwest Gondwana and represents the opening of the northern and southern branches of the Neotethys and the beginning of the Alpine cycle (Göncüoğlu, 2010).

In this study, it was aimed at investigating the detailed mineralogical and geochemical characteristics of Triassic-Cretaceous sedimentary and volcanic rocks of the Bozkır Unit in Bozkır-Hadim (Konya) region where the most typical outcrops of the Bozkır Unit are observed. Thus, the establishment of the degree of diagenesis-metamorphism related to rifting will give significant contributions for the interpretation of Lower Mesozoic evolution of the northern edge of the Taurus Belt; and so for the geology of Turkey. In other words; it will be possible to correlate other Taurus units which were previously studied by the authors, with the degree of diagenesis-metamorphism of the Antalya Unit (Alakırçay nappe) by means of findings that will be obtained from the Bozkır Unit.

2. Regional Geology

The Central Taurus carries the explicit characteristics, and it is one of the most significant sections of the Taurus Belt. It has been the subject of many investigations since 1940, and it has been understood that it had consisted of rock unit assemblages, which are tectonically in contact with each other, showing continuity along belt and reflecting different environmental conditions of the region in terms of stratigraphy, metamorphism and structural characteristics (Blumenthal, 1944, 1947, 1951, 1956; Özgül, 1971, 1976, 1984; Brunn et al., 1971; Özgül and Arpat, 1973; Monod, 1977; Gutnic et al., 1979). These assemblages, which are emplaced successively and gain the characteristic of a different tectono-stratigraphic unit as a result of horizontal displacements reaching hundreds of kilometers by means of Senonian and Lutetian movements were named as; Geyik Dağı Unit, Aladağ Unit, Bolkar Dağı Unit by Özgül (1976), Bozkır Unit, Alanya Unit and Antalya Unit (Figure 1).

Among the units, which can be observed both in Eastern and Western Taurus, it is known that the Bozkır Unit located in north and the Antalya Unit located in south consist of deep marine deposits and ophiolites; however, the Bolkar Dağı, Aladağ, Alanya and the Geyik Dağı units mainly comprise shelf type clastic and carbonated rocks, and they are all overlain by allochthonous units of the Geyik Dağı Unit which is relatively autochthonous (Özgül, 1976). Considering the stratigraphic and relative structural settings of the tectono-stratigraphic units of the Central Taurus, it is adopted that; all units formed a single platform a couple of thousand kilometers wide at the end of Cambrian-Early Triassic (Scythian) interval (Özgül, 1997). At the beginning of Anisian; this platform entered the rifting and re-rifting processes at sections corresponding to the Antalya Unit in south and the Bozkır Unit in north of this platform (Antalya Nappes; Marcoux, 1978) (Figure 2). It is also accepted that the northern and southern branches of the Tethys Ocean, which is represented by the Antalya and Bozkır units, were closed in Senonian and accordingly; the Bozkır Unit overlies the Bolkar Dağı and Aladağ units in north, and the Alanya Unit overlies the Antalya Unit in south (Özgül, 1984). It is claimed that "Dipsiz Göl Ophiolitic Complex" consisting of ophiolite, pelagic limestone and divergent turbidites was derived in Late Senonian-Early Tertiary interval between the Geyik Dağı and Aladağ units in north. It is also asserted that an short-lived basin might have developed and as being related with the closure of this basin in Lutetian, the Aladağ and Bolkar Dağı units overlain by the Bozkır Unit moved from north to south and the Antalya Unit overlain by the Alanya Unit moved from south to north to each other and overlaid the Geyik Dağı Unit (Özgül, 1997).

3. Stratigraphy and Lithology

In addition to sedimentary, volcano-sedimentary and volcanic rocks deposited in Triassic-Cretaceous time interval, the Bozkır Unit, which consists of blocks and slices in different sizes of rocks of the much older units (Özgül, 1976), appears as a big mélange and has been the subject to several studies. The outcrops of the unit, which remain at different sections outside the study area on Taurus, are known as; the Western Lycian Nappes (Graciansky, 1967), the Eastern Lycian Nappes around Korkuteli (Brunn et al., 1971), Beyşehir-Hoyran Nappe around Beyşehir-Seydişehir in the Central Taurus (Gutnic et al., 1979), Ophiolitic sequence around Hadim-Bozkır (Özgül, 1971), Schist-Radiolarite formation in Karaman (Konya) region (Blumenthal, 1956), and the nappes consisting of Triassic units in Hadim-Taşkent region are known as; the Bucakışla tectonic slice and Huğlu Group (Alan et al., 2014).

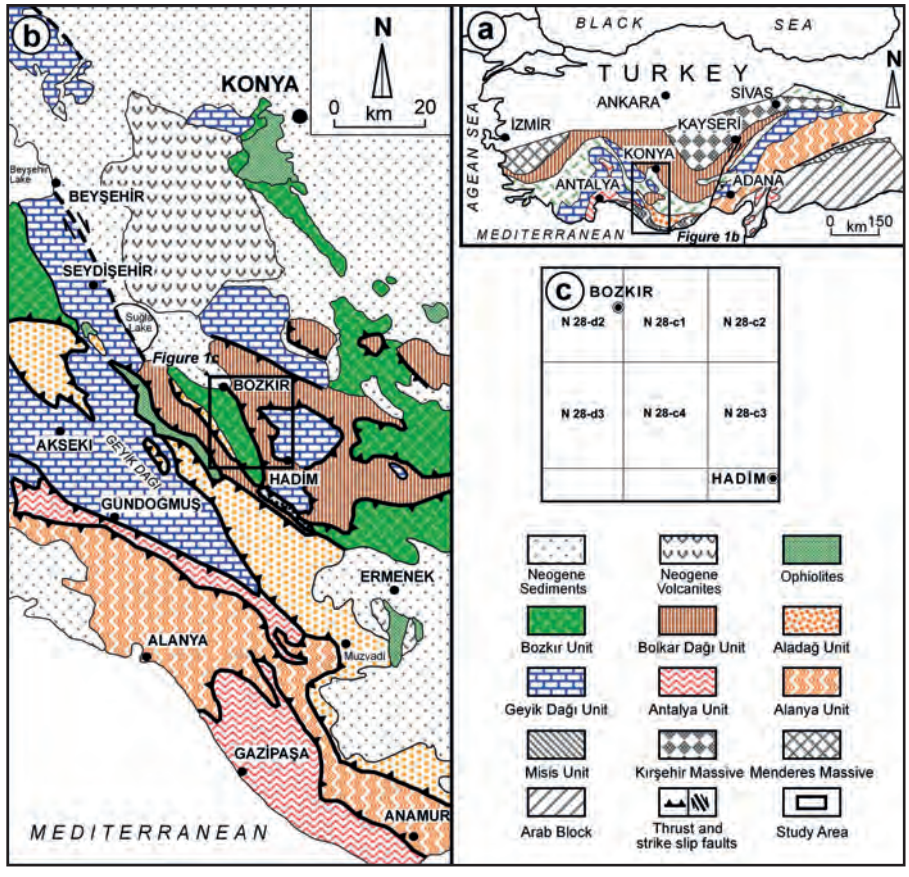

Figure 1- a) Tectonic units of the Southern Anatolia (Göncüoğlu et al., 1997; Özgül, 1976), b) The setting in the Tauride units (Özgül, 1984) outcropped in the Tauride of the study area, c) The distribution of the study area according to the sheets.

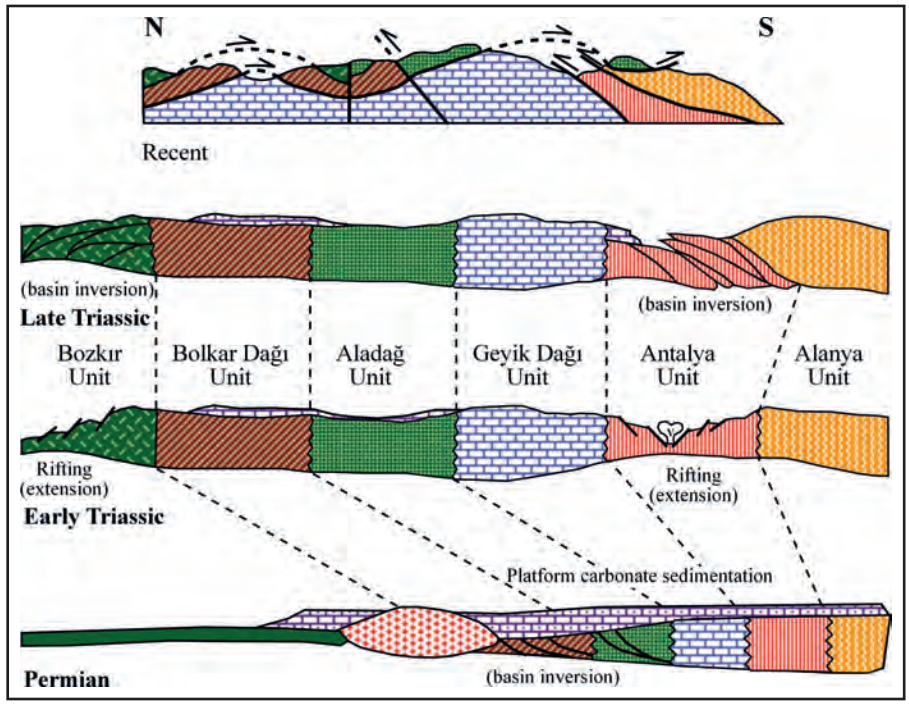

Figure 2- Schematic display of the geological evolution during the Permian-Triassic from Taurus Belt units (arranged from Özgül, 1984).

The outcrops, where units in different age intervals and lithologies in the Central Taurus in which the Bozkır Unit is located, and tectono-stratigraphic relationships were given in figures 3.1a and 3.1b, respectively. Among these; the Bozkır Unit, which consists of the subject of the study, was divided from bottom to top into units as; Upper Triassic Korualan Group (Kayabaşı formation, Başkışla Complex), Upper Triassic-Upper Cretaceous Huğlu Group (Dedemli formation, Mahmut Tepesi Limestone, Kovanlık Complex) and Jurassic-Cretaceous Boyalı Tepe Group (Soğucak Limestone/Kuztepe Limestone, Asar Tepe Limestone) units by Özgül (1997) according to recent structural settings. Besides, in the description of stratigraphic characteristics of the units Özgül (1976), Gutnic and Monod (1970), Monod (1977) and Gökdeniz (1981) have put significant contributions. Although the dominant lithology is limestone in the Mahmut Tepe Limestone among these units, it is more appropriate to name it as the Mahmut Tepe formation as it also consists of shale and siltstone intercalations. The locations of the samples collected from the Bozkır Unit and the details of the relationships between units related with the rift development were given in figure 4 with small scale geological map and field photos.

The Kayabaşı formation of the Korualan Group consists of dolomite, neritic foraminiferal limestone and shallow marine deposits containing reefal limestone, sandstone-shale intercalation with lensoidal reefal limestone at the bottom and nodular, radiolarian pelagic limestones with pelecypod shells and flintstone interlayers at the top. The formation represents the pre-rift carbonate deposition of the Bozkır Unit and has the characteristic of a sedimentary deposit which deepens towards upper layers.

Başkışla Complex is made up of shell traced (radiolarian and pelecypod) pelagic limestone, radiolarite, clastics with debris flow, andesitic blocks and from the mixture of rare green tuffs and fine grained debris flow clastics. The unit reflects the beginning of the rift and gives the image of mixture of blocks in similar characteristics (probably derived from them) with the rock units belonging to the other slices of the Bozkır Unit with dimensions reaching up to hundreds of meters. For example; green tuff and andesitic volcanic rocks, which are partially observed in the complex, show resemblance with the volcanics of the Dedemli formation; the pelagic limestones with radiolarite interlayers with the Mahmut Tepe formation and the neritic limestones resemble to the lower parts of the Boyalı Tepe formation.

The Dedemli formation of the Huğlu Group, which is synchronously or directly related with rifting, begins with the clastic layer consisting of unsorted limestone and pebbly, blocky debris flow accumulations with sandy-clayey groundmass. Then the section which is exclude the rare limestone and clastic intercalations is completely formed by tuff, tuffite, diabase and few andesitic submarine volcanics. Pale-dark green tuff and tuffites reflecting the volcanic products related with opening and/or extension (Andrew and Robertson, 2002) form the dominant rock type of the formation which can easily be recognized on the field.

The Mahmut Tepesi formation is fully formed by the pelagic limestone, which is flintstone interlayered and thin shale intercalated in lower parts, and ends up with red and thin layered micritic level located at the uppermost part. The unit exhibits a view reflecting the basin deepening with syn-sedimentary faults on the Dedemli formation (Figure 4).

The Kovanlık Complex, in addition to mainly pebble and small blocks, consists of radiolarite, pelagic and neritic carbonate (limestone, dolomite), volcanic slices and clastic rock (shale, sandstone) layers with heights reaching hundreds of meters. Spilitic volcanics are in different colors (black, dark brown, dark green) and easily disintegrate and occasionally show amygdaloidal pillow structures partly with zeolite infillings. In basaltic-andesitic volcanics, seldom high grade crystallized, dark red radiolarite and limestone patches are observed.

The Boyalı Tepe Group is composed of cream, dark red-pink, medium-thick layered, partly much fossilliferous neritic limestones with thin flintstone interlayers.

4. Material and Method

Total of 183 mineral and rock samples were collected in the study area. After the samples were washed, they were subjected to thin-section, crushing-pulverization-sieving, clay separation, X-ray diffraction (XRD) and optical microscopy (OM) processes in the Mineralogy-Petrography and Geochemical Research Laboratories (MİPJAL) of the

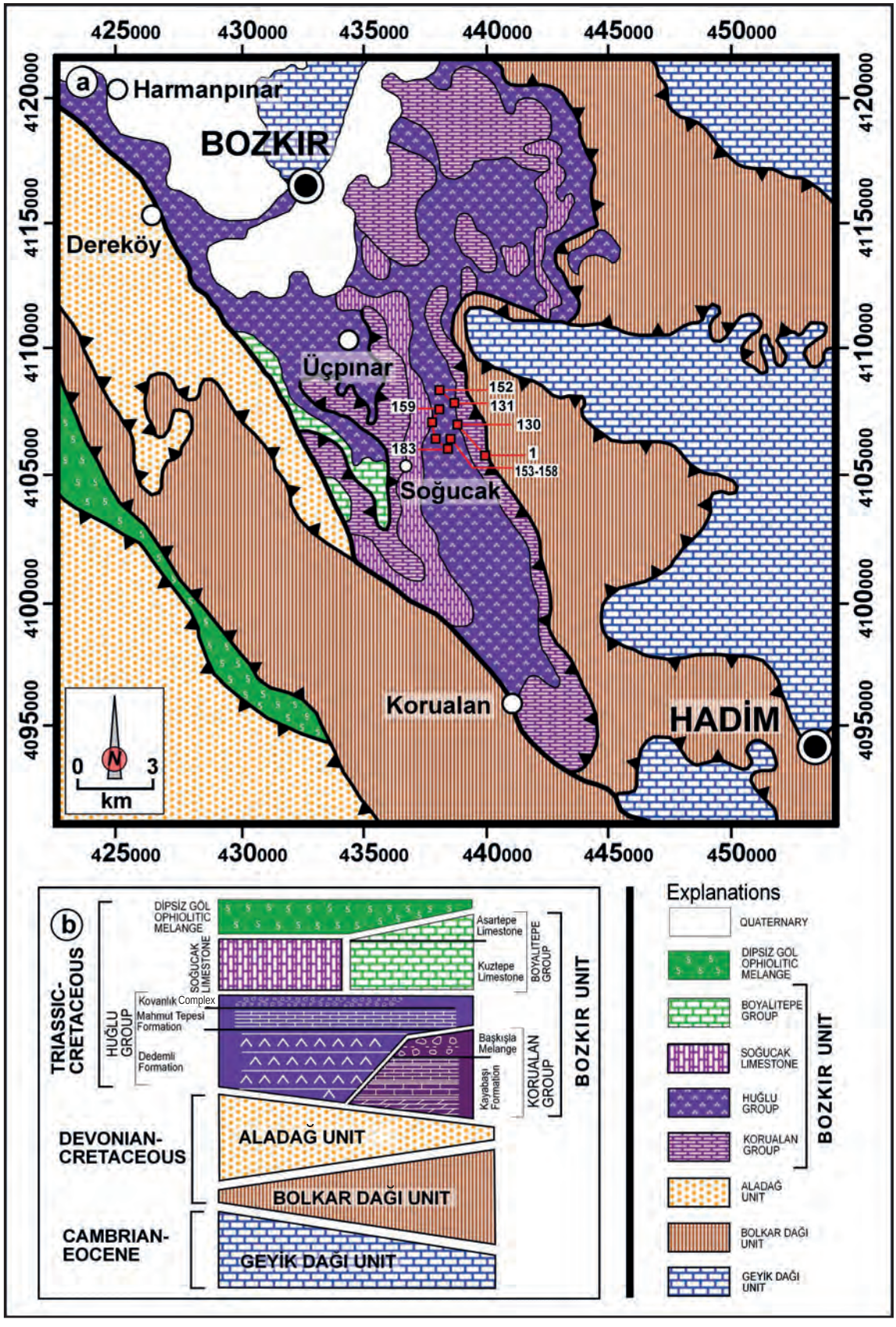

Figure 3- a) Geology map of the study area (adapted from MTA, 2002), b) The relative settings of the Units (arranged from Özgül, 1997).

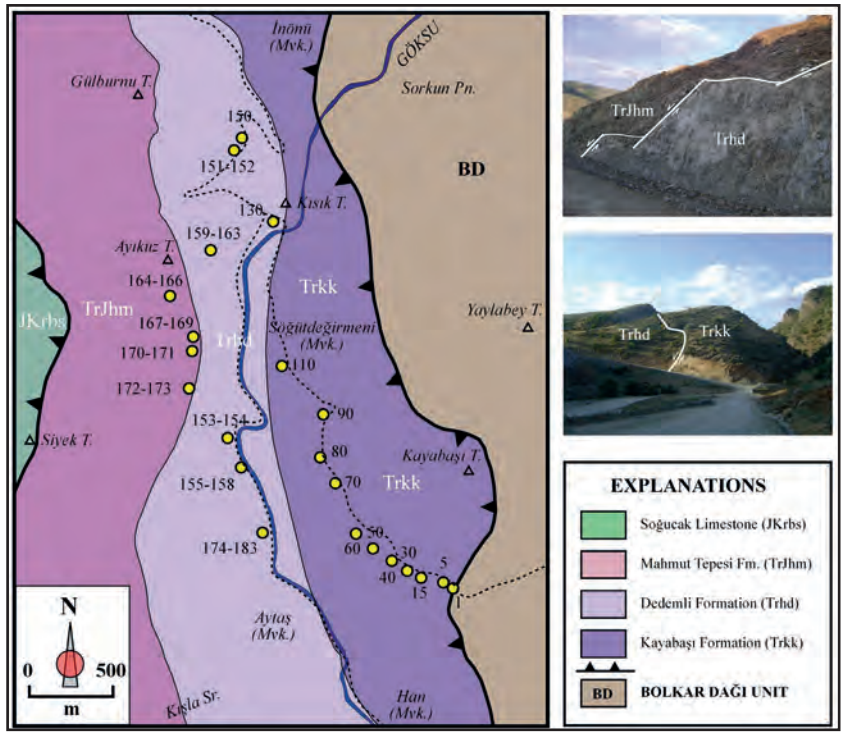

Figure 4- Geology map of the study area in the vicinity of sampling locations and field views showing rifting (arranged from MTA, 2002 and field observations).

Geological Engineering Department of the Cumhuriyet University (C.U.). The scanning electron microscope-secondary electron (SEM-SE), back scattered electron microscope (SEM-BSE) views and the energy dispersion spectrometer (EDS) analyses were carried out in the Laboratories of Scientific Research Center (Centro de Instrumentación Científica) of the Granada University (Universitad de Granada, Spain). For the major element analyses of illites, the trace and rare earth element (REE) analyses and the oxygen-hydrogen isotope geochemistry of illites; inductively coupled plasma spectrometer (ICP), inductively coupled plasma – mass spectrometer (ICP-MS) and the thermal ionization mass spectrometer (TIMS) were used, respectively in the Activation Laboratories Ltd. (Actlabs) in Canada.

The optical microscopy studies were performed by the transmitted light binocular polarized microscope (Nikon). By this method, the compositions and textural characteristics of the rocks were defined and described, and their alteration products were studied.

The XRD method was used in order to determine the whole rock mineralogical compositions (XRD-WR) of the rocks, the clay fraction (XRD-CF) and polymorphic changes in minerals, which are too small in grain size to study under the optical microscope (OM).

The samples used in XRD studies were first crushed by a hammer in 3-5 cm pieces and by the Fritisch brand jaw crusher into grains less than 5 mm, then pulverized by silicon carbide bowl grinder of the same brand for 10-30 minutes considering their hardness's. The dust materials obtained in this way were made ready to analysis after putting into nylon bags and stickered. XRD analyses were performed by DMAX IIIC model X-ray diffractometer of Rigaku (Anode = Cu (CuKα = 1.541871Å), Filter = Ni, Voltage = 35 kV, Current = 15 mA, Goniometer speed = 2°/min., Paper speed = 2cm/min., Time constant = 1 sec, Slits = 1° 0.15 mm 1° 0.30 mm, record interval = 2θ = 5-35°). As a result of XRD analyses, the whole rock and clay size components of the samples were defined (< 2μm) and semi-quantitative percentages were estimated based on the non-standard method (Brindley, 1980). The mineral intensity factors in XRD-WR and CF estimations and the reflections were measured in mm. In this method, the dolomite and kaolinite were taken as reference for the whole rock and clay fraction from the ethylene glycolation

pattern (Yalçın and Bozkaya, 2002). Quartz was used as the internal standard in measuring *d* distances. The description of clay minerals was mainly made according to (00l) basal reflections.

In phyllosilicate/clay bearing rocks, the process of separation of these minerals from the others are basically formed by chemical solution (the removal of non-clay fraction), centrifugation-decantation and leaching, suspension-sedimentation-siphoning-centrifugation and bottling. This process was accelerated by adding Calgon in cases when there had not been any siphoning process. The centrifugation was performed by the centrifuge of the Heraeus Sepatech brand Varifuge 3.2 S model with 5600 rev./min and 200 cc capacity metal codes. From each clay muds, the plastering or three oriented glass slides were prepared in the form of suspension for the ones that have swelled and cracked and then they were dried in room temperature. Clay fraction diffractograms were obtained by untreated-N (air-dried), ethylene glycolated-EG (to leave under ethylene glycol vapor in desiccator for 16 hours under the temperature of 60°C) and heating-F (4 hours heating under the temperature of 490°). During scanning, the goniometer speed and the recording interval were adjusted as 1°/min and 2θ=2-30° (error rate ± 0.04°).

In the polytype determination of pure or nearly pure illite minerals, the distinguishing peaks suggested by Bailey (1980 and 1988) and J.C.P.D.S. (1990) were used. For the detection of polytype, recording interval with 2θ = 16-36° and goniometer speed of 2°/min. were utilized.

Three dimensional morphological view studies were carried out on carbon coated samples which randomly broken into 1cm^3 sizes for SEM-SE analysis. Semi-quantitative EDS analyses were also utilized in minerals descriptions. For two-dimensional texture and mineral chemistry studies, the rock slices were cut and one of their sides were polished, and made ready to analysis coated with carbon. First; the mineral description and textural relationships were examined by BSE on polished sections, then EDS analyses were carried out in suitable points and areas. For EDS analyses; the Oxford INCA system was used and instrumental conditions were adjusted as 20 kV in voltage and with a probe size of 250 pA.

The results of oxygen and hydrogen isotopes have the accuracy of ± 0.2 ‰ and were estimated based on Vienna Standard Mean Ocean Water (V-SMOW). For stable isotope geochemistry and the description of isotopic standards, the processes of analyses were given by Clayton and Mayeda (1963) and by O'Neil (1986) in detail. Details of the analysis method and instrumental detection limits were given on the official web site of the firm (http://www.actlabs.com/).

5. Mineralogy-Petrography

5.1. Optical Microscopic Studies

Among lithologies forming the Korualan Group, the orthochem micritic and sparitic calcite and/or dolomites are seen in carbonate rocks, and the extraclastics are constituted by quartz, feldspar (mainly plagioclase), clay, opaque minerals (mainly hematite) and muscovite in order of abundance. In some samples, the fossil shell fragments and allochem components of radiolarian were encountered. According to Folk (1974); these rocks were defined as micrite, lithomicrite, micrite with quartz, micrite with radiolaira, dolomicrite, oomicrite, microsparite, sparite, sparite with quartz and dolomite, dolomicrosparite, dolosparite with calcite and dolosparite.

Sparites consist of coarse calcite minerals similar to crystallized limestones (Figure 5a). In oolites, the multi concentric oolites with lamellae are observed (Figure 5b). At the center of some oolites, the quartz minerals are encountered. Fossil remnants, radiolarians and fine grained opaque minerals are seen in bonding material.

In pores of the micrites; the euhedral rhombohedral and zone textured calcites (Figure 5c), in pores of the dolosparites; the euhedral rhombohedral dolomites are observed (Figure 5d). Dolosparites occasionally exhibit a gel texture and dolomites are surrounded by opaque minerals (hematite) in places.

The components of the siliciclastic rocks are constituted in order of abundance by monocrystalline and polycrystalline quartz, feldspar (mainly plagioclase), rock fragments (mainly metamorphic), mica minerals (muscovite and biotite), chlorite and opaque minerals (mainly hematite). However, tourmaline and zircon minerals are seldom observed. The bonding material is represented by the clay matrix and carbonate cement (calcite and dolomite). Siliciclastic rocks were

described as sandstone, siltstone, mudstone and shale according to grain size and mineral contents. The sandstones among these were defined according to quartz (Q), feldspar (F), rock fragments (L) and matrix (M) content (for M < % 15 Folk, 1974; for M > % 15 Pettijohn, 1975). These rocks were named as; quartz sandstone, arkose, litharenite and feldspathic litharenite (M<%15) or as lithic greywacke (M>%15) (Figure 5e). The sandstones, from mineralogical and textural points of view, are mainly mature-submature and of some are submature-immature. However, in pores of cherts with calcite and/or dolomite, the gel textured chalcedonic quartz (Figure 5f) is observed.

Volcanic rocks, which constitute one of the most widespread lithologies of the Huğlu Group exhibit three different textures as; hypocrystalline porphyritic, vitrophyric porphyritic and aphanitic-amygdaloidal. The pale colored components in these rocks are formed by plagioclase, and dark colored components are formed by augite, biotite and occasionally by opaque minerals (mainly hematite). The matrix is mainly represented by volcanic glass and plagioclase microlites in occasion. These rocks were described as basalt and andesite according to Streckeisen (1978) classification considering the primary magmatic composition and their textural characteristics.

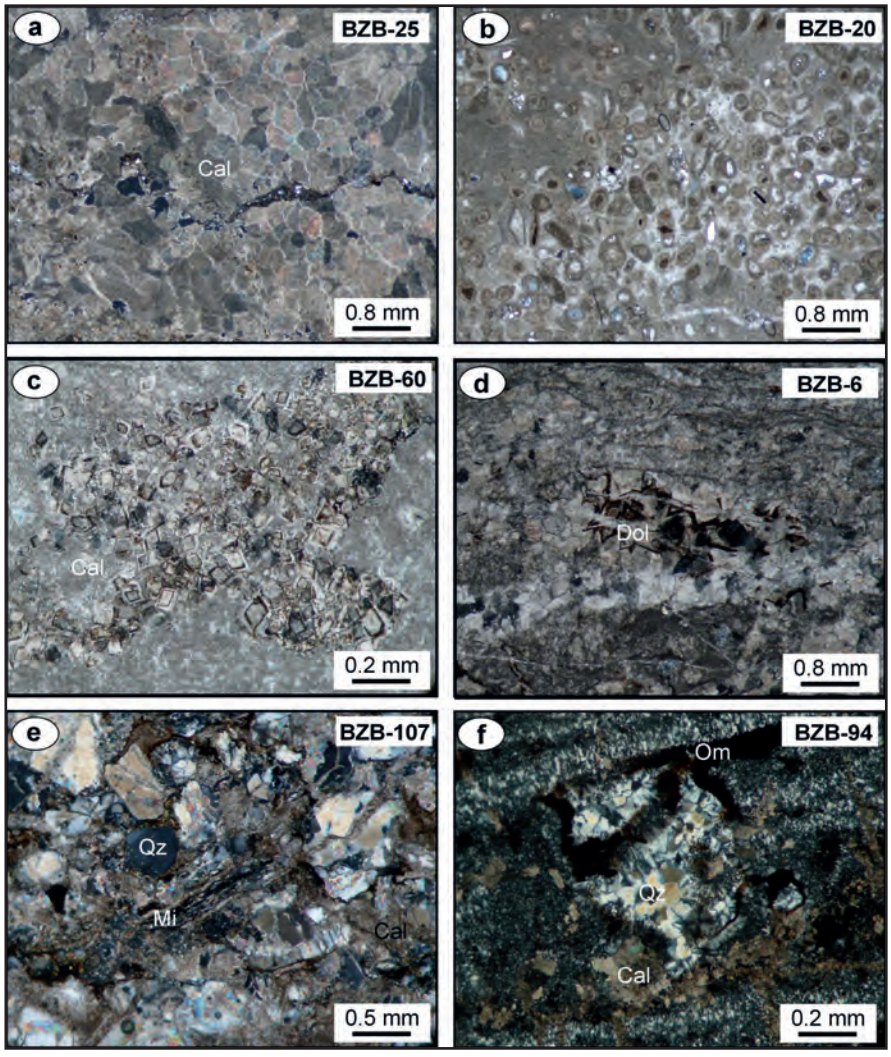

Figure 5- Optical microscopic views of carbonate rocks from the Korualan Group (crossed polarized light; Cal: Calcite, Dol: Dolomite, Qz: Quartz, Mi: Mica, Om: Opaque minerals), a) Sparites including coarse calcite crystals, b) Oomicrites with quartz and fossils, c) Micrites including euhedral, rhombohedral and zoned calcites within the pores, d) Dolosparites including euhedral, rhombohedral and zoned dolomite crystals within the pores and partly gel texture, e) Angular, monocrystalline and polycrystalline quartz within the calcite cement and detrital micas in the quartz sandstones, f) Chalcedonic quartz and gel texture within the pores of coarse-grained dolomitic chert.

In matrix and pores of the rocks, frequently the silicification, argillization and chloritization and partly zeolitization (analcime and heulandite/clinoptilolite) are observed (Figure 6a-b).

Pyroclastic rocks are vitroclastic in texture and contain quartz, plagioclase, opaque minerals and volcanic rock fragments. In bonding material, mainly the silicified and/or chloritized volcanic glass and carbonate minerals are encountered (Figure 6c-d). Pyroclastic rocks were defined as tuffaceous sandstone (tuffite) according to grain size and the ratios of pyroclastic (volcanic glass, pumice, crystal and volcanic rock fragments) / (epiclastic + chemical + organic) components (Schmid, 1981).

In carbonate rocks, also the silicified and/or carbonate textured radiolarian fossils are frequently encountered.

5.2. Electron Microscope Studies

SEM-SE (three dimensional) and SEM-BSE (two dimensional) views on polished surface of the rocks of the Bozkır Unit were given in figures 7 and 8, respectively.

Illite and chlorites are observed among quartz and feldspar grains in the form of flaky and plumy-like groups in shale (BZB-17) and mudstone (BZB-45) lithologies, which possess illite + quartz + calcite + feldspar + chlorite assemblage, of the Korualan Group (Figure 7a-b). Illite and chlorite minerals in authigenic or diagenetic recrystallized origin form the main components of the rock orientation. In the altered volcanic rock sample (BZB-100), which has illite + chlorite + quartz + feldspar + calcite paragenesis in the Huğlu Group, the illites are plumy-like and chlorites are flaky and form a distinctive orientation (Figure 7c). Among the coarse grain components in siltstone sample of the Huğlu Group (BZB-182), the completely authigenic fibrous

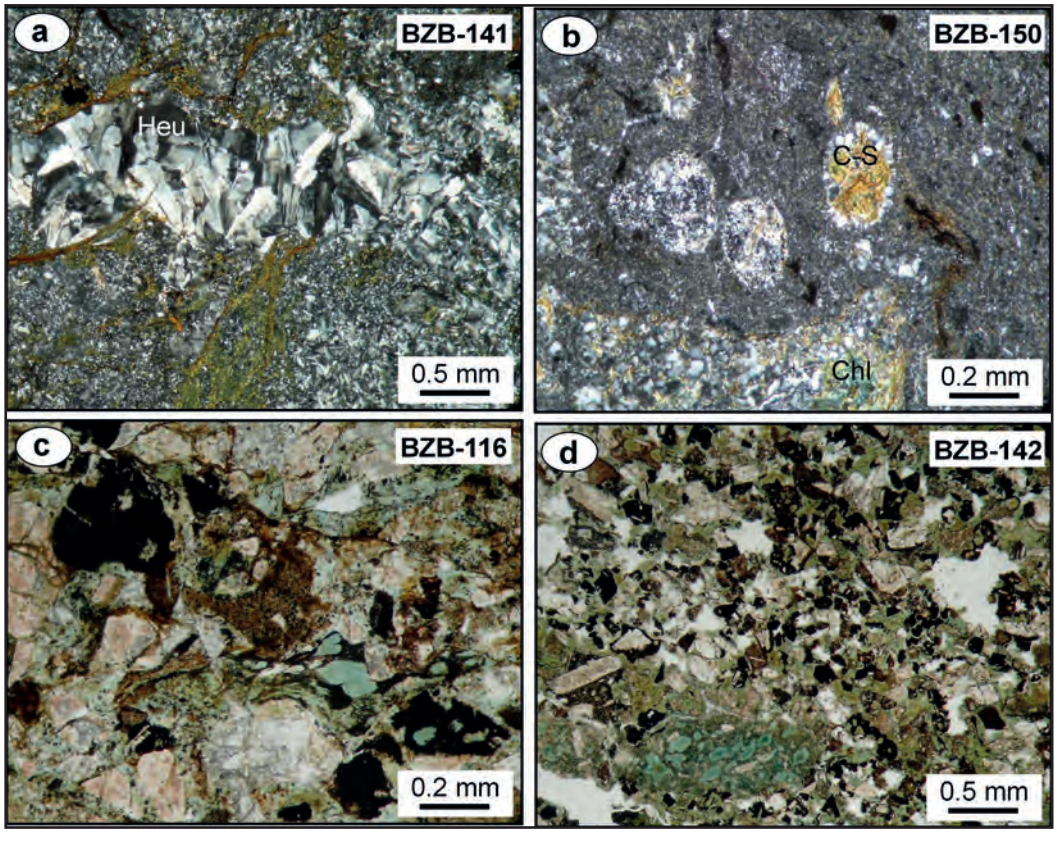

Figure 6- Optical microscopic views of Huğlu Group rocks (a-b: crossed polarized light, c-d: plane polarized light; Heu: Höylandit, Chl: Chlorite, C-S: Mixed-layered chlorite-smectite), a) Heulandites/clinoptilolites within the matrix and/or pores in the altered andesites, b) Chlorite and mixed-layered chlorite-smectite (C-S) within the matrix and/or pores in the altered andesites, c) Chloritization, carbonatization and volcanic rock fragments in the vitroclastic textured tuffaceous sandstones, d) Chloritizations in the vitroclastic textured tuffaceous sandstones.

I-C minerals are also observed in addition to feather and flaky illite and chlorites (Figure 7d).

The back scattered electron (BSE) microscope views of sandstone and mudstone samples of the Korualan Group have shown that the phyllosilicates, which are the main components of the orientation, are represented by fine grained illite and chlorite formations infilling the spaces of calcite, quartz and feldspar grains in addition to coarse dendritic micas (Figure 8a-b). In addition to silicate and carbonate minerals in mudstones, the framboidal pyrites, which formed as a result of probable bacterial reduction, were also observed (Figure 8b). In altered volcanic rock sample of the Huğlu Group, the pale gray-white iron rich components (chlorite, hematite) increase and also the orientation related with the burial can be observed in addition to the volcanic texture (Figure 8c). In siltstone sample, in which the clastic texture is dominant, the coarse grained platy mica (dark gray) and chlorites (pale gray) form a distinctive orientation (Figure 8d). The authigenic illite and chlorites are observed in the form of fine grained constituents which infill the grains.

5.3. X-Ray Diffraction Studies

5.3.1. Whole Rock and Clay Fraction Studies

In siliciclastic and carbonate rocks of the Korualan Group; the quartz, feldspar, clay and hematite minerals, and calcite and dolomite minerals are observed as dominant minerals, respectively in order of abundance. In siliciclastic rocks of the unit, mainly the illite, partly chlorite, smectite and mixed-layered I-S constitute clay minerals (Figure 9a-b).

The volcanic components of volcanic and pyroclastic rocks of the Huğlu Group in order of abundance are composed of feldspar (mainly plagioclase), augite, hornblende, biotite and hematite, and the post volcanic components are constituted by quartz, clay, calcite, dolomite, analcime and goethite. The mineralogy of silicilastic and carbonate rocks is similar to that of the Korualan Group except for their abundances. In volcanic-pyroclastic rocks of the unit (Dedemli Formation), the clay minerals are represented mainly by illite, chlorite, partly smectite and by the mixed-layered I-S. The deep marine silicified rocks

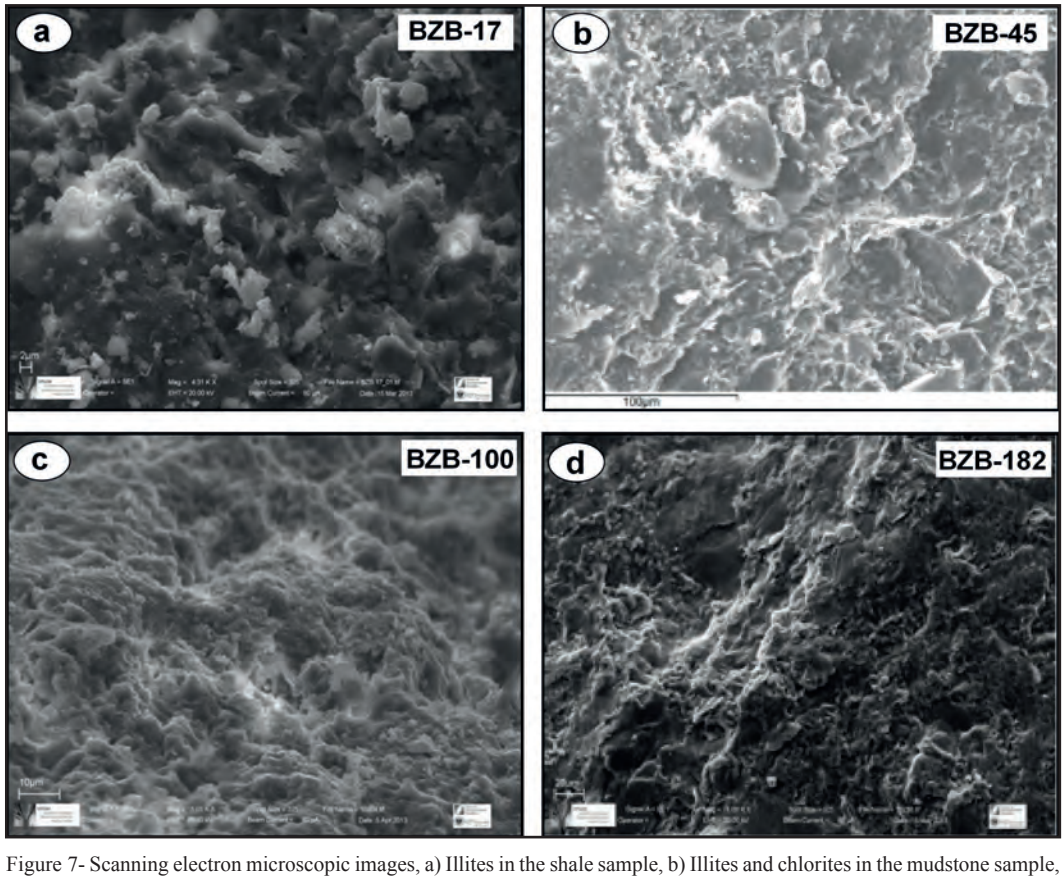

Figure 7- Scanning electron microscopic images, a) Illites in the shale sample, b) Illites and chlorites in the mudstone sample, c) Illites and chlorites in the altered volcanic sample, d) Illite, chlorite and mixed-layered illit-chlorite (I-C) in the siltstone sample.

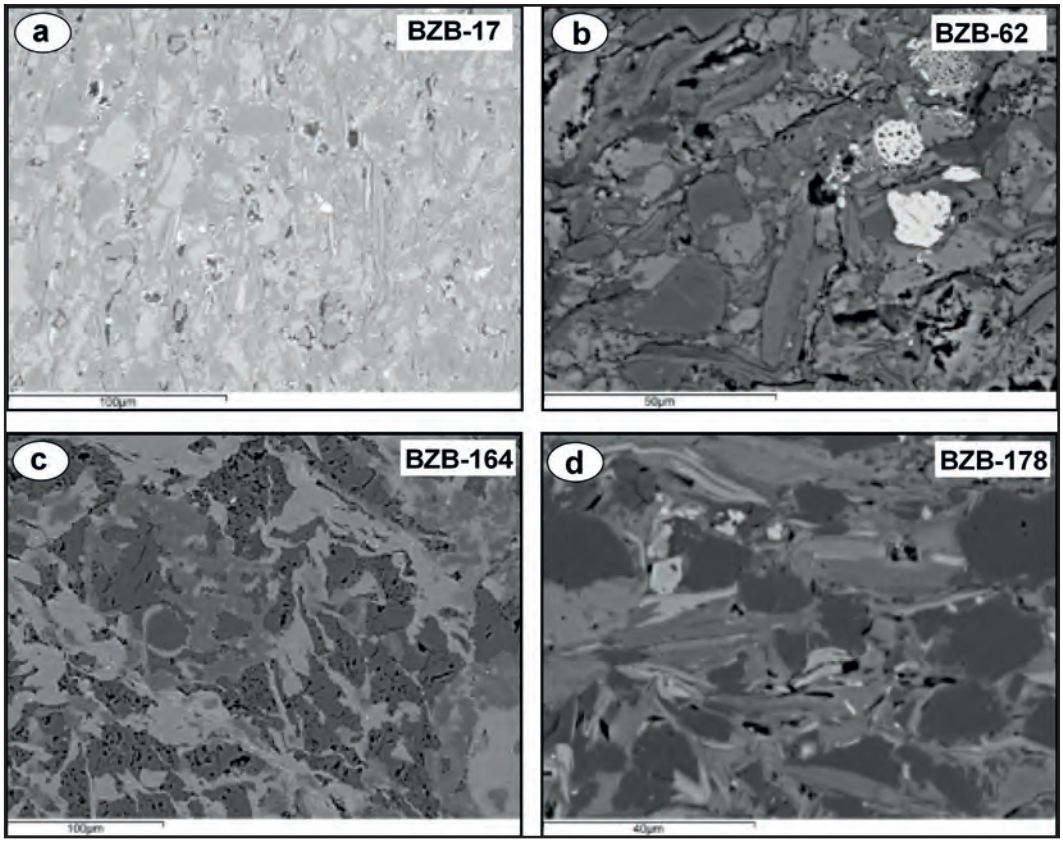

Figure 8- Backscattered electron microscopic images, a) Orientations of the illites in the shale sample, b) Detrital mica, authigenic illite and framboidal pyrite occurrences in the mudstone sample, c) Fine-grained hematites in the altered volcanic sample, d) Orientations of the micas and chlorites in the siltstone sample.

(Mahmut Tepesi Formation) contain C-V and C-S in addition to illite, chlorite and I-S minerals.

5.3.2. The Crystal Chemistry Studies of Phyllosilicates

The "crystallinity" values of illite and chlorite minerals of the Bozkır Unit obtained by the calibration of peak values (FWHM) in semi-height measured by means of WINFIT program were given in table 1. For illite and chlorite minerals the Kübler index (KI:Kübler, 1968) and the Arkai index (AI: Arkai, 1991; Guggenheim et al., 2002) were used, respectively.

The crystallinity measurement values for units were assessed in KI-I(002)/(001) diagram (Figure 10), and correspond with the Kayabaşı formation 1.48-2.31 $\Delta^o2\theta$ (mean 1.82 $\Delta^o2\theta$. low grade diagenesis), the Dedemli formation 0.54-0.81 $\Delta^o2\theta$ (mean 0.63 $\Delta^o2\theta$, high grade diagenesis) and the Mahmut Tepesi formation 0.35-0.76 $\Delta^o2\theta$ (mean 0.53 $\Delta^o2\theta$, anchizone and high grade diagenesis) values.

The relationship between the crystallinity degree (KI) and peak intensity ratio (Ir), which were determined in different lithologies of the Bozkır Unit, was given in figure 11. Accordingly; the Kayabaşı formation, the Dedemli formation and the Mahmut Tepesi formation reflect low grade diagenesis, high grade diagenesis and anchizone-high grade diagenesis, respectively.

The illites, which give a peak at 10 Å in N- and EG-patterns and do not show any extension in EG-pattern, might contain smectite even in fewer amounts. In case when illites contain smectite layer both the peak intensity of (003) reflection increases and 10 Å peak width decreases in EG-pattern. The peak intensity ratio suggested by Srodon (1984) ($Ir=I(003/001)_{air\text{-}dried}/I(003/001)_{glycolated}$) is one of the most widely used methods and Ir>1 means that illites contain smectite interlayer. Using the diagram generated according to crystallinity and Ir values of illites by Eberl and Velde (1989), it was assessed that illites had contained an expandable layer (smectite) (Figure 11).

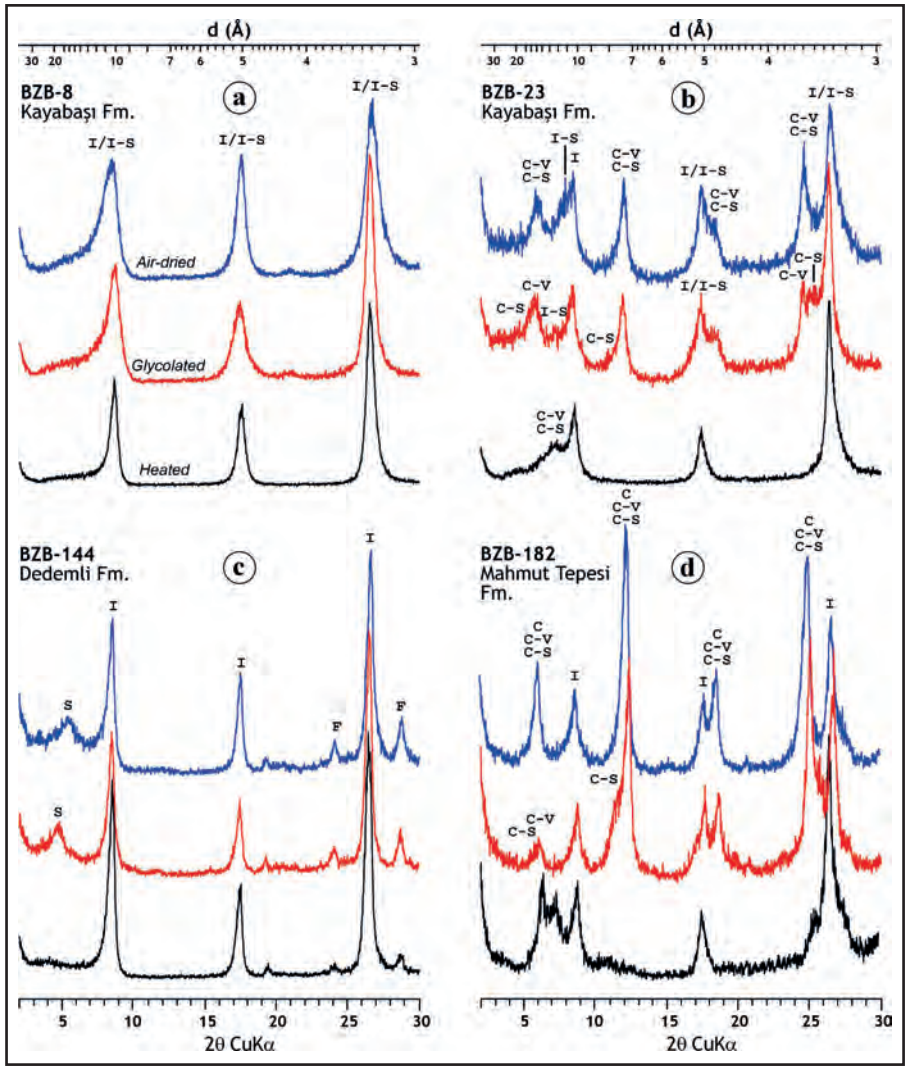

Figure 9- XRD-CF patterns of the Bozkır Unit rocks, a) Illite / I-S, b) Illite + I-S +C-V + C-S, c) Illite + Smectite, d) Illite + Chlorite + C-V + C-S.

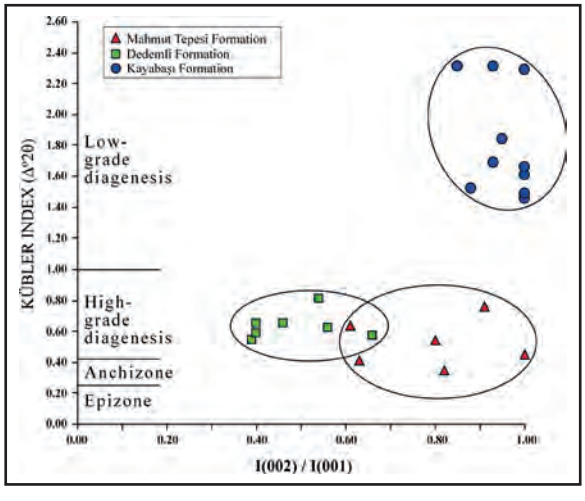

Figure 10- The distribution of KI-I(002)/(001) peak intensity ratios in the K-micas from the Bozkır Unit rocks.

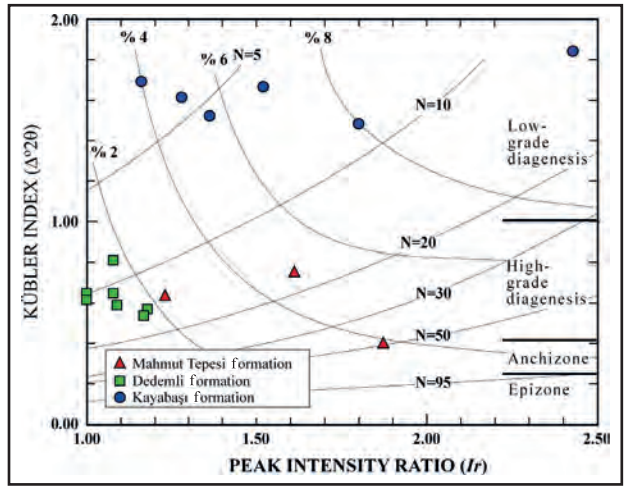

Figure 11- The relationship between expandable layer content (S %) and crystallite size of K-micas in the KI-[$I_{(003)}/I_{(001)N}$] / [$I_{(003)}/I_{(001)G}$] diagram (Eberl and Velde, 1989) from the Bozkır Unit rocks.

Thus, the expandable layer components of illites (smectite %) is in between 4-8 % in the Kayabaşı formation, less than 2 % in the Dedemli formation and between 2-5 % in the Mahmut Tepesi formation.

The crystalline size of illites, according to the formula (N_{001}=8.059/β; β=1.038949 x KI-0.8250323) suggested by Merriman et al. (1990), are 3-6 nm in the Kayabaşı formation (mean 5 nm), 11-17 nm (mean 14 nm) in the Dedemli Formation and 11-29 nm (mean 19 nm) in the Mahmut Tepesi formation (Table 1). The crystallite sizes of illites in KI-Ir diagram show a similarity with the values estimated from Merriman et al. (1990) (Figure 11).

The polytype and d_{060} measurements made in pure or nearly pure illites of the Kayabaşı Formation were given in figure 12. The illites mainly form from $2M_1$ and $1M_d$ polytypes, and a sample far from rifting (BZB-8) contains $1M$ polytype. According to d_{060} values (1.4996-1.5007 Å, mean 1.5002 Å), the illites are completely dioctahedral in composition (Octahedral Fe+Mg=0.18 atom).

6. Geochemistry

6.1. Major Element Geochemistry

Illite, smectite and vermiculites are clay minerals structurally related with micas, and they are distinguished from each other by the tetrahedral-octahedral-tetrahedral (T-O-T or 2:1) interlayer cation to be potassium. The ones that resemble to muscovite are dioctahedral; and the others resembling to biotite are trioctahedral. The general formula for illite can be expressed as; $K_yAl_4[Si_{8-y.0}Al_yO_{20}](OH)_4$ and here y<2 and mostly around 1.5.

The chemical compositions of some mica minerals that should be taken into consideration in the

Table 1- The results of "crystallinite", peak intensity ratio (Ir) and crystallite size (N, mm) measurements of illite and chlorite in the Bozkır Unit.

Sample No	FWHM-I	FWHM-C	KI-I	KI-C	Ir(*)	N(**)	I(002)/I(001)
Kayabaşı Formation							
BZB-8	1.450		1.61		1.28	5	1.00
BZB-17	1.523		1.69		1.16	5	0.93
BZB-23	1.376		1.52		1.36	5	0.88
BZB-28	1.319		1.46			6	1.00
BZB-45	2.038		2.29		1.77	4	1.00
BZB-69	1.651		1.84		2.43	4	0.95
BZB-71	1.493		1.66		1.52	5	1.00
BZB-89	2.055		2.31		2.33	3	0.93
BZB-105	2.055		2.31		1.86	3	0.85
BZB-131	1.337		1.48		1.80	6	1.00
Dedemli Formation							
BZB-100	0.621		0.65		1.00	14	0.46
BZB-117	0.592		0.62		1.00	14	0.56
BZB-140	0.755		0.81		1.08	11	0.54
BZB-144	0.549		0.57		1.18	16	0.66
BZB-161	0.526		0.54		1.17	17	0.39
BZB-164	0.566		0.59		1.09	15	0.40
BZB-165	0.622		0.65		1.08	14	0.40
Mahmut Tepesi Formation							
BZB-171	0.615		0.64		1.23	14	0.61
BZB-178	0.415	0.415	0.41	0.41	1.87	23	0.63
BZB-179	0.529	0.410	0.54	0.41		17	0.80
BZB-180	0.362	0.385	0.35	0.38		29	0.82
BZB-181	0.445	0.447	0.45	0.45		21	1.00
BZB-182	0.714		0.76		1.61	11	0.91

(*) Ir = $[I(003)/I(001)_{normal}] / [I(003)/I(001)_{glycole}]$

(**) N001 (nm) = 8.059/β; β=1.038949 x KI-0.8250323

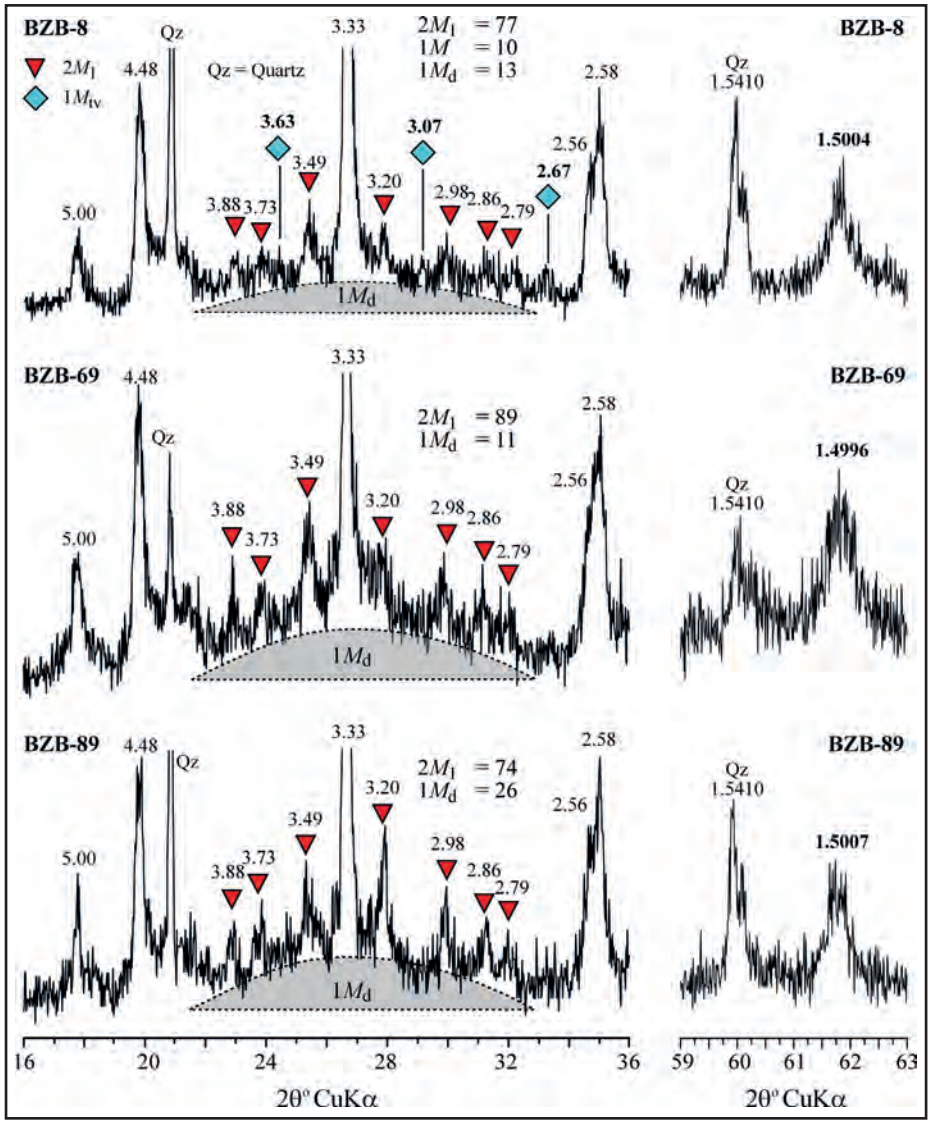

Figure 12- XRD patterns of polytypes and d_{060} values of illite in the Bozkır Unit rocks.

assessment of illites are given below. The structural and oxide formulae of theoretical muscovite and seladonite are successively; $K_2Al_4[Si_6Al_2O_{20}](OH,_F)_4$ ve $K_2O.3Al_2O_3.6SiO_2.2H_2O$ (SiO_2 45.26 %, Al_2O_3 38.40 %, K_2O 11.82 %, H_2O 4.52 %), $K_2(MgFe^{2+}Fe^{3+}{}_2)[Si_8O_{20}](OH)_4$ and $K_2O.Fe_2O_3.MgO.FeO.8SiO_2.2H_2O$ (SiO_2 54.45 %, Fe_2O_3 18.09 %, FeO 8.14 %, MgO 4.57 %, K_2O 10.67 %, H_2O 4.08 %). The structural and oxide formulae of theoretical biotite is $K_2Fe_6[Si_6Al_2O_{20}](OH)_4$ (K_2O 9.20 %, FeO 42.11 %, SiO_2 35.21 %, Al_2O_3 9.96 %, H_2O 3.52 %); and for phlogopite it is $K_2Mg_6[Si_6Al_2O_{20}](OH)_4$ (K_2O % 11.29, MgO 28.98 %, SiO_2 43.19 %, Al_2O_3 12.22 %, H_2O 4.32 %).

The major element contents of illite minerals detected by the ICP method and the structural formulae estimated based on 11 oxygen atom (Weaver and Pollard, 1973) were presented in table 2. The distribution of major oxides based on their content in illites shows nearly 50 times increase (SiO_2) and 100 times decrease (MnO) when 1 % value is taken as reference. The most distinctive difference according to samples is observed in ΣFe_2O_3, CaO and Na_2O contents.

Illites that have dioctahedral composition possess tetrahedral Al (0.04-0.49) substitution. The octahedral substitution and total octahedral cation amount related with Al, Mg, Fe, T, and Mn vary between 0.15-0.52 and 1.86-1.96, respectively. The major cation located between the interlayer is K, and its amount ranges from 0.37 to 0.51. The tetrahedral Al and interlayered K amount in ideal muscovite is 1, and the octahedral Al

amount is known as 2. The tetrahedral and octahedral substitutions and interlayer Ca and Na amounts in illites (0.05-0.12) make us consider that they are related with the expandable layer (smectite) component, the presence of other mica phases in clay fraction and most significantly with the diagenetic nature.

The major element compositions and structural formulae of illite and mixed-layered clay minerals (illite-chlorite I-C and chlorite-vermiculite C-V) by EDS method were given tables 3, 4 and 5; and the results were assessed with the ones performed by ICP method. The structural formulae of I-C and C-V mixed-layered clay minerals were estimated based on 12.5 atom (Weaver and Pollard, 1973).

Illites are located between montmorillonite and muscovite in the ternary diagram of tetrahedral substitution-octahedral substitution, but mostly in illite region (Figure 13a). Illites are located in montmorillonite − I-S − seladonite − phlogopite − muscovite pentagram in $M^{+}-4Si-R2^{+}$ diagram, but mostly between illite and muscovite (Figure 13b).

Illites are closer to Al^{IV} corner and have a composition between muscovite – phlogopite in the $Fe+Mg-Al^{IV}-Al^{VI}$ ternary diagram (Figure 14a). According to binary variation diagram of Na-K; Na low, but K presents a wide compositional interval (Figure 14b). However; they are aligned along muscovite-seladonite line, but close to muscovite corner in the Si-Al_{total} diagram (Figure 14c).

Illites are clustered in region parallel to the muscovite-seladonite line and closer to illite in the binary variation diagram of Si–(Na+K) (Figure 15a). However; in the Mg-Fe diagram they were aligned as parallel to the diagonal line of the rectangle showing a weak positive correlation (Figure 15b).

Illites were clustered close to muscovite corner in the binary variation diagram of Mg+Fe–Si in such a way that it shows a positive correlation though weak (Figure 16a). Interlayer cations possess a composition among muscovite-illite-phengite close to muscovite corner in Si/Al_{total} (Figure 16b).

The structural formulae of illite and mixed-layer clay minerals estimated starting from chemical analyses were given below:

Table 2- Major element chemical composition and structural formulas of illite minerals (ΣFeO: total iron, LOI: Loss on Ignition, TC: Tetrahedral charge, TOC: Total octahedral cation, OC: Octahedral charge, ILC: Interlayer charge, TLC: Total layer charge).

Oxide %	BZB-8	BZB-89	BZB-131	Mean
SiO_2	60.11	54.69	50.31	55.04
TiO_2	0.848	0.893	0.834	0.86
Al_2O_3	18.48	19.53	24.31	20.77
ΣFe_2O_3	5.70	7.13	4.88	5.90
MnO	0.010	0.019	0.011	0.01
MgO	1.45	1.95	1.86	1.75
CaO	0.72	0.88	0.34	0.65
Na_2O	0.12	0.37	0.18	0.22
K_2O	4.38	4.17	5.70	4.75
P_2O_5	0.21	0.22	0.20	0.21
LOI	7.43	8.59	10.06	8.69
Total	99.46	98.44	98.67	98.86
Si	3.96	3.75	3.51	3.74
Al	0.04	0.25	0.49	0.26
TC	0.04	0.25	0.49	0.26
Al	1.40	1.33	1.51	1.41
Ti	0.04	0.05	0.04	0.04
Fe	0.28	0.37	0.26	0.30
Mn		0.01		0.00
Mg	0.14	0.20	0.19	0.18
TOC	1.86	1.96	1.98	1.93
OC	0.52	0.38	0.15	0.35
Ca	0.05	0.07	0.03	0.05
Na	0.02	0.05	0.02	0.03
K	0.37	0.36	0.51	0.41
P	0.01	0.01	0.01	0.01
ILC	0.54	0.60	0.65	0.59
TLC	0.56	0.63	0.64	0.61

$(Ca_{0.05}Na_{0.03}K_{0.41}P_{0.01})(Al_{1.41}Ti_{0.04}Fe_{0.30}Mg_{0.18})[(Si_{3.74}Al_{0.26})O_{10}](OH)_2$ (Illite-ICP)

$(Mg_{0.02}Ca_{0.01}Na_{0.08}K_{0.77})(Al_{1.76}Ti_{0.02}Fe_{0.14}Mg_{0.12})[(Si_{3.23}Al_{0.77})O_{10}](OH)_2$ (Illite-EDS)

$(Mg_{0.23}Ca_{0.12}K_{0.07})(Al_{1.69}Fe_{1.05}Mg_{0.90})[(Si_{3.75}Al_{0.25})O_{10}](OH)_6$ (C-V-EDS)

$(Mg_{0.01}Ca_{0.12}K_{0.47})(Al_{1.90}Fe_{0.85}Mg_{0.80})[(Si_{3.28}Al_{0.72})O_{10}](OH)_6$ (I-C-EDS)

6.2. Trace Element Geochemistry

The trace element contents of illite minerals by ICP-MS method were presented in table 6. When distribution of trace elements with respect to their content is taken in 1 ppm reference interval; there is observed 385 times increase (Ba) and 100 times decrease (Bi and In). Looking at REE contents; 72 times increase (Ce) and

Table 3- EDS results (%) and structural formulas of illite minerals from the Kayabaşı formation (TC: Tetrahedral charge, TOC: Total octahedral cation, OC: Octahedral charge, ILC: Interlayer charge, TLC: Total layer charge).

Sample No.	BZB-17	BZB-45			BZB-71							
Mineral No.	m1	m1	m2	m3	m1			m2			m3	
Spectrum No.	s3	s8	s2	s1	s1	s2	s6	s2	s3	s9	s2	s10
SiO_2	50.234	50.784	48.890	50.567	48.075	50.895	50.049	48.482	47.145	49.498	47.620	50.420
TiO_2	0.685		0.593	0.361			0.613	0.642	0.368	0.450	0.400	
Al_2O_3	34.668	38.489	37.956	38.014	37.200	33.281	35.182	35.539	35.029	35.970	38.290	35.818
FeO	2.522	1.750	1.555	1.426	1.725	2.619	2.456	2.953	5.874	1.868	1.564	2.040
MnO												
MgO	1.5681	0.921	0.701	0.828	1.0989	2.282	1.507	1.409	2.4557	1.425	0.855	1.327
CaO		0.439					0.437		0.676	0.388		1.104
Na_2O	0.5530	0.639	0.560	0.708	0.895		0.644	1.112	0.656	0.984	1.213	0.728
K_2O	9.772	6.980	9.747	8.087	10.335	10.925	9.114	9.660	7.868	9.420	10.055	8.554
Total	100.00	100.00	100.00	99.99	99.33	100.00	100.00	99.80	100.07	100.00	100.00	99.99
Tetrahedral												
Si	3.18	3.14	3.08	3.14	3.07	3.23	3.16	3.09	3.02	3.12	3.02	3.17
Al	0.82	0.86	0.92	0.86	0.93	0.77	0.84	0.91	0.98	0.88	0.98	0.83
TC	0.82	0.86	0.92	0.86	0.93	0.77	0.84	0.91	0.98	0.88	0.98	0.83
Octahedral												
Al	1.76	1.94	1.89	1.92	1.87	1.72	1.77	1.76	1.67	1.80	1.88	1.82
Ti	0.03	0.00	0.03	0.02			0.03	0.03	0.02	0.02	0.02	
Fe^{2+}	0.13	0.09	0.08	0.07	0.09	0.14	0.13	0.16	0.31	0.10	0.08	0.11
Mn												
Mg	0.15		0.02	0.01	0.10	0.22	0.14	0.13	0.14	0.13	0.06	0.12
OC	0.04	0.00	0.01	0.00	0.01	0.12	0.03	0.02	0.01	0.06	0.00	0.08
TOC	2.07	2.01	2.02	2.02	2.06	2.08	2.07	2.08	2.14	2.05	2.04	2.05
Interlayer												
Mg		0.09	0.05	0.07					0.09		0.02	
Ca		0.03					0.03		0.05	0.03		0.07
Na	0.07	0.08	0.07	0.09	0.11		0.08	0.14	0.08	0.12	0.15	0.09
K	0.79	0.55	0.78	0.64	0.84	0.89	0.73	0.79	0.64	0.76	0.81	0.69
ILC	0.86	0.87	0.95	0.87	0.95	0.89	0.87	0.93	1.00	0.94	1.00	0.92
TLC	0.86	0.86	0.93	0.86	0.94	0.89	0.87	0.93	0.99	0.94	0.98	0.91
Sample No.	BZB-62											
Mineral No.	m1	m4	m4	m6	m6	m6	m6	m6	m6	m7	m9	
Spectrum No.	s3	s10	s12	s2	s3	s5	s6	s7	s9	s6	s3	
SiO_2	50.574	48.874	49.224	53.620	49.140	49.512	48.928	53.053	50.318	48.614	49.896	
TiO_2		0.352	0.445		0.661					0.658		
Al_2O_3	35.221	37.528	35.092	33.769	36.350	36.228	39.355	32.615	36.217	37.722	36.690	
ΣFeO	2.133	1.662	2.287	2.089	1.710	2.285	1.104	2.897	1.773	1.514	1.692	
MnO												
MgO	1.4382	0.861	1.364	2.497	1.4369	1.294	0.734	1.102	1.3107	1.110	1.3159	
CaO			1.202	0.760		0.748	0.801	0.476				
Na_2O	0.8706	1.092			0.4665	0.529	1.371	0.806	1.273	1.210	0.8347	
K_2O	9.765	9.633	10.389	7.265	10.237	9.406	7.710	9.052	9.070	9.174	9.570	
Total	100.00	100.000	100.00	100.00	100.00	100.00	100.00	100.00	99.96	100.00	100.00	
Tetrahedral												
Si	3.19	3.08	3.13	3.32	3.11	3.13	3.05	3.34	3.16	3.06	3.14	
Al	0.81	0.92	0.87	0.68	0.89	0.87	0.95	0.66	0.84	0.94	0.86	
TC	0.81	0.92	0.87	0.68	0.89	0.87	0.95	0.66	0.84	0.94	0.86	
Octahedral												
Al	1.81	1.87	1.76	1.78	1.82	1.83	1.94	1.76	1.84	1.86	1.86	
Ti		0.02	0.02		0.03					0.03		
Fe^{2+}	0.11	0.09	0.13	0.11	0.09	0.12	0.06	0.15	0.09	0.08	0.09	
Mn												
Mg	0.14	0.06	0.13	0.22	0.13	0.12	0.03	0.10	0.12	0.07	0.12	
OC	0.07	0.01	0.12	0.00	0.00	0.03	0.00	0.22	0.06	0.00	0.01	
TOC	2.06	2.04	2.04	2.11	2.07	2.07	2.03	2.01	2.05	2.04	2.07	
Interlayer												
Mg		0.02	0.01	0.01	0.01		0.04			0.03		
Ca			0.08	0.05		0.05	0.05	0.03				
Na	0.11	0.13			0.06	0.07	0.17	0.10	0.16	0.15	0.10	
K	0.79	0.78	0.84	0.57	0.83	0.76	0.61	0.73	0.73	0.74	0.77	
ILC	0.90	0.95	1.00	0.69	0.91	0.88	0.96	0.89	0.89	0.95	0.87	
TLC	0.88	0.93	0.99	0.68	0.89	0.90	0.95	0.89	0.90	0.94	0.86	

Table 4- EDS results (%) and structural formulas of illite minerals of the Mahmut Tepesi formation (TC: Tetrahedral charge, TOC: Total octahedral cation, OC: Octahedral charge, ILC: Interlayer charge, TLC: Total layer charge).

Sample No.	BZB-178									
Mineral No.	m3			m2	m8		m1			m2
Spectrum No.	s4	s6	s8	s3	s9	s12	s3	s5	s8	s4
SiO_2	62.490	56.650	60.410	59.544	57.676	58.292	52.140	51.760	51.074	50.347
TiO_2		0.330		1.610		0.409			0.389	
Al_2O_3	22.230	23.500	25.430	20.258	22.191	20.591	27.649	31.404	29.538	32.947
FeO	2.010	6.430	1.550	4.590	6.668	7.205	3.801	2.269	4.580	3.064
MnO										
MgO				2.643	3.417	3.495	3.689	2.584	2.847	2.654
CaO			0.330							
Na_2O					0.473			1.045		0.511
K_2O	12.370	10.690	10.840	11.355	9.574	10.007	11.779	10.485	11.572	10.476
Total	99.10	97.60	98.56	100.00	100.00	100.00	99.06	99.55	100.00	100.00
Tetrahedral										
Si	3.95	3.72	3.81	3.80	3.69	3.74	3.39	3.30	3.30	3.21
Al	0.05	0.28	0.19	0.20	0.31	0.26	0.61	0.70	0.70	0.79
TC	0.05	0.28	0.19	0.20	0.31	0.26	0.61	0.70	0.70	0.79
Octahedral										
Al	1.61	1.54	1.70	1.32	1.37	1.31	1.50	1.66	1.54	1.68
Ti		0.02		0.08		0.02			0.02	
Fe^{2+}	0.11	0.35	0.08	0.25	0.36	0.39	0.21	0.12	0.25	0.16
Mn										
Mg				0.25	0.33	0.34	0.36	0.25	0.27	0.25
OC	0.95	0.60	0.74	0.72	0.51	0.57	0.34	0.28	0.26	0.14
TOC	1.72	1.91	1.78	1.90	2.06	2.06	2.07	2.03	2.08	2.09
Interlayer										
Mg										
Ca			0.02							
Na					0.06			0.13		0.06
K	1.00	0.90	0.87	0.93	0.78	0.82	0.98	0.85	0.95	0.85
ILC	1.00	0.90	0.91	0.93	0.80	0.82	0.98	0.98	0.95	0.91
TLC	1.00	0.88	0.93	0.92	0.82	0.83	0.95	0.98	0.96	0.93

3 times decrease (Lu) is observed. Besides; the tracing of REE contents from La to Lu in the form of increase-decrease indicate the consistency of analyses and that illites are pure or nearly pure.

The chondrite-normalized distribution of trace element contents of illites (Sun and McDonough, 1989) was given in figure 17. The Nb and Y from Condie (1993) and the other elements were taken from Gromet et al. (1984) for NASC. When compared with chondrite values; the enrichment (579 times for U) - depletion (4 times for P) in elements based on the host-rock it derived vary and pattern minerals distinguish from NASC and each other. In other word; the illites exhibit distinctive differentiation / fractionation. The most distinctive positive and negative anomalies are recorded in La, Nd and Ti; and Sr and P elements, respectively.

The REE contents of illite minerals were normalized according to chondrite (Sun and McDonough, 1989) and their element abundances were compared (Figure 18). The values of the North American Shales (North American Shale Composite, NASC) were also added to the diagram (for Ho and Tm elements; Haskin et al., 1968, for other elements; Gromet et al., 1984).

According to chondrite values, illite minerals and NASC patterns resemble to each other, however; they differentiation from each other in term of abundances and show distinctive differentiation / fractionation. The REE contents of illites, except the La-Ce-Pr, are lower than NASC but increased with respect to chondrite (174 times for La, 10 times for Ho). Besides; LREE concentrations of illite minerals show a decrease with respect to HREE. There is also observed a small decrease for Eu.

Table 5- EDS results (%) and structural formulas of chlorite interlayered minerals in rocks of the Bozkır Unit (TC: Tetrahedral charge, TOC: Total octahedral cation, OC: Octahedral charge, ILC: Interlayer charge, TLC: Total layer charge).

Mineral	C-V	C-V	I-C
Sample No	BZB-45	BZB-71	BZB-178
Mineral No	1	3	2
Spectrum No	s6	s4	s6
SiO_2	42.926	43.440	43.470
TiO_2			
Al_2O_3	25.978	29.399	29.433
FeO	17.435	15.920	13.529
MnO			
MgO	11.959	8.390	7.189
CaO	1.303	1.726	1.452
Na_2O			
K_2O	0.402	1.123	4.925
Total	100.00	100.00	100.00
Tetrahedral			
Si	3.24	3.25	3.28
Al	0.76	0.75	0.72
TC	0.76	0.75	0.72
Octahedral			
Al	1.55	1.84	1.90
Ti			
Fe	1.10	1.00	0.85
Mn			
Mg	1.07	0.74	0.80
OC	0.01	0.00	0.00
TOC	3.72	3.58	3.55
Interlayer			
Mg	0.27	0.20	0.01
Ca	0.11	0.14	0.12
Na			
K	0.04	0.11	0.47
ILC	0.80	0.79	0.73
TLC	0.77	0.75	0.72

6.3. Stable Isotope Geochemistry

These analyses, which represent the oxygen and hydrogen isotope geochemistry of illites, are generally applied in two sections in order to determine the traces of geothermometer and fluid-rock interaction. The first is based on the differentiation between the two phases related to the formation temperatures, and the second is based on isotopic composition of fluid or rock in order to assess the origin of fluid or rock protoliths. In other words; if the origin of the water is known (sea water, meteoric, magmatic) then temperature conditions; if temperature conditions are known then the origin of water is detected. Oxygen and hydrogen isotope geochemistry analyses were carried out on 3 illite minerals (Table 7).

In addition to $\delta^{18}O$ and δD values of illite minerals, the sea water point, meteoric water and supergene-hypogene lines, which had been suggested by many investigators (Craig, 1961; Sheppard et al., 1969; Sheppard, 1986; Sheppard and Gilg, 1996; Wenner and Taylor, 1974), were also added to figure 19. In $\delta^{18}O$ – δD diagram according to isotopic change of water vs. increasing temperature, the isotopic composition of the water, which constitute I-S, is far from the sea water composition but is located between East Mediterranean Meteoric Water (EMMW, Gat et al., 1996) composition and the magmatic water composition. In the determination of illite-water equilibrium, which changes with temperature, R3 for oxygen; Savin and Lee (1988) equation for I-S (90 % I, 10 % S) and Yeh (1980) equation for hydrogen were used. It is considered that diagenetic waters forming

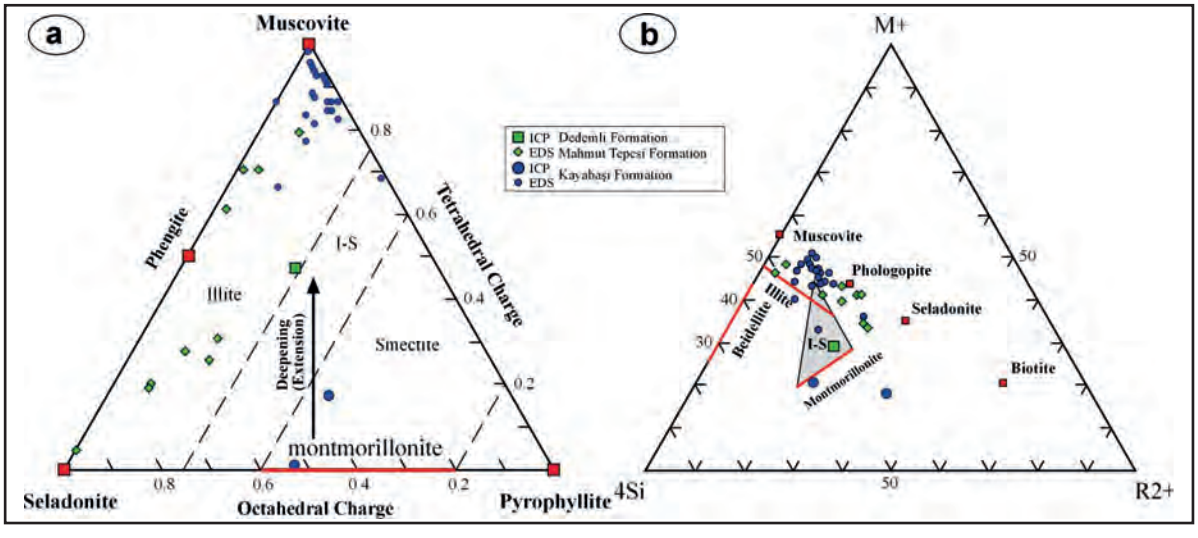

Figure 13- The distributions of cations from clay minerals in the triangular diagrams, a) Tetrahedral charge-octahedral charge, b) M^+-4Si-R^{2+}.

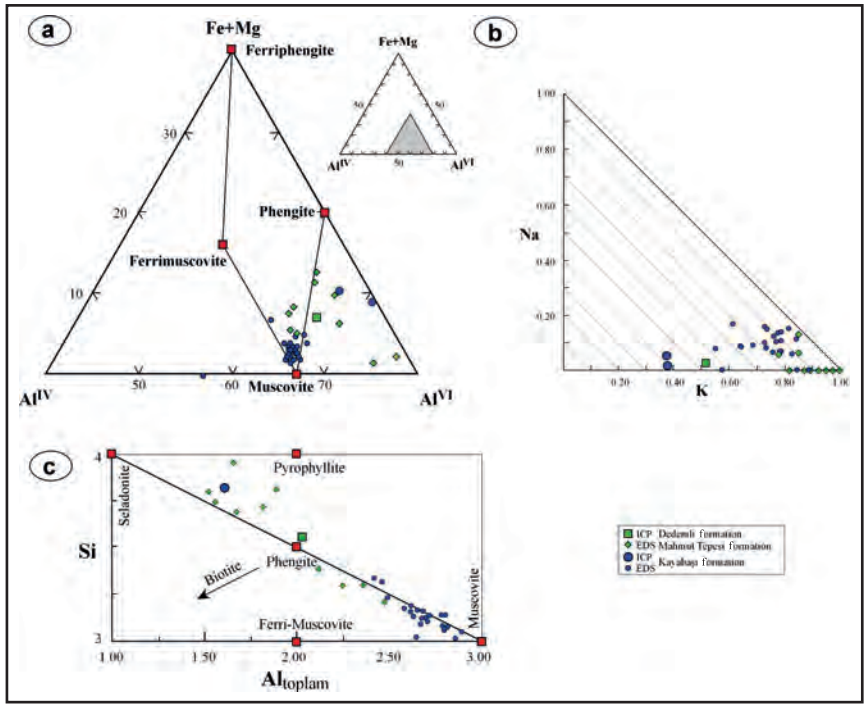

Figure 14- The distributions of cations from clay minerals in the triangular and binary diagrams, a) octahedral (Fe+Mg)-octahedral Al^{VI}-tetrahedral Al^{IV}, b) Interlayers Na-K, c) Tetrahedral Si-Al_{total}.

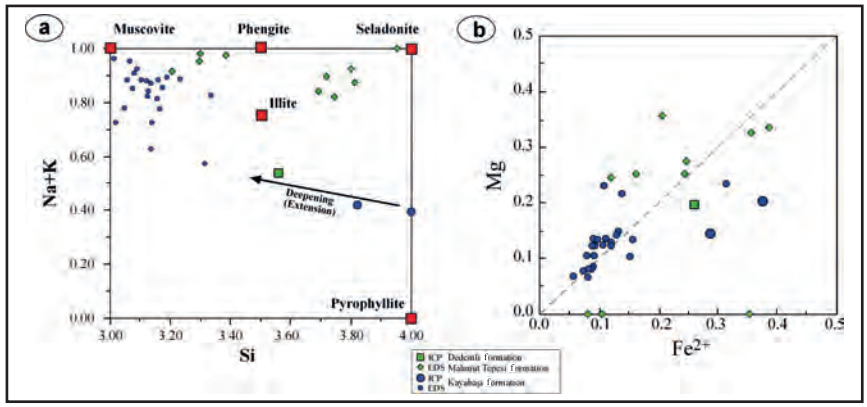

Figure 15- The distributions of cations from clay minerals in the variation diagrams, a) Interlayer Na+K-tetrahedral Si, b) Octahedral Mg-Fe.

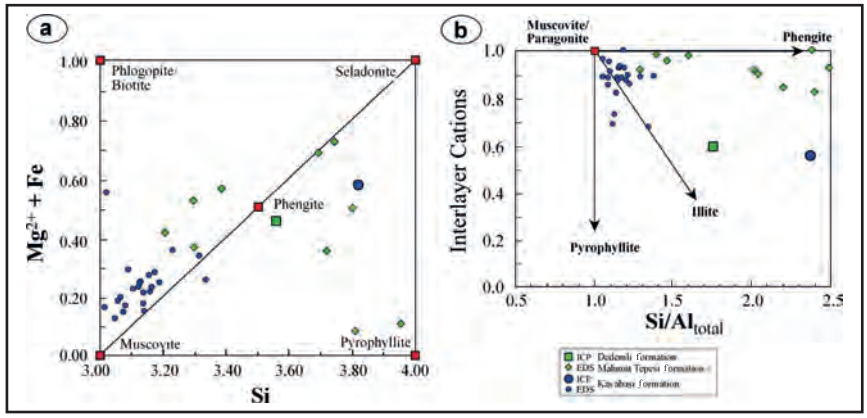

Figure 16- The distributions of cations from clay minerals in the variation diagrams, a) Octahedral Mg+Fe-tetrahedral Si, b) tetrahedral Si/Al_{total}.

Table 6- Trace element chemical compositions of illite minerals.

Element (ppm)	BZB-8	BZB-89	BZB-131	Mean
Cr	120	150	180	150
Ni	40	60	90	63
Co	6	9	13	9
Sc	14	16	17	16
V	160	187	224	190
Cu	30	30	40	33
Pb	15	11	15	14
Zn	150	310	130	197
Bi	0.1	0.3	<0.1	0.2
In	<0.1	<0.1	<0.1	0.1
Sn	4	5	6	5
W	2.7	5.7	2.1	3.5
Mo	<2	<2	<2	2
As	85	17	16	39
Sb	0.8	0.4	<0.2	0.5
Ge	2.0	2.6	2.8	2.5
Be	3	3	3	3
Ag	1.8	1.4	1.3	1.5
Rb	163	201	254	206
Cs	34.1	17.5	49.8	33.8
Ba	258	385	322	322
Sr	107	120	196	141
Tl	0.91	0.91	1.19	1.00
Ga	24	29	36	30
Ta	1.34	1.42	1.39	1.38
Nb	18.0	19.4	18.4	18.6
Hf	4.1	4.0	3.5	3.9
Zr	164	165	140	156
Y	13.2	16.5	16.8	15.5
Th	11.6	13.1	16.7	13.8
U	4.04	3.56	4.63	4.08
La	30.00	35.00	41.30	35.43
Ce	52.3	63.5	72.0	62.6
Pr	6.04	7.56	8.61	7.40
Nd	20.5	26.3	29.5	25.4
Sm	3.48	4.21	4.47	4.05
Eu	0.667	0.815	0.826	0.769
Gd	2.50	3.25	3.05	2.93
Tb	0.43	0.52	0.51	0.49
Dy	2.62	3.18	3.11	2.97
Ho	0.55	0.68	0.67	0.63
Er	1.67	2.04	2.08	1.93
Tm	0.279	0.322	0.352	0.318
Yb	1.91	2.25	2.37	2.18
Lu	0.301	0.342	0.342	0.328

Table 7- Stable isotope compositions ($\delta^{18}O$ ve δD) of illite minerals.

Sample No	Yield %	% H_2O	dD(SMOW)	$d^{18}O$(SMOW)
BZB-8	14.8	8.6	-72	20,8
BZB-89	14.1	10.7	-75	18.3
BZB-131	14.2	12.1	-71	19.7

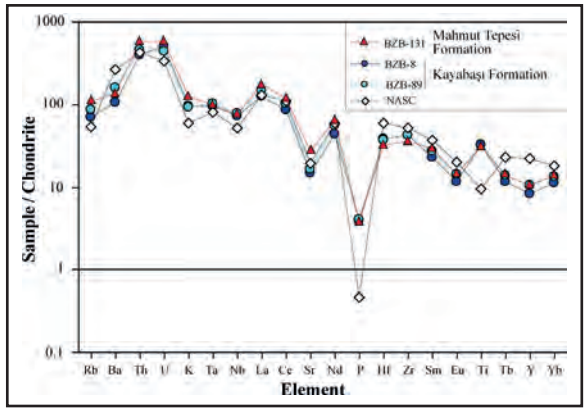

Figure 17- Chondrite-normalized trace element patterns of the illite minerals (Chondrite: Sun and McDonough, 1989; Nb and Y for NASC: Condie, 1993; other elements: Gromet et al., 1984).

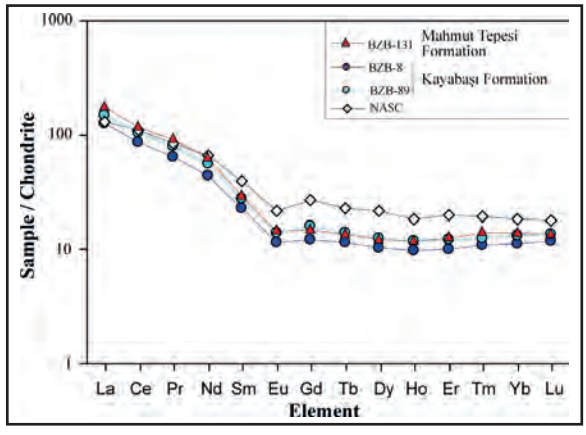

Figure 18- Chondrite-normalized REE abundances of the illite minerals (NASC: Ho and Tm elements from Haskin et al., 1968, other elements: Gromet et al., 1984; Chondrite: Sun and McDonough, 1989).

the illites which are closely located to the EMMW composition are mostly originated from groundwater and partly from volcanic-volcano-sedimentary waters.

According to $\delta_{18}O_{H2O}$ – temperature (°C) diagram, when the water forming the illites are completely assumed as EMMW then temperature conditions lower than 20 °C; and when it is assumed to be the magmatic water then temperature conditions higher than 80 °C were obtained (Figure 20). The crystal-chemical data (KI, crystallite size, d_{060}, polytype, etc.) of illites foresees temperature conditions higher than 20 °C and seems to be related with the mixture of two different waters. The isotope data of illites in sample BZB-8 representing the section away from the rifting of the Kayabaşı Formation and the illites in sample BZB-89 representing the section close to rifting indicate a temperature difference reaching 10 °C for

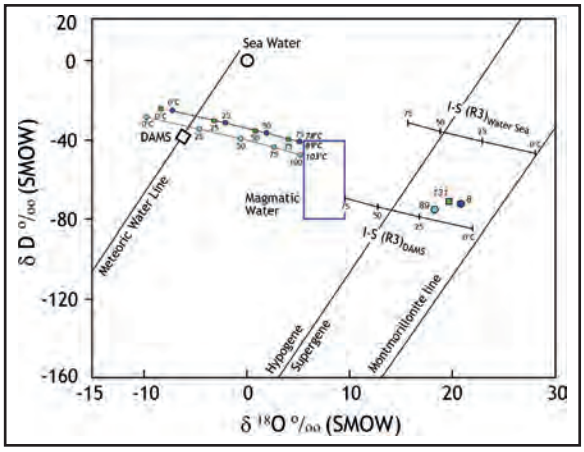

Figure 19- The setting of oxygen and hydrogen isotope compositions of the illite minerals in the $\delta^{18}O$ and δD diagram (Supergene-hypogene line: Sheppard et al., 1969; meteoric water line: Craig, 1961).

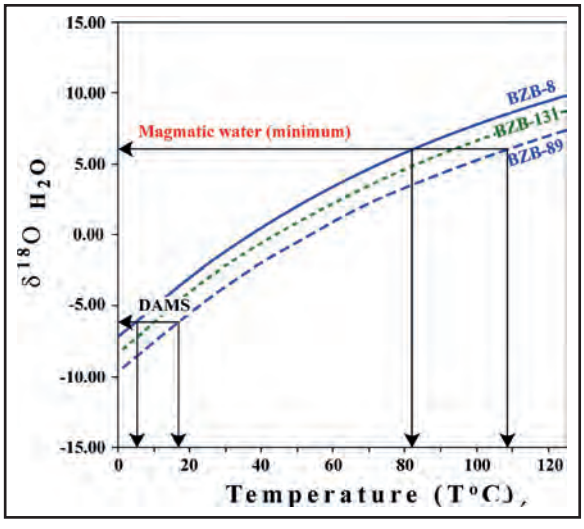

Figure 20- Relationships between ‰ $\delta^{18}O$ (SMOW) values and temperature of water forming illites (DAMS from Gat et al., 1996; magmatic water composition from Taylor, 1968).

the groundwater origin and 30 °C for the magmatic water origin. This situation makes us consider that the temperature increase of which the rifting had caused affected the illite isotope chemistry.

7. Discussion and Results

The results obtained from volcanic, pyroclastic, epiclastic and carbonate rocks of the Bozkır Unit between Triassic-Cretaceous intervals are mostly related with rifting, crustal thinning and partly with burial diagenesis and were mentioned below (Figure 21).

Illites are different in origin in diagenetic sediments (detritic / residual, authigenic) but there occurs ordering in their crystal structure by means of burial effects. With increasing diagenesis, the crystallographic parameters of illite can be used as the grading scale (especially KI). In addition to increasing heat flow related with rifting from diagenesis to metamorphism, there is observed a decrease in KI values (peak narrowing), and $1M_d$ and $1M$ polymorphic types are replaced by $2M_1$. Fine grained micas named as sericite as textural take the place of illites (Duyoner de Segonzac, 1970). The K_2O amount and total negative interlayer capacity of the illites increase in the direction of diagenesis → anchizone → epizone with increasing diagenetic / metamorphic grade (Hunkizer et al., 1986; Bozkaya and Yalçın, 1999).

According to OM and SEM analyses, illite/mica minerals encountered in the Bozkır Unit rocks are widely represented by diagenetic illite, few detritic and volcanogenic micas.

In addition to volcanic glass and/or matrix, typical in volcanogenic rocks, it is considered by many investigators (Yalçın and Gümüşer, 2000; Yalçın and Bozkaya, 2003; Yalçın et al., 2005), who studied in similar environments, that the cations, which occur by the decomposition of K-feldspars with sea water and not used in other phyllosilicate structure, caused the formation illite/muscovites:

(Volcanic glass and/or matrix → Aqueous Al- or Kal siicate gel → Illite/muscovite)

$$3SiO_2.2Al_2O_3+12H_2O \rightarrow 2Al_2(OH)_6.3Si(OH)_4+K^+ \rightarrow KAl_3(Si_3AlO_{10})(OH)_2+10H_2O+2OH^-$$

$$6SiO_2.3Al_2O_3.K_2O+21H_2O \rightarrow K_2O.6Al(OH)_3.6Si(OH)_4 \rightarrow 2KAl_2[AlSi_3O_{10}](OH)_2+19H_2O$$

(K-feldspar or feldspar → Illite/Muscovite and/or Quartz)

$$3(Na,K,Ca)Al_2Si_2O_8+4H^++2K^+ \rightarrow 2KAl_2[AlSi_3O_{10}](OH)_2+3(Na^+,K^+,Ca^{2+})$$

$$4KAlSi_3O_8+6H^+ \rightarrow KAl_3(Si_3AlO_{10})(OH)_2+9SiO_2+2H_2O+3K^+$$

In all geological times, the chlorites in sedimentary rocks are observed as residual in degradation profiles starting from the regressive metamorphism or diagenesis of the host-rock. However, they were

derived either from the alteration zones or completely from the alteration of green schists in which the whole component is chlorite in sedimentary basins. The chlorites are formed from irregular three layered clay minerals as a result of aggradation in marine environments. In the early diagenesis, irregular chlorites are subjected to aggradation because of Mg rich interstitial solutions. As the chlorites that occurred in the early diagenesis are generally rich in Fe, while the Mg content increases with increasing depth by the increasing diagenesis-metamorphism (Ahn and Peacor, 1985).

The chlorites in volcanic, pyroclastic and epiclastic rocks representing the rocks of the Bozkır Unit occur in bonding material and pores. OM and SEM analyses show that the chlorite developed authigenically in pores rather than dark-colored minerals. However; in volcanogenic rocks, it can be stated that the volcanic glass-chlorite transformation occurred passing through an aqueous MgFeAl-silicate gel interphase (e.g. Çerikçioğlu and Yalçın, 1998; Yalçın and Bozkaya, 2002; Yalçın et al., 2005):

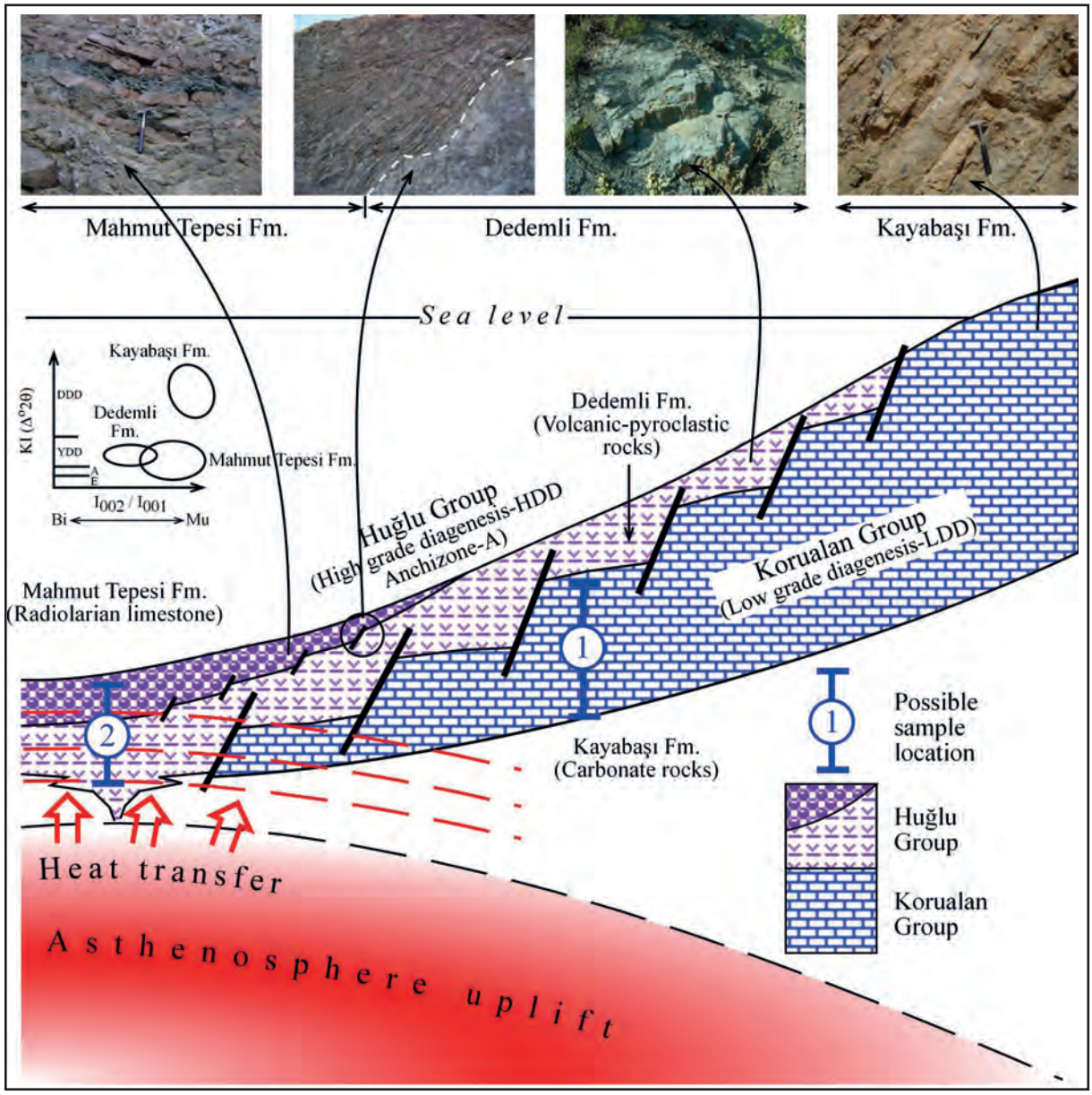

Figure 21- Schematic display of the thermal maturation (diagenesis / metamorpism grade) differrences related to rifting of Bozkır Unit rocks.

(Matrix and/or volcanic glass → Aqueous MgFeAl-silicate gel → Chlorite)

$7SiO_2.Al_2O_3.2MgO.2FeO+24OH^-+10H^+ \rightarrow 9MgO.2FeO.2Al(OH)_3.7Si(OH)_4 \rightarrow Mg_9Fe_2Al[AlSi_7O_{20}](OH)_{16}+9H_2O$

The diagenesis can only be possible by one interlayered phase stage (aggradation) such as the occurrence of these minerals, which have a special significance in studies related with very low grade metamorphism or by the transformation of smectite into illite or chlorite. Non-expanding layer components (illite or chlorite) of the mixed clay layers to increase towards deeper parts or expanding layer components (smectite) to decrease and the order of stacking give important clues on advanced diagenesis (Frey, 1987; Merriman and Peacor, 1999).

The mixed-layered clay minerals widely observed during the late diagenesis are C-S, C-V, I-C and I-S. Mixed-layered C-V is a stage in the aggradation of the 2:1 layered vermiculite type which shows evolution towards chlorite (Dunoyer de Segonzac, 1970; Hoffman and Hower, 1979). Mixed layers I-S and I-C show an evolution towards illite or chlorite by the participation of K or Mg and/or Fe. The permeability is also important for the mobility of solutions in the transformation of smectite into illite or chlorite and to play an active role.

The transformation of smectite into chlorite mostly occurs starting from regular interlayered stage, and 1:1 ordered C-S or C-V mixed layers called as corrensite is formed. Corrensite is widespread in basic and intermediate pyroclastic and volcanoclastic rocks (Evarts and Schiffman, 1983; Brigatti and Poppi, 1984; Inoue et al., 1984, 1987; Inoue, 1985, 1987; Bettison and Schiffman, 1988; Inoue and Utada, 1991), especially in the laumontite zone of the zeolite zone (Kübler et al., 1974; Boles and Coombs, 1977; Lippmann and Rothfuss, 1980; Kisch, 1980, 1981). These minerals are located at the contact metamorphism zones of shales (Blatter et al., 1973; April, 1980; Vergo and April, 1982) and besides in formations related with the burial diagenesis of octahedral clay minerals (Hoffman and Hower, 1979; Chang et al., 1986).

It is probable that the rocks, in which the mixed-layered clay minerals in siliciclastic and volcanic-volcanosedimentary units were derived, formed by the neoformation and/or transformation rather than detrital as being related with the origin material (e.g. Çerikçioğlu and Yalçın, 1998; Yalçın and Gümüşer, 2000; Yalçın and Bozkaya, 2002, 2003; Yalçın et al., 2005):

(Volcanic glass and/or matrix → Aqueous MgFeAl-silicate gel → C-S)

$7SiO_2.Al_2O_3.7MgO.FeO+11H_2O+12H^+ \rightarrow 7MgO.FeO.2Al(OH)_3.7Si(OH)_4 \rightarrow Mg_7FeAl[AlSi_7O_{20}](OH)_{12}+4H_2O+14H^+$

(Phlogopite-Biotite → I-V → Vermiculite)

$K(Mg,Fe)_3[AlSi_3O_{10}](OH)_2+0.50Ca^{+2}+4H_2O \rightarrow K_{0.5}Ca_{0.25}(Mg,Fe)_{3.0}[AlSi_3O_{10}](OH)_2.2H_2O$

$\rightarrow Ca_{0.5}(Fe,Mg)_3[AlSi_3O_{10}](OH)_2.4H_2O+K^+$

(Volcanic glass → Aqueous NaKAl-silicate gel → I-S)

$6SiO_2.3Al_2O_3.Na_2O.K_2O+19H_2O+4H^+ \rightarrow Na_2O.K_2O.6Al(OH)_3.6Si(OH)_4 \rightarrow KNaAl_4[Al_2Si_6O_{20}](OH)_4+18OH^-$

(Sanidine/Orthoclase or plagioclase → I-S)

$6KAlSi_3O_8+Na^++4H_2O \rightarrow KNaAl_4[Al_2Si_6O_{20}](OH)_4+12SiO_2+5K^++4OH^-$

$3(Na,Ca)Al_2Si_2O_8+2H_2O+K^++2H^+ \rightarrow KNaAl_4[Al_2Si_6O_{20}](OH)_4+2(Na^+,Ca^{2+})+2OH^-$

(Volcanic glass and/or matrix → Aqueous KMgFeAl-silicate gel → I-C)

$7SiO_2.4Al_2O_3.2FeO.9MgO.K_2O+25H_2O+2OH^- \rightarrow K_2O.9MgO.2FeO.8Al(OH)_3.7Si(OH)_4$

$\rightarrow K_2Mg_9Fe_2Al_5[Al_3Si_7O_{40}](OH)_{20}+4H_2O+24H^+$

According to KI and AI ($\Delta°2\theta$) data; The Kayabaşı formation has low grade diagenesis, the Dedemli formation has high grade formation and the Mahmut Tepesi formation has high grade digenesis and anchizone degree. With increasing degree of diagenesis the smectite component of illites decreases. The illite/micas of the Kayabaşı formation are muscovitic and the illite/micas of the Mahmut Tepesi formation related to rifting are phenitic and seladonitic in composition among pre-rift units. The chondrite based distribution of trace and REEs contents in illites present a similar orientation for the Kayabaşı and Dedemli formations, but the amounts of these elements increase few in the Dedemli formation.

According to $\delta^{18}O$–δD isotopic change of illite minerals with increasing temperature, the isotopic composition of the water which forms these minerals are away from the sea water composition, but it is located between EMMW and the magmatic water compositions. This situation makes us consider that the diagenetic fluids forming illites mostly originated from the groundwater (diagenetic water or the formation water), and partly from magmatic water (volcanic-volcanosedimentary). According to $\delta^{18}O_{H2O}$-temperature relationship; when the water, forming the illite minerals, are completely assumed as the East Mediterranean Meteoric Water (EMMW) then low (<20 °C) temperature conditions; and when it is assumed as the magmatic water then high (>80 °C) temperature conditions are satisfied. Thus; these diagenetic conditions can be explained by the interaction (rock-water interaction) of meteoric waters with volcanic rocks. The isotope data show that the probable rifting effect caused a temperature difference reaching up to 30 °C in the formation illite, that is; the temperature increase also reflected to the isotope chemistry of illite.

In conclusion; clay and very few observed zeolite minerals in the Bozkır Unit was formed by the neoformation mechanism starting from fluids / solutions that occur as a result of decomposition of the volcanic material with sea water. The clay minerals in diagenesis and very low grade metamorphism conditions on the other hand; were re-ordered by the transformation mechanism with diagenetic solutions subjected to interaction with volcanogenic rocks. The textural, mineralogical and geochemical data of the Bozkır Unit rocks present significant differences based on the temperature increase related to rifting. It seems that the rifting has also affected the chemical compositions of minerals in addition to lithological differences and the degree of diagenesis / metamorphism.

Acknowledgements

This study was supported by the project numbered as M-477 by the Scientific Research Projects of the Cumhuriyet University. We would like to thank to technical staffs in the laboratories of the Geological Engineering Department for their helps during thin-section and XRD analyses, to Geol. Eng. Deniz Hozatlıoğlu (MS) for his contributions during field studies and to Prof. Fernando NIETO for his logistical and scientific supports in SEM-EDS analyses in the Laboratories of the Granada University in Spain within framework of Erasmus. Besides; we would like to express our gratitude to referees and editors for their invaluable scientific criticisms during the preparation of this paper.

References

Ahn, J., Peacor, D.R. 1985. Transmission electron microscopic study of diagenetic chlorite in Gulf Coast argillaceous sediments. *Clays and Clay Minerals*, 33, 228-236.

Alan, İ., Şahin, Ş., Keskin, H., Kop, A., Balcı, V., Böke, N., Bakırhan, B., Altun, İ., Esirtgen, T., Elibol, H., Arman, S., 2014. Orta Toroslar'da Hadim-Taşkent (Konya) yöresinde tektono-stratigrafik istiflerde yeni bulgular: Kartal Dağı istifi. *67. Türkiye Jeoloji Kurultayı*, 14-18 April 2014, 60-61.

Andrew, T., Robertson, A.F., 2002. The Beyşehir–Hoyran–Hadim Nappes: genesis and emplacement of Mesozoic marginal and oceanic units of the northern Neotethys in southern Turkey. *Journal of the Geological Society, London*, 159, 529–543.

April, R.H. 1980. Regularly interstratified chlorite/vermiculite in contact metamorphosed red beds, Newark Group, Connecticut Valley. *Clays and Clay Minerals*, 28, 1-11.

Arkai, P. 1991. Chlorite crystallinity: an empirical approach and correlation with illite crystallinity, coal rank and mineral facies as examplified by Palaeozoic and Mesozoic rocks of northeast Hungary. *Journal of Metamorphic Geology*, 9, 723-734.

Bailey, S.W. 1980. Structure of Layer Silicates. In: Crystal Structures of Clay Minerals and Their X-ray Identification, G.W. Brindley and G. Brown (Eds.), Mineralogical Society, London, 1-123.

Bailey, S.W. 1988. X-ray diffraction identification of the polytypes of mica, serpentine, and chlorite. *Clays and Clay Minerals*, 36, 193-213.

Bettison, L.A., Schiffman, P. 1988. Compositional and structural variations of phyllosilicates from the Point Sal ophiolite, California. *American Mineralogist*, 73, 62-76.

Blatter, C.L., Roberson, H.E., Thompson, G.R. 1973. Regularly interstratified chlorite-dioctahedral smectite in dike-intruded shales, Montana. *Clays and Clay Minerals*, 21, 207-212.

Blumenthal, M.M. 1944. Bozkır güneyinde Toros sıradağlarının serisi ve yapısı. İÜFF Mec., SeriB, 9, 95-125.

Blumenthal, M.M. 1947. Seydişehir-Beyşehir hinterlandındaki Toros Dağlarının jeolojisi. *Bulletin of Min. Res. And Exp.*, Seri D, 2, 242 p.

Blumenthal, M.M. 1951. Batı Toroslarda Alanya ard ülkesinde jeolojik araştırmalar. *Bulletin of Min. Res. And Exp.*, Seri D, 5, 194 p.

Blumenthal, M.M. 1956. Karaman Konya havzası güneybatısında Toros kenar silsilesi ve şist-radyolarit formasyonu stratigrafi meselesi. *Bulletin of Min. Res. And Exp.*, 48, 1-36.

Boles, J.R., Coombs, D.S. 1977. Zeolite facies alteration of sandstones in the Southland Syncline, New Zealand. *American Journal of Science*, 277, 982-1012.

Bozkaya, Ö., Yalçın, H. 1996. Diyajenez-metamorfizma geçişinin belirlenmesinde kullanılan yöntemler. *Jeoloji Mühendisliği Dergisi*, 49, 1-22.

Bozkaya, Ö., Yalçın, H. 1997*a*. Aygörmez Dağı napı (Pınarbaşı-Kayseri) Devoniyen-Triyas yaşlı diyajenetik-çok düşük dereceli meta-sedimanter kayaçların mineralojik ve petrografik özellikleri. Çukurova Üniversitesinde Jeoloji Mühendisliği Eğitiminin 20. Yılı Sempozyumu, *Geosound*, Special Edition, Vol. II, 30, 807-832.

Bozkaya, Ö., Yalçın, H. 1997*b*. Bolkardağı Birliği (Orta Toroslar, Bozkır-Konya) Üst Paleozoyik-Alt Mesozoyik yaşlı diyajenetik-çok düşük dereceli metamorfik kayaçların mineralojisi ve petrografisi. H.Ü. *Yerbilimleri*, Baysal Batman Special Issue, 19, 17-40.

Bozkaya, Ö., Yalçın, H. 1998. Doğu Toros Otoktonu Paleozoyik kayalarında gömülme ile ilişkili diyajenez ve çok düşük dereceli metamorfizma. Bulletin of Turkish Association of the Petroleum Geologists, 10, 35-54.

Bozkaya, Ö., Yalçın, H. 1999. Doğu Toros Otoktonunda diyajenez-metamorfizma derecesi ile fillosilikatların kimyası arasındaki ilişkiler. 9. Ulusal Kil Sempozyumu, İstanbul Üniversitesi, İstanbul, 15-18 Eylül, Abstracts, 21-30.

Bozkaya, Ö., Yalçın, H. 2000. Very low-grade metamorphism of Upper Paleozoic-Lower Mesozoic sedimentary rocks related to sedimentary burial and thrusting in Central Taurus Belt, Konya, Turkey. *International Geology Review*, 42, 353-367.

Bozkaya, Ö., Yalçın, H., Göncüoğlu, M.C. 2002. Mineralogic and organic responses to stratigraphic irregularities: an example from the Lower Paleozoic very low-grade metamorphic units of the Eastern Taurus Autochthon, Turkey. *Schweizerische Mineralogische und Petrographische Mitteilungen*, 82, 2, 355-373.

Bozkaya, Ö., Yalçın, H. 2004. New mineralogic data and implications for the tectono-metamorphic evolution of the Alanya Nappes, Central Tauride Belt, Turkey. *International Geology Review*, 46, 4, 347-365.

Bozkaya, Ö., Yalçın, H. 2005. Diagenesis and very low-grade metamorphism of the Antalya Unit: mineralogical evidence of Triassic rifting, Alanya-Gazipaşa, Central Taurus Belt, Turkey. Journal of Asian Earth Sciences, 25, 109-119.

Bozkaya, Ö., Yalçın, H. 2010. Geochemistry of mixed-layer illite-smectites from an extensional basin, Antalya Unit, Southwestern Turkey. *Clays and Clay Minerals*, 58, 644-666.

Bozkaya, Ö., Gürsu, S., Göncüoğlu, M.C. 2006*a*. Textural and mineralogical evidence for a Cadomian tectonothermal event in the eastern Mediterranean (Sandıklı-Afyon area, western Taurides, Turkey). *Gondwana Research*, 10, 301-315.

Bozkaya, Ö., Yalçın, H., Dündar, M.K. 2006*b*. Maden Grubu (Malatya-Pütürge) kayaçlarında diyajenez/metamorfizma ve jeotektonik konum arasındaki İlişkiler. C.Ü. *Mühendislik Fakültesi Dergisi Seri A-Yerbilimleri*, 23, 1-24.

Brigatti, M.F., Poppi, L. 1984. Crystal chemistry of corrensite: A review. *Clays and Clay Minerals*, 32, 391-399.

Brindley, G.W. 1980. Quantitative X-ray mineral analysis of clays. In: Crystal Structures of Clay Minerals and their X-ray Identification, G.W. Brindley and G. Brown (Eds.), Mineralogical Society, London, 411-438.

Brunn, J.H., Dumont, J.F., Graciansky, P.C., Gutnic, M., Juteau, T., Marcoux, J., Monod, O., Poisson, A. 1971. Outline of the Western Taurides. Geology and History of Turkey, Angus S. Compbelli (Ed.), Petroleum Exploration Society of Libya, Tripoli, 225-255.

Chang, H. K., Mackenzie, F. T., Schoonmaker, J. 1986. Comparisons between the diagenesis of dioctahedral and trioctahedral smectite, Brazilian offshore basins. *Clays and Clay Minerals*, 34, 407-423.

Clayton, R.N., Mayeda, T.K. 1963. The use of bromine pentafluoride in the extraction of oxygen from oxides and silicates for isotopic analysis. *Geochimica et Cosmochimica Acta*, 27, 43-52.

Condie, K.C. 1993. Chemical composition and evolution of the upper continental crust: Contrasting results from surface samples and shales. *Chemical Geology*, 104, 1-37.

Craig, H. 1961. Isotopic variations in meteoric waters. *Science*, 133, 1702-1703.

Çerikcioğlu, B., Yalçın, H. 1998. Yıldızeli-Akdağmadeni arasındaki (Yavu çevresi) Eosen yaşlı volkanojenik kayaçlarla ilişkili kil minerallerinin mineralojisi ve jeokimyası. C.Ü. *Mühendislik Fakültesi Dergisi Seri A-Yerbilimleri*, 15, 87-100.

Dunoyer de Segonzac, G. 1970. The transformation of clay minerals during diagenesis and low-grade metamorphism: A review. *Sedimentology*, 15, 281-346.

Eberl, D.D., Velde, B. 1989. Beyond the Kübler index. *Clay Minerals*, 24, 571-577.

Evarts, R.C., Schiffman, P. 1983. Submarine hydrothermal metamorphism of the Del Puerto Ophiolite, California. *American Journal of Science*, 283, 289-341.

Folk, R.L. 1974. Petrology of Sedimentary Rocks. Second edition, Hemphill Press, Austin, TX, 182 p.

Frey, M. 1987. Very low-grade metamorphism of clastic sedimentary rocks. In: Low Temperature Metamorphism, M. Frey (Ed.), Blackie, Glasgow and London, 9-58

Gat, J.R., Shemesh, A., Tziperman, E., Hecht, A., Georgopoulus, D., Basturk, O. 1996. The stable isotope composition of waters of the eastern Mediterranean Sea. *Journal of Geophysical Research*, 101, 6441–6451.

Gökdeniz, S. 1981. Recherches géologigues dans les Taurus Occidentales enter Karaman et Ermenek, Turquie. Les series a "tuffites vertes" Triasiques: Univérsite de Paris Sud, C.d'Orsay, These, 202 p.

Göncüoğlu, M.C. 2010. Türkiye Jeolojisine Giriş: Alpin ve Alpin Öncesi Tektonik Birliklerin Jeodinamik Evrimi. Maden Tetkik ve Arama Genel Müdürlüğü, Monografi Serisi No: 5, 69 p.

Göncüoğlu, M.C., Dirik, K., Kozlu, H. 1997. General Characteristics of pre-Alpine and Alpine Terranes in Turkey: Explanatory notes to the terrane map of Turkey. *Annales Geologique de Pays Hellenique*, 37, Geological Society of Greece, 515-536.

Graciansky, P.C. 1968. Teke Yarımadası (Likya) Torosları'nın üst üste gelmiş ünitelerinin stratigrafisi Dinaro-Toroslar'daki yeri. *Bulletin of Min. Res. and Exp.*, 71, 73-92.

Gromet, L.P., Dymek, R.F., Haskin, L.A., Korotev, R.L. 1984. The "North American shale composite": Its compilation, major and trace element characteristics. *Geochimica et Cosmochimica Acta*, 48, 2469-2482.

Guggenheim, S., Bain, D.C., Bergaya, F., Brigatty, M.F., Drits, A., Eberl, D.D., Formoso, M.L.L., Galan, E., Merriman, R.J., Peacor, D.R., Stanjek, H., Watanabe, T. 2002. Report of the AIPEA nomenclature committee for 2001: order, disorder and crystallinity in phyllosilicates and the use of the "Crystallinity Index". *Clay Minerals*, 37, 389-393.

Gutnic, M., Monod, O. 1970. Un série Mésozoique condansée dans les nappes du Taurus Occidentale, la seri edu Boyalı Tepe. C.R., Somm., *Société Géologique de France*, 5, 166-167.

Gutnic, M., Poisson, A., Dumont, J.F. 1979. Géologie des Taurides Occidentales (Turquie). Société Géologique de France, Nouvelle Série, Mémoire, 58, 112 p.

Haskin, L.A., Haskin, M.A., Frey, F.A., Wildeman, T.R. 1968. Relative and absolute terrestrial abundances of the rare earths. In: Origin and Distribution of the Elements, L.H.Ahrens (ed.). Pergamon Press, 889-912.

Hoffman, J., Hower, J. 1979. Clay mineral assemblages as low grade metamorphic geothermometers: Application to the thrust faulted disturbed belt of Montana, USA. In: Aspects of Diagenesis, P.A. Scholle and P.R. Schluger (eds.), Society of Economic Paleontologists Mineralogists Special Publication, 26, 55-79.

Hunziker, J.C., Frey, M., Clauer, N., Dallmeyer, R.D., Freidrischen, H., Flehmig, W., Hochstrasser, K., Roggwifler, P., Schwander, H. 1986. The evolution of illite to muscovite: Mineralogical and isotopic data from the Glarus Alps, Switzerland. Contributions to Mineralogy and Petrology, 92, 157 -180.

Inoue, A. 1985. Chemistry of corrensite: a trend in composition of trioctahedral chlorite/smectite during diagenesis. *Journal of College of Arts and Sciences*, Achiba University, B-18, 69-82.

Inoue, A. 1987. Conversion of smectite to chlorite by hydrothermal and diagenetic alterations, Hokuroku Kuroko mineralization area, Northeast Japan. Proc. of Int. Clay Conf., Denver. Eds. L.G. Schultz, H.van Olphen, F.A.Mumpton. The Clay Minerals Society, Bloomington, Indiana, 158-164.

Inoue, A., Utada, M., Nagata, H., Watanabe, T. 1984. Conversion of trioctahedral smectite to interstratified chlorite smectite in Pliocene acidic pyrclastic sediments of the Ohyu District, Akita Prefecture, Japan. *Clay Science*, 6, 103-116.

Inoue, A., Kohyama, N., Kitagawa, R., Watanabe, T. 1987. Chemical and morphological evidence for the conversion of smectite to illite. *Clays and Clay Minerals*, 35, 111-120.

Inoue, A., Utada, M. 1991. Smectite-to-chlorite transformation in thermally meta-morphosed volcanoclastic rocks in the Kamikita area, Northern Honshu, Japan. *American Mineralogist*, 76, 628-640.

J.C.P.D.S. (Joint Committee on Powder Diffraction Standards), 1990. Powder Diffraction File. Alphabetical Indexes Inorganic Phases. Swarthmore, United States of America, 871 p.

Kisch, H.J. 1980. Illite crystallinity and coal rank associated with lowest-grade metamorphism of the Taveyanne greywacke in the Helvetic zone of the Swiss Alps. *Eclogae Geologicae Helvetiae*, 73, 753-777.

Kisch, H.J. 1981. Coal rank and illite crystallinity associated with the zeolite facies of Southland and the pumpellyite-bearing facies of Otago, southern New Zealand. *N.Z.J. Geol. Geophys*., 24, 349-360.

Kübler B. 1968. Evaluation quantitative du métamorphisme par la cristallinité de l'illite. *Bulletin-Centre de Recherches Pau*-SNPA, 2, 385-397.

Kübler, B., Martini, J., Vuagnat, M. 1974. Very low grade metamorphism in the Western Alps. Schweiz. Mineral. Petrogr. Mitt. 54, 461-469.

Liou, J.G., Maruyama, S., Cho, M. 1987. Very low grade metamorphism of volcanic and volcanoclastic rocks-mineral assemblages and mineral facies. In Low Temperature Metamorphism. Ed. Frey, M., Blackie, Glasgow and London, 59-113.

Lippmann, F., Rothfuss, H. 1980. Tonminerale in Taveyannaz-Sandsteinen. *Schweizerische Mineralogische und Petrographische Mitteilungen*, 60, 1-29.

Marcoux, J. 1978. A scenario for the birth of a new oceanic realm: The Alpine Neotethys. Abstract, 10. International Congress on Sedimentology, Jerusalem, 2, 419-420.

Merriman R.J., Frey M. 1999. Patterns of very low-grade metamorphism in metapelitic rocks. In: Low Grade Metamorphism, M. Frey and D. Robinson (Eds.), Blackwell Sciences Ltd., Oxford, 61-107

Merriman R.J., Peacor D.R. 1999. Very low-grade metapelites: mineralogy, microfabrics and measuring reaction progress. In: Low Grade Metamorphism, M. Frey and D. Robinson (Eds.), Blackwell Sciences Ltd., Oxford, 10-60.

Merriman, R.J., Roberts, B., Peacor, D.R. 1990. A transmission electron microscopy study of white mica crystallite size distribution in a mudstone to slate transitional sequence, North Wales, UK. *Contributions to Mineralogy and Petrology*, 106, 27-44.

Monod, O. 1977. Recherches géologiques dans le Taurus occidental au sud de Beyşehir (Turquie). These, Université Paris-Sud, Orsay, 442 p.

M.T.A. (Maden Tetkik ve Arama), 2002. 1:500.000 scaled Geological Map of Turkey. *General Directorate of Mineral Research and Exploratio*n, Ankara.

O'Neil, J.R. 1986. Terminology and standards, In: Stable Isotopes in High Temperature Geological Processes, J.W. Valley, H.P. Taylor and J.R. O'Neil (Eds.), *Mineralogical Society of America*, Chelsea, 561-570.

Özgül, N. 1971. Orta Torosların kuzey kesiminin yapısal gelişiminde blok hareketlerinin önemi. *Bulletin of the Geological Society of Turkey*, 14, 75-87.

Özgül, N. 1976. Torosların bazı temel jeoloji özellikleri. *Türkiye Jeoloji Kurumu Bülteni*, 19, 65-78.

Özgül, N. 1984. Stratigraphy and tectonic evolution of the Central Taurides. International Symposium on the Geology of Taurus Belt, Ankara, O. Tekeli and M.C. Göncüoğlu (Eds.), 77-90,

Özgül, N. 1997. Bozkır-Hadim-Taşkent (Orta Toroslar'ın kuzey kesimi) dolaylarında yer alan tektono-stratigrafik birliklerin stratigrafisi. *Bull. of Min. Res. and Exp.*, 119, 117-174.

Özgül, N., Arpat, E. 1973. Structural units of the Taurus orogenic belt and their continuations in neighboring regions: Selection of papers on the Eastern Mediterranean region, presented at 23rd Congress of CIESM in Athens, 1972, Bulletin *of Geological Society of Greece*, 10, 156-164.

Pettijohn, F.J. 1975. Sedimentary Rocks. Harper and Row, New York, 628 p.

Savin, S.M., Lee, M. 1988. Isotopic studies of phyllosilicates. In: Bailey, S.W. (Ed.), Hydrous Phyllosilicates. Mineralogical Society of America, Washington, DC, Reviews in Mineralogy, 19, 189–223.

Schmid, R. 1981. Descriptive nomenclature and classification of pyroclastic deposits and fragments: Recommendations of the IUGS Subcommission on the Systematics of Igneous Rocks. *Geology*, 9, 41-43.

Sheppard, S.M.F. 1986. Characterization and isotopic variations in natural waters. In: Stable Isotopes in High-temperature Geological Processes, J.W. Valley, Jr H.P. Taylor and J. O'Neil (Eds.), Mineralogical Society of America, Washington DC, *Reviews in Mineralogy*, 16, 165-184

Sheppard, S.M.F., Gilg, H.A. 1996. Stable isotope geochemistry of clay minerals. *Clay Minerals*, 31, 1-24.

Sheppard, S.M.F., Nielsen, R.L., Taylor, H.P. Jr. 1969. Oxygen and hydrogen isotope ratios of clay minerals from porphyry copper deposits. *Economic Geology*, 64, 755-777.

Srodon, J. 1984. X-ray powder diffraction identification of illitic materials. *Clays and Clay Minerals*, 32, 337-349.

Streckeisen, A. 1978. Classification and nomenclature of volcanic rocks, lamprophyres, carbonatites and melilitic rocks. IUGS Subcommission on the Systematics of Igneous Rocks. Recommendations and Suggestions. *Neues Jahrbuch für Mineralogie*, Stutgart, Abhandlungen, 31, 1-14.

Sun, S.S., McDonough, W.F. 1989. Chemical and isotopic systematics of oceanic basalts; implications for mantle composition and processes. In: Magmatism in Ocean Basins, A.D. Saunders and M.J. Norry (Eds.), *Geological Society of London, Special Publication 42*, 359-362.

Taylor, H.P., Jr. 1968. The oxygen isotope geochemistry of igneous rocks. *Contribution to Mineralogy and Petrology*, 19, 1-71.

Vergo, N., April, R.H. 1982. Interstratified clay minerals in contact aureoles, West Rock, Connecticut. *Clays and Clay Minerals*, 30, 237-240.

Weaver, C.E., Pollard, L.D. 1973. The Chemistry of Clay Minerals. *Elsevier, Amsterdam, Developments in Sedimentology 15*, 213 p.

Wenner, D.B., Taylor, H.P.Jr. 1974. D/H and O^{18}/O^{16} studies of serpentinization of ultramafic rocks. *Geochimica et Cosmochimica Acta*, 38, 1255-1286

Yalçın, H., Gümüşer, G. 2000. Mineralogical and geochemical characteristics of of Late Cretaceous bentonite deposits at the north of Kelkit valley, Northern Turkey. *Clay Minerals*, 35, 5, 807-825.

Yalçın, H., Bozkaya, Ö. 2002. Hekimhan (Malatya) çevresindeki Üst Kretase yaşlı volkaniklerin alterasyon mineralojisi ve jeokimyası: denizsuyu-kayaç etkileşimine bir örnek. C.Ü. *Mühendislik Fakültesi Dergisi Seri A-Yerbilimleri*, 19, 81-98.

Yalçın, H., Bozkaya, Ö. 2003. Sivas Batısındaki (Yıldızeli-Akdağmadeni) hidrotermal kaolin ve I-S oluşumlarının mineralojisi ve jeokimyası. *Bulletin of Turkish Association of Geology*, 46, 1-23.

Yalçın, H., Bozkaya, Ö., Tetiker, S. 2005. Kangal kömür yatağının kil mineralojisi ve jeokimyası. 12nd National Clay Symposium, Yüzüncüyıl University, Van, 5-9 September, Abstracts, 16-31.

Yeh, H.-W. 1980. D/H ratios and late-stage dehydration of shales during burial. *Geochimica Cosmochimica Acta*, 44, 341-352.

Bull. Min. Res. Exp. (2016) 153:91-111

Bulletin of the Mineral Research and Exploration

http://bulletin.mta.gov.tr

TRACE FOSSILS FROM DEEP SEA SEDIMENTS OF THE LATE EOCENE CEYLAN FORMATION, GELİBOLU PENINSULA (SW THRACE, TURKEY)

Huriye Demircan[a*] and Alfred Uchman[b]

[a] *General Directorate of Mineral Research and Exploration, Department of Geological Research, 06520, Ankara, Turkey*
[b] *Institute of Geological Sciences, Jagiellonian University, Oleandry 2a; 30-063 Kraków, Poland*

Research Article

Keywords:
Turbidites, Basin Plain, Late Eocene, Graphoglyptids, Trace Fossils.

Received: 26.01.2016
Accepted: 11.04.2016

ABSTRACT

In this study, trace fossils of the Ceylan Formation (Late Eocene) in the area NW of Fındıklı village and on the coast of the Ece Bay the Gelibolu Peninsula are identified for the first time. They occur in gray siltstones and mudstones intercalated with thin-bedded, parallel and ripple laminated sandstones, which were deposited on a basin plain in proximilt of a slopes in the Thrace Basin. The Late Eocene Ceylan Formation includes pre-depositionl (*Belorhaphe zickzack*, *Desmograpton* isp., *Helicolithus ramosus, Helminthorhaphe flexuosa, Paleodictyon majus, Paleodictyon minimum, Paleodictyon strozzii, Saerichnites* isp., *Urohelminthoida appendiculata*) and post-depositional (*Phycosiphon incertum, Spongeliomorpha oraviense, Trichichnus* isp., *Planolites* isp., *Ophiomorpha* isp., *Ophiomorpha annulata, Scolicia* isp., *Scolicia prisca*, and *Thalassinoides* isp.) trace fossils. This trace fossil assemblage is typical of the *Nereites* ichnofacies (*Paleodictyon* ichnosubfacies), which characterize deep-sea, thin bedded turbididitic sediments oxygenated sea floor.

1. Introduction

The Ceylan Formation is a characteristic Late Eocene lithostratigraphic unit of the Thrace Basin in the study area is located in badlands NW of Fındıklı village and in the coastal cliffs of the Ece Bay (Figure 1A). These areas were studied mainly in terms of stratigraphy and regional geology (Ternek, 1949; Druit, 1961; Önem, 1974; Saltık, 1974; Saner, 1985; Sümengen et al., 1987; Önal, 1987; Şentürk and Karaköse, 1987; Siyako et al., 1989; Okay et al., 1990; Sümengen and Terlemez, 1991; Erol, 1992; Temel and Çiftçi, 2002; Kesgin and Varol, 2003), palaeontology (Sönmez-Gökçen, 1964, 1973; Gökçen, 1967, 1971, 1972; Tekkaya, 1973; Taner, 1977, 1981, 1983, 1994; Freels, 1980; Toker and Erkan, 1985; Ünal, 1996; Şafak, 1999; Tunoğlu and Ünal, 2001*a, b*). Very few papers refer to ichnology (Demircan, 2008; Demircan and Uchman, 2016).

In this paper, trace fossils of the Ceylan Formation are presented and interpreted in reference to palaeoenvironment.

2. General Geology and The Ceylan Formation

The Gelibolu Peninsula is built of pre-Cenozoic basement units which are unconformably overlaid by Eocene deposits (Figures 1A–C).

In the Gelibolu Peninsula, the pre Cenozoic basement consists of the pre-Maastrichtian ophiolitic complex settled in and Maastrichtian-Paleocene limestones. They are covered by the Lower Eocene deep-sea mudstones and sandstones of the Karaağaç Formation. Generally, this formation shows an increase in grain sizes and bedding thicknesses up the section. The the Karaağaç Formation is overlain conformably by the fluvial red beds of the Early-Middle Eocene Fıçıtepe Formation. It is covered unconformably by *nummulitic*-reefal limestones of the Middle Eocene Soğucak Formation, which is locally accompanied by sandstones and conglomerates. Above, the deep-sea Late Eocene Ceylan Formation is present. It is dominated by calcareous, massive mudstones intercalated by turbiditic sandstone-mudstone beds. Contribution of the turbiditic sandstones is higher in the part of the sections studied. The overlying Mezardere, Osmancık and Armutburnu

* *Corresponding Author: Huriye DEMİRCAN, e-mail: asmin68@yahoo.com.tr*
http://dx.doi.org/10.19111/bmre.04255

formations, with a transition from shales to nearshore sandstone-dominated facies of a deltaic complex mark a regression, which started at the beginning of Oligocene. An extensive volcanism (Hisarlıdağ-Ayvacık volcanics) predominated during Early-Middle Miocene in the region. Sedimentary deposition that developed during Late Miocene continued until the beginning of Early Pliocene.

The Gazhanedere, Kirazlı and Alçıtepe formations have been formed in this time period. The Pliocene-Quaternary Ergene Formation, which does not outcrop on the land was detected in drills and seismic sections carried out by TPAO. All these units in the study area have then been unconformably covered by Quaternary alluvia (Siyako et al., 1989).

The Ceylan Formation was named by Ünal (1967), with its type sections in Fındıklı-1 and Ece Bay-1 in which basin plain deposits were interpreted.

In the study area, the Ceylan Formation sediment succession begins with volcanic tuffs and grades up into calcareous, massive mudstones. The tuffs are subdivided into two part: thin bedded and massive tuffs. The thin bedded tuff consists of fine-grained volcanic groundmass which contain mud pieces,

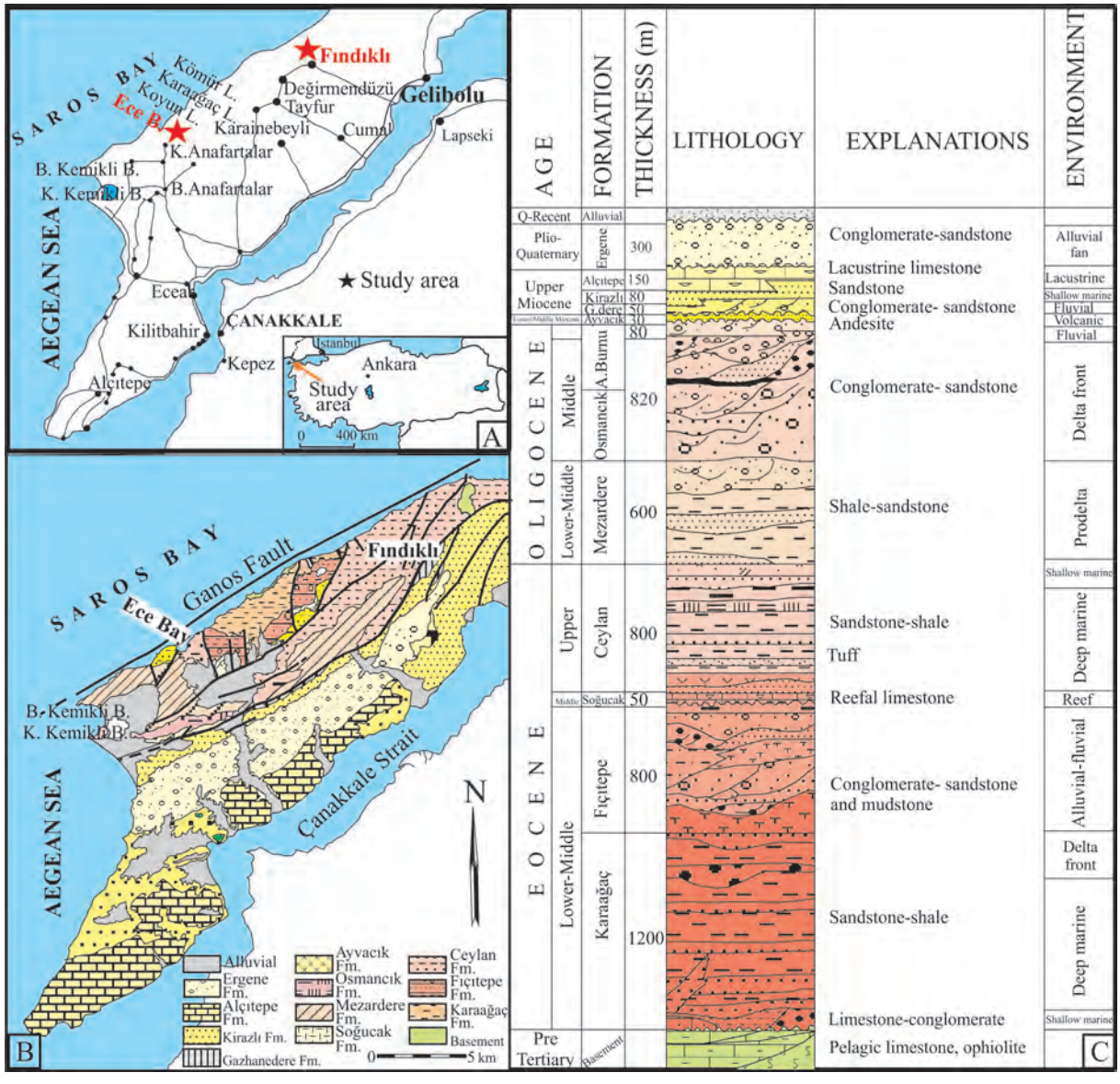

Figure 1- A) Location map of the study area. B) Geological map. C) Generalized stratigraphic column of the Gelibolu Peninsula (from Temel and Çiftçi, 2002).

pebble grains and volcanic rock fragments of various sizes. It passes gradually up into bedded and unbedded fine-grained tuffs. These tuffs also grade up into calcareous mudstones, which are rich in carbonates, structureless, and rarely interbedded by thin bedded, granular sandstone layers. The calcareous mudstones gradually pass up into gray massive mudstones, which contain vertical and horizontal trace fossils. In the lower and middle part, they contain intercalations of thin-bedded sandstones, which contribution increases up the section.

In average, The Ceylan Formation is 560 m thick, but it the thickness varies from 300 to 600 m depending on the geometry of the basin (Sümengen and Terlemez, 1991). The late Eocene age is based on *Pityosporites* spp., *Triletes* sp., *Echinatisporites* sp., *Batiacasphaera* sp., *Homotryblium plectilum, Diphyes colligerum, Deflandrea phosphoritica, Hystrichokolpoma* sp., *Ceistosphaeridium* sp., *Cordosphaeridium* sp., chitinous foraminiferal inner walls and the Hypae palynomorph assemblage obtained from the mudstone samples (Batı et al., 2002). The sandstone and shale dominated parts are referred to a deep sea turbiditic system (Kesgin and Varol, 2003).

3. The Studied Sections

3.1. The Fındıklı-1 section

Fındıklı-1 section is located in the NW part of the Gelibolu Peninsula, along the road between Fındıklı village and Kömür limanı (harbor) and gorges SW of the road (GPS coordinates: N40°26.866′; E026°31.700′; ±9 m). (Figures 1A, B).

The succession is formed by thin-bedded, fine-grained, turbiditic sandstone-siltstone beds intercalated with turbiditic and hemipelagic calcareous mudstones (Figure 2). The sandstones are parallel and ripple laminated. Lower bedding surfaces of the sandstone beds are rich in semi-reliefs of patterned, meandering, star- and net-shaped invertebrate trace fossils ascribed mainly to graphoglyptids.

The trace fossils include (from the bottom to the top) pre-depositional *Paleodictyon majus, Helminthorhaphe flexuosa, Urohelminthoida appendiculata, Belorhaphe zickzack, Phycosiphon incertum, Ophiomorpha annulata, Desmograpton* isp., *Saerichnites* isp. and post-depositional

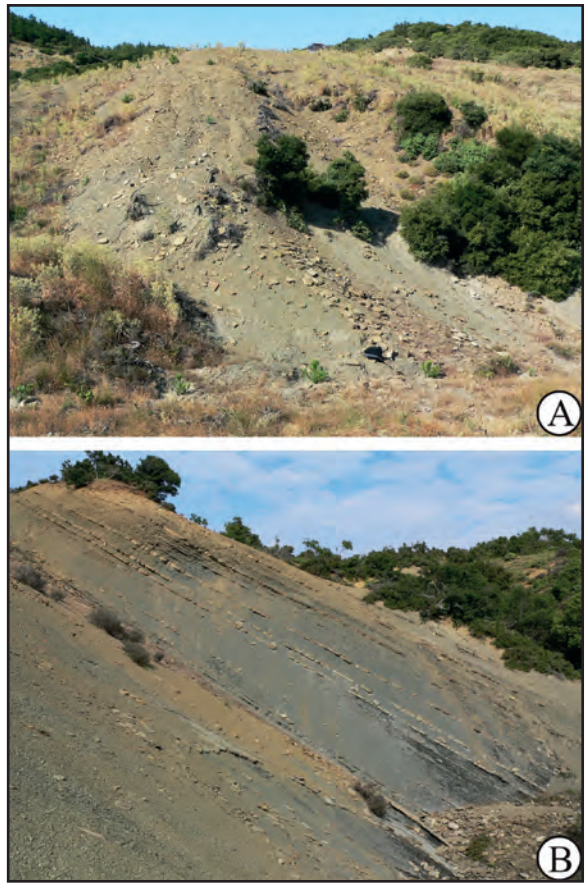

Figure 2- The Ceylan Formation in the Fındıklı-1 section. A) The outcrop with sandstones containing graphoglyptids of the Ceylan Formation (Fındıklı village). B) Thin-bedded sandstone intercalations in calcareous mudstones in the lower part of the gorge.

Spongeliomorpha oraviense and *Thalassinoides* isp., which occur on the lower bedding surfaces of the thin- and medium-bedded sandstone beds. Moreover, the trace fossils *Trichichnus* isp., *Phycosiphon incertum* are present in the gray mudstones (Figure 3).

3.2. The Ece Bay-1 section

The Ece Bay-1 (Ece Limanı-1) section is located in the cliffs of the Ece limanı coast, in the NW part of the Gelibolu Peninsula (GPS coordinates: N40°21.810′; E025°19.710′; ±9 m) (Figures 1-A, B).

The succession is formed by gray mudstone intercalated with thin-bedded, fine-grained sandstone beds (Figure 4). In the mudstones, *Trichichnus* isp., was recognized. The sandstone beds contain *Thalassinoides* isp., *Planolites* isp., *Ophiomorpha annulata*, *Scolicia* isp., *Scolicia prisca* (rare), *Helminthorhaphe flexuosa, Phycosiphon incertum* and *Helicolithus ramosus* (formerly known as *Punctorhaphe paralella*) (Figure 5).

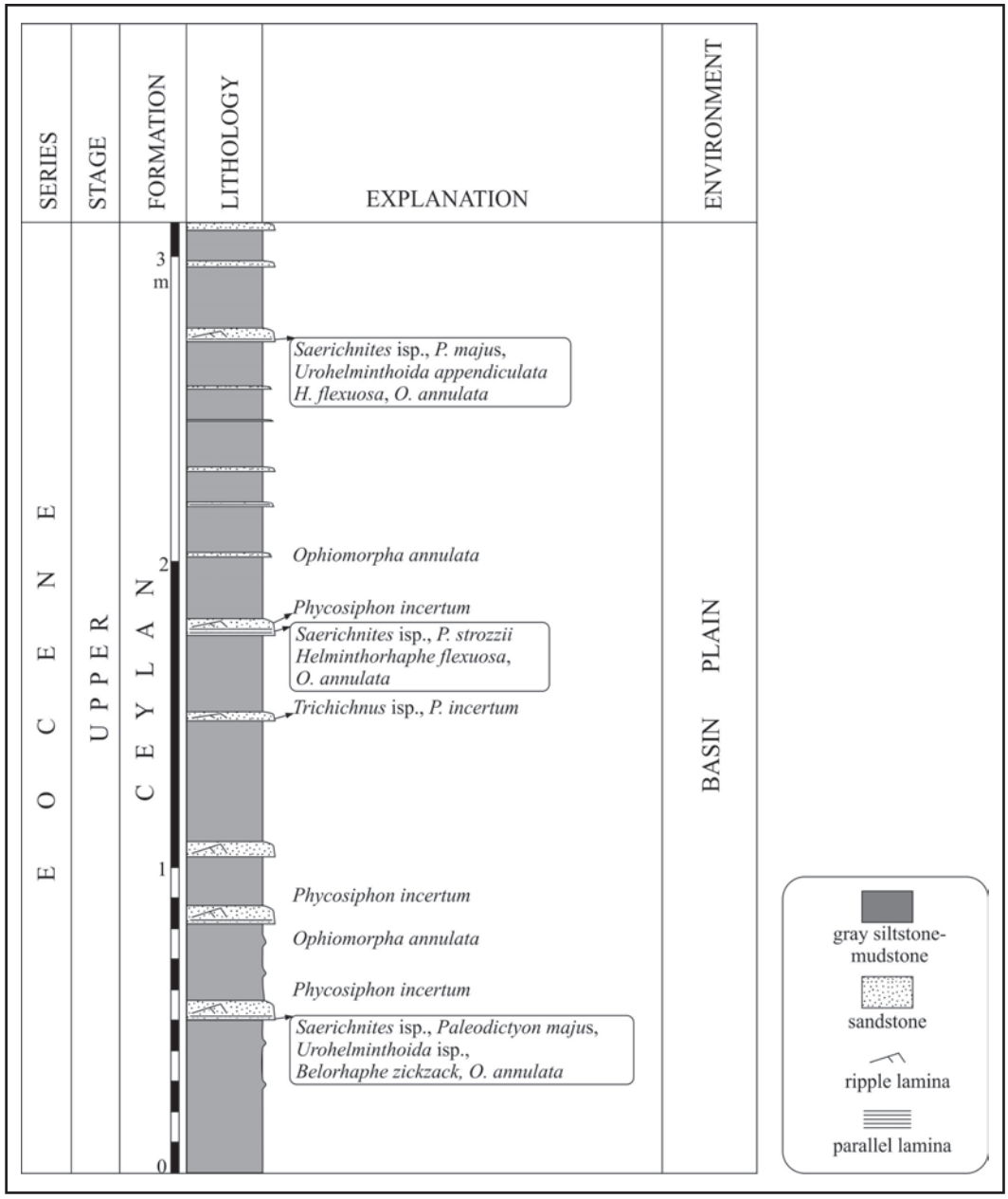

Figure 3- The Fındıklı-1 measured section with trace fossil distribution.

4. Trace Fossils

The section were studied "bed-by-bed", with registration of lithology and trace fossils, which were documented by photography, mostly in place.

Nineteen ichnotaxa are have been recognized in the study area. Their more extensive is in the monographs and papers by Häntzschel (1975), Książkiewicz (1977), Seilacher (1977), Fillion and Pickerill (1990), Crimes and Crossley (1991) and Uchman (1998).

4.1. Simple and Branching Structures

This group consists of mostly tubular, variable oriented structures, formed mainly by "worms" and "crustaceans" (e.g., Książkiewicz, 1977; Demircan and Toker, 2003).

***Planolites* Nicholson, 1879**

***Planolites* isp.**

Description: Horizontal, hypichnial, tubular structures, without wall, 2–4 mm in diameter.

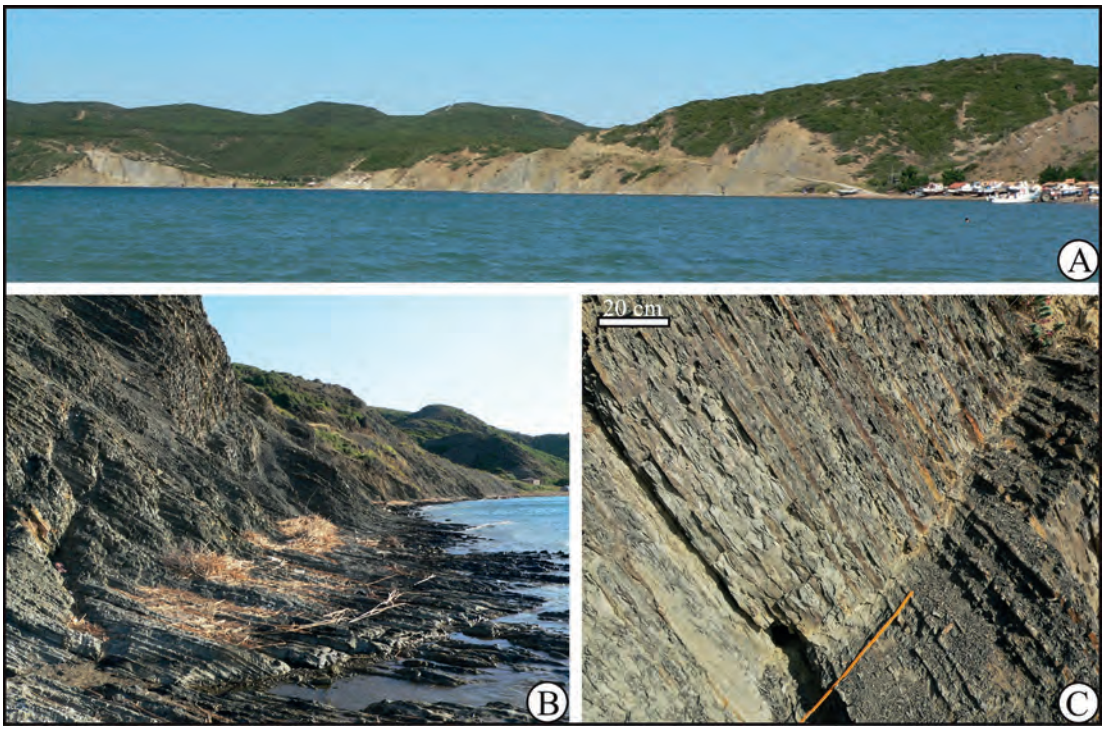

Figure 4- The Ceylan Formation in the Ece Bay-1 section A) General view of the Ceylan Formation outcrops along the Ece limanı coast. B, C) Intercalations of sandstone and siltstone beds in fine in mudstones.

Remarks: *Planolites* occurs in a great variety of facies and is formed mainly by deposit-feeding "worms" (Pemberton and Frey, 1982). It ranges from the Precambrian to the Recent (Häntzschel, 1975).

***Ophiomorpha* Lundgren, 1891**

***Ophiomorpha* isp.**

(Plate III, Figure B)

Description: Horizontal, hypichnial, tubular structures, with a wall, preserved in full relief, 8–9 mm in diameter, traced for a distance up to 60 mm.

Remarks: The described *Ophiomorpha* isp., resembles *Ophiomorpha rudis* Książkiewicz, 1977 (Uchman, 1991, 2009). *Ophiomorpha*, produced mainly by decapod crustaceans, can intergrade with *Thalassinoides, Spongeliomorpha* and *Gyrolithes* (e.g., Kennedy, 1967; Fürsich, 1973; Bromley and Frey, 1974; Kern and Warme, 1974.

***Ophiomorpha annulata* (Książkiewicz, 1977)**

(Plate I, Figure A)

Description: Mainly horizontal, tubular structure with a wall, 3.3 mm wide, observed on the distance up to 40 mm.

Remarks: This ichnospecies was described under *Granularia* Pomel or *Sabularia simplex* Książkiewicz, 1977) but it was included in *Ophiomorpha* (Uchman, 1995; Tunis and Uchman, 1996 *a*,*b*).

***Saerichnites* Billings, 1866**

***Saerichnites* isp.**

(Plate I, Figure B)

Description: A group of hypichnial hemispherical mounds, approximately 8.3 mm in diamneter.

Remarks: *Saerichnites* Billings, 1866 (see also Häntzschel, 1975) has then been interpreted by Uchman (1995) as casts of shafts connecting a burrow system with the sea floor.

***Spongeliomorpha oraviense* (Książkiewicz, 1977)**

(Plate I, Figure C)

Description: A short, tubular structure covered by oblique short ridges, about 10 mm in diameter.

Remarks: This trace fossil was described under *Halymenidium* by Książkiewicz (1977) and was included in *Spongeliomorpha* by (Uchman, 1998).

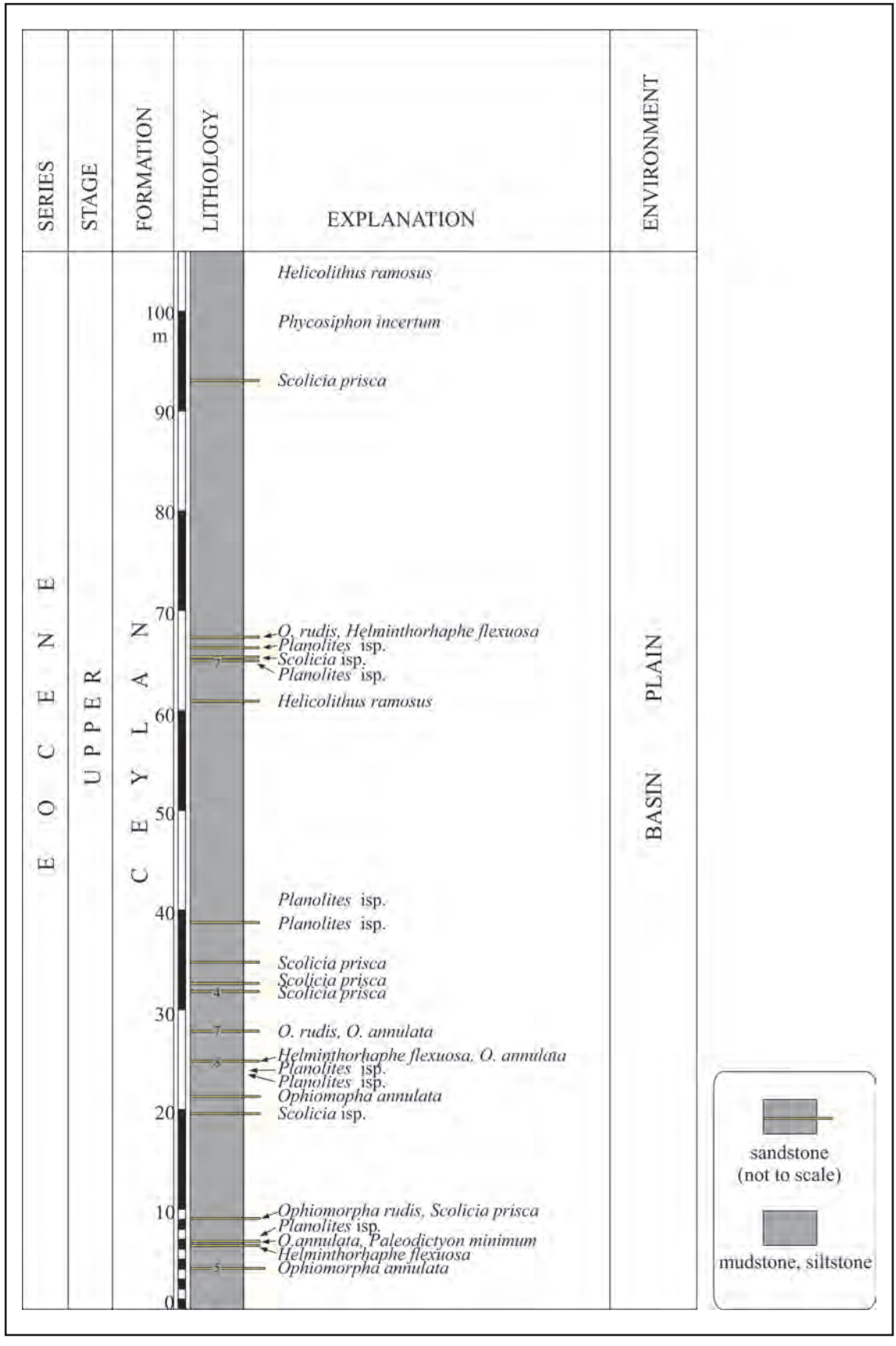

Figure 5- The Ece Limanı-1 measured section with distribution of trace fossils.

The ridges are interpreted as casts of scratch marks of crustaceans.

***Thalassinoides* Ehrenberg, 1944**

***Thalassinoides* isp.**

(Plate I, Figures D, E)

Description: Mostly horizontal, tubular, branched burrows, about 10 mm in diameter. They show Y- and T-shaped branches. They form three-dimensional burrow systems, which include shafts connecting the horizontal parts with the sediment surface.

Remarks: *Thalassinoides* is produced mainly by crustaceans, typically in shallow-marine environments, but also in the deep sea (Frey et al., 1984; Ekdale, 1992). According to Föllmi and Grimm (1990), the *Thalassinoides* crustacean tracemaker can survive transportation by turbiditic currents and make burrows even in anoxic conditions for a limited time. *Thalassinoides,* widely distributed in the Mesozoic and Cenozoic, occurs also in shallow-water sediments in the Paleozoic (e.g., Palmer, 1978; Archer and Maples, 1984; Sheehan and Schiefelbein, 1984; Stanistreet, 1989; Kulkov, 1991).

Large tubular burrow

(Plate I, Figure F)

Description: Horizontal, cylindrical structure, 27–30 mm in diameter, without branches.

Remarks: Usually, such large burrows are mainly formed by crustaceans in shallow-marine environments (Frey et al., 1984), but they can occur also in turbiditic systems (Uchman, 1991).

***Trichichnus* Frey, 1970**

***Trichichnus* isp.**

(Plate II, Figure A)

Description: Branched or unbranched, thread-like, cylindrical, straight or slightly winding structure, filled with pyrite or iron oxides, variable oriented, less than 1 mm in diameter.

Remarks: *Trichichnus*, formed by opportunistic organisms, was discussed by Fillion and Pickerill (1990) then by Uchman (1995, 1999). It is interpreted as a structure formed by sulphur bacteria in the transition between anoxic-dysoxic sediments (Kędzierski et al., 2015).

4.2. Winding and Meandering Structures

The studied trace fossils ascribed to this group include horizontal structures produced by irregular echinoids (*Scolicia*) and some graphoglyptids produced by small, unknown invertebrates.

***Scolicia* de Quatrefages, 1849**

***Scolicia* isp.**

(Plate II, Figure B)

Description: Hypichnial, trilobate, curved or meandering ridge, 25–30 mm wide.

Remarks: *Scolicia* is formed by irregular echinoids (Uchman, 1995) and ranges from Late Jurassic to Recent (Tchoumatchenco and Uchman, 2001).

***Scolicia prisca* de Quatrefages, 1849**

(Plate II, Figure C)

Description: Epichnial, trilobate, curved or meandering furrows, 15–25 mm wide and up to 3.5 mm deep. The middle lobe is convex up and 6 mm wide, covered with perpendicular ribs. The lateral lobes are covered by oblique ribs.

Remarks: This ichnospecies is formed by irregular echinoids at the transition between sandstone and mudstone within turbiditic beds (Uchman, 1995). It ranges from Late Jurassic to Recent (Tchoumatchenco and Uchman, 2001).

***Helminthorhaphe* Seilacher, 1977**

***Helminthorhaphe flexuosa* Uchman, 1995**

(Plate II, Figures D-E)

Description: Hypichnial meandering strings in fine-grained sandstones. The strings are 1.5-2 mm in diameter and the meanders are 55–60 mm deep and 2–3 mm wide, without bulges in the turns.

Remarks: This is graphoglyptid burrow produced by unknown worms, described also *Helminthorhaphe crassa* (see Seilacher, 1977).

***Helicolithus ramosus* (Vialov, 1971)**

(Plate II, Figure F; Plate III, Figure A)

Description: Hypichnial, tight meanders composed of aligned knobs, 0.8–1.0 mm in diameter, 1.5–2.0 mm.

Remarks: The aligned knobs are casts of shafts connecting spiral string arranged in meanders (Tunis & Uchman, 1996b). *Helicolithus ramosus* ranges from the Senonian (Książkiewicz, 1977) to the Miocene (D'Alessandro, 1980.

4.3. Branched Winding and Meandering Structures

***Belorhaphe* Fuchs, 1895**

***Belorhaphe zickzack* (Heer, 1877)**

(Plate III, Figure B)

Description: Hypichnial semi-relief zigzag meanders in fine grained turbiditic sandstones. The turning points of the zigzag are enlarged and are 5 mm wide. The zigzag turnsat the angle of approximately 50°. The string is 1.0–1.5 mm wide.

Remarks: *Belorhaphe zickzack* ranges from the Beriassian (Książkiewicz, 1977) to the Oligocene (Nowak, 1970) and occurs mainly in deep marine clastic sediments.

***Desmograpton* Fuchs, 1895**

***Desmograpton* isp.**

(Plate III, Figure C)

Description: Hypichnial rows parallel to sub-parallel ribs in fine grained turbiditic sandstones, preserved in semi-relief. The ribs are curved, their relief is semicircular od asymmetrically oval. The ribs are 5.5-6.0 mm, 1–1.5 mm wide.

Remarks: *Desmograpton* is a typical three dimensional graphoglyptid (Seilacher, 1977) showing a series of preservational variants (Uchman, 1995). It ranges from the Silurian (McCann, 1989, 1993) to the Miocene (D Alessandro, 1980; Uchman, 1995).

***Urohelminthoida* Sacco, 1888**

***Urohelminthoida appendiculata* (Heer, 1877)**

Description: Hypichnia meanders with protrusions in the turning points of the meanders, preserved in semi-relief in fine grained turbiditic sandstones. The string is undulating, 2 mm wide, and the meanders are 35-40 mm deep and 4 mm wide.

Remarks: This is a typical graphoglyptid (Seilacher, 1977; Uchman, 1995).

4.4. Networks Structures

***Paleodictyon majus* Meneghini in Peruzzi, 1880**

(Plate III, Figure E)

Description: Hypichnial hexagonal nets in fine-grained turbiditic sandstones. Meshes of the net are 6.0-7 mm wide and the string is 0.5 mm wide.

Remarks: This is common ichnospecies of *Paleodictyon* in Cenozoic turbidites (Książkiewicz, 1977). *Paleodictyon*, a typical graphoglyptid, is interpreted mainly as a farming structure (Seilacher, 1977), produced mostly in the deep-sea sediments, occasionally occurring in shelf sediments in the Paleozoic (Archer and Maples, 1984; Paczesnia, 1985) and in the Mesozoic (Häntzchel, 1964; Gierlowski-Kordesch and Ernst, 1987; Hantzpergue and Branger, 1992). *Paleodictyon* stratigraphically ranges from the Cambrian (Crimes and Anderson, 1985; Pacześna, 1985) to Recent (Ekdale, 1980; Miller, 1991).

***Paleodictyon minimum* (Sacco, 1888)**

Description: Hypichnial net composed of a string which is 0.25–0.3 mm wide and arranged in meshes which are1–2 mm wide.

Remarks: This ichnospecies is known mostly from Cenozoic turbidites (e.g.,Kindelan, 1919; Vialov & Golev, 1965).

***Paleodictyon strozzii* Meneghini in Savi & Meneghini, 1850**

(Plate III, Figures D, E)

Description: Hypichnial hexagonal nets in fine grained turbiditic sandstones. Their strings are 0.5–1.0 mm wide and the meshes are 3.6–4.5 mm wide .

Remarks: Individual meshes are of different size and can be elongated.

4.5. Spreite Structures

***Phycosiphon incertum* Fischer-Ooster, 1858**

(Plate III, Figure F)

Description: Small, horizontal lobes encircled by meandering marginal tunnel. The lobes are 1–3 mm wide and up to 10 mm long. The marginal tunnel is about 1 mm wide.

Remarks: *Phycosiphon incertum* is generally formed by sediment-feeders in the early stage of colonization of turbiditic fine-grained sediments (Wetzel and Uchman, 2001; Uchman et al,. 2004). For discussion of this trace fossil see Wetzel and Bromley (1994).

5. Discussion

Taking the morphological characteristics of the trace fossils into consideration, the determination of the trace fossil assemblages in the sections studied, composed of pre-depositional *Belorhaphe zickzack, Desmograpton* isp., *Helicolithus ramosus, Helminthorhaphe flexuosa*, *Paleodictyon majus, Paleodictyon minimum, Paleodictyon strozzii, Saerichnites* isp., *Urohelminthoida appendiculata* and post-depositional *Phycosiphon incertum, Planolites* isp., *Ophiomorpha* isp., *Ophiomorpha annulata, Scolicia* isp., *Scolicia prisca*, *Spongeliomorpha oraviense*, *Trichichnus* isp., and *Thalassinoides* isp. is typical of the *Nereites* ichnofacies; the high contribution of graphoglyptids points to the *Paleodictyon* ichnosubfacies, which is characteristic of thin-bedded sandy turbidites in different parts of depositional systems (Uchman & Wetzel, 2012). The turbidites studied formed in the basin plain or the lower slope, probably in fringes of small fans or isolated lobes. The trace fossils, especially these formed without permanent connection to the sea floor (*Planolites, Phycosiphon, Scolicia*), indicate good oxygenation in pore waters.

Acknowledgement

This study has been carried out within scope of the project "Güney Marmara Bölgesinde (Çanakkale-Armutlu Yarımadası-Balıkesir (GB Marmara)-Edremit Körfezi Arasında Kalan, Gelibolu Yarımadası) Yüzeyleyen Çökellerin İz Fosillere Dayalı Ortamsal Yorumu ve Paleoekolojik Değerlendirilmesi" (Environmental Interpretation and Paleoecological Assessment of Deposits Outcropping in the Southern Marmara Region (between Çanakkale (Dardanel)-Armutlu Peninsula (SW Marmara), Gelibolu Peninsula) based on Trace Fossils) coded as MTA 2012-30-14-08-4/2013-30-14-19.

References

Archer, A.W., Maples, C.G. 1984. Trace fossil distribution across a marine to nonmarine gradient in the Pennsylvanian of South Western Indiana. *Journal of Paleontology* 58, 448–466.

Batı, Z., Alişan, C., Ediger, V.Ş., Teymur, S., Akça, N., Sancay, H., Ertuğ, K., Kirici, S., Erenler, M., Aköz, Ö. 2002. Kuzey Trakya Havzası'nın Palinomorf, Foraminifer ve Nannoplankton Biyostratigrafisi. Trakya Litostratigrafi Birimleri Kitabı, *General Directorate of Mineral Research and Exploration.* 14.

Billings, E. 1866. Catalogues of the Silurian Fossils, 93, *Geological Survey of Canada, Dawson Brothers, Montreal.*

Bromley, R.G., Frey, R.W. 1974. Redescription of the trace fossil *Gyrolites* and taxonomic evaluation of *Thalassinoides, Ophiomorpha* and *Spongeliomorpha*: *Bulletin of the Geological Society of Denmark* 23, 311–335.

Crimes, T. P., Anderson, M. M. 1985. Trace fossils from Late Precambrian-Early Cambrian strata of southeastern Newfoundland (Canada): temporal and environmental implications. *Journal of Paleontology* 59, 310–343.

Crimes, T.P., Crossley, J.D. 1991. A diverse ichnofauna from Silurian flysch of the Aberystwyth Grits formation, Wales. *Geological Journal* 26, 27–64.

D'Alessandro, A. 1980. Prime osservacioni sulla ichnofauna miocenica della "formazione di Gorgolione" (Castelmezzano, Potenza). *Rivista Italiana di Paleontologia e Stratigrafia* 86, 357–398.

Demircan, H. 2008. Trace fossil associations and palaeoenvironmental interpretation of the late Eocene units (SW-Thrace). *Bulletin of the Mineral Research and Exploration* 136, 29–47.

Demircan, H., Toker, V. 2003. Trace fossils in the western fan of the Cingöz Formation in the northern Adana Basin (southern Turkey). *Bulletin of the Mineral Research and Exploration* 127, 15–32.

Demircan, H., Uchman, A. 2013*a*. Ichnological features of prodelta sediments from the Mezardere Formation (Late Eocene – Early Oligocene), Gökçeada Island, NW Turkey. Paper presented during conference: H. Demírcan (Ed.), XII. International ichnofabric workshop, 30th June– 5th July 2013, Çanakkale – Türkiye, Abstracts (pp. 24–25).

Demircan, H., Uchman, A. 2013*b*. 4th July 2013, Gökçeada Island. In H. Demírcan and A. Uchman (Eds.), Ichnological sites of the Gelibolu Peninsula and the Gökçeada Island, Thrace, NW Turkey. XII. International Ichnofabric Workshop, 30th June–5th July 2013, ÇanakkaleTürkiye. Field Guidebook (pp. 69–82).

Demircan, H., Uchman, A. 2016. Ichnology of prodelta deposits of the Mezardere Formation (late Eocene – early Oligocene) in the Gökçeada island, western Turkey. Geodinamica Acta 28, 86–100.

Druit, C. E. 1961. Report on the petroleum prospect of Thrace, Turkey: Turkish Gulf Oil Co. TPAO, Archive no: 1427 (unpublished).

Ekdale, A. A. 1980. Trace fossils in Deep Sea Drilling Project Leg 58 cores. *Initial Reports of Deep Sea Drilling Project.* 58, 601-605.

Ekdale A.A. 1992. Muckraking and mudslinging: the joys of deposit−feeding. In: C.G. Maples and R.R. West (eds) Trace fossils. Short Courses in Paleontology 5: 145–171. *The Paleontological Society,* Knoxville, Tennessee.

Erol, O. 1992. Çanakkale Yöresinin Jeomorfolojik ve Neotektonik Evrimi. *Bulletin of Turkish Association of Petroleum Geologists,* 4/1, 147–165.

Fillión, D., Pickerill, R. K. 1990. Ichnology of the Upper Cambrian? to Lower Ordovician Bell Island and Wabana groups of eastern Newfoundland, Canada. *Palaeontographica Canadiana* 7, 1–119.

Föllmi, K. B., Grimm, K. A. 1990. Doomed pioneers: Gravity-flow deposition and bioturbation in marine oxygen-deficient environments. *Geology* 18, 1069–1072.

Freels, D. 1980. Limnische Ostracoden aus Jungtertiar und Quaterder Turkei. *Geologisches* Jahrbuch, Reihe *B, Heft* 39, 172.

Frey, R. W., Curran, A.H., Pemberton, S.G. 1984. Trace making activities of crabs and their environmental significance: the ichnogenus *Psilonichnus. Journal of the Paleontology* 58, 511–528.

Fürsich, F. T. 1973. A revision of the trace fossils *Spongeliomorpha, Ophiomorpha* and *Thalassinoides*: *Neues Jahrbuch für Geologie und Paläontologie* Monatshefte, 1972, 719–735.

Gierlowski-Kordesch, E., Ernst, F., 1987. A flysch trace fossil assemblage from the Upper Cretaceous shelf of Tanzania: Mathies, G. and Schandelmeir, H., eds., Current Research in *African Earth Sciences, 14th Colloquium on African Geology,* Berlin, 18–22 August, 1987, p. 217–221.

Gökçen, S., L. 1967. Keşan Bölgesinde Eosen-Oligosen Sedimantasyonu, Güneybatı Türkiye Trakyası, *Bulletin Mineral and Research Exploration*, 69, 1–10.

Gökçen, S., L. 1971. Keşan Bölgesi Türbiditlerinde Sedimantasyon. *Hacettepe Fen ve Mühendislik Bilgileri Dergisi* 1, 1, 26–40.

Gökçen, S., L. 1972. Keşan Bölgesi Kumtaşlarının Yapısal, Dokusal Özellikleri ve Bölgenin Sedimanter Fasiyesleri. *Hacettepe Fen ve Mühendislik Bilgileri Dergisi*, 2, 1, 50–65.

Hantzpergue, P., Branger, P. 1992. L'ichnogenre *Paleodictyon* dans les depots neritiques de l'Oxfordien superieur NordAquitaine (France). *Geobios* 25, 195–205.

Häntzschel, W., 1964. Spurenfossilien und Problematica im Campan von Beckum (Westf.). Fortschritte in der *Geologie von Rheinland und Westfalen* 7, 295–308.

Häntzschel, W. 1975. Trace fossils and problematica. In: C. Teichert (ed.), Treatise on Invertebrate Paleontology. Part W, Miscellanea, Supplement I, W1–269. *Geological Society of America and University of Kansas Press,* Colorado, Boulder.

Kennedy, W.J. 1967. Burrows and surface traces from the Lower Chalk of southern England: *Bulletin of the British Museum (Natural History) Geology* 15, 127–167.

Kern, J.P., Warme, J. E. 1974. Trace fossils and bathymetry of the Upper Cretaceous Point Loma formation, San Diego, California. *Geological Society of America Bulletin* 85, 893–900.

Kędzierski, M., Uchman, A., Sawłowicz, Z. and Briguglio, A. 2015. Fossilized bioelectric wire – the trace fossil *Trichichnus*. *Biogeosciences* 12, 2301–2309. doi:10.5194/bg-12-2301-2015.

Kesgin, Y., Varol, B. 2003. Gökçeada ve Bozcaada' nın Tersiyer jeolojisi (Çanakkale), Türkiye. *Bulletin of Mineral Research Exploration,* 126, 49–67.

Kindelan, D.V. 1919. Nota sobre el Cretácico y el Eoceno de Güipozcoa, Espaňa: Inst. *Boletín del Instituto Geológico de Espaňa,* 20,165–198.

Książkiewicz, M. 1977. Trace fossils in the flysch of the Polish Carpathians. *Paleontologica Polonica* 36, 208.

Kulkov, N.P. 1991. The trace fossil *Thalassinoides* from the Upper Ordovician of Tuva: *Lethaia*, 24, 187–189.

McCann, T., 1989. The ichnogenus *Desmograpton* from the Silurian of Wales- first record from the Paleozoic. *Journal of Paleontology* 58, 950–953.

McCann, T., 1993. A *Nereites* ichnofacies from the Ordovician - Silurian Welsh Basin. *Ichnos* 3, 39–56.

Miller, M.F. 1991. Morphology and distribution of Paleozoic *Spirophyton* and *Zoophycos*: implications for the *Zoophycos* ichnofacies. *Palaios* 6, 410–425.

Nowak, W., 1970. Problematical organic traces of *Belorhaphe* and *Sinusites* in the Carpathian Lower Cretaceous and Paleogene flysch deposits. (In Polish, English summary). *Kwartalnik Geologiczny*, 14, 149–162.

Okay, İ. A., Siyako, M., Burkan, K. A. 1990. Biga Yarımadası' nın Jeolojisi ve Tektonik Evrimi. *Bulletin of Turkish Association of Petroleum Geologists,* 2/1, 83–121.

Önal, M., 1987. Gelibolu Yarımadası orta bölümünün çökelme istiflen ve tektoniği, KB Anadolu, Türkiye. *Yerbilimleri* 5, 21–38.

Önem, Y. 1974. Gelibolu ve Çanakkale dolaylarının jeolojisi. TPAO Report no: 877 (unpublished).

Pacześnia, J.I. 1985. Ichnorodzaj *Paleodictyon* ini z dolnego kambru Zbilutki (Góry Świętokrzyskie). *Kwartalnik Geologiczny* 29, 589–596

Palmer, T.J. 1978. Burrows at certain omission surfaces on the Middle Ordovician of the Upper Mississippi Valley. *Journal of Paleontology* 52, 109–117.

Pemberton, S. G., Frey, R. W. 1982. Trace fossil nomenclature and the *Planolites–Palaeophycus* dilemma. *Journal of Paleontology* 56, 843–881.

Saltık, O. 1974. Şarköy-Mürefte sahalarının jeolojisi ve Petrol olanakları: TPAO Raport no: 879, 30pp.

Saner, S. 1985. Saros Körfezi Dolayının Çökelme İstifleri ve Tektonik Yerleşimi, Kuzeydoğu Ege Denizi, *Geological Bulletin of Turkey* 28/l, 1–10.

Seilacher, A. 1977. Pattern analysis of *Paleodictyon* and related trace fossils: Crimes, T. P. &Harper, J. C. eds., Trace fossils 2. Geological Journal, *Special Issue* 9, 289–334.

Sheehan, P.M., Schiefelbein, J.D.R., 1984. The trace fossil *Thalassinoides* from the Upper Ordovician of the eastern Great Basin: deep Burrowing in the Early Paleozoic. *Journal of Paleontology* 58, 440–447.

Siyako, M., Burkan, K.A., Okay A.I. 1989. Biga ve Gelibolu Yarımadaları Tersiyer Jeolojisi ve Hidrokarbon olanakları: *Turkish Association of Petroleum Geologist Bulletin* 1, 183–199.

Sönmez-Gökçen, N. 1964. Notice sur le novvel age determine par les Ostracodes de la şerre a Congeria du Neogene des environs de Çatalca (Thrace). *Bulletin of Mineral Research Exploration,* 63, 47–58.

Sönmez-Gökçen, N. 1973. Etüde Paleontolowgique (Ostracodes) et Stratigraphique de nive aux du Paleogene du subest dela Thrace, Publ. D'Etud. *Bulletin of Mineral Research Exploration,* 147, 12.

Stanistreet, I.O. 1989. Trace fossil association related to facies of an Upper Ordovician low wave energy shoreface and shelf, Oslo – Asker district, Norway. *Lethaia* 22, 345–357.

Sümengen, M., Terlemez, İ., Şentürk., Karaköse, C., Erkan, E., Ünay, E., Gürbüz, M., Atalay, Z. 1987. Gelibolu Yarımadası ve GB Trakya Tersiyer havzasının stratigrafisi, sedimantolojisi ve tektoniği. General Directorate of Mineral Research and Exploration, *Report* No: 8218, (unpublished).

Sümengen, M., Terlemez, İ. 1991. Güneybatı Trakya Yöresi Eosen çökelleri Stratigrafisi. *Bulletin of Mineral Research Exploration,* 113, 17–30.

Şafak, Ü. 1999. Recent ostracoda assemblage of the Gökçeada - Bozcaada - Çanakkale Region, Yerbilimleri (Geosound), 4 th European Ostracodologists Meeting, 35, 149-172, Adana.

Şentürk, K., Karaköse, C. 1987. Çanakkale Boğazı ve Dolayının Jeolojisi. *General Directorate of Mineral Research and Exploration* Report No: 9333. (unpublished).

Taner, G. 1977. Gelibolu Yarımadası Neojen Formasyonları ile Baküniyen Molluska Faunasının İncelemesi, Ankara University, Doçentlik tezi, 66. (unpublished).

Taner, G. 1981. Gelibolu Yarımadası 'nın Denizel Kuvaterner Molluskaları, Die meerequatare mollusken der Halbinsel-Gelibolu. *Jeomorfoloji Dergisi* 10, 71–116.

Taner, G. 1983. Hamzaköy Formasyonu' nun Çavda (Baküniyen) Bivalvleri, Gelibolu Yarımadası. *Geological Bulletin of Turkey* 26, 59– 64.

Taner, G. 1994. Mollusk kavkılarında 8016/ 5018 izotopu araştırma metodu ile Çanakkale Boğazı'nın Romaniyen-Baküniyen çağma ait paleosıcaklık bulguları. *47. Türkiye Jeoloji Kurumu Bildiri Özleri Kitabı*, 12, 13

Tchoumatchenco, P., Uchman, A. 2001. The oldest deep-sea *Ophiomorpha* and *Scolicia* and associated trace fossils from the Upper Jurassic - Lower Cretaceous deep-water turbidite deposits of SW Bulgaria. *Palaeogeography, Palaeoclimatology, Palaeoecology* 169(1- 2), 85–99.

Tekkaya, İ. 1973. Çanakkale güneydoğusundaki Bayraktepe omurgalı faunası hakkında ön bildiri (proceeding). *Bulletin of Mineral Research Exploration*, 81,191-194.

Temel, R. Ö., Çiftçi, N. B. 2002. Gelibolu Yarımadası, Gökçeada ve Bozcaada Tersiyer çökellerinin stratigrafisi ve ortamsal özellikleri. *Bulletin of Turkish Association of Petroleum Geologists* 14, 17–40.

Ternek, Z. 1949. Keşan – Korudağ Bölgesinin Jeolojisi. İstanbul Üniversitesi Fen Fakültesi, Doktora Tezi, 79. (unpublished).

Toker, V., Erkan, E. 1985. Gelibolu yarımadası Eosen formasyonları nannoplankton biyostratigrafisi. *Bulletin of Mineral Research Exploration*, 101–102, 68–72.

Tunis, G., Uchman, A., 1996*a*. Trace fossils and facies changes in the Upper Cretaceous-Middle Eocene flysch deposits of the Julian Prealps, (Italy and Slovenia): consequences of regional and world-wide changes. *Ichnos* 4, 169–190.

Tunis, G., Uchman, A. 1996*b*. Ichnology of the Eocene flysch deposits in the Istria peninsula, Croatia and Slovenia. *Ichnos* 5, 1–22.

Tunoğlu, C., Ünal, A. 2001*a*. Biyostratigraphy and chronostratigraphy of Pannonian-Pontian sequence of Gelibolu Paninsula, NW Turkey. *Geological Bulletin of Turkey* 44, 1, 15–25.

Tunoğlu, C., Ünal, A., 2001*b*. Pannonian-Pontian ostracoda fauna of Gelibolu Neogene Basin (NW Turkey). *Hacettepe Üniversitesi Yerbilimleri Dergisi* 23, 167–187.

Uchman, A.1991. ''Shallow Water'' trace fossils in Palaeogene flysch of the southern part of the Magura Nappe, Polish Outer Carpathians. *Annales Societatis Geologorum Poloniae* 61, 61–75.

Uchman, A. 1995. Taxonomy and palaeoecology of flysch trace fossils: The Marnoso-arenacea Formation and associated facies (Miocene, Northern Apennines, Italy). *Beringeria* 15, 1–115.

Uchman, A. 1998. Taxonomy and ethology of flysch trace fossils: A revision of the Marian Książkiewicz collection and studies of complementary material. *Annales Societatis Geologorum Poloniae* 68, 105–218.

Uchman, A. 1999. Ichnology of the Rhenodanubian flysch (Lower Cretaceous-Eocene) in Austria and Germany. *Beringeria 25*, 65–171.

Uchman, A. 2009. The *Ophiomorpha rudis* ichnosubfacies of the Nereites ichnofacies: characteristics and constraints. *Palaeogeography, Palaeoclimatology, Palaeoecology* 276, 107–119.

Uchman, A., Drygant, D., Paszkowski, M., Porębski, S. J., Turnau, E. 2004. Early Devonian trace fossils in marine to non-marine redbeds in Podolia, Ukraine: palaeoenvironmental implications. *Palaeogeography, Palaeoclimatology, Palaeoecology* 214, 67–83.

Uchman, A., Wetzel, A. 2012. Deep-sea fans. In: Bromley, R.G. & Knaust, D. (Eds.), Trace Fossils as Indicators of Sedimentary Environments. *Developments in Sedimentology* 64, 643–671. Elsevier, Amsterdam.

Ünal, A. 1996. Gelibolu Yarımadası Neojen Ostrakod Biyostratigrafisi, MSc Thesis. *Hacettepe University, Institute of Science* 160 pp. (unpublished).

Ünal, O. T. 1967. l. Bölge (Marmara) Trakya Jeoloji ve petrol imkânları. *Turkish Petroleum Corporation Archive* No; 391.

Vialov, O. S., Golev, B. T. 1965. O drobnom podrazdieleni gruppy Paleodictyonidae. Byulletin Moskovskovo Obshczhestva Ispityvania Prirody. *Odtiel Gieologii* 40, 93–114.

Wetzel, A., Bromley, R.G. 1994. *Phycosiphon incertum* revisited: *Anconichnus* horizontalis is junior subjective synonym. *Journal of Paleontology* 68, 1396–1402.

Wetzel, A., Uchman, A., 2001. Sequential colonization of muddy turbidites: examples from Eocene Beloveža Formation, Carpathians, Poland. *Palaeogeography, Palaeoclimatology, Palaeoecology* 168, 171–186.

PLATE

PLATE - I

A - *Ophiomorpha annulata*

Hypichnial full reliefs in a fine grained turbiditic sandstone bed (Fındıklı-1 section).

B - *Saerichnites* isp.

Hypichnial semi-reliefs in a fine-grained turbiditic sandstone bed (Fındıklı-1 section).

C - *Spongeliomorpha oraviense*

Hypichnial full relief in a fin-grained turbiditic sandstone bed (Fındıklı-1 section).

D, E - *Thalassinoides* isp.

Hypichnial full reliefs in a fine-grained turbiditic sandstone bed (Ece Bay-1 section).

F - Large tubular burrow

Hypichnial full relief in fine-grained turbiditic sandstone bed (Ece Bay-1 section).

PLATE I

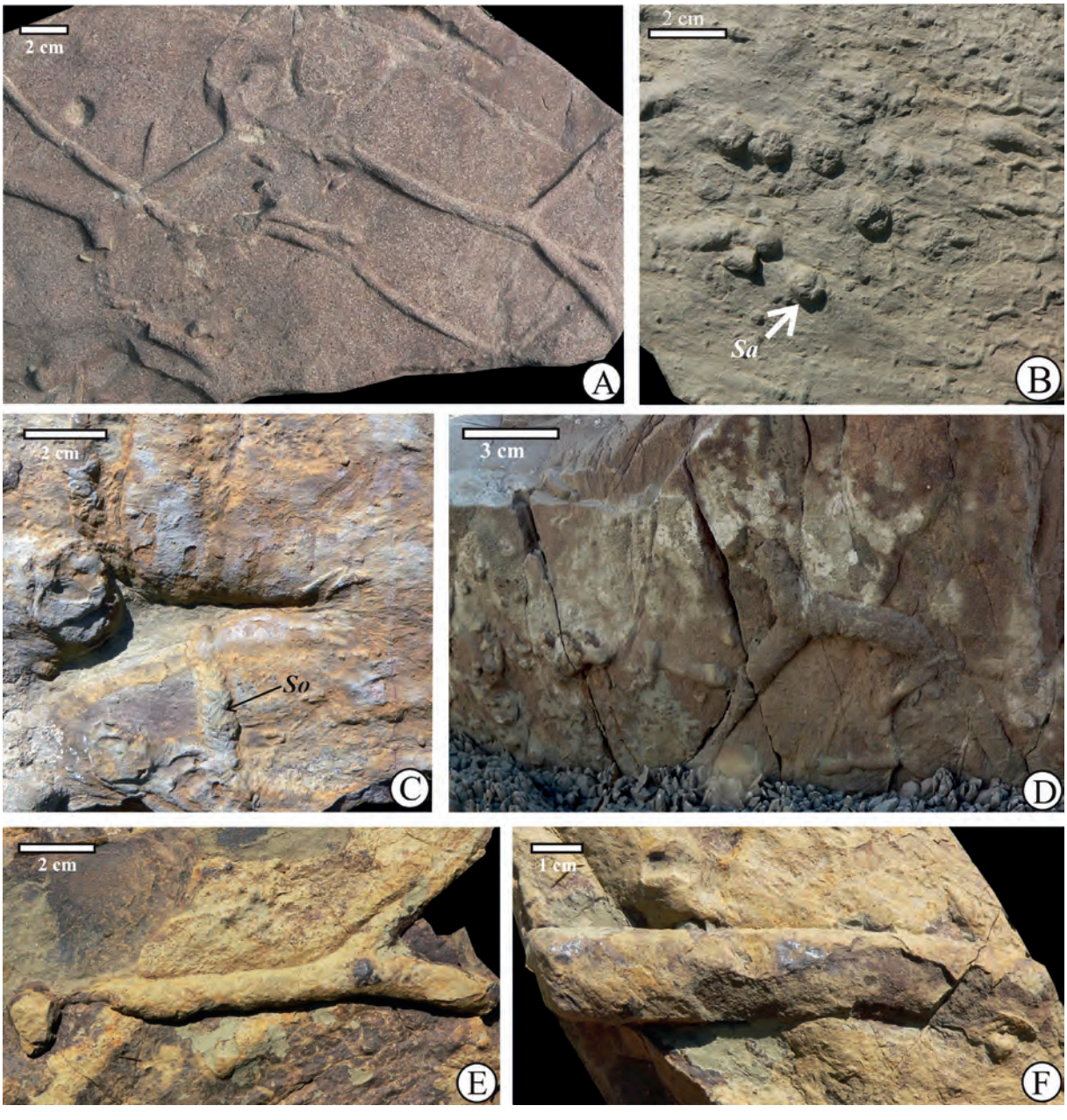

PLATE – II

A - *Trichichnus* isp.

Endichnial full relief in calcareous mudstone (Ece Bay-1 section).

B - *Scolicia* isp.

Hypichnial full relief in a fine-grained turbiditic sandstone bed (Ece Bay-1 section).

C - *Scolicia prisca*

Originally, full relief; its lower part is seen at the top of a turbiditic sandstone bed (Ece Bay-1 section).

D, E - *Helminthorhaphe flexuosa*

Hypichnial semi-relief in a fine-grained turbiditic sandstone bed (Ece Bay-1 section).

F - *Helicolithus ramosus*

Hypichnial semi-relief in a fine-grained turbiditic sandstone bed (Ece Bay-1 section).

PLATE II

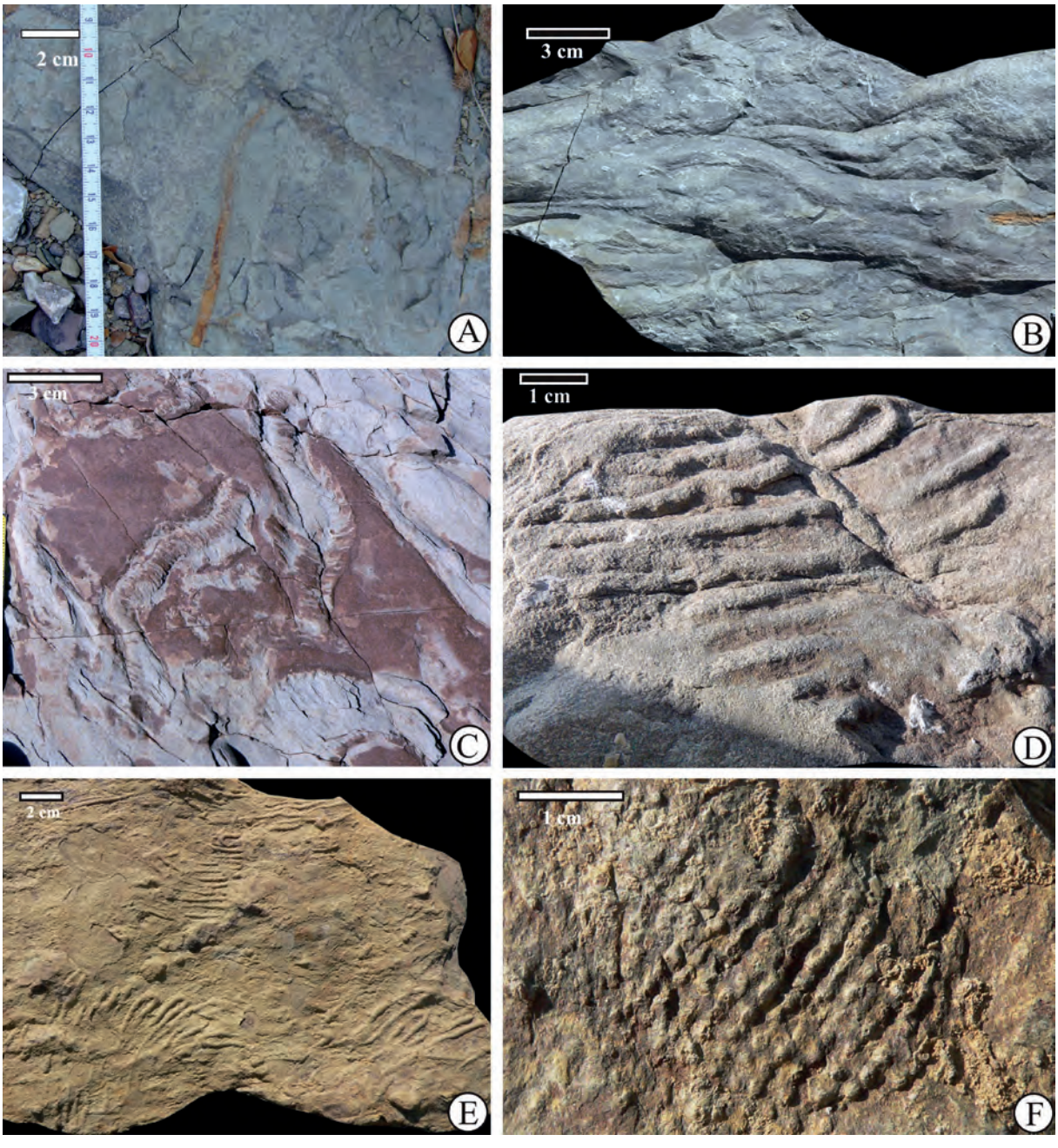

PLATE - III

A - *Helicolithus ramosus*

Hypichnial semi-relief in a fine-grained turbiditic sandstone bed (Ece Bay-1 section).

B - *Belorhaphe zickzack* and *Ophiomorpha* isp.

Hypichnial semi-relief (*Belorhaphe*) and hypichnial full relief (*Ophiomorpha*) in a fine-grained turbiditic sandstone bed (Fındıklı-1 section).

C - *Desmograpton* isp.

Hypichnial semi-relief in a fine-grained turbiditic sandstone bed (Fındıklı-1 section).

D - *Paleodictyon strozzii*

Hypichnial semi-relief in a fine-grained turbiditic sandstone bed (Fındıklı-1 section).

D - *Paleodictyon strozzii* and *Paleodictyon majus*

Hypichnial semi-reliefs in a fine-grained turbiditic sandstone bed (Fındıklı-1 section).

F - *Phycosiphon incertum*

Endichnial full relief in a fine grained turbiditic sandstone bed (Fındıklı-1 section).

PLATE III

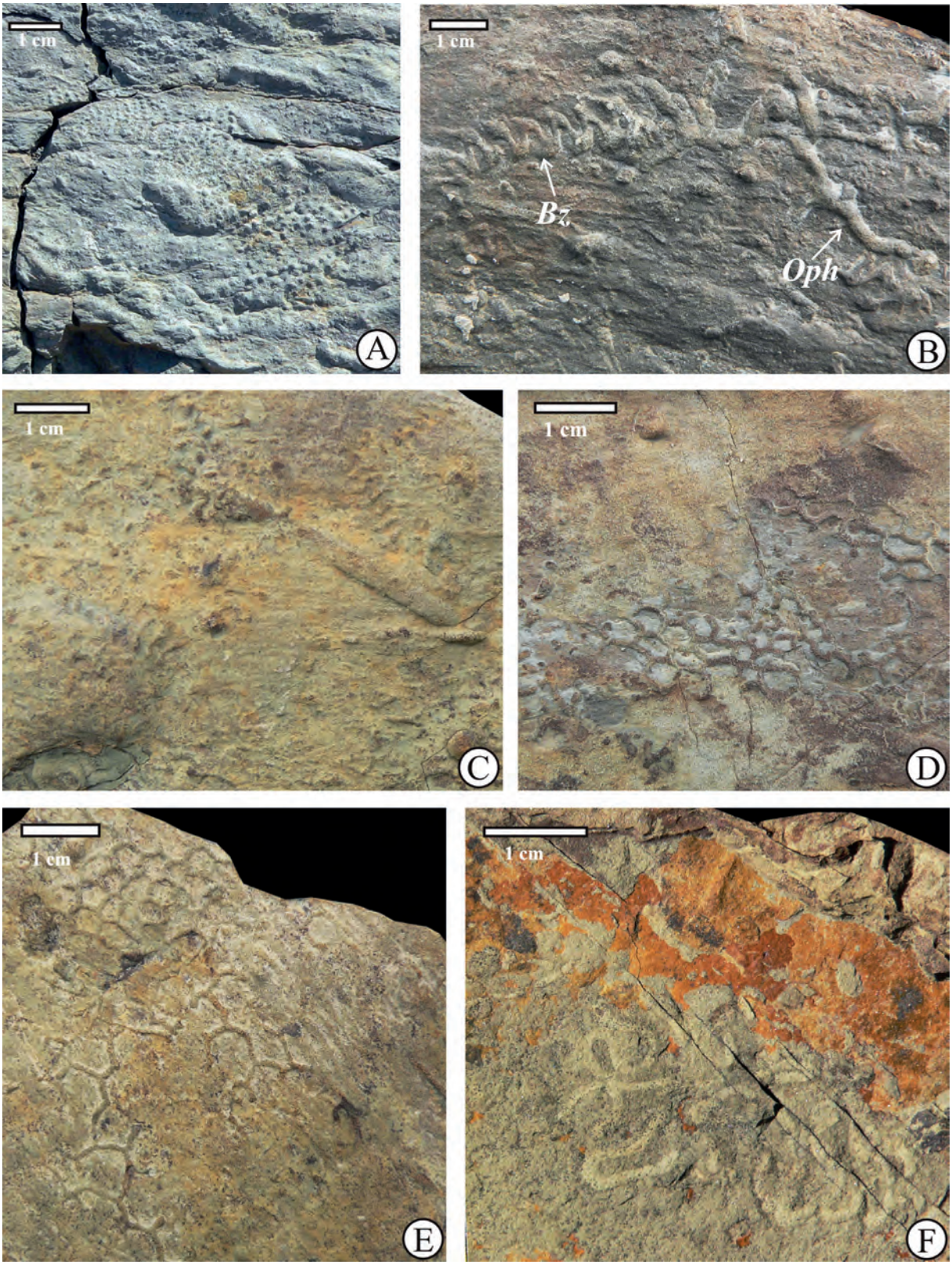

Bull. Min. Res. Exp. (2016) 153:113-137

Bulletin of the Mineral Research and Exploration

http://bulletin.mta.gov.tr

OSTRACOD FAUNA AND ENVIRONMENTAL CHARACTERISTICS OF KÖPRÜKÖY / ERZURUM (EAST ANATOLIA) REGION

Ümit ŞAFAK[a*] and Meral KAYA[b]

[a] *Çukurova University, Department of Geological Engineering, TR-01330 Adana*
[b] *Atatürk University, Department of Geological Engineering, 25030 Erzurum*

Research Article

Keywords:
Erzurum/East Anatolia, Ostracoda, Paleoenvironment, Late Miocene- Pliocene

ABSTRACT

The study was carried out within the Horasan Formation around Köprüköy located east of Erzurum. This formation outcrops in the region of Erzurum-Pasinler-Horasan forming the northernmost outcrop of neo-tectonic sediments in Eastern Anatolia. The unit is composed of pebble stones, clays and marl iterations. Ostracod, gastropod and pelecypod species are observed in the levels of clay stone with soft clasts and marl in the area. Generally, ostracod species which are unique to the Ponto-Caspian basin were described in these units within the scope of the study. These are ostracod species such as *Amnicythere idonea* Mandelstam, Markova, Rozyeva and Stepanajtys, *Candona (Caspiocypris) erzurumensis* Freels, *Candona* (*Caspiocypris*) *araxica* Freels, *Candona* (*Caspiocypris)* aff. *alta* (Zalanyi), *Candona (Lineocypris)* aff. *granulosa* Zalanyi, *Bakunella* cf. *dorsoarcuata* (Zalanyi), *Bakunella* cf. *subtriangularis* (Sveyer), *Candona* (*Candona*) *lycica* Freels, *Candona* (*Candona*) *armenia* Freels, *Candona* (*Candona*) aff. *elongata* (Svejer), and *Fossilyocypris sarızensis* (Şafak, Nazik and Şenol). There are also micro mollusk species such as *Gyraulus inornatus* and *Dreissena polymorpha* present in the sequence. Among these genera; *Candona* (*Candona*) is found in fresh water; *Candona (Caspiocypris), Candona (Lineocypris),* and *Fossilyocypris* indicate fresh - brackish water (oligohaline), *Bakunella* rarely characterizes fresh water but mostly brackish water, *Amnicythere* characterizes brackish water, and *Gyraulus, Dreissena* characterizes fresh water conditions. The ostracod fauna determined in this study indicates an age interval of Late Miocene-Pliocene for the formation and clearly supports previous studies in terms of age and environmental correlations.

Received: 07.10.2015
Accepted: 17.02.2016

1. Introduction

The study area is located east of Erzurum in the area surrounding Köprüköy (Figure 1).

The study area and close surroundings have been studied by many researchers. Arni (1939), Pamir and Baykal (1943), Erinç (1953), Erentöz (1954), Rathur (1965), Akkuş (1965), Acar (1975), Atalay (1978), Tokel (1979), Soytürk (1973), Gedik (1985), Yılmaz et al. (1988), Bozkuş (1990,1993,1998,1999), Arbaş et al. (1991), Şengüler and Toprak (1991), Tarhan (1989,1991), Gevrek and Şengüler (1992), Keskin (1994, 1998), Yılmaz (1997), Bozkuş (1990, 1993, 1998), Dağıstan (2001), Öner et al. (2006), Konak and Hakyemez (2008), Kibaroğlu et al. (2011) and Kalkan et al. (2012) investigated the general geology and volcanism. Stratigraphy-sedimentology studies were completed by Demirtaşlı et al. (1965), and Gürbüz and Gülbaş (1999). Tokel (1984), Erdoğan (1967), Özcan (1967), Şengör and Kidd (1979), Şengör (1980), Yılmaz and Şener (1984), Şaroğlu (1986), Şaroğlu and Yılmaz (1984), Koçyiğit (1985), Barka et al. (1987), Bayraktutan et al. (1996), Bayraktutan (1999), Bozkuş (1999), Beer et al. (2003), Keskin (2005), and Gelişli and Maden (2006) studied tectonics and magmatism. Paleontology was studied by Şafak (2013) and Vasilyan et al. (2014). This study determines the genus and species of ostracods and micro mollusks taken from measured sections in the Erzurum–Köprüköy region and provides new assessment of paleoenvironmental conditions.

2. Material and Method

The study material was retrieved from 25 washed samples taken from measured sections in the Erzurum-Köprüköy area. The samples obtained from two measured sections by Kaya in 2013-2014 underwent a washing procedure, were dated based on ostracod

* *Corresponding Author: Ümit ŞAFAK, Email: usafak@cu.edu.tr*
http://dx.doi.org/10.19111/bulletinofmre.266057

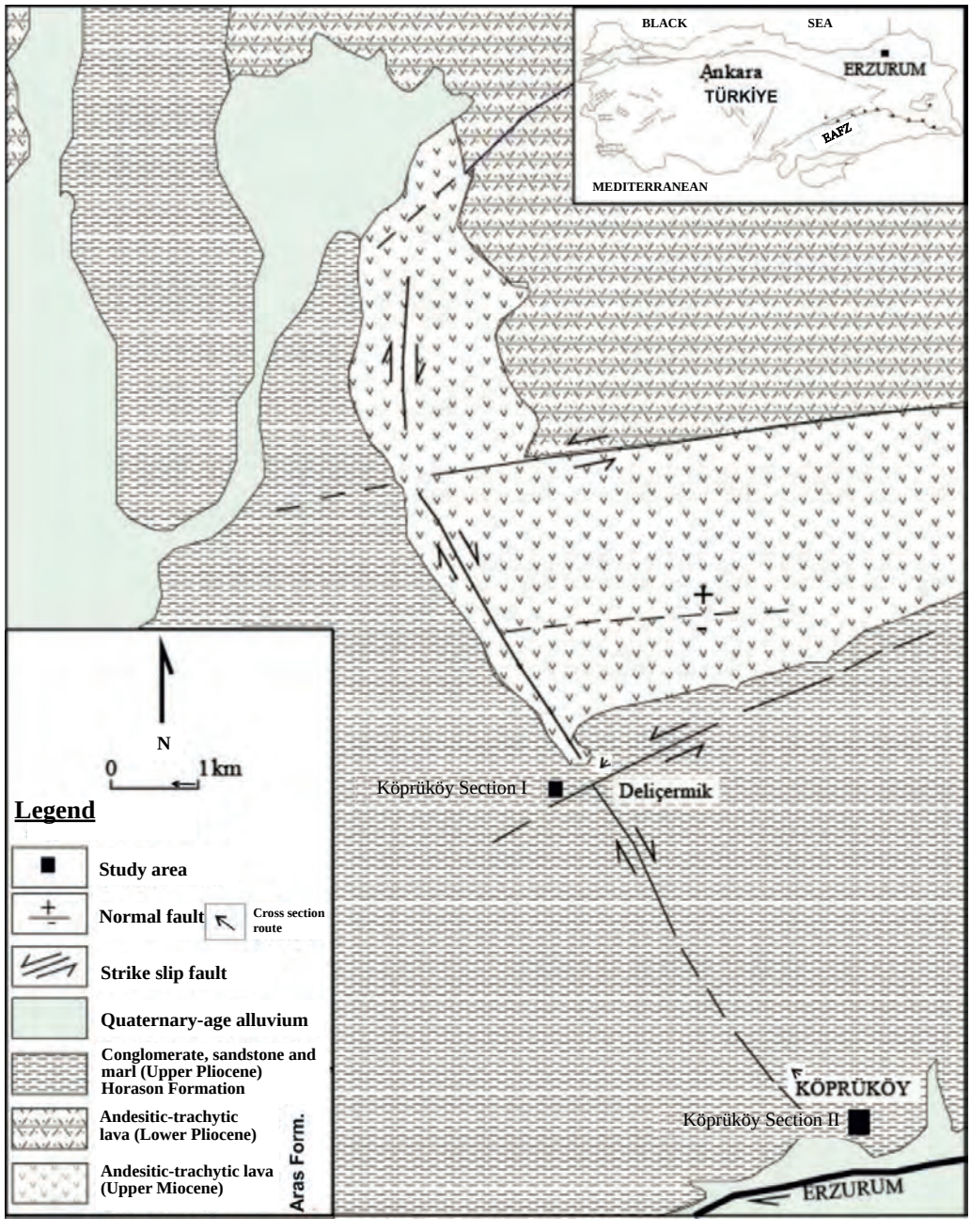

Figure 1- Geological map and section locations in the study area (adapted from Kalkan et al., 2012).

fauna and an attempt was made to infer environmental characteristics. The research identified 4 ostracod genera, 3 ostracod sub-genera and 11 ostracod species using the Hartmann and Puri (1974) classification for systematic identification. During the identification stage for mollusks, the studies by Sayar, 1991; Wenz, 1922; and Taner, 1980, 1997 were used. The SEM images of ostracod species and pelecypod species were taken at Meitam in Mersin University and are given in plates I-IV.

3. Stratigraphy

3.1. Horasan Formation

Definition: This formation was first described by Akkuş (1965) and Rathur (1965) and takes its name from Horasan county were it is best observed. It was studied in detail by Bozkuş (1993).

Distribution: Horasan formation outcrops around the Aras River near the Pasinler region.

Type location: 85 km from Erzurum province in Horasan county and surroundings.

Type section: Previous studies have emphasized the link with strike-slip faulting (Figure 2).

Reference sections: The measured sections in this study are reference sections controlled by strike-slip faulting.

Lithology: In the Middle Miocene ocean had retreated from the Erzurum-Pasinler-Horasan region, with terrestrial sediments specific to the neotectonic period deposited in the Late Miocene. In the Pliocene, basin specific formations were deposited, with increased uplift around the basin edges and resulting discontinuation of communication with other basins (Şaroğlu and Yılmaz, 1984).

The unit was described by Keskin (1994) as the Aras Formation, with the formation comprising terrestrial sediments including loosely consolidated pebble stone, sandstone, and claystone and marls with pyroclastic intercalations.

Yılmaz (1997) stated the Aras and Horasan formations comprised fluvial-lacustrine sediments of Pliocene age deposited in the Pasinler-Horasan basin developing above Late Miocene and older rocks controlled by strike-slip faults. Yellow-beige and grey color pebblestones, sandstone, siltstone and marl sequences from the Horasan formation westwards from Aliçeyrek village form a broad outcrop in the Pasinler-Horasan basin. The Horasan Fault zone, which controls the Aras River, comprises right and left strike-slip faults roughly parallel to the valley with mean strike N60-70E and 0.5-32 km length. The faults are dominated by left lateral strike-slip faults and they have affected the geomorphologic appearance of the basin.

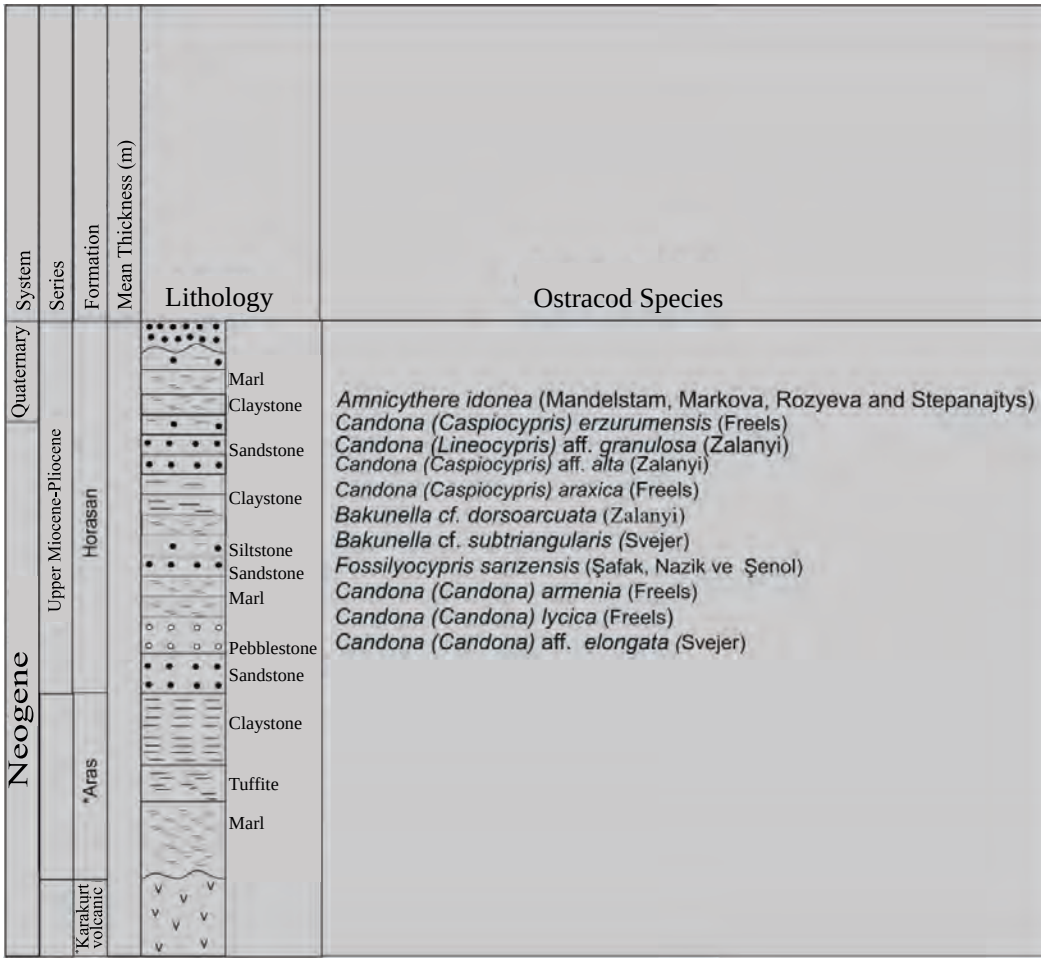

Figure 2- Generalized vertical section and ostracod findings in the study area (adapted from Bozkuş, 1993).

Konak and Hakyemez (2008) described the lower layers of the unit as brownish-greyish color loosely consoliated pebble stone and sandstones, grading up to yellow, grey, grayish, greenish pebble sandstone, sandstone with occasional pyroclastic lenses, siltstone, and marl intercalations. Especially at these levels siltstone and clayey marls with *Congeria* are common with intercalated thin lignite formations encountered.

As observed in photographs 1, 2 and 3, the lithology of the unit in the study comprises reddish, grading up to yellow, gray, grayish, greenish loosely consolidated sandstone, siltstone and marl intercalations.

Contact relations: According to Bozkuş (1993, 1999) within the left lateral strike slip basin, varying sizes of terrestrial sediments were deposited. The Aras Formation formed in a deep lake environment, while the conformably overlying large-fine clastic unit is the Horasan formation. These two units are emphasized as being Pliocene age. The Horasan formation has a conformable and transitional contact with the underlying Aras formation.

In the study by Konak and Hakyemez (2008), the lower limit of the Horasan Formation unconformably overlies Late Miocene volcanic rocks. In the southest of the mapped area, they stated small outcrops of underlying ophiolitic rocks were observed. The upper limit is overlain by Quaternary sediments above an unconformity. This formation comprised meandering river and delta deposits.

The base of the study unit conformably overlies Aras formation sediments, with the upper unit overlain by Quaternary sediments above an unconformity.

Thickness and Distribution: The thickness was 325 m (Bozkuş, 1993), while it was 50-60 m in this study.

Fossil Scope and Age: Previous studies (Erentöz, 1954*a,b*; Rathur, 1965; Arbas et al., 1991) have dated the unit as Late Pliocene-Early Pleistocene based on pelecypod, gastropod, ostracod and small mammalian fossils. Yılmaz and Şener (1984) stated the age of the formation was Late Pliocene.

According to the ostracod fauna described in this study, the age of the unit is Late Miocene-Pliocene.

Environment: According to the fauna in this study the unit developed in fresh water and brackish water (oligohaline) environmental conditions.

Correlation: The Horasan Formation (Bozkuş, 1993) is conformable and transitional with the underlying Aras formation and was described as the Aras Formation by Keskin (1994).

3.2. Measured Sections and Fossil Assemblages

In the study area within the Horasan formation, measured sections were examined with frequent sampling from lithologies related to the fault with high possibility of fossil levels. Two sections were studied.

3.2.1. Köprüköy Measured Section 1

On I47b1 sheet 1/25000 scale map beginning at coordinates X_1: 39°58'22. 74'', Y_1: 41°52'22.75'' and ending at X_2: 39°58'31.04'', Y_2: 41°52'0.17'', a total of 24 wash samples were obtained from this 60 m thick measured section.

In terms of ostracod species, samples numbered 4, 6, 15, 19 and 24 from 4.6 m, 10.2 m, 30 m, 44 m and 55.7 m contained *Candona* (*Caspiocypris*) *erzurumensis* Freels; samples numbered 3, 10 and 19 from 4.6 m, 18.8 m and 44 m contained *Candona* (*Caspiocypris)* aff. *alta* (Zalanyi); samples 10 and 24 from 18.8 m and 55.7 m contained *Candona (Caspiocypris) araxica* Freels, samples 6, 18, 21 and 24 from 10.2 m, 39.9 m, 47.8 m and 55.7 m contained *Bakunella* cf. *dorsoarcuata* (Zalanyi), samples 6, 13 and 20 from 10.2 m, 27.4 m and 45.5 m contained *Candona* (*Candona*) *lycica* Freels; samples 4 and 22 from 4.6 m and 51.2 m contained *Candona* (*Candona*) *armenia* Freels, and samples 21, 22 and 23 from 47.8 m, 51.5 m and 55 m contained *Fossilyocypris sarızensis* (Şafak, Nazik and Şenol) (Figure 3).

The ostracods such as *Candona* (*Caspiocypris*) *erzurumensis, Candona* (*Caspiocypris)* aff. *alta,* and *Candona (Caspiocypris) araxica* in this section are freshwater-brackish water (oligohaline), while ostracods like *Candona* (*Candona*) *lycica,* and *Candona* (*Candona*) *armenia* are freshwater, *Fossilyocypris sarızensis* is freshwater-brackish water (oligohaline) and *Bakunella* cf. *dorsoarcuata*

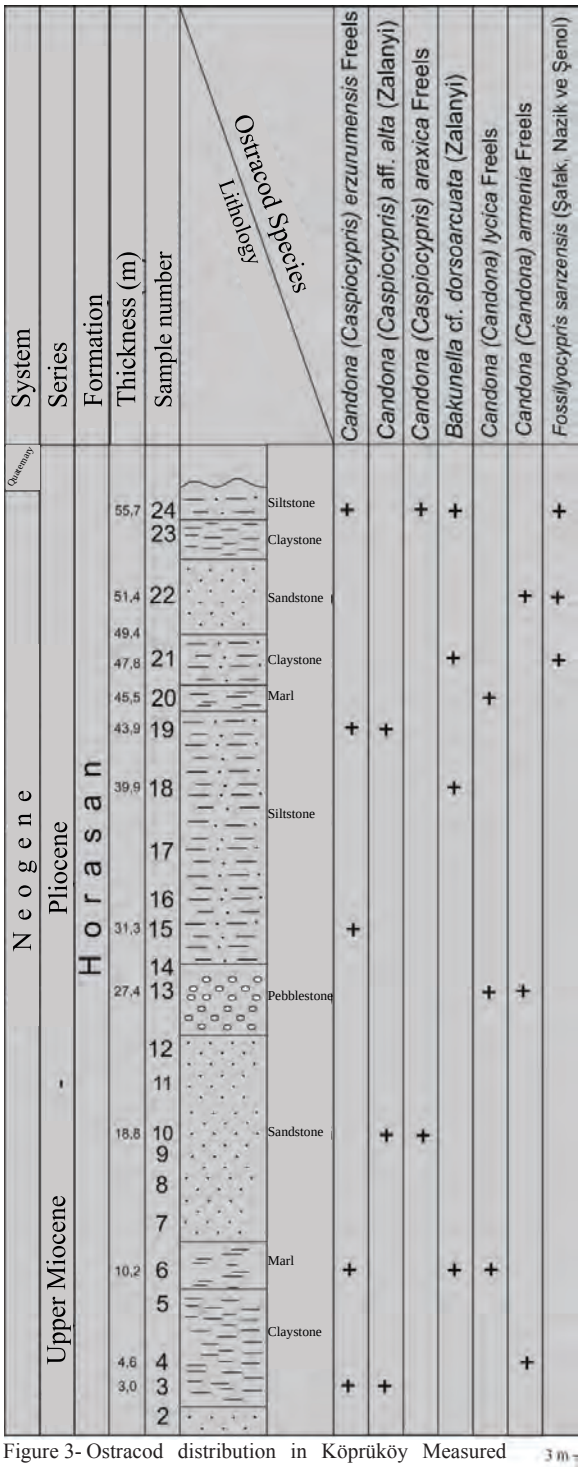

Figure 3- Ostracod distribution in Köprüköy Measured Section 1.

is generally found in brackish water and rarely in freshwater conditions (Remane, 1958) (Morkhoven, 1963).

These species indicate transition from fresh water to oligohaline conditions.

3.2.2. Köprüköy Measured Section 2

On 1/25000 scale I47b1 sheet map, a 10 m thick measured section beginning at X_1: 39°58'53.10'', Y_1: 41°51'38.27'' and ending at X_2: 39°58'50.87'', Y_2: 41°51'36.34'' was taken and a total of 9 wash samples were obtained.

In the sequence, samples number 6 and 8 from 5.6 m and 8.2 m contained *Amnicythere idonea* Mandelstam, Markova, Rozyeva and Stepanajtys; samples 1, 4 and 8 from 0.7 m, 3.8 m and 8.4 m contained *Candona (Caspiocypris)* aff. *alta* (Zalanyi); samples 4, 6 and 8 from 3.8 m, 5.6 m and 8.4 m contained *Candona (Caspiocypris) erzurumensis* Freels; samples 5 and 8 from 3.8 m and 8,4 m contained *Candona (Lineocypris)* aff. *granulosa* Zalanyi; samples 4 and 7 from 3.8 m and 7.2 m contained *Bakunella* cf. *subtriangularis* (Sveyer); and samples 6 and 8 from 5.6 m and 8.4 m contained *Candona (Candona) armenia* Freels; and sample number 6 from 5.6 m contained *Candona* (*Candona*) aff. *elongata* (Svejer) ostracod species. Also samples 1, 3, 5, 7 and 9 contained micropelecypods like *Dreissena polymorpha* (Pallas) and micro gastropod species like *Gyraulus inornatus* (Brusina) (Figure 4*a*, *b*).

In terms of environment, ostracods like *Candona (Caspiocypris)* aff. *alta*, *Candona (Caspiocypris) erzurumensis* and *Candona (Lineocypris)* aff. *Granulose* are freshwater-brackish water (oligohaline), while ostracods like *Candona (Candona) armenia* and *Candona* (*Candona*) aff. *Elongate* are freshwater species. Ostracods like *Amnicythere idonea* occur in brackish water, while *Bakunella* cf. *subtriangularis* generally occurs in brackish water and rarely in freshwater (Remane, 1958) (Morkhoven, 1963).

These species reflect the transition from freshwater to oligohaline conditions.

4. Systematics

The study identified a total of 11 ostracod species with 1 *Amnicythere*, 3 *Candona* (*Caspiocypris*), 1 *Candona* (*Lineocypris*), 2 *Bakunella*, 3 *Candona* (*Candona*), 1 *Fossilyocypris*, 1 *Dreissena*, and 1 *Gyraulus* species identified. Additionally 1 pelecypod and 1 gastropod species were identified. Ostracods are given in terms of their place in systematic classification.

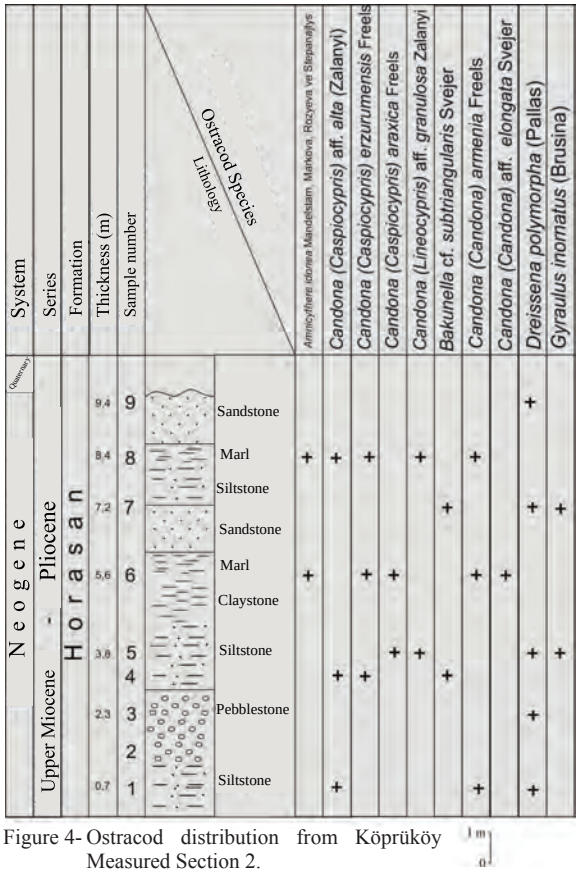

Figure 4- Ostracod distribution from Köprüköy Measured Section 2.

Photograph 1- General appearance of Horasan formation and measured section 1.

Photograph 2- General appearance of Horasan formation.

Photograph 3- General appearance of Horasan formation.

Systematic classification was made according to the classification of Hartmann and Puri (1974). Additionally, the classifications by Moore (1961), Morkhoven (1963) and Freels (1980) were used. Salinity of ostracod environments was determined according to Remane's (1958) criteria.

Subclass: Ostracoda Latreille, 1806

Order: Podocopida Sars, 1866

Superfamily: Cytheracea Baird, 1850

Family: Leptocytheridae Hanai, 1957

Genus: *Leptocythere* Sars, 1922-1928

Subgenus: *Leptocythere* Sars, 1922-1928 and *Amnicythere* Devoto, 1965

Species-type: *Cythere pellucida* Baird, 1850

Stratigraphic Distribution: Oligocene-Present

Environment: Some species typically occur in brackish water, others in shallow marine (littoral) environments (Morkhoven, 1963).

***Amnicythere idonea* Mandelstam, Markova, Rozyeva ve Stepanajtys, 1962**
(Plate 1, Figure 1)

1962 *Leptocythere idonea* Mandelstam, Markova, Rozyeva and Stepanajtys

1978 *Amnicythere idonea* (Mandelstam, Markova, Rozyeva and Stepanajtys), Carbonnel, page 112, plate 1, figure 18; plate 2, figures 4-5.

1999 *Leptocythere idonea* Mandelstam, Markova, Rozyeva and Stepanajtys, Gliozzi, plate 1, Figure a.

2016 *Amnicythere idonea* Mandelstam, Markova, Rozyeva and Stepanajtys, page 859, plate 5, figures 1-6.

Geographic and chronostratigraphic distribution: *A. idonea* in Turkmenistan (Caspian Basin) in the Pliocene (Mandelstam et al, 1962); west of Tethys by Carbonnel (1978) in Corsica (Aleria Basin), found in Spain (Vera Basin), in France (Ron Basin) in the Late Messinian, in Italy (Le Vicenne) in Late Messinian (Gliozzi, 1999). Stoica et al. (2016) studied Paratethys ostracods in the Lago-Mare region of Spain, with new evidence of variation in internal basins during high sea level in the Late Miocene-Pliocene and identified *Amnicythere idonea*.

Locations in this study: samples numbered 6 and 8 from Köprüköy Measured Section 2, Pliocene.

Superfamily: Cypridacea Baird, 1845

Family: Candonidae Kaufmann, 1900

Subfamily: Candoninae Kaufmann, 1900

Genus: *Candona* Baird, 1854

Subgenus: *Candona (Caspiocypris)* Mandelstam, 1956

Species-type: *Bairdia candida* Livental, 1929

Stratigraphic distribution: Oligocene (Eocene?) - Present

Environment: Freshwater, rarely brackish water (Morkhoven, 1963)

***Candona (Caspiocypris) erzurumensis* Freels, 1980**
(Plate I, Figures 2-3)

1980 *Candona (Caspiocypris) erzurumensis* Freels

2013 *Candona (Caspiocypris) erzurumensis* Freels, Şafak, page 78, plate II, figure 3.

Stratigraphic and Geographic distribution: Erzurum-Pasinler, Turkey - Late Miocene (Freels, 1980), Erzurum/Hınıs - Pliocene (Şafak, 2013).

Locations in this study: Samples 3, 6, 15, 19 and 24 in Köprüköy Measured section 1 and samples 4, 6 and 8 in Köprüköy Measured section 2, Late Miocene-Pliocene

***Candona (Caspiocypris) araxica* Freels, 1980**
(Plate I, Figure 4-8)

1980 *Candona (Caspiocypris) araxica* Freels

2001 *Candona (Caspiocypris) araxica* Freels, Tunoğlu, page 134, Figure 4; page 138, figure 5.

2013 *Candona (Caspiocypris) araxica* Freels, Şafak, page 79, plate II, figure 1-2.

Stratigraphic and Geographic Distribution: Erzurum-Pasinler, Turkey - Upper Miocene-Pliocene (Freels, 1980), Black Sea Region, Turkey - Middle-Late Miocene-?Pliocene (Tunoğlu, 2001), Erzurum/Hınıs - Pliocene (Şafak, 2013).

Locations in this study: samples 10 and 24 in Köprüköy Measured Section 1, samples 5 and 6 in Köprüköy Measured section 2, Late Miocene-Pliocene.

***Candona (Caspiocypris)* aff. *alta* (Zalanyi, 1929)**
(Plate II, Figures 1-7)

Aff. 1929 *Paracypris alta* n.sp., Zalanyi, Morpho-System, Studien, page 44, figure 14.

Aff. 1971 *Candona (Thaminocypris) alta* (Zalanyi), Krstic, Table II, 3-5.

1974 *Candona (Caspiocypris) alta* (Zalanyi, 1929), Hanganu, Table III, 10-12.

1980 *Candona (Caspiocypris)* aff. *alta* (Zalanyi, 1929), Freels, plate 4, figure 1-8.

1992 *Candona (Caspiocypris) alta* (Zalanyi), Şafak, Nazik and Şenol, pl. 4, Fig. 1.

1992 *Candona (Caspiocypris) alta* (Zalanyi), Nazik, Şafak and Şenol, plate II, figure 8.

2005 *Candona (Caspiocypris) alta* (Zalanyi), Vasiliev, Krijgsman, Stoica and Langereis, page 242, plate 1, figure 7.

2013 *Candona (Caspiocypris) alta* (Zalanyi), Şafak, page 78, plate II, figure 4-5.

Stratigraphic and Geographic Distribution: Caspian Basin (Zalanyi, 1929); Romania - Sarmatian (Hanganu, 1974); Sivas and Şebinkarahisar, Turkey - Late Miocene (Freels, 1980), Sarız and Tufanbeyli, Turkey - Pliocene (Şafak et al., 1992; Nazik et al., 1992); South Carpathians - Mio-Pliocene (Vasiliev et al., 2005); Hınıs/Erzurum - Early Pleistocene (Şafak, 2013).

Locations in this study: samples 10 and 19 in Köprüköy Measured Section 1, samples 1, 4 and 8 in Köprüköy Measured Section 2, Late Miocene-Pliocene

Subgenus: *Candona (Lineocypris)* Zalanyi, 1929

Species-type: *Lineocypris trapezoidea* Zalanyi, 1929

Stratigraphic distribution: (?Early Cretaceous) Pliocene-Present

Environment: Fresh water, generally deep lakes (Morkhoven, 1963)

***Candona (Lineocypris)* aff. *granulosa* Zalanyi, 1959**

(Plate II, Figure 8)

1959 *Candona granulosa* n. sp. Zalanyi, page 223, figure 5

1967 *Candona (Caspiocypris)* sp., Sokac, T. I: 4.

1972 *Candona (Lineocypris) granulosa* Zalanyi, Sokac, T. XXVI:7-13.

1980 *Candona (Lineocypris)* aff. *granulosa* Zalanyi, Freels, page 144, plate 6, figure 17-20.

Stratigraphic and Geographic Distribution: In the Pannonian Basin in the former Yugoslavia (Montenegro) – Pontian (Sokac, 1967, 1972); Turkey (Samsun, Erzurum) – Late Miocene (Freels, 1980).

Locations in this study: samples 5 and 8 in Köprüköy Measured section 2, Late Miocene-Pliocene.

Genus: *Bakunella* Schneider, 1958

Species-type: *Pontocypris dorsoarcuata* Zalanyi, 1929

Stratigraphic distribution: Pliocene-Present

Environment: brackish water, rarely freshwater (from Tunoğlu, 2003)

***Bakunella* cf. *dorsoarcuata* (Zalanyi, 1929)**

(Plate III, Figure 1-4)

1929 *Pontocypris dorsoarcuata n. sp.* Zalanyi, page 37, figure 11, 12.

1949 *Bythocypris guriana* (Lıvental) Svejer, t. III: 2.

1965 *Bakunella dorsoarcuata* (Zalanyi), Stancheva, page 15-16, plate 4, figure 8.

1967 *Bakunella dorsoarcuata* (Zalanyi), Agalarova, plate 3, figure 3-5.

1969 *Candona* (*Bakunella) dorsoarcuata* (Zalanyi) Gramann, page 495, plate 32, figure 5a,b.

1972 *Bakunella dorsoarcuata* (Zalanyi), Krstic, T. XXIII: 2-4.

1978 *Bakunella dorsoarcuata* (Zalanyi), Olteanu, page 1019, plate 6, figure 3-4.

1980 *Bakunella dorsoarcuata* (Zalanyi), Freels, page 32, plate 3, figure 10-15.

1991 *Candona* (*Bakunella) dorsoarcuata* (Zalanyi), Jiricek & Riha, pl. 6, fig. 4.

1998 *Candona* (*Bakunella) dorsoarcuata* (Zalanyi),Tunoğlu, Ünal and Bilen, page 96-97, plate 9, figure 1-3, 9, 10, plate 16, figure 1-4.

2001 *Candona* (*Bakunella*) *dorsoarcuata* (Zalanyi), Tunoğlu, page 131-133.

2003 *Candona* (*Bakunella*) *dorsoarcuata* (Zalanyi), Tunoğlu, page 31, plate 6, 1-3, 9, 10; plate 9, 1-4.

2011 *Bakunella dorsoarcuata* (Zalanyi), Olteanu, page 127, plate X, fig.

2011 *Bakunella dorsoarcuata* (Zalanyi), Floroiu, page 36.

2013 *Bakunella dorsoarcuata* (Zalanyi), Stoica, Floroiu, Krijgsman and Vasiliev**,** page 139, plate 1, figure 27.

2013 *Bacunella* cf. *dorsoarcuata* (Zalanyi), Vesel-Lukic, Tadesse and Poljak**,** page 413-414.

2013 *Bakunella dorsoarcuata* (Zalanyi), Pipik, Starek, Seko and Sykorova, page 291-294.

2013 *Bakunella dorsoarcuata* (Zalanyi), Floroiu, Stoica, Vasiliev and Krijgsman, page 131-132.

Stratigraphic and Geographic Distribution: Russia-Volga shore – Pliocene (Svejer, 1949); Kabistan, Azerbaijan, Ukraine, Bulgarian coast – Pontian (Stancheva, 1965); Black Sea coast – Pontian-Pliocene (Agalarova, 1967); Strimon Basin, Greece – Pontian (Gramann, 1969); Pannonian Basin, former Yugoslavia – Neogene (Krstic, 1972); Romania – Late Pontian (Hanganu, 1966); Pannon Lake – Late Miocene (Pipik et al., 2013); Dasic Basin, Eastern Carpathians, Romania – Late Miocene-Early Pliocene (Stoica et al., 2013); Eastern Slovenia – Late Miocene (Vesel-Lukic et al, 2013); Eastern Carpathians – Pontian (Floroiu et al., 2013); Black Sea coast, Turkey – Late Miocene (Freels, 1980); Araklı, Trabzon – Pontian (Tunoğlu et al.,1998); Eastern Black Sea region – Pontian (Tunoğlu, 2003); Bucharest, Romania (Dasic Basin) – Pontian-Maeotian (Floroiu, 2011).

Locations in this study: samples 6, 18, 21 and 24 in Köprüköy Measured Section 1, Late Miocene-Pliocene.

***Bakunella* cf. *subtriangularis* (Svejer, 1949)**

(Plate III, Figure 5-8)

1949 *Bythocypris subtriangularis* Svejer, Pliyosen, page 63, T. III: 6.,

1980 *Bakunella* cf. *subtriangularis* (Svejer), page 33, plate 3, figure 16-17.

Stratigraphic and Geographic Distribution: Lower Volga region, Russia – Pliocene (Svejer, 1949); Erzurum, Pasinler Basin, Turkey – Late Miocene; Konya-Beyşehir Basin – Pliocene-Early Pleistocene (Freels, 1980).

Locations in this study: samples 4 and 7 in Köprüköy Measured Section 2, Late Miocene-Pliocene.

Subgenus: *Candona (Candona)* Baird, 1845

Species-type: *Cypris candida* O.F.Müller, 1776

Stratigraphic distribution: (?Eocene) Oligocene-Present

Environment: Generally freshwater (Morkhoven, 1963)

***Candona (Candona) lycica* Freels, 1980**

(Plate IV, Figure 1-3)

1981 *Candona (Candona) lycica* n.sp. Freels, page 73 , plate 11, figure 12-13, plate 12, figure 1-6

Stratigraphic and Geographic Distribution: Suşehri, Sivas, Şebinkarahisar, Turkey – Late Miocene (Freels, 1980).

Locations in this study: samples 6, 13 and 20 in Köprüköy Measured Section 1, Late Miocene-Pliocene

***Candona (Candona) armenia* Freels, 1980**

(Plate IV, Figure 4-5)

1980 *Candona (Candona) armenia* n.sp. Freels, page 71 , plate 11, figure 9-11

Stratigraphic and Geographic Distribution: Erzurum-Pasinler-Horasan, Turkey – Late Miocene (Freels, 1980).

Locations in this study: samples 4, 13 and 22 in Köprüköy Measured Section 1, samples 6 and 8 in Köprüköy Measured Section 2, Late Miocene-Pliocene.

***Candona (Candona)* aff. *elongata* (Svejer, 1949)**

(Plate IV, Figure 6)

Aff. 1949 *Bythocypris elongata* Svejer, page 62, plate IV, figure 9-12.

1963 *Bythocypris elongata* Svejer, Mandelstam ve Schneider, page 138, plate 17, figure 2.

1980 *Candona (Candona)* aff. *elongata* (Svejer), Freels, page 82, plate 13, figure 9-12

2010 *Candona (Candona) elongata* (Svejer), Şafak, page 57, plate III, Figure 3.

Stratigraphic and Geographic Distribution: Lower Volga and Caspian Basin – Pliocene-Early Pleistocene (Mandelstam and Schneider, 1963); Denizli-Sarayköy-Güney-Babadağ, Turkey – Late Miocene (Freels, 1980; Şafak, 2010).

Locations in this study: sample 6 in Köprüköy Measured Section 2, Late Miocene-Pliocene.

Family: Ilyocyprididae Kauffmann, 1900

Genus: *Ilyocypris* Brady ve Norman, 1889

Species-type: *Cypris gibba* Ramdohr, 1808

Stratigraphic distribution: Triassic-Present

Environment: Freshwater – oligohaline salt falts and mainly muddy bottoms (Morkhoven, 1963)

***Fossilyocypris sarızensis* (Şafak, Nazik ve Şenol, 1992)**

(Plate IV, Figure 7)

1975 *Ilyocypris caspiensis* (Negadev) Kazmina, page 45-46, plate I, figure 16-17, plate XVIII, figure 5-6.

1988 *Ilyocypris caspiensis*? Krstic, Figure I.

1992 *Ilyocypris sarızensis* Şafak, Nazik and Şenol, page 177, plate II, figure 1-7.

2004 *Fossilyocypris sarızensis* (Şafak, Nazik and Şenol) Krstic, Markovic and Keyser, page 313, plate 2, figure 7-8.

Stratigraphic and Geographic Distribution: species originally described in southeast Turkey – Pliocene (Şafak et al., 1992). Global distribution west Siberia (Novosibirsk, Tomsk, Omsk) and different sections of the Altay mountains – generally lower-middle, rarely Upper Quaternary sequences (Kazmina, 1975); Vojvodina, north Serbia – Pliocene (Krstic, 1988); Central and eastern Europe – Late Pliocene and Middle Pleistocene (Krstic et al., 2004).

Locations in this study: samples 21, 22 and 24 in Köprüköy Measured Section 1, Pliocene.

5. Discussion and Conclusion

This study was conducted on units within the Horasan Formation near Köprüköy east of Erzurum. This formation is found in the Erzurum-Pasinler-Horasan region forming the northernmost section of deposits from the neotectonic period in Eastern Anatolia. Previous studis have determined that the sea retreated from the Erzurum-Pasinler-Horasan region in the Middle Miocene, with terrestrial sediments unique to the neotectonic period deposited in the Upper Miocene with basin formations deposited in the Pliocene as the basin edges were uplifted and connections with other basins were cut (Şaroğlu and Yılmaz, 1984). This study observed well-preserved ostracod, gastropod and pelecypod genera and species in soft clastic claystone, siltstone and marl levels of the Horasan Formation.

Amnicythere idonea is found in Turkmenistan (Caspian Basin), west of Tethys (Aleria and Vera Basins) and in Italy in the Pliocene and Late Messinian (Mandelstam et al., 1962, Carbonnel, 1978, Gliozzi, 1999); and in Spain in the Late Miocene-Pliocene (Stoica et al., 2016).

Candona (Caspiocypris) erzurumensis is found in Turkey in Erzurum Pasinler and Hınıs in the Late Miocene and Pliocene (Freels, 1980, Şafak, 2013).

Candona (Caspiocypris) araxica is found in Turkey in Erzurum-Pasinler and the Black Sea region in the Late Miocene-Pliocene, Middle-Late Miocene-?Pliocene and in the Pliocene (Freels, 1980; Tunoğlu, 2001, Şafak, 2013).

Candona (Caspiocypris) aff. *alta* is found in the Caspian Basin, Romania and Southern Carpathians in the Sarmatian and Mio-Pliocene (Zalanyi, 1929; Hanganu, 1974, Vasiliev et al., 2005). In Turkey it is

found in Sivas, Şebinkarahisar and Sarız, Tufanbeyli and Erzurum-Hınıs in the Late Miocene and Pliocene, and Pliocene-Early Pleistocene (Freels, 1980; Şafak et al.,1992; Nazik et al., 1992; Şafak, 2013).

Candona (Lineocypris) aff. *granulosa* is found in the Pannonian Basin in the former Yugoslavia in the Pontian (Sokac, 1967, 1972) and in Turkey in Samsun and Erzurum in the Late Miocene (Freels, 1980).

Bakunella cf. *dorsoarcuata* is found in Russia and on the Black Sea coast in the Pliocene (Svejer, 1949, Agalarova, 1967); in Azerbaijan, Ukraine, northern Bulgaria, on the Black Sea coast, in the Strimon Basin in Greece, Pannonian Basin in Romania, Eastern Carpathians, in the Black Sea region of Turkey near Trabzon, Araklı in the Pontian (Stancheva, 1965; Agalarova, 1967; Gramann, 1969; Hanganu, 1966; Pipik et al., 2013; Floroiu et al., 2013; Tunoğlu, 2003; Floroiu, 2011). It is also found in the eastern Carpathinas in the Late Miocene-Early Pliocene (Stoica et al., 2013), on the Black Sea coast in Turkey and in eastern Slovenia in the Late Miocene (Freels, 1980, Vesel-Lukic et al., 2013).

Bakunella cf. *subtriangularis* is found in Turkey in the Konya-Beyşehir Basin in the Pliocene-Lower Pleistocene and in the Erzurum-Pasinler Basin in the Late Miocene (Freels, 1980) and in the Lower Volga region of Russia in the Pliocene (Svejer, 1949).

Candona (Candona) lycica is found in Sivas-Suşehri and Şebinkarahisar in Turkey in the Late Miocene (Freels, 1980).

Candona (Candona) armenia is found in the Erzurum-Pasinler-Horasan region in Turkey in the Late Miocene (Freels, 1980).

Candona (Candona) aff. *elongata* is found in the Lower Volga and Caspian Basin in the Pliocene-Early Pleistocene (Mandelstam and Schneider, 1963) and in Denizli-Sarayköy-Güney-Babadağ in Turkey in the Late Miocene (Freels, 1980, Şafak, 2010).

Fossilyocypris sarızensis is found in Turkey and Serbia in the Pliocene (Şafak et al., 1992; Krstic, 1988), in the Mediterranean and Central and Eastern Europe in the Late Plicoene (Krstic et al., 2004) and in Siberia in the Quaternary (Kazmina, 1975).

Of these genera *Candona (Caspiocypris)* and *Candona (Lineocypris)* characterize freshwater-brackish water (oligohaline) conditions, while *Candona (Candona)* represents freshwater, *Bakunella* characterizes rarely freshwater and mainly brackish water, *Amnicythere* is found in brackish water and *Gyraulus* and *Dreissena* characterize freshwater conditions.

The ostracod fauna identified in this study, along with the micromollusk fauna clearly indicate an assemblage supporting these interpretations in terms of age and environmental correlations. According to the fauna, the age of the formation is determined as Late Miocene-Pliocene.

The ostracod and micromollusk species defined in the study and the environmental conditions represented by these species taken together and reviewed in light of previous studies indicate the Horasan Formation was deposited in the interval from the Late Miocene to Pliocene when generally freshwater and brackish water (oligohaline) conditions dominated.

Acknowledgements

The researchers thank Atatürk University Scientific Research Project Unit and Ass. Prof. Tuğbanur Özen Balaban and Çukurova University Department of Geological Engineering for contributions to field studies for project 2013/118. The authors acknowledge a debt of gratitude to the reviewers for their positive criticism and great contribution to this paper.

References

Acar, A. 1975. Tortum ve Çevresinin Jeolojisi ve Jeomorfolojisi Üzerine Bir Araştırma: Atatürk Üniversitesi, *Doçentlik Tezi*, Erzurum (unpublished).

Agalarova, D.A. 1967. Mikrofauna ponticeskih otlozenij Azerbajdzana I sopredel'nych rajonov. (Mikrofauna der pontischen Ablagerungen Aserbaidschans und der angrenzenden Gebiete), *Aznii po Dobyce Nefti*: 124 S., 21 Abb., 7 Tab., 24 Taf., Leningrad.

Akkuş, M F. 1965. Pasinler (Hasankale) Havzasının 1/25 000 Ölçekli Detay Petrol Etüdü Raporu: *Maden Tetkik ve Arama Rap.* No: 4037, Ankara (unpublished).

Atalay, İ. 1978. Erzurum Ovası ve Çevresinin Jeolojisi ve Jeomorfolojisi: *Atatürk Üniv., Fen-Edebiyat Fak. yayını*, No: 81.

Arbas, A., Gök. L., Ateş, M, İmik, M, Kılıç, F., Canpolat, M ve Aydın, A. 1991. Horasan (Erzurum ili) dolayının jeolojisi, *Maden Tetkik ve Arama Rap.* No: 9431 (unpublished).

Arni, P. 1939. Anadolu'nun umumi bünyesiyle mineral ve petrol yatakları arasındaki münasebetler, *Maden Tetkik ve Arama Mecmuası*, 2/15, Ankara.

Baird, W. 1845. Arrangement of British Entomostraca, with a list of species, particularly noticing those which have as yet been discovered within the bounds of the Club. Berwickshire Nat. Club (Hist.) Proc., 2.

Baird, W. 1850. The natural history of the British Entomostraca, *Roy. Soc.,* 18: 254-257, London.

Baird, W. 1854. The natural history of the British Entomostraca, *Roy. Soc.,* 1-364, London

Barka A, Toksoz N, Gulen L, Kandinsky-Cade K. 1987. Sedimentation, seismicity, and earthquake potential of the eastern part of the North Anatolian Fault Zone. *Earth Sci.* 14:337-352.

Bayraktutan, M.S. 1999. Active tectonics and evaluation of thrust bounded Pasinler Basin on the Erzurum Fault Zone, Eastern Anatolia. *Ann. Tectonicae*. 13(1-2):51-70.

Bayraktutan, M.S., Merefield, J.R., Grainger, P., Evans B.M., Yilmaz M., Kalkan, E. 1996. Regional gas geochemistry in an active tectonic zone, Erzurum Basin, Eastern Turkey. *Q. J. Eng. Geol*. 29:209-218.

Beer A. M., Jungirger H.E., Lukanov, J., Sagorchev, P. 2003. Evaluation of the permeation of peat substances through human skin in vito.Int. *J. Pharm* 253:169-175.

Bozkuş, C. 1990. Oltu-Narman Tersiyer Havzası kuzeydoğusunun (Kömürlü) stratigrafisi, *Türkiye Jeoloji Kurumu Bülteni*, C. 33, 47-56.

Bozkuş, C. 1993. Pasinler-Horasan (Erzurum) Havzası) doğusunun stratigrafisi, *Maden Tetkik Arama Dergisi*, 115, 43-53, Ankara.

Bozkuş, C. 1998. Kuzeydoğu Anadoluda (Oltu-Narman arası) Pontid/Anatolid kenet kuşağının stratigrafisi ve yapısal evrimi, *Pamukkale Üniversitesi Mühendislik Fakültesi Mühendislik Bilimleri Dergisi*, Cilt: 4, sayı1-2, 487-499.

Bozkuş, C. 1999. Karakurt (Kars) yöresinin jeomorfolojik evriminde volkanizma ve tektoniğin etkisi, *Pamukkale Üniversitesi Mühendislik Fakültesi Mühendislik Bilimleri Dergisi*, Cilt: 5, sayı1, 939-1000.

Brady, G.S., Norman, A.M. 1889. A monograph of the marine and freshwater ostracoda of the North Atlantic and of North-western Europe, Section I *Podocopa Sci. Trans. Roy.* Dublin Soc., 4 (2): 63-270.

Carbonnel,G.1978. La zoneà Loxoconcha djafarovi Schneider (Ostracoda,Miocène supérieur) oule Messinien de la vallée du Rhône, *Rev. Micropaléontol*.21,106–118.

Dağıstan, H. 2001. Geology of Erzurum-Köprüköy-Deliçermik spa area and its geothermal energy potentials. *General Directorate of Mineral Research and Exploration*, Ankara, Turkey (in Turkish). p. 44218.

Demirtaşlı, E., Tütüncü, K., Gedik, A. 1965.Tekman Havzasının 1/25.000 ölçekli jeoloji haritası, *Maden Tetkik ve Arama Enerji Hammadde Etüt ve Araştırma Dairesi Arşivi*, Ankara.

Devoto, G. 1965. Lacustrin Pleistocene in the lower Liri Valley, *Geologica Romana*, 4: 291-368.

Erdoğan, T. 1967. Erzurum-Hınıs Bölgesi 1/25.000 ölçekli Erzurum J-47 d1 paftalarının detay petrol etüdü, *Maden Tetkik ve Arama Genel Müdürlüğü Raporu.* No. 4340, Ankara (unpublished).

Erentöz, C. 1954a. Oltu 31/4, Kars 32/3 ve Hasankale 48/2 1/100.000 ölçekli jeolojik paftalara ait memuar: *Maden Tetkik ve Arama Genel Müdürlüğü Raporu*. No:2159 (unpublished).

Erentöz, C.1954b. Aras Havzası Jeolojisi, *Türkiye Jeoloji Kurumu Bülteni*, C: V, s. 1-2.

Erinç, S. 1953. Doğu Anadolu Coğrafyası: İstanbul. Üniv. Coğrafya Enstitüsü Yayınlarından, 15, İstanbul, 1245 s.

Floroiu, A. 2011. Analiza integrata (biostratigrafica, tectonica, stratigrafie seismica) a Paratethysului Oriental (Bazinul Dacic, Marea Neagra, Peninsula Taman) in timpul Pontianului, *Universitatea Din Bucuresti Facultatea de Geologie si Geofizica*, Teza.

Floroiu, A., Stoica, M, Vasiliev, I., Krijgsman, W. 2013. Pontian ostracods from Slanicul de Buzau section (eastern Carpathian foredeep), *Naturalista Siciliano*, S. IV, XXXVII(1), pp. 131-132.

Freels, D. 1980**.** Limnische Ostracoden aus Jungtertiaer und Quaterner Türkei, *Geol. Jahr.*, Reihe B, Heft 39, 1-172, Hannover.

Gedik, A. 1985. Tekman (Erzurum) Havzasının Jeolojisi ve Petrol Olanakları, *Maden Tetkik ve Arama Dergisi*, 103/104, 1-24, Ankara.

Gelişli, K. ve Maden, N. 2006. Analysis of potential field anomalies in Pasinler-Horasan Basin, Eastern Turkey, *Journal of the Balkangeophysical Society*, V. 9, No. 1, p. 1-7, 6 figs.

Gevrek, A.İ., Şengüler, İ. 1992. Markov Zinciri Analiz Yönteminin linyit içeren Zırnak formasyonuna (Pliyosen, Hınıs) uygulanması, *Jeoloji Mühendisliği*, 41, 84-90, Ankara.

Gliozzi, E. 1999. A late Messinian brackish water ostracod fauna of Paratethyan aspect from Le Vicenne Basin (Abruzzi, central Apennines, Italy), *Paleeogeography, Palaeoclimatology, Palaeoecology*, 151, 1, pp. 191-208 (18).

Gramann, F. 1969. Das Neogen im Strimon Becken (Griechisch Ostmazedonien). Teil: II Ostracoden und Foraminiferen aus dem Neogen des Strimon Beckens, *Geol. Jb.,* 87: 485-528, 2 Abb., 6 Taf., Hannover.

Gürbüz, K., Gülbaş, E. 1999. Tortum (Erzurum) güneybatısının Jeolojisi ve Pliyosen Yaşlı Gelinkaya Formasyonu'nun Sedimantolojisi, *Cumhuriyet Üniversitesi Mühendislik Mimarlık Fakültesi Dergisi*, Seri-AYerbilimleri, c. 16 (1), 39-46, Sivas.

Hanai, T. 1957. Studies on the Ostracoda from Japan. II. Subfamily Leptocytherinae n.subfam *J. Fac. Sci. Univ. Tokyo, Section II*, 10(3): 431-468.

Hanganu, E. 1966**.** Studiul stratigrafic al pliocenului dintre vaile Teleajen şi Prahova (Regiunea Ploieşti). (Franz. Résumé: Etude stratigraphique du Pliocène situé entre les vallées et de Prahova (Région de Ploieşti). A.a.O.S.110-127. *Comitetul de Stat al Geologiei, Institutul Geologic, Studii Tehnice şi Economice,* Seria J, Stratigrafie, 2: 127 S. (einschl. Franz. Résumé), 11 Abb., 52 Taf., 5 Tab., Bucureşti.

Hanganu, E. 1974. Observations sur l'ostracofaune pontienne de la région entre la vallée du Danube et la vallée du Motru, *Rev. Espanola Micropaleont*., 6, 3: 335-345, 3 Taf., Madrid.

Hartmann, G., Puri, H. 1974. Summary of neontological and paleontological classification of Ostracoda, *Mitteilungen aus dem hamburgischen Zoologischen Museum und Institut*, 70, 7-73.

Kalkan, E., Yıldırım Canbolat, M, Yarbaşi, N. Özgül, M. 2012 . Evaluation of thermal mud characteristics of Erzurum (Köprüköy) clayey raw materials (NE Turkey)**.** *International Journal of Physical Sciences* Vol. 7(40), pp. 5566-5576.

Kaufmann, A. 1900. Zur Systematik der Cypriden, *Mitt. Naturforsch. Ges. Bern*, 1900: 103-109.

Kazmina, T.A. 1975. Stratigraphy and ostracodes of Pliocene and early Pleistocene in southern West Siberian Plain (İn Russian): Trudy Inst. *Geol. Geophys*., Siberian branch Acad. Sci, USSr, 264, 1-108.

Keskin, M. 1994. Genesis of collision related volcanism on the Erzurum-Kars plateau, Northeastern Anatoli: *Ph.D. Thesis, University of Durham*, UK.

Keskin, M. 1998. Volcano-stratigraphy of collision-based volcanism of Erzurum-Kars (NE, Turkey) and its evolution by new findings. (in Turkish). J. Gen. Directorate *Miner. Res. Explor*. 120:135-157.

Keskin, M. 2005. Domal uplift and volcanism in a collision zone without a mantle plume: Evidence from Eastern Anatolia. *http://www.mantleplumes*. org/ Anatolia.html.

Kibaroğlu, M, Sagona, A., Satır, M. 2011. Petrographic and geochemical investigations of the Late Prehistoric ceramics from Sos Höyük, Erzurum (Eastern Anatolia). *Journal of Archaeological Science 38, 3072-3084.*

Kocyigit, A. 1985. Geotectonic properties of Çobandede fault zone between Muratbaşi-Balabantaş (Horasan, Erzurum, NE Turkey) and surface fractures of Narman (Erzurum, NE Turkey) earthquake. *Engineering Faculty of Cumhuriyet University*, (in Turkish). J. Earth Sci. 2(1):17-34.

Konak, N., Hakyemez, H. Y. 2008. 1: 100 000 ölçekli Türkiye Jeoloji Haritaları No :95 Tortum- H47 Paftası. *Maden Tetkik ve Arama Genel Müdürlüğü*, Jeoloji Etütleri Dairesi Ankara.

Krstic, N. 1972. Neue Ostracoden aus der Obermiozän von Donja mutnica (Paracin, Serbien), *Bulletin Scientifique* A17, 153-155.

Krstic, N. 1988. Some Quaternary ostracodes of the Pannonian Basin with a review of a few negloctoida: *Proc. 9th Internat. Symp. On ostracodes*, 1063-1072, (''Kodansha'' Ltd), Tokio.

Krstic, N., Markovic, Z., Keyser, D. 2004. Some important ostracodes from the late Pliocene (Akchagylian)of the Mediterranean and Central and Eastern Europe, *Bullettino della Paleontologica Italiana*, 43, 1-2, p. 307-320, 3pls, Modena.

Latreille, P.A. 1806, Histoire naturelle des crustaces et des insectes, 6-7, F. Dufart, Paris.

Livental, V.E. 1929. Ostracoda akcaglyskogo i apseronskogo jarusov po babazanonskomu razrezu, *Izv. Azerb. Politech. i Post Paleozoic Ostracoda*. Elsevier édit., 2: 1-478.n-ta, Baku.

Mandelstam, M.I. 1956. Order Ostracoda. In: Mandelstam MI, Shneyder G.F & Zanina J.E. (eds.), New families and genera. *All-Union Scientific Research*, Geological Institute, Moscow, (VSEGEI), 12, 87-144. (in Russian).

Mandelstam, M.I., Markova, L., Rosyeva, T., Stepanaitys, N. 1962. Ostracoda of the Pliocene and post-Pliocene deposits of Turkmenistan. *Turkmenistan Geological Institute*, Ashkhabad, 288 pp.

Mandelstam, M.I., Schneider, G. F. 1963. Iskopaemya Ostrakody SSSR. Semejstvo Cypridídea. *Trudy Vnıgrı*, 203: 331 S., 113 Abb., 42 Taf.; Leningrad.

Moore, R.C. (Ed.) 1961.Treatise on Invertebrate Paleontology, Q, Arthropoda 3, Crustacea, *Ostracoda*: XXIII, 442 s., 334 abb., Lawrence, Kansas.

Morkhoven, F.P.C.MVAN. 1963. Post Paleozoic Ostracoda. *Elsevier édit*., Volume 2, 477 s.

Mueller, O.F. 1776. Zoolgiaedanicae prodramus, seu animalium daniae et norvegiae indigenarum characteres, nomina et synonyma inprimis popularium, Lipsiae et Havniae, 1-282.

Nazik, A., Şafak, Ü., Şenol, M. 1992. Micropaleontological Investigation (Ostracoda) of the Pliocene sequence of the Tufanbeyli (Adana) Area, *Yerbilimleri, 1992 1st International Symposium on Eastern Mediterranean Geology, proceedings and abstracts*, 281-304, Adana.

Öner, F., Türkmen, S., Özbek, A., Karakaya, T. 2006. Engineering properties of Hınıs ignimbrites and their usability as a building stone (Erzurum / Turkey), *Environ Geol.,* 50: 275–284.

Özcan, A. 1967. Erzurum-Hınıs Bölgesinde Erzurum-J47a3 a4 paftalarının detay petrol etüdü, *Maden Tetkik ve Arama Genel Müdürlüğü Rapor* No. 4128, Ankara (unpublished)

Pamir, H.N. ve Baykal, F. 1943. Bingöl Bölgesi ve buranın şimal ve cenubundaki jeolojik yapı, *Maden Tetkik ve Arama Genel Müdürlüğü Raporu* 1447 (yayımlanmamış).

Pipik, R., Starek, D., Seko, M., Sykorova, M. 2013. Ostracods of the late Miocene long lived Lake Pannon, *Naturalista Siciliano*., S. IV, XXXVII(1), pp. 291-294.

Ramdohr, F.A. 1808. Über die gattung Cypris Mueller und drei zu derselben gehörige neue Arten, *Geselschaft Naturforsch.* Freunde Berlin, 2: 63-93.

Rathur, A.Q. 1965. Pasinler-Horasan (Erzurum) sahasına ait genel jeolojik rapor(H47c1-C2; H48-c4,d3,d4; İ47-b1, d2, b3, b4; I48-a1, a2, b1) *Maden Tetkik ve Arama Genel Müdürlüğü Raporu* No: 4168, Ankara (unpublished).

Remane, A. 1958. Die Biologie des Brackwassers. *In: THIENEMANN*, A: Die Binenge wasser, Einzeldarstellungen aus der Limnologie und ihren Nachbargebieten, Stuttgart, 22: 1-348.

Sars, G.O. 1866. Oversight of Norges marin: ostracoden, *Verhandl., videnkabs-Selskabat*, Christiania, 7: 1-130.

Sars, G.O. 1922-1928. An account on the Crustacea of Norway, *9. Ostracoda*, Parts 1 (1922)-16 (1928): 277s., 119 Taf., Bergen Museum (Norway).

Sayar, C. 1991. Paleontoloji Omurgasız Fosiller, İstanbul Teknik Üniversitesi Kütüphanesi Sayı: 1435, İstanbul.

Sokac, A. 1967. Pontska fauna ostrakoda jugoistrocnog pobocja Zagrebackegore. Deutsche Zusammenfassung: Pontische Ostracodenfauna an den südöstlichen Abhängen der Zagebacka gora., *Geol. Vjesnik*, 20: 63-86, 4 Taf., Zagreb.

Sokac, A. 1972. Pannonian and Pontian ostracode Fauna of Mt. Medvednica, *Palaeont.* Jugoslavica, 11: 140 s (S. 1-96: engl. Text+ Lit., Verz.: S. 97-140: serbokroat. Text), 47 Taf.; Zagreb.

Soytürk, N. 1973. Murat Baseni jeolojisi ve hidrokarbon imkanları, *TPAO Rapor* 791/1-2, Ankara (unpublished).

Schneider, G.F. 1958. New genera and species of ostracod. Trudy Vsesoyuznogo Neftyanogo Nauchno-Issledovatelskogo *Geologo-Razvedochnogo Instituta* (VNIGRI), 115: 244-245, 257, 263-264, 265, 267-269, 270-274.

Stancheva, M. 1965. Ostrakodna fauna ot Neogena v severozapadna Balgarija, 4. Pontski ostrakodi, Trud. Geol. Balgarija, Paleont., 7: 15-69, 8 Tab., 4 Taf., Sofija. (travaux sur la géologie de Bulgarie, *Sér. Paléontologie*, VII, 15-69, 8 Tab., 4 Taf., Sofia 1965).

Stoica, M., Floroiu, A. Krijgsman, W., Vasiliev, I. 2013. Upper Miocene ostracods from the Black Sea (Taman Peninsula, Russia), *Naturalista Siciliano*, S. IV, XXXVII(1), pp. 389-391.

Stoica, M ., Krijgsman, W., Fortuin, A., Gliozzi, E. 2016. Paratethyan ostracods in the Spanish Lago-Mare: More evidence for interbasinal exchange at high Mediterranean sea level *Palaeogeography, Palaeoclimatology, Palaeoecology,* 441 (2016) 854–870.

Svejer, A.V. 1949. Ob Ostracodah pliocena Severnego Kavkaza i Niznego Povolz'ja s nekotorymi novymi dannymi k sistematike iskopaemyh ostrakod, *Trudy Vnigri*, N.S. 30: 7-68, 10 Abb., 11 Taf., Leningrad, Moskva.

Şafak, Ü. 2010. Güney-Buldan-Yenicekent-Babadağ-Kale (Denizli, GB Anadolu) Çevresi Tersiyer Çökellerinin Ostrakod Topluluğu ve Ortamsal Özellikleri, *KSÜ Mühendislik Bilimleri Dergisi*, 13 (2), 44-62.

Şafak, Ü. 2013. Hınıs (Erzurum, Doğu Anadolu) yöresindeki volkano-sedimanter Yolüstü Formasyonu ostrakod faunası ve ortamsal özellikleri, *Maden Tetkik Arama Dergisi*, 146, 55-81, Ankara.

Şafak, Ü., Nazik, A., Şenol, M. 1992. Kayseri Güneydoğusu (Sarız) Pliyosen Ostrakod ve Gastropod Faunası, Ç. Ü. Müh. Mim Fak**.** *Dergisi*, Cilt 7, Sayı 1, s. 171-195, Adana.

Şaroğlu, F. 1986. Doğu Anadolu'da neotektonik dönemdeki jeolojik evrim ve havza modelleri, *Maden Tetkik ve Arama Dergisi* 107, 73-94, Ankara.

Şaroğlu, F., Yılmaz, Y. 1984.Doğu Anadolu'nun Neotektoniği ve ilgili Mağmatizması, *TJK İhsan Ketin Sempozyumu özel sayısı*, 149-162.

Şengör, A.M.C. 1980. Türkiye'nin Neotektoniğinin Esasları, *TJK Konferanslar Serisi*, No. 2, 40 s., Ankara.

Şengör, C. ve Kidd, W.S.F. 1979. Post-Collsional tectonic of the Turkish limnian a comparison with Tibet *Tectonoph*: yides 53, 363-365.

Şengüler, İ., Toprak, S. 1991. Varto, Hınıs, Bulanık, Malazgirt yöresi linyitlerinin petrografik özellikleri, *TJK Bülteni*, c. 34, 15-22, Ankara.

Taner, G. 1980. Das Neogen der Umgebung Yalova, Communications de la Faculté des Sciences de l'Université d'Ankara, Série C1, *Géologie*, Tome 23, Ankara.

Taner, G. 1997. Das Pliozan des östlichen Dardanellen Beckens, Türkei. Molluskenfauna und Stratigraphie. *Ann. Naturhist. Mus.* Wien, 98a, 35-67, Wien.

Tarhan, N. 1989. Hınıs-Varto (Erzurum-Muş) dolayının Jeolojisi ve Petrolojisi, İstanbul Üniversitesi Fen Bilimleri Enstitüsü *Doktora tezi*, 181 sayfa, İstanbul (unpublished).

Tarhan, N. 1991. Hınıs-Varto-Karlıova (Erzurum-Muş-Bingöl) Dolayındaki Neojen Volkanitlerinin Jeolojisi ve Petrolojisi, *MTA Dergisi*, 113, 45-60, Ankara.

Tokel, S. 1979. Erzurum-Kars yöresindeki Neojen çöküntüsüyle ilgili volkanizmanm incelenmesi: *Doçentlik tezi*, Karadeniz Teknik Univ., 106 s. (unpublished), Trabzon.

Tokel, S. 1984. Doğu Anadolu'da kabuk deformasyonunun mekanizması ve genç volkanitlerin petrojenezi: *Türkiye Jeol. Kur. İhsan Ketin Sempozyumu, Bildiri Özleri*, ODTÜ, Ankara.

Tunoğlu, C. 2001. Pontian aged *Loxoconcha* (Ostracoda) species from eastern Black Sea Region of Turkey, *Yerbilimleri*, 24, 127-142, Ankara.

Tunoğlu, C. 2003. Systematics and biostratigraphy of the Pontian Candonidae (Ostracoda) from the Eastern Black Sea region (Northern Turkey), *Geologica Carpathica*, 54, 1, 21-40, Bratislava.

Tunoğlu, C., Ünal, A., Bilen, C. 1998. The investigation of Tethys-Paratethys interaction and influence area along the Eastern Black Sea Coast of Turkey. *TÜBITAK, Project Number: YDABÇAG-133*, Ankara, 1—149.

Vasiliev, J., Krigsman, W., Stoica, M., Langereis, Cor, G. 2005. Mio-Pliocene magnetostratigraphy in the southern Carpathian foredeep and Mediterranean-Paratethys correlations, *Terra Nova*, 17, 376-384.

Vasilyan, D., Schneider, S., Bayraktutan, MS., Şen, Ş. 2014. Early Pleistocene freshwater communities and rodents from the Pasinler Basin (Erzurum Province, north-eastern Turkey), *Turkish Journal of Earth Sciences*, 23: 293-307.

Vesel-Lukic, M, Tadesse, V. H., Poljak, M. 2013. Late Miocene Ostracoda from Bizeljsko section (eastern Slovenia), *Naturalista Siciliano*, S. IV, XXXVII(1) pp. 413-414.

Wenz, W. 1922.Zur Nomenklatür tertiaerer Land und Süsswassergastropoden, *Senkenbergiana*, Bd. IV, Heft 5, 2, 75-86, Frankfurt.

Yılmaz, Ö. 1997. Aras Yarma Vadisi ve yakın çevresinin jeomorfolojisi ile morfotektonik evrimi (Kuzeydoğu Anadolu), *Türk Coğrafya Dergisi*, Sayı: 32, 121-142, İstanbul.

Yılmaz, O., Şener, M. 1984. Erzurum-Pasinler, Erzincan-Çayırlı, Kars-Tuzluca, Malatya-Hacılar stratigrafik açınsama kuyularına ait örneklerin X-ışınları tekniği ile incelenmesi, *Türkiye Jeoloji Kurumu Bülteni*, C. 27, 31-40.

Yılmaz, A., Terlemez, I., Uysal, Ş. 1988. Hınıs (Erzurum GD su) dolaylarının bazı stratigrafik ve tektonik özellikleri, *MTA Dergisi* 108, 38-56, Ankara.

Zalanyi, B. 1929. Morpho-systematische Studien über fosil: Muschelkrebse, *Geol. Hung., Ser. Paleontology*, 5:1-153.

Zalanyi, B. 1959. Tihanyi felsö Pannon Ostrakodak (Ober Pannonische Ostracoden aus Tihany) Hungary, *Annual Institute Geologie Publication Hungarici*, 48, 195-218.

PLATE

PLATE I

Figure 1. *Amnicythere idonea* Mandelstam, Markova, Rozyeva and Stepanajtys, 1962

Shell, right outer appearance, Köprüköy Measured Section 2, sample no. 6

Figures 2-3. *Candona (Caspiocypris) erzurumensis* Freels, 1980

Shell, left outer appearance, Köprüköy Measured Section 1, sample no. 19

Right shell, outer appearance, Köprüköy Measured Section 2, sample no. 6

Figures 4-8. *Candona (Caspiocypris) araxica* Freels, 1980

Left shell, outer appearance, Köprüköy Measured Section 2, sample no. 6

Shell, left outer appearance, Köprüköy Measured Section 2, sample no.5

Left shell, outer appearance, Köprüköy Measured Section 2, sample no. 6

Shell, left outer appearance, Köprüköy Measured Section 1, sample no. 24

Shell, left outer appearance, Köprüköy Measured Section 1, sample no. 10

PLATE I

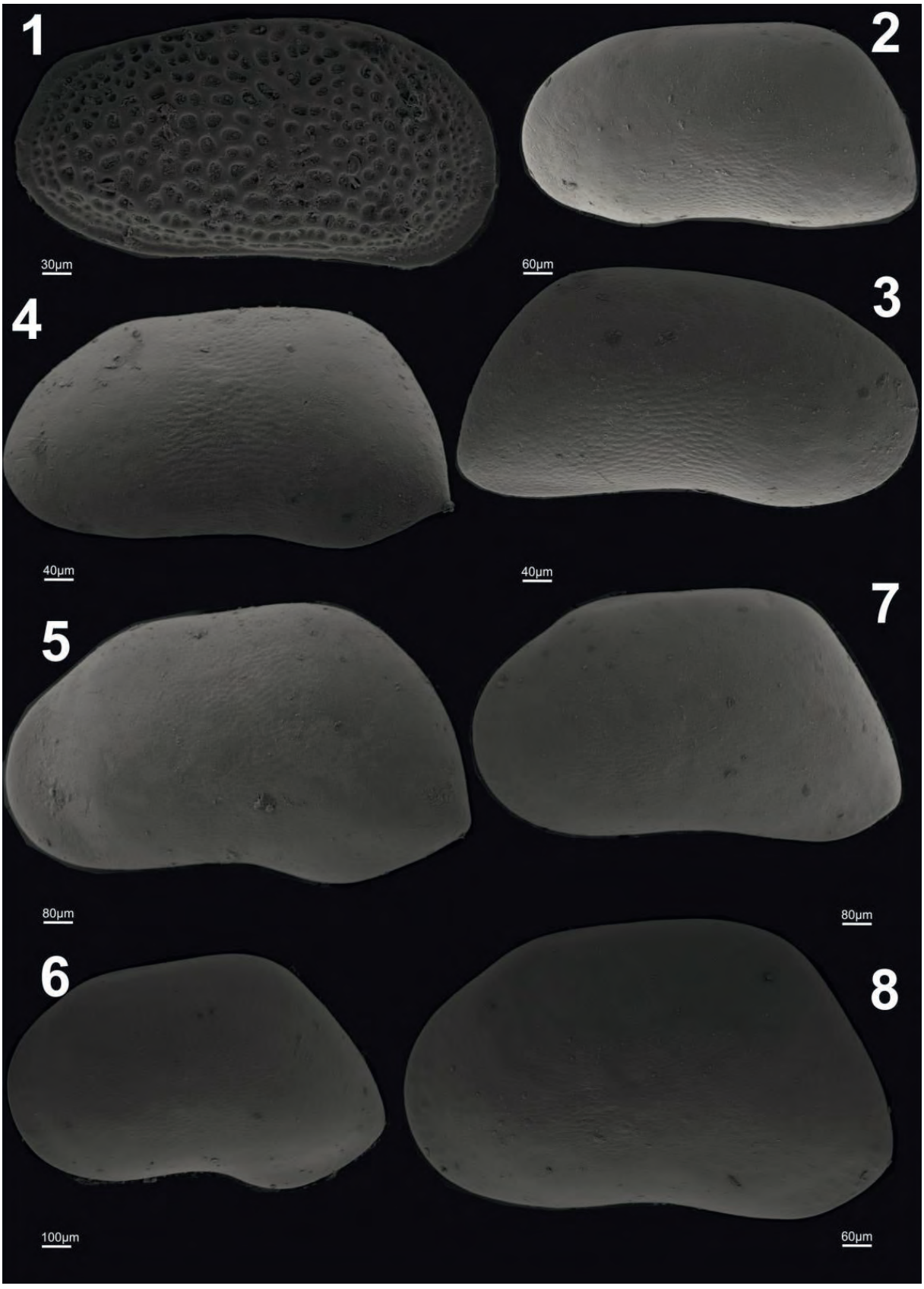

PLATE II

Figures 1-7. *Candona (Caspiocypris)* aff. *alta* (Zalanyi, 1929)

Shell, right outer appearance, Köprüköy Measured Section 2, sample no. 8

Right shell, outer appearance, Köprüköy Measured Section 2, sample no. 8

Shell, right outer appearance, Köprüköy Measured Section 2, sample no. 4

Shell, right outer appearance, Köprüköy Measured Section 2, sample no. 8

Right shell, outer appearance, Köprüköy Measured Section 2, sample no. 4

Shell, right outer appearance, Köprüköy Measured Section 1, sample no. 19

Shell, left outer appearance, Köprüköy Measured Section 1, sample no. 10

Figure 8. *Candona (Lineocypris)* aff. *granulosa* Zalanyi, 1959

Shell, left outer appearance, Köprüköy Measured Section 2, sample no. 5

PLATE II

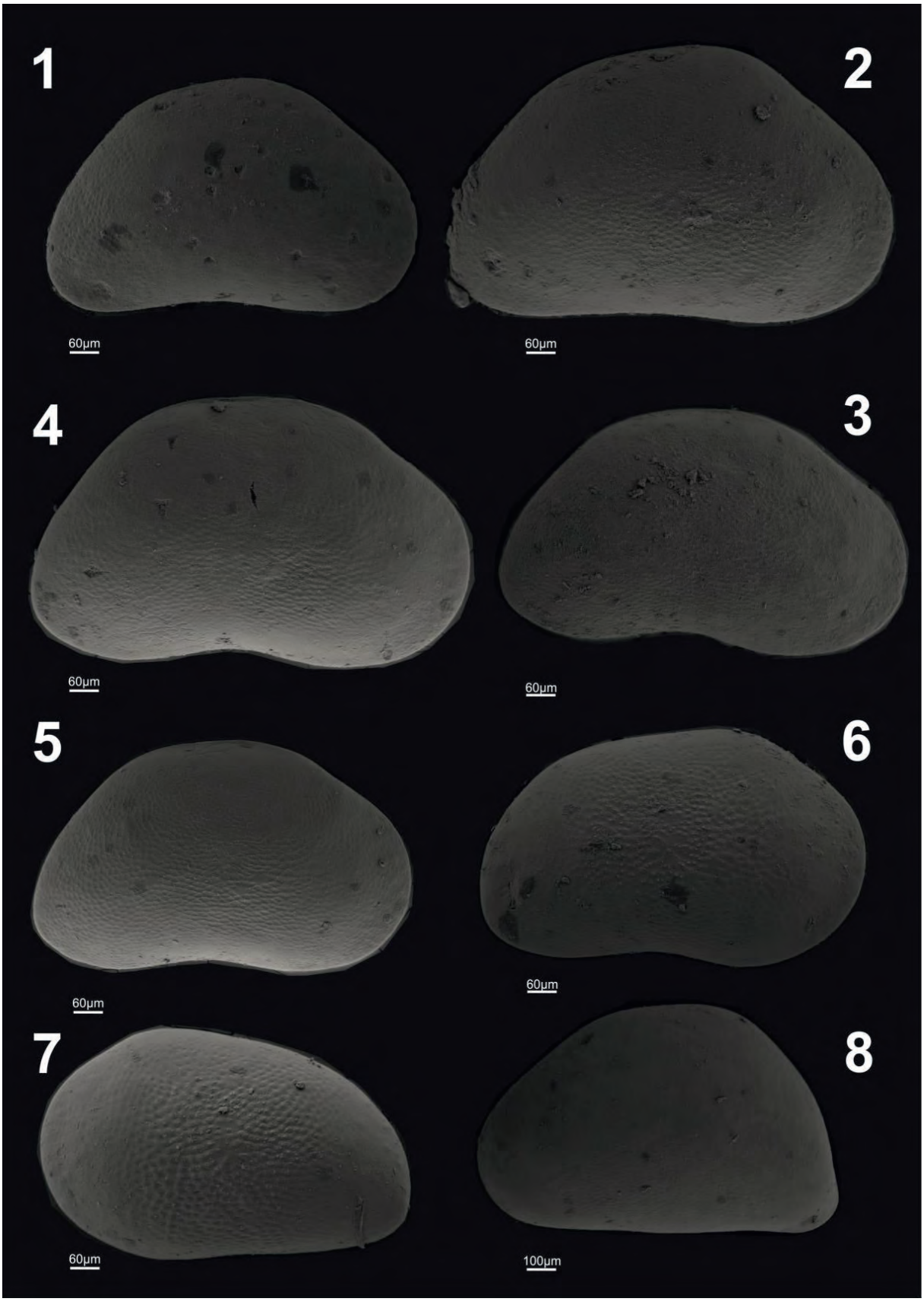

PLATE III

Figures 1-4. *Bakunella* cf. *dorsoarcuata* (Zalanyi, 1929)

Shell, left lateral appearance, Köprüköy Measured Section 1, sample no. 6

Shell, left outer appearance, Köprüköy Measured Section 1, sample no. 6

Left shell, outer appearance, Köprüköy Measured Section 1, sample no. 18

Shell, right outer appearance, Köprüköy Measured Section 2, sample no. 21

Figures 5-8. *Bakunella* cf. *subtriangularis* (Svejer, 1949)

Shell, left outer appearance, Köprüköy Measured Section 2, sample no. 4

Shell, right outer appearance, Köprüköy Measured Section 2, sample no. 4

Left shell, outer appearance, Köprüköy Measured Section 2, sample no. 4

Shell, left outer appearance, Köprüköy Measured Section 2, sample no. 7

PLATE III

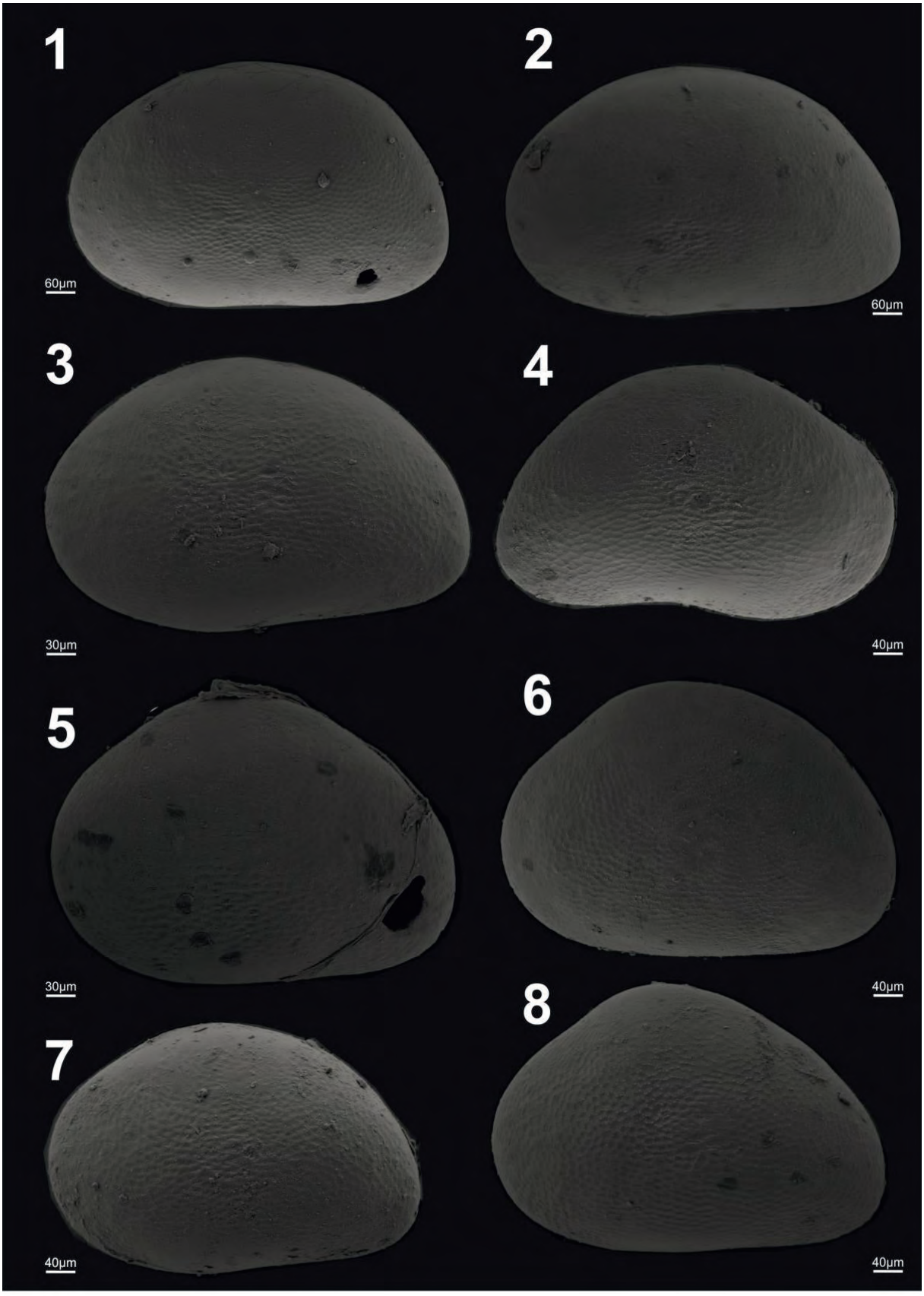

PLATE IV

Figures 1-3. *Candona (Candona) lycica* Freels, 1980

Right shell, outer appearance, Köprüköy Measured Section 1, sample no. 13

Shell, left lateral appearance, Köprüköy Measured Section 1, sample no. 13

Shell, left lateral appearance, Köprüköy Measured Section 1, sample no. 20

Figures 4-5. *Candona (Candona) armenia* Freels, 1980

Left shell, outer appearance, Köprüköy Measured Section 1, sample no. 13

Shell, left outer appearance, Köprüköy Measured Section 1, sample no. 4

Figure 6. *Candona (Candona)* aff**.** *elongata* (Svejer, 1949)

Right shell, outer appearance, Köprüköy Measured Section 2, sample no. 6

Figure 7. *Fossilyocypris sarızensis* (Şafak, Nazik and Şenol, 1992)

Right shell, outer appearance, Köprüköy Measured Section 1, sample no. 21

Figure 8. *Dreissena polymorpha* (Pallas,1771)

Right shell, outer appearance, Köprüköy Measured Section 2, sample no. 9

PLATE IV

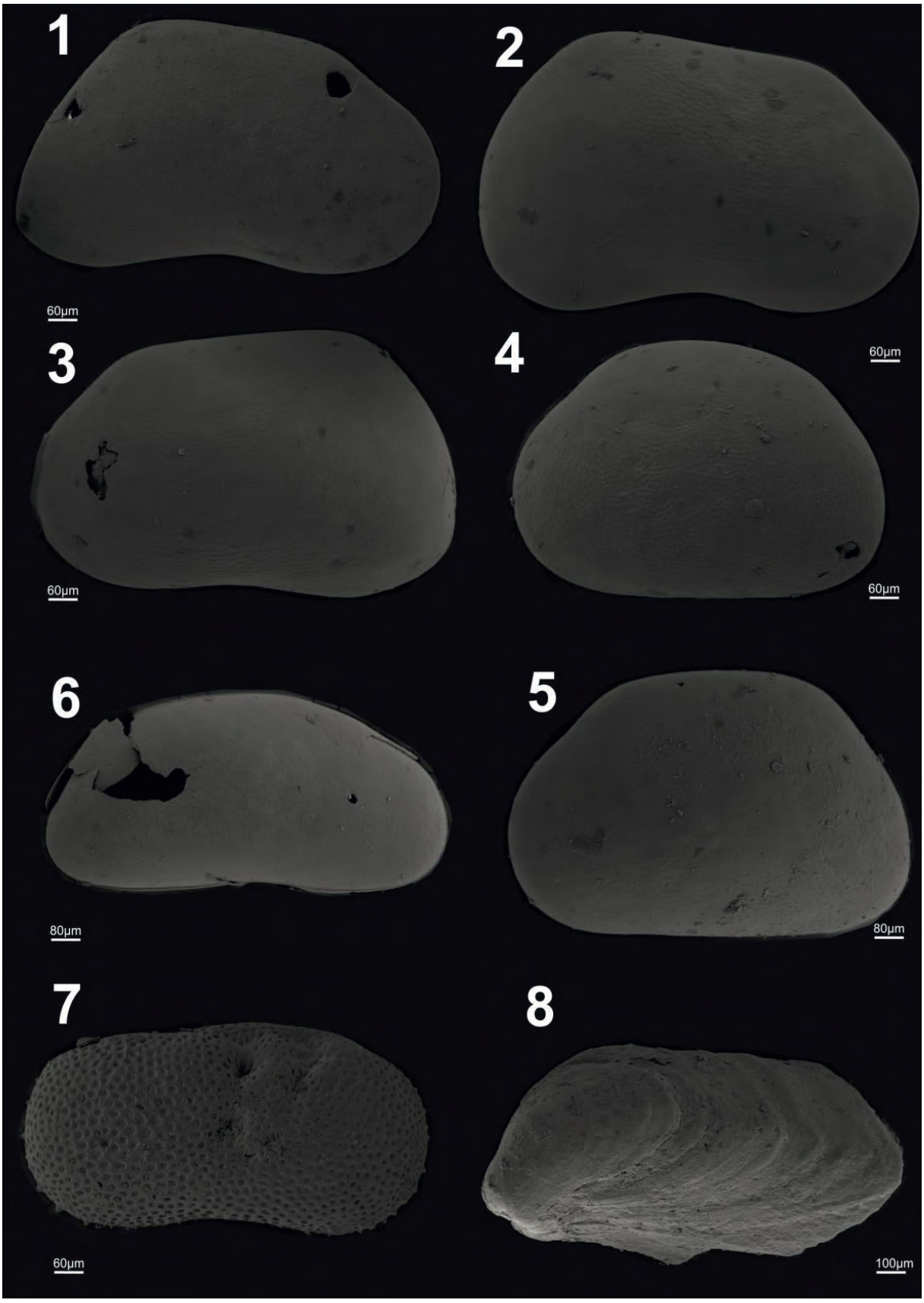

Bull. Min. Res. Exp. (2016) 153:139-158

Bulletin of the Mineral Research and Exploration

http://bulletin.mta.gov.tr

MINERALOGY AND GEOCHEMISTRY OF THE KOCADAL (TORUL, GÜMÜŞHANE, EASTERN BLACK SEA REGION, TURKEY) Zn-Pb-Ag, Au and Cu MINERALIZATIONS

İsmail CİHAN[a*], Levent TOSUN[a], Özcan DUMANLILAR[a], İsmet CENGİZ[a] and Taner ÜNLÜ[b]

[a]*Demir Export A.Ş., Maden Arama Müdürlüğü, 06440 Kızılay/Ankara*
[b]*Ankara Üniversitesi, Mühendislik Fakültesi, Jeoloji Mühendisliği, 06100 Tandoğan/Ankara*

Research Article

Keywords:
Eastern Pontides, Kocadal Gold Mineralization, Conglomerate-Sandstone, Quartz Veins.

Received: 08.12.2015
Accepted: 27.01.2016

ABSTRACT

The Kocadal base and precious metal mineralizations are located in the southwest of Gümüşhane province of the eastern Pontide orogenic belt. In the vicinity of the Kocadal mineralization, Gümüşhane granite, lithologies of the Hamurkesen, Berdiga, and Mescitli formations, dacite porphyry and andesite porphyry are present with abundant alluvium. Based on geological, mineralogical, and geochemical features, three mineralization styles have been recognized at the Kocadal area: (i) Mineralizations around Batarya tepe include (ia) Zn mineralization within the conglomerates and sandstones of the Hamurkesen formation and (ib) Zn-Pb-Ag-(Au) mineralization associated with dacite prophyry, (ii) Au mineralization, which occurs to the southwestern of Batarya tepe, and (iii) Cu mineralizations related to quartz veins and veinlets at Gözelerin Dere. Mineralized gravels within the conglomerates contains mainly sphalerite and pyrite, whereas hydrothermal mineralizations associated with porphyritic dacite comprise pyrite and sphalerite, with minor galena, chalcopyrite, pyrrhotite, arsenopyrite, marcasite, fahlerz, pyrargyrite, and proustite. Alteration patterns of hydrothermal mineralization in the field, from older to younger, are classified as: (i) tremolite-actinolite±garnet, (ii) quartz-sericite-chlorite, and (iii) carbonate-quartz. Mineralized gravels within the conglomerates contains mainly sphalerite and pyrite, whereas pyrite, chalcopyrite, and galena are common in quartz veins at Gözelerin Dere. Geostatistical studies based on the results of geochemical analysis of core samples reveal the presence of the distinct element associations for the different styles of mineralizations.

1. Introduction

Mineral deposits and mineral occurrences associated with the magmatic rocks in the southern part of the Eastern Black Sea Region form an E-W extending zone. This zone includes porphyry Cu-Mo, epithermal Au-Ag and vein type base metal and precious metal mineralizations (Figure 1). Kocadal base and precious metal mineralizations are located in the central part of this zone and are in the 24 km to the Southwest of Gümüşhane, in the 1/25000 scale map sheets H42-a2, a3, b1 and b4. Some of the mines operational in the region are Mastra Au, Midi (Zn-Pb-Cu-Au-Ag) and Hazine Mağara (Pb-Zn-Au-Ag). Apart from these, there are also numerous mineralization occurrences in the region.

There have been numerous studies concerning basic geology and mineralizations in and near Gümüşhane region. First studies on the mineralizations in the study area were carried out by Baytekin and Uslu (1974). Later on Çınar et al. (1983) and Türk (MTA)-Japan Joint Project (1985) (Türk (MTA)-Japon Ortak Projesi, 1985) carried out geological studies in the study area. All these studies were in the frame work of regional prospection and mineralizations in the Kocadal area were considered to be hydrothermal mineralizations developed along the fracture systems. In 2009-2014 Demir Export Inc carried out detailed geological mappings and surface geochemical studies to delineate mineralization areas and conducted core drillings to test dip down extensions of the mineralization. In this work some of Demir Export's data have been used to explain and discuss geological, mineralogical and geochemical characters of the Kocadal base metal and precious metal mineralizations and different types of mineralizations have been identified and described. By doing this it was meant to provide some information to help future mineral exploration activities in the region.

* *Corresponding Author: İsmail CİHAN, ismailc@demirexport.com*
http://dx.doi.org/10.19111/bulletinofmre.266067

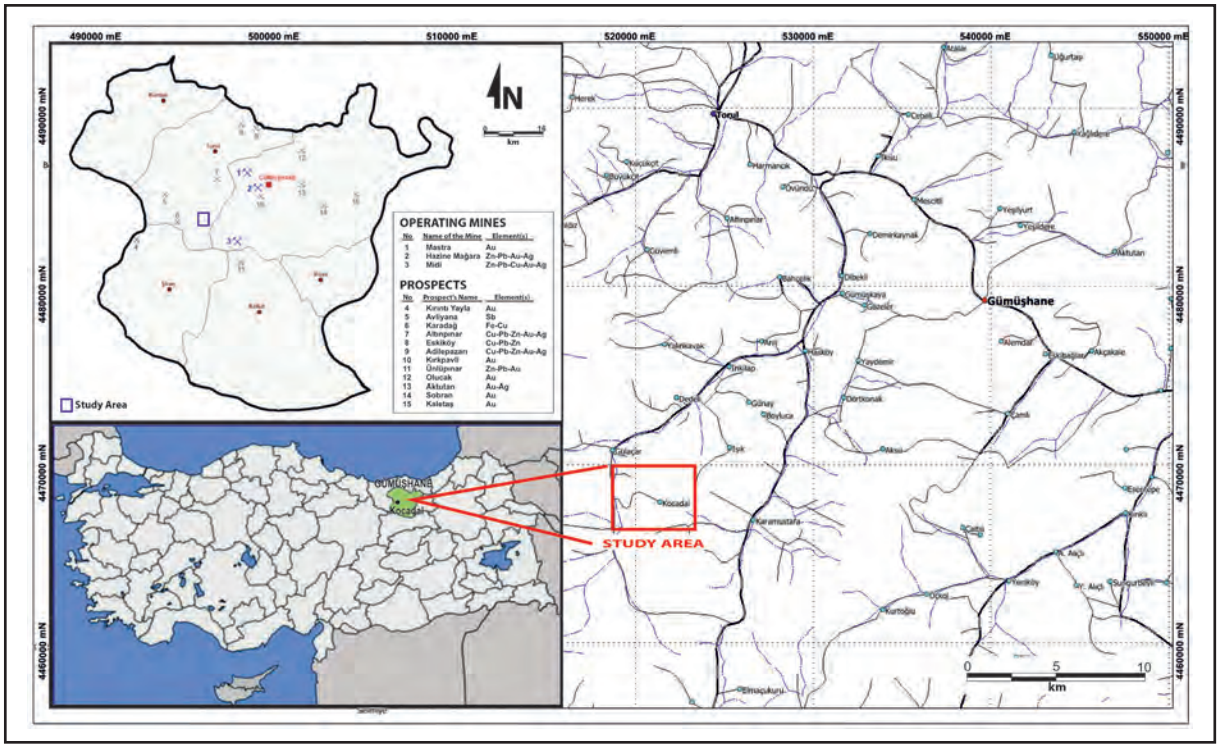

Figure 1- Location map of the study area.

2. Regional Geology

Study area is located in the Southern part of the Eastern Pontides (Hamilton, 1942; Ketin 1966; Ketin and Canıtez, 1972; Özsayar et al., 1981; Bektaş et al., 1984). The basal rock units present in the area are Paleozoic Kurtoğlu metamorphics (Yılmaz, 1972). These rock units were intruded by Permo-Carboniferous granitic intrusives (Çoğulu, 1970; Yılmaz, 1972), developed from the southern plunge of northern branch of Paleo Tethys (Dewey et al., 1973; Şengör and Yılmaz, 1981; Bektaş et al., 1999; Eyüboğlu, 2010; Eyüboğlu et al., 2012). These units were discordantly overlain by volcano-sedimentary Hamurkesen formation of Lower-Middle Jurassic, characterizing rifting in marine environment related to the extensional tectonics (Eyüboğlu et al., 2010, 2014). This succession at the next stage of rifting was concordantly overlain by Upper Jurassic-Lower Cretaceous Berdiga formation consisting platform limestones, characterizing shallow marine environment (Eyüboğlu et al., 2010, 2014). Berdiga formation is concordantly overlain by flysch like (Güven, 1993) Turonian-Paleocene, Mescitli formation (Pelin, 1977). All units in the area have been cut by Eocene dacite porphyries related to volcanic arch (Eyüboğlu et al., 2011). Dacite porphyries have intrusive relationships with the Hamurkesen formation and the Gümüşhane granite. Because of these relationships, dacite porphyries can be correlated with the Lower Eocene Zigane granitoid (Ketin 1966; Bektaş et al., 1995; Karslı, 1996) present in the area, related to the magmatic arch which was active during Late Cretaceous-Early Eocene (Şengör and Yılmaz 1981; Okay and Şahintürk 1997; Yılmaz and Karslı 1997; Yılmaz et al., 1997; Bektaş et al., 1999; Şengör et al., 2003), (Figure 2).

3. Local Geology

In the study area and in the surrounding areas various kinds of lithologies at various ages are present. From oldest to youngest they are; Gümüşhane granite, Hamurkesen (Zimoköy) formation, Berdiga formation, Mescitli formation, dykes and alluviums (Figure 3).

3.1. Gümüşhane Granite

In the study area Gümüşhane granite is the oldest unit. It was named as Gümüşhane pluton by Çoğulu (1970) and Yılmaz (1972). Lermi (2003) described Gümüşhane granite and said that it has granite, granodiorite, tonalite, quartz monzodiorite, quartz diorite and diorite mineralogy.

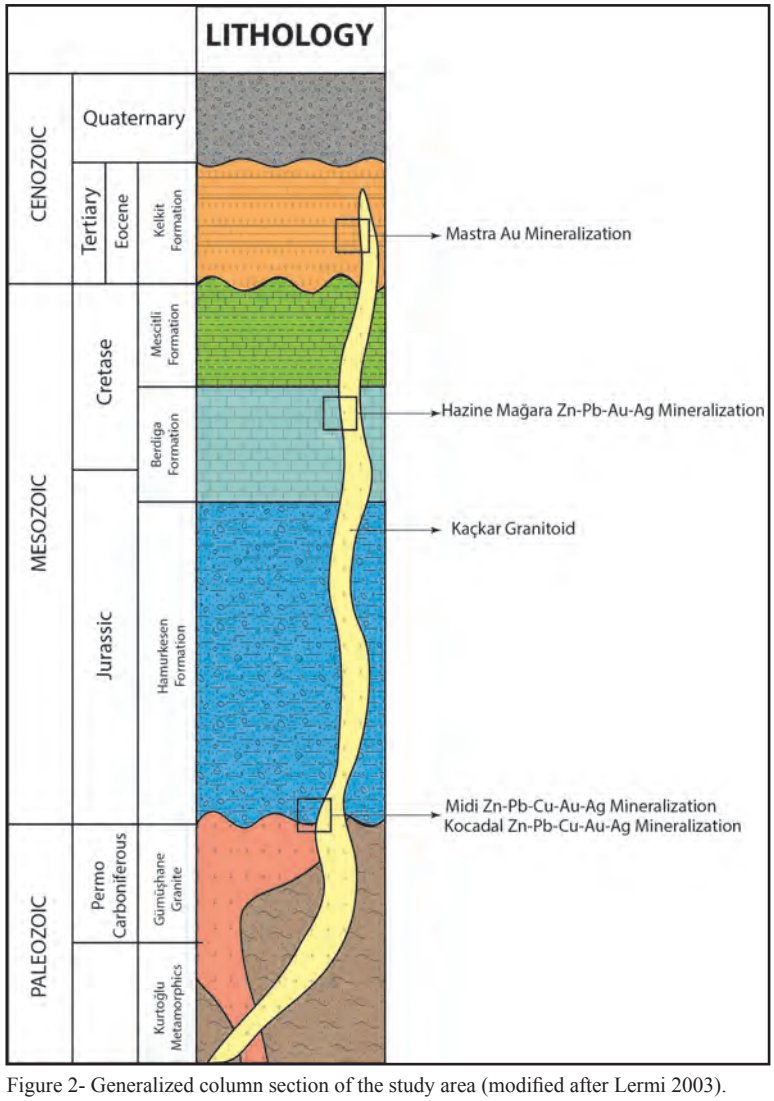

Figure 2- Generalized column section of the study area (modified after Lermi 2003).

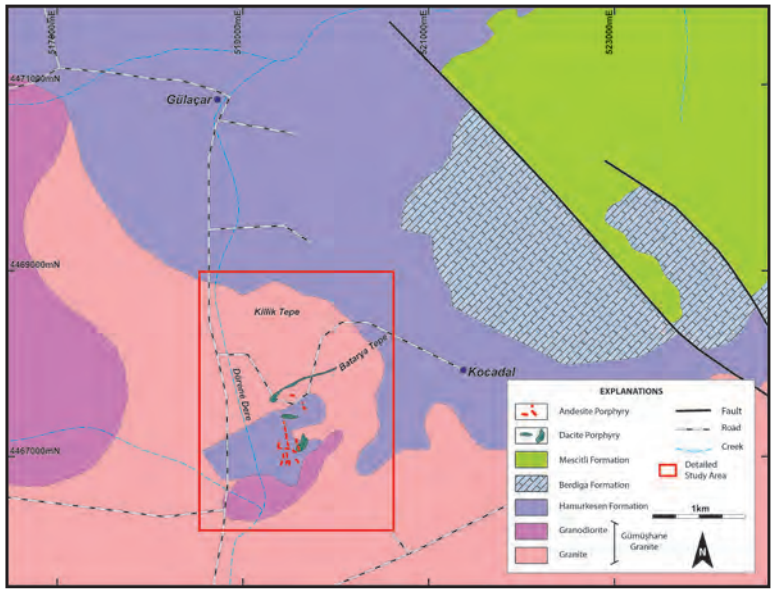

Figure 3- 1/500.000 scale geological map of the study area (modified after Şenel, 2002).

Rock units outcropping in the western and northern part of the study area are granite, granodiorite and quartz diorite. Gray-beige coloured granites and quartz diorites crop out around Killik Tepe (Killik Hill). These two rock units have intricate relationships and have various amounts of plagioclase, orthoclase and amphibole minerals, biotite, chlorite and small amount of pyroxenes. Size of minerals is up to 0.5 cm Diorites and quartz diorites considered to be last phase crop out around Batarya Tepe and have darker colours and smaller size minerals than granodioritic rocks. They are consist of 50% plagioclases and have alkali feldspars, quartz, amphibole, pyroxene minerals, epidote and chlorite (Lermi, 2003).

3.2. Hamurkesen Formation

Lower-Middle Jurassic volcano-sedimentary succession named as Hamurkesen formation by Ağar (1977) or Zimonköy formation as named by Eren (1983) overlays Gümüşhane granite with an unconformity. Based on the colour and lithological difference the Hamurkesen formation has been divided into two different members. The formation at the base starts with basalts, spilitic basalts, pyroclastics, dolerites of the İkisu member, concordantly overlain by andesites and pyroclastics with clayey limestone and sandstone lenses of the Karaca volcano-sedimentary member (Eyüboğlu et al., 2006).

The units cropping out around Batarya Tepe and in the southern part are conglomerates-sandstones with gray-black coloured sand to block size fragments (Figure 4A) and in places in limited narrow patches with volcanic interlayers (Figure 4B-4C). Bedding is not observed at the lower parts but in the upper parts as the grain sizes become smaller medium beddings become noticeable. The unit consists of magmatic rock fragments, quartz grains an lesser amounts of metamorphic rock fragments, the matrix is made of clay and sand size of similar materials. The unit also has magmatic rock pebbles with disseminated and massive ore mineralizations. In general in the unit semi rounded fragments with corners are dominant (Figure 4 D).

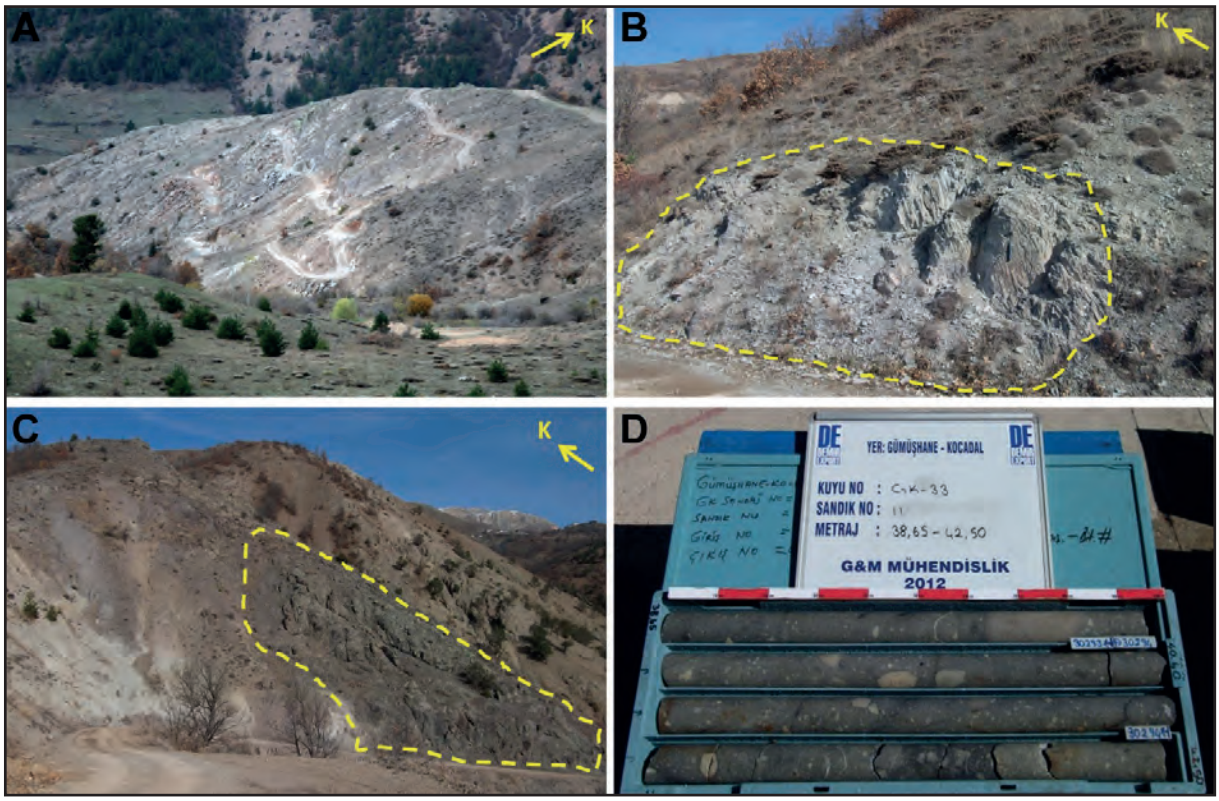

Figure 4- A) General field view of the conglomerates-sandstones of the Hamurkesen formation B) Volcanic (rhyolite) parts in the Hamurkesen formation C) Pyroclastic (agglomerate) parts in the Hamurkesen formation D) General view of the conglomerates-sandstones in the drill cores.

3.3. Berdiga Formation

Berdiga formation named by Pelin (1977) at the base starts with yellow coloured sandy limestones upward goes to red coloured limestones then to sandstone-siltstone-claystone-marl and limestone interbeds and also tuff intercalations concordantly overlies the Hamurkesen formation. The Berdiga formation is Upper Jurassic- Lower Cretaceous age (Taslı, 1984).

The unit is represented by gray-white coloured limestones, outcrops in the northern part of the study area at the high altitudes. The limestones display medium thick beddings and have extensive karsts structures.

3.4. Mescitli Formation

The unit was first named as Kermutdere formation by Tokel (1977). It is mainly made of flysch facieses sediments outcropping along the Southern Pontide zone. The unit later on was named as Mescitli formation by Güven (1993). The unit concordantly overlies the Berdiga formation. It starts with red-Bordeaux coloured clayey limestones and is a thick succession made of alternations of gray coloured marl-shale-clayey limestone with sandstones intercalations. In some locations tuff intercalations are also present. In Eastern Pontides All along Late Cretaceous, along with the products of developing active volcanisms Mescitli formation developed in deep marine environment. It is a thick succession at Turonian-Paleocene age (Güven, 1993).

The unit outcrops in the north-eastern part of the study area, is represented by red-bordeaux coloured clayey limestones with thin and thick beddings

3.5. Dikes

In the Eastern Pontides three different ages of magmatic activities are under considerations (Okay and Şahintürk, 1977); (I) First period is Early Jurassic-Middle Jurassic tholetiic rocks, related to extensional regime (Peccerillo and Taylor, 1975; Gedikoğlu, 1978; Akın, 1979; Eğin et al., 1979; Akıncı, 1984, Gedik et al., 1996). (II) In the region second period developed as a result of Turronian-Maestrichtien age subduction, generally sub alkaline related to oceanic island arc magmatisms (Adamia et al., 1977; Eğin et al., 1979; Kazmin et al., 1986; Çamur et al., 1996). Same magmatism has been claimed to be related to Late Cretaceous-Early Eocene magmatic arc (Şengör et al., 2003). It is quite possible that dikes present in the study area are related to the third of these activities.

In the study area there are dike systems with different phase and different chemical compositions cutting one another.

Dacite porphyries outcropping in the Batarya Tepe area located in the fracture systems varying between N60ºE and E-W strikes (Figure 5 A). Dacite porphyries in the field have white and beige colour, they have extensive quartz phenocryst in clayey matrix. Dacite porphyries have intrusive relations with the Hamurkesen formation and Gümüşhane granites and display 1-5 m thick topographic eaves in the field. As a result of alteration original texture and mineralogy of the rocks have been totally destroyed, but still signs of porphyritic texture are still identifiable. Mineralogical studies showed that apart from quartz all other minerals have been altered. In the specimens quartz, sericite, plagioclases (subjected to carbonate and clay alterations) and eroded quartz are present. Matrix materials are clay, carbonate sericite and quartz (Figure 5 B-C).

In the study area relatively younger dykes with andesitic (?) composition have N-S and E-W extensions (Figure 6 A) cut Hamurkesen formation and dacite porphyries in the south-western part of the Batarya Tepe. These dykes are maximum 4 m thick and are followed about 60 m along their strike directions. Andesitic dikes form relatively smoother features on the topography than porphyries. In the outcrops they are dark gray, mineralogical studies show that they porphyritic texture and include some phenocryst of plagioclases, mafic minerals and few quartz. Apart from quartz all other minerals have been fully altered. Plagioclases have been sericitized and carbonation. Mafic minerals (hornblende) have been altered to chlorite and carbonate and are seen as pseudomorphs. Matrix materials have also been altered and include plagioclase microlites, quartz, chlorite and a few opaque minerals (Figure 6 B-C).

As andesitic dikes (?) cut older porphyries and they have also been cut, so it is considered that andesitic dikes represent a later stage of magmatic activities.

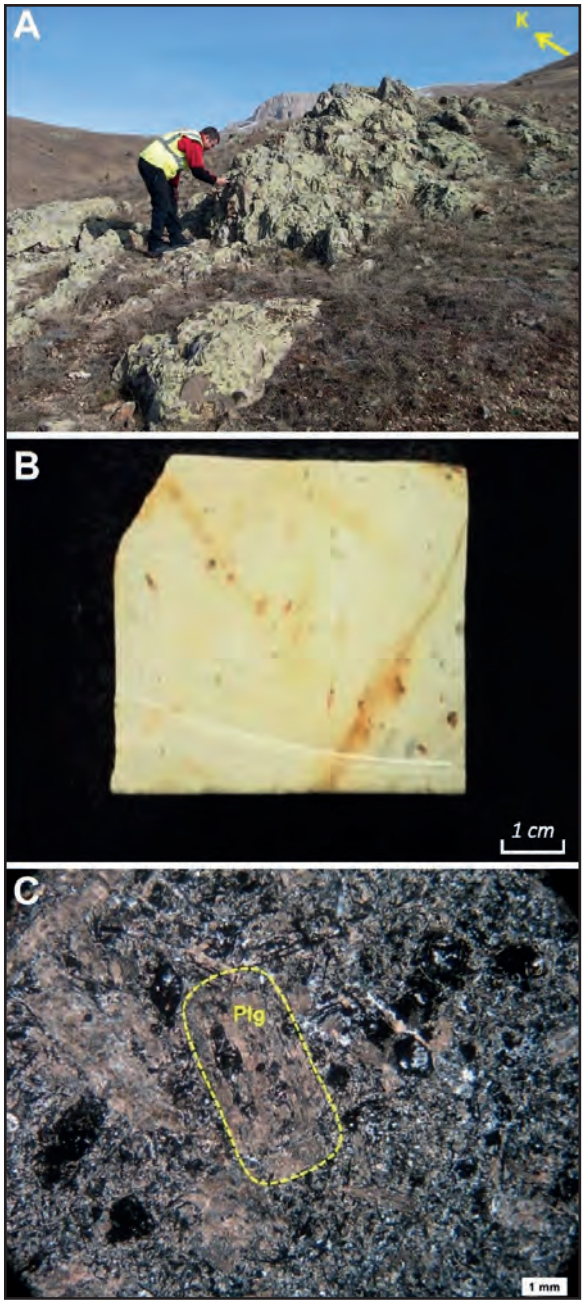

Figure 5- A) General field views of dacite porphyries, B) Hand specimen, C) Thin section view.

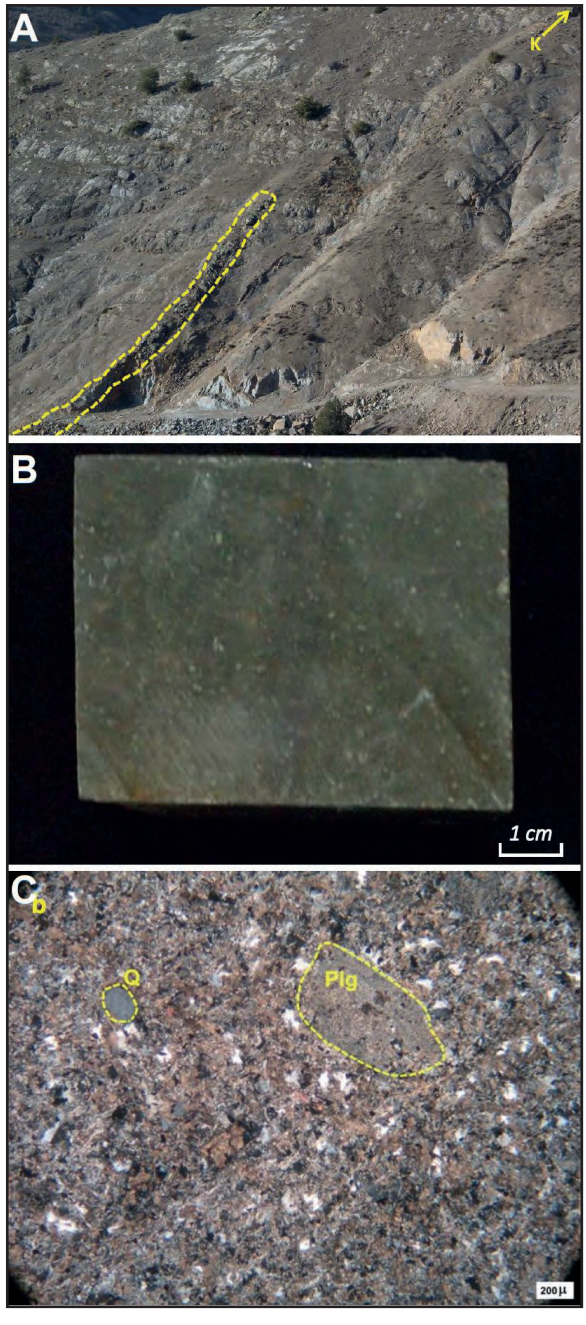

Figure 6- Andesitic dikes A) Field view, B) Hand specimen view, C) Thin section view.

These dykes in the study area have intercepting relations with older units, so they are considered to be Eocene age.

3.6. Alluvium

Stream sediments in the study area are present around Kara Dere. In the field in and around Kara Dere alluviums cover a 300 m long and 100 m wide area. Elements of the alluvium are rounded and are loosely cemented.

4. Structural Geology

In the study area as Lower-Middle Jurassic Hamurkesen formation overlies basement Permo-Carboniferous Gümüşhane granitoid with basal conglomerates indicating unconformity showing

that geological time gaps and long period of erosion during this time gap. Units of the Berdiga and Mescitli formations in the study area have concordant relationships indicating that in the area tectonically they had a quite sedimentation process.

In the study area 3 different fracture systems are present. They have NE-SW and NW-SE strike directions. Fracture system with NE-SW system has N60ºE and E-W strikes, dacite porphyries have developed in these fractures. N-S fracture system is closely associated with the andesitic dike systems, intercepting all older units in the study area NW-SE fractures area the youngest and intercept all other structure systems.

5. Mineralizations

In the study area mineralizations are present in three different locations. They are (ia) pebbles with sphalerites derived from the Gümüşhane granite (?), transported (magmatic) type mineralizations (ib) in the western slopes of Batarya Tepe Zn-Pb-Ag (Au) mineralizations in the N70ºE, E-W extending dacite porphyries in the conglomerates-sandstones of the Hamurkese formation, (ii) In the south-western part of the Batarya Tepe Au mineralizations in the dacite porphyries in the sandstones and (iii) around Gözelerin Dere Cu mineralizations in the N-S extending quartz veins and veinlets in the Gümüşhane granite (Figure 7) .

5.1. Batarya Tepe Zn-Pb-Ag-(Au) Mineralizations

Two different types and at two different ages mineralizations can be considered in the Batarya Tepe, they are (ia) transported type (magmatic origin) mineralizations, possibly associated with the Gümüşhane granite (Figure 8) and (ib) hydrothermal type mineralizations possibly related to the dacite porphyries intercepting granites and sandstones.

Presence of disseminated sphalerite bearing pebbles in the conglomerates-sandstones at the base of the Hamurkesen formation represent transported type (magmatic) mineralizations. The pebbles thought to have driven from the Gümüşhane granite is considered to be the right way to assume magmatic origin. Silicificiations argilizations and sericitization are extensive in these magmatic pebbles

Batarya Tepe Zn-Pb-Ag-(Au) mineralizations are associated with N60ºE, E-W striking and 60º-85º South

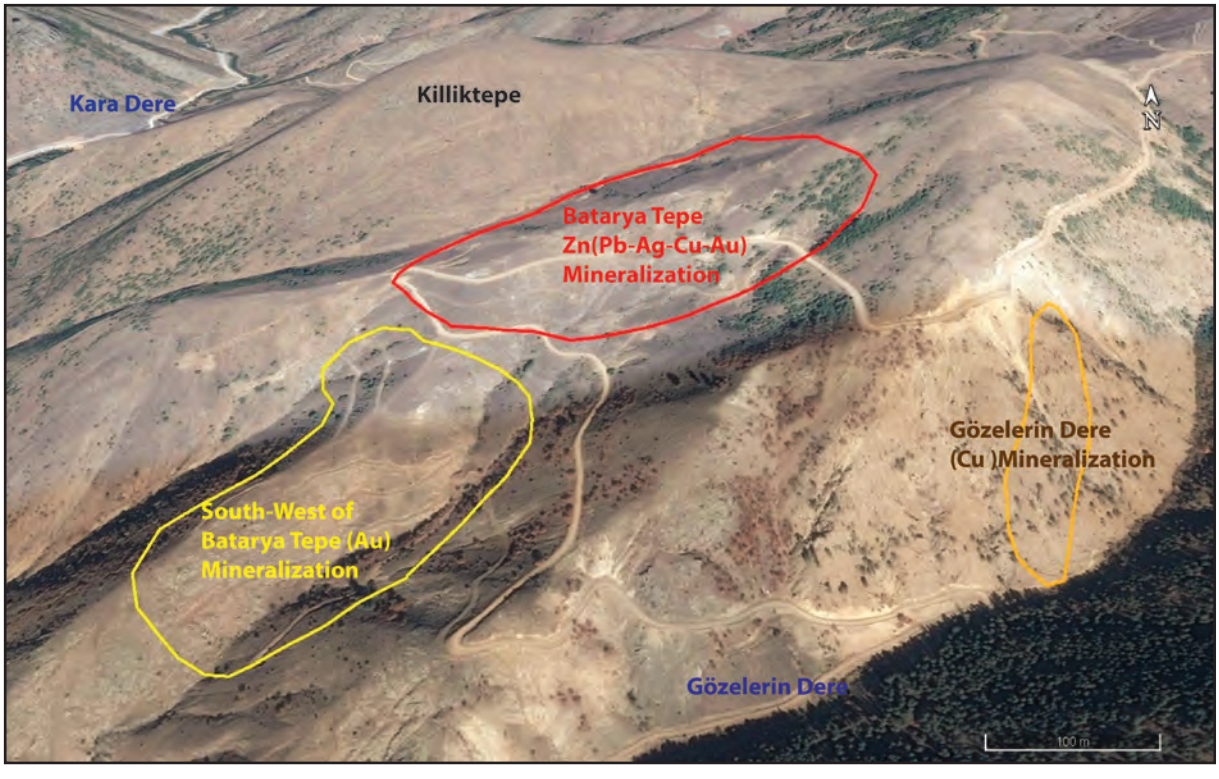

Figure 7- Google earth view of the mineralization areas.

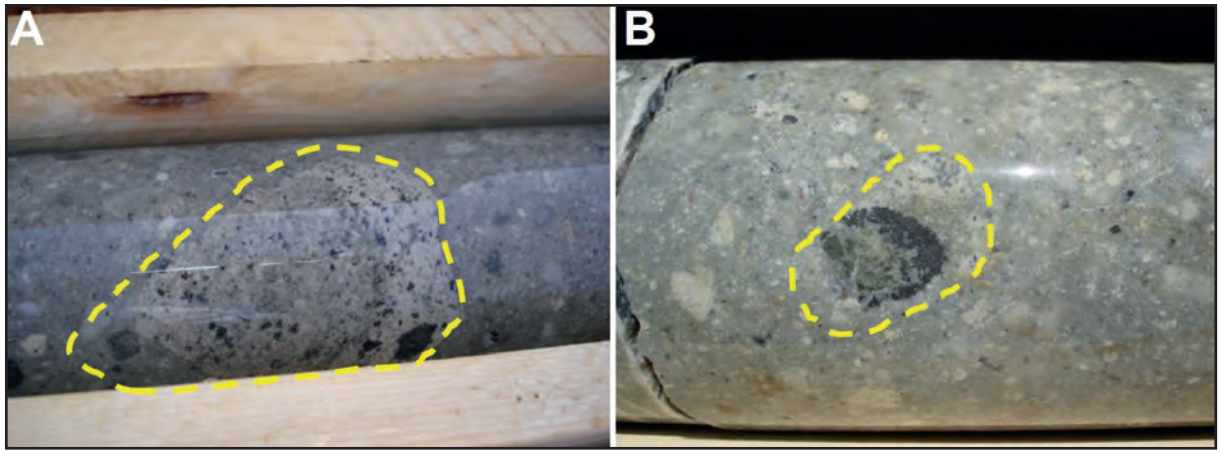

Figure 8- Mineralized pebbles in the conglomerates-sandstones of the Hamurkesen Formation A) Disseminated mineralizations in the pebbles, B) Massive mineralization in the pebbles.

dipping or vertical dacite porphyries. Conglomerates-sandstones of the Hamurkesen formation have been intercepted by dacite porphyries. Mineralizations and alterations have developed in dacite porphyries and in the rocks in contact with. Thickness, extension along the strike-dip directions of the mineralizations are connected and varied with thickness of the dacite porphyries, permeability, porosity, degree of fracturings of the host rock. On the surface alterations of silicificiation, argilization and limonitization and in places brecciations accompany mineralizations. In the Batarya Tepe these mineralized zones cover 150 x 400 m^2 area. With the surface and drill data it is concluded that these zones have 10-50 m continuation along the strike directions and are 1-5 m thick.

5.2. South-West of Batarya Tepe Au Mineralizations

Gold mineralizations in the south-western part of Batarya Tepe is associated with the conglomerates-sandstones of the Hamurkesen formation and with the N-S extending dacite porphyry dikes intercepting these units. In this part in the conglomerates-sandstones there are quartz, sphalerite and galenite bearing veinlets with limited extensions. On the surface carbonate-silica-chlorite-sericite alterations are observed in the dacite porphyries and in the conglomerates and in the sandstones. In this part sandstones-conglomerates and dacite porphyries have been cut by andesitic dikes. Taken surface and underground data together, it has been concluded that the mineralized zone is about 800 m long and up to 400 m wide.

5.3. Gözelerin Dere Cu Mineralizations

Gözelerin Dere Cu mineralizations are located in the ridge between Batarya Tepe and Gözelerin Dere. Within the zone milky quartz veins in varying thickness, varying degrees of silicificiations and argilizations are observed. Milky quartz veins may be up to 30 cm thick. Disseminated pyrite, very few chalcopyrite, galenite and in places malachite, azurite and limonite are present in the milky quartz veins and veinlets. Mineralizations are in the vertical tectonic lines with N10ºW and N-S strikes in the granodiorites of the Gümüşhane granite. They are up the 5 m thick and can be followed about 300 m along their strike directions

6. Mineralization Types

6.1. Transported (Magmatic) Type Mineralizations

In the Hamurkesen formation two different types mineralized rock fragments are present. Size of the mineralized rock fragments vary 1-5 cm. One type is granitic rock pieces (pebbles) with disseminated mineralizations (Rock pieces from the Gümüşhane granite) (Figure 8 A). Second type is massive ore pebbles (Figure 8 B).

6.2. Hydrothermal Type Mineralizations

In the study area hydrothermal mineralizations are observed in the granites, conglomerates-sandstones and dacite porphyries in the form of veins, veinlets, network, disseminations and smears.

6.2.1. Mineralizations in the Quartz Bearing Carbonate Veins-Veinlets

Sphalerite, galenite, pyrite and in places chalcopyrite minerals are present in the 0.5 cm – 1 m thick quartz-carbonate vein-veinlets (Figure 9 A). In places veins have been brecciated (Figure 9 B).

6.2.2. Network Type Mineralizations in Fractures and Cracks

Network type mineralizations are observed along the fractures and cracks in the rocks developed in various directions (Figure 9 C, D). These structures are filled with sulphide minerals and on the surface they are oxidized and have blackish-red coloured appearance.

6.2.3. Disseminated Type Mineralizations

Disseminated types of all kinds of ore minerals present in the region are encountered in the Batarya Tepe in the dacite porphyries and in their host rocks there. In the Gözelerin Dere copper mineralizations chalcopyrite, pyrite and galenite are also disseminated type (Figure 9 E).

6.2.4. Smear Type Mineralizations

Limonite smears are present in the cracks and fractures of all kinds of rock types present in the study area (Figure 9 F).

7. Alteration

By using drill cores alterations have been studied in detail and alteration patterns from old towards young have been grouped as (I) tremolite-actinolite ± garnet, (II) Quartz-sericite-chlorite and (III) Carbonate-silica alterations. During the processes of mapping because of surface effects and alterations masking one another alterations of silicification, argillization and quartz-sericite-chlorite-clay-carbonate minerals, have been marked with the dominant minerals present (Figure 10).

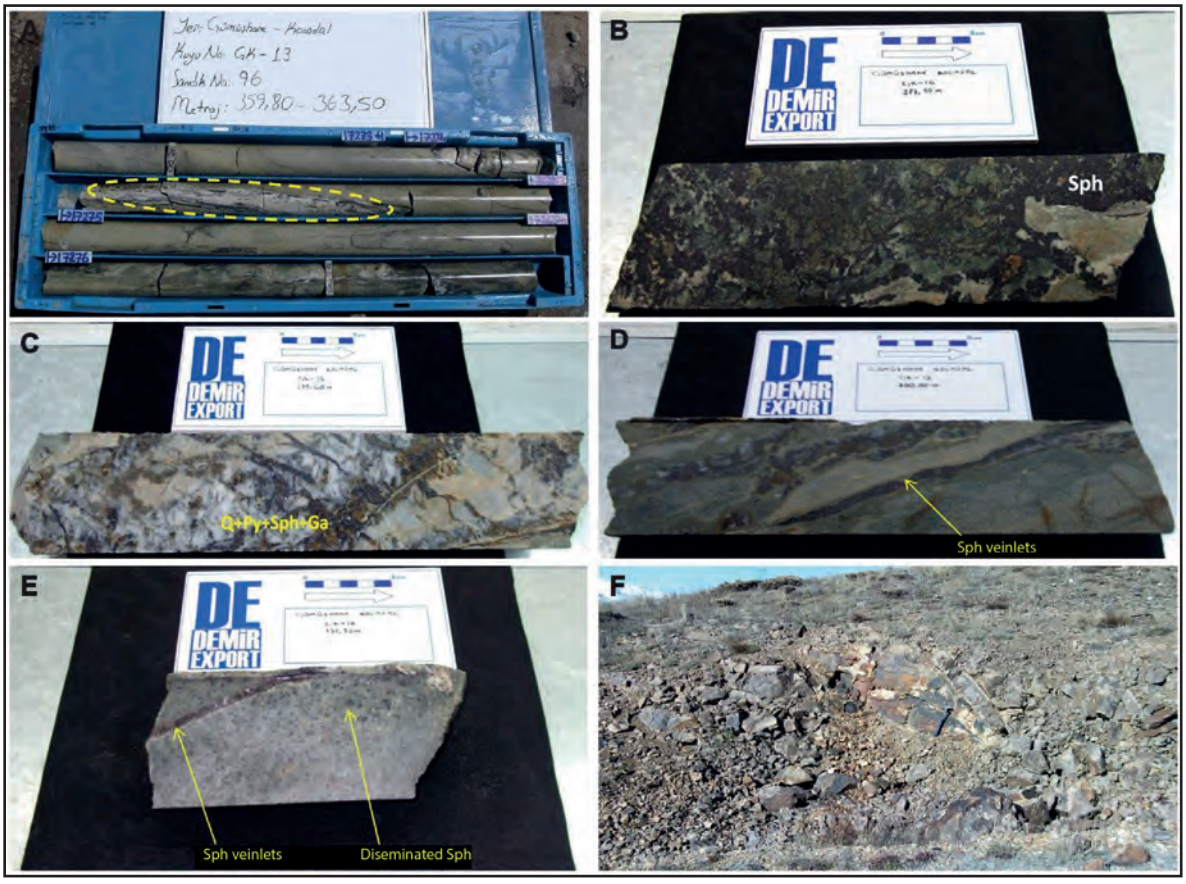

Figure 9- A) Quartz-carbonate vein with sphalerite, B) Mineralized (phalerite) brecciated zone, C) Network type mineralizations in cracks and fractures (Q: Quartz, Py: Pyrite, Sph: Sphalerite, Ga: Galenite), D) sphalerite vein along fractures and cracks, E) Disseminated type mineralization (Sphalerite), F) Smear type mineralization (limonite).

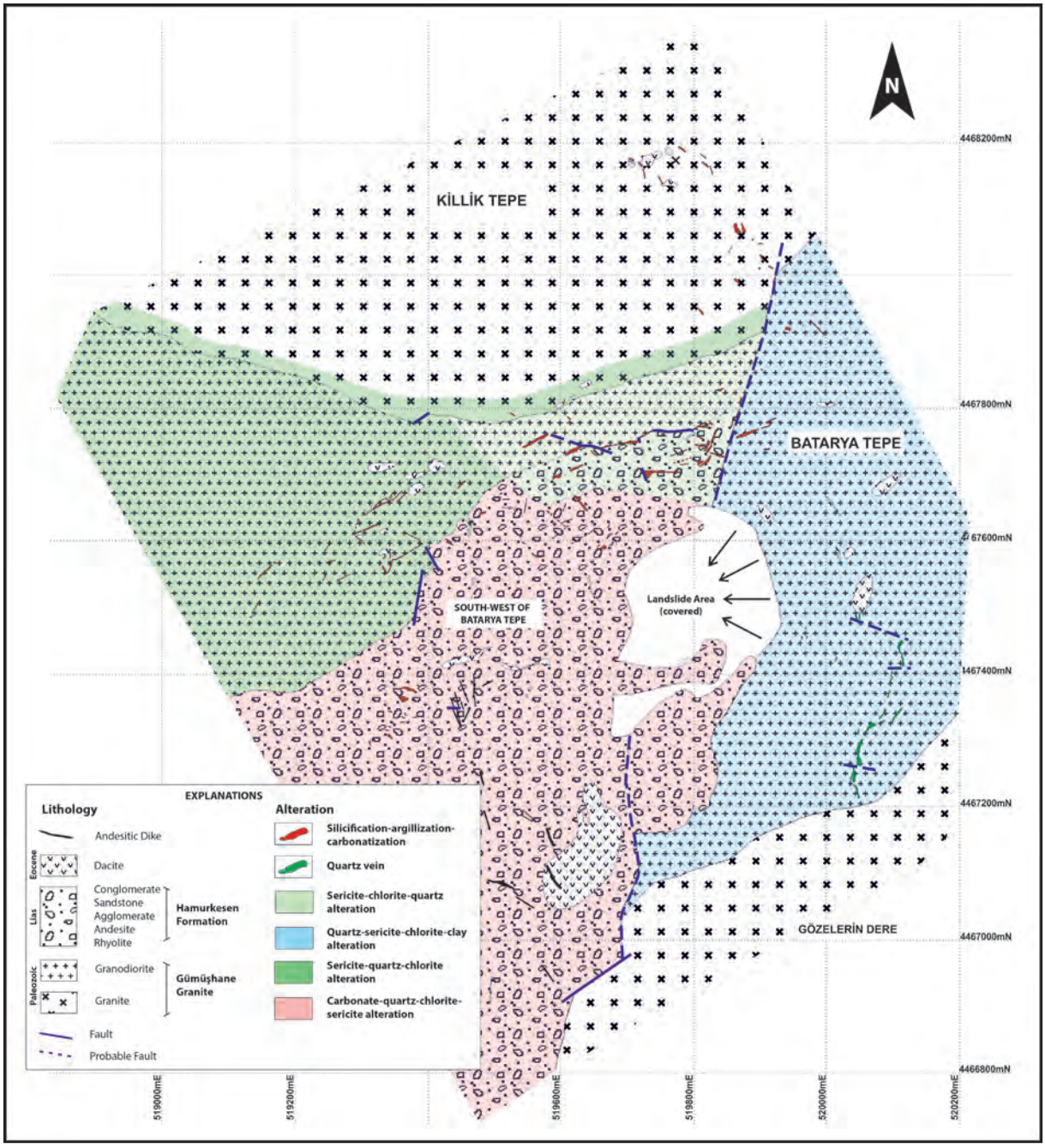

Figure 10- Geology of the Batarya Tepe Mineralizations and alterations map.

In Batarya tepe Tremolite-actinolite ±garnet alteration in general is observed as metasomatisms of veinlets of plagioclases and/or mafic minerals in dacite porphyries, conglomerates-sandstones and granites. Pyrrhotite, pyrite and sphalerite are the ore minerals in this alteration paragenesis.

In Batarya Tepe and south-west of Batarya Tepe, quartz-sericite-chlorite assemblage have developed from the changeover of feldspaths and mafic minerals or in the form of veinlets in the Conglomerates-sandstones and dacite porphyries present. Pyrite and sphalerite are the ore minerals present in this alteration paragenesis.

Last alteration period; carbonate (calcite-dolomite)-silica alteration is observed in Batarya Tepe and in the south of Batarya Tepe. While this

alteration in Batarya Tepe is seen to have developed from the mafic minerals in the granites and dacite porphyries or from the changeover of previously developed alteration minerals or have developed as veins intercepting the whole system, on the other hand they developed in the conglomerates-sandstones in association with the veins and veinlets. In the south-west of Batarya Tepe carbonate-silica alterations are seen as veins and veinlets. In the south-west of Batarya Tepe where carbonate-silica alterations are present as veins and veinlets, here sphalerite, galenite, fahlerz, arsenopyrite, pyrargyrite, proustite, chalcopyrite, bournonite and pyrrohotite minerals are present.

8. Mineralogy of the Ore Mineralizations

Ore microscopy studies carried out on the samples from transported (magmatic) and hydrothermal mineralizations in the study area showed that main minerals are pyrite and sphalerite. Along with these main minerals chalcopyrite, galenite, pyrrhotite, arseopyrite, marcasite, fahlerz, bournonite, pyrargyrite and proustite are also present. Secondary ore minerals; digenite, smithsonite, and limonite accompany to the paragenesis.

In Batarya Tepe mineralized pebbles in the conglomerates-sandstones of the Hamurkesen formation have sphalerite, pyrite. Sphalerites are xenomorph and have up to 3-4 mm varying grain size, rarely include pyrrohotite and chalcopyrite inclusions and exholitions. Pyrites are hypidiomorph and have up to 5 mm grain size.

Detailed informations on the minerals of hydrothermal mineralizations, which is present in three different locations in the area, are given below.

8.1. Pyrite

Two generations of pyrites are present. First generation of pyrites are hypidiomorphic (Figure 11 A, B), partly, among themselves forming interlocked crystal groups. They are about 0.5 mm size. First generation of pyrites are the oldest mineral of the paragenesis have cataclastic and mesh texture. They have been metasomatized by other minerals. They are interlocked with sphalerites. Second generations of pyrites are not too many and are the products, transformed from pyrrohotites (Figure 11 A, B). These types of pyrites in general are seen as skeletons interlocked with marcasites.

8.2. Sphalerite

Sphalerite minerals in general are xenomorph grains and have pyrite, pyrrohotite, inclusions and chalcopyrite and pyrrohotite exsolution lamellae. These features indicate that sphalerites started developing from hot hydrothermal solutions. Sphalerites have been cut by silver minerals (pyrargerite and proustite) and fahlerz (Figure 11 C) and galenite. Sphalerites have internal glare, indicating that they have excessive Fes in their crystal structure.

8.3. Chalcopyrite

Chalcopyrites are mostly large xenomorph grains and in general interlocked with sphalerites or intercepting them. They also are as exsolution lamellae and as inclusions in sphalerites

8.4. Galenite

Galenites are mostly observed in the quartz-carbonate veins and are the youngest mineral in this paragenesis. Grain sizes reach up to 1.1.5 mm. In galenites there are tiny pyrargerite and prusite grains.

8.5. Pyrrohotite

Pyrorrhotite is found in small amount, is present as exsolutions and inclusions in sphalerites and as inclusions in pyrites and arsenopyrites. In tremolite-actinolite±garnet veins and in places where quartz-sericite alterations are effective major part of the disseminated type pyrrohotites have been changed into marcasite or pyrite. Pyrrohotite lamellae changed into pyrite and marcasite have been filled with sphalerite and galenite (Figure 11 D).

8.6. Arsenopyrite

Arsenopyrites are commonly found in in quartz-carbonate veins. Idiomorph and hypidiomorph arsenopyrite crystals are found as rhombic and needle like. Size of arsenopyrite crystals may reach up to 1 mm. Galenite, tiny pyrrohotite, fahlerz and sphalerite grains are observed in marcasites. Arsenopyrites in parts are interlocked with each other and in parts, have

cataclastic textures, in places encircle pyrites and replace it by metasomatism.

8.7. Marcasite

Mascasite is found as alteration products of pyrites and hexagonal pyrrohotites. Marcasites changed from pyrrohotites are as lamellae. Marcasites resulted from the hydrothermal alteration of hexagonal pyrrohotites and pyrites have banded structure. With the development of sericite-clay-carbonate alteration pyrohotites and first stage pyrites have changed into marcasite. Marcasites are noticeable with high reflectivity, light yellow colour, reflection pleochroism and anisotropy.

8.8. Fahlerz (Tetrhedrite-Tennantite)

Fahlerz is commonly found in the quartz-carbonate veins, mostly xenomorphic fine grains with about 10-15 microns size. Fine grains of galenite, bournonite, pyrargyrite and proustite grains are found in fahlerz.

8.9. Pyrargyrite/Proustite

Pyrargyrite/Proustite is found small amount in quartz-carbonate veins. They encircle fahlerz grains and replaces them (Figure 11.E). Size of the largest interlocked pyrargyrite/proustite group is about 0.1-0.15 mm. They are also present as thin veinlets cutting sphalerites and as small grains in the galenites (Figure 11.F).

8.10. Bournonite

Bournonite grains are not very common in quartz-carbonate veins, they are found in fahlerz with galenite grains. Grain size is about 10-15 microns. Bournonites are found in chalcopyrites and in places in the cracks and partly display parallel twining.

8.11. Digenite

Digenites as secondary minerals are present small amount and generally found surrounding sphalerites and chalcopyrites as thin zone. They are also found filling the cracks of these minerals.

8.12. Smithsonite

Smithsonite is found as very fine grains in the cracks and fractures.

8.13. Limonite

Limonite is the alteration mineral of the sulphides found on the surface along the cracks and fractures.

By looking at the above given features and their mineralogical relations with each others of the minerals present, paragenesis of the hydrothermal minerals from old to young are; pyrrohotite, pyrite (I), sphalerite, chalcopyrite, galenite, bournonite, fahlerz, arsenopyrite, pyrite (II), pyrargyrite/proustite, digenite, smithsonite and limonite (Figure 12).

9. Geochemical Studies

In the study area to establish the dimensions, origin and economical potential of the mineralizations, geochemical studies carried out on the samples collected. In this connection first soil samples were collected then drill cores.

9.1. Soil Geochemistry

Soil geochemical studies have been carried out to establish surface extension of the mineralizations in and around Batarya Tepe. 12 sample lines along N-S direction with 100 m in between have been established. Length of the lines varied between 250 m to 850 m. Soil samples were collected along those established lines with 50 m intervals.

Collected samples without being subjected to any treatment like sieving etc. were sent to the ALS Chemex Laboratories for chemical analyses. In the laboratory the samples were dried, sieved through 50 mesh sieve and have been analysed 50 elements by ICP MS method.

Analyses of Au, Ag, Pb, Zn and Cu have been statistically studied. On average, standard deviations higher than +1 (+1 σ) have been considered weak anomaly and on average standard deviations higher than +2 (+2 σ) have been considered strong anomaly. In the study area, in three different parts contour maps have been prepared for Au, Ag, Pb, Zn and Cu for average+1 and +2 standard deviations. Certain anomaly groups have been established in three areas. They are; (I) Zn-Ag-(Au, Cu, Pb) anomaly district around Batarya Tepe, (II) Au anomaly district south-west of Batarya Tepe and (III) Cu anomaly around Gözelerim Dere district. When Strong Zn anomaly

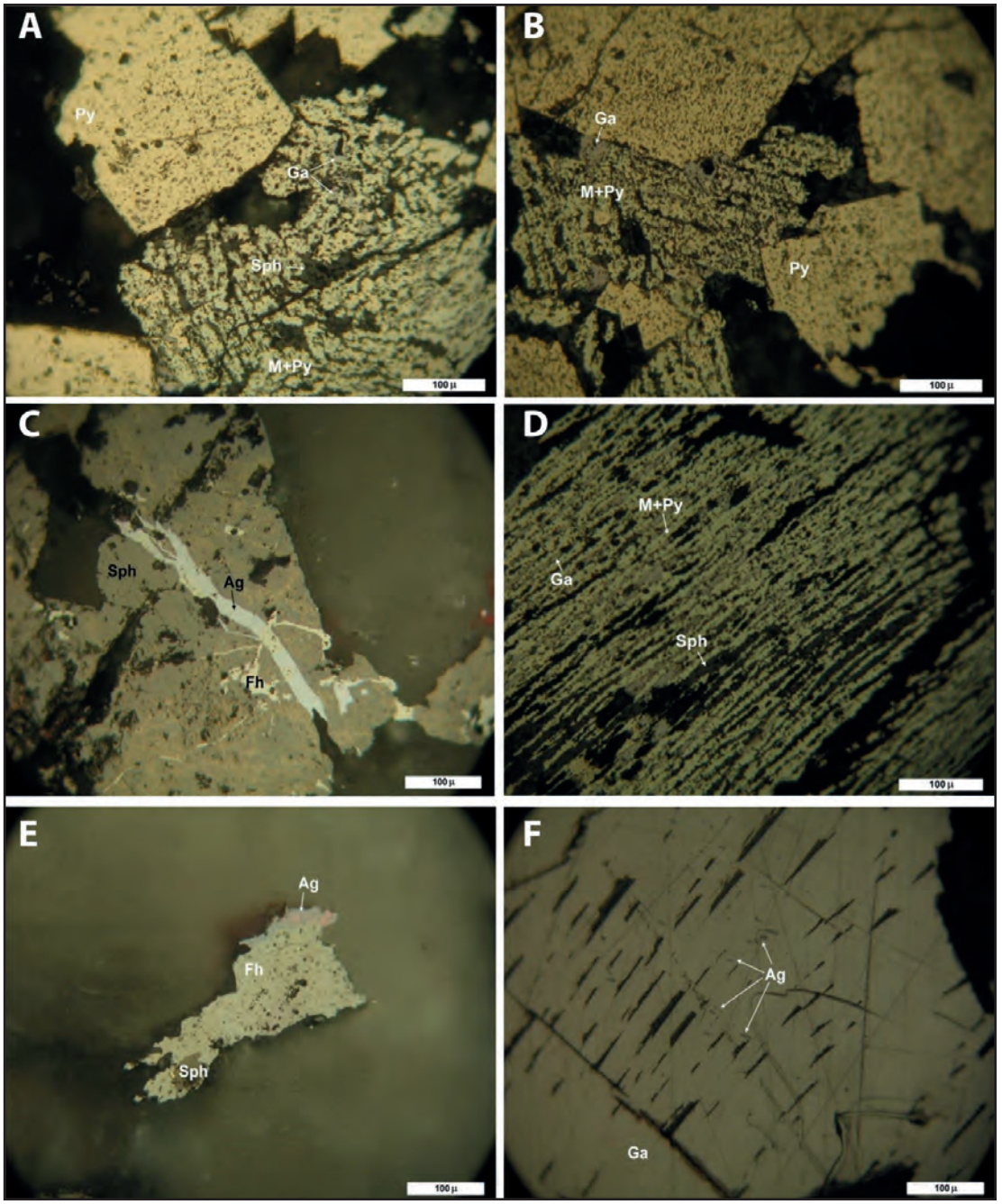

Figure 11- Hydrothermal mineralizations in the Batarya Tepe A,B) Change of first generation pyrite and arsenopyrite into marcasite and pyrite. Filling of pyrrohotite lamellae by sphalerite and galenite, C) Fahlerz and silver (pyrargyrite/proustite) cutting sphalerite, D) Change of pyrrohotite into pyrite and marcasite, filling of pyrrohotite lamellae by galenite and sphalerite, E) Silver mineral encircling fahlerz, and silver minerals in fahlerz, F) Silver minerals inclusions in galenite (Ag: Silver, Fh: Fahlerz, Ga: Galenite, M: Marcasite, Py: Pyrite, Sph: Sphalerite) .

around Batarya Tepe is considered together with the weak anomaly it is noticed that it is extending E-W direction. In the strong Zn anomaly area in Batarya Tepe there are also strong Ag, Au, Cu and Pb anomalies. In the south-west side of Batarya Tepe strong Au anomaly, accompanied by strong Pb anomalies has N-S extension. On the other hand in the northern part of the Gözelerin Dere there is a N-S extending Cu anomaly (Figure 13).

9.2. Core Samples Geochemistry

To be able to study the deep down distribution pattern of the soil geochemical analyses findings,

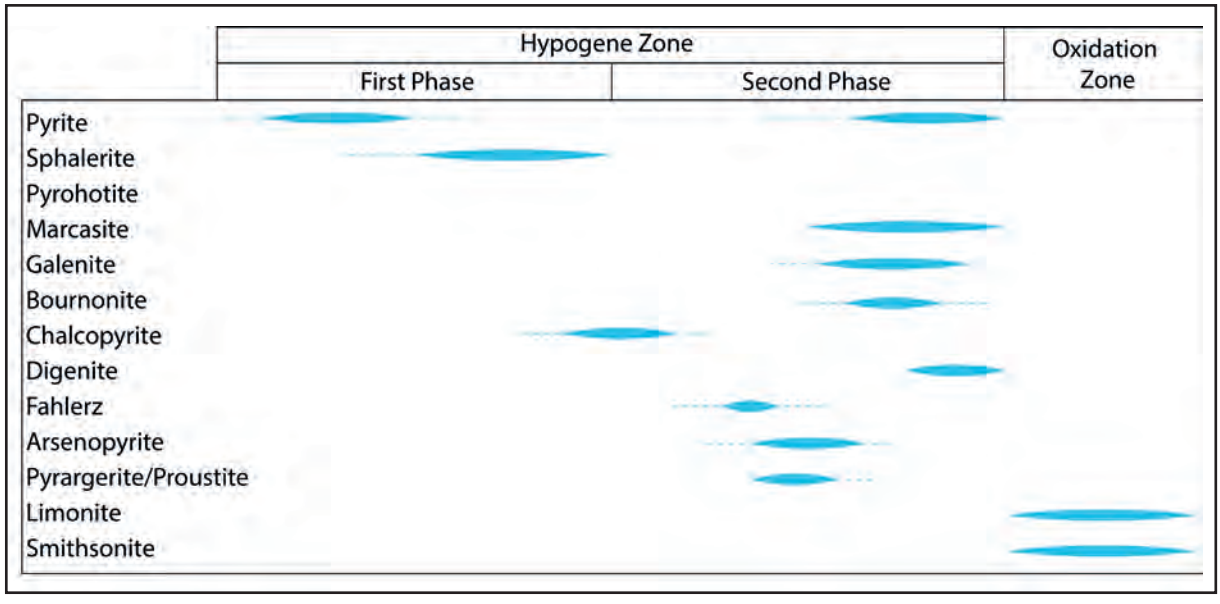

Figure 12- Paragenesis of the hydrothermal mineralizations.

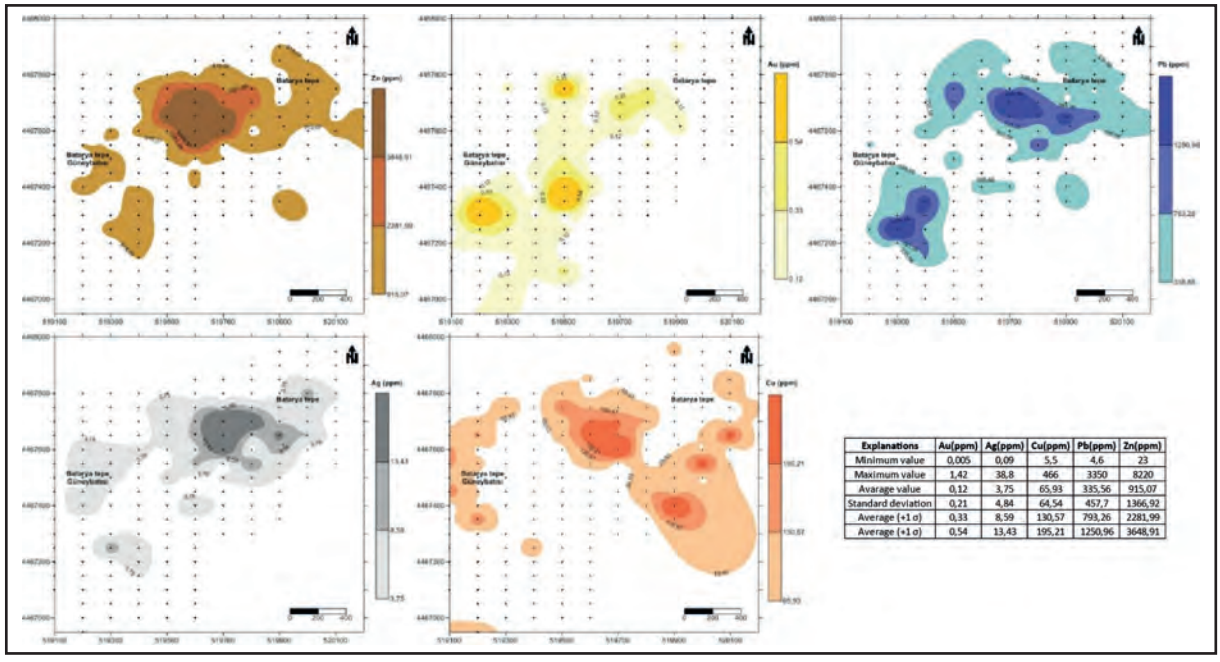

Figure 13- Zn, Au, Pb, Ag and Cu anomaly areas worked out from the soil geochemistry.

core samples of the mineralized zones of the drillings conducted on the Batarya Tepe and on the south-west of Batarya Tepe have been analysed and statistical data of the analyses of all elements are given in table 1.

In Batarya Tepe and in south-west part of it, to be able to understand elements togetherness of the analyses in different lithologies, correlation coefficients of 50 elements data set have been calculated. While evaluating correlation coefficients of the analyses, for Batarya Tepe mineralizations, over 5000 ppm values for Zn and over 0.1 ppm values for Au for the south-west part of Batarya Tepe have been selected. From the cumulative distributions of the coefficients, for positive correlations; coefficients 0.5 and over, for negative correlations; coefficients -0.5 and under have been accepted to be presenting meaningful correlation couples. Elements present in the mineralizations in different lithologies considered

Table 1- Statistical data on the analyses of the mineralized zones of the core samples.

Sector	Lithology	Statistics	Au_ppm	Ag_ppm	Al_pct	As_ppm	Ba_ppm	Be_ppm	Bi_ppm	Ca_pct	Cd_ppm	Ce_ppm
Batarya Hill Zn(Pb,Ag,Au,Cu) Mineralizaitons	Conglomerate-Sandstone (N=349)	Max	5.61	149.00	9.51	6490.00	1380.00	3.37	293.00	4.96	346.00	195.00
		Min	0.0025	0.62	0.28	7.30	10.00	0.25	1.02	0.15	14.45	19.00
		Average	0.08	9.33	6.64	270.76	285.30	1.60	16.70	1.03	42.93	57.07
	Dacite Porphyry (N=184)	Max	5.17	906.00	8.99	10000.00	7830.00	2.95	227.00	8.13	521.00	131.50
		Min	0.00	1.14	0.22	8.20	10.00	0.25	0.03	0.06	10.40	13.10
		Average	0.17	19.06	5.99	769.51	274.08	1.84	14.24	0.89	53.44	41.54
	Granite (N=545)	Max	4.14	110.00	9.88	10000.00	6060.00	3.14	422.00	9.20	347.00	215.00
		Min	0.00	0.30	0.29	1.00	20.00	0.25	0.14	0.07	16.10	14.00
		Average	0.08	7.74	6.78	421.05	273.52	1.79	14.78	1.55	51.34	49.34
South-West of Batarya Hill (Au) Mineralizaiton	Conglomerate-Sandstone (N=149)	Max	6.26	98.50	7.91	5080.00	1320.00	2.65	17.90	5.17	48.00	62.90
		Min	0.10	0.20	0.28	6.60	10.00	0.50	0.05	0.57	0.01	35.70
		Average	0.52	4.30	4.70	662.40	233.56	1.50	1.43	2.33	4.00	52.69
	Dacite Porphyry (N=80)	Max	14.80	454.00	8.43	5430.00	790.00	2.49	5.00	5.78	33.10	64.60
		Min	0.11	0.50	0.28	13.00	10.00	0.25	0.02	0.20	0.51	24.20
		Average	0.84	15.34	4.27	1068.98	216.75	1.41	0.85	1.08	7.98	36.58

Sector	Lithology	Statistics	Co_ppm	Cr_ppm	Cs_ppm	Cu_ppm	Fe_pct	Ga_ppm	Ge_ppm	Hf_ppm	In_ppm	K_pct
Batarya Hill Zn(Pb,Ag,Au,Cu) Mineralizaitons	Conglomerate-Sandstone (N=349)	Max	43.70	265.00	3.96	4870.00	14.25	23.10	0.41	6.40	37.30	4.77
		Main	2.80	2.00	0.95	12.20	2.04	5.00	0.05	0.50	0.07	0.22
		Average	11.00	24.61	1.86	246.65	5.38	17.02	0.18	2.18	4.95	3.21
	Dacite Porphyry (N=184)	Max	279.00	319.00	5.19	10150.00	14.35	23.30	0.34	5.10	24.10	4.03
		Min	0.60	0.50	0.65	27.90	1.12	5.00	0.05	0.50	0.02	0.19
		Average	10.10	21.85	2.03	309.77	4.24	15.60	0.14	2.06	4.52	2.79
	Granite (N=545)	Max	428.00	289.00	8.97	42170.00	14.40	27.00	0.40	4.20	72.10	4.69
		Min	1.80	0.50	0.92	8.50	1.15	5.00	0.05	0.50	0.07	0.19
		Average	13.91	21.24	3.33	275.72	6.03	17.11	0.17	1.65	5.42	2.74
South-West of Batarya Hill (Au) Mineralizaiton	Conglomerate-Sandstone (N=149)	Max	19.20	32.00	4.62	384.00	7.74	20.00	0.25	3.40	3.85	4.73
		Min	3.20	2.00	1.19	8.20	1.65	5.00	0.11	2.20	0.04	0.23
		Average	8.84	12.65	2.51	44.43	2.93	12.69	0.17	2.82	0.28	2.30
	Dacite Porphyry (N=80)	Max	20.00	103.00	4.93	220.00	4.65	17.85	0.19	2.70	1.17	4.05
		Min	0.50	0.50	0.97	4.00	0.55	5.00	0.03	1.30	0.04	0.27
		Average	2.31	5.58	1.71	52.46	1.65	10.93	0.12	1.99	0.33	2.06

Sector	Lithology	Statistics	La_ppm	Li_ppm	Mg_pct	Mn_ppm	Mo_ppm	Na_pct	Nb_ppm	Ni_ppm	P_ppm	Pb_ppm
Batarya Hill Zn(Pb,Ag,Au,Cu) Mineralizaitons	Conglomerate-Sandstone (N=349)	Max	92.80	36.20	2.52	14350.00	16.60	1.21	43.90	105.00	1680.00	14250.00
		Min	5.00	2.30	0.21	1000.00	0.31	0.01	6.30	1.60	240.00	12.70
		Average	26.34	5.99	0.98	5192.35	2.01	0.04	11.70	16.21	647.91	394.43
	Dacite Porphyry (N=184)	Max	82.30	37.20	4.35	47200.00	76.90	0.73	33.80	137.00	1460.00	24500.00
		Min	5.00	2.00	0.05	216.00	0.20	0.01	2.70	0.20	10.00	20.20
		Average	19.17	7.15	0.78	2924.57	1.95	0.05	9.10	6.51	347.50	917.06
	Granite (N=545)	Max	129.50	52.10	4.08	9210.00	14.60	2.28	18.20	121.50	1860.00	17050.00
		Min	5.00	1.90	0.22	402.00	0.16	0.01	2.00	0.20	10.00	12.80
		Average	22.08	11.47	1.46	3965.24	1.57	0.25	8.07	4.80	552.39	532.50
South-West of Batarya Hill (Au) Mineralizaiton	Conglomerate-Sandstone (N=149)	Max	32.30	16.40	2.39	11100.00	8.71	1.62	12.40	28.40	630.00	4460.00
		Min	5.00	2.30	0.46	752.00	0.50	0.01	8.50	5.10	380.00	3.00
		Average	19.84	5.78	1.10	3391.24	1.76	0.10	10.73	12.02	506.98	415.14
	Dacite Porphyry (N=80)	Max	26.40	25.50	2.78	8420.00	10.95	0.85	10.20	62.10	1530.00	8910.00
		Min	5.00	4.00	0.14	373.00	0.50	0.01	6.40	0.30	180.00	25.90
		Average	15.19	6.91	0.51	1676.66	1.58	0.04	8.61	4.25	288.63	869.78

Sector	Lithology	Statistics	Rb_ppm	Re_ppm	S_pct	Sb_ppm	Sc_ppm	Se_ppm	Sn_ppm	Sr_ppm	Ta_ppm	Te_ppm
Batarya Hill Zn(Pb,Ag,Au,Cu) Mineralizaitons	Conglomerate-Sandstone (N=349)	Max	197.00	0.004	9.34	169.50	29.00	7.00	17.80	132.00	2.81	1.07
		Min	63.10	0.001	0.07	0.87	2.00	0.50	1.10	2.00	0.35	0.03
		Average	128.50	0.001	2.17	7.57	10.71	2.00	7.28	26.65	0.88	0.18
	Dacite Porphyry (N=184)	Max	177.50	0.007	10.00	505.00	33.40	11.00	16.20	359.00	2.47	2.17
		Min	49.70	0.001	0.50	1.00	0.50	0.50	1.20	2.00	0.15	0.03
		Average	118.52	0.002	2.20	20.92	8.61	2.04	4.98	25.01	0.71	0.12
	Granite (N=545)	Max	288.00	0.010	10.00	184.50	32.90	10.00	16.20	510.00	3.12	1.40
		Min	37.40	0.001	0.01	0.74	1.60	0.50	1.10	3.70	0.13	0.03
		Average	132.20	0.001	2.16	9.97	16.57	1.85	5.36	43.12	0.69	0.12
South-West of Batarya Hill (Au) Mineralizaiton	Conglomerate-Sandstone (N=149)	Max	184.00	0.004	7.47	51.10	12.40	3.00	10.40	93.30	0.94	0.42
		Min	74.90	0.001	0.27	0.66	2.00	0.50	1.80	3.00	0.65	0.03
		Average	145.38	0.001	1.38	7.34	7.43	1.36	3.55	19.58	0.80	0.08
	Dacite Porphyry (N=80)	Max	153.00	0.007	3.12	214.00	16.80	2.00	4.20	203.00	0.82	0.29
		Min	64.30	0.001	0.06	1.00	0.50	0.50	0.70	3.00	0.35	0.03
		Average	120.67	0.001	0.81	15.16	2.34	0.98	1.44	18.06	0.70	0.05

Sector	Lithology	Statistics	Th_ppm	Ti_pct	Tl_ppm	U_ppm	V_ppm	W_ppm	Y_ppm	Zn_ppm	Zr_ppm	Hg_ppm
Batarya Hill Zn(Pb,Ag,Au,Cu) Mineralizaitons	Conglomerate-Sandstone (N=349)	Max	38.40	0.80	10.00	14.80	161.00	45.70	27.00	91200.00	500.00	1.00
		Min	1.50	0.01	0.40	0.30	3.00	2.80	6.40	5030.00	19.40	0.01
		Average	10.00	0.29	1.35	2.73	66.20	9.40	12.19	11660.20	76.42	0.13
	Dacite Porphyry (N=184)	Max	26.80	0.56	5.00	12.40	217.00	26.00	26.10	98200.00	183.50	6.20
		Min	0.90	0.01	0.32	0.50	0.50	1.10	4.20	5040.00	15.00	0.01
		Average	7.81	0.15	1.10	2.48	37.17	6.79	11.13	13058.86	57.17	0.24
	Granite (N=545)	Max	38.00	0.70	10.00	19.30	261.00	21.70	26.70	95800.00	99.40	3.04
		Min	1.20	0.01	0.36	0.50	1.00	1.10	4.30	5010.00	10.90	0.01
		Average	10.36	0.29	1.40	3.17	97.68	8.37	12.78	12267.08	41.36	0.22
South-West of Batarya Hill (Au) Mineralizaiton	Conglomerate-Sandstone (N=149)	Max	10.80	0.30	5.00	5.00	71.00	12.80	20.20	10600.00	109.50	1.00
		Min	6.20	0.01	0.60	1.40	2.00	1.40	10.10	12.00	70.80	0.01
		Average	9.29	0.16	2.44	3.18	38.70	5.07	13.86	1125.23	88.12	0.28
	Dacite Porphyry (N=80)	Max	10.00	0.43	5.00	5.00	122.00	8.20	13.90	9160.00	99.00	1.00
		Min	1.20	0.01	0.58	0.40	0.50	1.00	8.20	144.00	35.30	0.01
		Average	7.15	0.05	2.26	2.93	6.54	3.13	10.01	2105.83	53.58	0.36

to have different origin so those elements showing meaningful correlations with each other are given in table 2.

Elements togetherness have been worked out from the correlation coefficient studies for the Zn-Pb-Ag-(Au) mineralization of the samples collected from the conglomerates-sandstones in Batarya Tepe, is given in table 3. First group of togetherness is represented with Zn-Ag-Cd-S, Second group with Se-Cd and third group with Cd-Zn-In-Se. In the same district correlation coefficients of the mineralized zones in the dacite porphyries have also been studied and two elements togetherness have been worked out; first group is; Zn-Ag-Cd-Mo-Sb-Se-Sr and the second group is; Zn-In-S togetherness. Correlation coefficients of the analyses of the samples from the granites indicated Au-As-Sb, Zn-In-S and Zn-Cd-S togetherness's.

In Batarya Tepe south-west Au mineralizations, correlation coefficients of the analyses of samples collected from the conglomerates-sandstones showed 3 elements togetherness (Table 4). They are Zn-In-Cu; Zn-Pb-Cd and Zn-Te-Cu-In-Cd-Hg togetherness's. In the same area correlation coefficients of the samples from dacite porphyries also indicated 3 different elements togetherness, they are Au-As; Zn-Cd-Pb-In-S-Te and Ag-In-Sb. togetherness's.

In and south-west Batarya Tepe dacite porphyries are considered to be the source of hydrothermal solutions causing mineralizations. Mineralizations here present different elements combinations. These differences are also noticeable in the conglomerate-sandstone samples from these two areas and also in the granitic rock samples only from Batarya Tepe. Partial resemblances of the correlation coefficient groups of the analyses of the conglomerate-sandstone and granitic rock samples indicate that magmatic type (transported) mineralized pebbles derived from the Gümüşhane granites have been incorporated in the conglomerates-sandstones.

In two areas, elements combinations of the mineralizations, particularly observed in the dacitic rocks show noticeable variations. In the south-west of Batarya Tepe, it is noticeable that within the elements groups Au, Pb, As and Te are incorporated into the groups. This may mark zonings in the mineralizations and may also show different phases of dacite porphyry intrusions.

In the Gözelerin Dere analyses of the 5 samples collected from the Cu mineralizations in the quartz veins show following variations Cu: 97.2-160 ppm, Au: 0.005-0.111 ppm, Ag: 0.07-5.91 ppm and Pb: 16.8-1.160 ppm.

According to Stanton (1972) sulphides with magmatic origin mostly have smaller than 20.000 S/Se ratios. An S/Se ratio of the samples collected from the conglomerates-sandstones in Batarya Tepe is 10.85 and in the south-west Batarya Tepe is 10.146. These ratios indicate that hydrothermal solutions have magmatic origin (Table 5).

10. Conclusions

In the study area in Kocadal (Torul, Gümüşhane) mineralizations have been identified in three different areas. They are (I) Batarya Tepe Zn-Pb-Ag-(Au) mineralizations, (II) South-West Batarya Tepe Au mineralizations and (III) Gözelerin Dere Cu mineralizations.

Batarya Tepe Zn-Pb-Ag-(Au) mineralizations have two different origins; pebbles with sphalerite derived from Gümüşhane granite in the conglomerates-sandstones of the Hamurkesen formation, Zn-Ag-(Au) mineralizations associated with dacite porphyries which have intrusive relations with the conglomerates-sandstones of the Hamurkesen formation and with the Gümüşhane granite (Figure 14). In the South-west of Batarya Tepe Hydrothermal Au mineralizations have been identified in the dacite porphyries which has intrusive relations with the conglomerates-sandstones. Around Gözelerin Dere Cu mineralizations are present in the quartz veins and veinlets in the Gümüşhane granite. Kocadal Batarya Tepe and South-West Batarya Tepe mineralizations are genetically associated with Eocene dacite porphyries. Mineralizations display alterations in wide areas and include disseminated, veinlets/veins and stockwork type mineralizations.

Porphyry type Lengshuıkeng Pb-Zn ore deposit has developed in association with granite porphyries which has intrusive relation with Upper Jurassic volcanic rocks. Yijue (1985) studied this deposit and showed that alteration pattern from granite porphyry

Table 2- In whole of the drill core samples, elements showing meaningful correlations with each other.

	Batarya Hill Zn(Pb,Ag,Au,Cu) Mineralization		South-West of Batarya Hill (Au) Mineralizaiton		
	Conglomerate-Sandstone	Dacite Porphyry	Granite	Conglomerate-Sandstone	Dacite Porphyry
Au	–	As, Sb, Pb	As, Sb	–	As
Ag	Bi, Cd, Cu, Pb, S, Sb, Te, Zn	Ba, Cd, Mo, Sb, Se, Sr, Zn, Hg	Bi, Pb, Sb, Te	Fe, S, Sb	In, Sb
Zn	Ag, Cd, In, S, Se	Ag, Cd, In, Mo, S, Sb, Se, Sr Hg	Cd, In, S	Cd, Cu, In, Pb, S, Te, Hg	Cd, Cu, In, Pb, S, Te, Hg
Se	Zn, Hg, Cd, In	Ag, Cd, S, Sb, Sr, Zn, g, Mo	–	–	–
Pb	Ag, Zr	Sb	Ag, Cd	Zn, Cd	Cd, In, S, Sn, Te, Zn
Te	Ag, Bi	Bi	Ag, Bi, Cu	Zn, S, Cu, Co	Bi, Cd, Pb, S, Sn, Zn, In
In	Cd, S, Zn, Se	S, Zn, Bi	Zn	Cd, Cu, Zn, Hg	Ag, Bi, Cd, Cu, Pb, Zn, Hg
Bi	Ag, Te	In, Te	Ag, Te	Te	In, Te
Cd	In, S, Se, Zn, Ag, Cu	Mo, S, Sb, Se, Sr, Zn, Zr, Ag, Ba, Hg	Pb, S, Zn	In, Pb, Zn	In, Pb, Sn, Te, Zn, Hg, S
S	Ag, W, Zn, Cd, Co, Fe	Cd, In, Fe, Sb, Se, Zn	Cd, Zn	Ag, Co, Fe, Sb, Te	Cd, Fe, Pb, Sn, Te, Zn, In
Sb	Ag, As	Au, Ag, As, Mo, Pb, S, Zn, Hg	Au, Ag, As	Ag, Fe, S	Ag
Fe	Co, Mn, Ni, P, S, Se, Ti, V, W	Ge, Mg, Mn, P, S, Sc, Ti, V, W	Li, Mg, Mn, Sc, V / (Hf, La, Nb, Ta, Th, Zr)*	Ag, Co, S, Sb	Ca, Co, Cr, Cs, Li, Mn, Mg, Na, Ni, P, S, Sc, Sr / (Ta, Nb)*
Mo	–	Ag, Ba, Cd, Sb, Se, Sr, Zn, Hg	–	–	–

()* decribes meaningful negative correlation

Table 3- Zn-Pb-Ag-(Au) elements togetherness's in the Batarya Tepe mineralizations.

			Elements groups showing pozitive correlation (for r>0.5)
Batarya Hill Zn(Pb,Ag,Au,Cu) Mineralization	Conglomerate-Sandstone	1st group	Zn, Ag, Cd, S
		2nd group	Se, Cd, In
		3th group	Cd, Zn, In, Se
	Dacite Porphyry	1st group	Zn, Ag, Cd, Mo, Sb, Se, Sr
		2nd group	In, Zn, S
	Granite	1st group	Au, As, Sb
		2nd group	Zn, In, S
		3th group	Zn, Cd, S

Table 4- In Batarya Tepe South-West, elements togetherness in Au mineralizations.

			Elements groups showing pozitive correlation (for r>0.5)
South-West of Batarya Hill (Au) Mineralizaiton	Conglomerate-sandstone	1st group	Zn, In, Cu
		2nd group	Zn, Cd, Pb
		3th group	Zn, Te, Cu, In, Cd, Zn, Hg
	Dacite Porphyry	1st group	Au, As
		2nd group	Zn, Cd, Pb, In, S, Te
		3th group	Ag, In, Sb

Table 5- S/Se ratios of the mineralizations from different lithologies.

		S_pct	Se_pct	S/Se
Batarya Hill Zn(Pb,Ag,Au,Cu) Mineralization	Conglomerate-Sandstone	2,17	0,00020	10852,67
	Dacite Porphyry	2,20	0,00020	10791,36
	Granite	2,16	0,00018	11704,3
South-West of Batarya Hill (Au) Mineralization	Conglomerate-Sandstone	1,38	0,00014	10146,69
	Dacite Porphyry	0,81	0,00010	8249,902

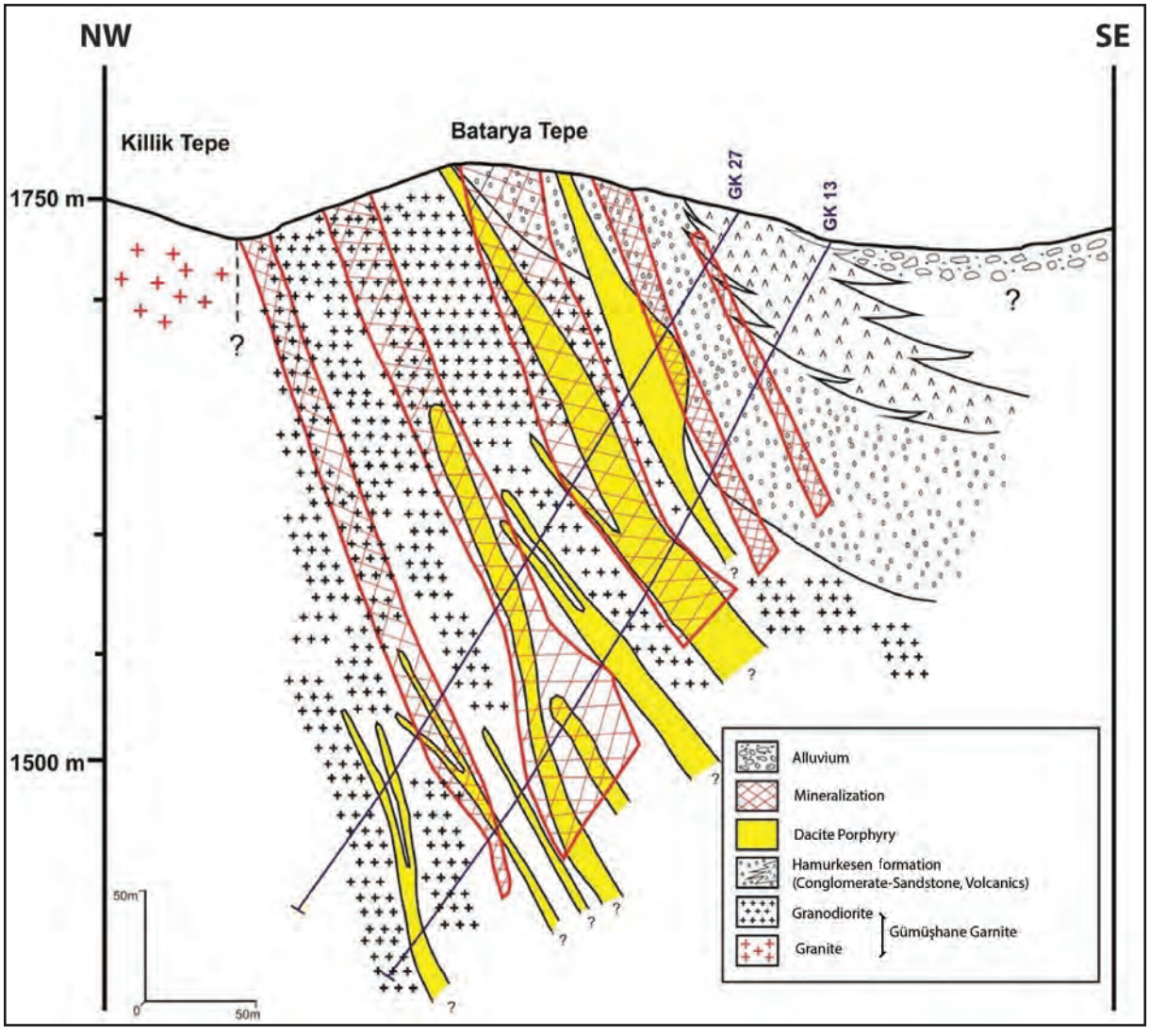

Figure 14- Geological cross section showing dacite porphyries and host rock-mineralization relations.

center towards the host rock have chlorite sericite and carbonate combinations. Lengshuıkeng is defined as low grade porphyry Zn-Pb deposit. As Batarya Tepe Zn (±Pb, Ag, Au, Cu) mineralizations has similar features, so it may also be considered to be a porphyry type mineralization.

Acknowledgement

This paper comprises the part of project conducted by Demir Export A.Ş. Exploration Department in Gümüşhane-Torul-Kocadal between the years 2011 and 2014. We are particularly grateful to Savaş Şahin, General Manager of Demir Export A.Ş., for his kind support during the project.

References

Adamia, S.A., Lordkipanidze, M.B., Zakariadze, G.S. 1977. Evolution of an active continental margin as exemplified by the Alpine history of the Caucasus. *Tectonophysics* 40, 183e189.

Ağar, Ö. 1977. Demirözü (Bayburt) ve Köse (Kelkit – Gümüşhane) Bölgesinin Jeolojisi, Doktora Tezi, KTÜ Fen Bilimleri Enstitüsü, Trabzon

Akın, H. 1979. Geologie, Magmatismus und Lagerstattenbildung im ostpontischen Gebirge/ Tiirkeiaus der Sicht der Plattentektonik. *Geol. Rundsch*., 68: 253-283.

Akıncı, Ö. T. 1984. The Eastern Pontide volcano-sedimentary belt and associated massive sulphide deposits. Geological Society, London, Special Publications, 17(1), 415-428.

Baytekin, A., Uslu, A. 1974. Gümüşhane – Torul – Ayana – Kocadal – Altıntaşlar sahasının 1/10.000 ölçekli jeoloji etüdü hakkında rapor, Ankara

Bektaş, O. 1984. Pontidlerde Üst Kretase yaşlı şoşonitik volkanizma ve jeotektonik önemi. *KTÜ Yerbilimleri Dergisi*, Jeoloji, 3/1 – 2, 53 – 62

Bektaş, O., Yılmaz, C., Taslı, K., Akdağ, K., Özgür, S. 1995. Cretaceous rifting of the eastern Pontide carbonate platform (NE Turkey): the formation of carbonates breccias and turbidites as evidences of a drowned platform. *Geologia* 57 (1–2), 233–244.

Bektaş, O., Şen, C., Atıcı, Y., Köprübaşı, N. 1999. Migration of the Upper Cretaceous subduction-related volcanism towards the back-arc basin of the eastern Pontide magmatik arc (NE Turkey). *Geological Journal*, 34(1-2), 95-106.

Çamur, M. Z., Güven, İ. H., Murat, E. R. 1996. Geochemical characteristics of the Eastern Pontide volcanics, Turkey: an example of multiple volcanic cycles in the arc evolution. *Turkish Journal of Earth Sciences*, 5(2), 123-144.

Çınar, S., Türk, O.; Er, M., Güç, A.R., Gümüşel, A., Özdemir, M., Kurtoğlu, T. 1983. Gümüşhane ili ve güneybatı yöresinin 1/25.000 ölçekli jeoloji ile maden zuhurlarına ilişkin rapor, *Maden Tetkik ve Arama Genel Müdürlüğü* (unpublished).

Çoğulu, E. 1970. Gümüşhane ve Rize granitik plütonlarının mukayeseli petrografik ve jeokronometrik etüdü: İst. Tek. Univ, Doktora Tezi (unpublished).

Dewey, J. F., Pitman, W. C., Ryan, W.B.F., Bonin J. 1973. Plate Tectonics and the evoluation of the the Alpine System, *Geol. Soc. Am. Bull.*, 84, 3137 – 3180

Eğin, D., Hirst, D.M. 1979. Tectonic and magmatik evolution of volcanic rocks from the northern Harşit area, NE Turkey: Geocome-l, Proceedings, 56-94, Ankara.

Eyüboğlu, Y. 2010. Late Cretaceous high-K volcanism in the eastern Pontide orogenic belt: Implications for the geodynamic evolution of NE Turkey. *International Geology Review*, 52(2-3), 142-186.

Eyüboğlu, Y., Bektaş, O., Seren, A., Nafız, M., Jacoby, W.R., Özer, R. 2006. Three-directional extensional deformation and formation of the Liassic rift basins in the eastern Pontides (NE Turkey), *Geologica Carpathica*, 57, No:5, 337-346.

Eyüboğlu, Y., Dilek, Y., Bozkurt, E., Bektas, O., Rojay, B., Sen, C. 2010. Structure and geochemistry of an Alaskan-type ultramafic–mafic complex in the Eastern Pontides, NE Turkey. *Gondwana Research*, 18(1), 230-252.

Eyüboğlu, Y., Chung, S.L., Santosh, M., Dudas, F.O., Akaryalı, E. 2011. Transition from shoshonitic to adakitic magmatism in the Eastern Pontides, NE Turkey: Implications for slab window melting. *Gondwana Research*, 19, 413-429.

Eyüboğlu, Y., Santosh, M., Yi, K., Bektaş, O., Kwon, S. 2012. Discovery of Miocene adakitic dacite from the Eastern Pontides Belt and revised geodynamic model for the late Cenozoic Evolution of eastern Mediterranean region. *Lithos*, 146-147, 218-232

Eyüboğlu, Y., Santosh, M., Yi, K., Tüysüz, N., Korkmaz, S., Akaryalı, E., Dudas, F., Bektaş, O. 2014. The Eastern Black Sea-Type Volcanogenic Massive Sulfide Deposits: Geochemistry, zircon U-Pb geochronology and an overview of the geodynamics of ore genesis. *Ore Geology Reviews*, 59, 29-54.

Gedikoğlu, A. 1978. Harşit granit karmaşığı ve çevre kayaçları, Doçentlik Tezi, KT Ü. Yer Bilimleri Fakültesi, Trabzon.

Gedik, İ., Kırmacı, M.Z., Çapkınoğlu, S., Özer, E., Eren, M. 1996. Doğu Pontidlerin jeolojik gelişimi, KTÜ Jeoloji Müh. Böl. 30. Yıl Semp. Bil., 2, 654-677.

Güven, I.H. 1993. Geological and Metallogenic Map of the Eastern Black Sea Region; 1:250000 Map. General Directorate Mineral Research and Eploration, Trabzon.

Hamilton, W.J. 1942. Researches in Asia Minor, Pontus abd Armenia, 1 rth Eds. Geol. Soc. London, 1842

Karslı., O. 1996. Zigana granitoyidi'nin mineralojik ve jenetik açıdan incelenmesi, Yüksek lisans tezi, KTÜ Fen Bilimleri Enstitüsü, Trabzon

Kazmin, V.G., Sbortshikov, I.M., Ricou, L.E., Zonenshain, L.P., Boulin, J., Knipper, A.L. 1986. "Volcanic belts as markers of the Mesozoic-Cenozoic Evolution of Tethys", *Tectonophysics*, 123, 123-152.

Ketin, İ. 1966. Anadolu'nun tektonik birlikleri. *Maden Tetkik ve Arama Dergisi,* 66, 22-34.

Ketin, İ., Canıtez, N. 1972. Yapısal Jeoloji, İTÜ Kütüphanesi, İstanbul

Lermi, A. 2003. High-potassium I-type Granitoid Magmatism in the Eastern Pontides: The Gümüşhane Pluton (NE Turkey), *Lithos*, 116, 92-110.

Okay, A.I., Şahintürk, Ö. 1997. Geology of the Eastern Pontides. In: Robinson, A.G. (Ed.), Regional and petroleum geology of the Black Sea and surrounding region. AAPG Mem., 68, pp. 291–311.

Özsayar, T., Pelin, S., Gedikoğlu, A. 1981. Doğu Pontidler'de Kretase, *KTÜ Yer Bilimleri Dergisi*, 2, 65 - 114

Peccerillo, A., Taylor, S. R. 1975. Geochemistry of Upper Cretaceous volcanic rocks from the Pontic chain, northern Turkey. *Bulletin volcanologique*, 39(4), 557-569.

Pelin, S. 1977. Alucra (Giresun) güneydoğu yöresinin jeolojisi ve petrol olanakları bakımından incelemesi. KTÜ Yayını No: 87, 103 s

Stanton, R. L. 1972. Ore petrology (Vol. 713). New York: McGraw-Hill, 771-p.

Şenel, M. 2002. Türkiye Jeoloji Haritası Trabzon Paftası, 1:5.00.000, *Maden Tetkik ve Arama Genel Müdürlüğü* Yayını, Ankara

Şengör, A.M.C., Yılmaz, Y., 1981. Tethyan evolution of Turkey: A plate tectonic approach. *Tectonophysics*, 75, 181 – 241

Şengör, A. M. C., Özeren, S., Genç, T., Zor, E. 2003. East Anatolian high plateau as a mantle-supported, north-south shortened domal structure. *Geophysical Research Letters*, 30(24).

Taşlı K. 1984. İkisu (Gümüşhane) İle Hamsiköy (Trabzon) yörelerinin jeolojisi ve Berdiga Formasyonun biyostratigrafik deneştirmesi, K.Ü. Fen Bil., Ens. MMLS Tezi, Trabzon (unpublished)

Tokel, S. 1977. Doğu Karadeniz bölgesinde Eosen yaşlı kalk-alkalen andezitler ve jeotektonizma, *Türkiye Jeoloji Kurumu Bülteni*, 20, 49-54

Türk Japon Ekibi, 1985. The cooperative Mineral Exploration of Gümüşhane Area, Phase 1, MTA Raporu No:334, Ankara

Yijue, L. 1985. Geological characteristics of the Lengshuikeng porphyry type Pb-Zn deposit in Guixi County, Jiangxi Province. *Mineral Deposits*, 4(4), 15-24.

Yılmaz, Y. 1972. Pertology and structure of the Gümüşhane Granite and Surrounding rocks, NE Anatolia, Ph. D. Thesis. Univ. London

Yılmaz, Y. 1972. Petrology and Structure Of The Gümüşhane Granite and Surrounding Rock, N.E. Andolin Ph.D Thesis, Uni.Of London,266 s.(unpublished).

Yılmaz, C., Karslı, O. 1997. Macka-Zigana yöresinde Üst Kretase sürecindeki çökel kayıtları ve bölge jeolojisindeki önemi. *Geosound*, 30, 331-340.

Yılmaz, C., Karslı, O., Aydin, F. 1997. Upper Cretaceous intra-arc sedimentation, magmatism, and tectonism in the south of Trabzon: IAS. In 18th Regional Meeting of sedimentology, Heidelberg, Abstracts (Vol. 369).

Bull. Min. Res. Exp. (2016) 153:159-167

Bulletin of the Mineral Research and Exploration

http://bulletin.mta.gov.tr

SPATIAL CLUSTER AND OUTLIER IDENTIFICATION OF GEOCHEMICAL ASSOCIATION OF ELEMENTS: A CASE STUDY IN JUIRUI COPPER MINING AREA

Tien Thanh NGUYEN[a*], Danh Tuyen VU[a], Le Hung TRINH[b] and Thi Le Hang NGUYEN[a]

[a] *Ha Noi University of Natural Resources and Environment, Ha Noi, Viet Nam*
Postal Address: No 41A Phu Dien Road, North-Tu Liem District, Ha Noi, Viet Nam
[b] *Le Quy Don Technical University, Ha Noi, Viet Nam*
Postal Address: 236 Hoang Quoc Viet Road, Cau Giay District, Ha Noi, Viet Nam

Research Article

Keywords:
Spatial Outliers, Spatial Clusters, Spatial Variability, Local Moran Statistic, Geochemistry.

ABSTRACT

Spatial clusters and spatial outliers play an important role in the study of the spatial distribution patterns of geochemical data. They characterize the fundamental properties of mineralization processes, the spatial distribution of mineral deposits, and ore element concentrations in mineral districts. In this study, a new method for the study of spatial distribution patterns of multivariate data is proposed based on a combination of robust Mahalanobis distance and local Moran's I_i. In order to construct the spatial matrix, the Moran's I spatial correlogram was first used to determine the range. The robust Mahalanobis distances were then computed for an association of elements. Finally, local Moran's I_i statistics was used to measure the degree of spatial association and discover the spatial distribution patterns of associations of Cu, Au, Mo, Ag, Pb, Zn, As, and Sb elements including spatial clusters and spatial outliers. Spatial patterns were analyzed at six different spatial scales (2km, 4 km, 6 km, 8 km, 10 km and 12 km) for both the raw data and Box-Cox transformed data. The results show that identified spatial cluster and spatial outlier areas using local Moran's I_i and the robust Mahalanobis accord the objective reality and have a good conformity with known deposits in the study area.

Received: 03.12.2015
Accepted: 15.03.2016

1. Introduction

The properties of living beings are distributed neither uniformly nor at random. They are aggregated in patches or formed gradients or other kinds of spatial patterns (Legendre and Fortin, 1989). Spatial patterns have been widely used in different research fields such as biometrics (Fuentes et al., 2006), landscape ecology (Bagchi et al., 2011; Irl et al., 2015), regional economics (Monastiriotis, 2009) and medicine (Waller and Gotway, 2004; McLaughlin and Boscoe, 2007; Goovaerts and Jacquez, 2004) etc. Extraction of spatial information for mineral exploration can be achieved through the study of spatial distribution patterns of regional geochemical elements such as spatial structures, spatial variability and spatial association patterns (spatial clustering and spatial outliers). Various methods and techniques have been proposed for spatial cluster and outlier identification such as Getis's G index (Getis and Ord, 1992), Geary's C (Geary, 1954), spatial scan statistics (Ishioka et al., 2007) and Tango's C index (Tango, 1995). The local Moran's I is by far the most commonly used test statistic (Anselin, 1995; Getis and Ord, 1996). The local Moran's I statistic has been successfully applied to the spatial cluster identification of diseases (Ruiz et al., 2004; Goovaerts and Jacquez, 2004), mortality rates (James et al., 2004; McLaughlin and Boscoe, 2007), environmental planning (Brody et al., 2006), and environmental sciences (McGrath and Zhang, 2003; Zhang and McGrath, 2004).

Many traditional methods for detecting outliers have been used for many years (Hawkins, 1980). However, the determination of outliers is still being extremely difficult (Rose et al., 1979; Reimann et al., 2005). A number of study (Rocke and Woodruff, 1996; Rousseeuw and Leroy, 1987 and Tyler, 1991) have shown that there have been many methods for the detection of multivariate outliers. Recently, Filzmoser et al. (2005) followed an idea of Gervini (2003) for increasing the efficiency of the robust estimation of multivariate location and scatter. However, this method can be seen as an automation of the method

* *Corresponding author: Tien Thanh NGUYEN, email: tdgis_ntthanh@163.com*
http://dx.doi.org/10.19111/bmre.01695

proposed by Garrett (1989). Filzmoser and Hron (2013) used the Mahananobis as a reliable distance measure for the analysis of multivariate data. For identifying outliers, it is crucial to estimate the mean and covariance from the data. However, geochemical data is a spatial data, all of the aforementioned methods have a common drawback that is they do not take the spatial distribution of data into account. Nguyen et al. (2014) identified spatial patterns for Cu geochemical univariable using local Moran's I, however, distance bands were chosen randomly without scientific basis and the effectiveness of spatial pattern identification for geochemical multiviables using local Moran's I was not investigated. Therefore, in this study, focuses will be made on the identification of spatial patterns of geochemical multivariables by means of a combination of robust Mahalanobis distance and local Moran's I statistic using 1341 stream sediment samples collected at scale of 1:200.000 in Jiurui copper mining area.

2. General Geological Setting of Study Area and Data Used

Jiurui area is a mining district in Jiangxi province (southeast China). Jiurui is rich in copper reserves. The Cu deposits in the Jiurui district are an important component of the Middle–Lower Yangtze River metallogenic belt, extending from Daye in Hubei Province in the west to Zhenjiang in Jiangsu Province in the east. Jiurui area are located at the edge of the active zone on the para platform. The exposed strata are Ordovician limestone, shale, sandstone in upper Silurian system, Huang long formation conglomeratic sandstone in upper carboniferous system, sandstone, dolomite, limestone, limestone in lower Daye, Changxing group's limestone, lower Triassic system Daye group's limestone, middle Jialing river group's limestone, dolomite limestone. Iron copper deposits in the area are one of the main ore deposits in the downstream. They are divided into two metallogenetic series: (i) submarine exhalative activities-related metallogenetic series are any hydrothermal deposits from the injection to the bottom of the sea environment, (ii) intermediate acid hypabyssal intrusive activities-activities-related ore deposits; refers to the formation of intrusive rocks of Carboniferous sand Triassic strata in contact zone and rock deposits. The main types are of skarn type iron and copper deposits, porphyry copper deposit, key, vein copper, gold deposits. Porphy, skarn, copper deposits in the study area belong to this series.

According to requirements of 1:200.000 regional stream sediment survey, a multi-element sediment geochemical survey of streams was carried out in Jiurui area. A total of 1482 composite samples representing about 5364 km^2 were collected. Some sampling areas at the upper part of the study area were not able to access. The sampling density was 1 composite sample per 4 km^2. There are more than 20 indexes in a composite sample, including Ag, As, Au, Be, Cd, Cu, Hg, Li, Mn, Mo, Nb, Pb, Sb, Sn, Th, V, W, Y, Zn, Al_2O_3, CaO, K_2O, Na_2O. Silver, gold, copper are three ore-forming elements. One of three geochemical associations of elements caused anomalous area in the study area is Cu, Au, Mo, Ag, Pb, Zn, As and Sb elements. There are two metallogenic series in the study area. A total of 13 ore deposits were found marked by numeric characters from 1 to 13 (Figure 1).

3. Methodology

3.1. Spatial Correlogram

Spatial correlation of a single variable can be measured by using Moran's I (1950) or Geary's c (1954) spatial correlation statistics (Cliff and Ord, 1981). The Moran's I seems to be the most commonly used statistic (Anselin, 1995; Getis and Ord, 1996), which is given by:

$$I(d) = \frac{N}{S_0} \frac{\sum_{i=1}^{N} \sum_{j=1}^{N} W_{ij}(x_i - \bar{x})(x_j - \bar{x})}{\sum_{i=1}^{N}(x_i - \bar{x})^2} \qquad (1)$$

where: x_i and x_j are the values of the observed variables at sites i and j, $\bar{x}$ is the average of an observed variable, d is the distance class considered in the calculation, S_o is the sum of the weights W_{ij} and N stands for the number of observations.

Spatial correlation coefficients I(d) are tested for statistical significance by computing the expected values (E) and the variance of the I.

3.2. Robust Distance-based Local Spatial Outlier and Cluster Identification

Standard methods for multivariate outlier detection are based on the Mahalanobis distance (Filzmoser, 2005) which is defined as

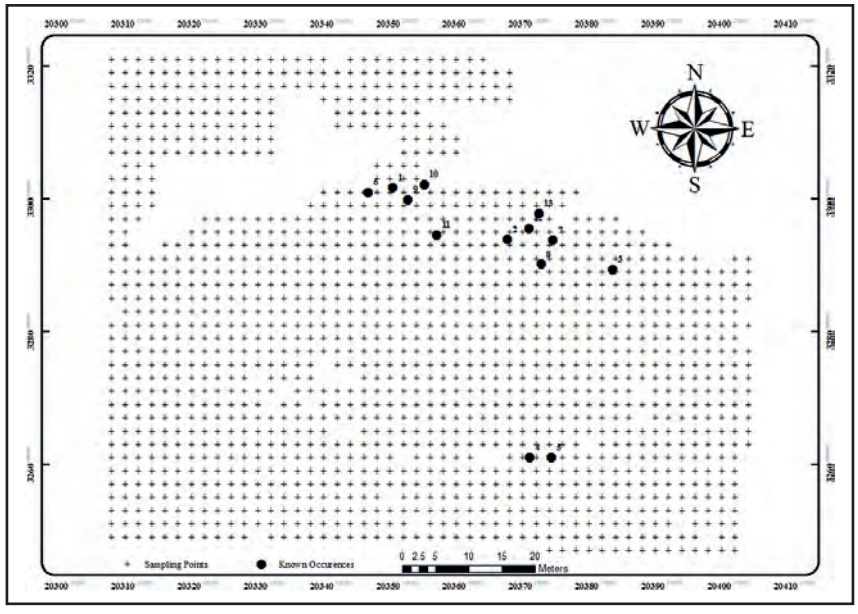

Figure 1- Location map of 1482 stream sediment samples and 13 ore deposits at scale 1:200.000.

$$MD_i = ((x_i - t)^T C^{-1}(x_i - t))^{\frac{1}{2}} \quad (2)$$

for a p-dimensional observation x_i and i = 1, 2,…, n. t is the multivariate arithmetic mean, the centroid, and C is the sample covariance matrix. The Mahalanobis distance is sensitive to the presence of outliers (Rousseeuw and Van Zomeren, 1990)

Using robust estimators of location and scatter in the formula for the Mahalanobis distance equation (2) leads to the so-called robust distances (RDs). Rousseeuw and Van Zomeren (1990) used these RDs for multivariate outlier detection. A global outlier is a measured sample point that has a very high or a very low value relative to all of the values in a dataset. If the squared RD for an observation is larger than $\chi^2_{2;0.98}$, it can be declared a global outlier. In the study, local outliers were considered. The robust Mahanalobis distance for the geochemical association of elements was first used as an investigated variable. Local spatial clusters and outliers were then identified by local Moran statistic using RD. Moran I statistic (Moran, 1948; Cliff and Ord, 1973, 1981) gives a formal indication of the degree of linear association between a vector of observed values y and a weighted average of the neighboring values, or spatial lag, Wy. When the spatial weight matrix is row-standardized such that the elements in each row sum to 1, Moran I is defined as (Anselin, 1995):

$$I = \frac{y'Wy}{y'y} \quad (3)$$

where, the y is in deviations from their mean, $(x_i - \bar{x})$, and $S_0 = N$. I is formally equivalent to the regression coefficient in a regression of Wy on y. A high positive local Moran's I value implies that the location under study has similarly high or low values as its neighbors, thus the locations are spatial clusters (Zhang et al., 2008). If $p(I_i)<\alpha$, $I_i>0$ and $x_i - \bar{x}>0$, then x_i and $x_{j\in Ji}$ belong to association between high values (high-high clusters) (Figure 2-a). If $p(I_i)<\alpha$, $I_i>0$ and $x_i - \bar{x}<0$, then x_i and $x_{j\in Ji}$ belong to association between low values (low-low clusters) (Figure 2-d). Spatial outliers are those values that are significantly different from the values of their surrounding locations (Lalor and Zhang, 2001). If $p(I_i)<\alpha$, $I_i<0$ and $x_i - \bar{x}>0$, then high value, x_i is surrounded by low values, $x_{j\in Ji}$ (high-low outliers) (Figure 2-c). If $p(I_i)<\alpha$, $I_i<0$ and $x_i - \bar{x}>0$, low value, x_i is surrounded by high values, $x_{j\in Ji}$ (low-high outliers) (Figure 2-b).

3.3. Data Processing

The robust Mahalanobis distances, the descriptive statistical parameters and exploratory data analysis plots were performed and conducted using the StatDA and MASS packages of Statistical Modeling and Computing - R Language (version i386 2.15.0). Moran's I spatial correlograms were carried out using

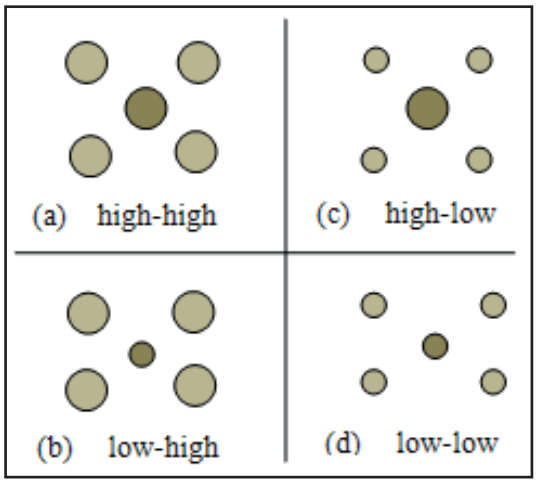

Figure 2- Spatial cluster and outlier schematic diagram (Zhang et al., 2008).

the *ncf* packages in R. The increment of the distance classes were 2 km. Testing for the significance of correlograms with each distance class was performed by a randomization test using 500 permutations. Spatial weight matrix and local Moran's I statistic were carried out with spatial statistics software - GeoDA (version 095i). The local Moran's I statistic was tested using 999 permutations, and the significance level (p-value) was set to 0.05 (5%). The results of spatial clusters and outliers were visualized using ArcGIS 9.3.

4. Results and Discussions

4.1. Distribution of Robust Mahalanobis Distances

Robust Mahalanobis distances (RMD) for original data were calculated using equation (2) are approximately chi-square distributed with a degree of freedom of 8. The distributions of RMDs can be seen in figure 3. The distribution of RMD is obviously strongly right-skewed, as a result typical asymmetrical (Figure 3a). The data points do not follow a straight line of normal Q-Q plots (Figure 3b). Box-Cox transformation was applied to make the distribution of RMD close to normality. The transformed RMD results in a symmetrical distribution and the histogram and density trace show symmetry as shown in figure 3c. The transformed data mostly follow straight lines of Q-Q plots (Figure 3d).

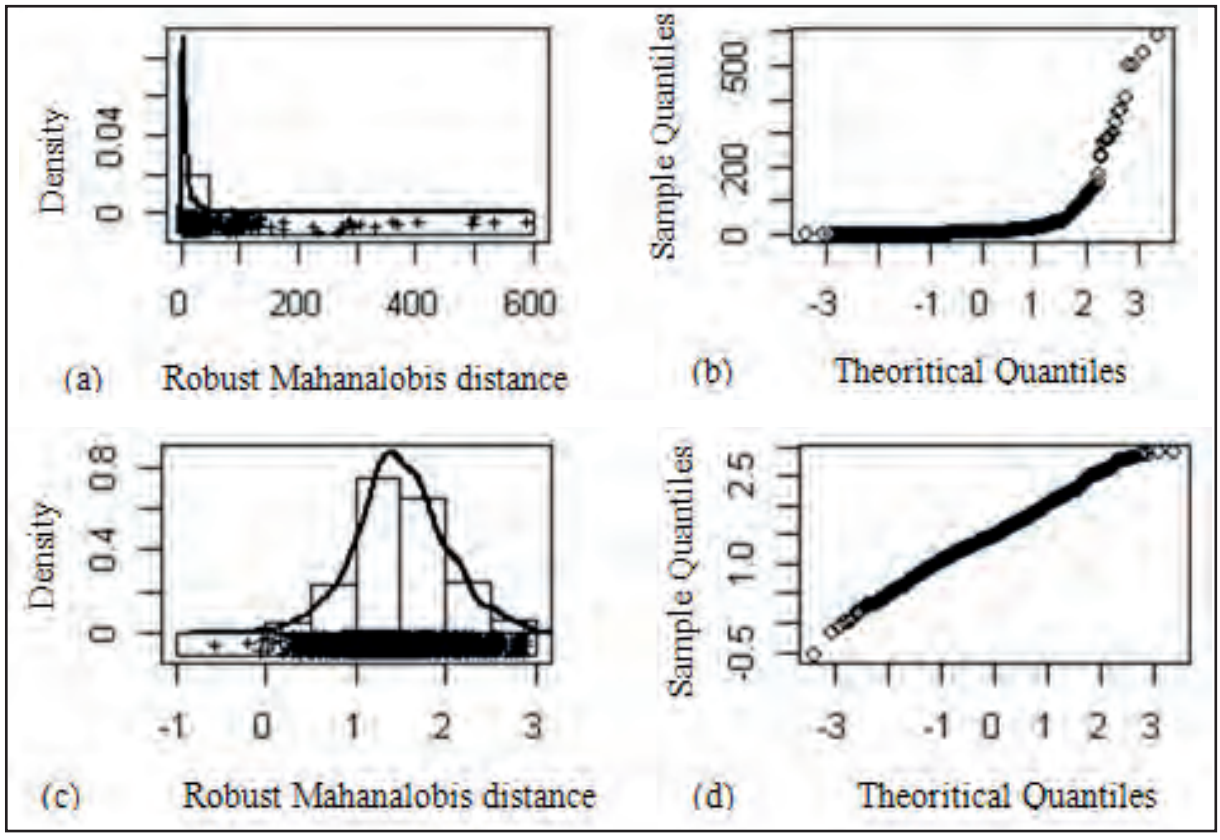

Figure 3- Histogram, density trace, 1-D scatter and Q-Q plot for the RMD of association of Cu, Au, Mo, Ag, Pb, Zn, As, Sb elements: raw data (upper), transformed data (lower).

4.2. Spatial Variability Analysis of RMDs

Both Moran correlograms for RMD and transformed RMD show a phenomenon that Moran correlation coefficients gradually decrease as distances get longer (Figure 4). Moran spatial correlogram found the strongest, positive and significant correlation at distance band ranging from 0 to 2 km for both non-transformed and transformed data. Spatial correlation decreased as distances increased. No significant spatial correlation was found at a distance above 11.1 km for non-transformed data (Figure 4a) and above 14.8 km for Box-Cox transformed data (Figure 4b). It can be concluded that spatial correlation for non-transformed RMDs and transformed RMDs are available when the distance is below 11.1 km. A distance of 12 km was thus applied to construct a spatial weight matrix.

4.3. Spatial Cluster and Outlier Analysis

Six different distance bands were used to construct spatial weights matrix including d = 2, 4, 6, 8, 10 and 12 km. The weights for neighboring locations were assigned 1 if the distances were within the band d, otherwise the weights were 0. To reduce the influence of high values (extreme values and outliers), Box-Cox transformation was applied for the identification of spatial clusters and outliers.

Table 1 shows the results of the identification of spatial clusters and spatial outliers for the association of elements. It can be seen that the number of significant spatial clusters (high-high, low-low) and spatial outliers (low-high, high-low) increased as distance bands increased for both the raw data and Box-Cox transformed data.

Table 1- Summary table of spatial clusters and outliers for association of Cu, Au, Mo, Ag, Pb, Zn, As and Sb elements using the raw RMD and Box-Cox transformed data.

Distance bands (km)	not significant	high-high	low-low	low-high	high-low
d=2	1191	65	145	26	4
d=4	1003	78	301	41	8
d=6	785	101	439	80	26
d=8	676	106	501	110	38
d=10	591	109	544	144	43
d=12	585	94	534	170	48
d*=2	1118	160	112	18	23
d*=4	908	231	199	38	55
d*=6	762	267	255	57	90
d*=8	643	274	295	82	137
d*=10	511	282	356	106	176
d*=12	464	284	384	107	192

For the raw data, the majority of samples were not significant, indicating no presence of spatial correlation or spatial dependence as distance bands were short, such as at 2 km with 1191 insignificant samples, at 4 km with 1003 insignificant samples and at 6 km with 785 insignificant samples in the southern part of the study area (Table 1 and Figure 5-1a, 1b, 1c). There were only 65 high-high samples clustered and 26 low-high, 4 high-low spatial outliers were detected at distance band of 2km (Figure 5-1a). When the distance band increased to 4 km, the number of clusters and outliers increased to 78 high-high samples clustered, 41 low-high and 8 high-low outliers (Figure 5-1a). Following this pattern, the number of clusters and outliers increased as distance bands increased to 6, 8, 10 and 12 km. Most of high-high spatial clusters were found in the north and in the east together with

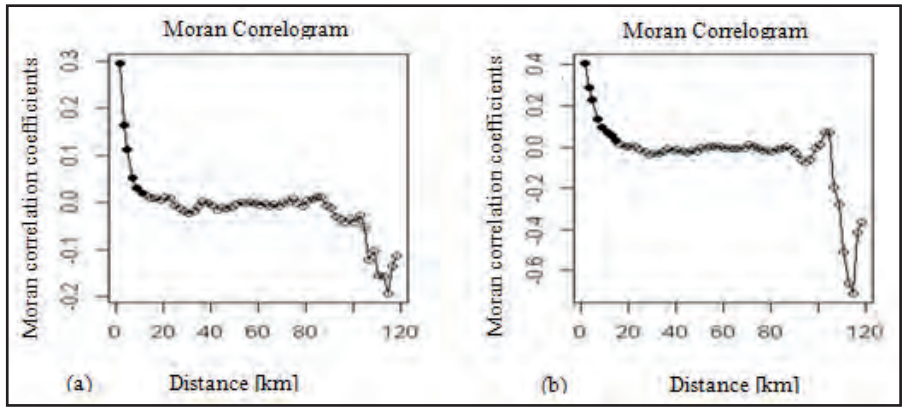

Figure 4- Moran correlograms for original Mahalanobis distance (a) and Box-Cox transformed one (b) of associations of Cu, Au, Mo, Ag, Pb, Zn, As and Sb elements.

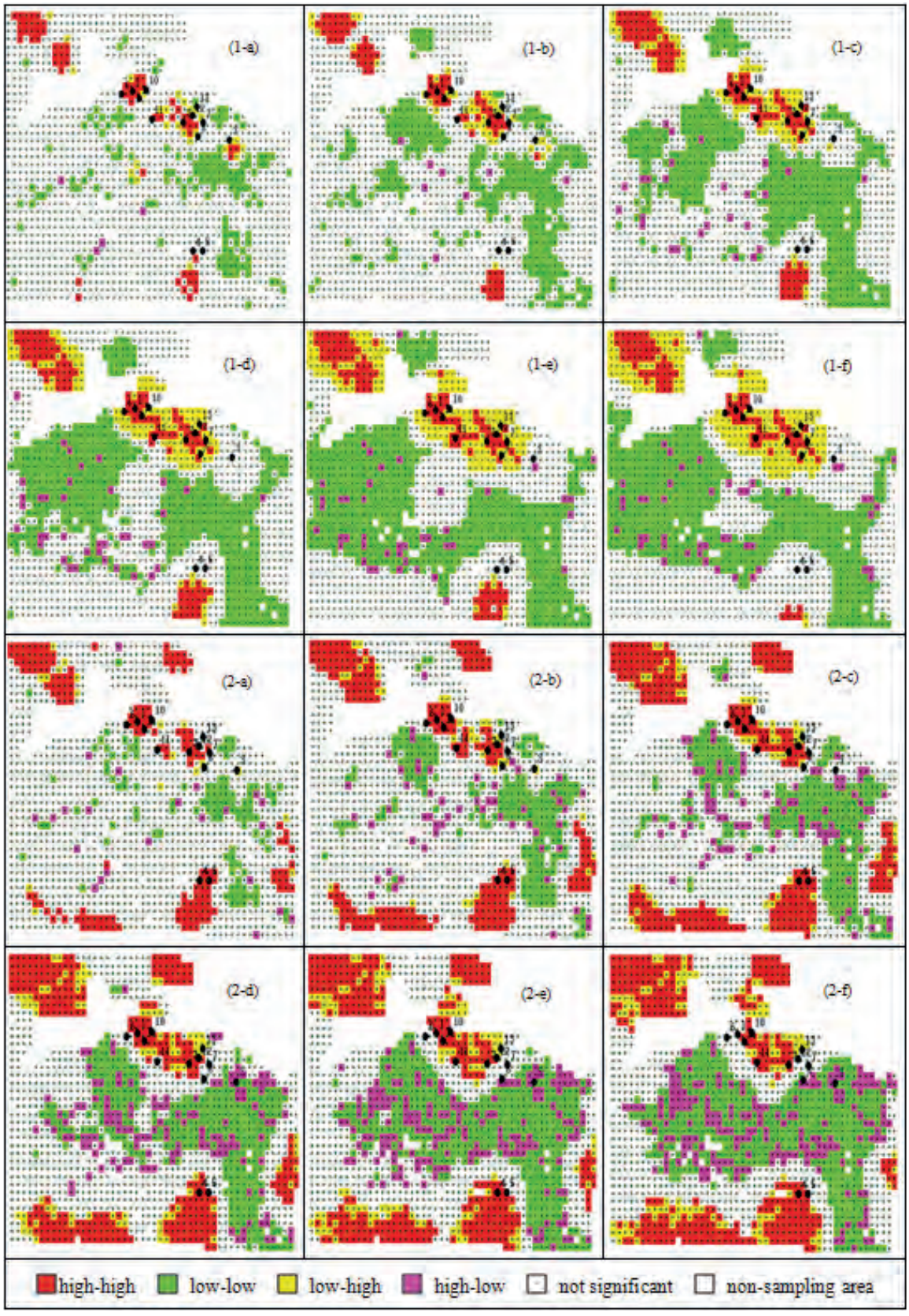

Figure 5- Spatial distribution maps of clusters and outliers of association of Cu, Au, Mo, Ag, Pb, Zn, As, Sb elements for Mahalanobis distances using raw data (1-a,b,c,d,e,f) and Box-Cox transformed data (2-a,b,c,d,e,f) at six different distance bands d = 2, 4, 6, 8, 10 and 12 km.

many low-high spatial outliers, where a metallogenic belt was found including Cu and multi-metal deposits marked by 6, 1, 9, 10, 2, 13, 7 and 8 in the east-northern part (Figure 5-1a, b, c, e, and f) except at a distance 8 km (Figure 5-1d). Moran's I_i also detected a significant high-high spatial cluster and low-high spatial outlier area in the north-west. Several significant high-low outliers were detected in the west, the south-west and the east, especially as distance bands increased. Significant low-low spatial clusters indicate that local stability occurred in these areas where no known ore deposits were found. The area of high-low outliers detected does not have conformity with known occurrences. It is therefore concluded that high-low spatial outliers played no role in the identification of ore deposits. No significant high-high clusters were found in the southern part where ore deposits 4 and 5 were located (Figure 5-1a, b, c, d, e, and f).

For Box-Cox transformed data, compared with the results of using the raw data, the number of spatial clusters and spatial outliers detected by local Moran's I_i are much more than that of non-transformed data. For example, at a distance of 2 km, there were 160 high-high spatial clusters, 18 low-high and 23 high-low spatial outliers for Box-Cox transformed data. There were 65 high-high spatial clusters, 26 low-high and 4 high-low spatial outliers for the raw data. In this case, high-low spatial outliers came into play. Moran's I_i did not detect spatial outliers or spatial clusters at distance bands of 2, 4 and 6 km where ore deposit 3 was found before (Figure 5-2a, b, and c), but it detected significant high-low spatial clusters at distances of 2 km, 4 km and 6 km (Figure 5-2d, e, and f). Also contrary to the case of non-transformed data, some significant high-high clusters were found in the southern part for Box-Cox transformed data where ore deposits 4 and 5 were located (Figure 5-2a, b, c, d, e, and f).

5. Conclusions

In this study, a new method to study spatial distribution patterns of multivariate data in an association of elements was proposed using robust Mahalanobis distance and local Moran's I_i. Four important issues can be concluded: (1) The results of the identification of spatial distribution patterns of clusters and outliers were strongly affected by the existence of high values (extreme values and outliers), as well as data transformation. It is suggested that data should be transformed first or high values (especially outliers) should be removed before calculation to reduce their influences on the results; (2) The results of the identification of spatial distribution patterns were also influenced by the construction of a spatial weights matrix. Generally, the number of spatial clusters and spatial outliers increased as distance bands increased. Therefore, it is suggested to study spatial distribution patterns at different bands; (3) High-high spatial clusters and low-high spatial outliers played an important role in the identification of local spatial instability and spatial heterogeneity in geochemical data. They may be influenced by extraneous and exotic processes such as those related to rare rock types and mineral deposit formation processes. High-high spatial clusters and low-high spatial outliers provided significant ore-finding information, which can help geochemists to have a better understanding of the potential for mineralization of element associations in the study area; (4) Low-high spatial outliers are a kind of multivariate outliers indicating the existence of local spatial instability and spatial heterogeneity, but they did not come into play in providing ore-finding information.

Acknowledgments

The authors thank Dr. Dieu Tien Bui (Associate Professor, Telemark University College (HiT), Norway) for assistance with suggested improvements to this manuscript and Dr. Peng Gong (formerly of China University of Geosciences) for the data collection.

References

Anselin, L. 1995. Local indicators of spatial association-LISA. *Geographical Analysis,* 27, 2, 93-115.

Bagchi, R., Henrys, P.A., Brown, P.E., Burslem, D.F.R.P., Diggle, P.J., Gunatilleke, C.V.S., Gunatilleke, I.A.U.N., Kassim, A.R., Law, R., Noor, S., Valencia, R.L. 2011. Spatial patterns reveal negative density dependence and habitat associations in tropical trees. *Ecology*, 92, 9, 1723-1729.

Brody, S.D. Highfield W.E., Thornton S. 2006. Planning at the urban fringe: an examination of the factors influencing nonconforming development patterns in southern Florida. *Environment and Planning B: Planning and Design*, 33, 1, 75-96.

Cliff, A.D., Ord, J.K. 1973. Spatial Autocorrelation. London - Pion.

Cliff, A.D., Ord, J.K. 1981. Spatial Processes, *Models and Applications*. London - Pion.

Filzmoser, P., Garrett, R.G., Reimann, C. 2005. Multivariate outlier detection in exploration geochemistry. *Computers and Geosciences*, 31,5, 579-587.

Filzmoser, P., Hron, K. 2013. Robustness for compositional data. In C. Becker, R. Fried and S. Kuhnt, editors, Robustness and Complex Data Structures, Festschrift in Honour of Ursula Gather, *Springer Verlag,* Heidelberg, 117-131.

Fuentes, M., Song, H.R., Ghosh, S.K., Holland, D.M., Davis, J.M. 2006. Spatial Association Between Speciated Fine Particles and Mortality. *Biometrics,* 62, 855-863.

Garrett, R.G. 1989. The chi-square plot: A tool for multivariate outlier recognition. Journal of *Geochemical Exploration*, 32, 1-3, 319-341.

Geary, R.C. 1954. The Contiguity Ratio and Statistical Mapping. *The Incorporated Statistician*, 5, 3, 115-145.

Getis, A., Ord, J.K. 1992. The analysis of spatial association by use of distance statistics. *Geographical Analysis,* 24, 3, 189-206.

Getis, A., Ord, J.K. 1996. Local spatial statistics: an overview. In: Longley P, Batty M, editors. Spatial Analysis: Modelling in a GIS Environment. Cambridge: *GeoInformation International*, 239-251.

Gervini, D. 2003. A robust and efficient adaptive reweighted estimator of multivariate location and scatter. *Journal of Multivariate Analysis*, 84,1, 116-144.

Goovaerts, P., Jacquez, G.M. 2004. Accounting for regional background and population size in the detection of spatial clusters and outliers using geostatistical filtering and spatial neutral models: the case of lung cancer in Long Island, New York. *International Journal of Health Geographics,* 3, 14-46.

Hawkins, D.M. 1980. Identification of Outliers. *Chapman and Hall* - London.

Irl, S., Harter, D., Steinbauer, M., Puyol, D., Fernández-Palacios, J., Jentsch, A., Beierkuhnlein, K. 2015. Climate vs. topography - spatial patterns of plant species diversity and endemism on a high-elevation island. *Journal of Ecology*, 103, 1621-1633.

Ishioka, F., Kurihara, K., Suito, H., Horikawa, Y., ONO, Y. 2007. Detection of hotspots for three-dimensional spatial data and its application to environmental pollution data. *Journal of Environmental Science for Sustainable Society*, 1, 15-24.

James, W.L., Cossman, R.E., Cossman, J.S., Campbell, C., Blanchard, T. 2004. A brief visual primer for the mapping of mortality trend data. *International Journal of Health Geographics,* 3, 1, 1-7.

Legendre, P., Fortin, M.J. 1989. Spatial pattern and ecological analysis. *Plant Ecology*, 80, 2, 107-138.

Lalor, G. C., Zhang, C. S. 2001. Multivariate outlier detection and remediation in geochemical databases. Sci. *Total Environ*, 281, 99-109.

McGrath, D., Zhang, C.S. 2003. Spatial distribution of soil organic carbon concentrations in grassland of Ireland. *Applied Geochemistry*, 18, 10, 1629-1639.

McLaughlin, C.C., Boscoe, F.P. 2007. Effects of randomization methods on statistical inference in disease cluster detection. *Health Place,* 13, 1, 152-63.

Monastiriotis, V. 2009. Examining the consistency of spatial association patterns across socio-economic indicators: an application to the Greek regions. *Empirical Economics*, 37, 1, 25-49.

Moran, P. A. P. 1948. *Biometrika*, 35, 255-60.

Moran, P. 1950. Notes on continuous stochastic phenomena. *Biometrika*, 37, 17-23.

Nguyen, T., Liu, X., Ren, Z. 2014. A Study Of Geochemical Exploration Spatial Cluster Identificaton Based On Local Spatial Autocorrelation. *Geophysical and Geochemical Exploration*, 38, 2, 370-376.

Reimann, C., Filzmoser, P., Garrett, R.G. 2005. Background and threshold: critical comparison of methods of determination. *Science of the Total Environment,* 346, 1-3, 1-16

Rose, A.W., Hawkes, H.E., Webb, J.S. 1979. Geochemistry in Mineral Exploration. *Academic Pres*s - London.

Rocke, D.M., Woodruff, D.L. 1996. Identification of Outliers in Multivariate Data. *Journal of the American Statistical Association,* 91, 435, 1047-1061.

Rousseeuw, P. J., Leroy, A. M. 1987. Robust regression and outlier detection. *John Wiley and Sons* - New York.

Rousseeuw, P.J., Van Zomeren, B.C. 1990. Unmasking multivariate outliers and leverage points. *Journal of the American Statistical Association*, 85, 411, 633-651.

Ruiz, M.O., Tedesco, C., McTighe, T.J., Austin, C., Kitron, U. 2004. Environmental and social determinants of human risk during a West Nile virus outbreak in the greater Chicago area, 2002. *International Journal of Health Geographics*, 3, 8, 2-11.

Tango, T. 1995. A class of test for detecting 'general' and 'focused' clustering of rare diseases. *Statistics in Medicine*, 14, 21-22, 2323-2334.

Tyler, D.E. 1991. Some issues in the robust estimation of multivariate location and scatter [C]. In W. Stahel and S. Weisberg, editors, Directions in Robust Statistics and Diagnostics 2. *Springer* - New York, 327-336.

Waller, L., Gotway, C.A. 2004. Applied Spatial Statistics for Public Health Data. *John Wiley and Sons* - New Jersey.

Zhang, C.S., McGrath, D. 2004. Geostatistical and GIS analyses on soil organic carbon concentrations in grassland of southeastern Ireland from two different periods. *Geoderma*, 119, 3-4, 261-275.

Zhang, C.S., Luo, L., Xu, W.L., Ledwith, V. 2008. Use of local Moran's I and GIS to identify pollution hotspots of Pb in urban soils of Galway, *Ireland. Science of the total environment,* 398, 1-3, 212-221.

Bull. Min. Res. Exp. (2016) 153:169-183

Bulletin of the Mineral Research and Exploration

http://bulletin.mta.gov.tr

INVESTIGATION OF THE WATER RESOURCES IN KÖPRÜÖREN BASIN (KÜTAHYA) WITH ENVIRONMENTAL ISOTOPES

Şebnem ARSLAN[a]*

[a] *Ankara Üniversitesi, Mühendislik Fakültesi, Jeoloji Mühendisliği Bölümü, 06100, Tandoğan, Ankara*

Research Article

Keywords:
Köprüören Basin, Isotopes, Carbon-14, Water-Rock Interaction, Surface Water, Groundwater.

ABSTRACT

In this study, the isotopic properties of the water resources located in Köprüören Basin are determined. $\delta^{18}O$ and δD contents of the samples respectively ranged from -10.84‰ to -7.09‰ and from -73.6‰ to -53.3‰ in dry season and ranged from -10.81‰ to -4.71‰ and -73.3‰ to -41.5‰ in wet season. Majority of the samples plotted along Global Meteoric Water Line although some of them show deviations from this line. The reason for the deviations are attributed to evaporative enrichment, modifying the original $\delta^{18}O$ and δD signatures of the samples. $\delta^{18}O$ content of the thermal samples are not modified as a result of water-rock interaction due to low wellhead and reservoir temperatures. Tritium concentrations for all samples range from ~0 to 6 TU in wet season and from ~0 to 8 TU in dry season. Accordingly, some of the groundwater samples are recharged from modern precipitation, their groundwater residence times are short and they have shallow circulation. Besides, samples with tritium concentrations close to detection limits (thermal water samples and two of the groundwater samples) were recharged before tritium from nuclear weapon tests and have relatively higher residence times. These samples were also analysed for $\delta^{13}C$ and ^{14}C to get information about the residence times. $\delta^{13}C$ ve percent modern carbon contents of five samples range from -5‰ to -14.6‰ and from 8.2 to 78 pmc, respectively. The corrected ^{14}C ages for these samples are up to 11500 years before present, thereby indicating the presence of paleowaters in the basin. $\delta^{13}C$ data indicate that ^{14}C contents of the thermal waters were diluted as a result of water-rock interaction.

Received: 24.02.2016
Accepted: 24.03.2016

1. Introduction

The importance of sustainable management of water resources has been increasing in recent years due to the rise in water consumption triggered with various factors including global population increase, industrial revolution and climate change. At the present time Turkey is not considered as one of the water-stressed countries, however, the pressure in our water resources increase with urbanization, industrialization, population and irrigation water requirement. Therefore, it is necessary to use advanced techniques, besides the classic methods to contribute to the research carried out towards safe and sustainable development of the available water resources which are renewable but limited (Çifter and Sayın, 2002). Isotope techniques have commonly been employed in hydrological and hydrogeological investigations. Humans cannot control the signature of environmental isotopes found naturally in water, therefore, in hydrology monitoring and evaluation of isotopic variations give information about the origin and renewability of waters, recharge areas and circulation mechanisms, mixing processes, surface water- groundwater interactions, and the subsurface processes affecting the quality of waters (Clark and Fritz, 1997). Many researchers have employed environmental isotopes in investigations involving determination of groundwater flow paths, groundwater residence times and water circulation (Schlosser et al., 1988; Clark et al., 1997; Bayarı et al., 2009; Çelik et al., 2013; Arslan et al., 2015).

Köprüören Basin is located to the west of the Kütahya province, upstream of Kütahya and Eskişehir plains (Figure 1). The total catchment area of the basin is 320 km^2; however, both the quality and the quantity of the basin influences a broader region than the catchment area itself involving Enne Dam, Felent and Porsuk streams. The only exploited silver deposit of Turkey is developed in the metamorphic basement rocks, Early Miocene volcanics and Pliocene units. The cyanide-rich wastes of the silver plant are stored in waste pools. The safety of this facility has been discussed and investigations have been carried out to put forward

* *Corresponding Author: Şebnem ARSLAN, E-mail: sebnem_okten@yahoo.com, Phone: +90 312 2033416, Fax: +90 312 2150487*
http://dx.doi.org/10.19111/bmre.81859

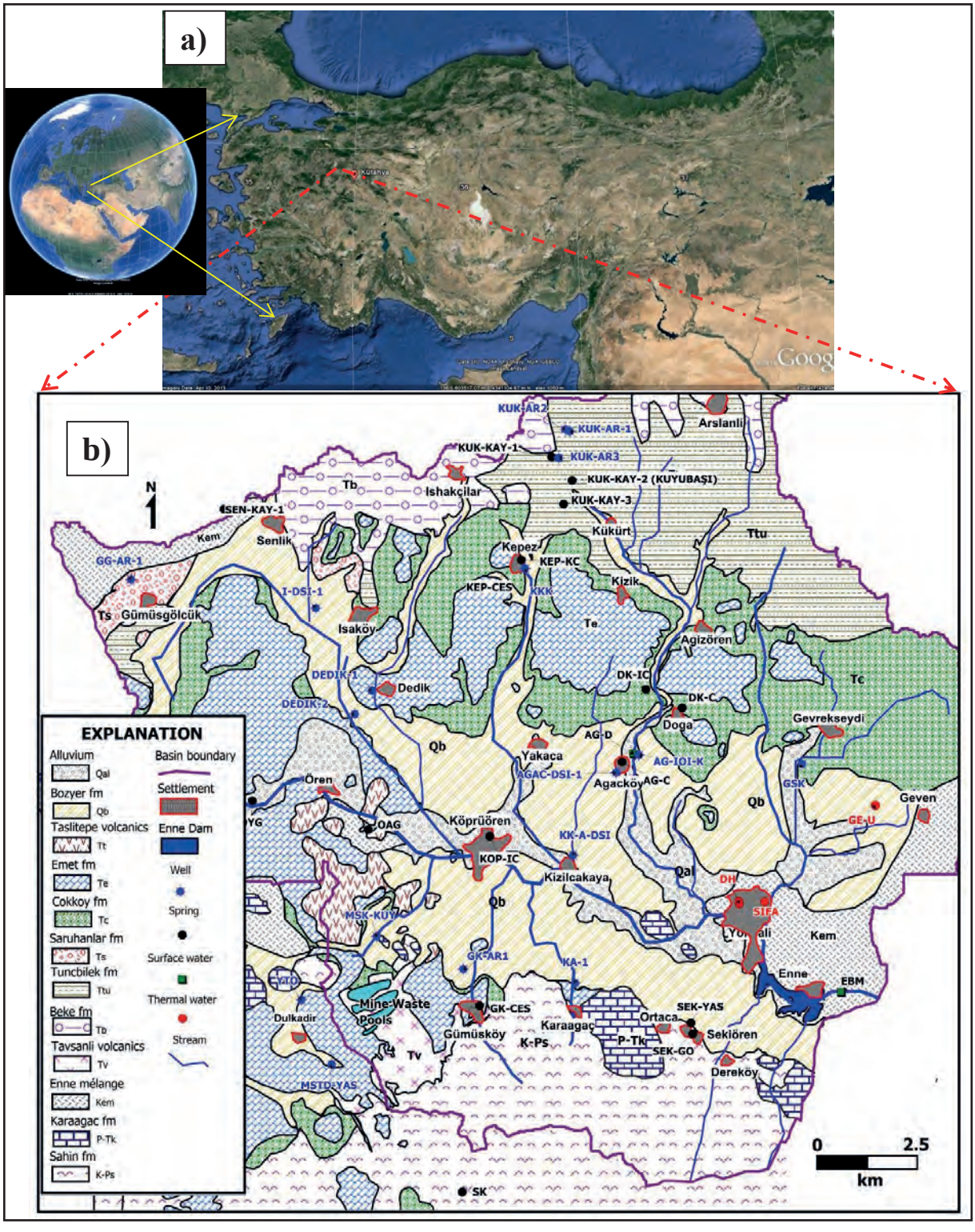

Figure 1- Figure showing a) location map b) geological map of the study area with sampling locations (Modified from Arik, 2002).

the damage to the environment after a major collapse occurred in one of the pools (Arslan et al., 2013; Arslan and Çelik, 2015)

The aim of this study is to present the isotopic signatures and origin of the water resources in Köprüören Basin as well as to determine the groundwater residence times and to identify different processes (evaporation, water-rock interaction etc.) involved in the modification of the isotopic composition of the waters. To this end, the stable isotopes of oxygen, hydrogen and carbon ($\delta^{18}O$, δD and $\delta^{13}C$) and the radioactive isotopes of hydrogen and carbon (^{3}H and ^{14}C) are utilized.

1.1. Geographical Setting, Climate and Topography

Köprüören Basin is located in Inner West Anatolia, to the north of Kütahya province and to the south of Tavşanlı district. The effects of both continental and Mediterranean climates can be seen in the area. Summers are generally hot and dry whereas winters are moist and cold. The annual average mean temperature, precipitation, average relative humidity and potential evapotranspiration recorded at Kütahya Meteorological Station between years 1970-2913 by Turkish State Meteorological Service are 10.7 °C, 546.5 mm, 65% and 800 mm, respectively. The elevation within the basin varies between 900 m and 1600 m and the average elevation is 1250 m. Northern and southern parts have rugged terrains, whereas the central part is flat (Figure 2).

1.2. Geological and Hydrogeological Settings

The geologic units outcropping in the study area are represented by metamorphic, magmatic, volcanic and sedimentary rocks formed between Paleozoic and Quaternary periods (Figure 1) Arık, 2002). Basement rocks in the area are Palezoic (Carboniferous- Permian) metamorphics which are composed of metasandstones, metaconglomerates and schists (Baş, 1983; 1986; 1987; Arık, 2002). Paleozoic metamorphics are also known as Şahin formation. Şahin formation is conformably overlain by Karaağaç Formation consisting of Permian-Triassic marbles (Arık, 2002). These marbles are

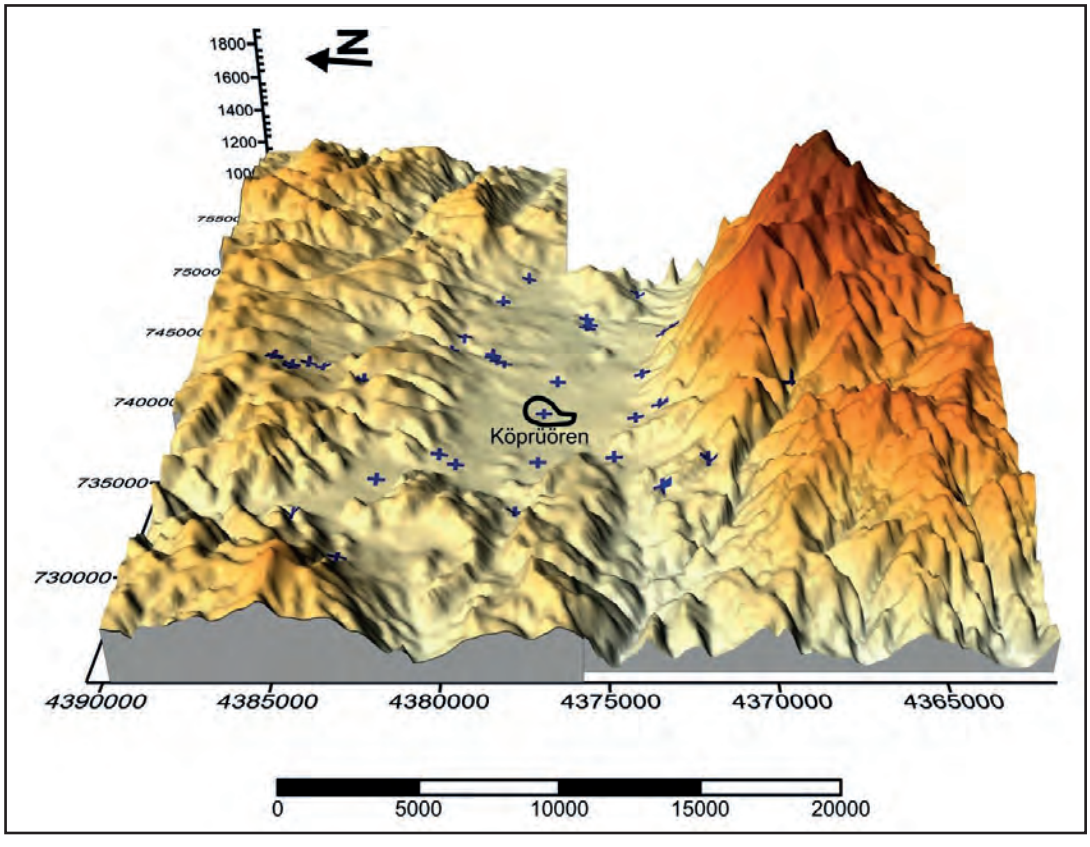

Figure 2- Digital elevation model of the study area. Sampling locations are shown with blue plus signs.

dark grey colored, thick layered at the bottom and thin to medium layered at the top. The older units are tectonically overlain by Upper Cretaceous Enne mélange consisting of serpentinite, cherts and radiolarites (Arık, 2002). Due to the block faulting in Late Oligocene- Early Miocene two different depositional settings were formed in the area. In the northern part, pre-Cenozoic units are unconformably overlain by Early Miocene Beke formation. Beke formation contains pebble stone, sandstone, mudstone, shale, bituminous levels rich in organic matter and coal lenses (lignites) (Konak, 1979; Baş, 1983; Çelik ve Kerey, 1999; Arık, 2002). The pebbles of this formation are derived from schists, carbonate rocks and serpentinites. Beke formation is conformably overlain by Miocene Tunçbilek formation which is composed of claystone-siltstone alternations, laminated tuffite and calcareous claystone at the base; coal lenses represented by dark brown, black colored lignites (Çelik and Kerey, 1999) in the middle followed by laminated marls, clayey limestones, claystones and silicified tuffs at the top. In the southern part of the study area, pre-Cenozoic units are unconformably overlain by Tavsanli volcanics which consist of altered dacites, rhyodacites, tuffs and agglomerates. The oldest unit of Pliocene, Saruhanlar formation can be observed throughout the basin and it covers the older units unconformably. This formation is composed of conglomerates, sandstones and alternations of limestone and tuffs (Baş, 1983). Late Pliocene Çokköy formation overlies Saruhanlar formation conformably and consists of marls, claystones, sandstones, conglomerates and tuff. Çokköy formation is conformably overlain by Early Pliocene Emet formation. Emet formation is composed of highly porous, white limestones, clayey, silicified and dolomitic limestones (Akdeniz and Konak, 1979). At the bottom of this formation, clayey limestones and marls are abundant. Limestones of Emet formation show thin laminations and in between them there are clayey and cherty levels. Furthermore, Arik (2002) stated that there are cavities formed due to dissolution. There is volcanic input in early Pliocene during which Taşlıtepe volcanics formed. Taşlıtepe volcanics are characterized by black, highly porous basalts and dark pink colored andesites (Baş, 1983). Quaternary Bozyer formation and alluvium deposits unconformably overlie the older units. Bozyer formation shows a wide distribution in the basin and contains red pebbles, sands and clays. Today, weathering still continues contributing to the formation of alluvium (Arık, 2002).

Kocasu stream and its tributaries are the surface waters of the basin with a drainage area of 320 km^2 (Figure 1). Kocasu stream flows from west to east into Enne Dam in Yoncalı. This stream joins to Felent Stream, flows to east until it reaches Porsuk River. Enne Dam is the main reservoir in the basin and is used for irrigation and for cooling purposes in Seyitömer thermal plant located to the north of the basin.

State Hydraulic Works (DSİ) carried out hydrogeological investigations in 1981 and determined the locations of the alluvium springs which were formed along the contact of the water table and topography and the karstic springs. Moreover, there are some thermal springs located around Yoncalı village. These springs emerge along the faults in Paleozoic marbles. The main aquifer units in the area were determined by the geological and geophysical investigations and exploration drilling carried out by DSİ (DSİ, 1981). Accordingly, Quaternary units are clayey and they are not considered as a productive aquifer. Limestones and tuffs in Neogene series, on the other hand, are the water bearing units in the area and the main aquifer. The groundwater flow in the plain part of the basin is from north to south and south to north towards Kocasu stream and there is discharge to Enne Dam. There are 6 irrigation cooperatives throughout the basin (Dedik, Yakaca, Ağaçköy, Kızılcakaya, Köprüören, Gümüşköy) which were established to employ groundwater for irrigation purposes. Only the ones located in Dedik, Gümüşköy, Kızılcakaya and Ağaçköy are active. In other parts of the basin, there are a limited number of wells used for irrigation.

According to the hydrogeochemical studies conducted by Arslan and Çelik (2013) the dominant cations in the waters of the basin are Ca and Mg, whereas the dominant anions are HCO_3 and SO_4 (Table 1). The chemical characters of the samples are in general Ca-Mg-HCO_3 and Mg-Ca-HCO_3 except for one well located in Gümüşgölcük village which is Na-HCO_3 type (Arslan and Çelik, 2013).

Table 1- The coordinate and altitude information, sample explanations, water types and the in-situ electrical conductivities of the samples determined in May 2012 and September 2012.

Sample ID	X	Y	Altitude (m)	EC (µS/cm)		Chemical Character (Arslan and Çelik, 2013)	Explanation
				May 2012	September 2012		
OAG	734678	4377301	1024	573	518	Mg-Ca-HCO_3	Spring emerging from volcanics (sample taken from discharge point inside a lake)
KK-A-DSI	739718	4376655	1035	518	774	Mg-Ca-HCO_3	Kızılcakaya village DSİ irrigation well No: 41052
GG-AR-1	728846	4383426	1108	402	389	Na-HCO_3	Gümüşgölcük village well (artesian)
SK	736997	4368394	1233	484	507	Ca-Mg-HCO_3	Fountain located in the entrance of Şahin village
I-DSI-1	733384	4382727	1055		881	Mg-Ca-HCO_3	İsaköy village DSİ irrigation well No: 55505
EBM	746560	4373445	998	485		Mg-Ca-HCO_3	Surface water sample located downstream of Enne Dam
YTO	733039	4373105	1080			Ca-Mg-HCO_3	Well located in Yılmazlar stone quarry
KUK-KAY-1	739192	4386460	1150			Mg-Ca-HCO_3	Kükürt village spring
KUK-KAY-2 (KUYUBAŞI)	739699	4385874	1125	1600	1572	Mg-Ca-SO_4-HCO_3	Kükürt village spring
KUK-KAY-3	739489	4385299	1128		1101	Mg-Ca-HCO_3	Kükürt village spring
GSK	745350	4378900	1034	820		Mg-Ca-HCO_3	Gevrekseydi village DSİ irrigation well No: 55227
KUK-AR-1	739641	4387068	1171	760		Mg-Ca-HCO_3	Kükürt village artesian well
SIFA	744435	4375525	1000			Ca-Mg-HCO_3	Şifa hotel well- Mixture of thermal water and groundwater
YKK	743794	4375531	1007		990	Ca-Mg-HCO_3	Yoncalı Thermal Hotel well- thermal water
DH	743807	4375477	1006			Ca-Mg-HCO_3	Dübecik Hamam well- thermal water
SEN-KAY-1	731131	4385175	1077			Mg-HCO_3	Şenlik village spring
KKK	738535	4383710	1135			Mg-Ca-HCO_3	Kepez village well
AG-C	740923	4378959	1047	356		Mg-Ca-HCO_3	Ağaçköy fountain
AG-IOI-K	741337	4379120	1038	1194		Mg-Ca-HCO_3-SO_4	Ağaçköy Special provincial Administration well
AG-D	741210	4379158	1035	1600		Mg-Ca-SO_4-HCO_3	Ağaçköy stream
DK-C	742403	4380288	1058	1345	1122	Mg-Ca-HCO_3-SO_4	Doğaköy fountain
DK-IC	741511	4380739	1054	378	352	Mg-Ca-HCO_3	Doğaköy drinking water fountain
OYG	731833	4378007	1032	613	956	Mg-Ca-HCO_3	Spring located west of Ören village
SEK-YAS	742618	4372554	1071	671	1010	Ca-Mg-HCO_3	Sekiören village fountain
SEK-GO	742666	4372278	1100	551	381	Mg-Ca-HCO_3	Sekiören village spring located prior to a pond
KOP-IC	737670	4377130	1018	569		Mg-Ca-HCO_3	Köprüören village drinking water fountain
KEP-CES	738444	4383924	1153	573	600	Mg-Ca-HCO_3	Kepez village fountain
KUK-AR2	739530	4387123	1173	870		Mg-Ca-HCO_3	Kükürt village artesian well
KUK-AR3	739367	4386420	1146	958		Mg-HCO3	Kükürt village artesian well
GK-AR1	737018	4373857	1049	590	704	Ca-MgHCO_3	Gümüşköy DSİ irrigation well No: 52884
GE-U	747156	4377891	1038	533	1102	Mg-Ca-HCO_3	Thermal water well located in Geven village (Belongs to Dumlupınar University)
Y-YAG	744060	4375408	990			Ca-HCO_3-SO_4	Rain sampled in Yoncalı village
MSK-KUY	734890	4374659	1031	410		Ca-Mg-Na-HCO_3	Well located downstream of mine site
MSTD-YAS	733788	4371522	1113	426		Ca-HCO_3	Well close to Dulkadir village
AGAC-DSI-1	740779	4378690	1043		823	Mg-Ca-HCO_3	Ağaçköy DSİ irrigation well No: 36813
GK-CES	737419	4372971	1094		636	Ca-HCO_3	Gümüşköy fountain
KA-1	739768	4373513	1068		736	Ca-Mg HCO_3	Karaağaç village well
DEDIK-1	734779	4380705			660	Mg-Ca-HCO_3	Dedik village DSİ irrigation well No: 41946
DEDIK-2	734350	4380125	1042		665	Mg-Ca-HCO_3	Dedik village DSİ irrigation well No: 41949
KEP-KC	738444	4383924	1137		600	Mg-Ca-HCO_3	Kepez village fountain

2. Sampling and Analysis Procedures

Three field trips were carried out between years 2011 and 2012 and in-situ electrical conductivity (EC) measurements were performed in surface waters, groundwaters, springs and thermal springs in 40 different locations. Deuterium (δD) and oxygen-18 ($\delta^{18}O$) samples were collected from each of these locations. Besides, 20 samples were collected for tritium analyses (^{3}H) and 5 samples were collected for carbon-13 ($\delta^{13}C$) and carbon-14 (^{14}C) analyses. For radiocarbon samples, in order to prevent post-collection biological activity from altering the carbon concentration and isotopic concentration, the samples were preserved by adding approximately 0.2 ml of saturated $HgCl_2$ solution.

Samples collected in October 2011 and September 2012 represent dry periods whereas the samples collected in May 2012 represent wet period. For $\boldsymbol{\delta}^{18}O$ and δD analyses, 17, 25 and 22 samples were collected in October 2011, May 2012 and September 2012, respectively. In selected locations, to observe the seasonal changes, samples were taken in all of the three sampling periods. For ^{3}H analyses, 5, 12 and 14 samples were collected in October 2011, May 2012 and September 2012, respectively (Table 2). Sampling was carried out only in September 2012 for $\delta^{13}C$ and ^{14}C (Table 3).

The water samples were analyzed for their $\delta^{18}O$ and δD stable isotope ratios in the Stable Isotope Laboratory of Hacettepe University by using laser spectroscopic methods. VSMOW (Vienna Standard Mean Ocean Water) was used as a reference standard and analytical precisions were reported to be within 0.2‰ for $\delta^{18}O$ and 1‰ for δD. ^{3}H concentrations were determined in the Environmental Tritium Laboratory of Hacettepe University with an ultra-low level liquid scintillation counting unit. Analytical uncertainties are reported as ±0.4 TU. $\delta^{13}C$ and ^{14}C analyses were carried out in Beta Analytical Laboratories (U.S.A.) from dissolved inorganic carbon (DIC). $\delta^{13}C$ contents were determined by using a Stable Isotope Mass Spectrometer whereas carbon-14 analyses were carried out by using an accelerator mass spectrometry (AMS) system

3. Results and Discussion

3.1. Relationship of Oxygen-18 ($\delta^{18}O$) and Deuterium (δD)

According to the electrical conductivity measurements carried out during the field trips in May 2012 and September 2012, EC values vary between 356 µS/cm and 1600 µS/cm for 24 samples in May 2012 and they vary between 352 µS/cm and 1572 µS/cm for 22 samples (Table 1).

Results of the environmental isotopic analyses are reported in Table 2 for October 2011, May 2012 and September 2012. Accordingly, not much seasonal difference can be observed in samples collected from the same location in different periods (dry and wet periods) except for samples EBM, SEK-GO, KEP-CES and GE-U. For samples collected in dry period, $\delta^{18}O$ and δD values range from -10.84‰ to -7.09‰ and from -73.6‰ to -53.3‰, respectively (Table 2). Deuterium excess values, calculated by using formula $d= \delta D-8* \delta^{18}O$, are also presented in Table 2 and they vary between 3.5 ‰ and 13.9 ‰ in October 2011, between -3.8 ‰ and 13.2 ‰ in May 2012 and between 5.22 ‰ and 14.94 ‰ in September 2012.

To understand the relationship between $\delta^{18}O$ and δD, $\delta^{18}O$ vs. δD graphs were prepared for each sampling season and data were compared to Global and Mediterranean Meteoric Water Lines (GMWL and MMWL) (Figure 3, 4, 5). According to figure 3, some of the samples collected in October 2011 plotted along GMWL whereas some of them show deviations from the GMWL. Deviations from meteoric water lines are usually caused by different processes like evaporation, condensation, water-rock interaction. During evaporation, lighter isotopes enter the vapor phase immediately, therefore, the remaining water phase enriches in heavy isotopes (Clark and Fritz, 1997). An evaporation line with a slope of approximately 5 was formed with the samples showing deviation from GMWL. The slope of this line (s) depends on the relative humidity since oxygen and hydrogen are affected by moisture differently and if the relative humidity is between 25% and 75% the slope is usually between 4 and 5 (Clark and Fritz, 1997). The average relative humidity in the area is reported as 65% by Turkish Meteorological Service and the slope of the evaporation line is coherent with the relative humidity. In figure 3 one sample, which shows maximum

Table 2- Oxygen-18, deuterium, deuterium excess and tritium data for October 2011, May 2012 and September 2012.

Sample ID	Deuterium (‰)			Oxygen-18 (‰)			Döteryum fazlalığı (‰)			Trityum (TU)		
	October 2011	May 2012	September 2012	October 2011	May 2012	September 2012	October 2011	May 2012	September 2012	October 2011	May 2012	September 2012
OAG	-60.3	-61.8	-61.2	-8.57	-8.56	-8.55	8.3	6.7	7.2		3.44	
KK-A-DSI	-62.5	-63.3	-65.3	-8.71	-8.8	-9.01	7.2	7.1	6.7		0.6	-0.4
GG-AR-1	-71.5	-72.1	-72.8	-10	-9.98	-10.19	8.5	7.8	8.7		-0.41	0.87
SK	-68.3	-73.3	-73.6	-10.29	-10.81	-10.62	14.0	13.2	11.4	4.11	5.41	
I-DSI-1	-65.1		-66.4	-9.05		-9.24	7.3		7.6			5.66
EBM	-53.3	-68.2		-7.09	-9.67		3.5	9.2				
YTO	-63.3			-8.88			7.7					
KUK-KAY-1	-61.1			-8.59			7.6			7.87		
KUK-KAY-2 (KUYUBAŞI)	-62.2	-61.3	-63.9	-8.6	-8.48	-8.82	6.6	6.5	6.7			6.3
KUK-KAY-3	-60.1		-63.5	-8.4		-8.59	7.1		5.2			
GSK	-63.4	-64.7		-8.68	-8.95		6.0	6.9		2.44	0.79	1.69
KUK-AR-1	-60.6	-61.1		-8.63	-8.55		8.4	7.3		2.55	4.58	6.57
SIFA	-65.3			-9.23			8.5					
YKK	-68.3		-70.0	-9.86		-9.88	10.6		9.1	0.3		
DH	-66.8			-9.78			11.5					
SEN-KAY-1	-63.2			-9.03			9.0					2.95
KKK	-61.2			-8.76			8.9					
AG-C		-64.5			-9.11			8.4				
AG-IOI-K		-60.8			-8.28			5.5				
AG-D		-58.4			-8.05			6.0				
DK-C		-62.6	-63.0		-8.78	-9.11		7.6	9.9		1.18	
DK-IC		-65.3	-63.6		-9.11	-9.03		7.6	8.6			
OYG		-61.4	-62.0		-8.5	-8.7		6.6	7.6		6.11	6.44
SEK-YAS		-71.6	-68.4		-10.55	-10.08		12.8	12.2		5.33	6.74
SEK-GO		-71.6	-69.9		-10.47	-10.61		12.1	14.9			
KOP-IC		-60.6			-8.3			5.8				
KEP-CES		-61.9	-65.0		-8.87	-9.19		9.1	8.6			7.23
KUK-AR2		-62.2			-8.84			8.5			3.48	
KUK-AR3		-62.4			-8.78			7.9				
GK-AR1		-67.3	-69.1		-9.72	-10.23		10.4	12.7		5.06	3.61
GE-U		-64.7	-73.4		-8.73	-10.53		5.2	10.9		1.02	0.48
Y-YAG		-34.5			-5.79			11.8				
MSK-KUY		-41.5			-4.71			-3.8				
MSTD-YAS		-63.3			-9.33			11.4				
AGAC-DSI-1			-63.8			-8.71			5.9			1.33
GK-CES			-72.6			-10.84			14.2			
KA-1			-66.9			-9.81			11.6			
DEDIK-1			-63.3			-8.95			8.3			4.31
DEDIK-2			-62.7			-8.58			6.0			
KEP-KC			-65.9			-9.07			6.7			

Table 3- $\delta^{13}C$ and ^{14}C data, radiocarbon ages without correction, q-factor, apparent radiocarbon ages corrected with carbon-13 method.

Sample ID	$\delta^{13}C$ (‰)	^{14}C (pmc)	^{14}C Error (pmc)	Unadjusted ^{14}C age (BP*)	^{14}C age error (BP)	q factor	Corrected ^{14}C ages (BP)
GE-U	-5.0	8.18	0.09	20110	90	0.26	9420
KK-A-DSI	-11.4	19.10	0.12	13300	50	0.48	7375
GG-AR-1	-14.6	13.99	0.1	15800	60	0.59	11500
GSK	-13.3	77.96	0.28	2000	30	0.54	-2920
YKK	-4.8	13.18	0.09	16280	60	0.26	5380

* Radiocarbon ages were calculated by assuming an initial ^{14}C content of 100 pmc for the water samples. Libby half-life ($t_{1/2}$ =5568 years) was used in the calculations.

evaporative enrichment, was collected from Enne Dam and this sample was exposed to evaporation under high temperature conditions during the dry period. For other samples located along the evaporation line there is also evaporative enrichment. Some of the fountain samples were not collected from their original sources where they emerge, so evaporative enrichment is possible during storage. For shallow wells, evaporation before recharge can be the reason of the evaporative enrichment of these samples.

Thermal water samples do not show evaporative enrichment and they have depleted $\delta^{18}O$ and $\delta^{2}H$ values. Besides, these samples are plotted along GMWL although deviations in $\delta^{18}O$ due to the water-rock interaction are common in thermal waters. The thermal waters, under high temperatures, usually interact with rocks and during this interaction there is enrichment in $\delta^{18}O$ values of the waters (the hydrogen contents of the rocks are usually lower compared to the hydrogen contents of water so during water-rock interaction δD contents doesn't show variations.) (Güleç and Mutlu, 2002). The wellhead temperatures of thermal waters sampled in Yoncali are around 40 °C (Arslan and Çelik, 2013). Besides, the reservoir temperatures calculated by using chalcedony and quartz geothermometers (Fournier, 1977) ranges between 49-84 °C for Yoncalı, and between 68-99 °C for Geven (Arslan and Çelik, 2013). Therefore, due to the reason that thermal waters have relatively low wellhead and reservoir temperatures, the $\delta^{18}O$ contents of these samples are not affected from the water-rock interaction. One of the samples collected from Yoncali has got $\delta^{2}H$ and $d^{18}O$ content similar to the $\delta^{2}H$ and $d^{18}O$ of cold waters (Figure 3). This sample was collected from a pool in which a mixture of thermal and cold waters was present. Therefore, this sample reflects the isotopic content of a mixture instead of reflecting the isotopic contents of a thermal water sample. There are two samples having relatively depleted stable isotope contents compared to the thermal waters (Figure 3). One of these samples was collected from an artesian well located in Gümüşgölcük village and it will be evaluated in the following sections. The other sample was collected from a fountain in the entrance of Şahin village (SK, discharge elevation: 1233 m). The tritium content of SK is 4.11 TU and due to the presence of tritium, it can be argued that this sample is recharged with modern precipitation falling into high altitudes.

According to figure 4, which was prepared by using stable isotope data obtained during wet period sampling, there is an evaporation line formed with a slope of 5 in accordance with the relative humidity. This evaporation line is similar to the one presented in figure 3. Herein, the sample showing maximum evaporation effect is collected from a well sample located downstream of the silver mine site. In this well it was not possible to discharge the water prior to sampling so the sample was taken from the evaporated water mass inside the well. Another sampling point which is on the evaporation line is stream water sampled near Ağaçköy and observation of evaporation effect in surface water is an expected result. Another noteworthy point about evaporation is that in Enne Dam samples, the dry period sample is under the influence of evaporation although the sample collected in wet period does not show evaporation effects according to $\delta^{2}H$- $\delta^{18}O$ contents. In the sample location, the difference in dam water level between dry and wet periods and the change in isotope content with the effect of rain is stunning. In this period, rain water sampling was possible following heavy rains in Yoncalı region. $\delta^{2}H$- $\delta^{18}O$ content of this sample almost plotted along Global Meteoric Water Line (Figure 4). In May 2012, thermal water sampling was carried out in one station which belongs to Dumlupınar University located

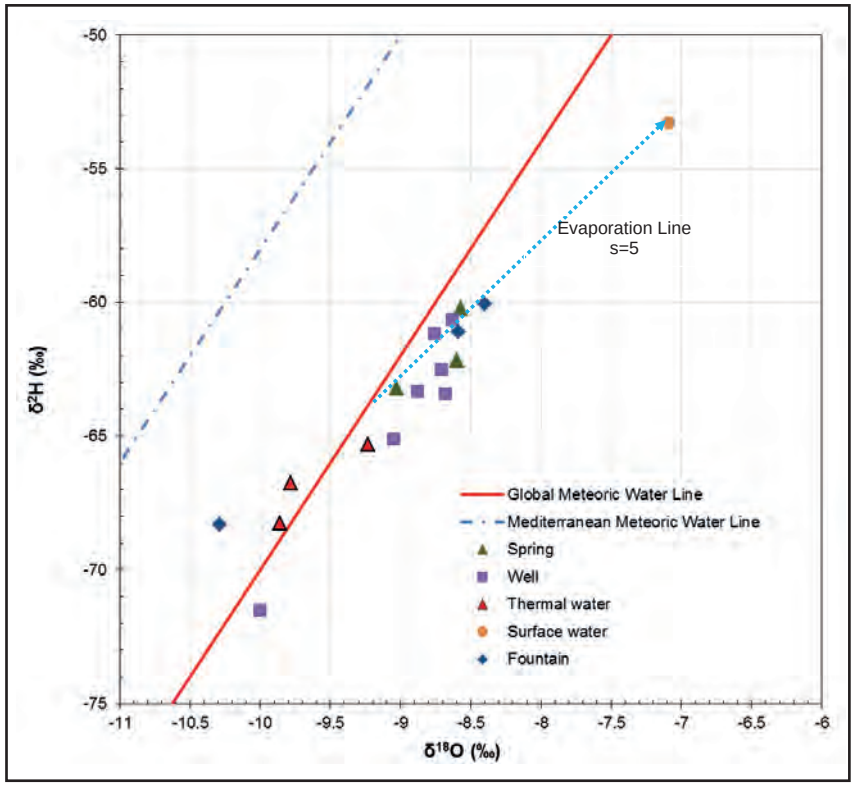

Figure 3- δ^2H vs. $\delta^{18}O$ diagram for October 2011 (dry period). Global Meteoric Water Line is defined by equation $\delta^2H = 8\delta^{18}O+10$ (‰ SMOW) (Craig, 1961), Mediterranean Meteoric Water Line is defined by equation $\delta^2H = 8\delta^{18}O+22$ (‰ SMOW) (Gat and Carmi, 1970).

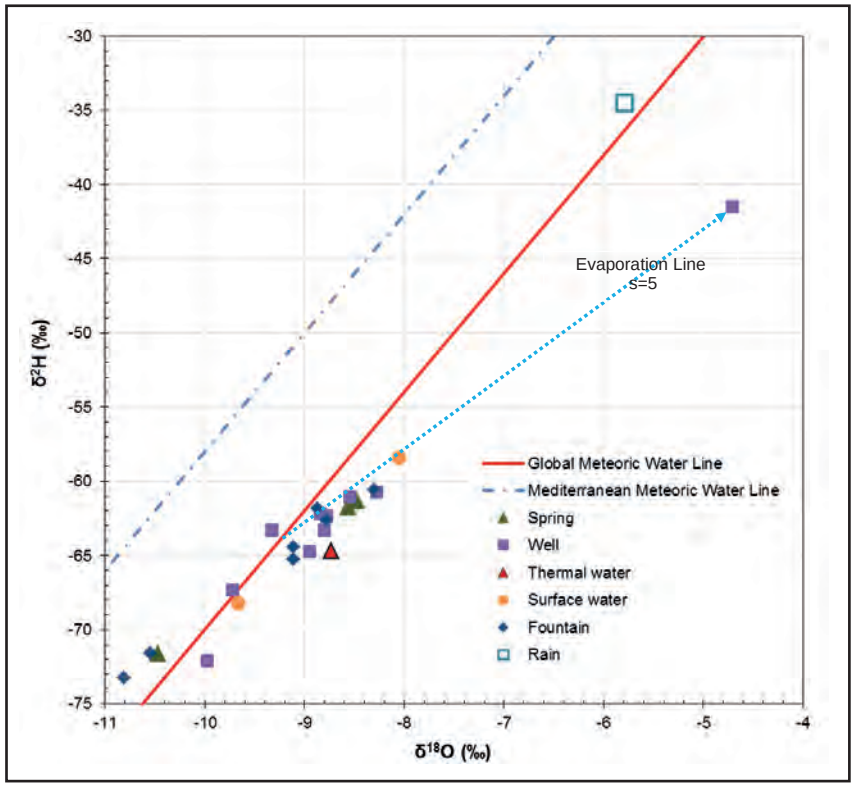

Figure 4- δ^2H vs. $\delta^{18}O$ diagram for May 2012 (wet period). Global Meteoric Water Line is defined by equation $\delta^2H = 8\delta^{18}O+10$ (‰ SMOW) (Craig, 1961), Mediterranean Meteoric Water Line is defined by equation $\delta^2H = 8\delta^{18}O+22$ (‰ SMOW) (Gat and Carmi, 1970).

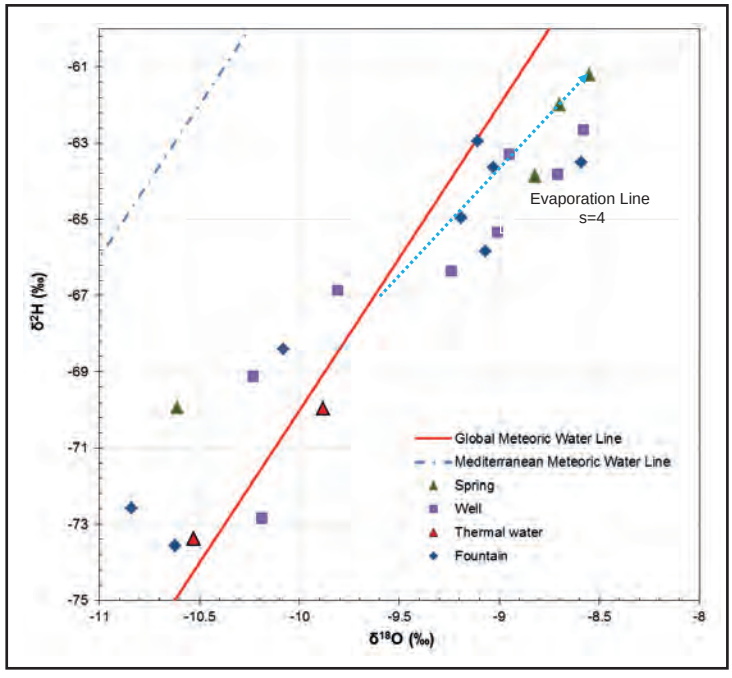

Figure 5- δ^2H vs. $\delta^{18}O$ diagram for September 2012 (dry period). Global Meteoric Water Line is defined by equation $\delta^2H = 8\delta^{18}O+10$ (‰ SMOW) (Craig, 1961), Mediterranean Meteoric Water Line is defined by equation $\delta^2H = 8\delta^{18}O+22$ (‰ SMOW) (Gat and Carmi, 1970).

in Geven village. It was impossible to approach the wellhead during sampling so the sample was collected from a creek formed by the water leaking from the well. As a result, the sample was not only unable to reflect the actual isotopic content of the thermal water but also shows evaporation. This well was also sampled in September 2012, this time from the wellhead. For sampling periods May 2012- September 2012, the difference in $\delta^{18}O$ and δD contents are reported as 1.8‰ and 8.7 ‰, respectively. These differences are far from reflecting seasonal changes, they are rather related to sampling.

δ^2H vs. $\delta^{18}O$ graph prepared by using the stable isotope contents of samples collected in September 2012 reveals out that there is another evaporation line formed for some samples collected from springs, wells and fountains. This time, slope is slightly smaller than the slopes calculated for previous periods (s~4). In this period, samples depleted in heavy isotopes are collected from fountains Şahin and Sekiören villages, thermal well of Dumlupınar University in Geven village and from Gümüşköy village well.

When deuterium excess values obtained throughout three sampling periods are evaluated, the lowest deuterium excess values are observed in samples under evaporation effect and the maximum value is observed in one sample from Şahin village. This sample is enriched in heavy isotopes, doesn't show evaporation effect and its discharge elevation is relatively higher.

3.2. Relationship of Elevation and Oxygen-18 for Precipitation

Oxygen-18 content of precipitation changes with temperature, altitude and latitude. The temperatures drop at higher altitudes and precipitation gets depleted in heavy isotopes. This depletion varies between -0.15 and -0.5 per 100 m rise in altitude for $\delta^{18}O$ (Clark and Fritz, 1997). In the content of this study, it has been aimed to get information about the isotopic character of precipitation falling into different altitudes; however, it was impossible to find enough number of seasonal springs discharging from different altitudes. Therefore, the comments about this subject were carried out by relatively comparing the recharge altitudes of groundwater and thermal water samples. In the light of this information, throughout the basin, the isotopically most depleted samples are Gümüşgölcük artesien well (GG-AR-1), Şahin village spring (SK), Sekiören village fountain (SEK-YAS), Sekiören spring collected previous to pond (SEK-GO), Gümüşköy fountain (GK-CES) and well (GK-

AR-1). These samples are recharged by precipitation from higher altitudes.

3.3. Evaluation of Tritium Data

In this study, besides stable isotopes, the radioactive isotopes of hydrogen and carbon were also utilized. Tritium, which is a short-lived isotope of hydrogen, is formed as a result of the reaction of ^{14}N isotope with cosmic rays. Besides, there is tritium input to the atmosphere as a result of nuclear tests. In groundwater systems, tritium is an excellent tracer since it is part of a water molecule. Because it is radioactive (half-life 12.43 years), it is commonly used to determine the relative age of groundwater (Clark and Fritz, 1997). Concentration of tritium in meteoric waters is reported in Tritium Unit (TU) (1 TU=1 atom ^{3}H /10^{18} atom H). The concentration of tritium, especially in the northern hemisphere, has changed as a result of nuclear tests. Before 1963, the concentrations were about 5 TU and with the tritium input as a result of nuclear tests the concentrations reached to a maximum of 3000 TU. (Mazor, 1991). If the tritium content of precipitation before 1963 is assumed to be 5 TU, then until sampling date (year 2012- 49 years of radioactive decay) the expected tritium concentration in precipitation becomes 0.32 TU. Therefore, when the tritium content of groundwater is interpreted it can generally be said that if groundwater does not contain tritium or contains less than 0.32 TU then the water sampled should have been recharged by precipitation occuring before nuclear tests (year 1963).

According to tritium data (^{3}H) obtained during this study, the tritium content of the samples vary from ~0 TU to 6.11 TU in wet period and from ~0 TU to 7.87 TU in dry period. Accordingly, in the basin there are waters present that are recharged both by precipitation before the start of the nuclear tests (year ~1963) (<0.32 TU) and after (>0.32 TU). Most groundwater samples are recharged by recent precipitation, does not have a high residence tie and they have shallow circulation. The samples from Gümüşgölcük and Kızılcakaya village artesian wells and thermal waters contain very low tritium and they are probably recharged before the nuclear tests. For these samples, detailed interpretations will be done in the following section during the evaluation of carbon-14 data.

During wet period (May 2012), according to the relationship between tritium and $\delta^{18}O$, two spring samples are recharged by recent precipitation falling into higher altitudes (Figure 6). The samples with relatively low ^{3}H content are recharged by precipitation falling into lower altitudes. When all of the samples with shallow circulation (high tritium samples) are examined, it can be said that these samples are recharged by precipitation from different altitudes. Since some of the samples are under evaporation effect (Especially thermal water sample: GE-U), accurate estimations about the relative recharge elevations cannot be done by using $\delta^{18}O$ data. During dry period (September 2012), ^{3}H vs. $\delta^{18}O$ graph revealed out that the samples having the highest recharge elevation and residence time are the thermal waters (Figure 7). Besides, two groundwater sample with low tritium content (GG-AR-1 and KK-A-DSI) are recharged from different elevations (the recharge elevation of GG-AR-1 is relatively lower). In figure 7, for all samples there isn't any relationship between ^{3}H and $\delta^{18}O$.

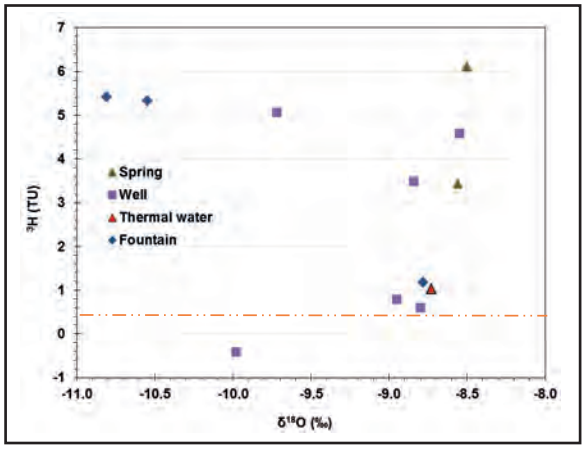

Figure 6- Tritium vs. $\delta^{18}O$ for the water samples in wet period (May 2012).

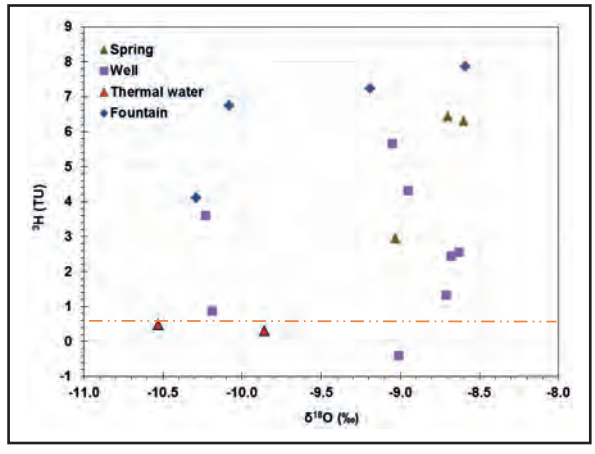

Figure 7- Tritium vs. $\delta^{18}O$ for the water samples in dry period (September 2012).

The relationship between tritium and electrical conductivity in wet and dry periods are presented in figure 8 and 9. According to figure 8, ^{3}H and EC are inversely proportional. With the decreasing ^{3}H content EC is expected to increase (with increasing groundwater residence time within the aquifer the amount of dissolved ions also increases). Relatively deep circulated samples have EC values ranging from 400 to 1400 µS/cm. According to Figure 9, shallow and relatively deep circulated waters have similar EC values and there is not any relationship between ^{3}H and EC.

3.4. Evaluation of Carbon-13 ($\delta^{13}C$) and Carbon-14 Data

Within the scope of this work, in the samples having the lowest tritium contents radiocarbon analyses were also carried out to determine the residence times. Radiocarbon method is a standard method allowing dating up to 40000 years before present. This method relies on the measurement of carbon-13 ($\delta^{13}C$) and carbon- 14 (^{14}C) in Dissolved Inorganic Carbon ($DIC = CO_{2(aq)} + HCO_3^- + CO_3^{-2}$). Radioactive isotope of carbon is (Libby half-life 5568±30 years, Cambridge half-life is 5730±40 years) present in the atmosphere and it dissolves in the unsaturated zone until it reaches water table and starts decaying to nitrogen in the groundwater system.

According to table 3, modern carbon contents (^{14}C) of 5 samples range from 8.18 pmc to 77.96 pmc, the highest content observed in Gevrekseydi artesian well and the lowest one observed in the thermal water well located in Geven. $\boldsymbol{\delta}^{13}C$ contents of groundwaters range between -11.4 ‰ and -14.6 ‰, whereas $\boldsymbol{\delta}^{13}C$ contents of thermal waters are about -5 ‰. The difference between $\boldsymbol{\delta}^{13}C$ contents of thermal waters and groundwaters can be attributed to water-rock interaction. In other words, the enrichment in $\boldsymbol{\delta}^{13}C$ contents, especially in thermal waters, suggests that there is isotopic exchange between water and aquifer material.

Determination of groundwater residence times with ^{14}C method is based on the measurement of the loss of the parent radionuclide, ^{14}C (Clark and Fritz, 1997). Equation 1 is used to calculate the radiocarbon ages of waters.

$$A = A_0 e^{-\lambda t} \qquad \text{(Equation 1)}$$

In Equation 1, A is the measured or observed activity of the sample, λ is the decay constant and t is the time passed after recharge. If the initial radiocarbon activity, A_0 is not assigned correctly, then the above equation would not give accurate results. It is hard to assign a correct value to the initial activity since there are various processes that have an effect upon ^{14}C in water. In addition, the final concentration of ^{14}C in the groundwater is also modified by isotopic exchange as a result of recrystallization and precipitation reactions.

3.4.1 Carbon-13 in the Carbonate System

Clark and Fritz (1997) indicated that carbon-13 is an excellent tracer for the evolution of carbonates in groundwaters. The cause of this is that different carbon reservoirs have different carbon-13 values. The development of Dissolved Inorganic Carbon

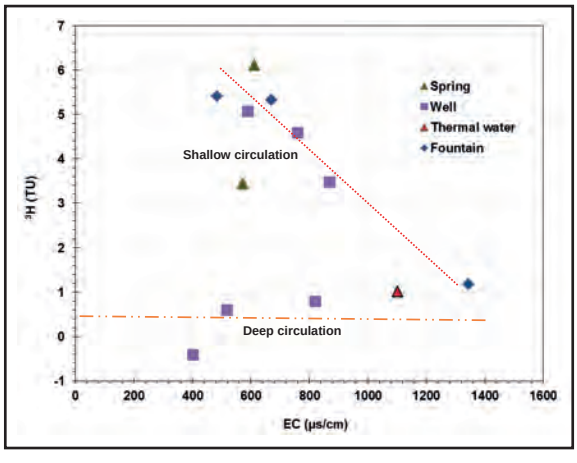

Figure 8- Tritium vs. Electrical Conductivity in wet period (May 2012).

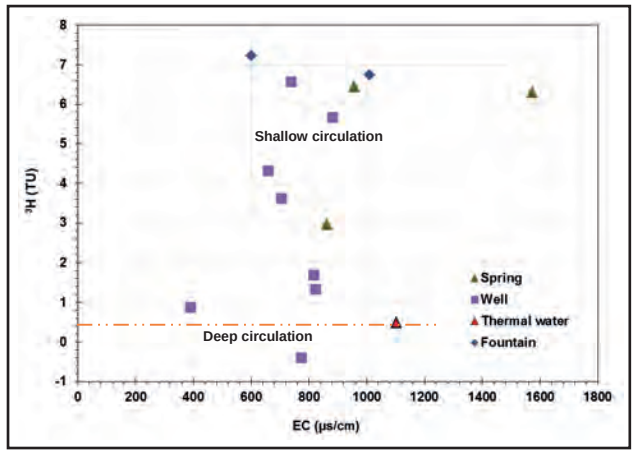

Figure 9- Tritium vs. Electrical Conductivity in dry period (September 2012).

(DIC) and $\delta^{13}C_{DIC}$ begins with atmospheric CO_2. At this point, $\delta^{13}C$ value is approximately -7 ‰ VPDB. Photosynthetic uptake of $CO_{2(atm)}$ cause a visible depletion in $\delta^{13}C$ values. This uptake occurs during CO_2 diffusion from leaf pores and during carbon fixation (transformation of CO_2 to CH_2O) which is carried out by chloroplast of leaves (Clark and Fritz, 1997). The depletion in the amount of ^{13}C differs according to the observed photosynthetic cycle. There are three main known photosynthetic cycles. These are Calvin or C_3 cycle, Hatch-Slack or C_4 cycle and Crassulacean acid metabolism (CAM) cycle (Clark and Fritz, 1997). Calvin cycle is observed in 85% of the plants and $\delta^{13}C$ values of the plants following this cycle is approximately -27 ‰ (Vogel, 1993). At higher temperatures, the plants follow C_4 cycle and $\delta^{13}C$ values are approximately -12.5 ‰ (Vogel, 1993).

3.4.2 Correction of ^{14}C Ages for Carbonate Dissolution

There are different methods to calculate apparent ^{14}C ages and application of these methods are generally decided according to chemical system and the data available. $\delta^{13}C$ mixing model, suggested by Pearson (1965) and Pearson and Hanshaw (1970), was used in order to be able to perform an estimated age calculation according to the data obtained in this study. This model enables using carbonate dissolution in open system conditions together with radiocarbon dilution in closed system conditions (Clark and Fritz, 1997). Every process adding carbon to DIC pool and removing carbon from the pool, affect $\delta^{13}C$ concentrations. The change of DIC in groundwater in one area could demonstrate to what degree carbon-14 concentrations influenced by the addition of dead carbon (Clark and Fritz, 1997). The dilution factor (q) is a number used to prevent factors affecting carbon-14 concentrations to produce false results in age calculation. This factor is demonstrated in the below equation (Equation 2) (Pearson and Hanshaw, 1970).

$$q = \frac{\delta^{13}C_{çik} - \delta^{13}C_{karb}}{\delta^{13}C_{toprak} - \delta^{13}C_{karb}} \qquad \text{(Equation 2)}$$

In Equation 2, $\delta^{13}C_{DIC}$ is $\delta^{13}C$ measured from dissolved inorganic carbon ; $\delta^{13}C_{soil}$ is $\delta^{13}C$ of CO_2 in soil (it depends on the vegetation, C_3 plants -27‰, C_4 plants approximately -12.5‰); and $\delta^{13}C_{carb}$ is $\delta^{13}C$ dissolved in calcite (generally very close to 0 ‰, 2‰ for marine carbonates). Within the scope of the current study, a sample was taken from the aquifer material carbonate rocks which host the groundwater in the area (microcrystalline limestone, close to Ören village) and $\delta^{13}C$ content in this sample was determined as +2.9‰. Thus, only unknown variable during the calculation of q is $\delta^{13}C$ content of the soil which changes according to vegetation cover. C_4 plants mostly grow in tropic and semitropic regions. The dominant vegetation in the basin is generally forest and steppe and these plants follow C_3 cycle predominantly during photosynthesis. According to this, it is appropriate to accept this content as -27‰ for current samples. On the other hand, this value might not be constant from past to present. However, it is difficult to estimate the vegetation in the study area for the last 20,000 years before present. So it should be considered that there would be some uncertainity in calculation of age for samples which are not modern due to the uncertainities in $\delta^{13}C_{soil}$ values. While performing age calculations with carbon-13 correction, if $t_{1/2}$ is taken as 5568 years, then Equation 1 becomes Equation 3 (Clark and Fritz, 1997). Radiocarbon ages were calculated by assuming A_0 as 100 pmc in Equation 3 and these ages are presented in table 3.

$$t = -8035 * \ln\left(\frac{A_t{}^{14}C}{q * A_0{}^{14}C}\right) \qquad \text{(Equation 3)}$$

When the radiocarbon ages presented in table 3 are compared, it can be seen that as the corrections for carbonate dissolution for thermal waters are high, the apparent ages are considerably lower than uncorrected ages. The reason for this is the water-rock interaction during which there is contribution of "dead carbon" from millions of years old carbonate aquifer matrix having a carbon content of 0 pmc. As a result of the contribution of "dead carbon" ^{14}C concentrations measured in the sample are diluted and the ages come up to be older than the actual ages (Ingebridsten and Sanford, 1998). Thus, as carbon 13 content of the sample becomes positive, in other words as the dead carbon contribution increases so as the difference between the corrected and uncorrected ages increases.

It could be understood that the sample obtained from the artesian well in Gümüşgölcük (GG-AR-1) has the highest groundwater residence time without taking high amounts of dead carbon to its system from the aquifer material whereas modern recharge is predominant in the sample obtained from

Gevrekseydi well. The residence time of sample (GG-AR-1) is determined as 11.500 years and the results indicate presence of fossil groundwaters in the basin. Kızılcakaya artesian well has similar duration of stay in underground with thermal water samples so it can be stated that there is hot water mixture to this water in the light of the temperature and chemical data. (Arslan and Celik, 2013). According to the diagram demonstrating the relation between radiocarbon activity and oxygen-18 content, the samples depleted in heavy isotopes have lower modern carbon activities (Figure 10).

4. Conclusions

Utilization of the isotopes having known behaviour in the hydrologic system offers researchers beneficial information. In this study, isotopic features of the surface waters and groundwaters in Köprüören Basin are presented. According to the results, $\delta^{18}O$ and δD contents of some samples show deviations from Global Meteoric Water Line. The $\delta^{18}O$ and δD signature of these samples are modified as a result of evaporation. Evaporation is an expected situation in surface waters. The evaporation lines determined for each different sampling periods have slopes in accordance with the relative humidity in air. The thermal water samples plot along Global Meteoric Water Line and for these samples $\delta^{18}O$ signatures were not modified due to water-rock interaction. The reason for this is attributed to the relatively low wellhead and reservoir temperatures of thermal water samples. In the context of this study, it was impossible to relate $\delta^{18}O$ to altitude and recharge altitude calculations could not be carried out. Therefore, the comments about the subject matter are made on the basis of relative comparisons. Tritium data revealed out that some of the groundwater samples are recharged by recent precipitation, did not stay long in the aquifer and they have shallow circulation. In addition to this, the low tritium contents of thermal water samples and two groundwater samples pointed the existence of waters which entered the system before nuclear tests (before last 50 years) and have relatively long residence times. In order to obtain more information about the residence times of these samples, $\delta^{13}C$ and ^{14}C data are evaluated. For these samples, the apparent ^{14}C ages, corrected against carbonate dissolution, reach up to 11500 before present. Accordingly, these results indicate the existence of fossil (paleo) waters. As a result of water-rock interaction, there is addition of dead carbon to thermal waters and the ^{14}C concentrations of these samples are diluted. Therefore, the correction against carbonate dissolution is considerably high.

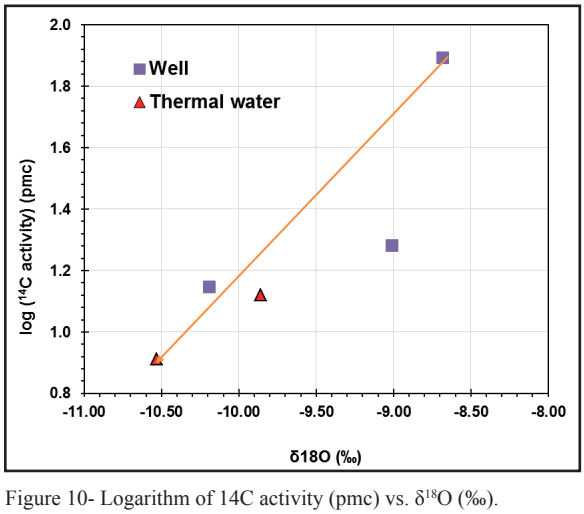

Figure 10- Logarithm of 14C activity (pmc) vs. $\delta^{18}O$ (‰).

Acknowledgements

This study was supported by The Scientific and Technological Research Council of Turkey Project No. 110Y225. The author would like to thank the locals and Mehmet Çelik, Uğur Erdem Dokuz and Orhan Arslan for their support in the field.

References

Akdeniz, N. Konak, N. 1979. Geology of Simav-Emet-Tavşanlı-Dursunbey-Demirci area. *Mineral Research and Exploration Institute of Turkey* Report *No: 6547*, 108 s. Ankara (unpublished).

Arık, F. 2002. Geochemical modeling of Gumuskoy (Kutahya) silver deposit. PhD Disseration, *Selçuk Üniversitesi Fen Bilimleri Enstitüsü, Jeoloji Mühendisliği Bölümü*, 318 s. Konya (unpublished).

Arslan, Ş., Çelik, M. 2013. Investigation of the arsenic contamination in the surface water and groundwater of the Kopruoren Basin (Kutahya) by using hydrogeochemistry and environmental isotopes. *The Scientific and Technological Council of Turkey,* Ankara No: 110Y225, 149 s. Ankara (unpublished).

Arslan, Ş., Çelik, M., Dokuz, U.E., Berhe, B.A. 2013. Antropogenic water contamination in Köprüören Basin (Kütahya). *2nd Medical Geology Workshop*, 4-6 Aralık 2013, Antalya, 213-219.

Arslan, Ş., Çelik, M. 2015 Assessment of the Pollutants in Soils and Surface Waters around Gümüşköy Silver Mine (Kütahya, Turkey). *Bulletin of Environmental Contamination and Toxicology* 95, 499-506.

Arslan, Ş., Yazıcıgil, H., Stute, M., Schlosser, P., Smethie, W.M. 2015. Analysis of groundwater dynamics in the complex aquifer system of Kazan Trona, Turkey, using environmental tracers and noble gases. *Hydrogeology Journal* 23, 175-194.

Baş, H. 1983. Tertiary geology of Domaniç-Tavşanlı-Kütahya-Gediz region and petrology of the volcanics. *Mineral Research and Exploration General Directorate of Turkey Report No. 7293,* Ankara (unpublished).

Baş, H. 1986. Tertiary geology of the Domanic-Tavşanlı-Kutahya-Gediz region. *Journal of Geological Engineering* 27, 11-18.

Baş, H. 1987. Characteristics of the Tavşanlı-Domaniç (Kütahya) volcanics and their significance in Western Anatolian Cenozoic volcanism. *Geological Bulletion of Turkey* 30, 67-80.

Bayarı, C.S., Özyurt, N.N., Kilani, S. 2009 Radiocarbon age distribution of groundwater in the Konya Closed Basin, central Anatolia, Turkey. *Hydrogeology Journal* 17, 347-365.

Clark, I., Fritz, P. 1997. Environmental Isotopes in Hydrogeology. *CRC Press*, 342 s.

Clark, J.F., Stute, M., Schlosser, P., Drenkard, S. 1997. A tracer study of the Floridan aquifer in southeastern Georgia: implications for groundwater flow and paleoclimate. *Water Resources Research* 33, 281–289.

Çelik, M., Dokuz, U.E., Türköz, P.E., Güllü, Ö., Arslan, Ş. 2013. Hydrogeochemical and isotopic investigation of Nasrettin Hoca springs, Eskişehir, Turkey. *Bulletin of the Mineral Research and Exploration* 146, 93-104.

Çelik, Y., Kerey, İ.E. 1999. Lithofacies and deposition environments of coal bearing sediments of Domanic Neogene Basin. *52nd Geological Congress of Turkey*, 10-12 May 1999, Ankara, 318-325.

Çifter, C., Sayın, M. 2002. Using of Isotopes in Hydrology, *Isotope Techniques in Hydrology symposium*. State Hydraulic Works, 21-25 October 2002, Adana, 1-14.

DSİ. 1981. Hydrogeological Investigation report of Kutahya-Kopruoren Plains, *State Hydraulic Works,* 64 s, Ankara (unpublished).

Fournier, R.O. 1977. Chemical geothermometers and mixing models for geothermal systems. *Geothermics* 5, 41-50.

Güleç, N., Mutlu, H. 2002. Isotope Geochemistry of Geothermal Areas. Earth Sciences application in Geothermal, Summer School Lecture Notes. Dokuz Eylül University Faculty of Engineering Publications No. 306, 64-88 s. İzmir

Ingebritsen, S.E., Sanford, W.E. 1998. Groundwater in Geologic Processes. *Cambridge University Press,*564 p.

Konak, N. 1979. Simav graben and related problems of urbanization. Turkish Geological Engineering 1st Scientific and Technological Congress book, 157-164.

Mazor, E. 1991. Applied chemical and isotopic groundwater hydrology. *Wiley,* 256 p.

Pearson, F.J. 1965. Use of C-13/C-12 Ratios to Correct Radiocarbon Ages of Material Initially Diluted by Limestone. Chatters R.M., Olsen, E.A. (Eds.) Proceedings of the 6th International Conference on Radiocarbon and Tritium Dating. *US Atomic Energy Commission, CONF-650652*. Washington, 357-366.

Pearson, F.J., Hanshaw, B.B. 1970. Sources of dissolved carbonate species in groundwater and their effects on carbon-14 dating. *International Atomic Energy Agency Symposium on Use of Isotopes in Hydrology*, 1970, Vienna, 271-285 p.

Schlosser, P., Stute, M., Horr, C., Sonntag, C., Munnich, K.O. 1988. Tritium/^{3}He Dating of Shallow Groundwater. *Earth and Planetary Science Letters* 89, 352-363.

Vogel, J.C. 1993. Variability of carbon isotope fractionation during photosynthesis. Ehleringer, J.R., Hall, A.E., Farquhar, G.D. (Eds.). Stable Isotopes and Plant Carbon-Water Relations. *Academic Press*. San Diego, 29-45.

Bull. Min. Res. Exp. (2016) 153:185-202

Bulletin of the Mineral Research and Exploration

http://bulletin.mta.gov.tr

INVESTIGATION OF THE SEISMIC VELOCITY DISTRIBUTION AND CRUSTAL STRUCTURE OF TURKEY BY MEANS OF GRAVITY DATA

Uğur AKIN[a*]

[a] *General Directorate of Mineral Research and Exploration, Dept. of Geophysical Researches, Ankara, Turkey*

Review Article

Keywords:
Seismic Velocity, Apparent Density, Continental Crust, Conrad Discontinuity, Moho

Received: 27.01.2016
Accepted: 15.03.2016

ABSTRACT

In this study, the apparent gravity density data was measured for Turkey using apparent density filter, and the seismic velocity distribution map was generated from this data cluster. By interpreting these two measured data clusters, three dimensional structure of the Conrad discontinuity was investigated. The apparent gravity filter is a kind of filter which is used in the apparent gravity measurements for different depth levels different than gravity data. In this study, considering previously measured distribution of the continental crustal thickness of the Anatolia, the density maps for different depth levels were formed and interpreted. The lowest and highest densities in different levels of Turkey are 2.23 gr/cm^3, and 3 gr/cm^3, respectively; and the mean density is 2.698 gr/cm^3. The lowest and highest seismic velocities for different thicknesses were measured as 3.20 km/sec and 6.83 km/sec, respectively. However; the mean seismic velocity of Turkey for depths increasing up to 10 km until MOHO discontinuity was estimated as 5.66 km/sec. The density and seismic velocity in the first 20 km of the continental crust have reached its highest values as 2.74 gr/cm^3 and 5.86 km/sec, respectively. This zone is also the Conrad discontinuity between the lower and upper crusts, and its average depth is 16 km in Turkey. The Conrad discontinuity boundary, which developed between SIAL-SIMA, not to be observed in the East Anatolian High Plateau made us consider that SIMA had disappeared as a result of the geological evolution, and the available crust could only be SIAL in origin.

1. Introduction

Studies of seismic velocity distribution have been carried out by various investigators for different regions of the Anatolia. Zor et al. (2003) measured seismic velocities of the crustal structure of the East Anatolian Plateau by receiver function and determined the shearing velocity in between 3.5-3.8 km/sec. Canbaz and Karabulut (2010, 2011) used environmental seismic noises to measure the regional group velocity changes in Turkey. They obtained high resolution velocity structure of Turkey by passive monitoring techniques and interpreted group velocity maps with known tectonic structures and geology. They defined the East Anatolia as low velocity, the Pontide, Bitlis and Pötürge massif as high velocity, the Central Anatolia as homogenous velocity, Isparta angle as low velocity, and the Aegean region, where the crust thins out, as the high velocity region. Karabulut et al (2013) studied velocity changes (*Vp/Vs*) for the western Turkey (Thrace, Sea of Marmara, Sakarya Zone, Bornova Flysch zone, Menderes massif, Lycian nappes). Ersan and Erduran (2010) used P wave receiver function analysis in order to determine the structure of crust and upper mantle velocity beneath the Central Anatolia. Warren et al. (2013) generated the maps of shear wave velocity for the Central and East Anatolia at different depths (10, 20, 30 and 40 km). In these maps, the East and Central Anatolia regions were presented as in low and high velocities, respectively. Vanacore et al. (2013) estimated the velocity ratio map of Turkey (*Vp/Vs*). They indicated that volcanisms in tectonically active regions in Eocene and post Eocene times in East and the Central Anatolia had shown variations in (*Vp/Vs*) ratios. Ozacar et al. (2008) investigated discontinuities in the upper mantle beneath the East Anatolian Plateau and measured *Vp* velocity as 6.30 km/sec between 0-40 km's in the crust. Çıvgın and Kaypak (2012) produced (1D) one dimensional seismic wave velocity model belonging to the upper mantle beneath Ankara and its vicinity using local earthquake data. They detected that; while the P-wave velocity of the first 8 km thick layer is 5.25 km/sec, the P-wave velocities of the underlying layers increase with depth and reached the velocity of 6.47 km/sec at a depth of 30 km.

* *Corresponding Author: Uğur AKIN, ugurakin11@gmail.com*
http://dx.doi.org/10.19111/bmre.01024

Toksöz et al. (2003) measured the crustal thickness nearly as 36 km in the vicinity of Kırıkkale. They stated that the crust in the region formed in two layers, the mean P-wave velocity in the upper mantle, which is 5-10 km thick, was 5 km/sec, and the velocity in the lower thick layer was 6.4 km/sec. They also specified that the velocity increased with depth and reached around 7.8-7.9 km/sec in upper mantle. The crustal thickness of Turkey, as well as seismic velocities, has been the point of interest of several investigators, and studies have been carried out in different disciplines such as; seismology, seismic and gravity. Özelçi (1973) assessed that there had been a linear relationship between gravity values and topographical elevations along the lines taken in the Anatolia. Akçığ (1988) obtained that there had been an approximate crustal thickness of 30 km in the Aegean Sea, and this thickness reached 35-40 km in West Anatolia using the power spectrum. Maden et al. (2005) applied experimental relations to gravity data and measured that the crustal thickness in the Anatolia had changed in between 26.4-49.5 km Maden et al. (2009), in other studies, measured the maximum crustal thickness of the Eastern Pontides as 43.8 km using back analysis method. Bekler et al. (2005) have used in-well explosions in stone quarries as artificial seismic source and measured the crustal thickness in the Central Anatolia as 36-40 km Arslan et al. (2010) measured the crustal thickness of Turkey as 31.4 km (shallowest) and as 50 km (deepest) using the gravity data. Karabulut et al. (2013) estimated the MOHO depth as 31 km in Thrace basin, as 25 km in the Sea of Marmara, as 32 km in İzmir-Ankara Suture Zone, as 25 km in the Menderes Massif using receiver function. Vanocore et al. (2013) measured the MOHO depth as 55 km for the East Anatolia, as 37-47 km for the Central Anatolia and much thinner for the West Anatolia using receiver function. Kahraman et al. (2015) have shown lithological and structural variations in lower, middle and upper crusts by means of the receiver function. Pamukçu et al. (2007) in their studies determined the crustal thickness nearly 45 km. Pamukçu et al. (2011) determined low density level approximately 10 km thick below the ductile zone in the Eastern Anatolia. Pamukçu et al (2015) applied the 2nd Trend Method to gravity data, and derivations in both vertical and horizontal directions in order to investigate the structure of lithosphere. According to the results of derivative, which they obtained within scope of the study, they determined that structure transitions with Bitlis-Zagros Thrust Fault increased much.

Simeoni and Brückle (2009) applied the power spectrum to gravity Bouguer anomalies, and distinguished the components consisting of low and high wavelengths in gravity data from each other. They assessed in the power spectrometer analysis that the effects consisting of relatively high wave numbers had originated from structures in the upper mantle. In addition; they also observed that the density variations with long wavelength originating from the upper mantle were rather affective. They defined the main tectonic elements of geology of the region and MOHO depth using gravity density and seismic data together. They also determined the density difference between the lower and upper crusts as 0.3 gr/cm^3.

However; in this study, the seismic velocities corresponding to the apparent density data estimated from the gravity Bouguer data were measured using the equivalence given by Barton (1986). Thus; the seismic velocity distribution in both vertical and horizontal directions of Turkey and the Conrad discontinuity boundary were studied. Besides; considering the geological units of the country, 7 seismic velocity depth sections in different directions, the crustal thickness and Conrad discontinuity were interpreted with earthquakes having magnitudes greater than 4; and as a result, the crustal model was generated using the result obtained.

2. Geology of Turkey

The geological structure of Turkey is located within the Alpine-Himalayan Orogeny system. It was shaped by the continental zones formed by the evolution of the Pan-African basement and Tethys Ocean (Paleo and Neo Tethys) exposing in a couple of regions, and by paleotectonic zones which was formed by the oceanic suture belts located among them. The shape, location, distribution, contact relationships, regional correlations and tectonic evolutions of the tectonic units extending generally in E-W directions, shown in Figure 1, have been studied by different investigators (Ketin, 1966; Özgül, 1976, 1984; Şengör and Yılmaz, 1981; Şengör 1985; Görür, 1987, 1988, 1991; Okay 1989; Koçyiğit et al., 1991; Tüysüz, 1993; Görür et al., 1983; Yılmaz et al., 1994, 1995; Okay et al., 1996; Okay and Tüysüz, 1999).

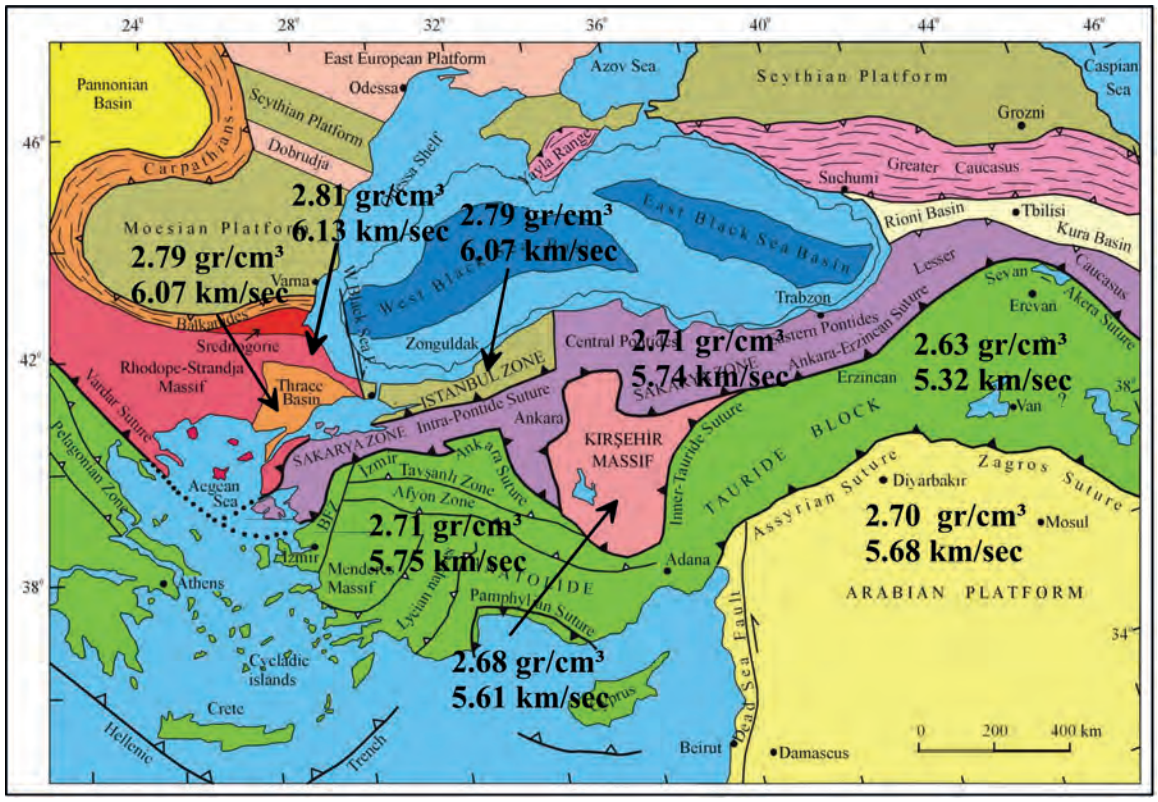

Figure 1- Tectonic units and structural zones of Turkey (modified from Okan and Tüysüz, 1999).

When the continental zones, which are tectonically in contact with each other, and suture belts are studied from north to south, the Strandja zone is located in northwest of Turkey. Gneiss and metagranitoids are observed at the basement of Strandja zone, which is formed by the Strandja massif and Thrace basin. These lithologies are overlain by Triassic-Early Jurassic clastic and carbonate rocks which metamorphosed in Late Jurassic. These metamorphic rocks were then unconformably overlain by the succession of Thrace Basin which was formed by carbonate and clastic rocks deposited between Middle Eocene to recent (Aydın, 1974; Kasar and Okay, 1992; Okay et al., 2001). The Strandja zone separates from the İstanbul Zone with a strike slip tectonic contact in East (Okan and Tüysüz, 1999). At the bottom of the İstanbul Zone, the Pan-African basement rocks composed of Precambrian gneiss, metagranite and amphibolite exist. This basement is then overlain by a sedimentary deposit which is composed of an unmetamorphosed Ordovician-Carboniferous clastic and carbonate rocks (Kozur and Göncüoğlu, 1999; Özgül, 2011). Triassic clastic and carbonate rocks unconformably overlie the underlying succession (Şengör and Yılmaz, 1981; Yılmaz et al., 1995). Late Cretaceous-Eocene volcanoclastic and carbonate rocks constitute cover rocks of the İstanbul-Zonguldak zone (Okay et al., 1994; Görür and okay, 1996). The Inner Pontide suture separates the İstanbul Zone from the Sakarya Zone in south (Şengör and Yılmaz, 1981). Late Cretaceous-Paleocene ophiolitic mélange and Late Cretaceous-Eocene blocky flysch are observed in the Inner Pontide Suture (Okay and Görür, 1995; Görür and Okay, 1996). In the southern part of the Inner Pontide Suture, the continental rock assemblage extending from the Biga Peninsula to Eastern Black Sea constitutes the Sakarya Zone. Metamorphic massifs composed of gneiss, marble and metaperidotites at the basement of the Sakarya zone (Kazdağ, Uludağ and Pulur massifs) were influenced by Hercynian orogeny. These massifs are tectonically overlain by Late Paleozoic-Triassic volcanosedimentary rock assemblages (Karakaya Complex). This complex is highly deformed and consists of limestone blocks and was influenced from the low grade metamorphism, (Bingöl et al., 1973; Okay et al., 1996; Duru et al., 2004). These rocks are then transgressively overlain by Early Jurassic-Eocene carbonate and flysch deposits in which the volcanic products especially in the Black Sea are widely observed starting from Late Cretaceous.

Besides; dense granitic intrusions are observed in the Sakarya Zone between Late Paleozoic-Miocene intervals. İzmir-Ankara-Erzincan suture in the southern part of the Sakarya Zone presents northerly dipping subduction zone of the Neo-Tethys Ocean (Şengör and Yılmaz, 1981). These ophiolitic rocks are accompanied by Triassic-Cretaceous aged, densely sheared ophiolitic rocks, Late Cretaceous blocky flysch in western Anatolia (Bornova Flysch Zone) and by blueschists in Tavşanlı Zone (Okay, 1984; Okay, 1986; Erdoğan et al, 1990). In the southern part of İzmir-Ankara-Erzincan Suture, the Central Anatolian Massif consisting of high graded metamorphic rocks are observed. This crystalline massif, which is cut by the Late Cretaceous granitic intrusions, is unconformably overlain by clastic and carbonate rocks deposited between Late Maastrichtian to recent (Erkan, 1975; Göncüoğlu, 1981; Seymen, 1982; Gökten, 1986). The Central Anatolian Massif separates from Tauride platform in south by the Inner Tauride Suture which is composed of Late Cretaceous-Eocene ophiolitic rocks (Şengör and Yılmaz, 1981). The Menderes Massif and Taurus platform take place towards the south of the İzmir-Ankara Suture and Inner Tauride Suture. The Menderes Massif consists of a core and surrounding cover units (Dürr et al., 1978; Şengör and Sungurlu, 1984; Konak, 2003). The core is formed by lensoidal gneiss and migmatites representing the Pan-African metamorphic basement. However; the cover units are composed of Late Paleozoic-Eocene carbonate and clastic deposits which were affected from the regional metamorphism in Paleocene-Eocene. The Taurus Platform is composed of different tectono-stratigraphical units and nappes in Paleocene-Eocene. These units and nappes, which consist of the platform, the continental margin and oceanic lithologies deposited in between Paleozoic-Tertiary times thrusted on each other by Late Cretaceous-Eocene movements and occasionally affected from metamorphism (Özgül, 1976; Özgül, 1984). The Bitlis Suture forms the boundary of Taurus Platform and the Arabian Platform, and it represents the southern branch of the Neo-Tethys Ocean which existed from Late Triassic to Early Miocene. Extensive ophiolitic nappes in the Eastern and Southern Anatolia are the remnants of this ocean (Şengör and Yılmaz, 1981; Dewey et al., 1986). The Arabian platform located at the southern part of the Bitlis Suture is represented by highly deformed basement consisting of Precambrian oceanic and continental fragments and by overlying clastic rocks deposited in pre Late Permian. These units are then transgressively overlain by Late Permian-Tertiary carbonate deposit on and around the Arabian Platform (Perinçek, 1980; Perinçek et al., 1991; Şengör and Natal, 1996).

3. Geophysical Data and Applied Data Process

The gravity method, which is one of the potential areal methods of the geophysics, provides significant information in investigating the locations, depths and geometries of buried structures in small, medium and large scale fields with the help of geological data. The General Directorate of Mineral Research and Exploration (MTA) has taken gravity measurements in 60648 stations in 3-5 km intervals in the country. The measurement points, as 1st, 2nd and 3rd degree triangulations being the first, were taken at certain points such as; school, mosque, crossroads, bridges and river junctions in 1/25 000 scale topographical maps. The collection of regional gravity data cluster of Turkey began in 1973 and has continued 15 years by several geophysical teams. The Turkish Petroleum Corporation (TPAO) and the General Command of Mapping (HGK) have made significant contributions in collecting these data. MTA has spread the international base value, which it had been taken by HGK from postdam and carried out airports, across the country and formed the Turkish National Gravity Base Network. Worden Master, LaCoste Romberg 344 and 347 gravimeters were used during the collection of regional gravity data.

In this study, the gravity apparent density filter was applied to Bouguer data of Turkey and the apparent density map was generated (Figure 4).

The apparent density filter and lateral distribution of the density in a horizontally layered environment can be estimated by the gravity area. The main assumption here is that the density in vertical axis does not show any variation. The apparent density filter is expressed by the formula of Gupto and Grant, (1985).

Here, the apparent density: ($\rho(x,y)$)

$$\rho(x,y) = \rho_o + (1/2\pi G)\, F^{-1}\{(\omega / 1\text{-}e^{-\omega h}) \,.\, \Delta g(u,v)\}$$

where;

ρ_o : estimated background density,

G: gravitational constant,

ω: total wave number

h : thickness,

u : number of waves in x direction,

v : number of waves in y direction,

F^{-1}: inverse Fourier Transformation.

As it is understood from the equation; the apparent density wave filter is a linear filter expressed in wave number medium.

The velocity and density data generated by Barton (1986) were used in each grid cells of the apparent density map (Table 1). So; linearly, a transition into the seismic velocities were made and the seismic velocity map of Turkey was generated (Figure 6).

The tectonic units of Turkey stated in the study of Okan and Tüysüz (1999) were plotted on all the maps generated. In addition, there are several fault systems in Anatolia, and two of the most important fault among them (the North Anatolian Fault Zone (NAFZ) and the East Anatolian Fault Zone (EAFZ)) was plotted on generated maps.

While the gravity Bouguer signature of the general tectonic structures like; the Sakarya Zone, İstanbul, Anatolide-Tauride Block, Kırşehir and Menderes Massifs are clearly observed for some geological structures, the gravity response of some tectonic structures shows some differences (Figure 2). The eastern boundary of the İstanbul Zone and Sakarya Zone cannot be discriminated clearly from each other, and the diversity of the Bornova Flysch Zone with its surround is not clearly observed in the Bouguer map. Besides; while the eastern part of the Anatolide-Tauride Block is represented by low amplitude Bouguer values, it distinctively separates from the Arabian Platform in south and from the Sakarya Zone in north. NW-SE orientation of Tavşanlı and Afyon Zones were also observed in the gravity map (Figure 2). In this study, the relationship of tectonic structures with gravity apparent density and seismic velocity distributions were also investigated.

The map was reproduced by using data of the crustal thickness map of Turkey given by Arslan et al. (2010). The regressional equivalence, Y=-72.2E+7.77, found for the Bouguer anomaly type

Table 1- Seismic velocities measured for different densities (Barton, 1986).

Density (gr/cm³)	Velocity (km/sec)	Density (gr/cm³)	Velocity (km/sec)	Density (gr/cm³)	Velocity (km/sec)
1.47	1.5	2.36	3.8	2.80	6.1
1.66	1.6	2.38	3.9	2.83	6.2
1.73	1.7	2.39	4.0	2.85	6.3
1.80	1.8	2.41	4.1	2.87	6.4
1.86	1.9	2.43	4.2	2.90	6.5
1.92	2.0	2.44	4.3	2.93	6.6
1.98	2.1	2.46	4.4	2.95	6.7
2.01	2.2	2.48	4.5	2.98	6.8
2.03	2.3	2.50	4.6	3.01	6.9
2.06	2.4	2.52	4.7	3.04	7.0
2.09	2.5	2.53	4.8	3.07	7.1
2.11	2.6	2.55	4.9	3.10	7.2
2.13	2.7	2.57	5.0	3.13	7.3
2.15	2.8	2.59	5.1	3.16	7.4
2.18	2.9	2.61	5.2	3.19	7.5
2.21	3.0	2.62	5.3	3.22	7.6
2.23	3.1	2.64	5.4	3.25	7.7
2.24	3.2	2.66	5.5	3.28	7.8
2.26	3.3	2.68	5.6	3.31	7.9
2.28	3.4	2.70	5.7	3.34	8.0
2.30	3.5	2.72	5.8	3.38	8.1
2.32	3.6	2.74	5.9	3.42	8.2
2.34	3.7	2.77	6.0		

was used in Woollard (1959) equation and equation T=32-0.08(-72.2E+7.77)=31.38+5.77E was obtained, thus the crustal thickness map of Turkey was prepared. In the crustal thickness map in Figure 3, the shallowest and the deepest crustal structures were measured as 29.54 km and 50.62 km, respectively. The difference between the shallowest and the deepest crustal structures is 21 km across Turkey. The thinnest parts of the continental crust have been the Thrace Basin and seasides. The continental crust in the west of the country thins out until Denizli. This area overlaps with the SE boundary of the Menderes Massif at the same time. Areas, where the continental crust thins out, have clearly revealed graben regions in which the geothermal activity is the most. Another area, where the continental crust thins out, is the Isparta Bend in south. The separations of İstanbul and Sakarya Zones, which cannot be observed between Karabük and Kastamonu in the Gravity Bouguer map, have become distinctive in the crustal thickness map (Figure 3). The crustal thinning in the İstanbul Zone has differed from the Sakarya Zone by crustal thickening. The crustal thickness of NW-SE extending Tavşanlı and Afyon Zones have increased towards west. The crustal thickness between the eastern and western parts of the Kırşehir Massif to display a difference is remarkable. The crustal thickness of the Lake Tuz and its surround is observed as one of the shallowest regions of the massif. The deepest region of Turkey in crustal thickness is the East Anatolian Plateau with 40-50 km. The Arabian Platform with a depth of 35 km has separated from the deeper Anatolide-Tauride Block by the Bitlis Suture Belt (Figure 3).

Applying the apparent density filter to gravity Bouguer data, the gravity apparent density map was obtained (Figure 4). The apparent density values range in between 2.55 gr/cm^3 and 2.98 gr/cm^3 and the difference is 0.43 gr/cm^3. The continental crust to be thick in the East Anatolian Plateau causes the density of the region to decrease. However, the continental crust to thin out at seasides as well has caused an increase in apparent densities in these areas (Figures 3 and 4). The NS boundary of the İstanbul Zone and the Sakarya Zone separation, which is not clear between Karabük and Kastamonu settlement areas in the gravity Bouguer map, were not well observed also in the density map. The mean density distributions of each tectonic units of the Anatolia in figure 1 were measured, and these were given in table 3.

The thickest value of the crustal thickness map of Turkey is nearly 50 km. Therefore; the apparent density values and seismic wave velocities were measured in 10 km increments until the depth of 50 km (Figure 5). The mean seismic velocity and densities have the lowest values between 0-10 km. However, the densities and velocities show an increase in between 10-20 km. The mean velocities of levels located in deeper parts show a relative decrease with respect to this level. However, the numerical values of the information observed in figure 5 were given in table 2.

The wave velocity map of Turkey was obtained by using the apparent density map of Turkey generated from gravity data. Also; an assessment was made between the seismic velocities of the rocks and their densities by means of the relationship between

Table 2- Density and seismic velocity data measured for different depth levels.

	0-10 km			10-20 km			20-30 km			30-40 km			40-50 km		
	Min.	Max.	Ort.	Min.	Max.	Ort.	Min.	Max.	Ort.	Min.	Max.	Ort.	Min.	Max.	Ort.
Density (gr/cm^3)	2.23	2.95	2.60	2.55	2.98	2.74	2.58	2.96	2.71	2.62	2.98	2.72	2.63	2.99	2.72
Seismic velocity (km/sec)	3.20	6.7	5.13	4.90	6.83	5.86	5.05	6.73	5.72	5.30	6.80	5.79	5.35	6.83	5.78

Table 3- Mean density and seismic velocities of the structural elements.

	Anatolide Tauride Block	Thrace Basin	Arabian Platform	Istanbul Zone	Strandja Massif	Kırşehir Massif	Sakarya Zone
Density (gr/cm^3)	2.67	2.79	2.7	2.79	2.81	2.68	2.71
Seismic Velocity (km/sec)	5.52	6.07	5.68	6.07	6.13	5.61	5.74

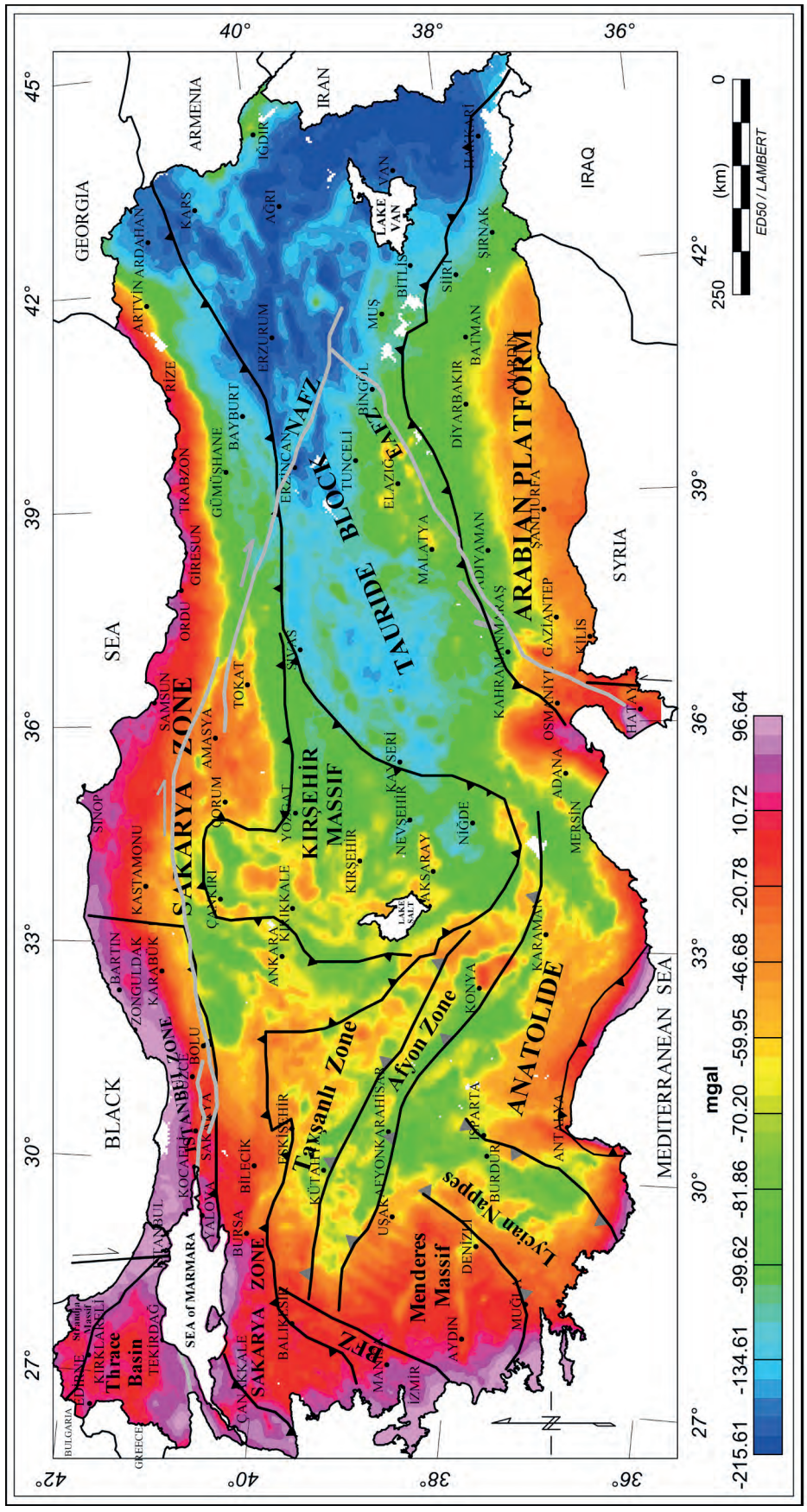

Figure 2- Gravity Bouguer map of Turkey.

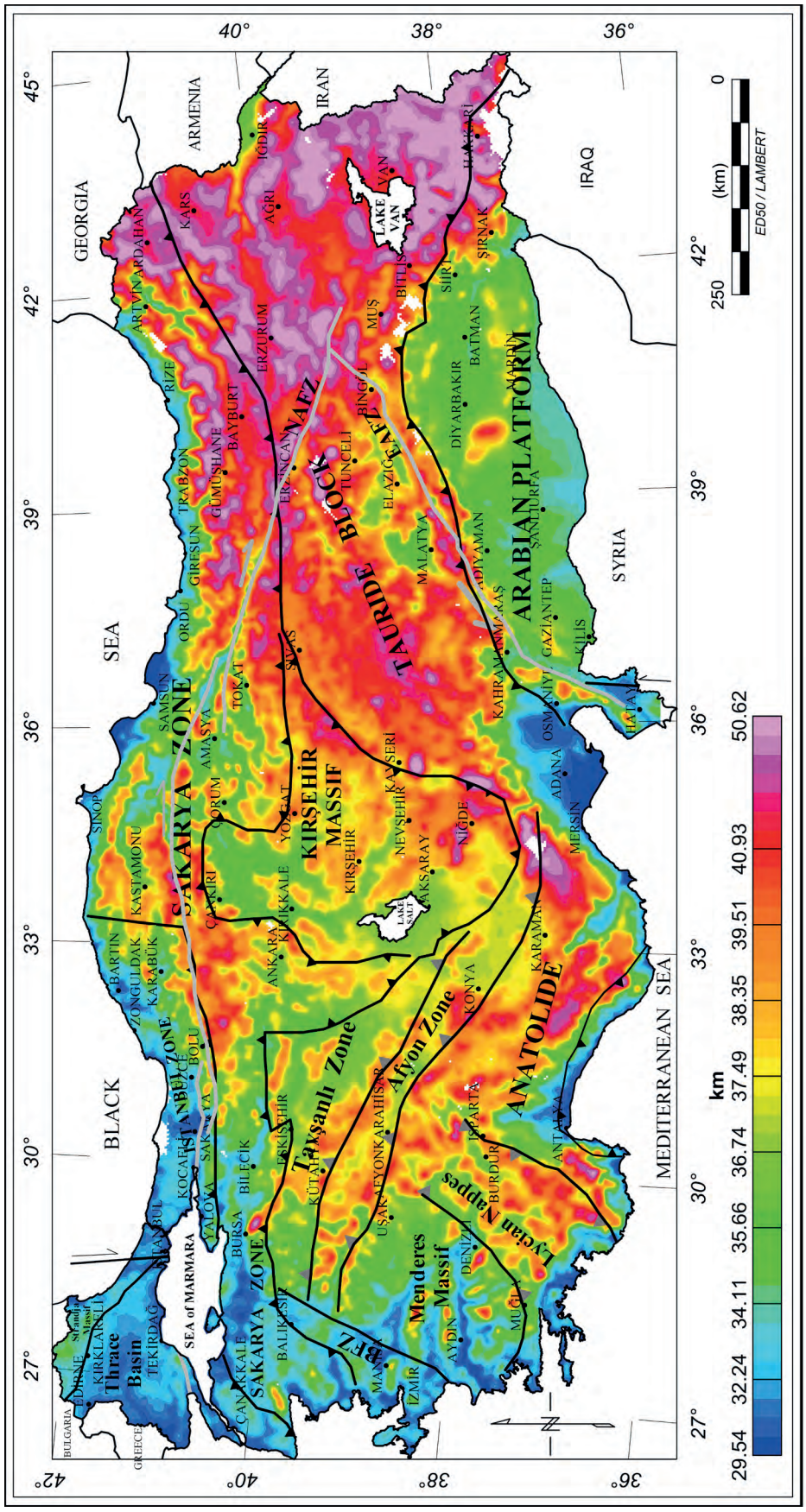

Figure 3- Continental crustal thickness map of Turkey.

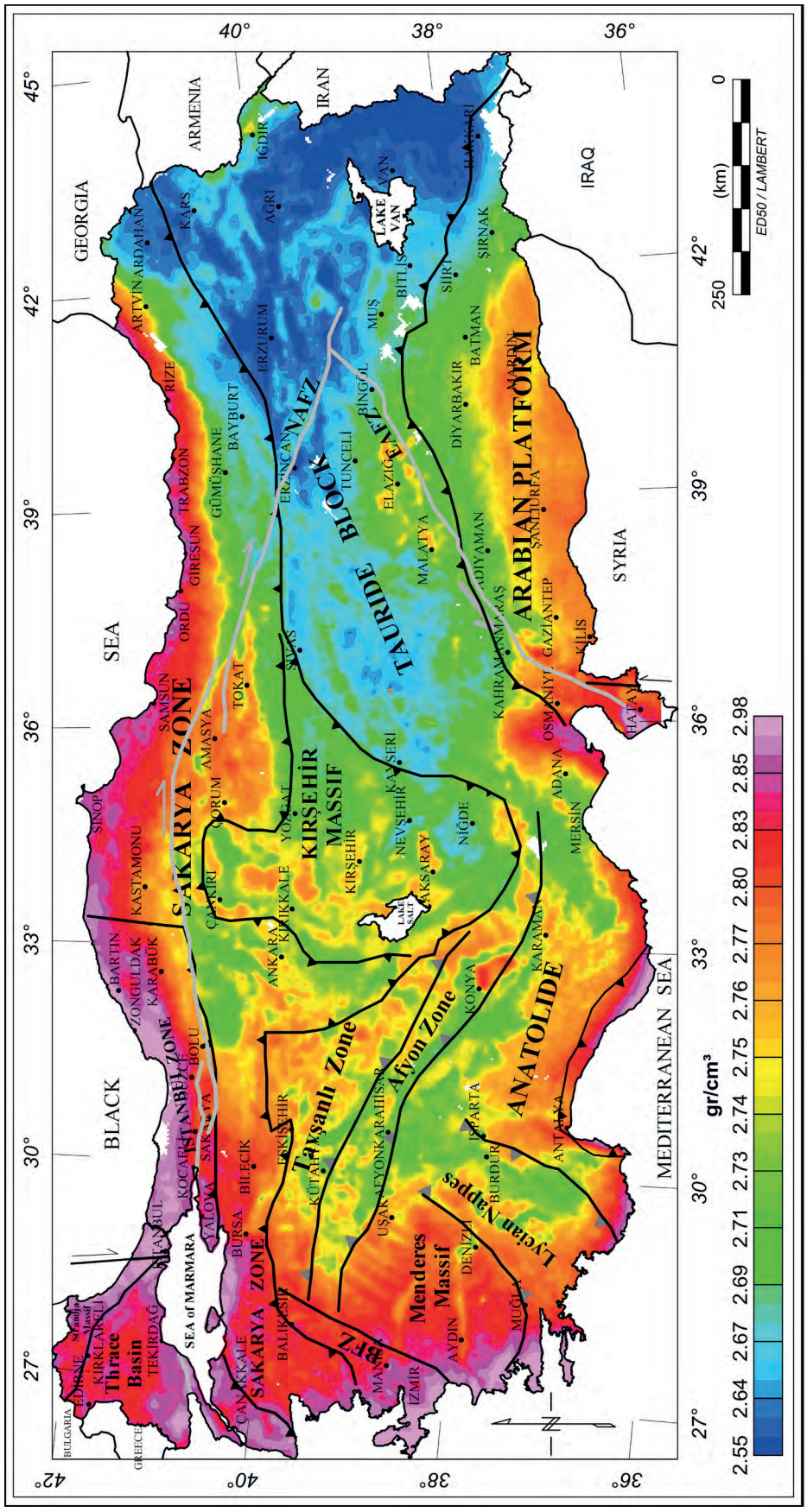

Figure 4- Gravity apparent density map of Turkey (measured 20 km thickness).

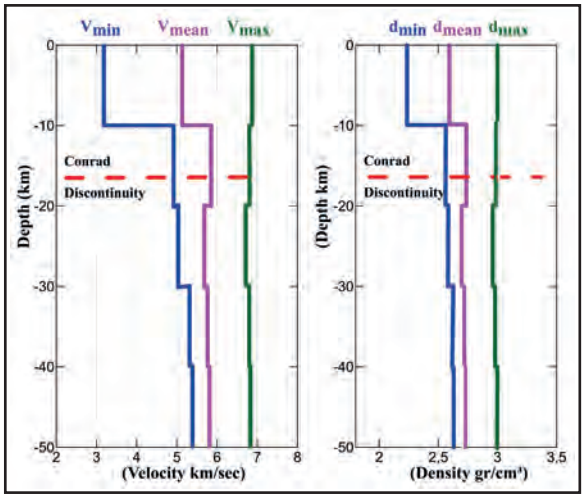

Figure 5- The variation of seismic velocity and apparent densities at depths of 0-50 km.

seismic and gravity, which are the two disciplines of the geophysics. From each density and seismic velocities, the information related to the rock type can be acquired and the structural models of the earth crust can be obtained. Nafe and Drake (1957) and Ludwig et al. (1970) carried out velocity-density measurements from several collected rock types. They also graphed density and velocity values in their measurements and acquired a mean linear function. Barton (1986), Nafe and Drake (1957) and Ludwig et al. (1970) presented a mutual density and velocity values in tabular form. The seismic velocity values of this investigation were taken from the table of density-velocity values of Barton (1986).

The seismic wave velocity map, which had been obtained from the map of gravity apparent map of Turkey, was given in figure 6. Seismic velocities vary in between 4.91-6.78 km/sec and the velocity difference across the country is 1.87 km/sec. The average of seismic wave velocities of each structural element was measured and their results were given in table 3 considering the tectonic units of Turkey. Since Anatolide and Tauride Blocks present some differences in density and velocity, their eastern and western parts were investigated separately. As the East Anatolian Plateau has a deep crustal thickness, its mean density and velocity values are 2.63 and 5.32 gr/cm^3, respectively. However; its western side reaches a much higher mean density and velocity values (2.71, 5.75 gr/cm^3) with respect to the eastern side (Figures 1 and 6).

When mean velocities given in table 3 were studied, it was seen that the Strandja Massif had the maximum seismic velocity with 6.13 km/sec among the tectonic units of Turkey. The İstanbul Zone and Thrace Basin has the same seismic velocity with 6.07 km/sec, and then the Sakarya Zone, the Arabian Platform, Kırşehir, Anatolide and Tauride Blocks follow order successively.

In order to fully investigate the depth at which high velocity and density values are observed, the thicknesses in the apparent density filter were linearly incremented as 1 km. It was revealed that the boundary, where the maximum velocity and density are observed, was nearly at a depth of 16 km for Turkey in data (Figure 5). In addition; the distribution of seismic velocities, which had been estimated from the apparent density data with 1 km increments in thickness, were investigated, and it was seen that 74% of the total data had occurred within a band of 10-20 km depth. Only a very few portion of the high velocity data (4%) occurred in 40-50 km depths (Table 4).

Table 4- The distribution of the Conrad discontinuity (measured for different depth levels).

0-10 km	10-20 km	20-30 km	30-40 km	40-50 km
% 0	% 74	% 11	% 11	% 4

Zor et al. (2003) constructed a network with 29 seismographs at an elevation of 2 km in the East Anatolian High Plateau. They measured the mean crustal thickness of the region as 45 km and (*Vp/Vs*) mean seismic velocity as 3.7 km/sec by interpreting *V* and *S* seismic wave velocities from the seismic data collected. Şengör et al (2003) explained that the closure of the Neo-Tethys Ocean occurred between Early Eocene to Late Eocene and the rigid Arabian Plate dipped into the Pontide arc and then steepened in Middle and Late Miocene. The plate was then broken and subducted into the asthenosphere and lost its mantle crust. They also emphasized that the asthenosphere had entered from this broken region and uplifted the Eastern Anatolia. They also attributed the density decrease in the crust to this high temperature effect. Keskin (2003) explains that the reason, why the region was extensively covered with volcanism in Neogene and Quaternary in Eastern Anatolia, reflects only a small portion of the melt exposing in the area and the presence of plutonic intrusions in deeper parts

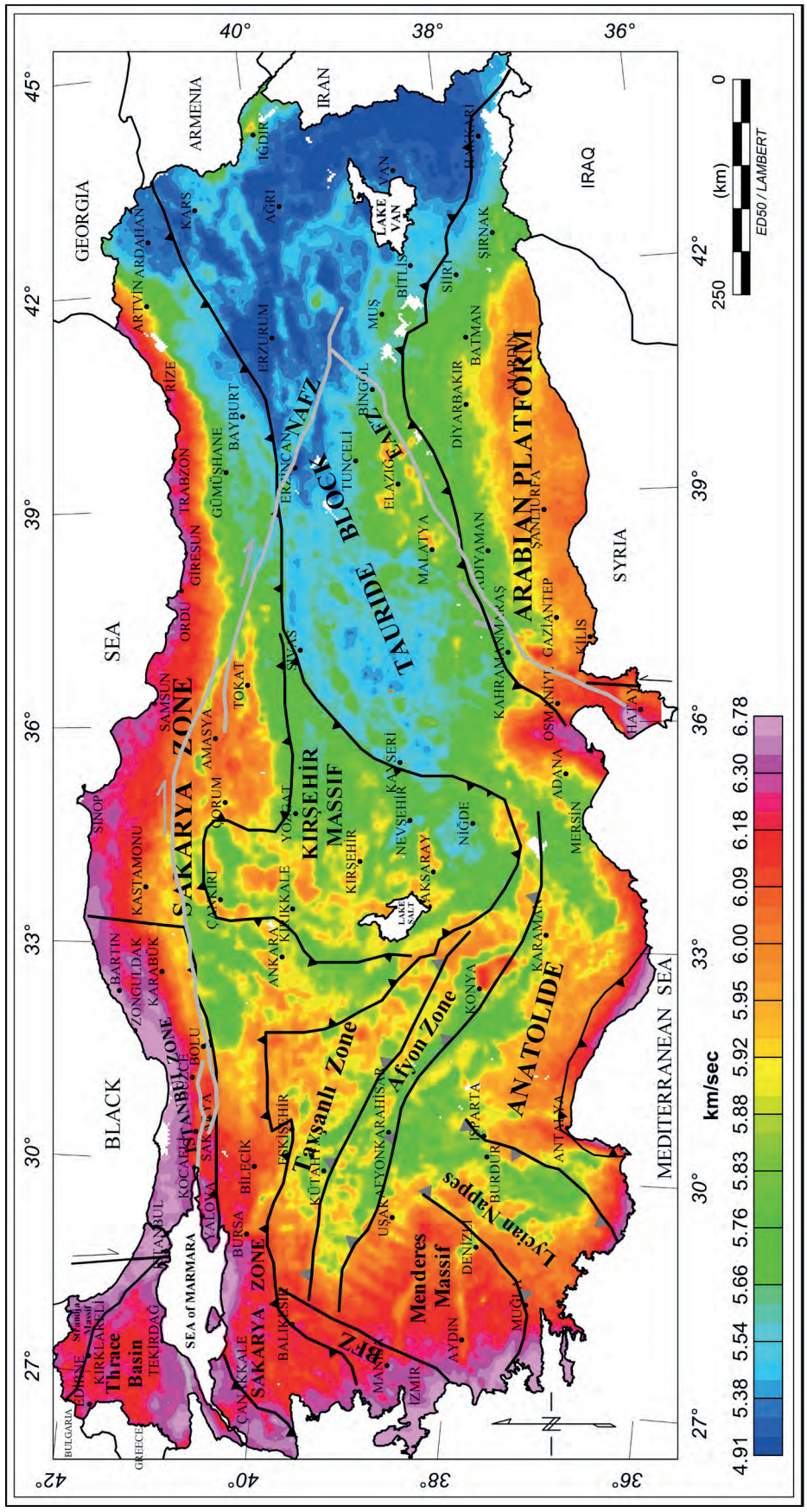

Figure 6- Seismic velocity map of Turkey (measured for 20 km depth).

of the crust. Pamukçu and Akçığ (2011) mentioned about the presence of several vertical discontinuities in the region between EAFZ and NAFZ, and the flexible region starting at a depth of 10 km within crust structure.

The Conrad discontinuity has taken its name from seismologist Victor Conrad and is the discontinuity area where the seismic wave velocity increases in horizontal direction in the continental crust. The depths of this boundary are generally in between 15-20 km, and there is not observed any Conrad discontinuity on the oceanic crust (Figure 9). The continental crust is divided into two parts; as the upper and lower crusts. While the upper crust consists of felsic rocks such as; granite etc. (silica, aluminum, SIAL), the lower crust is composed of mafic rocks such as; basalt etc. (silica, magnesium, SIMA). The average of this depth, in which there is a compositional difference between SIAL and SIMA, was found as 16 km for Turkey (Figure 7).

Considering the tectonic units of Turkey, cross sections were taken along 7 lines (Figure 8). In cross sections, which show the variation of seismic velocities with depth, the compatibility between the deep crustal structure of the Eastern Anatolia in figure 3 and high values of the Conrad discontinuity in figure 7 actually indicates an unconformity. This unconformity is also observed clearly in cross sections (Figure 8), because the high velocity zone (Conrad discontinuity), that should occur between SIAL-SIMA, does not exist in east. It is quite remarkable that the high velocity level exists in deeper most parts of the crust and sometimes at depths closer to mantle within crust. This study also brought up a question whether one of SIAL-SIMA layers might be missing in the East Anatolian continental crust.

The crustal depths, the Conrad discontinuity and earthquakes with magnitudes equal or greater than 4 were plotted on cross sections in figure 8. The majority of earthquakes have occurred along the Conrad discontinuity and at depths very close to this discontinuity. As seen in figures 8a, b and d, the Conrad discontinuity were distinctively observed along lines taken in West Anatolia and the Central Anatolia. There was not detected any Conrad discontinuity in Anatolide and Tauride Blocks in figures 8c, e and f. The high velocity zone in figure 8g have existed on the crust-mantle boundary.

The Conrad discontinuity, which is observed in west of the Anatolia, could not be traced in the Anatolide-Tauride Block in east. The reason, why the Conrad discontinuity is not observed but the high velocity zone in crust-mantle boundary in the East Anatolian High Plateau is seen, made us consider that the crust might have formed only from SIAL. If this argument is right, then there is not SIMA in the crustal structure of the East Anatolia. According to this inference the crustal model of Turkey was given in figure 9, schematically.

4. Results

With this study, the crustal thickness map generated from our previous study was updated, and the crustal thickness in related sections was taken from this map. The apparent density filter was applied to Gravity Bouguer data and "The Apparent Density Map of Turkey" was obtained. For each grid cell of the apparent density map, the corresponding seismic velocities were taken and the "Seismic Wave Velocity map of Turkey" was generated.

The graph of seismic velocity and apparent density with respect to depth was formed and the "high velocity zone" between 10-20 km intervals was determined according to this graph. This zone was determined as the "Conrad Discontinuity". In order to determine the position of the "Conrad Discontinuity" across the country, the measurements were made by incrementing thicknesses as 1 km intervals. As a result of the measurements, the "Mean Conrad Discontinuity" was estimated as 16 km's, and the "Conrad Discontinuity Map of Turkey" was obtained.

The variations of seismic velocities with depth were investigated in 7 cross sections together with crustal thickness, the Conrad discontinuity and the tectonic units of Turkey. It was seen that the Conrad discontinuity was not available in the East Anatolian High Plateau, and high velocity zone along the crust-mantle boundary.

The Conrad discontinuity boundary, which developed between SIAL-SIMA, not to be observed in the East Anatolian High Plateau made us consider that SIMA has disappeared as a result of the geological evolution, and the available crust could only be SIAL in origin. Keskin (2003) explains that the magma generation in this region is related with the subduction

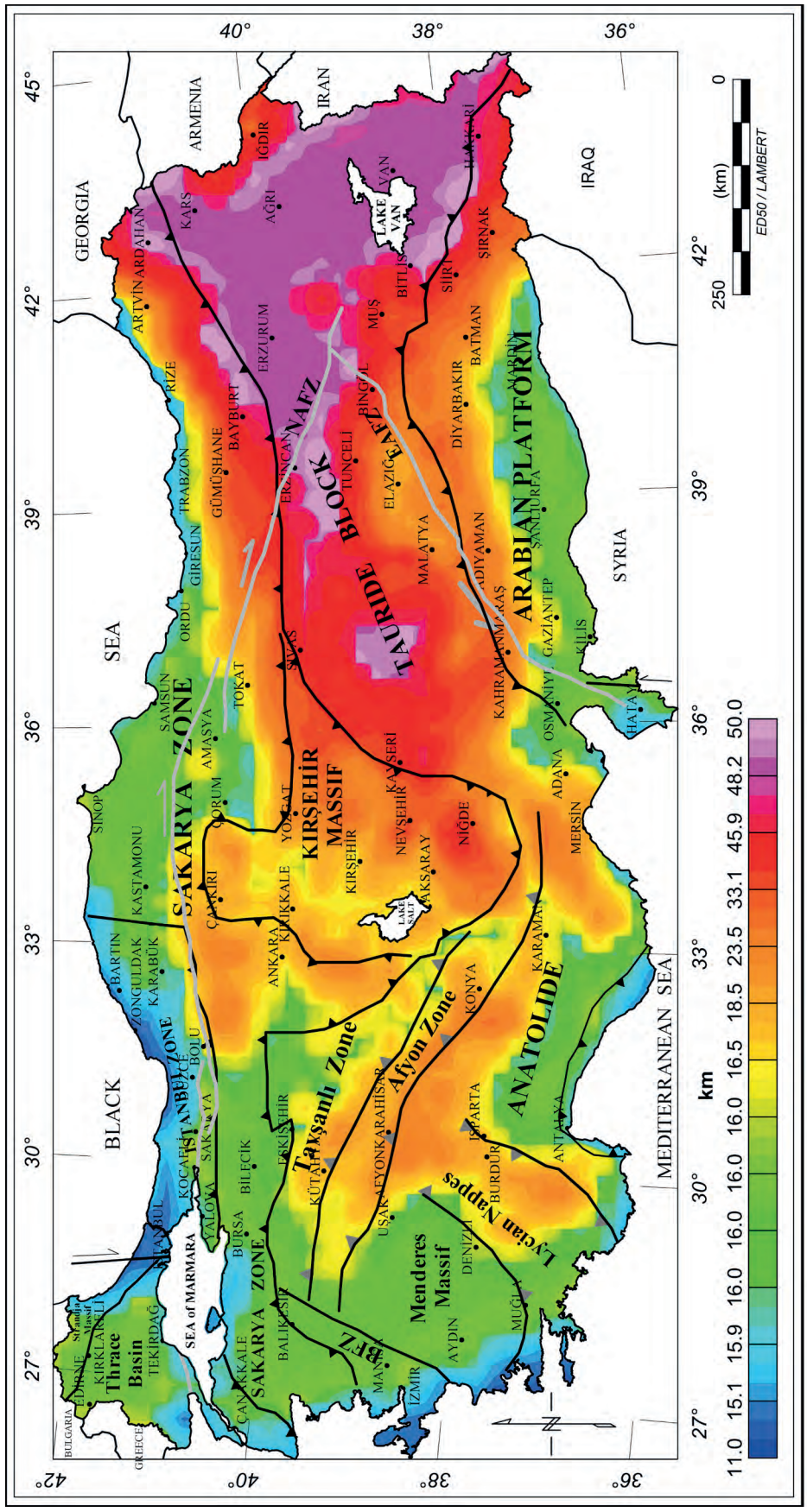

Figure 7- Conrad discontinuity depth map of Turkey.

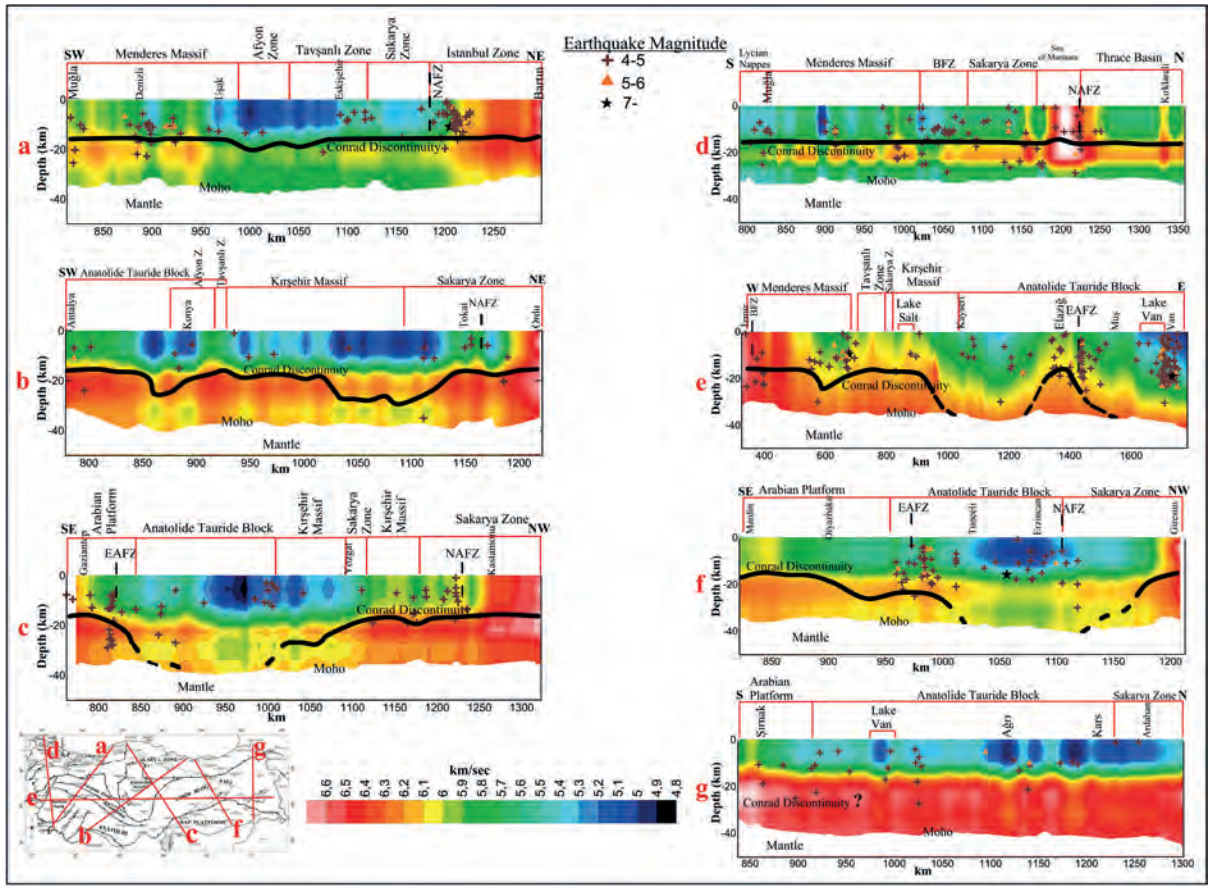

Figure 8- The variation of seismic velocities with depth.

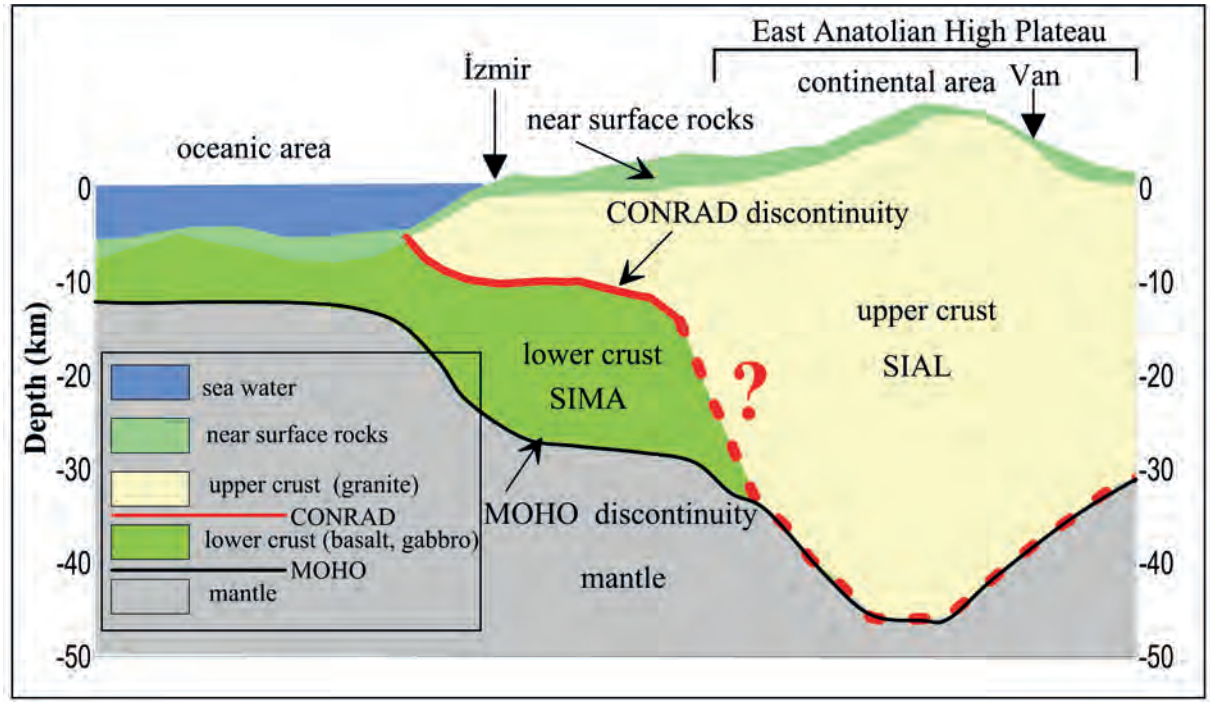

Figure 9- Crustal model (disappearance of the Conrad discontinuity and the appearance of the maximum seismic velocities between continental crust and mantle at depths (thick, dotted red line)).

between the Arabian and Eurasian plates and with the subduction related lithospheric slab breakoff in the model which he had generated for the volcanism related with the collision in East Anatolia. According to the model proposed by Keskin (2003), the Arabian Oceanic lithosphere, which subsides beneath the East Anatolian Accretion Prism, detached 11-13 million years ago, so the asthenosphere was uplifted from the detached segments and formed the volcanism in the East Anatolia ranging from 6 million years ago to recent. Another suggestion, which supports this idea, is the shallow Curie depths belonging to the East Anatolian region obtained in the study carried out by Pamukçu et al (2014). It can be interpreted that the uplifting asthenosphere material through these geodynamical processes might have melted-depleted the lower crust beneath the East Anatolian Accretion Prism (SIMA).

Acknowledgements

I am grateful to Prof. Aral Okay, Prof. M. Emin Candansayar and Assoc. Prof. Oya Pamukçu who reviewed this article to be more clear and compatible with scientific criteria. I also would like to express my special thanks to computer engineer Halit Emre Sayılır, who made significant contribution to data processing with the software he developed, to Dr. Akın Kürçer, Dr. Ahmet Üçer and Dr. Muzaffer Özgü Arısoy, who I exchanged ideas with, about the article.

References

Akçığ, Z. 1988. Batı Anadolu'nun yapısal sorunlarının gravite verileri ile irdelenmesi. *Türkiye Jeoloji Bülteni,* C.31, 63-70.

Arslan, A., Akın, U., Alaca, A. 2010. Investigation of Crustal Structure of Turkey By Means of Gravity Data. *Bull. Min. Res. Exp.,* 140, 55-71.

Aydın, Y. 1974. Etude petrographique et géochimique de la partie centrale du Massif d'Istranca (Turquie). Thése de Docteur Ingénieur, Univ. Nancy, France 1, 131 p.

Barton, P.J. 1986.The relationship between seismic velocity and density in the continental crust - a useful constraint? *Geophys. J. R. astr. SOC.* 87,195-208.

Bekler, T., Gürbüz, C., Kalafat, D., Toksöz N. 2005. Anadolu'da Kontrollü Sismik Kaynak Kullanarak Kabuk Yapısı Araştırmaları, *Deprem Sempozyumu* Kocaeli.

Bingöl, E., Akyürek, B., Korkmazer, B. 1973. Biga Yarımadası'nın jeolojisi ve Karakaya Formasyonu'nun bazı özellikleri. *Cumhuriyetin 50. Yılı Yerbilimleri Kongresi*, 17-19 Aralık 1973, Proc., Maden Tetkik ve Arama Genel Müdürlüğü, Ankara, 70-76.

Canbaz, M.D., Karabulut, H. 2010. Love-wave group velocity maps of Turkey and surrounding regions. *Geophys. J. Int.* 181. 502-520.

Canbaz, M.D., Karabulut, H. 2011. Velocity Structure of Turkey and Surroundings by passive imaging Technique. *1. Deprem Mühendisliği ve Sismoloji Konferansı,* ODTÜ-Ankara.

Çıvgın, B., Kaypak, B. 2012. Ankara ve Dolayında Kabuğun bir-boyutlu Sismik Hız Yapısının Araştırılması. *Hacettepe* Üniversitesi Yerbilimleri Uygulama ve Araştırma Merkezi Bülteni, Yerbilimleri, 33 (2), 131-150.

Dewey, J.F., Hempton, M.R., Kidd, W.S.F., Şaroğlu, F., Şengör, A.M.C. 1986. Shortening of continental lithosphere: the neotectonics of eastern Anatolia-a young collision zone. In: Covard, M.P. and Ries, A.C., (eds.), Collision Tectonics. *Geol. Soc. London Spec. Publ*., 19, 3-36.

Duru, M., Pehlivan, Ş., Şentürk, Y., Yavaş, F., Kar, H. 2004. New results on the lithostratigraphy of the Kazdağı Masif in NW Turkey. TUBİTAK, *Turkish Journal of Earth Sciences*, 13/2, 177-186.

Dürr, S., Altherr, R., Keller, J., Okrusch, M., Seidel, E. 1978. The Median Aegean crystalline belt: Stratigraphy, structure, metamorphism, magmatism. In: Cloos, H., Roeder, Schmidt, K., (eds), *Alps, Apenines, Hellenides*. Stuttgart: E. Schweizbart'sche Verlag, 455-477.

Erdoğan, B., Altıner, D., Güngör, T., Özer, S. 1990. Karaburun Yarımadasının stratigrafisi. *Maden Tetkik ve Arama Dergisi,* 111, 1-21. (Foreign Edition: Stratigraphy of Karaburun peninsula. *Bull. Min. Res. Exp.*, 111, 1-20).

Erkan, Y. 1975. Orta Anadolu Masifi'nin güneybatısında (Kırşehir bölgesinde) etkili rejyonal metamorfizmanın petrolojik incelenmesi. Thesis of Associate Professorship, *H.Ü. Yerbilimleri Enst.*, Ankara, 147.

Ersan, A., Erduran, M. 2010. Orta Anadolu'nun kabuksal hız yapısının araştırılması. *Dicle Üniversitesi Mühendislik Fakültesi* Vol. 1, Number 1, 49-60.

Gökten, Y.E. 1986. Paleocene carbonate turbidites of the Şarkışla region, Turkey - Their significance in an orogenic basin. *Sedimentary Geology*, 49, 143-165.

Görür, N. 1987. Earth Science Problems Along The First Turkish Geotraverse. *Tübitak, Basic Sciences Research Group And Research Institute For Basic Sciences*, Earth Sciences Department, Gebze, Kocaeli, Turkey, 5-33.

Görür, N. 1988. Timing of Opening of The Black Sea Basin. *Tectonophysics*, 14, 247-262.

Görür, N. 1991. Aptian-Albian Palaeogeography of Neo-Tethyan Domain. *Palaeogeo., Palaeoclm., Palaeoec*., 871, 267- 288.

Görür, N., Şengör, A.M.C., Akkök, R., Yılmaz, Y. 1983. Pontidler'de Neo-Tetis'in Kuzey Kolunun Açılmasına İlişkin Sedimentolojik Veriler. *TJK Bülteni*, 26/1, 11-20.

Görür, N., Okay, A.İ. 1996. A fore-arc origin for the Thrace Basin, NW Turkey. *Geol. Rundsch*, 85, 662-668.

Göncüoğlu, M.C. 1981. Niğde Masifi'nin jeolojisi. *35. Türkiye Jeoloji Bilimsel ve Teknik Kurultayı, Ankara, İç Anadolu'nun Jeolojisi Simpozyumu*, 16-19.

Gupta, V.K., Grant, F.S. 1985. Mineral-exploration aspects of gravity and aeromagnetic surveys in the Sudbury-Cobalt area, Ontario; in The Utility of Regional Gravity and Aeromagnetic Anomaly Maps. *Society of Exploration Geophysicists*, Ed. Hinze, J., Special Volume, 392-411.

Kahraman, M., Cornwell, D.G., Thompson, D.A., Rost, S., Houseman, G.A., Türkelli, N., Teoman, U., Poyraz, S.A., Utkucu, M., Gülen L. 2015. Crustal-scale shear zones and heterogeneous structure beneath the North Anatolian Fault Zone, Turkey, revealed by a high-density seismometer array. *Earth and Planetary Science Letters,* volume 430, pages 129–139.

Karabulut, H., Paul, A., Ergün, T.A., Hatzfeld, D., Childs D.M., Aktar, M. 2013. Long-wavelength undulations of the seismic Moho beneath the strongly stretched Western Anatolia. *Geophysical Journal International*, doi:10.1093/gji/ggt100.

Kasar, S., Okay, A. İ. 1992. Silivri-Kıyıköy-İstanbul Boğazı arasındaki alanın jeolojisi. T.P.A.O. raporu, No: 3119, 79 s.

Keskin, M. 2003. Magma generation by slab steepening and breakoff beneath a subduction-accretion complex: An alternative model for collision-related volcanism in Eastern Anatolia, Turkey. *Geophysical Research Letters*, vol. 30, No. 24, 8046, doi:10.1029/2003GL018019.

Ketin, İ. 1966. Anadolu'nun tektonik birlikleri. *Maden Tetkik ve Arama Dergisi*, 66, 20-34.

Koçyiğit, A., Altıner, D., Farinacci, A., Nicosia, U., Conti, M.A. 1991. Late Triassic - Aptian Evolution of The Sakarya Divergent Margin: Implications For The Opening History of The Northern Neo-Tethys, In North-Western Anatolia, Turkey. In: Farinacci, A., Et Al., (Eds.), Pontides, Turkey; Jurassic - Early Cretaceous Stratigraphy, Tectonics and Paleogeographic Evolution. Cnr - *Tubitak Project*, 81-100.

Konak, N. 2003. Menderes Masifi'nin güneydoğusundaki naplı yapılar. *56. Türkiye Jeoloji Kurultayı, Bildiri Özleri (Abstracts)*, 304-306.

Kozur, H.W., Göncüoğlu, M.C. 1999. Differences inthe geological evolution of the Istanbul and Zonguldak terranes, northern Turkey. In: Talent, J., Khan,F., Mawson, R. (Eds.), IGCP 421: *Mid - Palaeozoic bioevent / biogeography patterns in relation to crustal dynamics.* North Ryde (Macquarie University Printery), Peshawar, Pakistan, pp. 16-18.

Ludwig, J. W., Nafe, J. E., Drake, C. L. 1970. Seismic refraction, in Maxwell, A**.** E**.,** (ed)**,** *The Sea***,** vol. 4, Wiley, New York, 53-84.

Maden, N., Gelişli, K., Bektaş, O., Eyüboğlu, Y. 2005. Anadolu'da Kabuk Yapısı ve Tektonik Yapı ile İlişkisi. *II. Mühendislik Bilimleri Genç Araştırmacılar Kongresi,* MBGAK 2005, İstanbul, 17-19 Kasım.

Maden, N., Gelişli, K., Eyüboğlu, Y., Bektaş, O. 2009. Two-and-Three-Dimensional Crustal Thickness of the Eastern Pontides (NE Turkey). *Turkish Journal of Earth Sciences*, vol. 18, 2009, 225–238. doi:10.3906/yer-0703-3.

Nafe, J.E., Drake, C. L. 1957. Variation with depth in shallow and deep water marine sediments of porosity, density and the velocities of compressional and shear waves. *Geophysics,* 22(3), 523-552.

Okay, A.I. 1984. Distribution and characteristics of the north-west Turkish blueschists. In: Dixon, J.F. and Robertson, A.H.F. (eds.), The Geological Evolution of the Eastern Mediterranean. *Geol. Soc. London, Spec. Publ.*, 17, 297-308.

Okay, A.I. 1986, High pressure/low temperature metamorphic rocks of Turkey. *Geol. Soc. Amer. Mem.*, 164, 333-348.

Okay, A.I. 1989. Tectonic Units And Structures In The Pontides, Northern Turkey. In: Şengör, A.M.C.(Ed.), Tectonic Evolution of The Tethyan Region. Nato Advanced Asi Series. *Kluwer Academic Publishers*, Dordrechd, 109-116.

Okay, A.I., Şengör, A.M.C., Görür, N. 1994. Kinematic history of the opening of the Black Sea and its effect on the surrounding regions. *Geology*, 22, 267-270.

Okay, A.I., Görür, N. 1995. Batı Karadeniz ve Trakya havzalarının kökenleri arasında zaman ve mekan ilişkisi. *Trakya Havzası Jeolojisi Simpozyumu, Bildiri Özleri (Proc.)*, TPAO - Ozan Sungurlu Bilim, Eğitim ve Yardım Vakfı, 9-10.

Okay, A.I., Satır, M., Maluski, H., Siyako, M., Monie, P., Metzger, R., Akyüz, S. 1996. Paleo-And Neo-Tethyan Events In Northwestern Turkey: Geological and Geochronological Constraints. In: Yin, A. and Harrison, T.M. (Eds), *The Tectonic Evolution of Asia*, Cambridge Univ. Press, 420-441.

Okay, A.I., Tüysüz, O. 1999. Tethyan sutures of northern Turkey. *Geological Society of London Special Publication*, 156, 475-515.

Okay, A.I., Satır, M., Tüysüz, O., Akyüz, S., Chen, F. 2001. The tectonics of the Strandja Massif; late Variscan and mid- Mesozoic deformation and metamorphism in the northern Aegean. *International Journal of Earth Sciences*, 90 (2), 217-233.

Ozacar A.A., Gilbert, H., Zandt, G. 2008. Upper mantle discontinuity structure beneath East Anatolian Plateau (Turkey) from receiver functions. *Earth and Planetary Science Letters*, 269, 426–434.

Özelçi, F. 1973. Doğu Akdeniz Bölgesi Gravite Anomalileri. *MTA Dergisi*, Issue 80, 54-89.

Özgül, N. 1976. Torosların Bazı Temel Jeoloji Özellikleri. *TJK Bülteni*, 19/1, 65-78.

Özgül, N. 1984. Stratigraphy and Tectonic Evolution of the Central Taurides. In: Tekeli, O. and Göncüoğlu, M.C. (Eds), Geology of the Taurus Belt. *Int. Symp. Proc.,* Maden Tetkik ve Arama Genel Müdürlüğü, Ankara, 77-90.

Özgül, N. 2011, İstanbul il alanının jeolojisi. İstanbul Büyükşehir Belediyesi, 308.

Pamukçu, A. O., Akçığ, Z., Demirbaş, Ş., Zor, E. 2007. Investigation of crustal thickness in Eastern Anatolia using gravity, magnetic and topographic data. *Pure and Applied Geophysics,*164, 11, 2345-2358.

Pamukçu, A. O., Akçığ, Z. 2011. Isostasy of the Eastern Anatolia (Turkey) and discontinuities of its crust. *Pure and Applied Geophysics,* 168, 5, 901-917.

Pamukçu, O., Akçığ, Z., Hisarlı, M., Tosun. S. 2014. Curie Point Depths and Heat Flow of Eastern Anatolia (TURKEY), *Energy Sources, Part A: Recovery, Utilization, and Environmental Effects*, 36, 2699-2706.

Pamukçu, O., Gönenç, T., Çırmık, A.Y., Demirbaş, Ş., Tosun, S. 2015. Vertical And Horizontal Analysis Of Crustal Structure In Eastern Anatolia Region. *Bull. Min. Res. Exp.*, 151: 217-229.

Perinçek, D. 1980. Arabistan kıtası kuzeyindeki tektonik evrimin kıta üzerinde çökelen istifteki etkileri. *Türkiye 5. Pet. Kong., Jeoloji-Jeofizik Bildirileri*, 77-94.

Perinçek, D., Duran, O., Bozdoğan, N., Çoruh, T. 1991. Stratigraphy and paleogeographical evolution of the autochthonous sedimentary rocks in the SE Turkey. *Ozan Sungurlu Semp. Bildirileri*, Kasım 1991, Ozan Sungurlu Bilim, Eğitim ve Yardım Vakfı, 274-305.

Seymen, I. 1982. Kaman dolayında Kırşehir Masifi'nin jeolojisi. *Thesis of Assoc. Prof., ITÜ Maden Fak.*,164.

Simeoni, O., Brückl, E. 2009. The Effect of Gravity Stripping on the Resolution of Deep Crustal Structures in the Eastern Alps and Surrounding Regions. *Austrian Journal of Earth Sciences*, Vol 1002/2, 157-169.

Şengör, A.M.C., Yılmaz, Y. 1981. Tethyan Evolution of Turkey: A Plate Tectonic Approach. *Tectonophysics,* 75, 181-241.

Şengör, A.M.C., Sungurlu, O. 1984. Tectonics of the Mediterranean Cimmerides: Nature And Evolution of The Western Termination of Paleo-Tethys. In: Dixon, J.F. And Robertson, A.H.F. (Eds.), The Geological Evolution of The Eastern Mediterranean. *Geol. Soc. London, Spec. Publ.*, 17, 117-152.

Şengör, A.M.C. 1985. Türkiye'nin Tektonik Tarihinin Yapısal Sınıflaması. *Ketin Simpozyumu, TJK*, Ankara, 37-61.

Şengör, A.M.C., Natal'in, B. 1996. Palaeotectonics of Asia: Fragments of a synthesis. In: Yin, A. and Harrison, M. (eds), The tectonic evolution of Asia. Rubey Colloquium, *Cambridge University Press*, Cambridge, 486-640.

Şengör, A. M. C., 2, Özeren, S, Genç, T., Zor, E., 2003. East Anatolian high plateau as a mantle supported, N–S shortened domal structure. *Geophysical Research Letters,* 30(24), 8045.

Toksöz, M.N., Kuleli, S., Gürbüz, C., Kalafat, D., Bekler, T., Zor, E., Yılmazer, M., Öğütçü, Z., Schultz, C.A., Harris, D.B. 2003. Calibration of regional seismic stations in the Middle East with shots in Turkey. *Proceedings of the 25th Annual Seismic Research Review*, vol. I, 162-171.

Tüysüz, O.1993. Karadeniz'den Orta Anadolu'ya bir jeotravers; Kuzey Neo-Tetisin Tektonik Evrimi. *Türkiye Petrol Jeologları Derneği Bülteni*, 5/1, 1-33.

Ustaömer, T., Robertson, A.H.F. 2005. Tectonic evolution of the Intra-Pontides suture zone in the Armutlu Peninsula, NW Turkey; reply. *Tectonophysics,* 405 (1-4), 223-231.

Vanacore, E.A., Taymaz, T., Saygin, E. 2013. Moho structure of the Anatolian Plate from receiver function analysis. *Geophys. J. Int.,* 193, 329–337.

Yılmaz Y., Genç, Ş. C., Yiğitbaş, E., Bozcu, M., Yılmaz, K. 1994. Kuzeybatı Anadolu'da Geç Kretase Yaşlı Kıta Kenarının Jeolojik Evrimi. *Türkiye 10. Pet. Kong. ve Sergisi, Bildiriler,* Jeoloji, 37-55.

Yılmaz, Y., Genç, Ş. C., Yiğitbaş, E., Bozcu, M., Yılmaz, K. 1995. Geological Evolution of The Late Mesozoic Continental Margin of Northwestern Anatolia. *Tectonophyscics*, 243, 155-171.

Warren, L.M.,Beck, S.L., Biryol, C.B., Zandt, G., Ozacar, A.A. Yang, Y. 2013. Crustal velocity structure of Central and Eastern Turkey from ambient noise tomography. *Geophysical Journal International,* doi: 10.1093/gji/ggt210.

Woollard, G.P. 1959. Crustal Structure from Gravity and Seismic Measurements. *J. Geophys. Res*., 64 (10), 1524-1544.

Zor, E., Sandvol, E., Gürbüz, C., Türkelli, N., Seber, D., Barazangi, M. 2003. The crustal structure of the East Anatolian plateau (Turkey) from receiver functions. *Geophysical Research Letters*, vol. 30, no. 24, 8044, doi:10.1029/2003GL018192.

Bull. Min. Res. Exp. (2016) 153:203-222

Bulletin of the Mineral Research and Exploration

http://bulletin.mta.gov.tr

GEOPHYSICAL REGIONAL GRAVITY MAPS OF TURKEY AND ITS GENERAL ASSESSMENT

Selim ARSLAN[a*]

[a] *Gravity and Magnetic Division, General Directorate of Mineral Research and Exploration (MTA)*

Review Article

Keywords:
Gravity, Free Air, Bouguer, Isostasy, Crust Thickness, Density.

Received: 26.10.2015
Accepted: 15.03.2016

ABSTRACT

In this study, the maps generated from the regional gravity data, which had been measured within scope of "Türkiye Rejyonal Gravite Haritaları Projesi" (Regional Gravity Map of Turkey) project were introduced. The topography, Free Air, Bouguer gravity, isostatic residual, isostatic regional, density and crust thickness maps of Turkey in 1/1.500.000 scale were prepared using database which started in 1973 and ended in 2011. The boundaries of the main tectonic members were determined by crust thickness, isostatic residual and Bouguer gravity maps of Turkey. Within this scope, a database that will illuminate the investigation of crustal structure, the development of the scientific database and the solution of geological problems were established.

1. Introduction

The maps presented in this study were prepared by data obtained in the project of "Türkiye Jeofizik Rejyonal Gravite Haritaları Projesi" (Geophysical Regional Gravity Anomaly Map of Turkey), in the General Directorate of Mineral Research and Exploration (MTA) in 1973 by Dr. Erdoğan ORAY. The project initiated in 1973 and was completed by the estimation of all regional gravity data of Turkey in 1988. A small portion of these data were taken from the gravity data of the General Commandership of Turkey (HGK) and Turkish Petroleum Corporation (TPAO). In total; 60166 gravity data were measured and planned such that at least 10 points would fall into 1/25.000 scale topographical sheet with nearly 5-6 km intervals. Besides; in addition to regional gravity data of Turkey, 25.000 gravity data, which had been estimated within scope of TUBITAK project named as "Türkiye Kuzey Batı Anadolu'nun Kabuk Yapısının Jeofizik Yöntemlerle Araştırılması" (Candansayar et al., 2011) (Investigation of the Crustal Structure of the Western Anatolia, by means of Geophysical Methods, Turkey", which started in 2006 and ended in 2011, were also added. The point interval within scope of this project was selected as nearly 2.5 km, and it was also paid attention for 25 data to be in 1/25.000 scale sheet with previous points.

Elevation and coordinate measurements in gravity field studies were taken from 1/25.000 scale topographical maps by means of 1st, 2nd and 3rd degree triangulations. Besides; the points such as; school, mosque, crossing road, river junctions, bridge etc. were detected in which elevations and coordinates could be read on 1/25.000 scale topographical map. The regional gravity and TUBITAK data were measured by Worden Master, Lacoste Romberg gravimeters and Lacoste Romberg and Scintrex CG5 gravimeter instruments, respectively. The coordinate data in TUBITAK Project were measured by Hemishere A 100 DGPS, which has accuracy less than one meter, and orthometric elevations in all data were utilized.

The purposes of the "Regional Gravity Maps of Turkey" project are as follows; to reveal the unexposed deep seated fault systems, to investigate horst-graben structures, to determine surface, deep mass distributions in the project area, the boundaries of the main tectonic units, distributions and relationships, the elastic layer thickness of the continental upper crust, the regional variation and MOHO depth of which isostatic models are suitable and realistic, to increase the international scientific competition by providing information to investigators who make research about the crustal structure, which requires additional research in investigating deep basin structures, and to develop scientific environment and infrastructure

* *Corresponding Author: Selim ARSLAN, sarslan1823@gmail.com - selim.arslan@mta.gov.tr*
http://dx.doi.org/10.19111/bmre.96652

for the utilization of both geophysical and geological studies.

The earth crust is not made up of only one piece but has been separated into several pieces. Each piece is called as the "plate". The compositions, densities, depths and thicknesses display different characteristics. These various blocks, of which their thicknesses, compositions and densities are different, are observed in the form of equilibrium in depths of the earth. In other words; the pressure that these blocks exert in the mantle is balanced at a certain depth or equalized. This equilibrium is called as the "isostatic equilibrium", and it is reached nearly at a depth of 40-50 km. Although the isostatic equilibrium is at a risk of imbalance, it is always protected by motions occurring on earth crust. These movements, which occur for the protection of isostatic equilibrium is called as the "isostatic movements". The events that cause isostatic movements to happen or isostatic equilibrium to fail are erosion, depositional events, glaciation and volcanism. Briefly; the variations that happen as a result of all internal and external phenomena in earth crust is explained by the isostatic equilibrium.

"Isostasy" is the equilibrium of large plates of which their densities and masses are different on crust. The addition or removal of large loads on crust disturbs the isostatic equilibrium. The failure in equilibrium is compensated by the substitution of mantle material on the boundary of crust-mantle. The effective elastic thickness estimation was taken as 6 km for the western Anatolia based on admittance and coherence between gravity, free air and topographical data (Pamukçu et al., 2008). Using the east Anatolian gravity and topography data, this thickness was estimated as 13 km by misfit function (Pamukçu et al., 2011). The admittance function Z(k) from isostatic response functions were defined by making an equation between Fourier Transformations of G(k) gravity and T(k) topography anomaly (Dorman and Lewis, 1970). Later on; Mckenzie and Bowin (1976) have developed the admittance function in their studies. For the eastern America, T_e was estimated as 10 km; and for the Central America and Siberia T_e values were estimated as 18 and 15.5 km's, respectively (McKenzie and Fairhead, 1997).

Many investigators have carried out studies related to the crustal thickness of Turkey by means of gravity data. The crust thickness was estimated as 35-40 km by means of data-process and theoretical modelling using Bouguer gravity data in western Anatolia (Akçığ, 1988). Estimating the power spectrums of the East Anatolian Gravity data, it was stated that the depths had been in between 35.6-45.1 km (Maden et al., 2005). The crust thickness for the eastern Anatolia was found in between 38-52 km by means of the east Anatolian gravity, magnetic and topography data (Pamukçu et al., 2007). The gravity Bouguer anomaly, free air and isostatic residual anomaly data of Turkey were associated with elevation data; and it was seen that the Bouguer anomaly data had given the best result. The crustal thickness of Turkey was estimated as 31.4 km (shallowest) and as 50 km (deepest) (Arslan et al., 2010). Pamukçu et al., (2015) have given information with gravity data about the characteristics of various structural elements observed in the region from their studies called "Doğu Anadolu Bölgesindeki kabuk yapısının düşey ve yatay yönlü analizi" (Vertical and Horizontal Analysis of the crustal structure in the eastern Anatolia Region).

2. Geophysical Regional Gravity Maps of Turkey

The topography, free air, Bouguer anomaly, isostatic regional, isostatic residual, crustal thickness and density maps of Turkey introduced in this article had been prepared using the geophysical Regional Gravity data of Turkey in 2012 making all gravity corrections by copyrighted MTA Geosoft Oasis Montaj Software, and these were published by the General Directorate of Mineral Research and Exploration as a result of referral inspections (Arslan, 2012 a, b, c, d, e, f, g). Each of them was printed as 1000 numbers and still could be obtained by cash as they are available at General Directorate of Mineral Research and Exploration (MTA), Department of Scientific Documentation and Publicity.

2.1. Topographical Map of Turkey

For isostasy correction, elevation data between 24°-48° longitudes and 34°-45° latitudes were used, and a large zone was selected in order to make the isostasy correction until 166.7 km also including sea depths (Hayford Zone). These data were obtained from NOAA's National geophysical http://www.ngdc.noaa.gov/mgg/topo/gltiles.html web site. In Figure 1, Caucasian, Zagros, East Anatolian and Taurus Mountains are observed. Elevations vary between 0-3685 meters on lands and 0-2825 meters in seas.

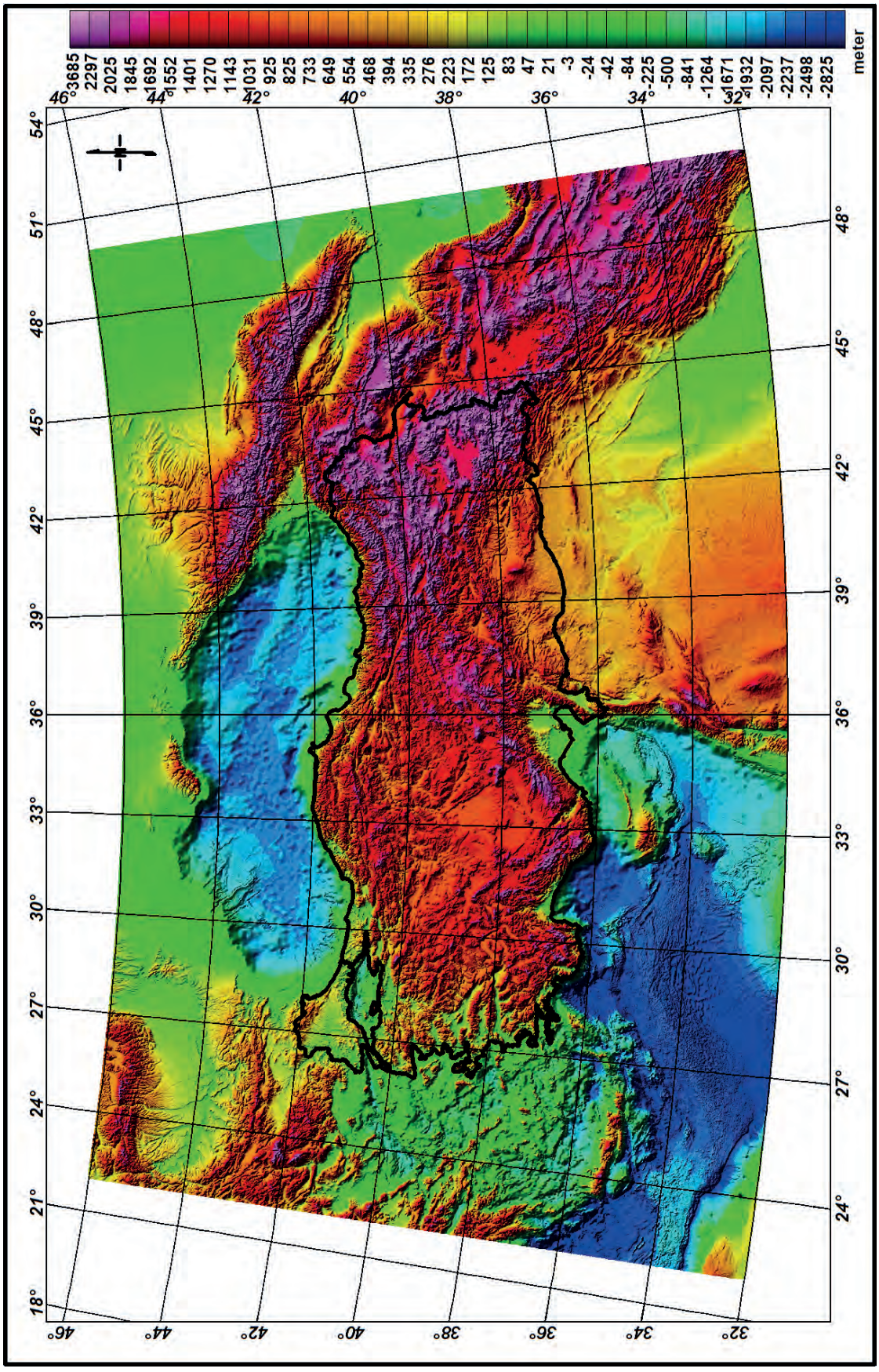

Figure 1 - Topographical map (modified from Arslan, 2012*a*).

The elevation data, which were subjected to isostasy correction, were used in 500 meters' grid interval, and the topographical map of the study area was drawn in order to compare with free air corrected map (Figure 1).

2.2. Free Air Anomaly Map of Turkey

The equation given below was used for the Free Air Correction;

According to the latitude of the measured point;

g_φ = - (0.30877 -0.00044 $\sin^2\varphi$). h_m -0.073 h^2_{km} = 0.3086.h mgal (Erden, 1979)

where;

h: Height of the measurement point above the sea level (h_m meter and h_{km} kilometer)

φ: Latitude of the measurement point.

For $\varphi = 30^o$ latitude;

g_φ is 0.3086.h mgal, and this value changes according to the latitude of each point.

In the study carried out, the latitude correction (g_l) was subtracted from the observed gravity g_{obs} and the free air effect was added.

Free Air Anomaly= $g_{obs} - g_l + 0.3086h$

When the gravitational effect of the topographical mass is equalized as the equivalent of mass in depths, these values in this map will approximately be zero. At regional elevations corresponding to zero free air anomalies, the elevation is related with the isostatic equilibrium. When zero free air values are formed as a result of the formation of the effect that had occurred due to the local mass distribution, such zero values are not used for regional estimations in the Bouguer gravity area (Wollard, 1959). Gravity free air maps generally reflect the topography if there is not any disruptive mass in underground. When the topography map in Figure 1 and free air anomaly map in Figure 2 are compared, there is seen a negative belt located in Edirne and south of Kırklareli in Thrace region. It shows here the presence of a low density cover and it is highly compatible with topographical map. Gravity free air anomaly maps are generally quite useful in detailed researches and mineral explorations. Because, there is considered a disruptive mass below anomalies which show incompatibility with topography.

2.3. Bouguer Anomaly Map of Turkey

Latitude, elevation, geoid and terrain corrections were made in the gravity Bouguer anomaly map. It is crucial to make geoid correction, which varies due to latitude and longitude, since all gravity data of Turkey were used. The density was taken as; 2.4 gr/cm^3 for terrain correction (Nagy, 1966). Some investigators have regarded density as; 2.67 gr/cm^3 for terrain correction, as it was in the elevation correction. The mass calculation in elevation correction is taken from the sea level. Since the utilization of densities of deeper masses is intended, it was regarded that the density for terrain correction should be less than 2.67 gr/cm^3. The mass of the difference among the measurement point and the tilt of the topography, and accordingly; the effect of shallower masses is estimated in terrain correction. The points in TUBITAK project were also measured up to J zone (6652 meter) for compatibility, since previous regional gravity points had been estimated up to J zone by using Hammer chart (Hammer, 1939). Terrain corrections were estimated by elevation data taken from HGK. HGK digitized elevation contours of the 1/25 000 scale topographical maps and prepared in 1 sec x 1 sec ASCII grid format. MTA have purchased the elevation data of 5547 1/25 000 scaled topographical maps of all Turkey in ASCII grid format. Terrain corrections in MTA researches are made by these elevation data. Actually; terrain corrections are made up to 166.7 km (Hayford zone). However, the technical facilities are not suitable for this.

Latitude correction was measured by 1967 geodetic reference formula given below;

g_e = 978031.85* (1 + 0,005278895*sin2φ + 0,000023462*sin4φ) mgal

g_e= 0.8122 sin(2φ) mgal/km

Elevation Correction (E.C.) = (0.3086 - 0.04191ρ) h mgal, h=H+N

where;

h: Ellipsoidal height of the measurement point,

H: Orthometric height

These parameters were read by differential GPS during measurements in TUBITAK project number 105G145. However; in the regional gravity project of

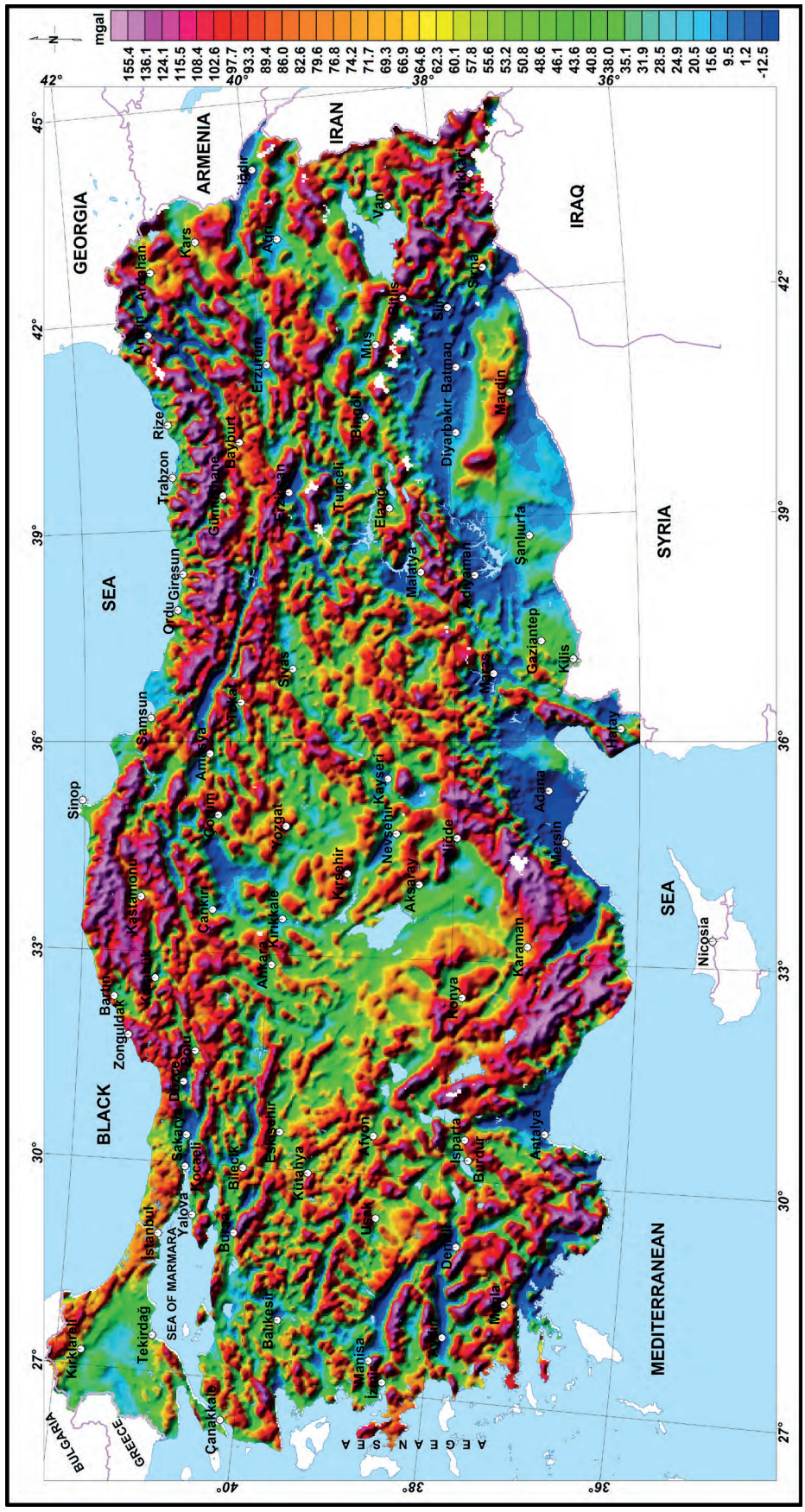

Figure 2- Regional gravity free air anomaly map of Turkey (Arslan, 2012*b*).

MTA these parameters were read by eye from 1/25 000 scale maps. As elevation and coordinates were read by eye in the regional gravity project of MTA using 1/25 000 scale topographical maps, the measurement points were selected in places such as; triangulation points, elevated hill, school, mosque and crossing roads. N geoid height is ρ=2.67 gr/cm^3 which is the upper crust density. The N value was estimated from Geodetic Reference System (GRS) 1980 ellipsoid by entering the data set, in which the geographical coordinates of each point are available, into the licensed Oasis Montaj software

In figure 3, the gravity Bouguer anomaly map is seen. When this map is studied there is observed a negative belt in southwest of Bolu, in Köroğlu Mountains and its southern part. This situation most probably represents low density formations. The Strandja Mountains were bounded by positive indications and the Gediz graben is clearly distinguished on map. The North Anatolian Fault (NAF) is also observed on the map. There might be some granitic intrusions or crustal thickening in most parts where gravity values decrease (Singh et.al., 1999). There is observed also in this study that gravity values in the eastern Anatolia are quite low and the crust is thicker in this area. High gravity values on shores of the Black Sea, Aegean and Mediterranean Sea correspond to areas where the crust thins out. Besides; one can also consider that a magmatic lopolith have revealed gravity increases. In some parts, gravity increases may also correspond to suture belts. As it is known; the gravity values become high as the high density magmatic material approaches the surface in suture belts. Low density granitic intrusions can be represented by negative anomalies. The Eğrigöz granite located in Emet, Kütahya is a good example for that.

2.4. Isostatic Regional Anomaly Map

The "isostasy" is the state of equilibrium of continental pieces which have different thickness, compositions and densities in the mantle, and it defines the state of equilibrium behavior in which there is not any other disturbing effects between the crust and the underlying mantle (Watts, 2001). The concept of isostatic equilibrium was explained by two different hypotheses (Airy and Pratt, 1855). The theory of isostasy explains the state of equilibrium of the outermost layer of the earth with respect to the average densities of underlying rocks. As a result of this theory, the earth surface moves upward or downward because of loading and unloading. Therefore; the concept of isostasy is significant for the definition of lithosphere. Isostatic correction is made in order to remove the gravity effect of isostatic root part.

For isostatic correction, the theory of Airy-Heiskanen was accepted and corrections were estimated up to 166.7 km (Hayford Zone). The topographical data used for the isostatic correction had been taken from the website (http://www.ngdc.noaa.gov/mgg/topo/gltiles.html) of NOAA's National Geophysical Data Center (NGDC). In calculations, the elevation and bathymetrical data between longitudes of 24°-48° and latitudes of 34°-45° were utilized.

During estimations of isostatic regional values, the topographical grid interval was taken as 500 meters. The crustal density was regarded as; 2.8 gr/cm^3, the mantle density as; 3.3 gr/cm^3 and the sea density as; 1.027 gr/cm^3, and approximately 33 km was used for MOHO depth.

Long wave isostatic effect as a response to regional topography consists of a large area in Bouguer anomaly (Figure 3). These anomalies are observed as big negative values as it was seen in the eastern Anatolia. In order to resolve this low density, effect the isostatic correction was made considering the equilibrium surface. When we have a look at the isostatic regional anomaly map in figure 4, it can be considered that the negative belts in the eastern Anatolia have deeper roots compared to west. Because negative belts in the eastern Anatolia have not still become lost though they became small and fragmented despite isostatic correction had been made. However; almost all negative anomalies located on Bouguer anomaly map in western Anatolia (Figure 3) are not seen on the isostatic regional anomaly map (Figure 4). Isostatic regional anomaly values vary between -203.09 and -15.23 mgal as seen in figure 4.

2.5. Isostatic Residual Anomaly Map

Gravity isostatic residual anomaly map (Figure 5) was prepared in order to remove the effect of deep structures. In this study the equilibrium limit was used as 33 km. The isostatic residual anomaly values show distribution compatible with geometries of

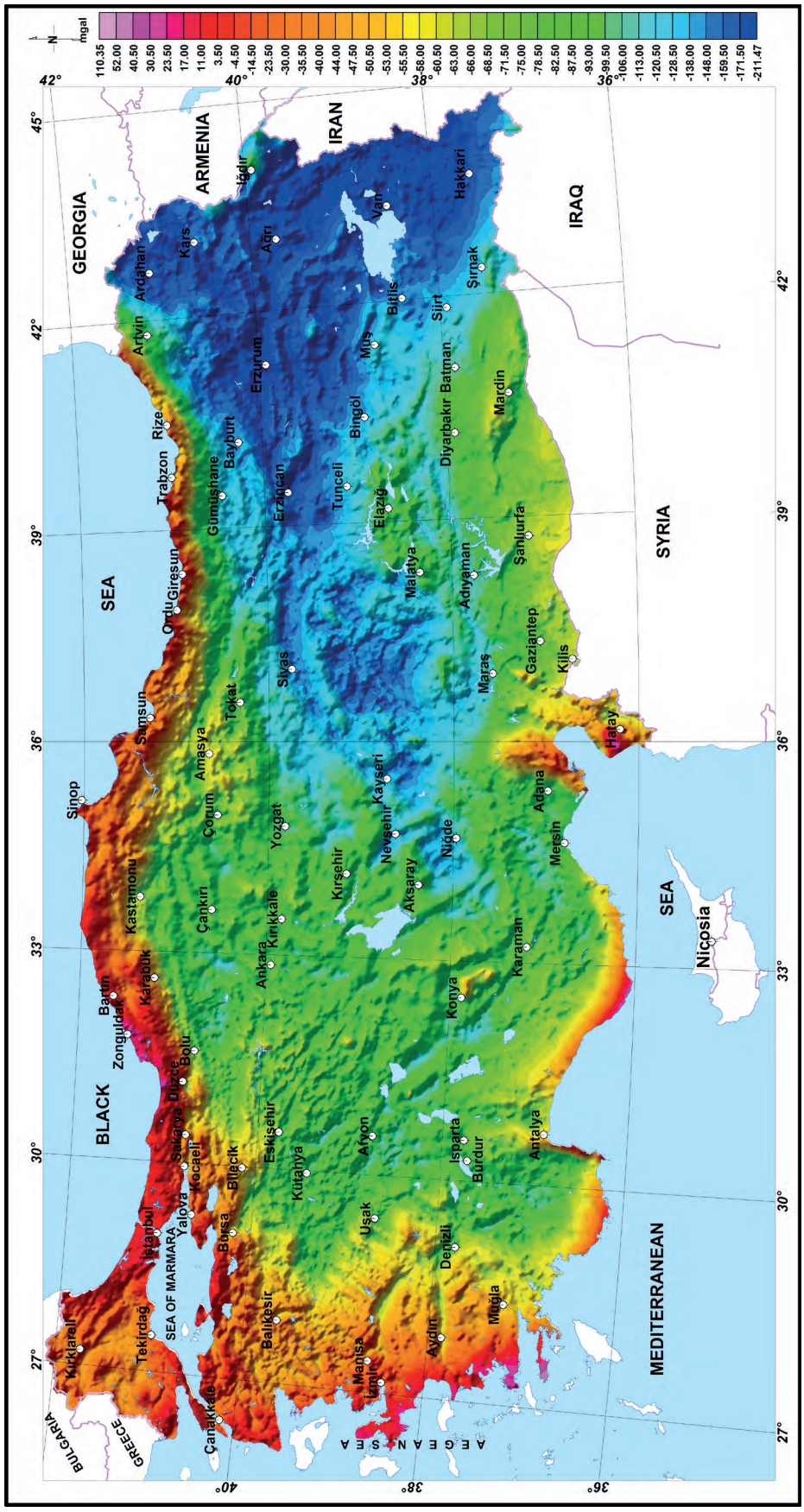

Figure 3- Regional gravity Bouguer anomaly map of Turkey (Arslan, 2012*c*).

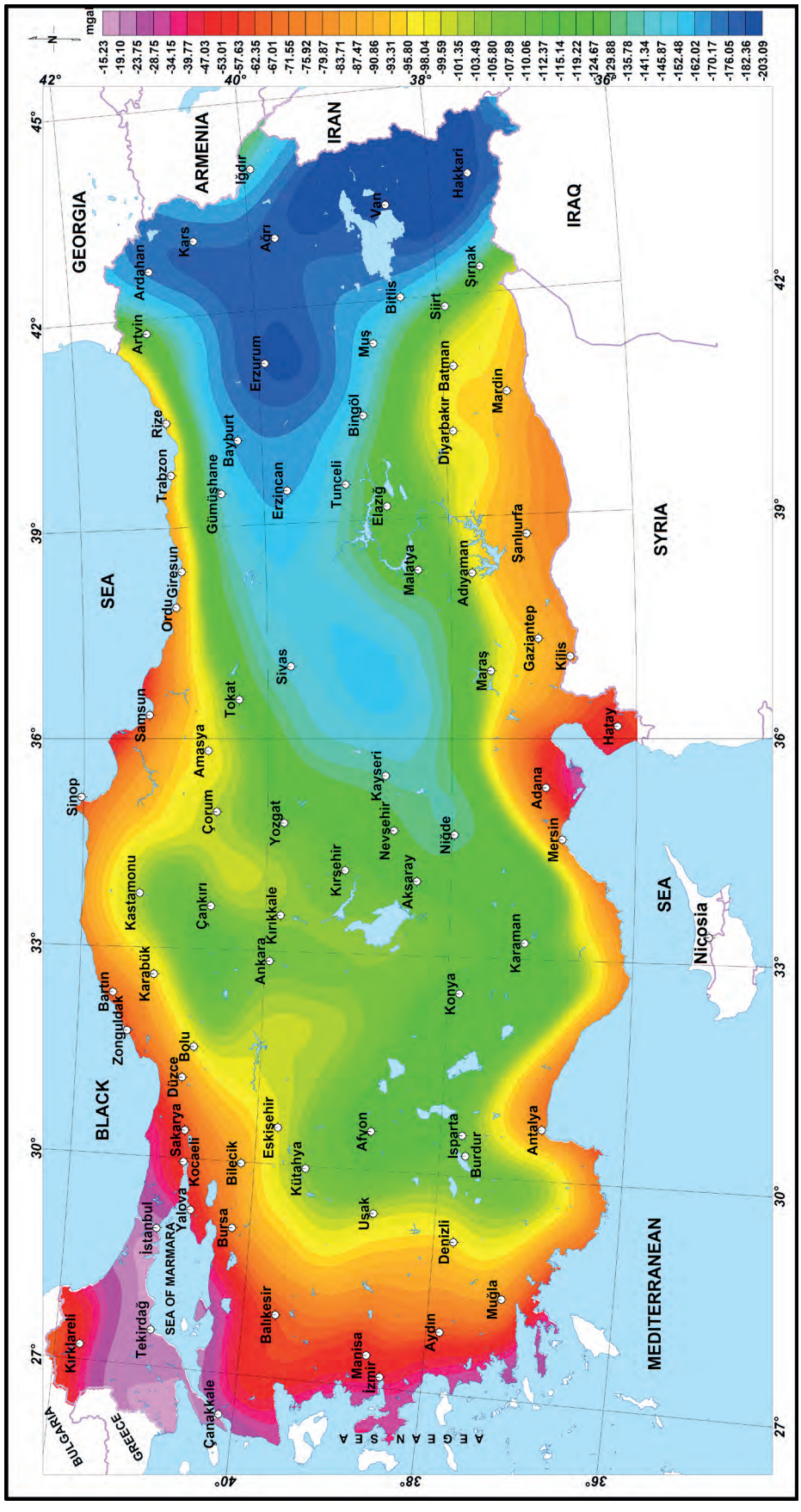

Figure 4- Regional gravity isostatic anomaly map of Turkey (Arslan, 2012*d*).

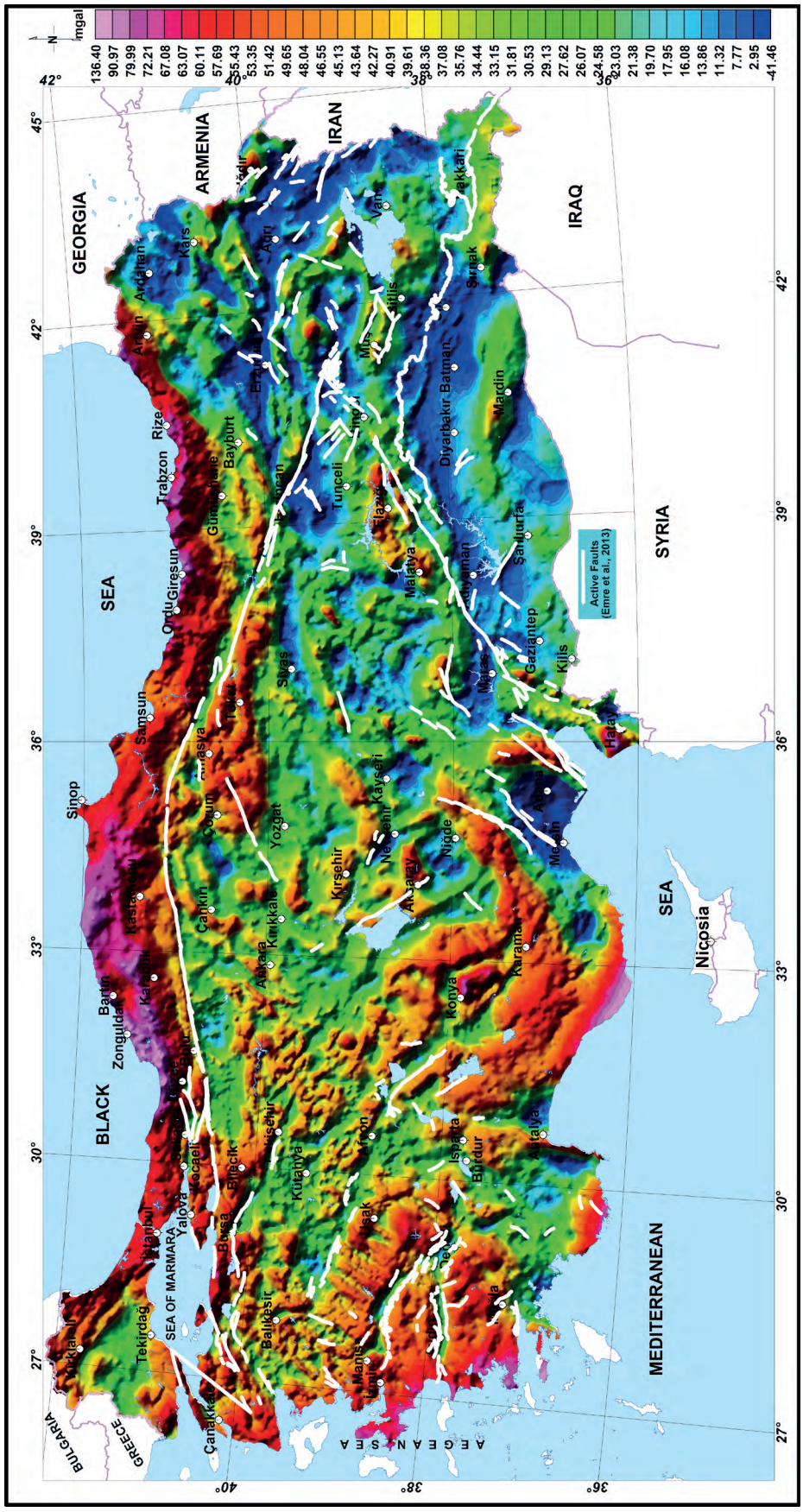

Figure 5- Regional gravity isostatic residual anomaly map of Turkey (Arslan, 2012*e*, active faults data were taken from Emre et.al., 2013).

the main tectonic structures. Negative belts located in south of Kütahya and in west of Kırşehir massif were isostatically corrected, and the effect of root was mostly removed in the gravity isostatic residual map. The negative belt located in Thrace, Edirne and in south of Kırklareli is quite clearly seen here. It shows that the negative belt in Thrace does not have any root but a really thick density and a low cover compared to surround. Big negative anomaly belt in the east Anatolian region in Bouguer anomaly map (Figure 3) was broken into pieces, and the value of the anomaly located in this region on this map has dropped from -168 to -41 mgal. While studying big geological structures and basins of Turkey, both the geological map of Turkey and geophysical gravity isostatic residual anomaly map of Turkey must be interpreted together (Figure 5). For mineral exploration and geological researches in small areas the gravity Bouguer anomaly map can be utilized (Figure 3), but for larger and bigger areas the gravity isostatic residual anomaly maps must be used. There is a big compatibility between the geological map of Turkey and the geophysical isostatic residual map of Turkey in Thrace section. There is a low density deep structure in both maps. Big faults in the active fault map of Turkey were plotted in white color over isostatic residual map (Emre et al., 2013). The North Anatolian Fault (NAF), the Menderes basins and the East Anatolian Fault (EAF) are clearly observed on both maps and are very compatible with each other.

2.6. Crustal Thickness Map Prepared by Using Elastic Thickness

In estimating the crustal thickness, the crust thickness package software prepared for MTA by Geosoft firm was used (Watts, 2001). This program has three steps. In the first step, the effective elastic thickness T_e is predicted by Admittance function. In the second step, the isostatic regional is estimated (Airy, 1855). In the third step, the crust thickness is calculated by isostatic response function. In the first step, gravity Bouguer anomaly values of Turkey and topographical data were entered into Fourier Transform, and the gravity admittance Z(k), wave number and T_e=10 km were predicted (Kirby and swain, 2009). The equilibrium depth of the sea level was used as; 33 km, Bouguer density as; 2.8 gr/cm^3, sea density as; 1.027 gr/cm^3 and Moho density was used as 3.30 gr/cm^3.

Admittance (using distance 1/d), effective elastic thickness prediction;

The effective elastic thickness of the lithosphere T_e is predicted by the Fourier transformation of gravity and topography in regional scale.

Z(k)=[G(k)*H(k)] / [H(k)H*(k)] (Kirby and Swain, 2009) Equation 1

where;

G(k): Fourier Transformation of the gravity data

H(k): Fourier Transformation of the topography

H*(k): Complex equivalence of the topography in the activity area of Fourier

In Air's model, the gravitational area G is formed from the gravity effect of the topography G_{topo} and the equilibrium G_{comp} gravitational effect (root or anti-root). Watts (2001) defines the gravity admittance as a function modifying the topography to generate a gravitational area.

$$Z(k)_{Airy} = 2\,\pi\,g\,(\rho_c - \rho_w)e^{-kd}(1 - e^{-kt})$$ (Watts, 2001) Equation 2

where;

g : Newton's gravitational constant,

ρ_c : Crust density,

ρ_w : Sea water density and

d : Average sea depth.

In Pratt's model, the gravitational area G is formed by the gravitational effect of the topography G_{topo} and the equilibrium gravitational effect (root or anti-root). The admittance in the elastic layer model was developed as follows;

$$Z(k)_{Flex} = 2\,\pi\,g\,(\rho_c - \rho_w)e^{-kd}(1 - \varphi(k)e^{-kDc}$$ Equation 3

where;

g: Newton's gravitational constant,

ρ_o: Sea bottom density,

ρ_w: Sea water density and

D_c: Equilibrium depth.

Flexure response function φ(k)

$$\varphi(k) = \left[\frac{D(T_e)k^4}{(\rho_m-\rho_c)g} + 1\right]^{-1} \quad \text{Equation 4}$$

Flexural rigidity, D is the function of effective elastic thickness (T_e). According to the formula given below;

$$D(Te) = \frac{ETe^3}{12(1-v2)} \quad \text{Equation 5}$$

where;

E: Young's modulus and

V: Poisson's ratio.

The limit equilibrium states of Airy's and Pratt's flexure and admittance are shown in Figure 6.

If it is regarded that the lithosphere has a finite resistance and rigidity, the isostatic equilibrium will be compensated by vertical flexure as the flexure of the plate is prevented in lateral direction because of morphological and abnormal loads over plate. In Bouguer correction it is regarded that the crust has an infinite rigid and it compensates for all loads.

Bouguer gravity and topography data of all Turkey were gridded in 1500 and 500 meters, respectively. In the first stage, the Bouguer and topography data were subjected to FFT. Then in the second stage, T_e=10, 20, 30 and 40 km's were entered in the admittance part of the crust program, and the Airy values by the Equation 2 and flexure by the Equation 3 were calculated and their graphs were drawn. Among these graphs, T_e=10 km, which is the closest to Airy equilibrium depth, was used (Figure 7). In the third stage, from the Airy root part of the MTA crust thickness program the isostatic regional (Airy.grd) was calculated. And in the last stage, the crust thickness was calculated from the crust thickness part (Crust10.grd).

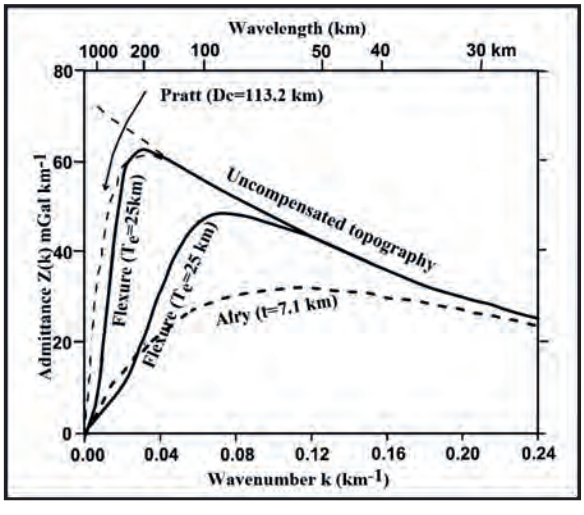

Figure 6- Isostasy and lithosphere flexure (Watts, 2001).

Points on green lines denote for the Fourier transforms of the Bouguer anomaly values, red line denotes for the vertical flexure calculated by the Equation 3 in the elastic layer model, and blue line denotes for Airy isostasy admittance value which was calculated by the Equation 2. If it is considered that the lithosphere has a finite resistance and rigidity, then the isostatic equilibrium will be compensated by the vertical flexure as the lateral flexure of the plate is prevented because of the morphology and abnormal loads on the plate. It is regarded that the crust is infinite and compensates for all loads in the Bouguer correction.

In the third stage, the gravity isostatic regional root depth was estimated by 500-meter topographical grid (Figure 8). The output format was selected as the root depth. The calculation was made by selecting the Bouguer density as 2.8 gr/cm^3, the Moho density as 3.3 gr/cm^3, and the equilibrium depth of the sea level as 33 km. Then the depth of root was estimated until 166.7 km by 3D gravity response (Simpson, 1983).

In the fourth stage (i.e. the estimation of the crust thickness), Airy.grd T_e=10 km, Young's modulus 100 GPa, Poisson's ratio 0.25 and Moho contrast 0.50 gr/cm^3 were used. The output was recorded as crust10.grd. So, the crust thickness map was drawn by crust10.grd in Figure 9.

Regional crust thickness maps were prepared for T_e=10 km in Figure 9 and for T_e=40 km in Figure 10. As T_e value becomes higher, then the crust thickness becomes smaller but the contours become more linear. The crust thickness difference is only 2.6 km looking at both maps. However; T_e=40 km is too high for Turkey.

The crustal thickness map of Turkey was prepared for T_e=10 km; (Figure 11) using the regional crustal thickness map (Figure 9). The crust thickness in this study was estimated in between 33-46 km's. As seen in the crustal thickness map in Figure 11, the shallowest parts of the crust are the northwestern Anatolia, Tekirdağ, Çanakkale (Dardanel) and shores of the Black Sea with 33

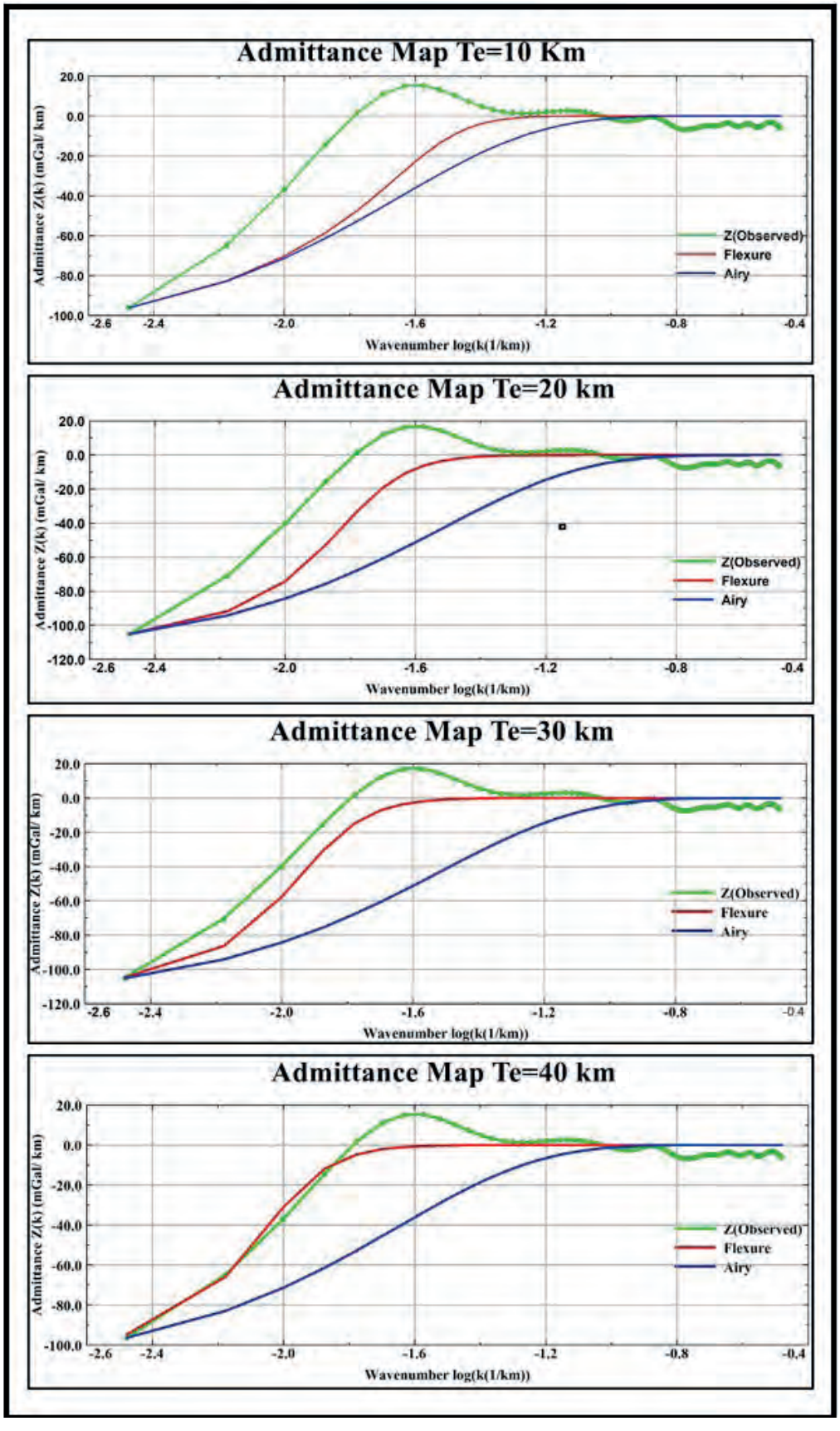

Figure 7- Admittance maps.

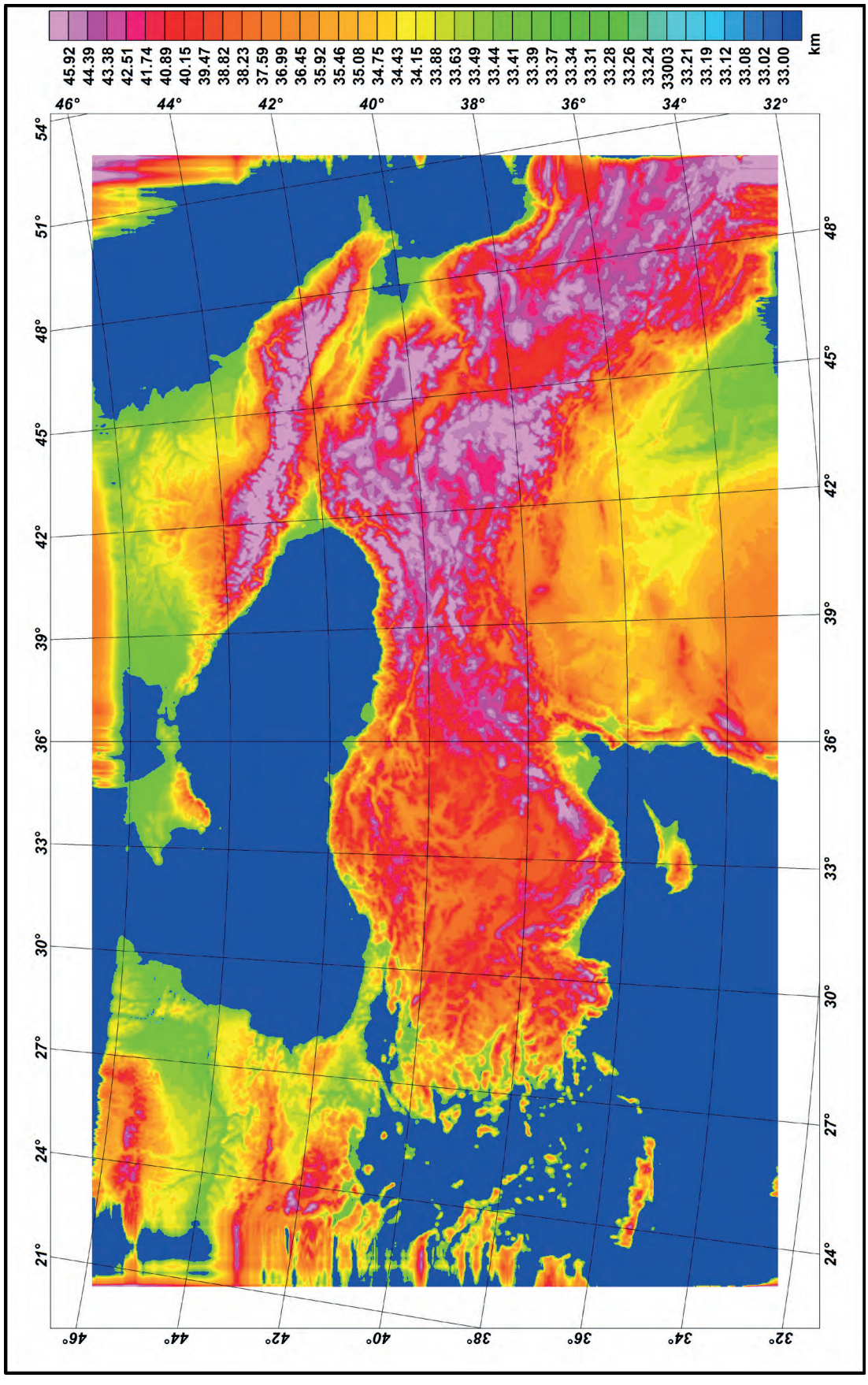

Figure 8- Airy isostatic regional root depth map (Airy.grd).

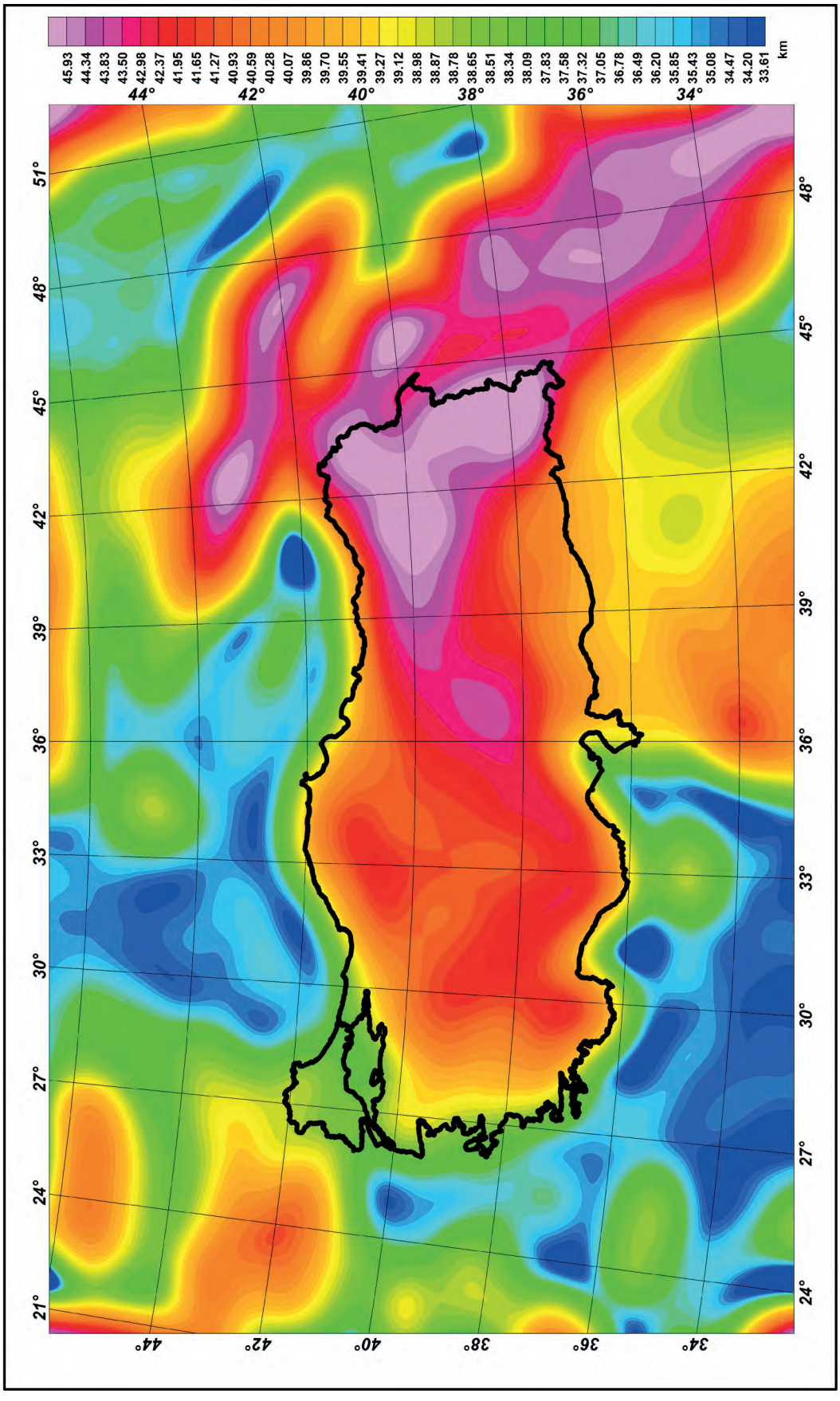

Figure 9- Regional crust thickness map of Turkey for T_e=10 km (Crust10.grd).

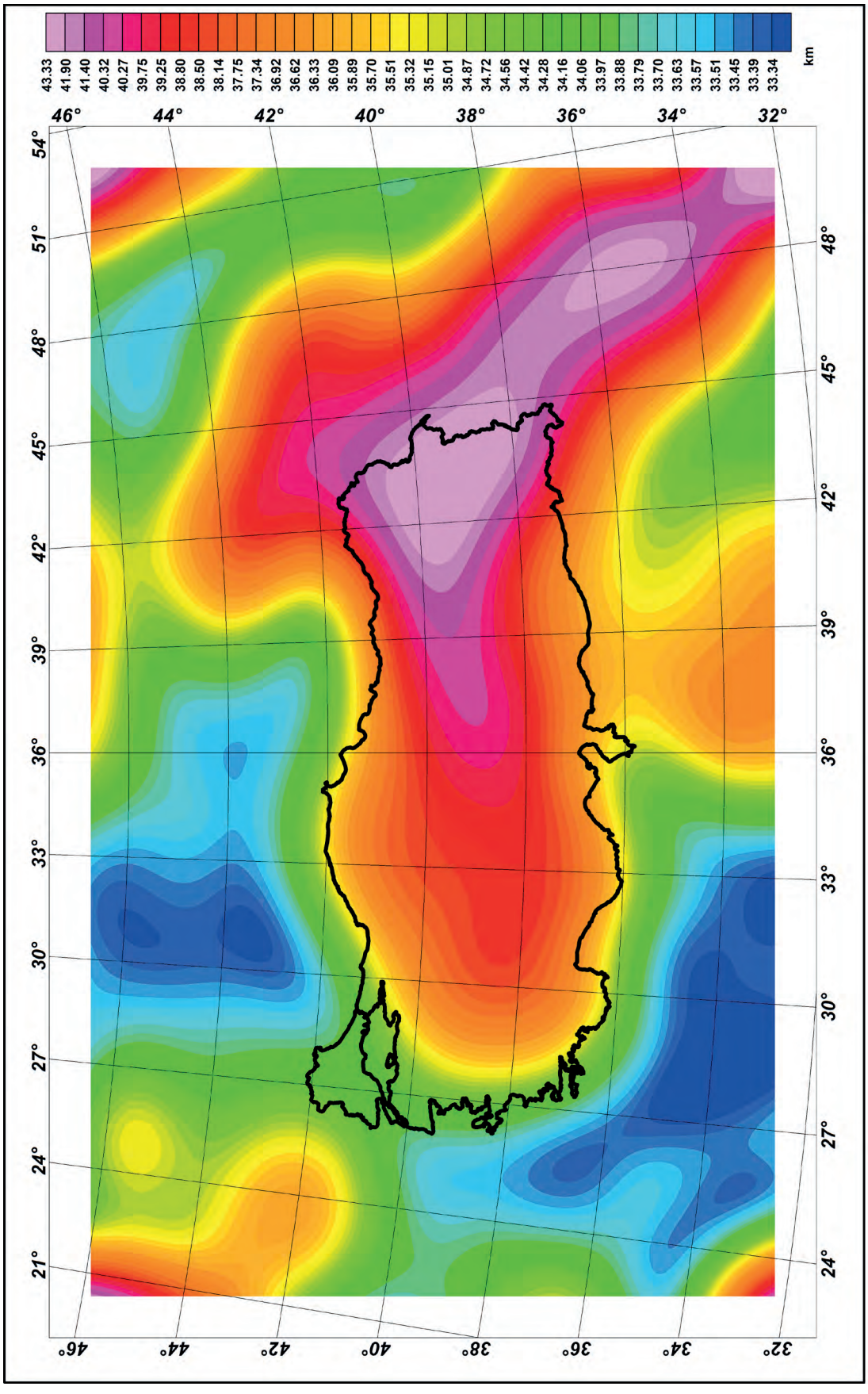

Figure 10- Regional crust thickness map of Turkey for T_e=40 km (Crust40.grd).

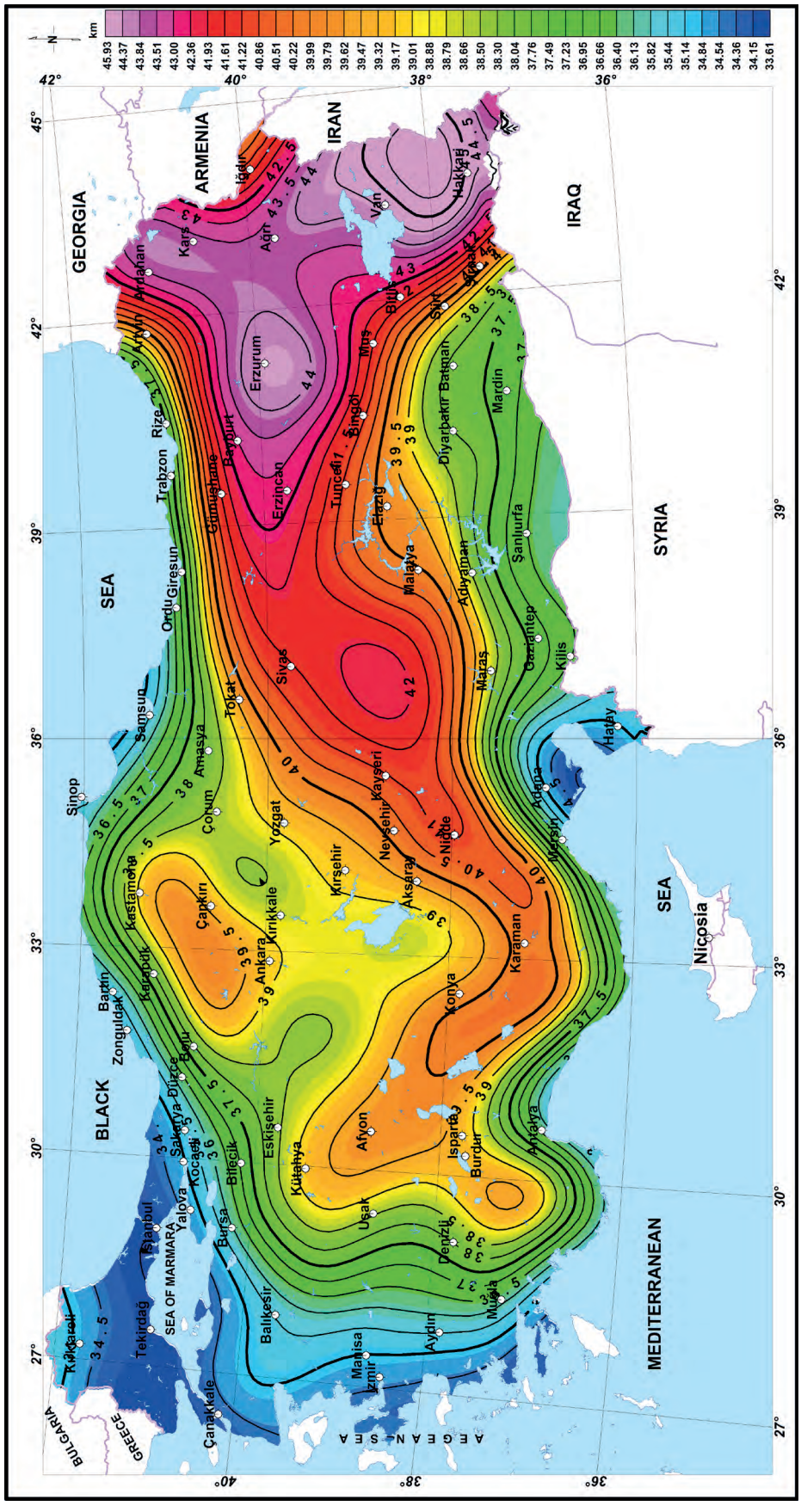

Figure 11- Regional gravity crust thickness map of Turkey (Arslan, 2012*f*).

km. However, the inner parts are relatively thicker. Afyon and its southern part, the northern part of Ankara are the thickest sections of the crust with 39.8 km. The crustal thickness in the eastern Anatolia is around 46 km.

2.7. Density Map

In preparation stages of density maps, 10 km thick horizontal layer represents the upper crust (Singh et al., 1999)

Apparent density;

$\rho(x,y) = \rho_o + (1/2\pi G)\, F^{-1}\{(\omega / 1\text{-}e^{-\omega h}) \,.\, \Delta g(u,v)\}$ (Gupta et al.., 1985)

where;

ρ_o: Predicted background density,

G: Gravitational constant,

H: Thickness,

U: Wave number in x direction,

v : Wave number in y direction and

F^{-1}: Inverse Fourier Transformation.

As it will be understood from the equation, the apparent density filter is a linear filter expressed in the wave number state.

The gravity density map (Figure 12) was obtained by gravity isostatic residual anomaly values using licensed Oasis Montaj software. For the gravity density map, isostatic gravity values were gridded to 1500 meters. First; the trend was removed from the grid, then values were produced to spaces from grids. Lastly; the densities were calculated by applying FFT. As seen in figure 12, the densities vary in between 2.29-2.90 gr/cm^3. This map is as same as the isostatic residual anomaly map in appearance (Figure 5), because the isostatic residual anomaly map in a sense originates from densities of the formations in underground. Only the unit of density map is gr/cm^3 and the unit of isostatic residual anomaly map is mgal. Gravity changes are proportional with the densities of geological structures but inversely proportional with depth and masses of disruptive bodies in underground.

3. Discussion and Results

The thickness of the East Anatolian plateau was found as 46 km by seismic method (Zor et al., 2003). The crustal thickness of Turkey was estimated as 33 km in west and as 46 km in east in this study, and surface densities were estimated as 2.29 and 2.90 gr/cm$_3$. Gravity values in the eastern Anatolia are low; however, the crust depth is quite high. High gravity anomalies on shores coincide with areas where the crust thins out. It can also be considered that these anomalies reveal gravity increases of a magmatic lopolith. In some places the increases in gravity can also match with dyke formation. Low density granitic intrusions can be represented by negative anomalies and the Eğrigöz granite is a good example to this phenomenon.

As a result of this study, isostatic residual anomaly values show a distribution compatible with geometries of the main tectonic structures. The North Anatolian Fault Zone (NAFZ), the Menderes Massive and the East Anatolian fault are clearly seen on map. The large negative anomaly seen in the eastern Anatolia in Bouguer anomaly map (Figure 3) has been broken into pieces and its value has dropped from -168 to -41 mgal. The gravity isostatic residual map in basin analysis (Figure 5) should be assessed with geological maps of Turkey, because geological formations are best reflected by the isostatic residual map.

The maps prepared in this study were generated by using the regional gravity database of Turkey. This database was formed starting from 1973 and have been modified according to changing conditions since then. These maps reflect the projection of large scale geological structures on earth surface. The geometries and changes of these structures towards the deeper parts of the earth crust can be modelled by using other data process methods; and if possible, using geophysical data which give information about depth.

Acknowledgements

I would like to thank to all of my friends who have studied in the project of "Regional Gravity Maps of Turkey" with me and the others who are not with us. I am also grateful to referee Assoc. Prof. Dr. Oya Pamukçu and to the other referee whose name is unknown.

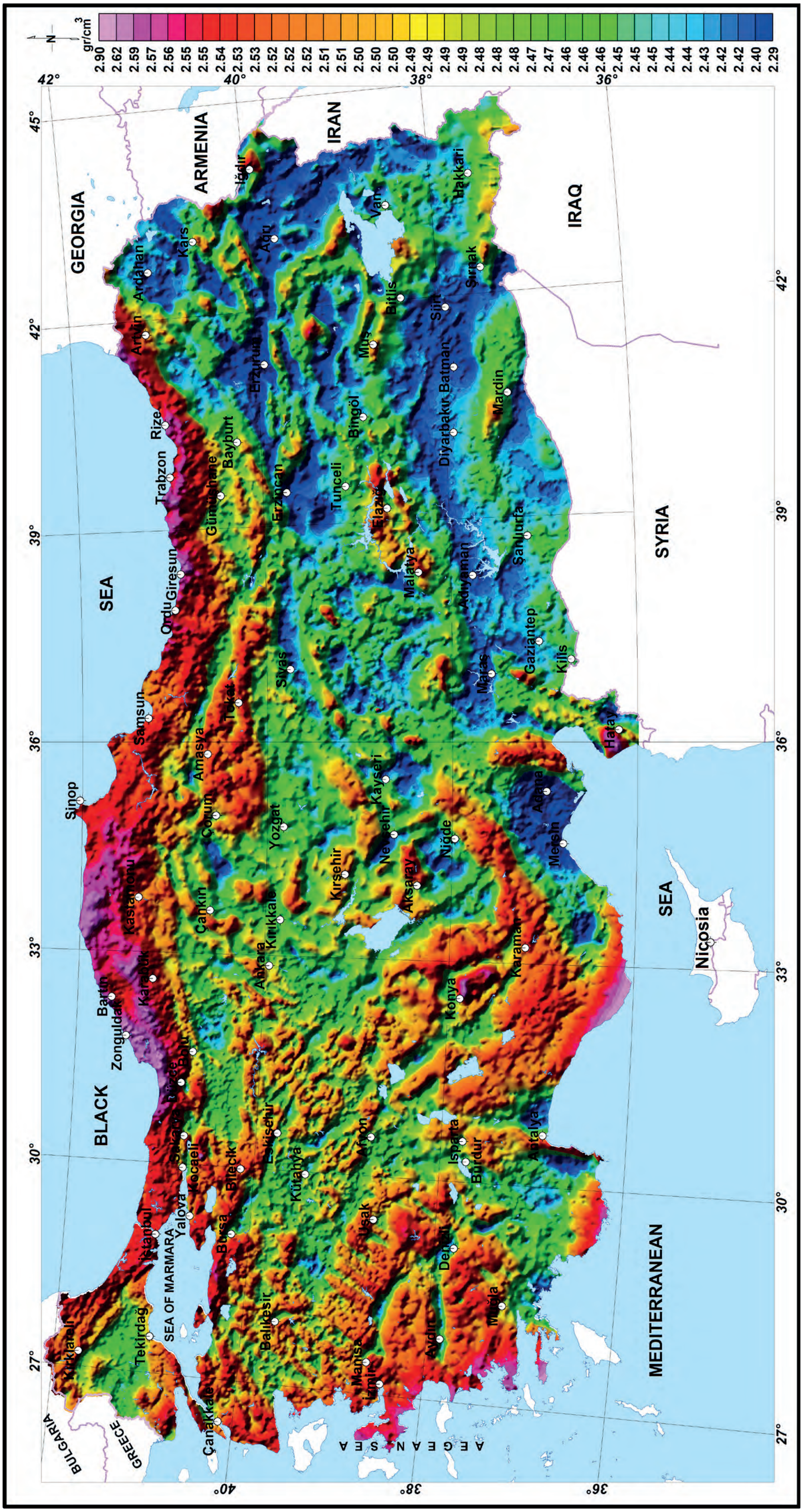

Figure 12- Regional gravity density map of Turkey (Arslan, 2012*g*).

References

Airy, G. B. 1855. On the computation of the effect of the attraction of mountain masses as disturbing the apparent astronomical latitude of stations in geodetic surveys. *Philosophical Transactions of the Royal Society of London* 145. 10 1-104.

Akçığ, Z., 1988. Batı Anadolu'nun yapısal sorunlarının gravite verileri ile irdelenmesi. *Geol. Bull. Of Turkey*, 31, 63-70.

Arslan, S., Akın, U., Alaca, A., 2010. Investigation of Crustal Structure of Turkey by Means of Gravity Data. *Bulletin of the Mineral Research and Exploration,* 140, 55-71.

Arslan, S., 2012a. Türkiye 1/1.500.000 Ölçekli Topoğrafya Haritası. Maden Tetkik ve Arama Genel Müdürlüğü Yayını, Ankara.

Arslan, S., 2012b. Türkiye 1/1.500.000 Ölçekli Gravite Serbest Hava Anomali Haritası. Maden Tetkik ve Arama Genel Müdürlüğü, Ankara.

Arslan, S., 2012c. Türkiye 1/1.500.000 Ölçekli Gravite Bouguer Anomali Haritası. Maden Tetkik ve Arama Genel Müdürlüğü, Ankara.

Arslan, S., 2012d. Türkiye 1/1.500.000 Ölçekli Gravite İzostatik Rejyonal Anomali Haritası. Maden Tetkik ve Arama Genel Müdürlüğü, Ankara.

Arslan, S., 2012e. Türkiye 1/1.500.000 Ölçekli Gravite İzostatik Rezidüel Anomali Haritası. Maden Tetkik ve Arama Genel Müdürlüğü, Ankara.

Arslan, S., 2012f. Türkiye 1/1.500.000 Ölçekli Gravite Kabuk Kalınlığı Haritası. Maden Tetkik ve Arama Genel Müdürlüğü, Ankara.

Arslan, S., 2012g. Türkiye 1/1.500.000 Ölçekli Gravite Yoğunluk Haritası. Maden Tetkik ve Arama Genel Müdürlüğü, Ankara.

Dorman, L.M., Lewis, B.T.R. 1970. Experimental isostasy 1: theory of determination of the Earth's response to a concentrated load. *Journal of Geophysical Research,* 75, 3357–3365.

Emre, Ö., Duman, T.Y., Özalp, S., Elmacı, H., Olgun, Ş., Şaroğlu, F., 2013. 1:1 250.000 Türkiye Diri Fay Haritası. Maden Tetkik ve Arama Genel Müdürlüğü Ankara.

Erden, F., 1979. Uygulamalı Gravite. Maden Tetkik ve Arama Enstitüsü Yayınları, Eğitim Serisi no 21.

Gupta, V.K., Grant, F.S., 1985. Mineral-exploration aspects of gravity and aeromagnetic surveys in the Sudbury-Cobalt area, Ontario; in The Utility of Regional Gravity and Aeromagnetic Anomaly Maps, Society of Exploration Geophysicists, Ed. Hinze, J., Special Volume, p.392-411.

Hammer S., 1939. Terrain corrections for gravimeter stations. *Geophysics*, 4, 184–194.

Hayford, J.F., Bowie, W., 1912. The effect of topography and isostatic compensation upon the intensity of gravity. USCGS, special publication, 10. G.P.O., Washington DC

Heiskanen, W.A., Moritz, H., 1967. Physical Geodesy, W.H. Freeman, San Francisco

Kane, M.F., 1962. A Comprehensive System of Terrain Corrections Using a Digital Computer. *Geophysics,* 27 (4), 455–462

Kirby, S.H., Swain, C.J., 2009. A reassessment of spectral T_e estimation in continental interiors: The case of North America, J. *Geophysical research* v.114, B08401.

Lockwood, A. M., 2004, Western Australia: isostatic residual gravity anomaly and depth to basement model: Western Australia Geological Survey, Record 2004/14, 31.

Maden, N., Gelişli, K., Bektaş, O., Eyüboğlu, Y., 2005. Anadolu'da Kabuk Yapısı ve Tektonik Yapı ile İlişkisi. II. Mühendislik Bilimleri Genç Araştırmacılar Kongresi MBGAK İstanbul.

McKenzie, D.P. Bowin, C.O., 1976. The relationship between bathymetry and gravity in the Atlantic Ocean. *Journal of Geophysical Research,* 81, 1903–1915.

Mckenzie, D.P., Fairhead, D. 1997. Estimates of the effective thickness of the continental lithosphere from Bouguer and free air gravity anomalies. *Journal of Geophysical Research,* B12, 27.523-27552.

Nagy., D., 1966. The Gravitational Attraction of a Right Rectangular Prism. *Geophysics,* 31(2), 362-371.

Pamukçu, O., Akçığ, Z., Demirbaş, Ş., Zor, E. 2007. Investigation of Crustal Thickness in Eastern Anatolia Using Gravity, Magnetic and topographic Data. *Pure appl. Geophys*. 164, 2345-2358.

Pamukçu, O., Yurdakul. A., 2008. Isostatik Compensation in Western Anatolia with Estimate of Efective Elastic Thickness. *Turkish Journal of Earth Scinces*, 17, 545-557.

Pamukçu, A.O., Akçığ, Z., 2011. "Isostasy of the Eastern Anatolia (Turkey) and Discontinuities of its Crust", *Pure Applied Geophysics*, 168/901-917.

Pamukçu, O., Gönenç, T., Yurdakul Çırmık, A., Demirbaş, Ş., Tosun, S., 2015. Vertical and horizontal analysis of crustal structure in eastern Anatolia region. Bull. Min.Res.Exp., 151, 217-229

Pratt, J. H., 1855. On the attraction of the Himalaya Mountains and of the elevated regions beyond upon the plumb-line in India. Philosophical Transactions of the Royal Society of London 145:53- 100.

Qureshy, M. N., 1970. Relation of gravity to elevation, geology and tectonics in India. Proceedings of the second symposium on upper mantle project 28-31 December 1970, Hyderabad.

Simpson, R.W., Jachens, R. C., Blakely, R.J., 1983. Airy root: A Fortran Program for Calculating the Gravitational Attraction of an Airy Isostatic Root Out to 166.7 KM: U.S.G.S. Open-File Report 83-883, 66.

Simpson, R. W., Jachens, R.C., Blakely, R. J., Saltus, R. W., 1986. A New Isostatic Residual Gravity Map of the Conterminous United States with a Discussion on the Significance of Isostatic Residual Anomalies, *Journal of Geophysical Research,* 91, 8348-8372.

Singh A.P., Mishra, D.C, Laxman, G., 2003. National Geophysical Research Institute, Uppal Road, Hyderabad-500 007, Apparent Density Mapping and 3-D Gravity Inversion, of Dharwar Crustal Province. *J. Ind. Geophys*. Union, 7(1), 1-9

Candansayar, M.E., Kaya, C., Gürer, A, Dikmen, Ü., Akın, U, Arslan, S., Kadıoğlu, Y.K., Konak, N., Başokur, A.T., Kaypak, B., Okay, H., Emre, Ö., Kılıç, A.R., Yılmaz, H., Ulugergerli, E.U., 2011. 105G145 nolu "Kuzey Batı Anadolu'nun Kabuk Yapısının Jeofizik Yöntemlerle Araştırılması Projesi" raporu. TÜBİTAK Report

Zor, E., Sandvol, E., Gürbüz, C., Türkelli, N., Seber, D.i Barazangi, M., 2003. The crustal structure of the East Anatolian plateau (Turkey) from receiver functions. *Geophysical Research Letters,* 30, (24), 8044

Watts, A.B., 2001. Isostasy and Flexure of the Lithosphere, 478p, Cambridge University Press.

Woollard, G.P., 1959. Crustal structure from gravity and seismic measurements, *J. Geophys. Res.,* 64, 1521-1544.

Bull. Min. Res. Exp. (2016) 153:223-238

Bulletin of the Mineral Research and Exploration

http://bulletin.mta.gov.tr

PROPOSALS FOR THE STANDARD PRESENTATION OF ELEMENTS OF NATURAL AND CULTURAL HERITAGE WITHIN THE SCOPE OF GEOPARK PROJECTS

Yahya Çiftçi[a*] and Yıldırım Güngör[b]

[a] *General Directorate of Mineral Research and Exploration, Department of Mineral Research and Exploration, Ankara*
[b] *İstanbul University Engineering Faculty, Department of Geological Engineering, Istanbul.*

Review Article

Keywords:
Geopark, Geosite, Natural-Cultural Heritage, Geotourism, Geopark Classification System, Standard Identity Card.

ABSTRACT

The aim of this work is to develop suggestions for designated standards for the display of natural and cultural assets in the design of a Geopark. During a continuing dynamic period detailed work continues to be carried out by experts on the natural and cultural assets found within Geosites that are part of Geoparks according to National laws and guidelines and international agreements. This article proposes standard identity cards, to be used during the period of preparation of a Geopark Project within an area that encompasses a known number of natural and cultural assets. This enables a shared organisation and language to be used within the organisation process relating to the consolidation of data, set-up of visitor centres and route planning activity organisation. The identity cards in question should be prepared in such a way that they give short, interesting summary information about the characteristics of these natural and cultural assets that fits well with, and can be used in conjunction with, other information, brochures and map materials. There is also the potential to prepare graduated identity cards according to the interests of different age groups and levels of understanding. The cards, easy to carry and containing safety information, will therefore be useable by every visitor of whatever age or level of interest (professional, amateur), and will also therefore be useable as educational materials. This work will also open up debate about the new classification and assessment system it proposes in the light of legal definitions and terms and other measures practiced across the world. To develop a classification system is the product of long and hard work and the discussions necessary for the progress of the system may last for years. Indeed some classification systems in use for years come to the point of being inadequate in the light of scientific developments and need to be re-designed. This is the path of scientific thought. There is no doubt that conceptual discussion of these developments that are new both in Turkey and in the wider world will continue in the future. Although consciousness of safeguarding as well as legal policies for cultural assets have progressed to a certain point, unfortunately the same is not true for natural assets. This article presents a contribution to all works in this field both through proposals for standard identity cards for natural and cultural assets and for a classification system for geosites.

Received: 16.09.2015
Accepted: 11.03.2016

1. Introduction and Legal Framework

As a result of the geodynamic processes that have taken place since the formation of the earth's crust the globe on which we live, which is constantly changing and evolving, can be characterised as a living ecosystem. Humans were not witness to a large portion of this development. However in the last few million years anthropological development, and in the last few tens of thousands of years of cultural accumulation and transfer, socialisation has been achieved. During the development of the industrial and information ages humans began to feel a gradual interest in the past and with the help of scientific fields such as archaeology, anthropology and palaeontology began to voyage into both their and nature's past.

On the other hand, the production carried out in industrial societies opened the path to the fast consumption of natural resources; this conscious/unconscious destruction continues to this day. To meet the ever increasing variety of human 'requirements' almost all existing natural resources of the earth, metallic and non-metallic mineral bodies (ores, industrial materials, natural stones) and other natural assets have started to be consumed with disregard for their non-renewability. Thus natural assets have become elements of "natural geological heritage" and at the point where they are not protected they will be consumed and disappear. Equally when it became clear that our links to the earth's past would be broken some protection reflexes came into action. It should not be forgotten that this protection reflex concurrently places protection and reorganisation

* *Corresponding Author: Yahya ÇİFTÇİ, yahyaciftci@gmail.com*
http://dx.doi.org/10.19111/bmre.80846

ahead of industry, which has gained resources at next to no cost, as well as the finances for improvement. The protection reflex also includes the slowing down of the untamed consumption economy in favour of some collectivist approaches. To put it another way, together with the appearance of the safeguarded areas has come a situation where the provision of natural resources has become increasingly difficult and cost is continually increasing.

The first steps towards the safeguarding of Geological Heritage go as far back as the 1750s with the protection works to the Baumann Cave in France and the Giants' Causeway in Ireland (Burek and Prosser, 2008; Doughty, 2008; Erikstad, 2008). Likewise in 1872 the Yellowstone National Park in the USA was brought under special protection status. Later, despite the addition of the Grand Canyon and Karlsbad Caves (Kazancı, 2001), due to lack of an established legal framework and lack of widespread knowledge of safeguarding these efforts were not successful. One of the reasons for this was the beginning of industrial development and the intensive use of material sources and reserves, meaning that such parks might have been seen as an economic risk.

The IUCN (*International Union for the Conservation of Nature*), founded in 1948, and its 1964 "species in danger" and "red list" can be counted as the first systematic and international practices. The signing of the "International UNESCO cultural and natural heritage protection agreement" and the "World Heritage List" published at the same time, although initially awakening great excitement was not particularly effective in the development of safeguarding politics and practice. From the notes of Turkish scientists during this period we know that particularly in northern European countries there was swift development in the conscious protection of rare geological formations (Ketin, 1970). Although this term started to be systematically used in Europe in the 1970s, it was in 1991 at an initiative organised by earth scientists in the town of Digne in France that a proposal for the organisation of the newly-termed Geoparks was published in a manifesto. The document in question was signed by delegates from more than 30 countries (Kazancı, 2001). Although this was heralded as 'the awakening of earth scientists' (Barettino vd., 1999*a, b*), the level reached by the subject in the intervening 25 years cannot be characterised as very hopeful. A short time later the 1995 European Association for the Conservation of Geological Heritage; ProGEO, played an important role in the contemporary and scientific approach to the subject. Meetings were particularly organised on developing solutions to how and by whom these elements of geological heritage should be safeguarded (ProGEO Group, 1998). It was in the same period that these terms rapidly began to be debated (Wimbledon et al., 1995; Wimbledon, 1996; Sol and Ünder, 1999). In 2002 UNESCO put together its own directive on how the safeguarding of geological heritage should be put into practice within the framework of sustainable development and founded the International Geopark Network (GG, 2015; GGN, 2015).

Work on the characterization and protection of the geological heritage of Turkey began in the 1970s (Ketin, 1970; Canik, 1972). Important analyses of outstanding geological heritage elements have been carried out, these rare and special geological formations particularly include caves (Güldalı, 1972; Şenol and Şenol, 1978; Güldalı et al., 1981; Atalay, 1982; Güldalı et al., 1983), chasms (Güldalı and Şaroğlu, 1983), lagoon lakes (Gedik, 1977) and glacier lakes (Perinçek, 1979), waterfalls (Ulakoğlu, 1978), meteorite craters (Arpat and Yılmaz, 1976) and human footprint fossils (Arpat, 1976; Tekkaya, 1976). In the same period proposals oriented towards the protection of natural monuments began to be put forward (Öngür, 1976). Work undertaking the Geotourism concept together with mythology and geology underlines how seriously the subject was approached in Turkey during this period (Yüksel and Korkmaz, 1982; Şaroğlu, 1983). In this period open air museums and their roles were also moved into the scientific realm and public agenda (Altınlı, 1978*a, b*). Works proposing a different perspective on the perception of nature are also found in the same period (Durmaz, 1983). Law number 1710 on Ancient Artefacts (R.G., 1973) and Law number 2873 on National Parks (R.G., 1983), show that the state had started action in this area. Unfortunately these well intentioned works did not move far beyond those engaging with the subject at a professional level and was not transformed into a public preservation reflex. The socio-political and economic conditions of the period in question were likely a great influence in the inadequate legal organization and lack of preparation of education programmes. Even today economic conditions are

seen to be an impediment to the provision of resources and time by the targeted relatively middle to high income groups to such activities. The ÇED regulation that was published in the 21489 Official Newspaper on 07/02/1992 can be added to the organization of the legal protection of nature and countryside that began in the 1980s (R.G., 1993). This regulation was revised on 23/06/1997, 06/06/2002, 16/12/2003, 17/07/2008, 3/10/2013 and 25/11/2014 (RG, 2014). The right of decision making used by the Ministry since 2013 allows 'when seen necessary partial or complete transfer to the Provincial Governors'. This particularly strengthened the central authority on mining or large construction projects that directly interfere with nature and opened the way to some social discomforts. The mining law that can be discussed in the same frame was enacted with statute 6309 from 1954 to 1985 (R.G., 1954) at which date it was re-worked with important changes (RG, 1985*a,b*), in 2004 it was exchanged with statute 5177 (R.G., 2004). However, the new varied rules that defines the conducts in this subject which have resulted considerable unclarity on work programmes, authorization and conduct problems (R.G., 2007). The subject of interest in this article is the complexity created by the interrelated mining law and environment regulation and the uncertainty relating to the safeguarding of elements of geological heritage. Because of the lack of direct reference to geological heritage in the 1980s National Parks Law (R.G., 1983), the deficiencies came to the attention of professional associations and some suggestions for the removal of the deficiencies were put forward (Gürler, 1997; 1999). When we come to the 2000s more comprehensive publications start to be made on the subject (Gürler, 2001; Gürsoy, 2001; Saraç, 2001, Yılmaz, 2002). In addition to assessment works on specific landslide areas and the advent of geotourism (Avcı, 2001), works addressing ecotourism (Akıllı, 2004), special recommendations for the landscaping of areas with geological heritage characteristics (Polat, 2006), geological heritage in National Parks (Kazancı, 2007) and methods for the protection and use of geoparks (Gürler and Timur, 2007) were also put forward in this period.

Recently this subject shows a more striking development. Kazancı's "approaches to the phenomenon of Geosites, Geoparks and Geoheritage in the World and Turkey" and "geological safeguarding: the concept and Fundamentals" (2010*a, b*) act as handbooks for work carried out in Turkey in this field. In the subsequent short period of time in various regions of Turkey proposals for Geoparks have been developed and presented for public attention (Koçan, 2012*a, b*; Akbulut, 2014; Kumsar et al., 2014; Gümüş and Zouros, 2014; Güngör et al., 2014*a, b*). In fact the standard proposals relating to this subject were arrived at during this period (Çiftçi and Güngör, 2014).

Since the year 2000 in the world in general much effort has been given, and continues to be given, to the determination of geological heritage, its safeguarding and orienting towards Geotourism as an element of sustainable development (Wimbledon and Smith-Meyers, 2012; Theodossiou - Drandaki et al., 2002; Brilha et al., 2005; Dowling and Newsome, 2005). In fact, the "European Geopark Network" (EGN) founded in 2000 and the "Global Geopark Network" (GGN) founded by UNESCO in 2002 made clear the rules for contemporary work on the subject and won the position of fundamental organisations at the global scale.

In Turkey, during the same recent period both MTA (TUJEMAP) and some civilian organisations (JEMİRKO) have put forward many elements of geological heritage that are suggested to need safeguarding (MTA, 2015; JEMİRKO, 2015). The process of preparing a project to place these within the organisation of a Geopark and combine them with other elements of natural and cultural heritage is still very new in Turkey. Again in recent years this work has begun to bear fruit and in 2014 Turkey's first National Geopark (Kula Volcanic Geopark) was successfully accessioned into the UNESCO Geopark network. Thus for the first time Turkey's say in the UNESCO-GGN decision making mechanism (Representation right), the right to vote (voting right) and the right to partner status in European and UNESCO-GGN projects (Right to authority) was expressed (Gümüş ve Zouros, 2014).

Although, as highlighted above, in Turkey the basic legal organisation of natural assets and natural heritage are to be found (RG, 1973; RG, 1983), no definition has been made of the contents and standards relating to the terms Geopark and Geosite. This legal inadequacy hinders the formation of a set scientific standard in Geopark planning projects. At the "Workshop for Geoparks and Geological Heritage within the Framework of the UNESCO agreement" held in Ankara on 16/01/2014 the Ministry of Culture and the

General Directorate of Natural Assets' representatives made clear that the disorder in authority in this area had come to an end with decree law 644 (MADDE 13/A – (Ek: 8/8/2011-KHK-648/10 md.) (R.G., 2011). According to the results of the inventory carried out by representatives of the Environment and Planning Ministry with the 2013 "Protected Area Administration System" (SAYS) around 1700 natural protected areas and 49110 folders were included in the system. At the same meeting, according to the regulation prepared by the Ministry for the Countryside and Town Planning (R.G., 2012 and 2013) and published in the official newspaper issue 28358 on 19/07/2012, new safeguarding categories were designated, these are:

Sensitive areas definitely to be protected (Article 7): areas where all uses are restricted excepting scientific work.

Well-qualified protection areas (Article 8): areas protecting traditional lifeway's relating to natural life,

Sustainable protection and controlled use areas (Article 9): areas in which permission can be given to low intensity activities, tourism and settlement.

In papers in the workshop session entitled "Geopark enterprises in Turkey, Protected Areas and Legal Accountability, Area Administration, Geological Heritage and Nature Tourism" there were talks about the Geoparks and Geological Heritage concepts in the UNESCO agreement. In these talks the subject of making joint decisions towards benefiting from Turkey's geographical and geological wealth with international bodies that have an input into the subject of "Geoparks and Geological Heritage" on "legal regulation", "the need for a national network" and "sustainability" was voiced. As can be seen, apart from moving onto the national stage, the concept of "Geological Heritage" does not seem close to having high quality regulations within itself.

In the acceleration of Geopark organization projects in Turkey since the middle of the 2000s unfortunately the term "Geotourism" has taken priority over "Geological Heritage". The Geotourism concept is only one component in the planning of geoparks. The geopark concept really has the characteristic of a "cultural organisation" formulated within the framework of "sustainable development". In fact the main aim here is the determination of natural assets with the characteristics of geological heritage (geosite) and to safeguard them as part of the human experience, and in so doing to both increase awareness and give education relating to nature at every level as well as to transfer these assets to future generations by blocking their rapid exploitation/destruction. Alongside the rapid industrialization during the last 50 years, Turkey's elements of geological heritage have entered a period of rapid destruction, and it should not be left too late to take broad steps in this regard.

Above all a Geopark must contain a certain number of characteristic geosites. In addition, the region's natural and cultural heritage assets must have a place in a specific configuration within the Geopark Project. By looking at their spatial relationships and potential all these natural and cultural assets can be grouped from the point of view of designated scientific, social and cultural activities, activity routes with different aims can be put together and a fit must be found with people's needs. If this is done, in other words, if all the natural and cultural assets are related to one another, there will be a much greater total potential of these natural and cultural heritage elements to raise awareness. Naturally, without local ownership, organisations on this scale will not survive. For this reason it is important that 'local ownership' should be a primary proviso for this sort of project. The ownership of this sort of Geopark Organisation by local administrators and civil organisations at the same time ensures the formation of continuity in organisation and importantly brings about the capability to recruit experts.

2. Terms, Definitions, Principles

In this section previously established systematic approaches to the grouping of Geosites will be explained; firstly the terms Geopark, Geological Heritage, Geotourism and Geosite are discussed. In addition, in explaining the "Framework List" term, this subject's importance will be discussed. Apart from these, other natural and cultural assets that might be included in Geopark Planning will be briefly defined and the proposals developed for their introduction cards are explained.

2.1. Geopark

The name Geopark is given to large areas that encompass several Geosites, as well as other

natural and cultural heritage elements, museums and administration centres. The Geopark area is a cultural organisation that primarily takes under protection networks characterised by geological heritage and natural and cultural heritage and in so doing has the aim of socio-economic development. The Geopark area can be encompassed within one or more of a previously defined "national park", "natural monument" or "special protection area". Thus according to up to date legal regulations a geopark can encapsulate previously formed areas of special status or can be made for any small area within a nature preservation area. Together with geosites, these areas will have a role in preservation as well as raising awareness about safeguarding.

As of June 2015 there were 111 geoparks tied into the "Global UNESCO Network of Geoparks" programme (GGN, 2015*a*), a number that is increasing daily. The number of geoparks in the European Geoparks Network (EGN) is 58. For a geopark project making an application to the Global UNESCO Network of Geoparks (GGN) a form is sent and an assessment made. In this assessment, apart from standard information (country, place, location, geological environment, etc.), the geopark is presented to a commission for suitability assessment and suggestions according to whether it has its own logo, safeguarding strategies for geological site areas and other natural and cultural assets, the infrastructure allowing the geopark's sustainability must be in place, the geopark's geotourism potential must have an established link with the region's tourism sector, the geopark must have local stakeholders, the necessary provision must be made for education opportunities for visitors, the geopark administration must have strategic partnerships, administration structure and sustainable development (GGN, 2015*b*).

As can be seen from the assessment form, the geopark is not solely a concept made for special geological assets or groups of geosites. At the same time a Geopark encompasses other tourist areas such as nature tourism together with geotourism, religious tourism and health tourism. Such an organisation gives the opportunity to present all of these activities under a single umbrella and thus presents the most important cultural organisation servicing sustainable regional development. This is the reason for the rapid increase in the number of Geopark organisations across the World.

In Turkey work on Geoparks began systematically in 2003 with the MTA, JEMİRKO and Kula Volcanic Geopark Project. The Kula Volcanic Geopark Project became part of the UNESCO Geopark Network in 2013. Apart from this in Turkey there are also both yet to be completed or completed Geopark projects such as Çamlıdere (JEMİRKO), Karapınar (Gürler ve Timur, 2007), Levent Valley (Güngör vd. 2012*a, b*, Akbulut, 2014), Gökçeada (Güngör vd., 2014*a*), Nemrut-Süphan (Güngör vd., 2014*b*) and Narman Fairy Chimnies (Güngör, 2014*c*) for which applications have yet to be made to EGN or the UNESCO Geopark Network. Manisa Celal Bayar University was at the forefront of the implementation and research centres showing activity in this area in Turkey (R.G., 2013). This development shows that this subject will quickly move into the academic realm.

Although there is widespread effort and literature relating to Geopark organisation, there is still not a standard proposal for the definition of the term Geosite. The aim of this article is to develop suggestions on this subject and open a discussion.

2.2. Geological Heritage (Geoheritage)

A geosite is a region that is rare, under threat of destruction, with which destruction information about the area and a geological testimonial will be lost (Wimbledon, 1996; Kazancı, 2010*b*). The name "geological heritage" is given to formations or found forms such as regions, rocks, fossils, minerals and ground formations that came into existence at any point in the 4.6 billion year formation period of the earth that are viewed as a finite natural monument that if not taken under safeguard will be destroyed.

The fact that there are hundreds of geological heritage elements in Turkey that fall into this category was dealt with above in description of work on this subject. Apart from these, there are many items of natural heritage that, because protection measures are not yet sufficient, are waiting, identified but not published, both in the inventories of MTA and of civil organisations such as JEMIRCO. Which of these have value as geosites and which might be assessed as the main themes of geoparks are subjects that cannot be decided ab initio.

2.3. Geotourism

Geotourism is an activity, and forms one element of nature tourism that encompasses all types of winter and summer nature sports, that encompasses scientific organisation and attracts high income groups. Geoparks fulfil their regional development role (in a large part) through geotourism (Koçan, 2012*a*). Geotourism, while in some respects at one with nature, also provides the opportunity for the investigation of geological heritage elements and a better understanding of nature. Visits and excursion activities organised with the aim of investigating nature and geological heritage come under the umbrella of "Geotourism" (Kazancı, 2010*b*). In Turkey there are examples of established tours organised in part for archaeological sites and in part to visit cave formations (Damlataş Cave, The Cave of Heaven and Hell). Within this frame, the Nemrut caldera, in the Bitlis-Tatvan region is one of the geological heritage sites in Turkey that is host to hundreds of local and international visitors every year and is an important item of geotourism.

2.4. Geosite

A Geosite is a natural structure such as group of rocks, minerals or fossils, stratum, ground formation or geological structure resulting from an event during the creation or evolution of the earth's crust, that put a process or formation into existence, that has a need for scientific documentation and in some cases visual attraction qualities (Wimbledon, 1996; ProGEO Group, 1998; www. progeo.se).

A geosite is inside a Geopark and carries the characteristic of geological heritage. The geosites in question could themselves be part or all of the geological heritage entity with which they are related. Within this category of geosite can be evaluated not only geological or morphological elements, but also things reminiscent of the earth's formation, as well as ecological history and culture related formations showing human-earth relations.

Elements of "Geological heritage" can be taken under protection by the state. The terms "protection area" and "site" were made only for areas with "archaeological" and "cultural" elements according to the regulations in operation. In Turkey, while there are terms such as National Park, Nature Park and Natural Monument within the protection regulations, there is not as yet a legal framework directly relating to the protection of "geological heritage", the term Geosite could be adapted for the sort of geological heritage that is defined as a "geological heritage protection area".

2.5. The Grouping of Geosites and the Framework List

The ProGEO Group, collected together ten different categories or groups that cover all areas of earth sciences (ProGEO, 1998). These are: a- stratigraphic, b- environmental, c- volcanic-metamorphic- sedimentary petrology, fabrics and structures, events and provinces, d- mineralogical, economic, e- structural, f- geomorphological structures, erosion-deposition events, landscapes and topography, g- events relating to asteroids, h- continental and oceanic scale phenomena, plate relations, i- under-sea, j- historical and cultural geosites (www.progeo.se) (Table 1).

As a general grouping, this division is not detailed. Within each group it is possible to formulate sub-groups by looking at shared characteristics and these sub-groups are known as the Framework List (Brilha et al., 2005). In this way it becomes easier to formulate lists bringing together almost identical characteristics and compare them. Even if the framework lists are not accepted as countries' inventory lists they are an important contribution towards achieving this purpose (Brilha et al., 2005; De Lima at al., 2010). Efforts towards achieving the Framework List for Geosites in Turkey within the structure of JEMİRKO and TUJEMAP, the need for which was suggested by Kazancı and Şaroğlu (2009), have increased in recent years (Kazancı et al., 2005; Kazancı et al., 2012). Kazancı et al. (2015) define the purpose of the Framework List as, "to indicate the occurrence of Geosites, representation of the geosites and indication of the cases without naming them".

All of the effort of creating Framework Lists will of course be shaped by various public and private organisations as well as independent researchers. In this article the focus is on proposals for the definition, classification and formulation of standard identity cards for Geosites.

Indeed the "Natural site inventory form" and "The Technical Assessment In order to Evaluate Natural Sites" prepared by the General Directorate for the Safeguarding of Natural Assets are already

Table 1- Geosite classification by classes and sub-classes, and point system.

Jeosit Sınıf Numarası	Jeosit Sınıfı (*)	Jeosit Alt Sınıfı (Çatı Liste Adı ve Kodu)	Çatı Liste Açıklaması	Jeosit Kodu	Geosite value and points		
					A (5) (Aesthetic)	B (5) (Scientific)	C (A+B) (10)
JS-1	Stratigraphic						
JS-2	Environmental	(Ex: Lakes: G)	(Every types of lacustrine environment)	(JS-2/G-A)	(5)		
JS-3	Volcanic - Metamorphic - Sedimanter Petrology / Textures and Structures, Cases and Provinces						
JS-4	Mineralogical, economic						
JS-5	Structural,						
JS-6	geomorphological structures, erosion-deposition events, topography and land views						
JS-7	Meteorite related events						
JS-8	continental and oceanic scale phenomena, plate relations						
JS-9	Under-sea						
JS-10	Historical and cultural						

(*) Divisions used in the classification system proposed by ProGEO (ProGEO, 1998).

readily available (ÇŞB, 2013). The classification system and standard identity card proposals presented below are not official in character. These proposals are formulated with the intention of easing the communication both within the teams preparing "Geopark Planning Projects" and with official and private parties in any region of Turkey, to be a contribution to the formulation of a shared language. Being the first works on this subject in Turkey, these proposals will progress discussion between interested experts and new proposals. In time this work should be viewed as a well–intentioned start to a potential meeting point on a shared platform with the public.

2.6. Other Natural and Cultural Heritage Components

A Geopark area's essence is to encompass more than one Geosite and in addition other natural and cultural heritage elements within its structure. These 'Natural Heritage' elements consist of wetlands that can shelter flora and fauna and their endemic species, and all types of geomorphological formations.

Cultural Heritage elements are: all types of artefacts and remains pertaining to the activities of people before the present. All types of remains from Palaeolithic caves to Neolithic settlements, younger settlements and artefacts have a place within this class. These cultural remains can be anything from a bead to a road continuing for kilometres (Roman road), a water cistern (Byzantine Yerebatan Cistern), or a canal (Urartu Şamran Canal). The Ministry of Culture has developed standard record forms for every type of find and the director of the museum to which the artefact is related is responsible for it. The subject that interests us in this article is the cultural assets that remain with the area of Geopark projects and the development and introduction of identity cards of different levels according to the age and level of interest of the visitors to the area. The suggested identity cards can initially be considered in three categories. The first category is cards designed to be used by visiting children of primary school age. The second is to be developed for adults. The third type of identity card can be designed with contents suitable for visitors interested at a more professional level. The cards in question can also be translated into different languages and when necessary can be printed within the visitor centre in suitable numbers, or shared digitally. Of course the role of specialist professional groups within the preparation of the cards is essential.

In relation to the research methodology that should be used for the other natural assets, flora and

fauna, the General Directorate for the Safeguarding of Natural Assets' "technical principles" (TVKGM, 2013) presents details. However, these regulations do not contain standard proposals for Geosites and Geological Heritage and it should be emphasised that these subjects are treated in the most superficial way.

The proposed identity cards should be filled in by the subject's experts and presented to the Geopark project group. The experts in question (archaeologists, anthropologists, biologists, botanists, ethno botanists etc.) will of course make a detailed inventory work of the flora and fauna within the scope of the Geopark Proposal Project and will report according to their own legal framework. The identity card suggested here will provide clear characteristic information on stocks of natural assets in abstract format that will help bring together other information and documentation more easily. Here it is enough to say that a Cultural Asset Identity Card, resembling the Geosite Identity Card, would be very useful. The contents of these identity cards, and their pre-preparation, as well as being the subject of a separate study, would help the Geopark Planning Project group to carry out much sounder planning and achieve a sustainable Geopark Administration.

3. Geosite Classification System and Proposal for a Standard Identity Card

It is necessary to be able to describe all Geosites on a standard form, in an easily explicable and indexable classification. Firstly it is suggested that on the basis of general contents 10 Geosite groups should be formed (ProGEO, 1998). In this classification, not including any order of importance, each class is host to a very wide range of geological components and can be divided into sub-groups on the basis of shared characteristics. The sub-groups, as emphasised above, can also be used as headings for the Framework List and these can be scored using a points system in three groups, A, B and C, according to geological importance, scientific value, rarity and aesthetic characteristics (Table 1). In this way a Geopark Project's Geosite richness is shown by the total of the site's Geosite points.

The first and most important scientific activity is the production of the inventory of the Geosite elements within the designated Geopark area. After first placing the geosites within specific groups according to contents and scope and point-scoring them, they must be included in the inventory, having had their other physical and environmental qualities accurately specified. There are various rules for the accession of such natural formations with high scientific or visual value to the inventory. After all the geological specifics of these geological elements have been recorded, the environmental and technical characteristics must also be recorded carefully. The preparation of a standard "Geosite Identity Card" (Table 2) is proposed for the purpose of this recording system.

The inventory studies, based on the identification of specific case studies within a certain time segment, are important and aim to protect the geological sites and their monitoring. In this way, every kind of Geosite in the Geopark area will be recorded and when these cards are used transfer of information will be very practical and fast. The identity cards in question must be made by earth scientists chosen by the Geopark Planning Project Group. Academically trained earth scientists specialised in a specific area and tied to the Geosite field should be commissioned on this subject. The identity cards in question, as discussed in the above 'Cultural asset' section, can be prepared in different styles according to the different intended age and interest groups. Here we will introduce the proposed standard adult format.

On the face of the Geosite Identity Cards are four sections. Starting at the top left and moving clockwise, the first section (blue) gives geographical situation information. The second section (green) gives the Geosite's name, class, sub-class and points, physical dimensions and geological classification measures. The third section (orange) contains information on the physical environment, security and logistics. The fourth section (yellow) gives information on the geosite's geological heritage qualities, what the visitor will find when they visit the site, and what they should bring with them in preparation for their visit.

The back of the identity card also consists of four sections. Moving clockwise, as above, in the top left section (red) the geosite's safeguarding and protection specifics; top right (grey) the geosite's inventory details; bottom right (dark Brown) if it is represented in any way in the visitor museum (photograph, mineral or rock, fossil etc.) and a photograph where necessary; bottom left (pink) a physical view of the inventoried item.

Table 2- Geosite inventory identity card (front and back details).

NATURAL HERITAGE TYPE: GEOLOGICAL HERITAGE (GEOSITE)

GEOGRAPHIC LOCATION	GEOSITE DESCRIPTION
X: Y: Z: COORDINATE SYSTEM: PROJEKTION: 1:25.000 SCALE SHEET Nr: TIME ZONE: PROVINCE: Erzurum COUNTY:Narman VILLAGE: Yoldere LOCALITY: Göndere ROAD ACCESS: 11th km of the Erzurum -Pasinler Road, turn right, first valley.	**GEOSITE NAME:** Gönderi Fairy Chimney **GEOSITE CODE:** GeoCode-1 **GEOSITE CLASS:** Geomorphologic-Erossional Feature **SUBCLASS and SCORE:** Fch-A) ; 5 **DIMENSIONS:** X=20 (mt); Y=20(mt); Z=13(mt) **GEOLOGICAL CLASSIFICATION:** **LITHOLOGY** : Gravelstone-Sandstone **AGE** : Plio-Quaternary **STRATIGRAPHIC UNIT:** Yoldere Formation
GEOLOGICAL HERITAGE SPECIFICATIONS	**PHYSICAL ENVIRONMENT, SAFETY and LOGISTICS**
DESCRIPTION: **IMPORTANCE:** **SCIENTIFIC IMPORTANCE and SIMILAR FEATURES:** **BEST POINT FOR OBSERVATION and VIEW:** **TECHNICAL EQUIPMENT FOR BEST OBSERVATION:** (Binokular, magnify, ruler, textbook, camera, etc.)	**DISTANCE FROM VISITOR CENTER:** (optimum route, km) **NAME and Nr. of the ROUTE :** (on which route of the Geopark?) **NEAREST WATER STATION:**(spring or others, km?) **NEAREST LOGISTCS STATION:**(numbered or coded stations including emergency phone line and other equipment) **NEAREST SAFETY SIGNBOARD :**(signboards that are located in fixed and well known locations by the safety team; includes special marks and sign, phosphoreschent/dark yellow colored, in 50x50 cm diameter and 2 meters high) **NATURAL HAZARD RISK:** (possible risks like flooding, lightning, landslaide, rockfall, snowslide, or any attack wild animals, etc.) **EMERGENCY CALL NUMBERS:** (Police, Gendarme, Forest ranger, Emergency of health and Visitor Emergency Center)

(FRONT)

GÖNDERE FAIRY CHIMNEY (GeoCode-6/Fch-A)	TURKISH NATIONAL GEOSITE INVENTORY Nr:.....
CONSERVATION/PROTECTION PROPERTIES	**GEOSITE INVENTORY PROPERTIES**
PHYSICAL CONDITION AND DAMAGES: (i.e., no artificial damage, but rock fall is possible in heavy rain or wind errosion) **OUTCROP CONSERVATION AND PRECAUTIONS:** (no damagable actions allowed like sampling or digging, etc.) **GEOSITE PROTECTION ADVICES:** (drainage or landscaping, precautions against settlement, pcnic place, agricultural activities or mining, etc.)	**GEOPARK NAME :** **GEOSITE ID :** **NAMES OF THE PEOPLE PREPARED THIS CHARD:** **DATE:** **FIRST DISCOVERY:** **RELATED PAPERS:** **REPRESENTATION IN VISITOR CENTER:** (Geological map, cross/column section, thin/polished section, hand sample, souvenir materials, etc.) **FURTHER INFORMATION ADRESS:**
CURRENT PHYSICAL VIEW	**REPRESENTATIVE SAMPLE IN VISITOR CENTER**
(high-definition photo)	(high-definition photo of the sample in the visitor center)

(REVERSE SIDE)

The "Turkish National Geosite Inventory Number" takes its place on the top right section of this card. This number will be very useful in the preparation of the central Turkish catalogue of geosites and in accordance with proposals to be developed later about the nature of the coding system, a decision can be made. At the same time this number will be used on maps, brochures, route maps and booklets and will be easy to understand in excursion programmes and among the regional population, as well as visitors.

The proposed information to be included in the Geosite inventory identity card are presented in the example in table 2.

4. Geopark Identity Card Proposal

All the natural and cultural elements introduced above will be the elements of the geopark that are combined to prepare a Geopark Project. Therefore when the proposed standard identity cards are completed, they will bring about a situation where a standard assessment form for the Geopark area can be prepared (Table 3).

The Geopark assessment form can be in either standard A4 or A3 sizes. This assessment form, together with the other natural and cultural heritage identity cards presented, will become the key documents for the region. The sections on this standard Geopark assessment form and the information they contain are all proposals that are open to discussion and will progress with the experience of the researchers leading the project. The information proposed to be found on the first page is as follows:

1- Legal foundation and framework: is there a defined safeguarding status for the area of the Geopark organisation? If there are natural monuments or special protection areas, forest assets and protection status, a water reservoir protection area or other such within the Geopark then the national or international safeguarding status should be recorded.

2- Geographical characteristics: The geographic coordinates, settlements in the vicinity and transportation facilities as well as administrative divisions should be recorded on a topographic map of specific scale.

3- Geopark area's geographical borders: The placement of the Geopark area within a wider geographical region should be shown.

4- Geological scope of the Geopark area (general geological characteristics): The Geopark area's regional geology map and legend should be provided. On this map the Geopark's defined Geosites can also be shown.

5- Potential of the Geopark: In this area the Geopark's activity identification is given. The numerical inventory and characteristic information of all types of natural and cultural assets within the geopark area can be given in this space.

On the second page should be the Geopark settlement plan and activity route. On this settlement plan, apart from the main transportation and settlement components, the topographic characteristics (preferably three dimensional), the Geopark's visitor centre and all the natural and cultural items with an identity card within the Geopark should be shown, the routes arranged according to aims should be shown in different colours. The settlement plan in question can be made more complex or more basic according to the ages of the activity groups or the requirements of the groups using it and then printed in the correct numbers.

5. Conclusions

Today there are 111 Geoparks linked to the "Global UNESCO Network of Geoparks" and 58 linked to the European Geoparks Network. Apart from these there are also examples that are not connected with the Geopark networks. The reason for the rapid increase in these types of organisations is both the quickly increasing potential of the educational characteristics of the areas and awareness and consciousness of the protection of nature and the input of Geotourism activities directly into regional economies. One part of Nature Tourism, Geotourism, in contrast to the former which includes all forms of summer and winter nature sports, encompasses a scientific organization and is an activity that attracts high income groups. Meanwhile the Geopark phenomenon encompasses Nature Tourism and Geotourism together with Cultural Assets (archaeology and ethnography), Religious Tourism, and Health Tourism and gives the opportunity for the presentation of all these activities in a designated

Table 3- Details of an example of a standard Geopark identity card.

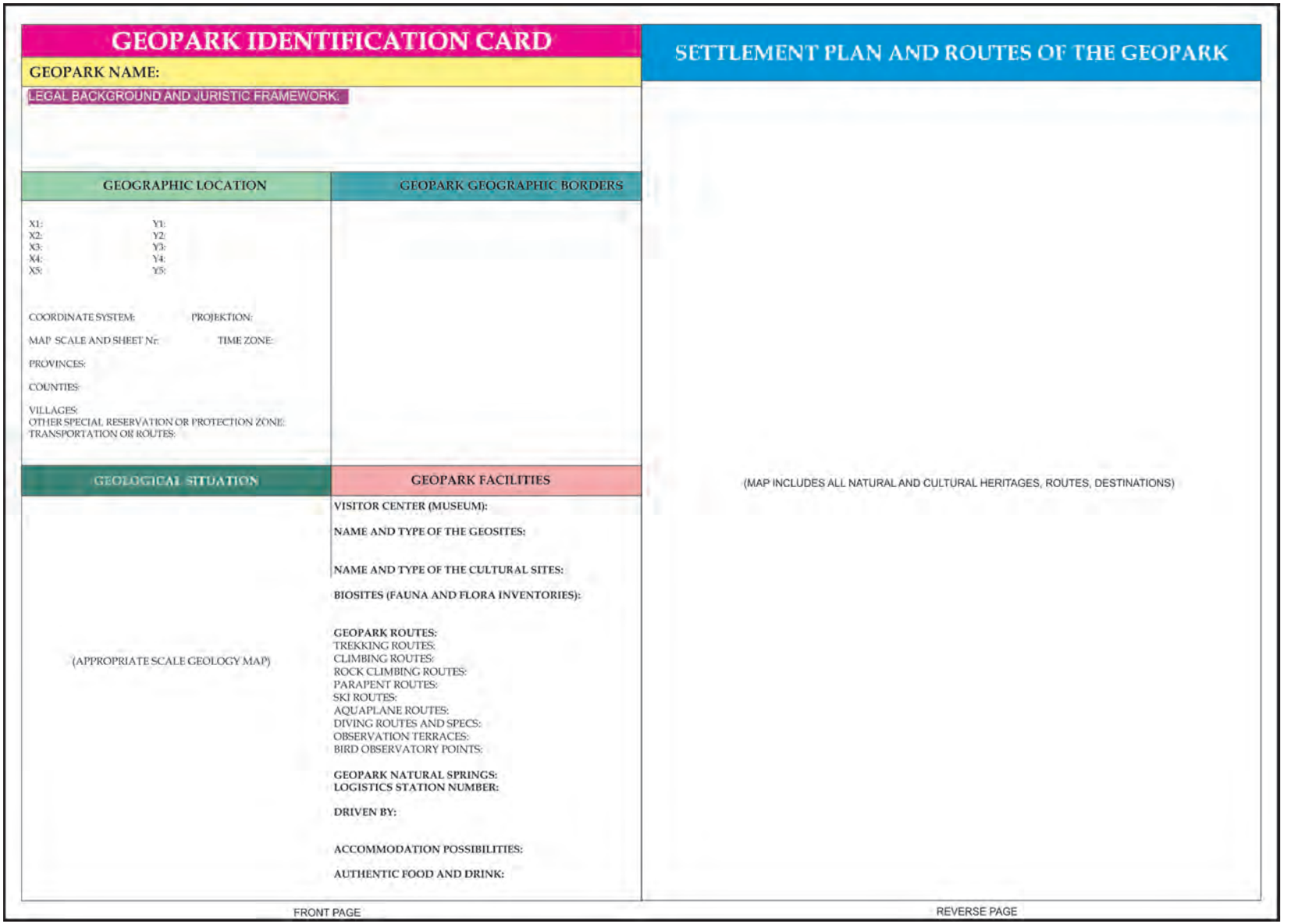

organisation, in a planned fashion (Table 4). Thus, this is the most important cultural contribution to "sustainable regional development". This is the reason for the rapid global increase in Geopark numbers.

In Turkey systematic work on Geoparks started in 2003 with the MTA and JEMIRKO – organised Kızılcahamam Silicified Tree Forest and the Kula Volcanic Geopark. The Kula Volcanic Geopark was included in the UNESCO Geopark Network in 2013. Apart from that the other completed or in-progress Geopark projects have not yet been included in the UNESCO Geopark Network.

Although there are many reasons for this it remains outside the scope of this article. In fact the importance of this subject has not yet been realised. In terms of legal arrangements or local administrations and serious and scientific concentration on this subject there are serious deficiencies. The legal arrangements to be made on this subject can both open recruitment of technical experts from many different branches of science and can ensure the knowledgeable inclusion of these national assets into people's lives. In this way sustainable activities can ensure a contribution to the development of an effective and efficient consciousness of safeguarding.

A Geopark project's success comes from; correct project formation, scientific team work, effective financial structure, stable project administration, the ownership of the project by local communities and sufficient distribution of education and information. Unless all these elements come together a sound Geopark Project is not a realistic proposition.

The aim of Geopark projects is the winning of natural and cultural assets for the public within a known system and in doing this to awake awareness from the point of view of nature, present an addition to education and teaching and in learning to present enjoyment and sustainable regional development. The preparation of this type of project is very complicated both from the scientific and social points of view. The declaration of the natural and cultural assets within this sphere by the use of standard identity cards or forms can achieve convenience as well and advantages for both the experts working in this field and for the people who will benefit from it.

Acknowledgements

The reviewers who carried out the scientific assessment of this article ensured the clearer and more

Table 4- Elements of a Geopark Project.

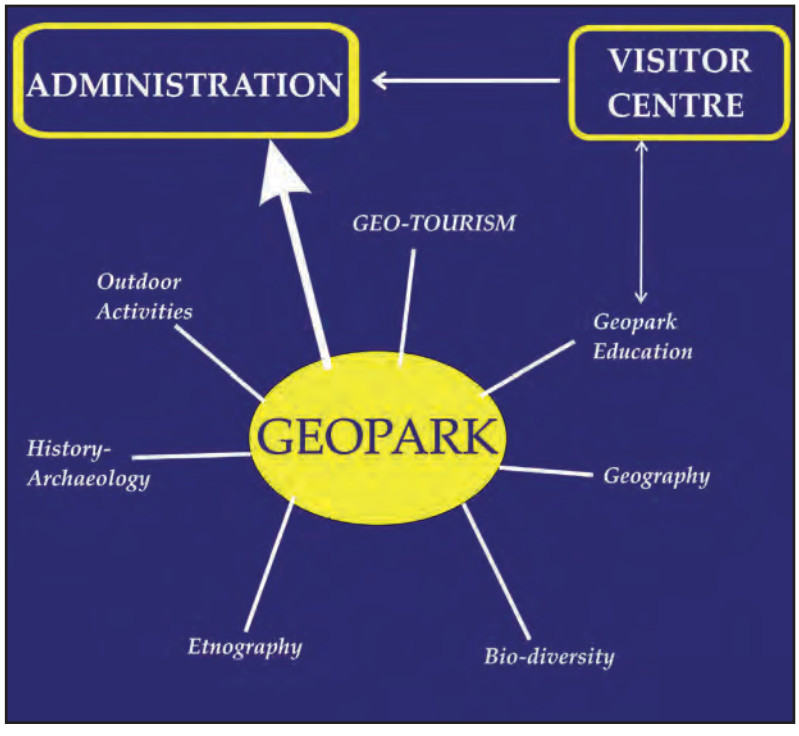

open expression of some terms. For these contributions we offer our thanks. In addition, whether in relation to how cultural assets should be handled or for views on the whole of this article we would like to thank our friend, archaeologist Dr. Adnan Baysal for his time and important contributions.

References

Akbulut, G. 2014. Önerilen Levent Vadisi Jeoparkı'nda Jeositler. *C.Ü. Sosyal Bilimler Dergisi*, Haziran 2014, Volume: 38, No: 1, Sivas

Akıllı, H. 2004. Ekoturizmin Sosyokültürel, Ekonomik, Yönetsel ve Çevresel Etkiler Bakımından İrdelenmesi, Antalya Köprülü Kanyon Milli Parkı Örneği. *Akdeniz Üniversitesi, Sosyal Bilimler Enstitüsü, Yüksek Lisans Tezi*, pp.120, Antalya.

Altınlı, İ. E. 1978*a*. Niçin Açık Hava Müzesi? *Yeryuvarı ve İnsan*, V. 3, No. 3, 29-30.

Altınlı, İ. E. 1978*b*. Bilecik Açık Hava Müzesi. *Yeryuvarı ve İnsan*, V. 3, No. 3, 30.

Arpat, E. 1976. İnsan ayağı izi fosilleri: Yitirilen bir doğal anıt. *Yeryuvarı ve İnsan*, V. 1, No. 2, 3-4.

Arpat, E., Yılmaz, G., 1976. Göktaşı çukuru mu? Çökme çukuru mu?. *Yeryuvarı ve İnsan*, V. 1, No. 1, 12-14.

Atalay, E. Ö. 1982. Kırklareli – Dupnisa Mağara Sistemi. *Yeryuvarı ve İnsan*, 7/2, 22-25.

Avcı, M. 2001. Ağrı Dağı'nda karmaşık bir yerakması: Nuh'un Gemisi. JMO-*Mavi Gezegen*, 4, 3 2-36, Ankara.

Barettino D.,Vallejo M., Gallego E. (Eds), 1999*a*. Towards the Balanced Management and Conservation of the Geological Heritage in the New Millenium. ProGEO- European Association for Conversation of Geological Heritage and Sociedad Geologica de Espana, Madrid, p 459.

Barettino D., Wimbledon W.A.P., Gallego E. (Eds), 1999*b*. Geological Heritage: Its Conservation and Management. ProGEO European Association for the Conservation of the Geological Heritage and Sociedad Geologica de Espana, Madrid, p 212.

Brilha J.,Andrade C., Azerêdo A., Barriga F.J.A.S., Cachão M., Couto H., Cunha P.P., Crispim J.A., Dantas P., Duarte L.V., Freitas M.C., Granja M.H., Henriques M.H., Henriques P., Lopes L., Madeira J., Matos J.M.X., Noronha F., Pais J., Piçarra J., Ramalho M.M., Relvas J.M.R.S., Ribeiro A., Santos A., Santos V., Terrinha P. 2005. Definition of the Portuguese frameworks with international relevance as an input for the European geological heritage characterisation. *Episodes*, 28(3), pp. 177-186.

Burek, C.V.,Prosser, C.D. 2008. The History of Geoconservation. Geological Society, Spec. Pub. 300, London, p 312.

Canik, B. 1972. Jeoloji mostralarına saygı. *TJK Yıllık Bülteni*, 1972.

Çiftçi, Y., Güngör, Y. 2014. Jeosit Tanımlama Ve Jeopark Düzenleme Standartları Üzerine Bir Çalışma, 67. TJK. Bildiri özleri kitabı, p 422, Ankara.

ÇŞB, 2013. Doğal Sit Alanlarının Değerlendirilmesine İlişkin Yönetmelik, Çevre ve Şehircilik Bakanlığı, Tabiat Varlıklarını Koruma Genel Müdürlüğü.

de Lima, F.F.,Brilha, J.B., Salamuni, E. 2010. Inventorying Geological Heritage in large territories: a methodological proposal applied to Brazil. *Geoheritage* 2, 91-99.

Doughty, P. 2008. How things began: the origin of geological conservation. In: The History of Geoconservation (Ed. Burek ve Prosser), *Geol. Soc. Spec. Pub.* 300, London, 7-16.

Dowling, R.,Newsome, D. (eds), 2005. Geotourism. *Elsevier,* Amsterdam.

Durmaz, L. 1983. Yeryüzünü Algılayan Yeni Gözler. Yeryuvarı ve İnsan, 7/4, 18-20.

Erikstad, L. 2008. History of geoconservation in Europe. In: The History of Geoconservation (Ed. Burek ve Prosser), *Geol. Soc. Spec. Pub*. 300, London, 249-256.

Gedik, A. 1977. Korunması gerekli doğal anıtlarımızdan Akyatan Gölü (Lagün). *Yeryuvarı ve İnsan*, V. 2, No. 3, 38-44.

Güldalı, N. 1972. Mağaralar: Yıkıma uğrayan doğal güzelliğimiz. *Yeryuvarı ve İnsan*, V. 2, No. 1, 70-72.

Güldalı, N., Önal, Ö., Nazik, L. 1981. Türkiye'de Mağara Araştırmaları. *Yeryuvarı ve İnsan*, V. 6, No. 3-4, 5-7.

Güldalı, N., Şaroğlu, F. 1983. Konya Yöresi Obrukları. *Yeryuvarı ve İnsan*, 7/4, 14-18.

Güldalı, N., Nazik, L., Derici, Ş. 1983. Narlıkuyu Dilek Mağarası: Turizme açılmakta olan bir mağaranın öyküsü. *Yeryuvarı ve İnsan*, 8/4, 18-21.

Gümüş, E., Zouros, N. 2014. Kula jeoparkı Türkiye'nin ilk ve tek Avrupa ve UNESCO Global Jeoparkı. 67. TJK. Bildiri özleri kitabı, 412-413, Ankara.

Güngör, Y., Çiftçi, Y., Şerifoğlu, T. E., Yıldırım, M. A., Çelik, E. 2014*a*. Türkiye'de Jeopark Çalışmalarına Bir Örnek: Nemrut – Süphan Jeopark, Bitlis. 67. TJK. Bildiri özleri kitabı, p. 424, Ankara.

Güngör, Y., Çiftçi, Y., Kasapçı, C., Azaz, D. 2014*b*. Gökçeada'nın Jeopark Potansiyeli. 67. TJK. Bildiri özleri kitabı, p. 436, Ankara.

Güngör,Y., İskenderoğlu, L., Azaz, D., Güngör, B. 2012*a*. Levent Vadisi (Akçadağ - Malatya) Jeopark envanter çalışması. 65. Türkiye Jeoloji Kurultayı, Bildiri özetleri Kitabı, 322-323.

Güngör, Y., İskenderoğlu, L., Azaz, D., Güngör, B. 2012*b*. Geopark Inventory Study of Levent Valley, Akçadağ- Malatya (Eastern Turkey) 12. International Multidisplinary Scientific Geoconferance, Proceedings, 125 -137.

Güngör, Y. 2014*c*. Narman Peri Bacaları'nın jeosit özellikleri ve jeopark düzenleme projesi. İ.Ü BAP ÖNAP Projesi (unpublished).

Gürler, M. 1997. Doğal koruma alanlarının belirlenmesi ve planlanmasında jeoloji. JMO Semineri; Aynı yazı ve yazar: Birlik Haberleri, 46-48.

Gürler, M. 1999. Ekolojik planlamada jeolojik oluşumlar için öneri bir sınıflama modeli. TMMOB Birlik Haberleri, May-June issue, 1999, Ankara.

Gürler, M. 2001. Anıt nitelikli jeolojik oluşumlar ve koruma çalışmaları. JMO *Mavi Gezegen Popüler Bilim Dergi*si, No. 4, 10-11, Ankara.

Gürler, G., Timur, E. 2007. Jeoparkların Koruma Kullanım Yöntemlerinin Belirlenmesi; Karapınar Potansiyel Jeopark Alanı İçin Bir Değerlendirme, Türkiye. Proceedings of The Second International Symposium on Development Within Geoparks Environmental Protection and Education, Lushan, Jiangxi Province, China, 12-15 June, 2007.

Gürsoy, F. D. 2001. Ürgüp'teki Jeolojik Miras Etkinliği Üzerine. JMO – *Mavi Gezegen Popüler Bilim Dergisi,* 4, No .25, Ankara.

GGN, 2015. http://www.globalgeopark.org/aboutGGN/list/index.htm

GG, 2015. http://www.globalgeopark.org: Evalution Mission/Revalidation Model Report.

JEMİRKO, 2015. www.jemirko.org.tr

Kazancı, N. 2001. Jeolojik Miras Üzerine. JMO *Mavi Gezegen Popüler Bilim Dergisi,* No. 4, 4-9, Ankara.

Kazancı, N. 2007. Milli Parklarda Jeolojik Miras 1, Soğuksu Milli Parkı (Kızılcahamam-Ankara), Çevre, Atmosfer, Yer ve Deniz Bilimleri Araştırma Grubu, 61, Ankara.

Kazancı, N. 2010*a*. Dünyada ve Türkiye'de Jeosit-Jeopark-Jeomiras Olgusuna Yaklaşımlar. Kızılcahamam-Çamlıdere Jeopark ve Jeoturizm Projesi Raporu, p 76, Ankara.

Kazancı, N. 2010*b*, Jeolojik Koruma (Kavram ve Terimler), Jemirko ve TMMOB Jeoloji Mühendisleri Odası Yayınları, p 60, Ankara.

Kazancı, N., Şaroğlu, F., Kırman, E., Uysal, F. 2005. Basic threats on geosites and geo-heritages in Turkey. Proceedings of Second Conference on Geoheritage of Serbia, June 2004 Belgrade, pp. 149-153, Belgrade, Sebia-Montenegro.

Kazancı, N., Şaroğlu, F. 2009. Türkiye Jeositleri Çatı Listesi. 62. Türkiye Jeoloji Kurultayı (13-17 Nisan 2009) Bildiri Özleri Kitabı-I, Jeoloji Mühendisleri Odası, Ankara, pp. 266-267.

Kazancı, N.,Şaroğlu, F., Doğan, A., Mülazımoğlu, N. 2012. Geoconservation and geo-heritage in Turkey. In: Geoheritage in Europe and its Conservation (Ed. W.A.P. Wimbledon ve S. Smith-Meyer), *ProGeo Spec. Pub*, Oslo, Norway, pp. 366-377.

Kazancı, N., Şaroğlu, F., Suludere, Y. 2015. Jeolojik Miras ve Türkiye Jeositleri Çatı Listesi. *Maden Tetkik ve Arama Dergisi* (2015) 151: 263-272, Ankara.

Ketin, İ., 1970. Türkiye'de önemli jeolojik aflörmanların korunması. *TJK Bülteni*, 13/2, 90-93, Ankara. (Aynı yazı Mavi Gezegen 4. Sayı, s.18-19'da (2001) tekrar yayınlanmıştır).

Koçan, N. 2012*a*. Ekoturizm ve Sürdürülebilir Kalkınma: Kızılcahamam-Çamlıdere (Ankara) Jeopark ve Jeoturizm Projesi. Karadeniz Fen Bilimleri Dergisi, 2/6, 69-82, Trabzon.

Koçan, N. 2012*b*. Kızılcahamam-Çamlıdere jeoparkında kırsal peyzaj ve rekreasyon planlama. Erciyes Üniv. *Fen Bil. Dergisi*, 28 (1), 38-46, Kayseri.

Kumsar, H., Aydan, Ö., Ulusay, R., Öztürk, P., Bozlak, F., Orhan, N., Ganız, İ. 2014. Gündoğdu (Babadağ-Denizli) Heyelan Alanının Jeopark Kapsamında Değerlendirilebilirliği, 67. TJK. Bildiri özleri kitabı, 408-409, Ankara.

MTA. 2015. http://www.mta.gov.tr/v2.0/birimler/jeolojik_miras/

Öngür, T. 1976. Doğal anıtların korunmasında yasal dayanaklar. *Yeryuvarı ve İnsan,* V. 1, No. 4, 35-38.

Perinçek, D. 1979. Cilo Dağı, Sat Gölleri. *Yeryuvarı ve İnsan*, V. 4, No. 3, 25-35.

Polat, A.T. 2006. Karapınar İlçesi ve Yakın Çevresi Peyzaj Özelliklerinin Ekoturizm Kullanımları Yönünden Değerlendirilmesi Üzerine Bir Araştırma. Selçuk Üniversitesi, Fen Bilimleri Enstitüsü, Doktora Tezi, p 305, Konya.

ProGeo Group, 1998. A first attemt at a geosites frameworkfor Europe -an lUGS initiative to support recognition of World heritage and European geodiversity. *Geologica Balcanica* 28, 5-32.

Resmi Gazete, 1954. 11.03.1954 tarih ve 8655 Sayılı RG. 6309 sayılı Maden Kanunu.

Resmi Gazete, 1973. 25.04.1973 tarih ve 1710 Sayılı Eski Eserler Kanunu.

Resmi Gazete, 1983. 11.08.1983 tarih ve 2873 Sayılı Milli Parklar Kanunu.

Resmi Gazete, 1985*a*. 15.06.1985 tarih ve 18785 Sayılı RG. 3213 sayılı Maden Kanunu.

Resmi Gazete, 1985*b*. 15.06.1985 tarih ve 18785 Sayılı RG. 5995 Sayılı Kanun İle Değişik 3213 Sayılı Maden Kanunu.

Resmi Gazete, 1993. 07.02.1993 tarih ve 21489 Sayılı RG. Çevresel Etki Değerlendirmesi Yönetmeliği.

Resmi Gazete, 2004. 05.06.2004 tarih ve 25483 Sayılı RG. 5177 sayılı "Maden Kanununda ve Bazı Kanunlarda Değişiklik Yapılmasına İlişkin Kanun".

Resmi Gazete, 2007. 21.04.2007 tarih ve 26500 Sayılı RG. Madencilik Faaliyetleri İzin Yönetmeliğinde Değişiklik Yapılmasına Dair Yönetmelik.

Resmi Gazete, 2012. Çevre ve Şehircilik Bakanlığı, Korunan Alanların Tespit, Tescil ve Onayına İlişkin Usul ve Esaslara Dair Yönetmelik. 19.07.2012 tarihli R.G., Sayı No: 28358.

Resmi Gazete, 2013. 04.07.2011 tarihli ve 27984 Mükerrer sayılı R.G. 29.06.2011 tarihli 644 sayılı KHK. Çevre Ve Şehircilik Bakanlığının Teşkilat Ve Görevleri Hakkında Kanun Hükmünde Kararname.

Resmi Gazete, 2013. 19.02.2013 tarihli ve 28564 sayılı R.G. Çevre ve Şehircilik Bakanlığı, Korunan Alanların Tespit, Tescil ve Onayına İlişkin Usul ve Esaslara Dair Yönetmelikte Değişiklik Yapılmasına Dair Yönetmelik.

Resmi Gazete, 2013. Celal Bayar Üniversitesi Jeopark Uygulama ve Araştırma Merkezi Yönetmeliği. 06.10.2013 tarih ve 28787 sayılı RG.

Resmi Gazete, 2013. 25.11.2014 tarih ve 29186 sayılı RG. Çevresel Etki Değerlendirmesi Yönetmeliği. Çevre ve Şehircilik Bakanlığı.

Saraç, G. 2001. Anadolu'nun bilinen en eski sakinleri. JMO - *Mavi Gezegen Popüler Bilim Dergisi*, 4, 12-17, Ankara.

Şaroğlu, F. 1983. Bingöl Dağı ve Öyküleri. *Yeryuvarı ve İnsan*, 8/3, 3-4.

Sol, A.,Ünder, H. 1999. A model for the conservation of geological remains as documents, *Environmental Geology*, 37, 26-28.

Şenol, F., Şenol, M. 1978. KB Bulgaristan'da bulunan Panora Karst Sistemi'ne bağlı bazı mağaralar ve Türkiye'de mağaracılık. Yeryuvarı ve İnsan, V. 3, No. 1, 11-14.

Tekkaya, İ. 1976. İnsanlara ait fosil ayak izleri. Yeryuvarı ve İnsan, 1/2, 8-12.

Theodossiou-Drandaki,I, R. Nakov, W.A.P. Wimbledon, A.Serjani, A. Neziraj, H. Hallaci, G. Sijaric, P. Begovic, T. Todorov, Pl. Tchoumatchenco, A. Diakantoni, Ch. Fassoulas, N. Kazancı, F. Saroglu, A. Dogan, M. Dimitrijevic, D. Gavrilovic B. Krstic, D. Mijovic, 2004, IUGS Geosites Project progress - a first attempt at a common framework list for southeastern European countries. In: M. Parkes, Ed., Natural and Cultural Landscapes- the Geological foundation. Proceedings of a Conference 9-11 September 2002, Dublin Castle, Ireland, RoyalIrish Academy, Dublin, pp. 81-90.

TVKGM, 2013. Doğal Sit Alanlarının Değerlendirilmesine İlişkin Teknik Esaslar. T.C. Çevre ve Şehircilik bakanlığı, Tabiat Varlıklarını Koruma Genel Müdürlüğü yayını, Ankara.

Ulakoğlu, M. S. 1978. Yeni bir çağlayanlar dizisi. Yeryuvarı ve İnsan, V. 3, No. 1, 8-11.

Wimbledon, W. A., Benton, M. J., Bevins, R. E., Black, G. P., Bridgland, D. R., Cleal, C. J., Cooper, R.G., May, V. J. 1995. The development of a methodology for the selection of British geological sites for conservation: Part 1. *Modern Geology*, 20 (2), 159.

Wimbledon, W.A.P., 1996. National site election, a stop on the road to a European Geosite List. *Geologica Balcanica* 26, 15-27.

Wimbledon, W.A.P., Smith-Meyers, S (eds), 2012. Geoheritage in Europe and Its Conservation. *PeoGEO Spec*. Pub., Oslo, Norway, p 405.

www. progeo.se

Yılmaz, A., 2002. Jeolojik Mirasımız. Bilim ve Teknik, 416, 92-93, Ankara.

Yüksel, V., Korkmaz, S., 1982. Mitoloji, Jeoloji, Jeoturizm: Olimpos'un sönmeyen Alevi. *Yeryuvarı ve İnsan*, 7/2, 3-4.

ACKNOWLEDGEMENT

We gratitude to the following reviewers for their valuable contributions to the Bulletin of The Mineral Research and Exploration in 2016.

Adile Melis SOMAY
Ahmet ŞAŞMAZ
Akın KÜRÇER
Alaaddin VURAL
Ali AYDIN
Ali Ekber DAYA
Alican KOP
Alper BABA
Ana PARAS
Aral OKAY
Arie W. JANSSEN
Asuman KAHYA
Atike NAZİK
Atilla ÇİNER
Aynur HAKYEMEZ
Ayşegül YILDIZ
Azad Sağlam SELÇUK
Baki VAROL
Bedri KURTULUŞ
Bilal SARI
Bülent ORUÇ
Cahit HELVACI
Can AYDAY
Cemal BÖLÜCEK
Cemal GÖNCÜOĞLU
Cihat ALÇİÇEK
Coşkun SARI
Çağlar ÖZKAYMAK
Çetin HOŞTEN
Deniz TİRİNGA
Emin CANDANSAYAR
Emin ÇİFTÇİ
Emrah PEKKAN
Engin MERİÇ
Ercan AKSOY
Ercan AKYOL
Ercan KUŞÇU
Erdal ŞEN
Erdinç YİĞİTBAŞ
Erhan TERCAN
Erol KAYA
Evren TUNCA
A.Feyzi BİNGÖL
Frank WESSELİNG
Füsun YİĞİT FETHİ
Ghasam NABATIAN
Gönül ÇULHA
Güldemin DARBAŞ
Günay ÇİFÇİ
Hakan NEFESLİOĞLU
Halil İPEK
Halim MUTLU
Hasan SÖZBİLİR
Hasan YAZICIGİL
Hülya İNANER
Ioan SEGHEDİ
İbrahim GEDİK
Kimon CHRİSTANİS
Levent GÜLEN
Leyla KALENDER
Mefail YENİYOL
Mehdi ESHAGH
Mehmet ASLAN
Mehmet ÇELİK
Mehmet EKMEKÇİ
Mehmet ÖZKUL
Mehmet ŞENER
Muhittin GÖRMÜŞ
Muhterem DEMİROĞLU
Mustafa AFŞİN
Mustafa DÖNMEZ
Mustafa ERGİN
Mustafa KARABIYIKOĞLU
Mustafa KUŞÇU
Muzaffer Özgü ARISOY
Nail YILDIRIM
Nazire ÖZGEN ERDEM
Necati TÜYSÜZ
Neşe OYAL
Nilgün GÜLEÇ
Nizamettin KAZANCI
Nuretdin KAYMAKÇI
Nurullah HANİLÇİ
Okan TÜYSÜZ
Orhan TATAR
Orkun ERSOY
Osman BEKTAŞ
Osman CANDAN
Osman GÜNAYDIN
Osman PARLAK
Oya PAMUKÇU
Ömer Faruk ÇELİK
Önder KAYADİBİ
Özcan DUMANLILAR
Özlem Öztekin OKAN
Peyman AFZAL
Pınar ŞEN
Recep KILIÇ
Sabah YILMAZ ŞAHİN
Sacit ÖZER
Selahattin KADİR
Selami TOPRAK
Selçuk ALEMDAĞ
Selim ÖZALP
Serdar BAYARI
Serdar KESKİN
Sevinç KAPAN YEŞİLYURT
Shah FAİSAL
Sherif FAUROK
Solmaz BABAKAN
Sönmez SAYILI
Ş. Can GENÇ
Şebnem ARSLAN
Şükrü DURGUN
Şükrü PEHLİVAN
Tahir EMRE
Tekin YÜRÜR
Thanh NGUYEN TİEN
Timur USTAÖMER
Tolga AKEVLİ
Tolga GÖNENÇ
Türker YAKUPOĞLU
Utku BAĞCI
Ümit ŞAFAK
Veysel IŞIK
Vural OYAN
Xurxo COSTOYA NOGUEROL
Yalçın ERSOY
Yeşim BÜYÜKMERİÇ
Yurdal GENÇ
Yüksel ÖRGÜN
Zeki HASSAN
Zihni Mümtaz HİSARLI
Zülfü GÜROCAK